**UNITED STATES DEPARTMENT OF THE INTERIOR**

**GEOLOGICAL SURVEY**

---

PROCEEDINGS OF

WORKSHOP XIV

# EARTHQUAKE HAZARDS OF THE PUGET SOUND REGION, WASHINGTON

Convened Under Auspices of
NATIONAL EARTHQUAKE HAZARDS REDUCTION PROGRAM

Sponsored by
U.S. GEOLOGICAL SURVEY

EARTHQUAKE HAZARDS REDUCTION PROGRAM

13-15 October, 1980 Lake Wilderness, Washington

---


OPEN-FILE REPORT 83-19



*Menlo Park, California*
*1983*

CONFERENCES TO DATE

| | |
|---|---|
| Conference I | Abnormal Animal Behavior Prior to Earthquakes, I<br>Not Open-Filed |
| Conference II | Experimental Studies of Rock Friction with Application to Earthquake Prediction<br>Not Open-Filed |
| Conference III | Fault Mechanics and Its Relation to Earthquake Prediction<br>Open-File No. 78-380 |
| Conference IV | Use of Volunteers in the Earthquake Hazards Reduction Program<br>Open-File No. 78-336 |
| Conference V | Communicating Earthquake Hazard Reduction Information<br>Open-File No. 78-933 |
| Conference VI | Methodology for Identifying Seismic Gaps and Soon-to-Break Gaps<br>Open-File No. 78-943 |
| Conference VII | Stress and Strain Measurements Related to Earthquake Prediction<br>Open-File No. 79-370 |
| Conference VIII | Analysis of Actual Fault Zones in Bedrock<br>Open-File No. 79-1239 |
| Conference IX | Magnitude of Deviatoric Stresses in the Earth's Crust and Upper Mantle<br>Open-File No. 80-625 |
| Conference X | Earthquake Hazards Along the Wasatch and Sierra-Nevada Frontal Fault Zones<br>Open-File No. 80-801 |
| Conference XI | Abnormal Animal Behavior Prior to Earthquakes, II<br>Open-File No. 80-453 |
| Conference XII | Earthquake Prediction Information<br>Open-File No. 80-843 |
| Conference XIII | Evaluation of Regional Seismic Hazards and Risk<br>Open-File No. 81-437 |
| Workshop XIV | Earthquake Hazards of the Puget Sound Region, Washington<br>Open-File No. 83-19 |

Open-File Services Section
Branch of Distribution
U.S. Geological Survey
Box 25425, Federal Center
Denver, Colorado 80225

UNITED STATES DEPARTMENT OF THE INTERIOR

GEOLOGICAL SURVEY

---

# PROCEEDINGS OF

# WORKSHOP XIV

# EARTHQUAKE HAZARDS OF THE PUGET SOUND REGION, WASHINGTON

Convened under Auspices of
NATIONAL EARTHQUAKE HAZARDS REDUCTION PROGRAM

13 - 15 October 1980 Lake Wilderness, Washington

Sponsored by

U.S. GEOLOGICAL SURVEY

EARTHQUAKE HAZARDS REDUCTION PROGRAM

Editors and Convenors

James C. Yount
U.S. Geological Survey
Branch of Western Regional Geology
345 Middlefield Road
Menlo Park, California 94025

and

Robert S. Crosson
Geophysics Program AK-50
University of Washington
Seattle, Washington 98195

OPEN-FILE REPORT 83-19
Compiled by
Muriel Jacobson



MENLO PARK, CALIFORNIA
1983

TABLE OF CONTENTS

ABSTRACTS

# INTRODUCTION AND ACKNOWLEDGEMENTS

This conference, the fourteenth in a series sponsored by the Earthquake Hazards Reduction Program, was held October 13-15, 1980 at Lake Wilderness, Washington. The stated purpose of the conference was to assess progress and the state of knowledge of earthquake hazards in the Puget Sound region of Washington. The small size of the group and the pleasant informal setting of the Lake Wilderness Conference Facility created conditions which encouraged abundant discussion, expansion of ideas and impromptu presentation that went well beyond the scheduled topics, most of which are covered in this volume.

Initially it was hoped that some fundamental questions about earthquake causes and hazards could be answered during the Proceedings. In particular, 1) What tectonic mechanisms are responsible for observed earthquakes in Puget Sound? 2) What is the largest expectable earthquake in Puget Sound, and at what depth would it likely occur? 3) What are the probable hazardous geologic effects of such expectable earthquakes?

It became evident early in the conference that educated guesses, rather than convincing answers, were all that would come out of our present state of knowledge.

Significant progress has been demonstrated for suggesting plausible tectonic mechanisms for observed earthquakes. Recognition of shallow (less than 30 km) and deep suites (40 to 70 km) of earthquakes (Crosson, Rogers; this volume) that might be caused by compression in the upper plate (shallow) and tension in the lower plate (deep), gives a starting point for interpreting the neotectonics of the region. The north-south compression documented for upper plate earthquakes (Crosson, Rogers, Yelin and Crosson) was most logically attributed to stress generated by oblique northeasterly subduction of the Juan de Fuca Plate, and the general northward motion of the Pacific Plate relative to North America.

However, it has long been a puzzle that even though subduction of the Juan de Fuca Plate is going on all the way from southern British Columbia to northern California, as evidenced by Holocene activity in most of the volcanoes in the Cascade Range, the seismicity associated with this subduction occurs almost entirely in the Puget Sound-Georgia Strait region. Stress concentration at triple junctions (Fox and Engebretson) and bends or bulges in the lower plate (Rogers) may explain the concentration of deep earthquakes around Puget Sound, with aseismic creep taking place to the south (Weichert and Hyndman).

Estimates of the largest possible earthquake and its probable location in the region are hampered by the short duration of high quality seismic location data (network operating since 1970) and the short historic record of seismicity. Intensive study of historic earthquakes has been undertaken for the region for purposes of siting numerous nuclear power plants in western Washington and Oregon. And, although an 1872 earthquake of Modified Mercalli intensity VIII has been recognized to have occurred in the Pacific Northwest, its probable location has been greatly debated. Much of the location difficulty stems directly from the lack of geologic structures known to be capable

of generating earthquakes in the Pacific Northwest. Whether this is confirmation that most large earthquakes occur in the lower plate, or that geologic investigation has not been detailed enough to delineate active faults with surface expression, is not clear. The investigations by Wilson and by Wagner and Wiley would suggest that active faults may be more common in Puget Sound than was once believed.

Finally, the problem of geologic consequences of large earthquakes is one that has not been solved in Puget Sound. In a general way, liquefaction, landsliding and intensified ground shaking are phenomena that have been observed in past earthquakes (Keefer), particularly in 1949 and 1965. But, apparently owing to large possible variations in source depth, the highly variable thickness and physical properties of unconsolidated and semi-consolidated sediments that underlie Puget Sound, and the highly irregular basement topography of the region, prediction of the behavior of specific sites for postulated earthqukes has been difficult (Langston, Yount), as has interpretation of observed response from past earthquakes.

Any success this conference had was due, in large part, to the effort of Jessie Reeves of the U.S. Geological Survey and Peggy Ruthstrom of Lake Wilderness and their efficient handling of accommodations and logistics. Robert Page, past program manager of the Earthquake Hazards Program, suggested the need for the conference and Robert Brown, Jr., present program manager, supported the effort. Thanks are due to Howard Gower and Gordon Greene for their numerous suggestions for participants and topics in the planning stage of the conference. Jesse Reeves and Muriel Jacobson assisted greatly in the assembly of the conference volume.

List of Participants

Dr. Gary Anttonen
Golder Associates
10628 NE 38th Place
Kirkland, WA 98033
8-399-0111, (206) 827-0777

Dr. Robert Brown
U.S. Geological Survey
345 Middlefield Rd., MS 77
Menlo Park, CA 94025
323-8111 x 2565

Dr. Don Caldwell
Golder Associates
10628 NE 38th Place
Kirkland, WA 98033

Dr. Paul Carroll
U.S. Geological Survey
1107 NE 45th Street
Seattle, WA 98105

Dr. Robert S. Crosson
University of Washington
Geophysics Program
Seattle, Washington 98195
8-392-2100 x 6505

Dr. F. Danes
Dept. of Physics
University of Puget Sound
Tacoma, WA 98416
8-390-6111, (206) 756-3127

Dr. David Engebretson
Dept. of Geophysics
Stanford University
Stanford, CA 94305
(415) 497-2537, 326-7399

Dr. Kenneth Fox
U.S. Geological Survey
345 Middlefield Road, MS 75
Menlo Park, CA 94025
(415) 323-8111 x 2032

Mr. Gordon W. Greene
U.S. Geological Survey
345 Middlefield Road, MS 83
Menlo Park, CA 94025
(415) 323-8111 x 2764

Dr. M. H. Hait, Jr.
Engineering Geology Branch
U.S.G.S. MS 903
Denver Federal Center
Denver, CO 80225

Mr. Renner B. Hofmann
Golder Associates Inc.
10628 NE 38th Place
Kirkland, WA 98033

Dr. Mark Holmes
U.S. Geological Survey
"U" District Building
1107 NE 45th St., Suite 110
Seattle, WA 98105
8-399-1995

Dr. Phil Justus
U.S. NCR
P-314
Washington, D. C. 20555

Dr. David K. Keefer
U.S. Geological Survey
345 Middlefield Rd., MS 98
Menlo Park, CA 94025
(415) 323-8111 x 7115

Dr. Charles A. Langston
Dept. of Geosciences
Pennsylvania State University
University Park, PA 16802
8-455-4700, (814) 865-0085

Dr. Robert Morris
U. S. Geological Survey
National Center, MS 908
Reston, VA 22092

Ms. Linda Noson
Geophysics Program AK-50
University of Washington
Seattle, WA 98195

Dr. Fred Pessl
U.S. Geological Survey, Suite 125
"U" District Building
1107 NE 45th Street
Seattle, WA 98105
(206) 442-7300

Dr. Norman H. Rasmussen
Geophysics Program AK-50
University of Washington
Seattle, Washington 98195
8-392-8020

Mrs. Jessie F. Reeves
U.S. Geological Survey
345 Middlefield Rd., MS 83
Menlo Park, CA 94025
(415) 323-8111 x 2765

Dr. Garry C. Rogers
Pacific Geoscience Center
Earth Physics Branch
P. O. Box 6000
Sidney, B. C. V8L 4B2
Canada
(604) 656-8269

Dr. Stewart W. Smith
Geophysics Program AK-50
University of Washington
Seattle, WA 98105
8-392-8020

Dr. Carl Stepp
Fugro Associates
3777 Long Beach Blvd.
Long Beach, CA 90807
8-213-595-6611

Dr. D. Stuart-Alexander
U.S. Geological Survey
345 Middlefield Road, MS 75
Menlo Park, CA 94025
(415) 323-8111 x 2238

Mr. Richard Sylvester
U.S. Geological Survey
Suite 110
1107 NE 45th Street
Seattle, WA 98105

Mr. John Taber
Geophysics Program AK-50
University of Washington
Seattle, WA 98195

Mr. G. W. Thorsen
Dept. of Natural Resources
Div. of Geology & Earth Resources
Olympia, WA 98504

Dr. Robert Thorsen
University of Alaska Museum
Fairbanks, Alaska 99701

David D. Tillson
Washington Public Power Supply
Box 968, MS 540
Richland, WA 99352

Dr. Joseph A. Vance
Dept. of Geological Sciences
University of Washington
Seattle, WA 98195
8-392-1913

Dr. Holly Wagner
U.S. Geological Survey
345 Middlefield Rd., MS 99
Menlo Park, CA 94025
(415) 323-8111 x 7013

Dr. Craig S. Weaver
U.S. Geological Survey
Geophysics Program AK-50
University of Washington
Seattle, WA 98195

Dr. D. H. Weickert
Pacific Geoscience Center
Earth Physics Branch
P. O. Box 6000
Sidney, B. C.
Canada
(604) 656-8428

Dr. John Whetten
U.S. Geological Survey
1101 NE 45th St., #125
Seattle, WA 98105

Mr. Joseph R. Wilson
Dept. of Geology
Washington State University
Pullman, WA 99164
(509) 335-3009

Dr. T. Yelin
Geophysics Program AK-50
University of Washington
Seattle, WA 98195
8-392-1913

Dr. Les Youd
U.S. Geological Survey
345 Middlefield Rd., MS 98
Menlo Park, CA 94025
(415) 323-8111 x 7117

Mr. James Yount
U.S. Geological Survey
345 Middlefield Rd., MS 75
Menlo Park, CA 94025
(415) 323-8111 x 2905

# REVIEW OF SEISMICITY IN THE PUGET SOUND REGION FROM 1970 THROUGH 1978

Robert S. Crosson
Geophysics Program
University of Washington
Seattle, Washington 98195

In an attempt to improve our knowledge of earthquake hazards in the Puget Sound region, earthquakes recorded with the western Washington regional seismograph network from 1970 through 1978 were reviewed. The most obvious characteristic of the spatial distribution of earthquakes is the diffuse zone of high seismicity in the central Puget Sound region. Within this central basin distribution, several clusters of earthquakes exist which are either long term swarms, aftershock sequences, or just persistent source zones (Figure 1). An apparent epicenter lineation passes through the southwest corner of the central basin earthquake zone. This lineation is due mainly to small earthquakes (M less than 2) and its significance remains uncertain.

A significant division of earthquakes into shallow and deep suites (Figure 2) is based on spatial separation, energy release statistics, and b value determinations as well as focal mechanism evidence (Figures 3, 4, 5, 6, and 7). The deep suite forms a sub-planar zone which dips at an azimuth of about 60 degrees between the depths of 40 and 70 km (Figure 8). This group of earthquakes may be subduction related although the focal mechanisms and spatial distribution do not yield simple interpretations.

Central basin earthquakes of the shallow suite have a bi-modal depth distribution (Figure 9), influenced to an extent by the existence of swarms. This bi-modal distribution is not so clearly apparent in the energy release distribution. However, both energy release and occurence rate are maximum in the interval from 20 to 25 km depths for the shallow suite.

Earthquakes above magnitude 4 are confined largely to the central Puget Sound basin and north to the Strait of Georgia, with a distinct preference for the deepest earthquakes to be on the west side of Puget Sound (Figure 10). Magnitude statistics indicate that the deep suite of earthquakes appears to have a significantly lower b value than the region as a whole, indicating a population enriched in larger magnitude earthquakes. It is obviously dangerous to extrapolate directly to large magnitude earthquakes (magnitude 6 and 7) but evidence

to date indicates that potentially destructive Puget Sound earthquakes occur in the zone from 40 to 70 km depths.

A suitable regional tectonic model has still not emerged from these data. The seismically quiet zone from 30 to 40 km depths beneath Puget Sound could well represent a weak stress decoupling between shallow and deep parts of the lithosphere, possibly where shear strain rates due to subduction are highest. Among the major problems facing us are the better resolution of the vertical and lateral crustal seismic velocity distribution, explanation of the localization of both shallow and deep seismicity beneath Puget Sound, and the establishment of direct evidence for or against continued subduction beneath western Washington.

## Figure Captions

Figure 1. Epicenters of all earthquakes with depths less than 35 kilometers, 1970 through 1978.

Figure 2. Epicenters of all earthquakes with depths of 35 kilometers or greater, 1970 through 1978.

Figure 3. Depth distributions for number of earthquakes (dots) and cumulative energy release (solid) for all earthquakes, 1970 through 1978.

Figure 4. Recurrence curve for all earthquakes shallower than 35 kilometers, 1970 through 1978.

Figure 5. Recurrence curve for all earthquakes 35 kilometers deep or deeper, 1970 through 1978.

Figure 6. Lower hemisphere, equal area plot of distribution of tectonic compressional axes (P) and tensional axes (T) determined from focal mechanisms of magnitude 3 and above earthquakes with depths greater than 35 kilometers.

Figure 7. Same as Figure 6, except for earthquakes in shallow suite above 35 kilometers depth.

Figure 8. Cross-section projecting all hypocenters onto a plane which strikes at an azimuth of 60 degrees. Total aperture width for projection is 300 km. The center of the projection is at 47, 30' N and 122, 30' W. Includes earthquakes from 1970 through 1978 with magnitudes 2.0 or greater.

Figure 9. Depth-count histogram of central basin earthquakes only. All events from 1970 through 1978.

Figure 10. Epicenters of earthquakes of magnitude 3.5 and greater, with symbols showing depth ranges and symbol sizes showing magnitude ranges. Earthquakes from 1970 through 1978.

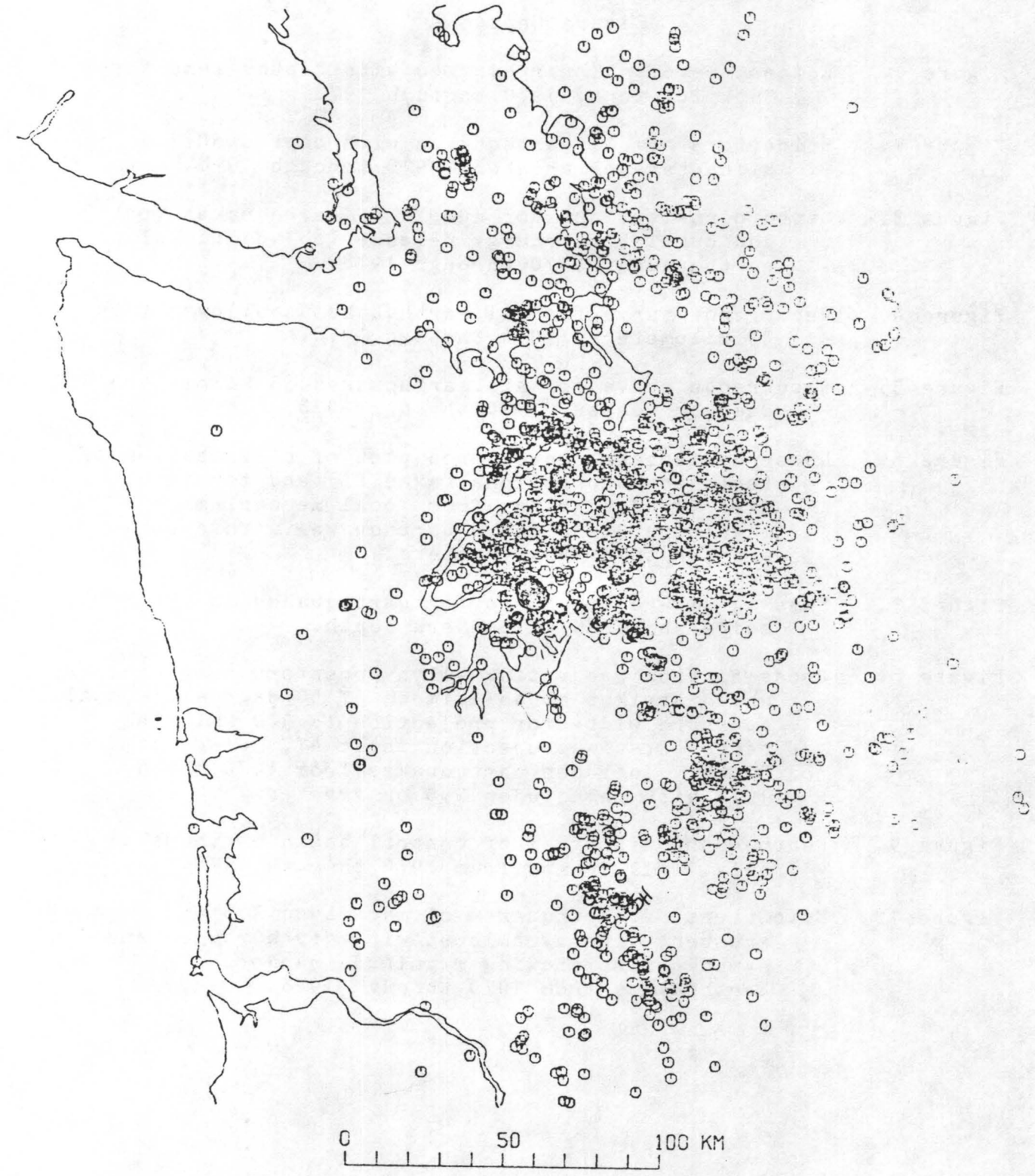


**FIGURE 1**

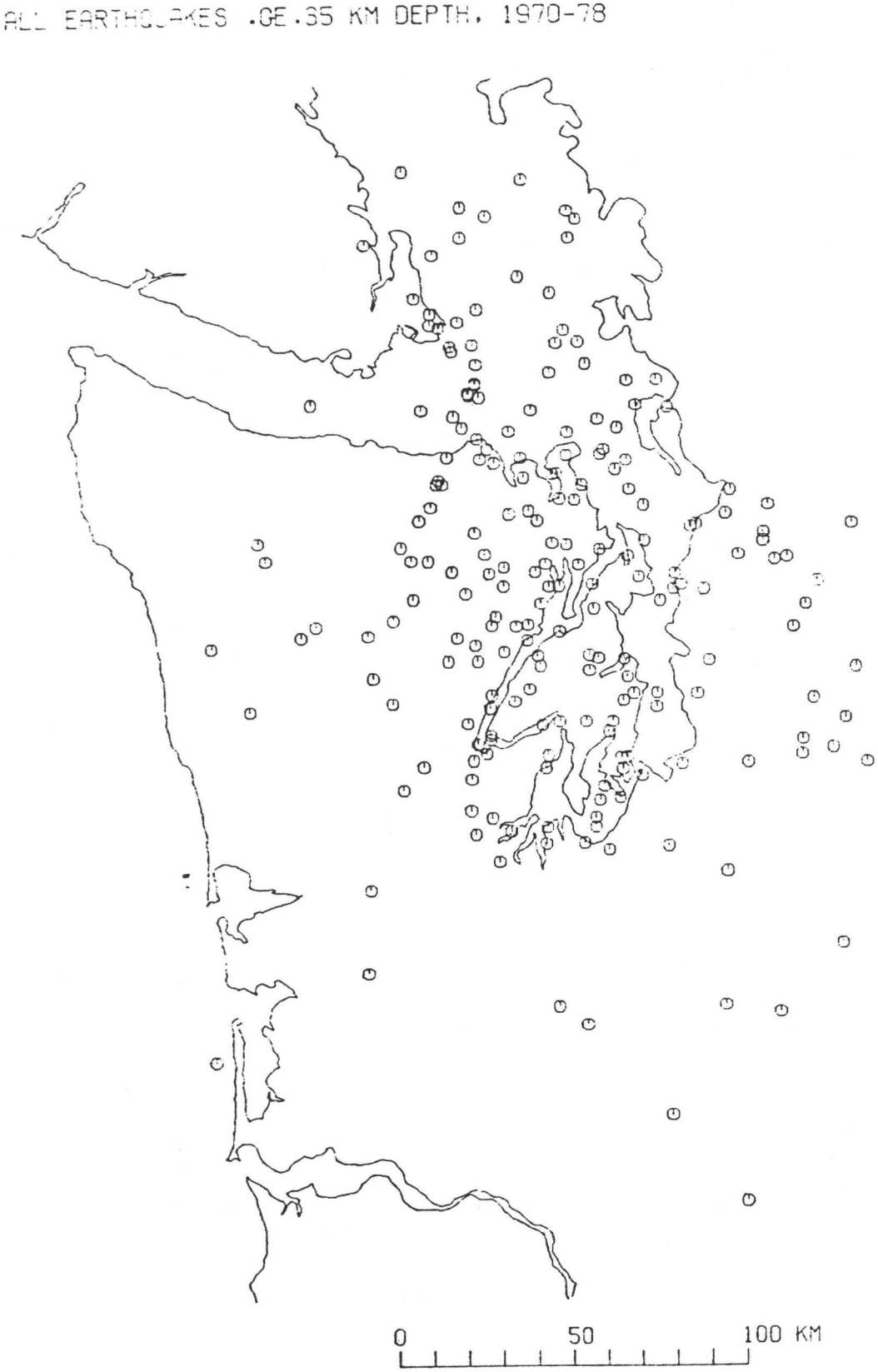


**FIGURE 2**

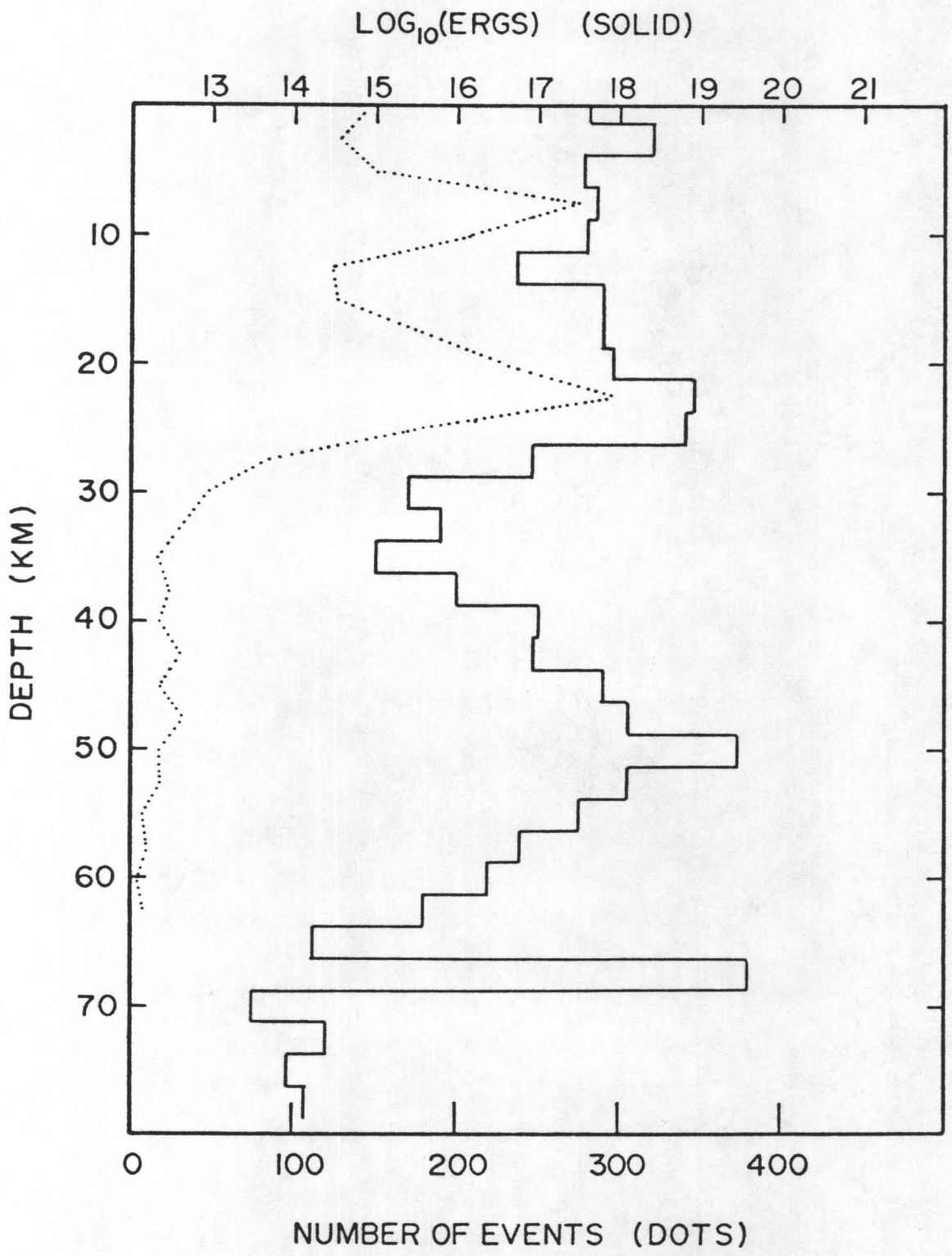
LOG10(ERGS) (SOLID)
13
14
15
16
17
18
19
20
21
10
20
30
40
50
60
70
DEPTH (KM)
0
100
200
300
400
NUMBER OF EVENTS (DOTS)

**FIGURE 3**

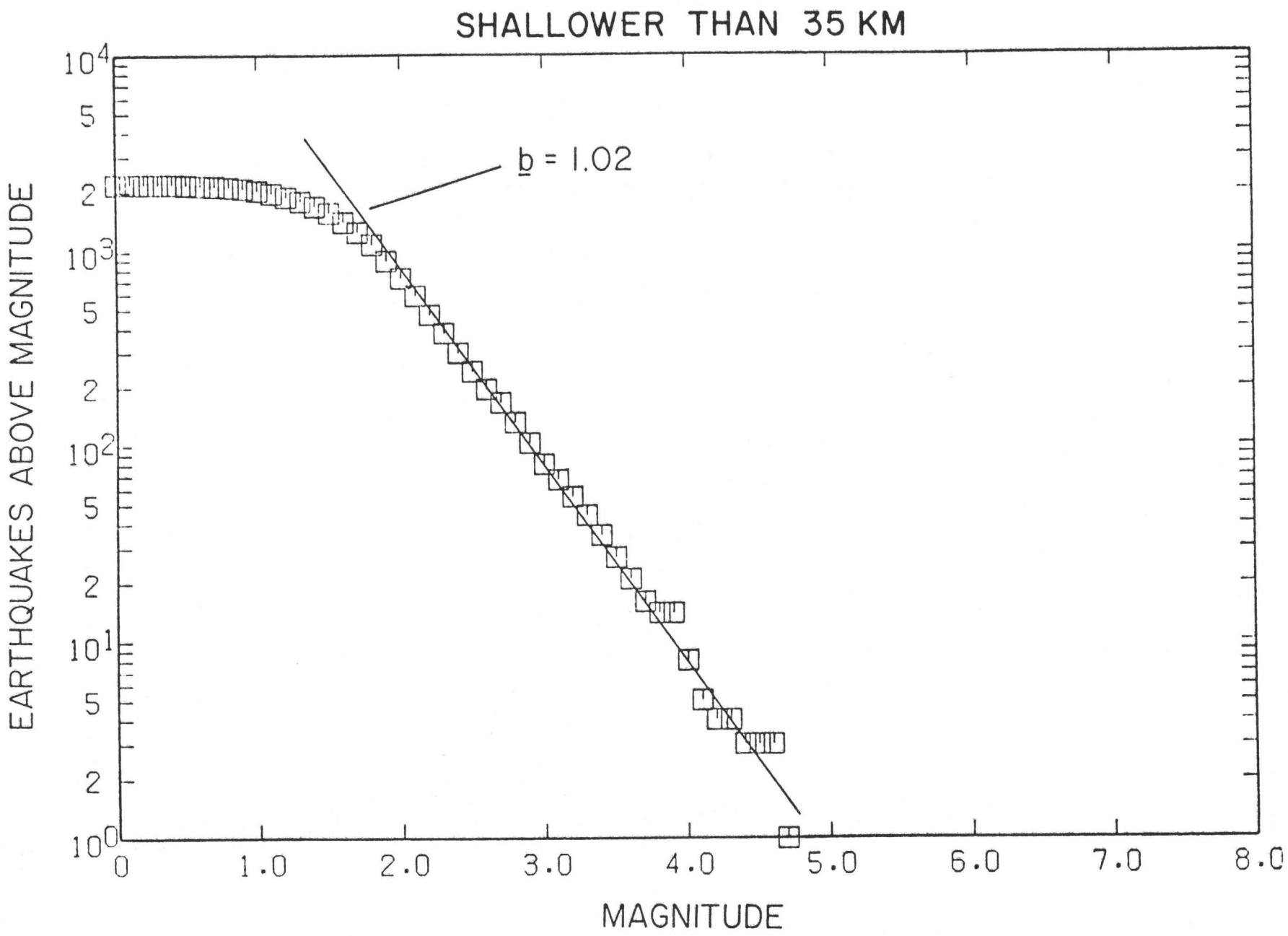
SHALLOWER THAN 35 KM
b = 1.02
EARTHQUAKES ABOVE MAGNITUDE
MAGNITUDE
10^4
5
2
10^3
5
2
10^2
5
2
10^1
5
2
10^0
0
1.0
2.0
3.0
4.0
5.0
6.0
7.0
8.0

**FIGURE 4**

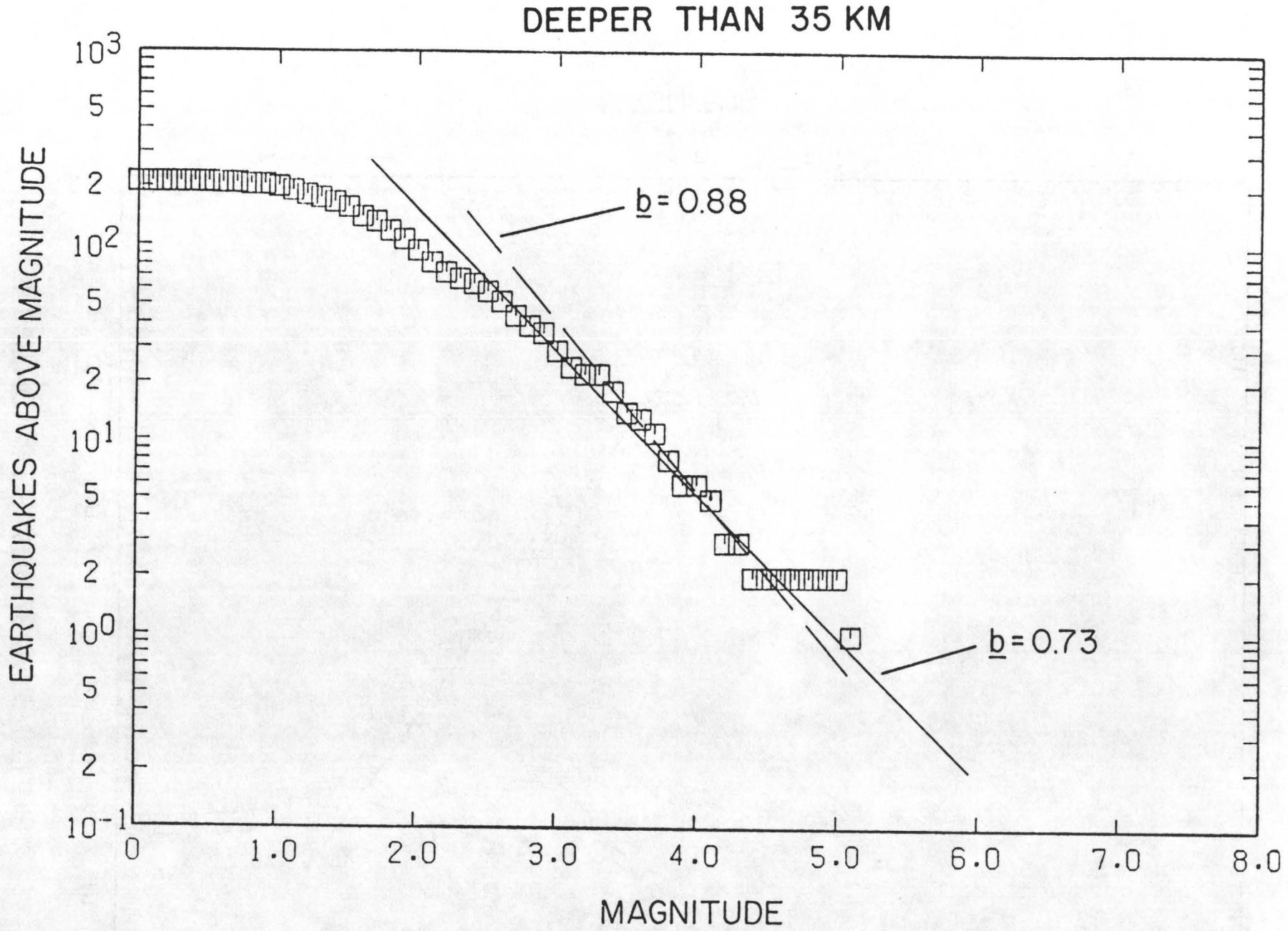
DEEPER THAN 35 KM
EARTHQUAKES ABOVE MAGNITUDE
MAGNITUDE
b = 0.88
b = 0.73
10^3
5
2
10^2
5
2
10^1
5
2
10^0
5
2
10^-1
0
1.0
2.0
3.0
4.0
5.0
6.0
7.0
8.0

FIGURE 5

1974-78; MAG .GE. 3.0; DEPTHS .GT. 35 KM

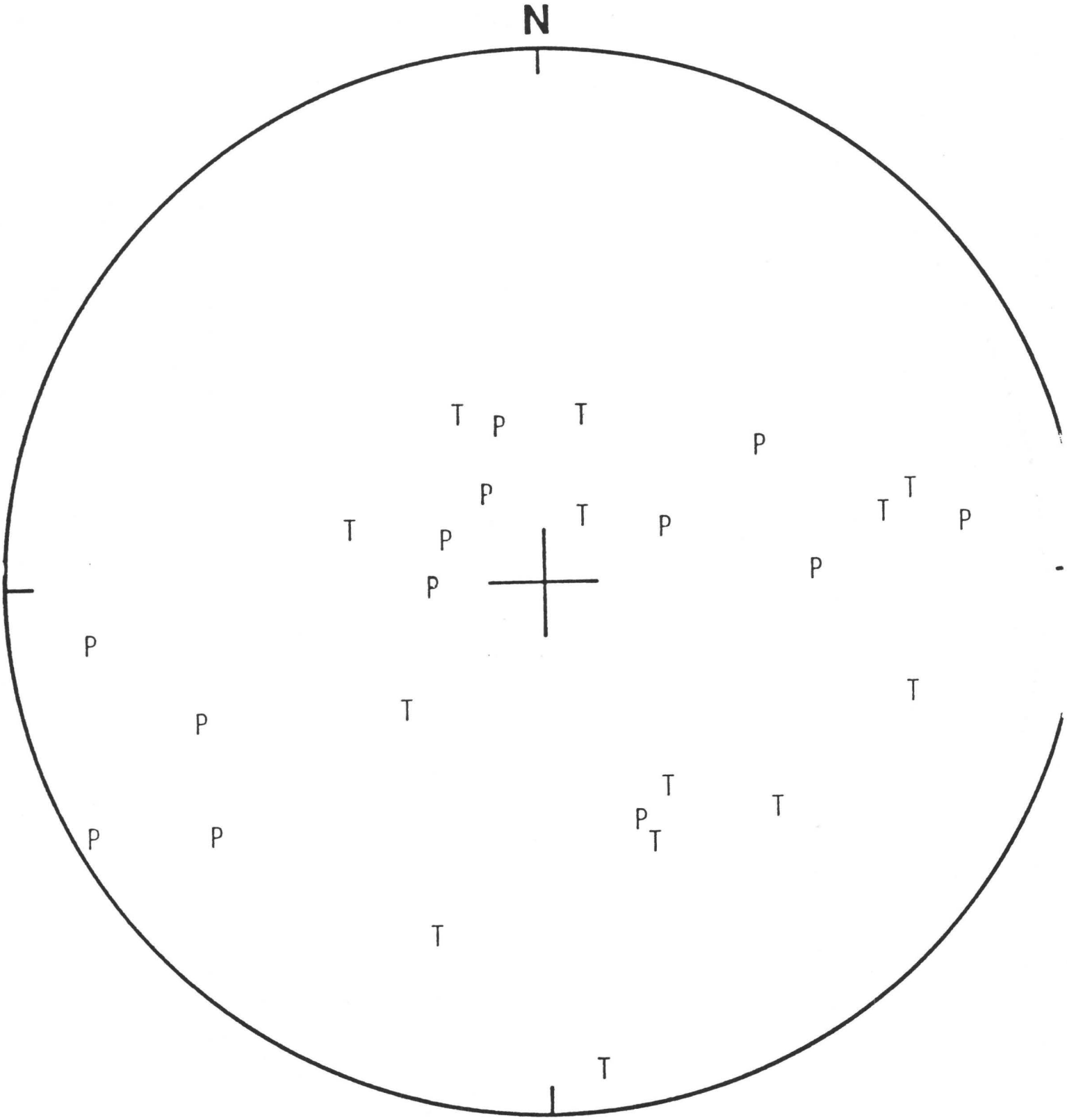


LOWER HEMISHPERE; EQUAL ANGLE

**FIGURE 6**

1974-78; MAG .GE. 3.0; DEPTHS .LE. 35 KM

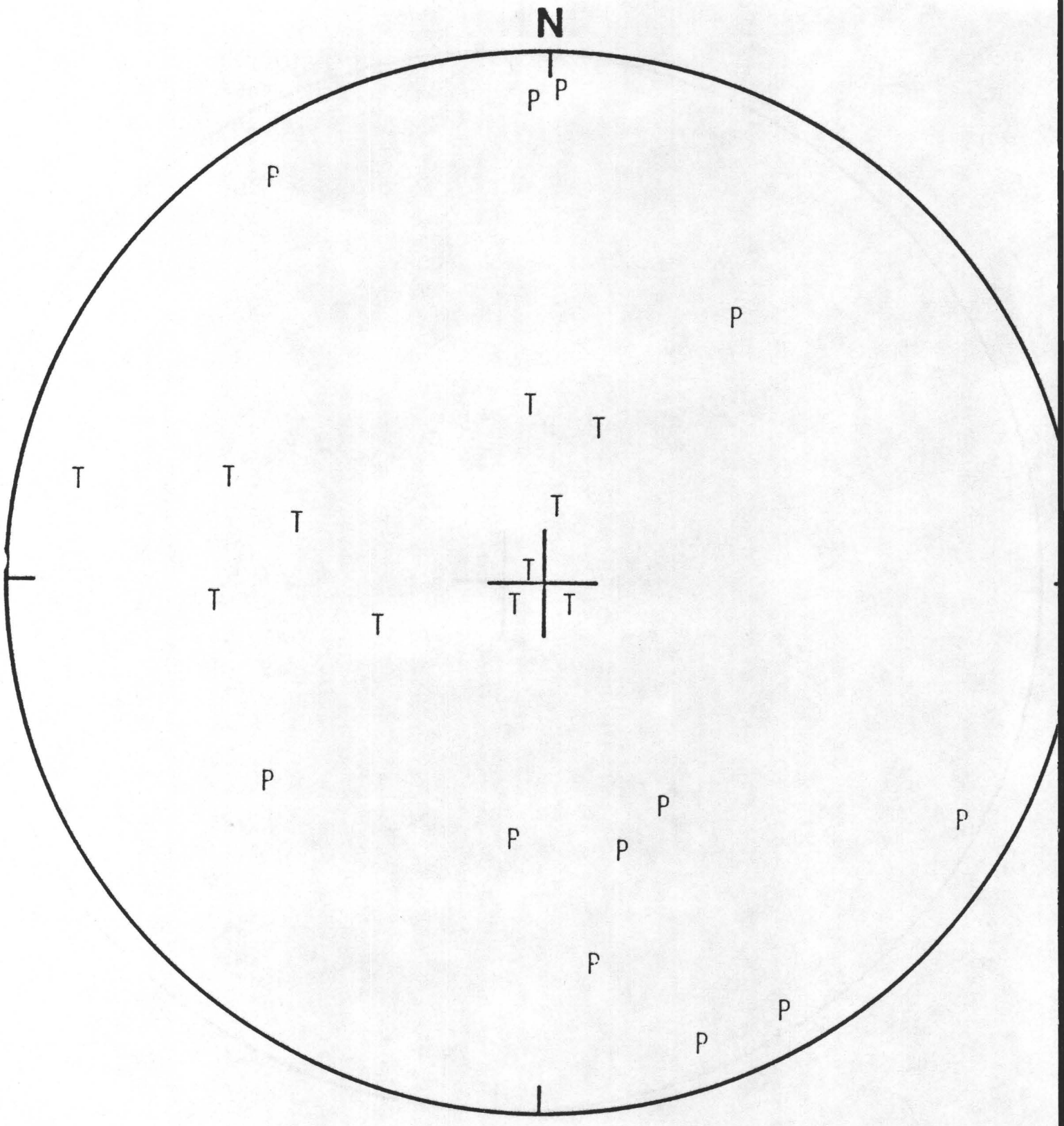


LOWER HEMISPHERE; EQUAL ANGLE

**FIGURE 7**

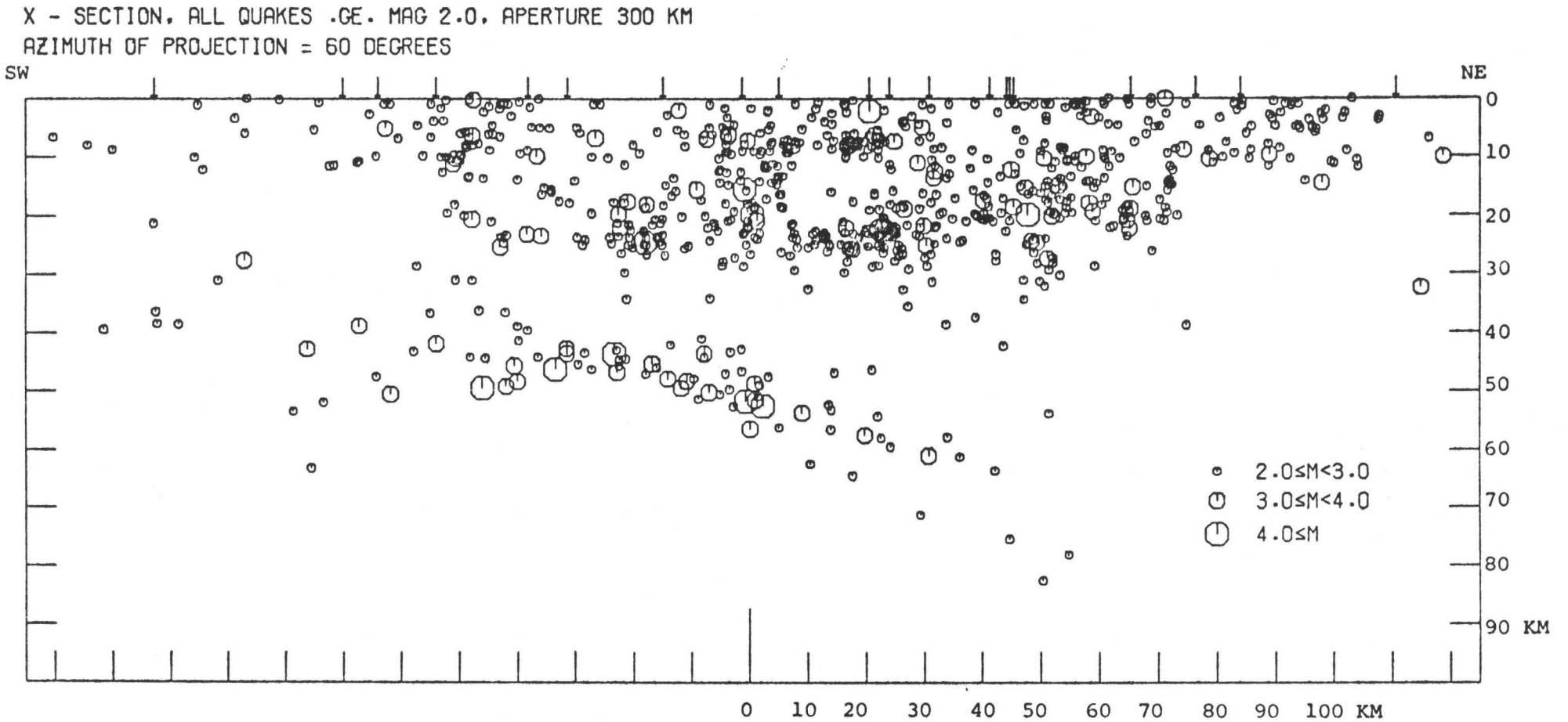
X - SECTION. ALL QUAKES .GE. MAG 2.0. APERTURE 300 KM
AZIMUTH OF PROJECTION = 60 DEGREES
SW
NE
0
10
20
30
40
50
60
70
80
90 KM
2.0≤M<3.0
3.0≤M<4.0
4.0≤M
0 10 20 30 40 50 60 70 80 90 100 KM

**FIGURE 8**

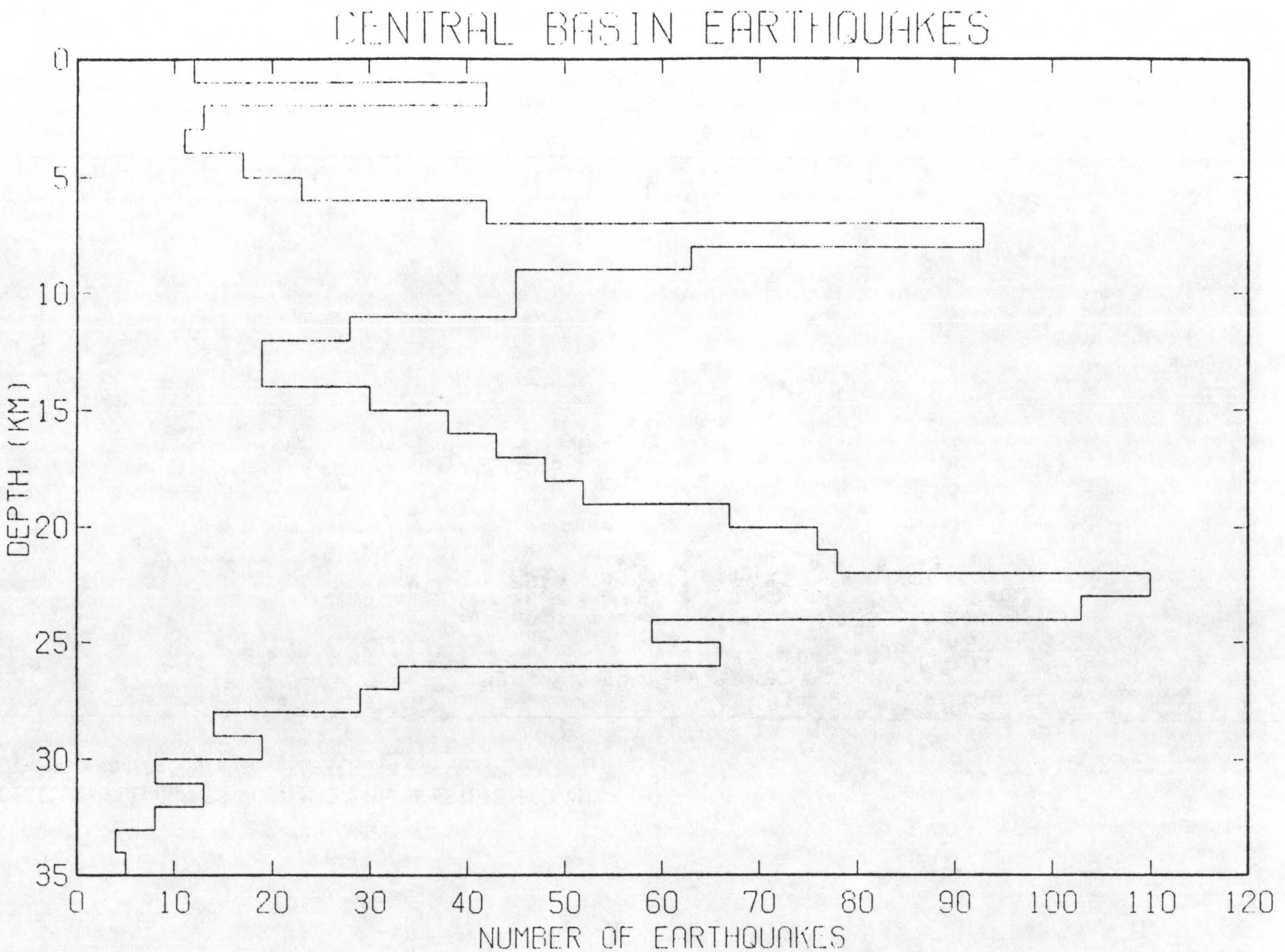
CENTRAL BASIN EARTHQUAKES
DEPTH (KM)
0
5
10
15
20
25
30
35
0
10
20
30
40
50
60
70
80
90
100
110
120
NUMBER OF EARTHQUAKES

**FIGURE 9**

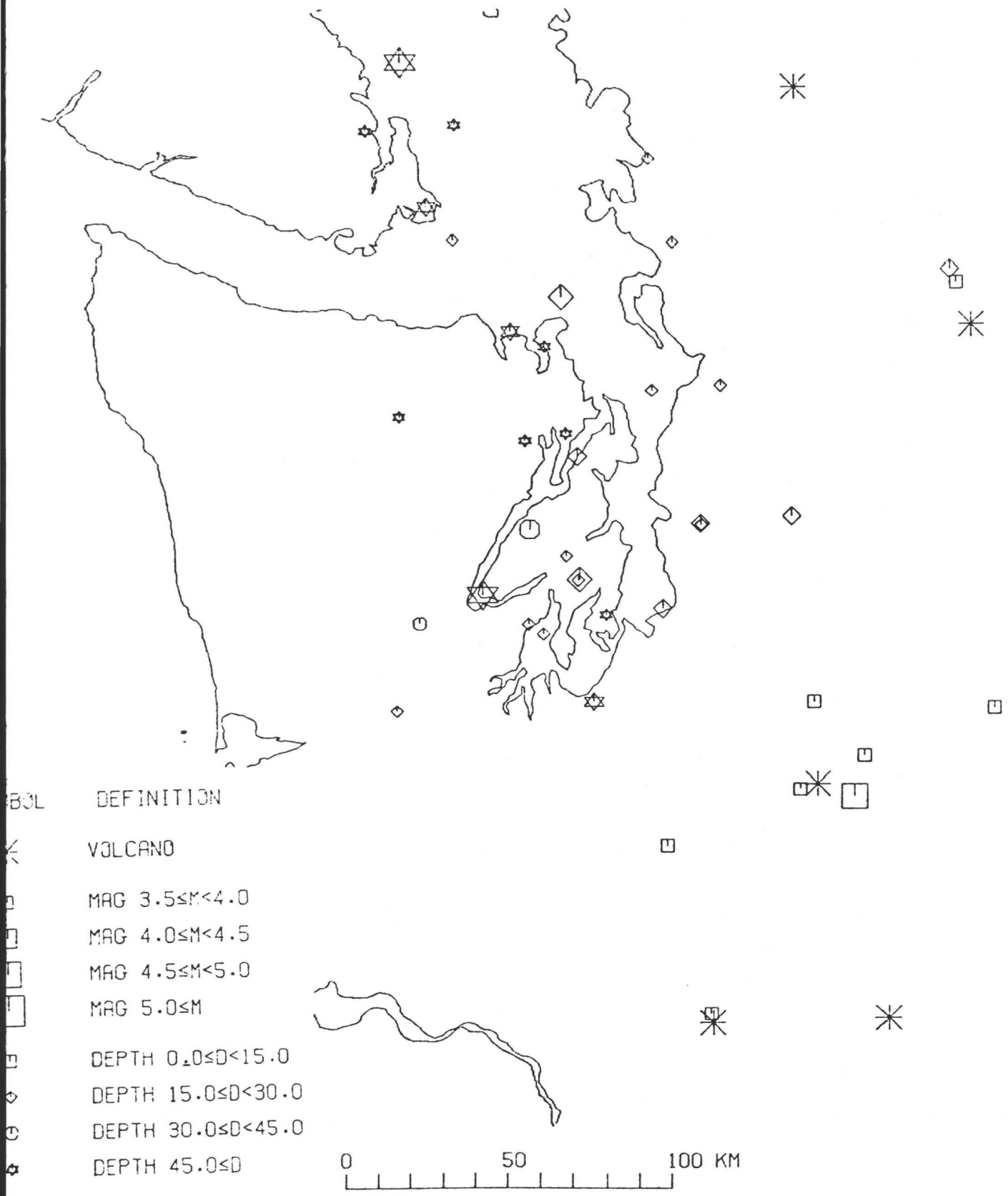
EARTHQUAKES, MAGNITUDE 3.5 AND LARGER
BOL DEFINITION
VOLCANO
MAG 3.5≤M<4.0
MAG 4.0≤M<4.5
MAG 4.5≤M<5.0
MAG 5.0≤M
DEPTH 0.0≤D<15.0
DEPTH 15.0≤D<30.0
DEPTH 30.0≤D<45.0
DEPTH 45.0≤D
0
50
100 KM

**FIGURE 10**

# SOME COMMENTS ON THE SEISMICITY OF THE NORTHERN PUGET SOUND - SOUTHERN VANCOUVER ISLAND REGION

Garry C. Rogers
Pacific Geoscience Centre
Earth Physics Branch
P.O. Box 6000
Sidney, B.C., Canada V8L 4B2

## Introduction

The seismicity of the southern Vancouver Island - Puget Sound region, particularly the deep seismicity, is similar in character from north to south. This is demonstrated by examining three data sets: the historical seismicity from 1900 to 1950, the graphically located data set from 1951 to 1969 and the very high quality data set from 1970 to 1978. These divisions are based on significant changes in the distribution of seismograph stations (Figure 1). A statistical argument is used to infer that much of the known seismicity prior to 1950 consisted of deeper events. The focal mechanisms of the two largest deeper earthquakes in recent times are used to infer that the fundamental stress regime is the same in the north and the south and it is consistent with that predicted by the plate tectonic model. Finally, a model is proposed to explain the character and lateral extent of both the deep and shallow seismicity.

## Seismicity 1900 - 1950

The first seismograph station in the region was established in Victoria in 1898, but the first high gain station suitable for studying local earthquakes was not introduced into the region until 1948. (Figure 1). Thus, much of the information from this period comes from international catalogues and local felt reports. The standard references for the region are the International Seismological Summary, which started systematic publication of all locatable earthquakes in 1917, and the publication U.S. Earthquakes which started in 1928. Earthquakes occurring prior to these publications are listed in the original catalogues of McAdie (1907), Bradford (1935) and Townley and Allan (1939). The summaries of Coombs (1953), Milne (1956) and Rasmussen (1967) collected most of the work in the earlier publications and extended the original lists.

The larger events north of 48° have been re-examined in this study and in several cases relocated or assigned different magnitudes (see Table I and Table II). The earthquakes larger than magnitude 4.5 from 1900 to 1950 are plotted in Figure 2. Magnitudes have been assigned mainly on the basis of felt area as listed in the publication Earthquake History of the United States(Coffman and von Hake, 1973) or as estimated from newspaper reports. The relationships used are those of Toppozada (1975). The maximum observed intensity has been used to assign magnitudes in some cases, again using the relationships of Toppozada (1975). This is less accurate and is likely to underestimate the

magnitude,(see Toppozada, 1975) particularly for the deeper earthquakes which occur in this region.

The most notable features of the revised data set are that the seismicity does not occur on Vancouver Island but is confined in an east-west sense mainly to the northern extension of the Puget Sound lowland and at the northern end it does not extend past the Gulf Islands region into Georgia Strait.

Seismicity 1951 - 1969

During this period the only agency systematically publishing epicentres for small earthquakes in the Puget Sound - Southern Vancouver Island region was the Dominion Observatory in Canada (predecessor of the present Earth Physics Branch). Data were gathered from U.S. stations in the Pacific Northwest for larger events but most epicentres were produced using only data from Canadian stations. Epicentres of some larger events appeared in the publication U.S. Earthquakes and sometimes in the Bulletin of the Seismograph Station of the University of Washington. If these epicentres were distant from Canadian stations they were often incorporated as published into the Canadian catalogues. The data set as it presently exists is reproduced in Figure 3.

Epicentres of all but the largest earthquakes in Figure 3 were located graphically assuming a shallow focal depth. Thus most of the deeper events will be pushed away from the triangle formed by the 3 Canadian stations and will be mislocated a few 10's of kilometers to the southeast.

Although the seismicity represented by this data set is more diffuse, the main features apparent in the previous data set are repeated here. The northern end of the Puget Sound seismicity stops near 49°N and, again, the east-west extent of the epicentres is concentrated mainly in the Puget Sound lowland and Gulf Islands region.

Seismicity 1970 - 1978

There is a very high quality data set for this time period because of the density of seismograph stations (Figure 1). Two agencies, the Earth Physics Branch in Canada and the University of Washington independently published earthquake catalogues for this region during this time period. Raw data were exchanged for the largest events and for investigations of specific earthquakes, but were not integrated on a routine basis for most events.

In this study P arrivals from both agencies for all events between 48°N and 49°N and 122°W and 124°W were combined to produce one set of epicentres. The deep suite of earthquakes (see Crosson, 1981) is perhaps most interesting and is reproduced in Figure 4. Those events south of 48° are from catalogues published by the University of Washington, those north of 48°N are the relocated epicentres. Figure 5 is a cross-section perpendicular to the coast through A and B in Figure 4. Events north of 48°N are projected on to the cross section and a hypothetical position for

the Juan de Fuca plate is drawn assuming the earthquakes delineate the brittle portion of the subducting lithosphere.

The main points to be emphasized are, again, that the seismicity stop abruptly near the 49th parallel in the north and it is confined in east-west extent. Also, the distribution of the seismicity is similar from the north end to southern Puget Sound and the cross section through the northern section of deeper events reveals that the structure is not different from that of central Puget Sound (Crosson, 1981).

The total thickness of the lithosphere as it starts to subduct is calculated to be about 30 km using the square root formula of Oldenburg (1975) (Figure 5). This is the thermal thickness assuming a melting temperature of about 1200°C on the bottom edge. The brittle thickness where earthquakes can occur must be much thinner, as earthquakes can only occur in the portion of the slab that is cold enough to support elastic stress. Estimates for the maximum temperature of the lithosphere that can support earthquake stress range from 300°C to 700°C (e.g. Brace and Byerlee, 1970; Burr and Solomon, 1978; Caldwell and Turcott, 1979). In Figure 5 the brittle thickness is depicted as 10 km in the region of seismicity without any attempt to allow for thinning as the slab gets deeper and warms up (e.g. see Keen and Hyndman, 1979). The bend in the slab where it dips at a steeper angle (e.g. Riddihough, 1979) has been drawn to accommodate the depths to the subducting slab under the Cascade volcanoes suggested by Dickinson (1970) and the average world wide depth of about 100 km (e.g. Isacks and Barazangi, 1977). There are subduction zones where the depth to the top of the subducted plate is less than 100 km) (e.g. the North Island of New Zealand as shown by Reyners, 1980 and the northeastern Japan arc as shown by Hasegewa et al. 1978) thus, a bend may not be required here.

Earthquake Statistics

A recurrence relationship calculated from earthquakes magnitude 4 and greater from the whole Puget Sound data set gives a b value of about 0.7, which will vary slightly depending on the assumptions made about the completeness of the data set (e.g. Stepp 1972; Weichert and Hyndman, 1981). A value of 0.7 can be compared to Crosson's (1981) b values for small earthquakes, calculated for the 1970 to 1978 period, of 0.73 for deep events and 1.02 for shallow events. Since the b value of the larger earthquakes is close to that of the deep suite of small earthquakes the inference is that most of the larger events are deeper ones. This can also be seen by overlaying Crosson's (1981) b value plots and noting that the two curves cross at above magnitude 4-1/2 inferring a higher proportion of deep events above this magnitude.

Thus, since most of the larger events are probably deep it is not surprising that the pattern of the 1900-1950 earthquakes has similar lateral extent to the 1970 to 1978 deep earthquakes, while the 1950-1969 data set, which contains more small shallow earthquakes,

is similar but more diffuse. The four damaging earthquakes that have occurred in this century have all been deep (Figure 6). The similarity of the 3 data sets suggest that there is potential for larger earthquakes anywhere within this zone of deep seismicity.

Deeper Earthquakes

There have been only two deeper earthquakes in recent times that have been large enough to record on enough seismograph stations to enable well constrained teleseismic fault plane solutions to be calculated. These are the 1965 Seattle earthquake and the 1976 earthquake in the Canadian Gulf Islands. These earthquakes are at extreme ends of the suite of deeper earthquakes but their fault plane solutions are remarkably similar (Figure 7). The preferred solution for the 1976 event (not shown) contains data from near stations as well and is slightly different. However, since there were so few near stations in 1965, the 1976 teleseismic solution is compared with 1965 teleseismic solution of Isacks and Molnar (1971).

Crosson (1981) has presented focal mechanisms of several smaller deep Puget Sound earthquakes. Only a few of these smaller earthquakes have mechanisms similar to the 1965 and 1976 events, but these two earthquakes are much larger than the earthquakes in Crosson's studies and likely fractured all the way through the brittle portion of the subducted lithosphere (see Figure 5). Thus, these two events probably reflect the stress regime acting on the whole lithosphere. The smaller events may reflect more complex stress involved in the north-south shortening or bulging due to the subducting plate accommodating the 45° bend in the coast line (from north-south off Washington and Oregon to northwest-southeast off Vancouver Island.) (see Figure 8). The forces acting on the plate as a whole are likely those driving the plate motion and, indeed, they are consistent with downdip tension seen elsewhere in subducting lithosphere (Isacks and Molnar, 1971). The azimuth and dip direction are consistent with that predicted by the plate tectonic model, particularly if a secondary bend to a steeper angle of 25° to 30° is real (Table III).

Figure 8 attempts to show how both north-south shortening, vertical compression (suggested by the mechanisms of several small earthquakes presented by Crosson, 1981) and downdip tension can be accommodated. The lateral compression that must occur in the subducted plate as it bends down and around the 45° bend is depicted here as taken up in a number of undulations, similar to the folds that appear when a table cloth is draped over the 90° corner of a table. Lateral compression resulting from a subducting plate encountering a convex bend has been discussed by Isacks and Molnar (1971) and has been modelled in this region by Keen and Hyndman (1979) as an overlap in the subducted Juan de Fuca plate (e.g. see Figure 7 of Weichert and Hyndman, 1981). The motivation for the model shown in Figure 8 comes from the work of Dickinson (1970), where he indicates varying depths to the magma sources under the Cascade volcanoes (see Figure 4 of Dickinson, 1970). While the model may not represent the true case, it provides a rationale for having a zone of confused deformation in the subducting plate that could give rise to the observed mechanisms of small earthquakes (Crosson, 1981).

The model also provides for downdip tension in the subducted plate at the appropriate dip of 25° to 30° if the lithosphere dives at a steeper angle to meet a 100 km depth beneath the volcanoes.

Shallow Earthquakes

The model Figure 8 also gives an explanation for the extent and character of the increased level of shallow seismicity in the Puget Sound region. Bulging or convolutions in the subducted Juan de Fuca plate may increase the effective dynamic coefficient of friction in the Puget Sound region to a level where sufficient strain is coupled across the subduction interface to cause earthquakes in the overlying plate. It is apparent from the strain measurements of Savage et al. (1981) that only a portion of the 3.5 cm per year northeast interaction (Atwater, 1970; Riddihough, 1977) is being coupled across this subduction boundary. The shallow seismicity corresponds closely in areal extent to the region of deeper seismicity which is what would be expected if the bulging, outlined by the deeper seismicity, is the reason for the shallow earthquakes. The orientation of the pressure axes in the focal mechanism solutions of the shallow earthquakes, which suggests north-south compression or right lateral shear in Puget Sound (Crosson, 1972; 1981) and surrounding area (Malone et al., 1975; Rogers, 1979), may be a result of the oblique subduction direction in the region (Rogers, 1979). Fitch (1972) and Walcott (1978) have discussed the theory of oblique subduction and give examples in other areas of the world where a zone of continuous shear has developed inland and parallel to the coastline (Figure 9). Thus, much of the observed seismicity, both shallow and deep, does not seem to be typical of the normal subduction process, which at present seems largely aseismic along the Juan de Fuca-America plate bounday, but it is a second order effect, which can be explained by a model taking into account the special geometry of the region.

Conclusions

1) Data sets from three different time periods, 1900-1950, 1951-1970 and 1970-1978 show a truncation of the seismicity at about the 49th parallel similar to the truncation that occurs at the south end of Puget Sound.

2) Data from the 3 data sets show a similarity in character from north to south even though the largest earthquakes have occurred in the south.

3) Recurrence relationships calculated from earthquakes greater than magnitude 4 give b values of about 0.7, close to the b value for smaller deep events of 0.73 (Crosson, 1981), suggesting most of the larger events are deep.

4) Focal mechanisms of two earthquakes large enough to have fractured the entire portion of the brittle section of the subducted lithosphere are very similar even though at opposite ends of the seismic zone suggesting the same stress regime is acting on the whole subducted lithosphere.

5) The confused pattern of focal mechanisms of smaller deep earthquakes can be explained by a model showing north-south shortening and bulging due to the subducting plate deforming as it negotiates the 45° change of angle in the coastline.

6) The areal extent of the shallow seismicity and the consistent north-south orientation of pressure axes from focal mechanism solutions of shallow earthquakes can be explained by a model requiring oblique subduction and an increased dynamic coefficient of friction on the subduction interface in the Puget Sound region.

References

Atwater, T. 1970. Implications of plate tectonics for the Cenozoic tectonic evolution of western North America. Geological Society of America Bulletin, 81, pp. 3513-3536.

Brace, W.F. and Byerlee, I.D. 1970. California earthquakes: Why only shallow focus. Science, 1968, pp. 1573-1575.

Bradford, D.C. 1935. Seismic history of the Puget Sound Basin. Bulletin of the Seismological Society of America, 25, pp. 138-158.

Burr, N.C. and Solomon, S.C. 1978. The relationship of source parameters of oceanic transform earthquakes to plate velocity and transform length. Journal of Geophysical Research, 83, pp. 1193-1205.

Caldwell, J.G. and Turcott, D.L. 1979. Dependence of the thickness of the elastic oceanic lithosphere on age. Journal of Geophysical Research, 84, pp. 7572-7576.

Coffman, J.L. and von Hake, C.A. 1973. Earthquake history of the United States. Publication 41-1 (Revised edition - through 1970), U.S. Department of Commerce, Washington, D.C. 208 p.

Coombs, H.A. 1953. A summary of Washington earthquakes, Bulletin of the Seismological Society of America, 43, pp. 1-5.

Crosson, R.S., 1972. Small earthquakes, structure, and tectonics of the Puget Sound region. Bulletin of the Seismological Society of America, 62, pp. 1133-1172.

Crosson, R.S., 1981. Review of seismicity in the Puget Sound region from 1970 through 1978. This volume.

Dickinson, W.R. 1970. Relations of andesites, granites and derivative sandstones to arc-trench tectonics. Reviews of Geophysics and Space Physics, 8, pp. 813-860.

Fitch, T.J. 1972. Plate convergence, transcurrent faults, and internal deformation adjacent to southeast Asia and the western Pacific. Journal of Geophysical Research, 77, pp. 4432-4460.

Hasegawa, A., Umino, N. and Takagi, A. 1978. Double-planed structure of the deep seismic zone in the northeastern Japan arc. Tectonophysics, 47, pp. 43-58.

Isacks, B. and Molnar, P. 1971. Distribution of stresses in the descending lithosphere from a global survey of focal mechanism solutions of mantle earthquakes. Reviews of Geophysics, 9, pp. 103-174.

Isacks, B.C. and Barazangi, M. 1977. Geometry of Benioff zones: lateral segmentation and downwards bending of the subducted lithosphere in Island Arcs, Deep Sea Trenches and Back-Arc Basins, Am. Geophys. Union, Maurice Ewing Series 1, eds. Talwani,M. and Pitman, W.C., pp. 243-258.

Keen, C.E. and Hyndman, R.D. 1979. Geophysical review of the continental margins of eastern and western Canada. Canadian Journal of Earth Sciences, 16, pp. 712-747.

Malone, S.D., Rothe, G.H. and Smith, S.W. 1975. Details of micro-earthquake swarms in the Columbia Basin, Washington. Bulletin of the Seismological Society of America, 65, pp. 855-864.

McAdie,A.G. 1907. Catalogue of earthquakes on the Pacific coast, 1897 to 1906. Smithsonian Miscellaneous Collections, B. 1721 (part of Vol. XLIX).

Milne, W.G. 1956. Seismic activity in Canada west of the 113° meridian, 1841-1951. Publications of the Dominion Observatory, Ottawa, 18, pp. 119-145.

Oldenburg, D.W. 1975. A physical model for the creation of the lithosphere. Geophysical Journal of the Royal Astronomical Society, 43, pp. 425-451.

Rasmussen, N.H. 1967. Washington State earthquakes, 1840 through 1965. Bulletin of the Seismological Society of America, 57, pp. 463-476.

Rasmussen, N.H., Millard, R.C. and Smith, S.W. 1974. Earthquake hazard evaluation of the Puget Sound region, Washington State. University of Washington Press, 99 p.

Reyners, M. 1980. A microearthquake study of the plate boundary, North Island, New Zealand. Geophysical Journal of the Royal Astronomical Society, 63, pp. 1-22.

Riddihough, R.P. 1977. A model for recent plate interactions off Canada's west coast. Canadian Journal of Earth Sciences, 14, pp. 384-396.

Riddihough, R. 1979. Gravity and structure of an active margin - British Columbia and Washington. Canadian Journal of Earth Science, 16, pp. 350-363.

Rogers, G.C. 1979. Earthquake fault plane solutions near Vancouver Island. Canadian Journal of Earth Sciences, 16, pp. 523-531.

Savage, J.C., Lisowski, M. and Prescott, W.H. 1981. Geodetic strain measurements in Washington, Journal of Geophysical Research, (in press).

Stepp, J.C. 1972. Analysis of completeness of the earthquake sample in the Puget Sound area and its effect on statistical estimates of earthquake hazard. Proceedings of the international conference on microzonation, Seattle, Washington, pp. 897-909.

Toppozada, T.R. 1975. Earthquake magnitude as a function of intensity data in California and western Nevada. Bulletin of the Seismological Society of America, 61, pp. 1223-1238.

Townley, S.D. and M.N. Allen. 1939. Descriptive catalogue of earthquakes of the Pacific coast of the United States 1769 to 1928. Bulletin of the Seismological Society of America, 29, pp. 1-20.

Weichert, D.H. and Hyndman, R.D. 1981. A comparison of seismic activity and several estimates of deformation in the Puget South area. This volume.

Walcott, R.I. 1978. Geodetic strains and large earthquakes in the axial tectonic belt of North Island, New Zealand. Journal of Geophysical Research, 83, pp. 4419-4429.

Figure Captions

Figure 1 Distribution of seismograph stations through time. Numbers indicate the year the station was established. The first seismograph appeared in the region in 1898, the first seismograph suitable for studying small local earthquakes appeared in 1948 and the first dense local network in 1970.

Figure 2 Known earthquakes 1900-1950 magnitude 4.5 and larger extracted from Table I. Population distribution suggests that the lack of earthquakes above magnitude 4.5 on southern Vancouver Island and the Georgia Strait during this time period is real.

Figure 3 Earthquakes 1951 to 1969 located mainly with data from Canadian stations. Dots are events magnitude 3 and larger. X's represent smaller earthquakes for which the detection level is not uniform.

Figure 4 Deeper earthquakes larger than magnitude 2, 1970-1978. Epicentres south of 48° are from catalogues published by the University of Washington. Epicentres north of 48° are calculated from data from both the University of Washington and Canadian stations. One well located 1969 event is also included. A and B mark the location of the cross section in Figure 5.

Figure 5 Cross section perpendicular to the coastline from A to B in Figure 4. Earthquakes north of 48°N are projected onto the cross section. The bend in the descending lithosphere is speculative and may not exist but satisfies inferred depths under the volcanic zone. Larger dots are larger earthquakes. Earthquake distribution is similar to that in central Puget Sound shown by Crosson (1981). Hypocentres shallower than 30 km are not shown.

Figure 6 Damaging earthquakes in the Puget Sound - southern Vancouver Island region.

Figure 7 Fault plane solutions for 1965 and 1976 earthquakes. The projection is lower hemisphere equal angle projection with shaded areas representing compressional quadrants. Not all of the data are plotted to avoid confusion. The 1965 solution is that of Isacks and Molnar (1971) and the 1976 solution is calculated using teleseismic data only. The similarity suggests the same stress regime exists at both the north and south ends of the deeper suite of earthquakes. These mechanisms are consistent with the stress regime expected for down dip tension in the subducting lithosphere.

Figure 8 (a) A proposed model for the subducted Juan de Fuca plate.

Figure 8 (b) The plate in the Puget Sound region is subjected to both north-south and vertical compressive forces due to the plate accommodating the 45 degree bend in the coastline and the downdip forces of the sinking lithosphere. The arcuate shaded region represents the extent of the zone of deeper seismicity. Undulations in the subducting plate could increase the effective dynamic coefficient of friction on the subduction interface allowing sufficient stress to be coupled to the upper plate to cause a higher level of shallow seismicity in the Puget Sound region.

Figure 9 Fitch (1972) and Walcott (1978) have proposed oblique subduction models where a zone of shear develops inland and parallel to the coast. Such a mechanism would explain the north-south orientation of pressure axes in the focal mechanisms of shallow earthquakes in Puget Sound and surrounding regions.

TABLE 1

LARGER SOUTH VANCOUVER ISLAND - NORTH PUGET SOUND EARTHQUAKES, 1900-1950[1]

| DATE | | COORDINATES | | FELT AREA/ MAX. INTENSITY[2] | MAGNITUDE[4] | COMMENT |
|---|---|---|---|---|---|---|
| 1901 | JAN 11 | 48.7 | 122.8[5] | 150,000[3] | 6.0 | Lack of severe intensities suggests deep focus |
| 1911 | SEP 28 | 48.8 | 122.7 | VI | 4.8 | |
| 1915 | AUG 15 | 48.5 | 121.4 | 77,000 | 5.6 | |
| 1916 | FEB 22 | 48.8 | 122.6 | V | 4.3 | |
| 1920 | JAN 24 | 48.6 | 123.0[5] | VII | 5.3 | S-P of 4 s at Victoria |
| 1923 | FEB 12 | 49.0 | 122.7 | V | 4.3 | |
| 1926 | DEC 04 | 48.5 | 123.0[5] | 15,000[3] | 4.5 | |
| 1928 | FEB 09 | 48.5 | 125.0 | 27,000 | 4.9 | |
| 1931 | APR 18 | 48.7 | 122.2 | 13,000 | 4.4 | |
| 1932 | JAN 05 | 48.0 | 121.8 | 4,000 | 3.6 | |
| 1932 | JUL 18 | 48.0 | 121.8 | 36,000 | 5.1 | |
| 1933 | OCT 05 | 49 | 124[5] | V | 4.3 | |
| 1934 | MAY 05 | 48 | 123 | 27,000 | 4.9 | |
| 1934 | NOV 03 | 48 | 121 | 27,000 | 4.9 | |
| 1943 | NOV 29 | 48.4 | 122.9 | 23,000 | 4.8 | |
| 1945 | JUN 15 | 49 | 123.5[5] | V | 4.3 | |
| 1950 | APR 14 | 48 | 122.5 | 18,000 | 4.6 | |
| 1950 | DEC 02 | 48.0 | 122.3 | V | 4.3 | |

[1] Material different from Coffman and van Hake (1973) is underlined.
[2] Felt area in $km^2$ and maximum Modified Mercalli Intensity.
[3] Newspaper reports suggest larger felt area than Coffman and van Hake (1973).
[4] Magnitude from felt area or maximum intensity using Toppozada (1975).
[5] Epicentre adjusted to fit available felt information.

TABLE II

EPICENTRES MOVED FROM SOUTHERN VANCOUVER ISLAND

| DATE | COORDINATES | FELT AREA | MAGNITUDE | COMMENT |
|---|---|---|---|---|
| 1904 MAR 16 | 47.8 123 | 51,000 | 5.3 | was 48.5, 122.8 Adjusted to centre of felt area |
| 1918 DEC 06 | 49.7 126.5 | 725,000 | 7 | was 124 49 in ISS |
| 1919 OCT 10 | delete | not felt | 5.5 | was 124 49 in ISS |
| 1921 JUN 25 | delete | not felt | 5.0 | was 124 49 in ISS |
| 1926 SEP 17 | 50 123 | not felt | 5.5 | was 124 49 in ISS, re-calculated with ISS data |
| 126 SEP 22 | 50.2 121.9 | not felt | 5.5 | was 124 49 in ISS, re-calculated with ISS data |
| 1927 MAY 08 | 50.2 127.9 | not defined | 5.5 | was 124 49 in ISS, adjusted to fit felt reports |

TABLE III

TENSION AXES FROM EARTHQUAKE MECHANISMS AND PREDICTED PLATE MOTION

| | Earthquake Mechanisms Tension Axes | | Azimuth from Plate Interaction Model | Dip from Figure 5 |
|---|---|---|---|---|
| | AZ | Dip | AZ[1] | Dip |
| 1965[2] | 63 | 26 | 63 | 25-30 |
| 1976 | 61 | 30 | 61 | 25-30 |

[1]Azimuth of Juan de Fuca plate motion at the coordinates of each earthquake computed by R.P. Riddihough.

[2]From the solution of Isacks and Molnar, 1971.

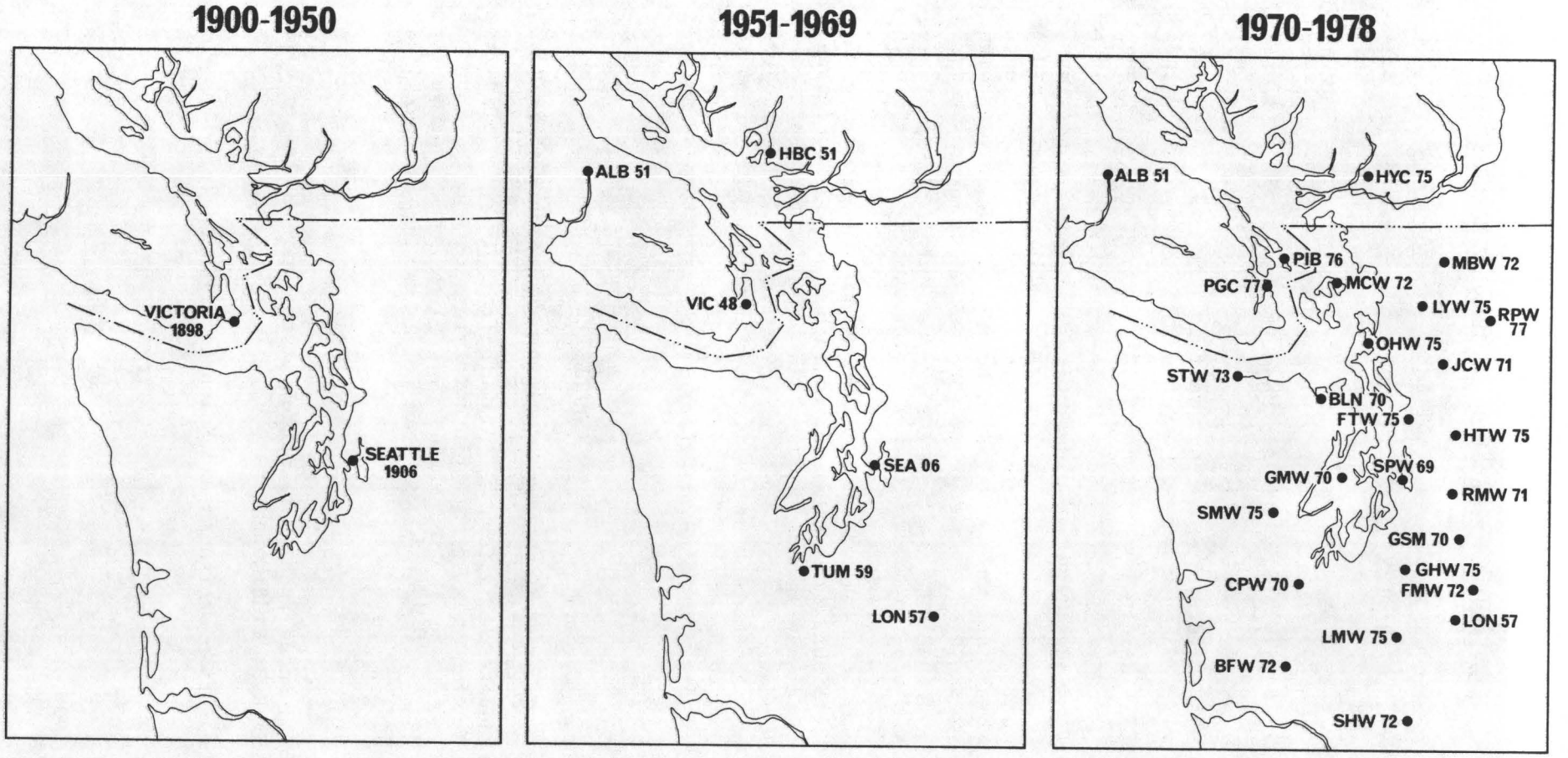
1900-1950
VICTORIA
1898
SEATTLE
1906
1951-1969
HBC 51
ALB 51
VIC 48
SEA 06
TUM 59
LON 57
1970-1978
ALB 51
HYC 75
PIB 76
MBW 72
PGC 77
MCW 72
LYW 75
RPW
77
OHW 75
JCW 71
STW 73
BLN 70
FTW 75
HTW 75
GMW 70
SPW 69
RMW 71
SMW 75
GSM 70
GHW 75
CPW 70
FMW 72
LON 57
LMW 75
BFW 72
SHW 72

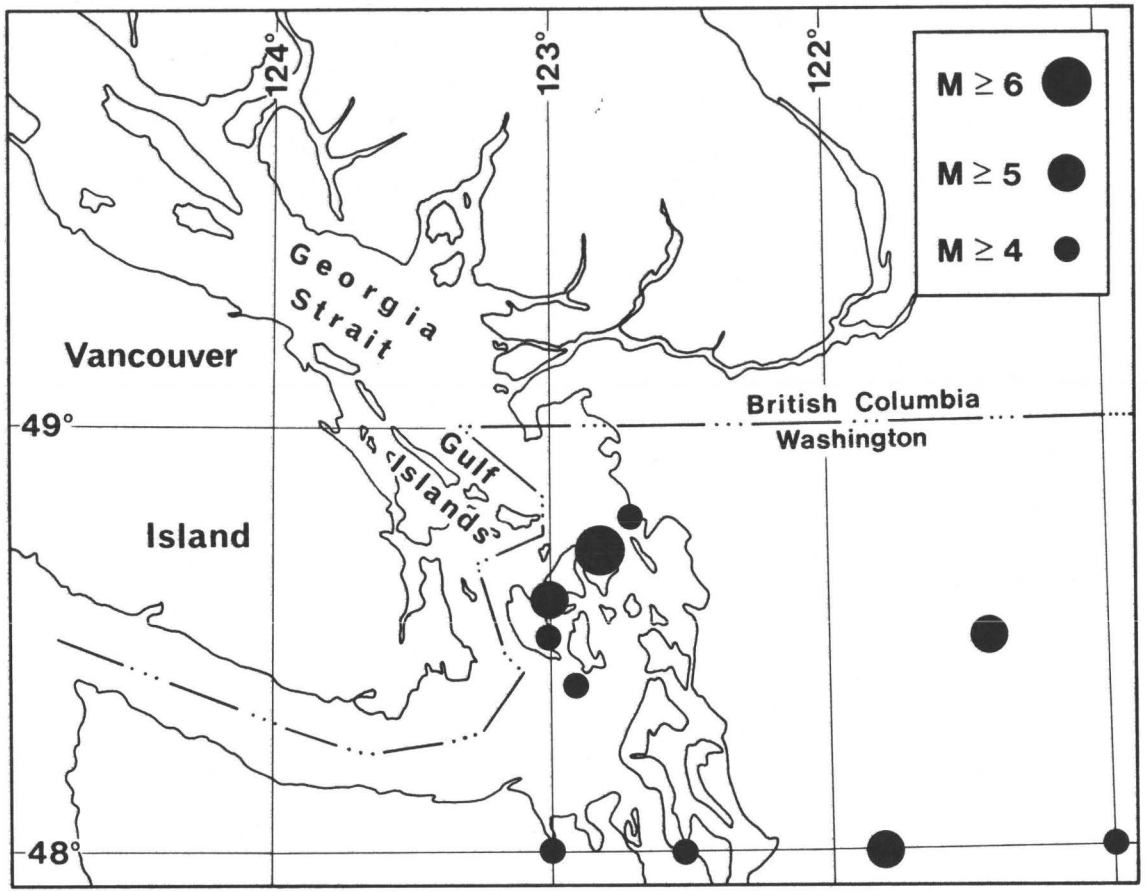
124°
123°
122°
M ≥ 6
M ≥ 5
M ≥ 4
Georgia Strait
Vancouver
Island
Gulf Islands
British Columbia
Washington
49°
48°

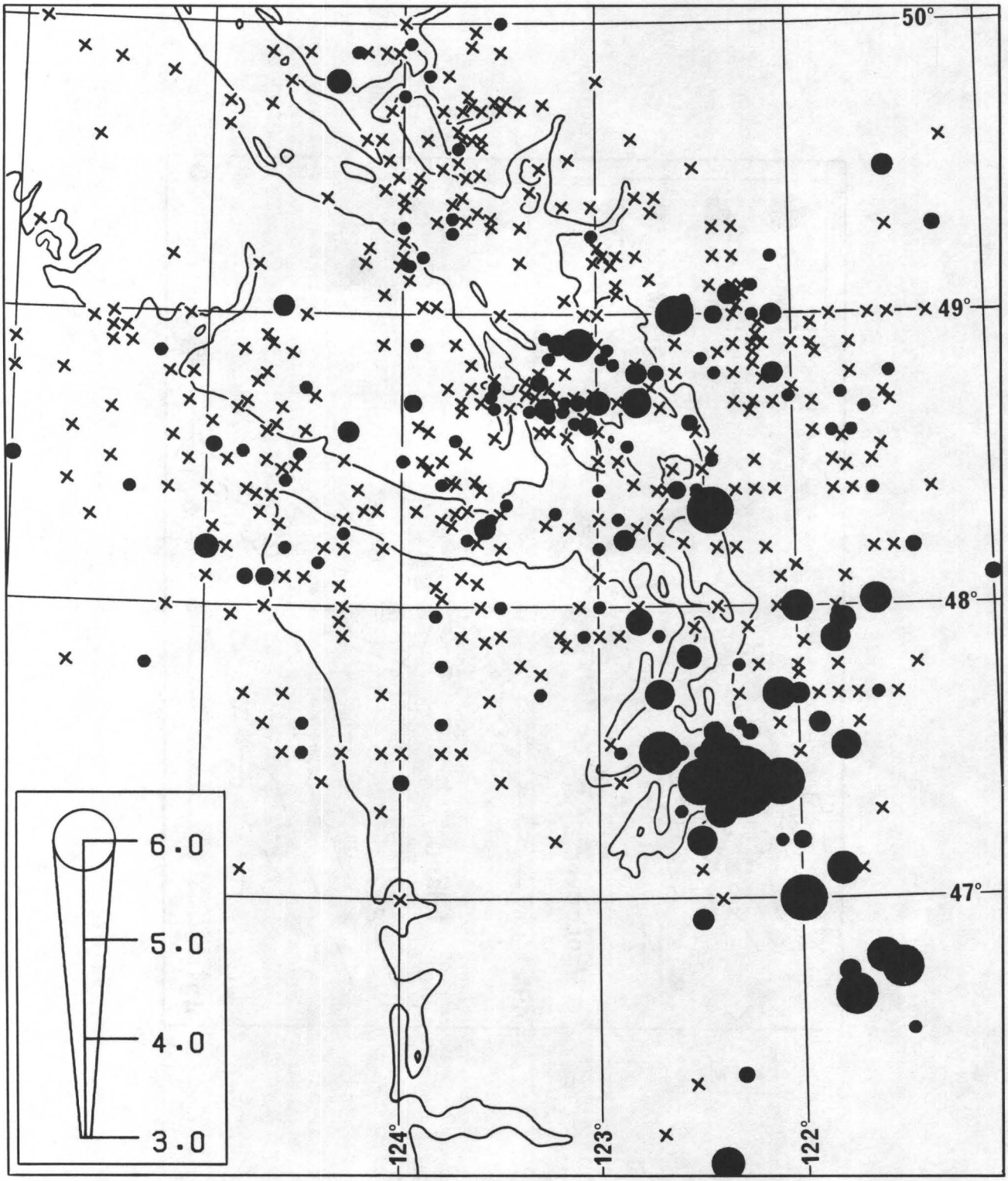
50°
49°
48°
47°
124°
123°
122°
6.0
5.0
4.0
3.0

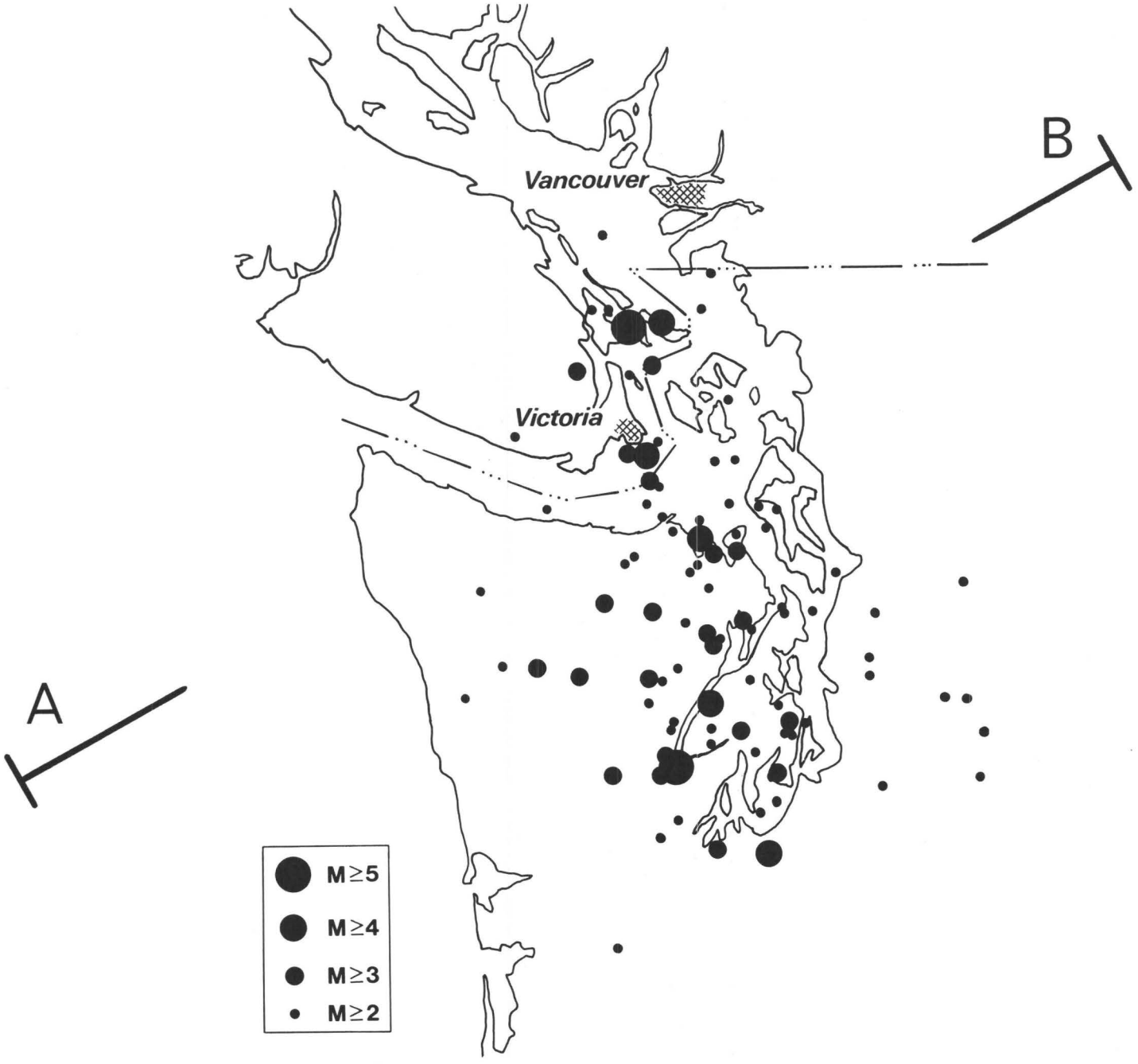
Vancouver
Victoria
A
B
M≥5
M≥4
M≥3
M≥2

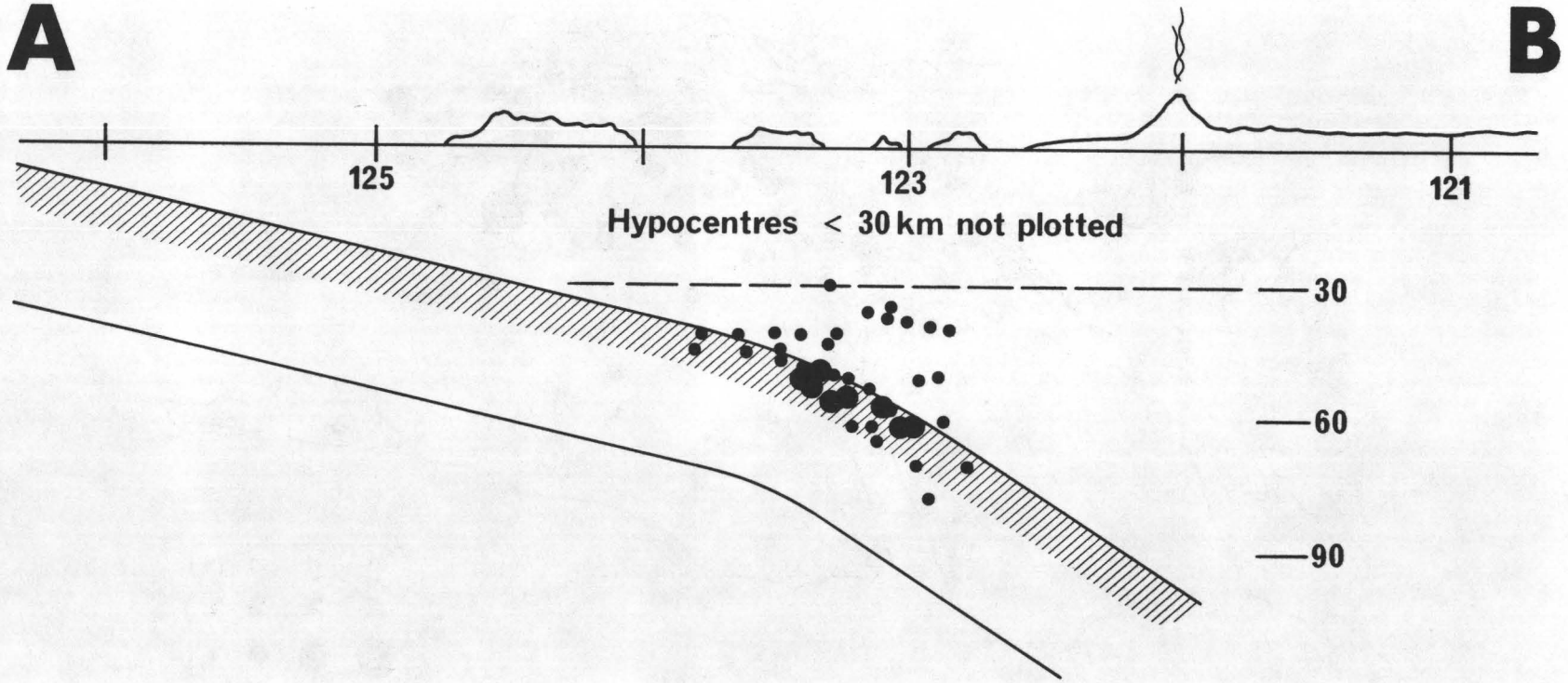
A
B
125
123
121
Hypocentres < 30 km not plotted
30
60
90

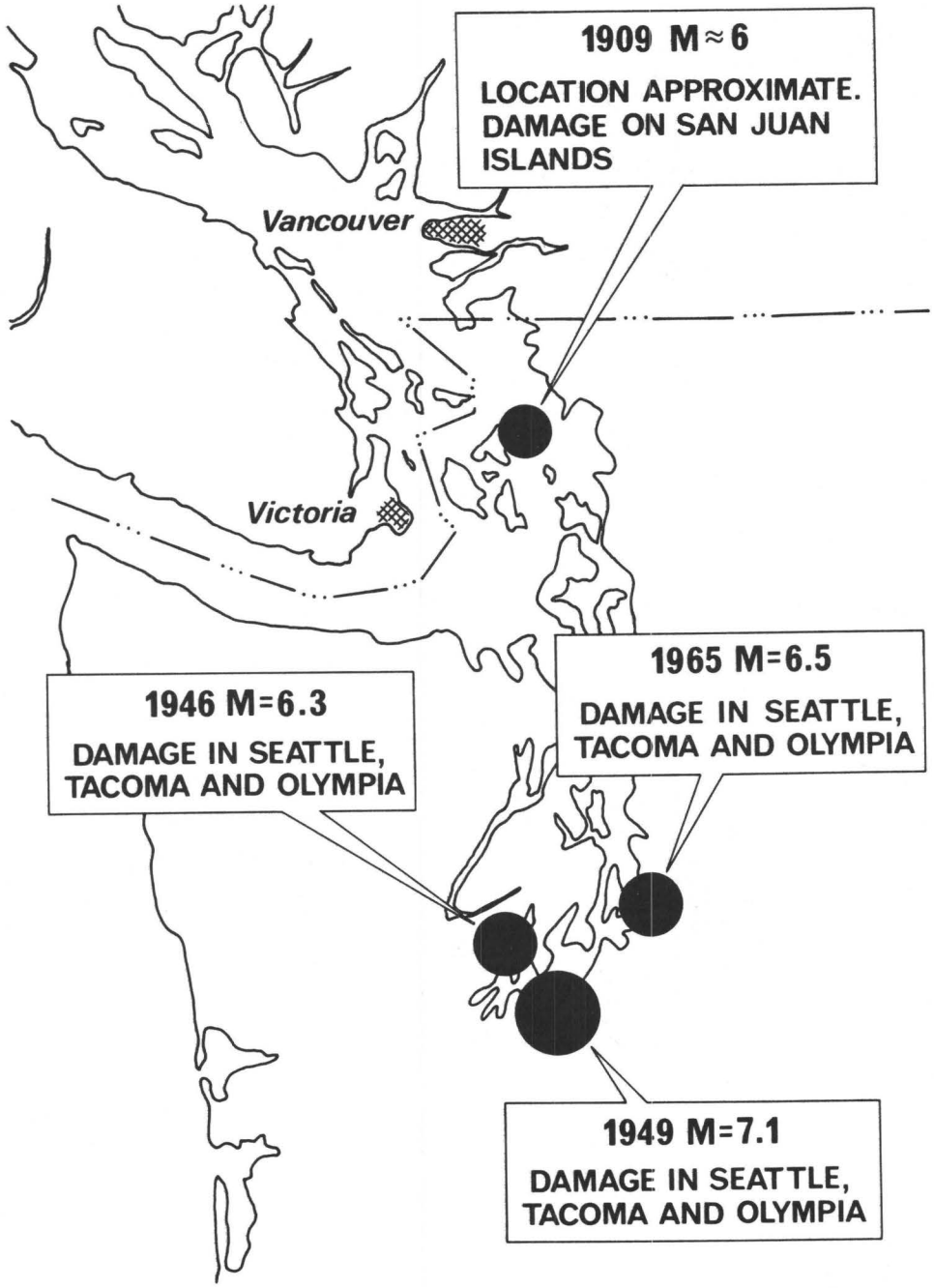
1909 M≈6
LOCATION APPROXIMATE. DAMAGE ON SAN JUAN ISLANDS
Vancouver
Victoria
1965 M=6.5
DAMAGE IN SEATTLE, TACOMA AND OLYMPIA
1946 M=6.3
DAMAGE IN SEATTLE, TACOMA AND OLYMPIA
1949 M=7.1
DAMAGE IN SEATTLE, TACOMA AND OLYMPIA

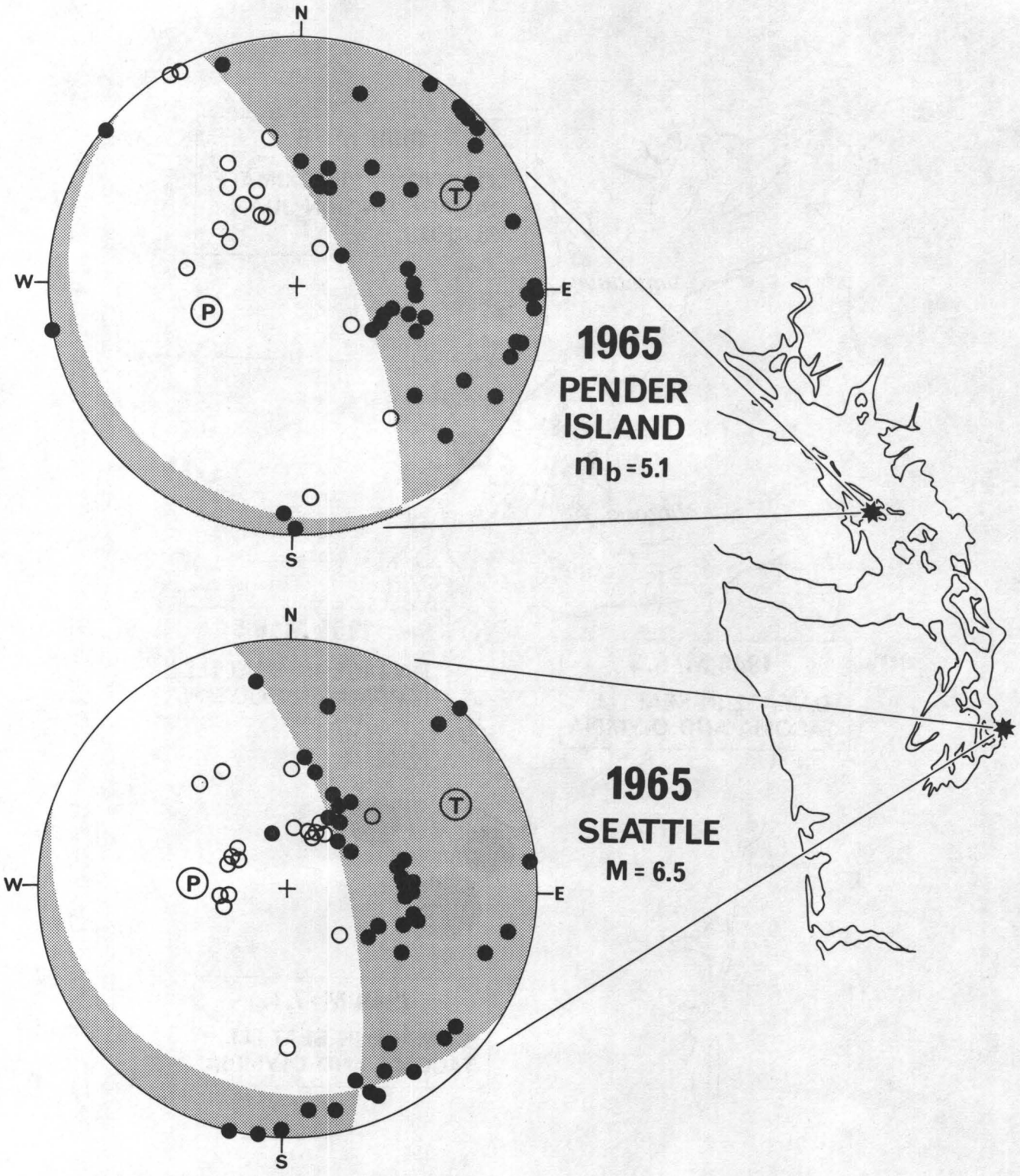
N
W
E
S
T
P
1965
PENDER
ISLAND
$m_b$ = 5.1
N
W
E
S
T
P
1965
SEATTLE
M = 6.5

b
a

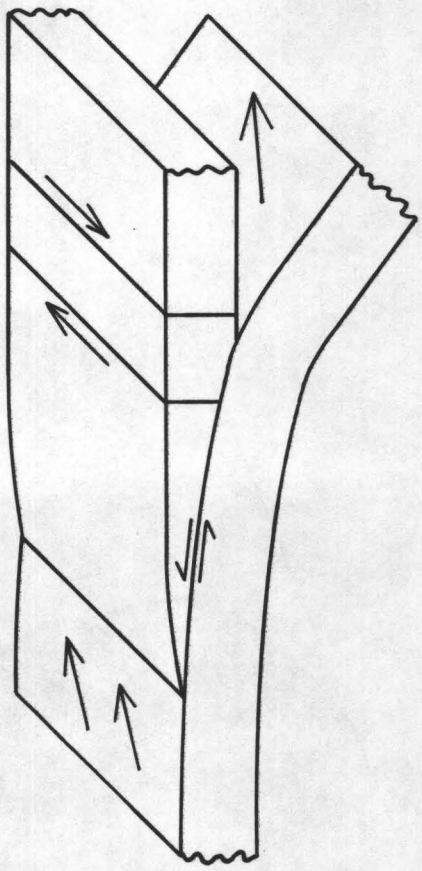

# THE MAGNITUDE 4.6 SOUTH PUGET SOUND EARTHQUAKE OF MARCH 11, 1978: MAIN SHOCK AND AFTERSHOCKS

Thomas S. Yelin and Robert S. Crosson
Geophysics Program AK-50
University of Washington
Seattle, Washington 98195

On March 11, 1978, a magnitude 4.6 earthquake occurred 35 km southwest of Seattle at a depth of about 24 km beneath the Kitsap Peninsula, in the south-central Puget Sound basin (we define the Puget Sound basin to extend approximately from Olympia on the south to Port Townsend on the north and from Seattle on the east to the Hood Canal on the west). The earthquake was felt widely over the south-central basin but there were no reports of significant property damage. In the nine months following the March 11 earthquake, 44 aftershocks occurred in the immediate vicinity of the main shock. Only two of them had magnitudes greater than 2. The rate of aftershock occurrence decayed with time in approximately a 1/t fashion (Figure 1).

This sequence of earthquakes is noteworthy for two reasons. The main shock is the largest earthquake recorded in the south-central basin since 1970. It is also the first well-defined example of a classical main shock-aftershock sequence observed in the Puget Sound basin since the western Washington regional seismographic network began operation in 1970.

Epicenters for the years 1970-1977 in the region adjoining the immediate area of the 1978 sequence are shown in Figure 2. The distribution is generally diffuse, with only a few distinct areas of clustering. The hypocenter region of the March 11 earthquake had only a moderate amount of seismicity during the years 1970-1977.

We first located the earthquakes in this sequence with the velocity model and station corrections developed by Crosson (1976). The locations resulting from this initial analysis are summarized in Figures 3 and 4. Figure 3 is an epicenter map which suggests a fault plane striking N45°W. Figure 4a is a projection of the hypocenters onto a vertical plane striking N45°E. The alignment of hypocenters in this cross section supports the idea of a nearly vertical fault plane striking N45°W. Figure 4b is a projection of the hypocenters onto a vertical plane striking N45°W, at right angles to the plane of Figure 4a. This cross section indicates that the distribution of hypocenters dips to the northwest.

We constructed first motion projections for the main shock using both a constant gradient velocity model and the layered model used to locate the earthquakes. Polarity readings from the USGS network in the vicinity of Mount Hood were helpful in providing some additional constraint on the focal mechanism. The mechanisms obtained from the two different models are essentially identical, with conjugate fault planes striking N18°W and N78°E and dipping, respectively, 80° to the east and 60° to the south (Figure 5). Very similar focal mechanisms were obtained for the largest aftershock (M=4.0) and a composite of three smaller aftershocks. Thus, there is a discrepancy in orientation between the fault plane determined by the first motion projections and the fault plane suggested by epicentral and hypocentral alignments. This discrepancy may be due to several causes. The locations and/or fault planes may be influenced by the lateral heterogeneities which we know exist in the crust of this region. Another possibility is that poor location control in certain spatial directions may be influencing the locations and also indirectly influencing the focal mechanisms determined.

In an attempt to evaluate these effects we carried the analysis further by calculating error ellipsoids (Flinn, 1965) for each location to reveal directions in space along which relatively poor location control exists.

Figure 6 is a lower hemisphere stereographic plot of the three axes of each error ellipsoid. Twenty five (53%) of the earthquakes have error ellipsoids whose major axis to minor axis ratio is 3:1 or greater and whose intermediate to minor axis ratio stands as 1.5:1 or less. No ellipsoid had a major to minor axis ratio of less than 2:1. The axis orientations of these 25 ellipsoids are plotted in Figure 7. All the major axes in this group have plunges of 60° or greater. This reflects the fact that, in general, depth is the most poorly controlled hypocenter coordinate. The orientation of the minor and intermediate axes are seen to be rather evenly distributed in azimuth compared to the orientations of the major axes. The majority of minor and intermediate axes have plunges of less than 20°. Thus, the majority of the earthquakes have error ellipsoids which are considerably elongated, with their axis of elongation plunging steeply to the northwest and north-northwest. The lengths of the major axes range from about 1 km to 2.4 km. These probably represent lower limits on the true errors and in any event should be interpreted only in relative terms. The major axis errors are a significant fraction of the apparent spatial extent of the sequence. The results of this error analysis indicate that there is a true lack of control of hypocenters along the major axis directions indicated in Figure 7. The approximate direction of hypocenter alignment (as determined from Figures 3 and 4b) is also indicated in Figure 7 by the the solid square. We believe this direction is close enough to the average direction of elongation of the error ellipsoids that the hypocenter alignment could be at least partially the result of the relatively poor control of hypocenters parallel to that elongation.

In an effort to reduce the error of relative location, with the hope that we might be able to detect a spatial structure which was less likely to be a product of location error, we relocated the earthquakes using the master event technique (Evernden, 1969), as applied to tightly grouped local earthquake sequences. Residuals from a single well-located earthquake were used in the location procedure as station corrections. The main shock of March 11 was used as the master event. Figure 8 is an epicenter map of the solutions obtained with the master event technique. Comparison with Figure 3 shows that the epicenters have generally become more tightly grouped, suggesting that the source area is smaller than previously indicated. There is an apparent alignment of epicenters trending NNW, much closer to the NNW nodal plane of Figure 5. Figures 9a and 9b are projections of the master event hypocenters onto vertical planes striking N70°E and N20°W, respectively. Comparison of Figures 4a and 9a show that the vertical alignment of hypocenters is preserved. Comparison of Figures 4b and 9b also show that the distribution of hypocenters still seems to plunge in a linear alignment. A near-vertical fault plane trending north-northwest appears to be favored although the evidence is somewhat ambiguous, due to the small aftershock volume. Focal mechanisms for the master event locations, which are essentially identical to the initial mechanisms, are in accord with this conclusion. The identical nature of the initial and master event mechanisms is not suprising in light of the fact that the locations of most of the earthquakes were not changed by more than a kilometer or two.

We proceeded to calculate error ellipsoids for the master event solutions

and plotted the three axes of each ellipsoid on a stereo net (Figure 10). Twenty two (49%) of the master event ellipsoids were significantly elongated, with major to minor axis ratios of 3:1 or greater and intermediate to minor axis ratios of 1.5:1 or less. As was the case with the initial solutions, no ellipsoid had a major to minor axis ratio of less than 2:1. The axes of these 22 ellipsoids are plotted on Figure 11. Once again, these ellipsoids have directions of elongation that plunge steeply (60° or greater) to the northwest and north-northwest. The other two axes of the ellipsoids are again distributed relatively evenly in azimuth with most plunging less than 20°. For the most part, the length of the major axes lie between .75 km and 1.5 km. These lengths should again be interpreted in relative terms. The approximate axis of hypocenter alignment (as determined from Figures 8 and 9b) is plotted as a solid square on Figure 11.

The alignment of epicenters and hypocenters obtained with the master event technique may well be a real feature of the spatial distribution of this sequence of earthquakes. Unfortunately, clear resolution of the problem for this case is not possible in view of the small source region and the fact that the alignment that does exist is close to but not exactly in the direction of poorest location control. It is difficult to determine how different the alignment and location control bias must be before alignment may be regarded as a real feature of the distribution. However the focal mechanism evidence, when combined with the spatial alignment provides a stronger indication of the true fault orientation than either does alone. It is clear that both error ellipse calculation and master event locations are extremely valuable when evaluating the spatial distribution of tightly clustered hypocenters.

There is no geologic evidence for any through-going fault in this region along which these earthquakes might have occurred. This is not suprising in view of their depth and the glacial overburden which obscures the basement structure in this region. If the spatial arrangement of hypocenters is real, the area of fault surface involved is approximately 12-15 $km^2$ (roughly $2.5x5km^2$). For either choice of conjugate fault planes the dominant component of motion is strike slip. The axis of maximum compression (P) has an azimuth of 32° and a plunge of 14° to the northeast. Other shallow earthquakes (depth less than 30 km) in the Puget Sound region seem also to result from a roughly north-south compression of the crust (Crosson, 1972).

## References

Crosson, R.S. (1972). Small earthquakes, structure, and tectonics of the Puget Sound region, Bull. Seism. Soc. Am. 62, 1133-1171.

Crosson, R.S. (1976). Crustal structure modeling of earthquake data, 2. velocity structure of the Puget Sound region, Washington, J. Geophys. Res. 81, 3047-3054.

Evernden, J.F. (1969). Identification of earthquakes and explosions by use of teleseismic data, J. Geophys. Res. 74, 3828-3856.

Flinn, E.A. (1965). Confidence regions and error determinations for seismic event location, Rev. Geophys. 3, 157-185.

## CAPTIONS FOR FIGURES

Figure 1: Distribution of south Puget Sound sequence in time.

Figure 2: Epicenters in south Puget Sound for the years 1970-1977 (box contains area of 1978 sequence).

Figure 3: Map of initial epicenters of 1978 sequence.

Figure 4a: Projection of initial hypocenters onto a vertical plane striking N45°E.

Figure 4b: Projection of initial hypocenters onto a vertical plane striking N45°W.

Figure 5: Fault plane solutions for main shock using both linear and layered velocity models for the focal sphere projections (open circles = dilatation, closed circle = compression, P = axis of maximum compression, T = axis of maximum tension).

Figure 6: Lower hemisphere stereographic plot of the three principle axes of the error ellipsoids of all the initial hypocenter solutions. Solid square denotes direction of hypocenter alignment as determined from Figures 3 and 4b. All other solid figures denote two or more axes with essentially identical orientations.

Figure 7: Same as Figure 6 except that only initial ellipsoids with major to minor axis ratios of 3:1 or greater and intermediate to minor axis ratios of 1.5:1 or less are plotted. Symbols as in Figure 6.

Figure 8: Map of master event epicenters.

Figure 9a: Projection of master event hypocenters onto a vertical plane striking N70°E.

Figure 9b: Projection of master event hypocenters onto a vertical plane striking N20°W.

Figure 10: Lower hemisphere stereographic plot of the three principle axes of the error ellipsoids of all the master event hypocenter solutions. Solid square denotes direction of hypocenter alignment as determined from Figures 8 and 9b. Other symbols as in Figure 6.

Figure 11: Same as Figure 10 except that only master event ellipsoids with major to minor axis ratios of 3:1 or greater and intermediate to minor axis ratios of 1.5:1 or less are plotted. Solid square as in Figure 10. Other symbols as in Figure 6.

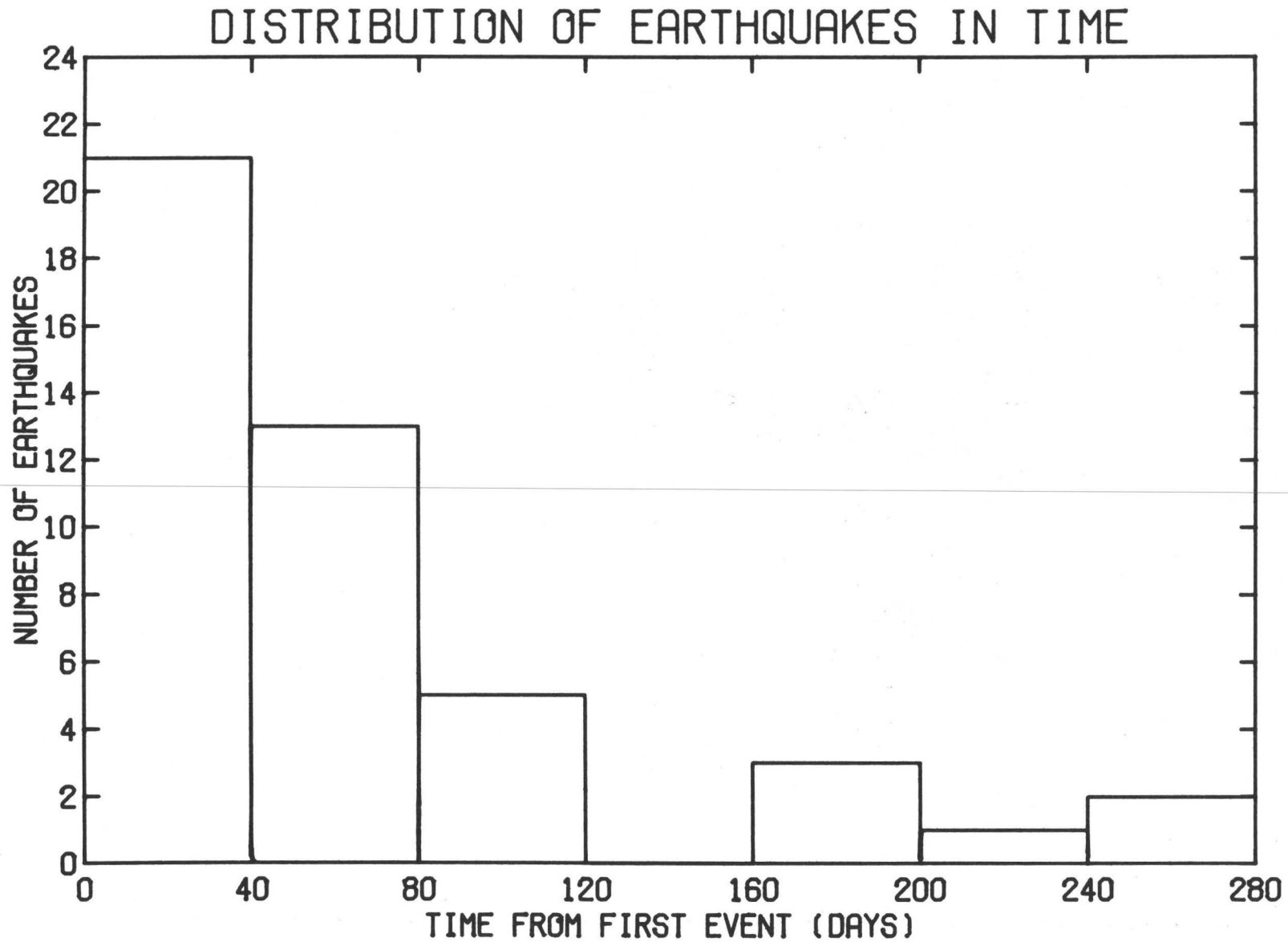
DISTRIBUTION OF EARTHQUAKES IN TIME
NUMBER OF EARTHQUAKES
0
2
4
6
8
10
12
14
16
18
20
22
24
0
40
80
120
160
200
240
280
TIME FROM FIRST EVENT (DAYS)

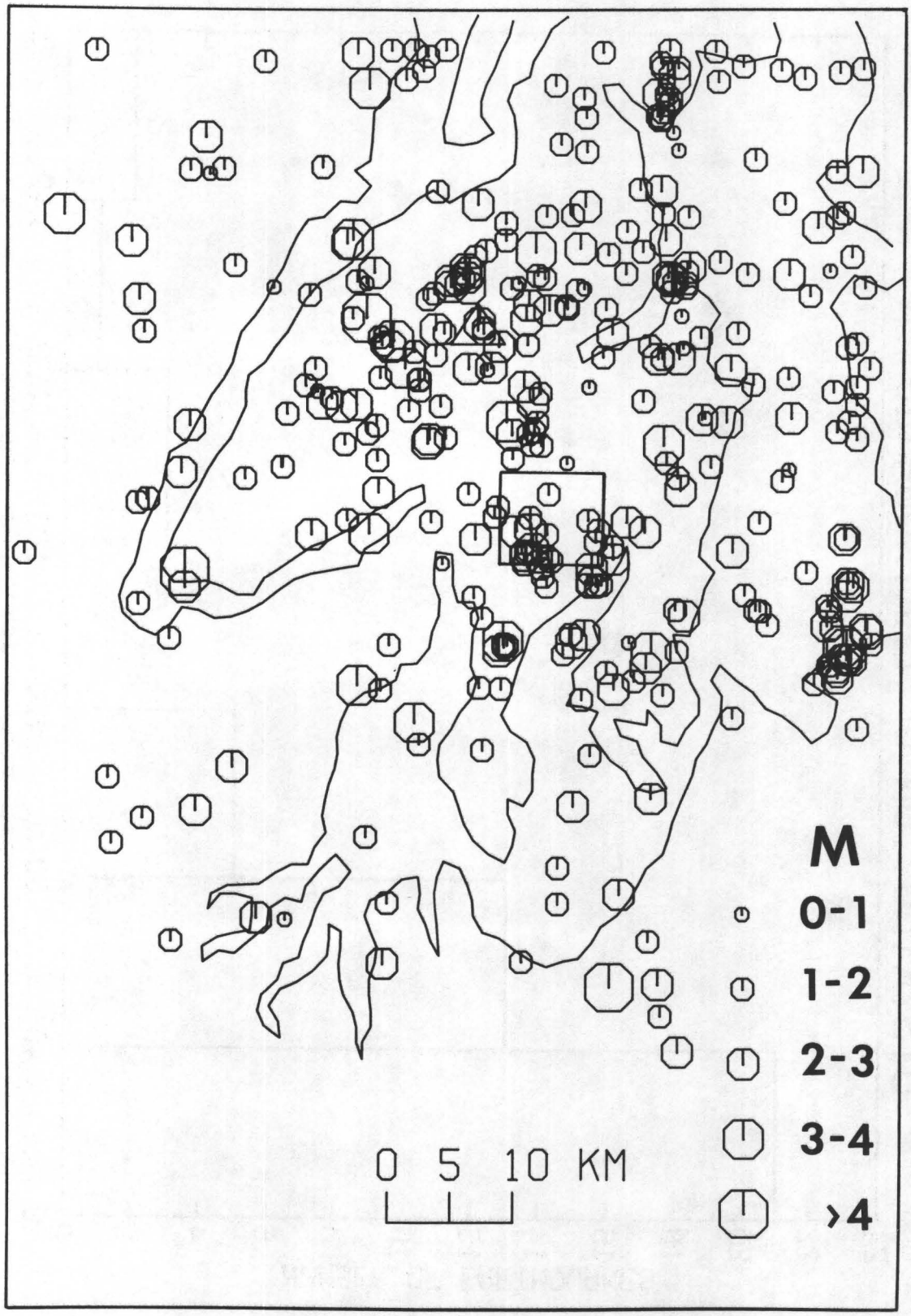
M
0-1
1-2
2-3
3-4
>4
0 5 10 KM

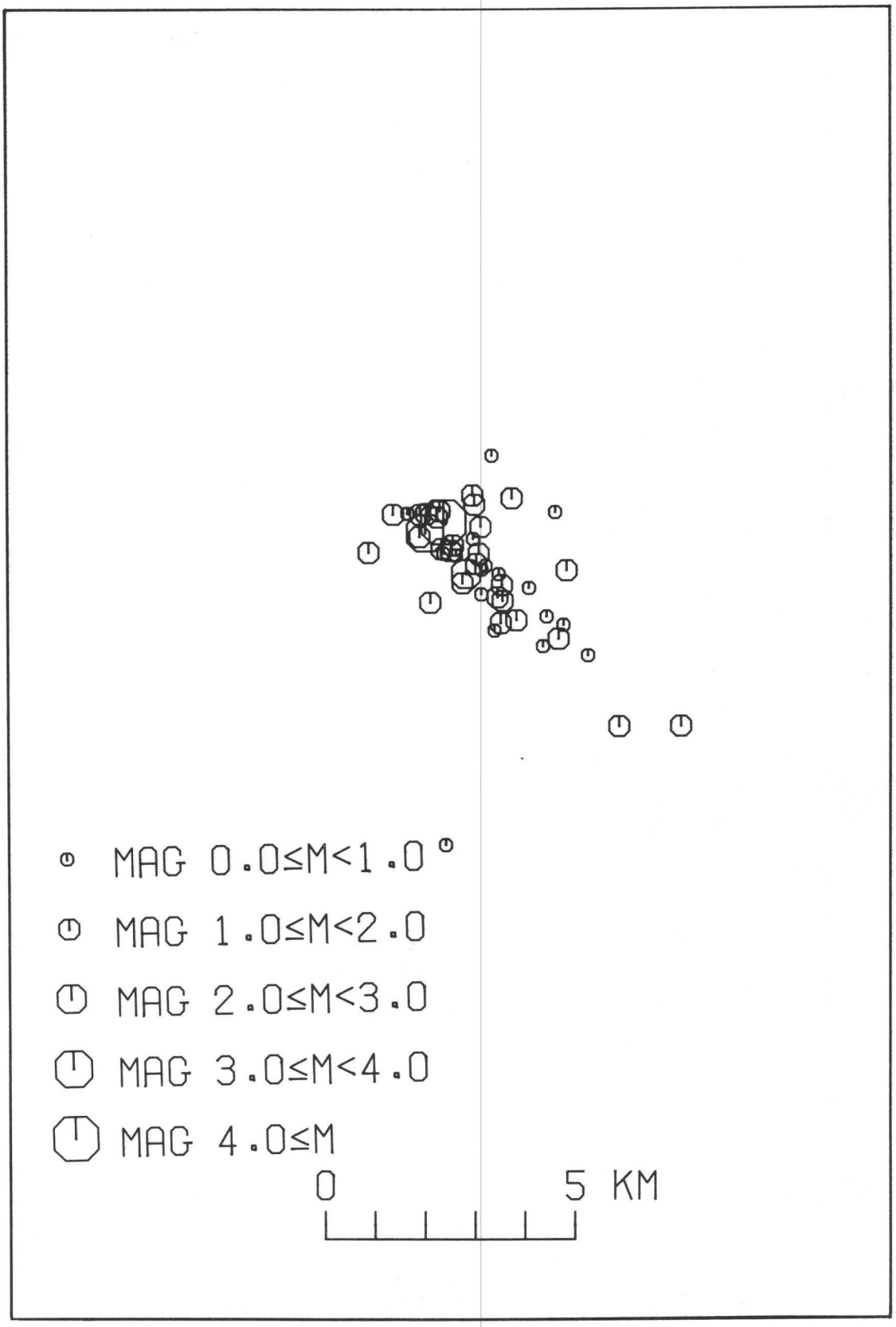
MAG 0.0≤M<1.0
MAG 1.0≤M<2.0
MAG 2.0≤M<3.0
MAG 3.0≤M<4.0
MAG 4.0≤M
0
5 KM

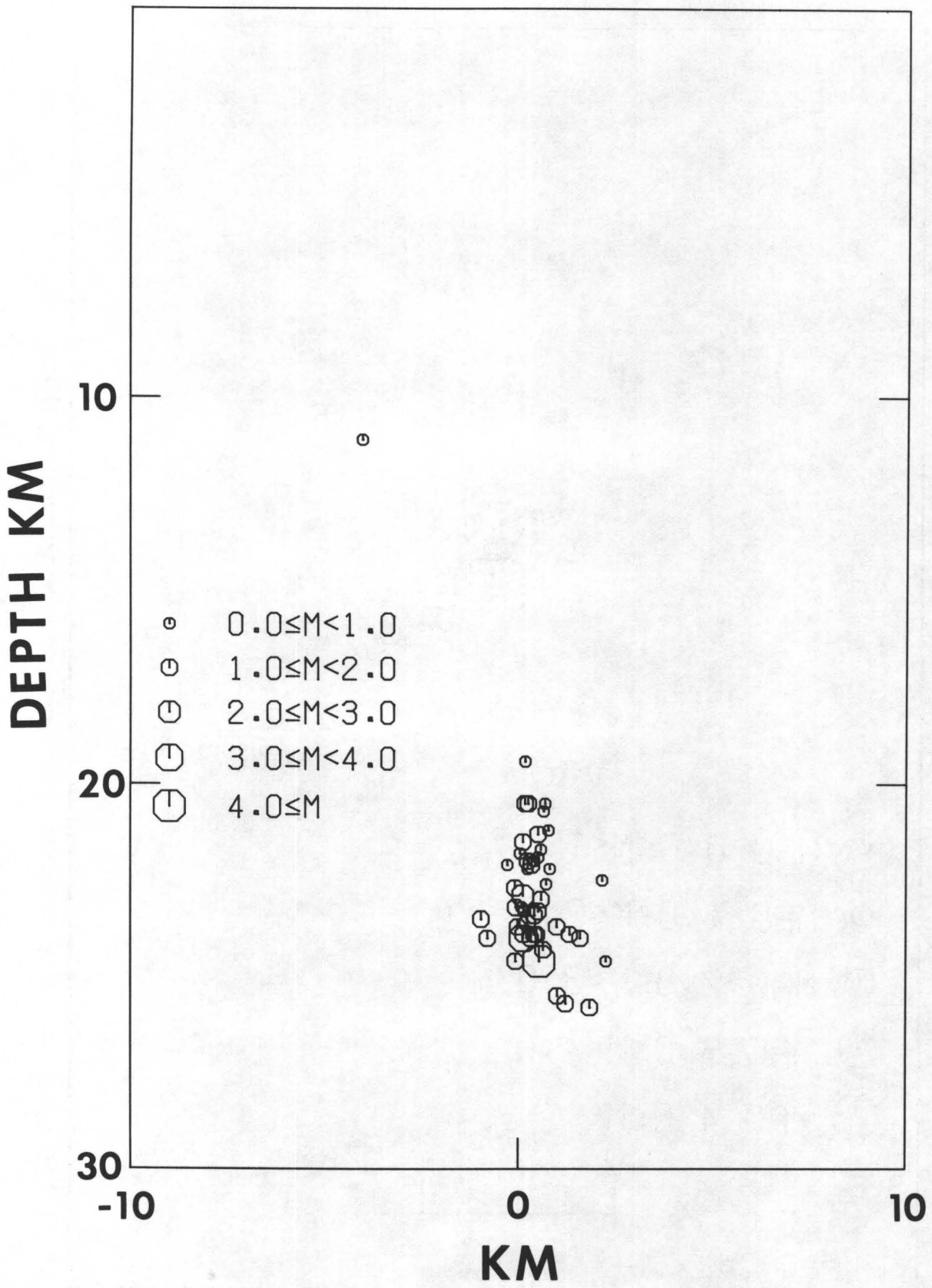
DEPTH KM
10
20
30
-10
0
10
KM
0.0≤M<1.0
1.0≤M<2.0
2.0≤M<3.0
3.0≤M<4.0
4.0≤M

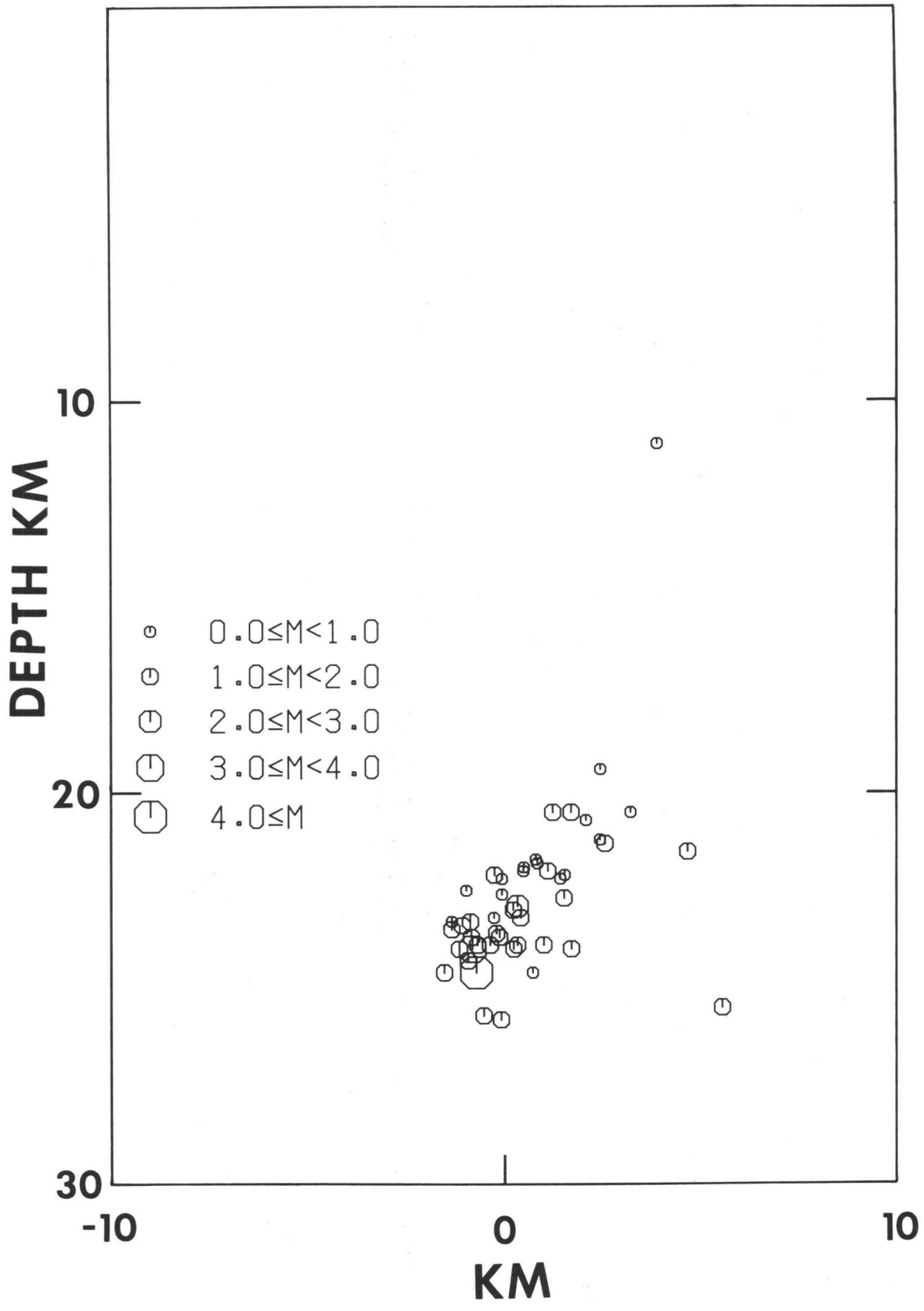
DEPTH KM
10
20
30
-10
0
10
KM
0.0≤M<1.0
1.0≤M<2.0
2.0≤M<3.0
3.0≤M<4.0
4.0≤M

N
P
T
LAYERED
N
P
T
LINEAR

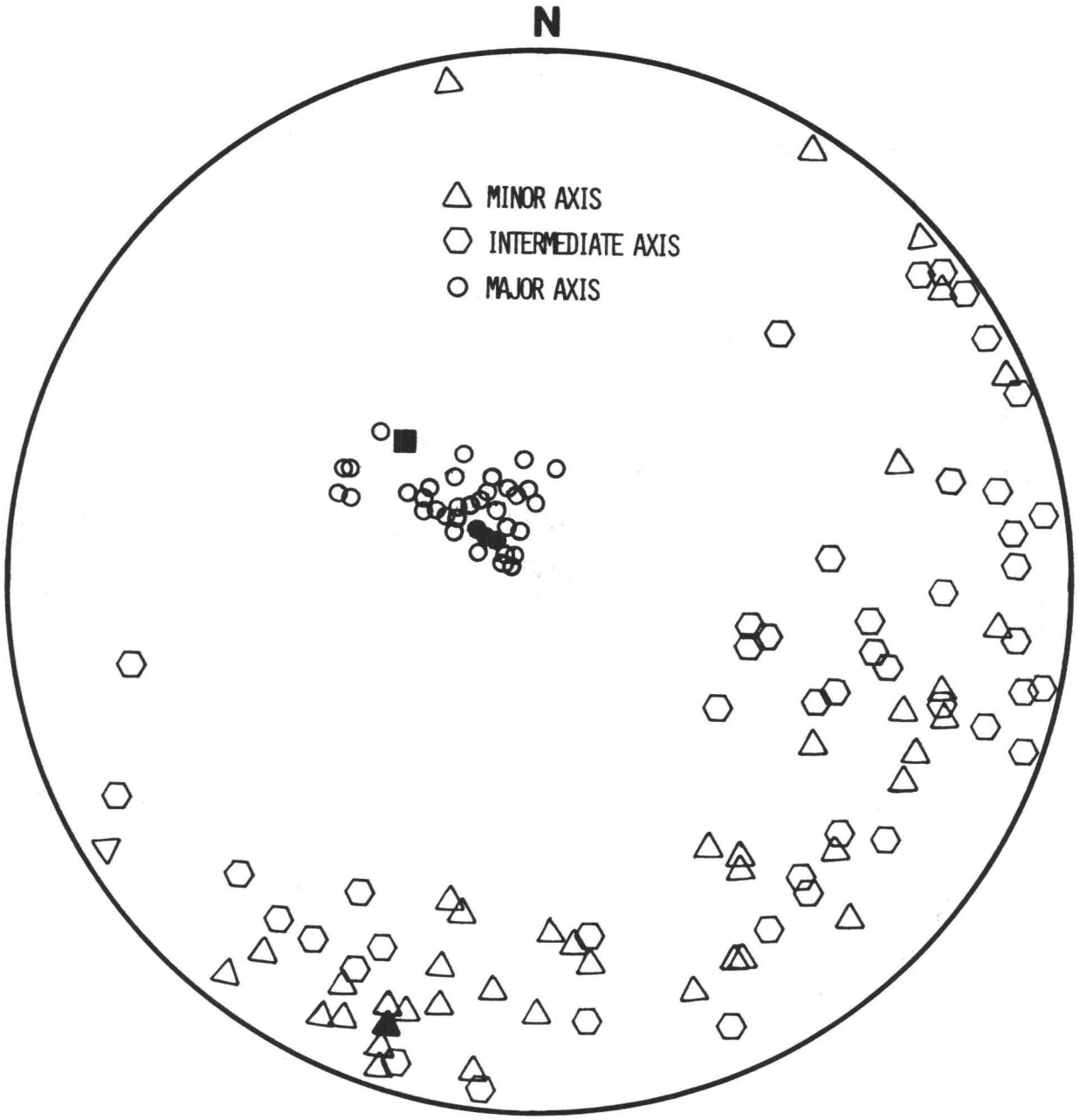
N
MINOR AXIS
INTERMEDIATE AXIS
MAJOR AXIS

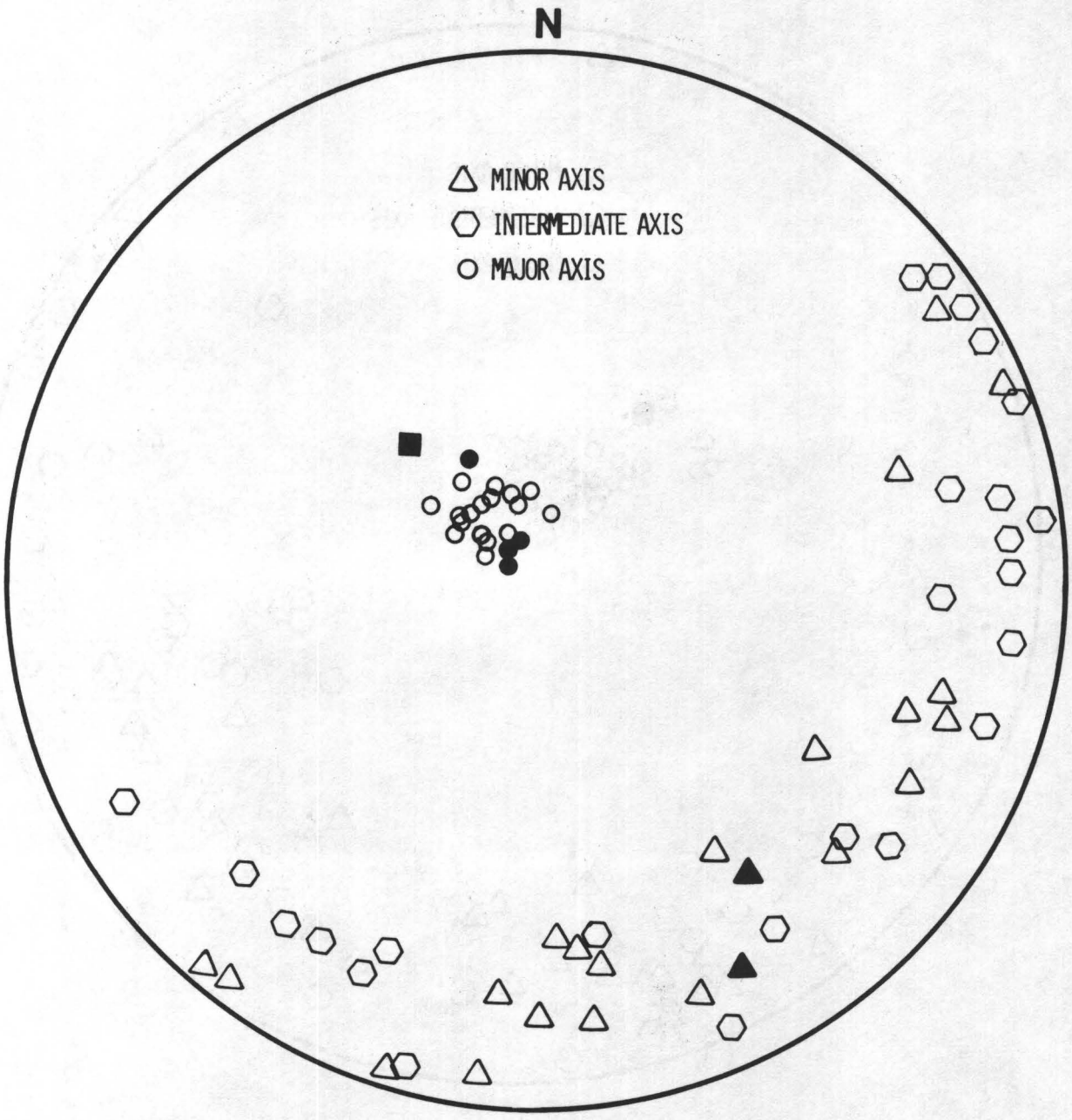
N
MINOR AXIS
INTERMEDIATE AXIS
MAJOR AXIS

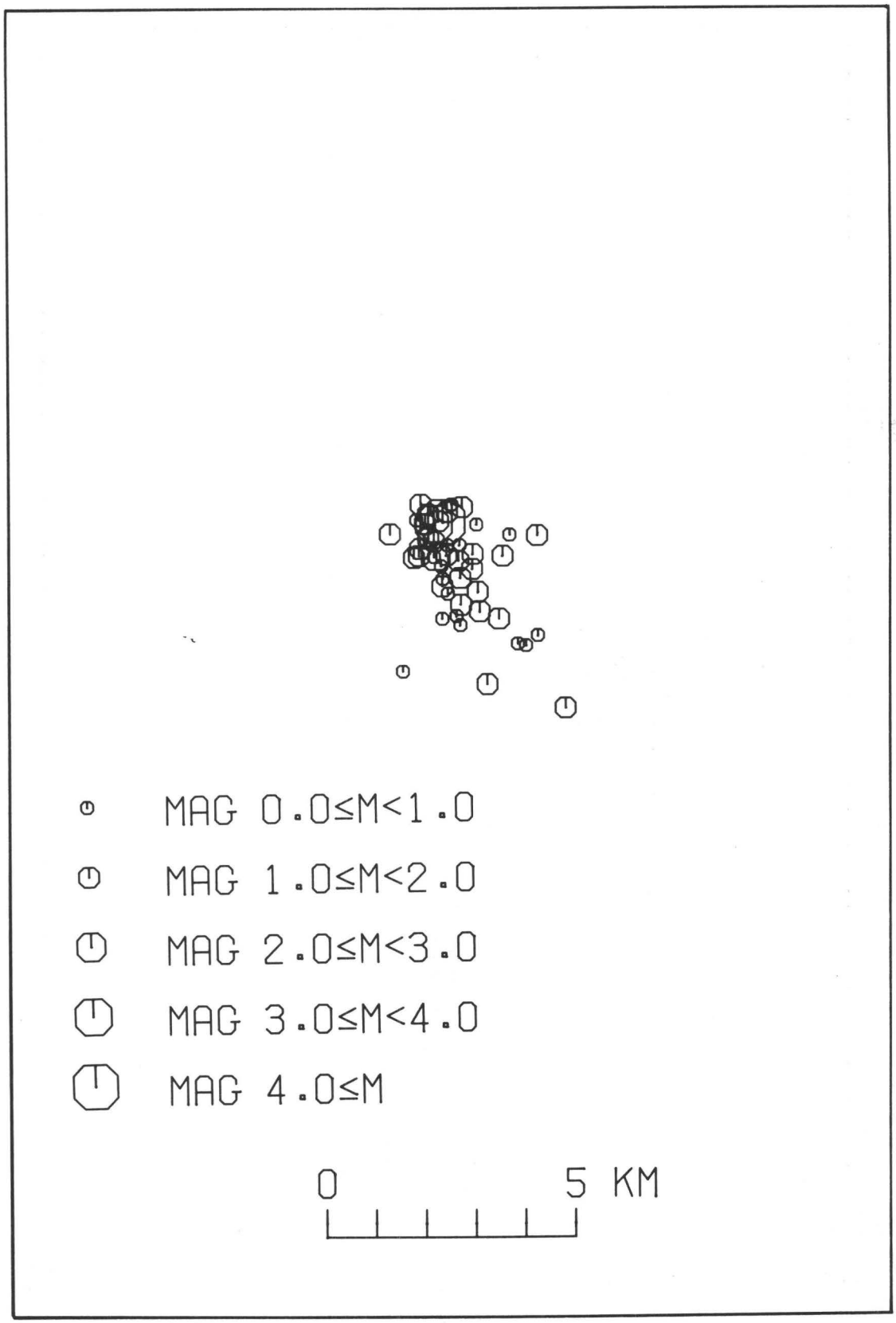
MAG 0.0≤M<1.0
MAG 1.0≤M<2.0
MAG 2.0≤M<3.0
MAG 3.0≤M<4.0
MAG 4.0≤M
0
5 KM

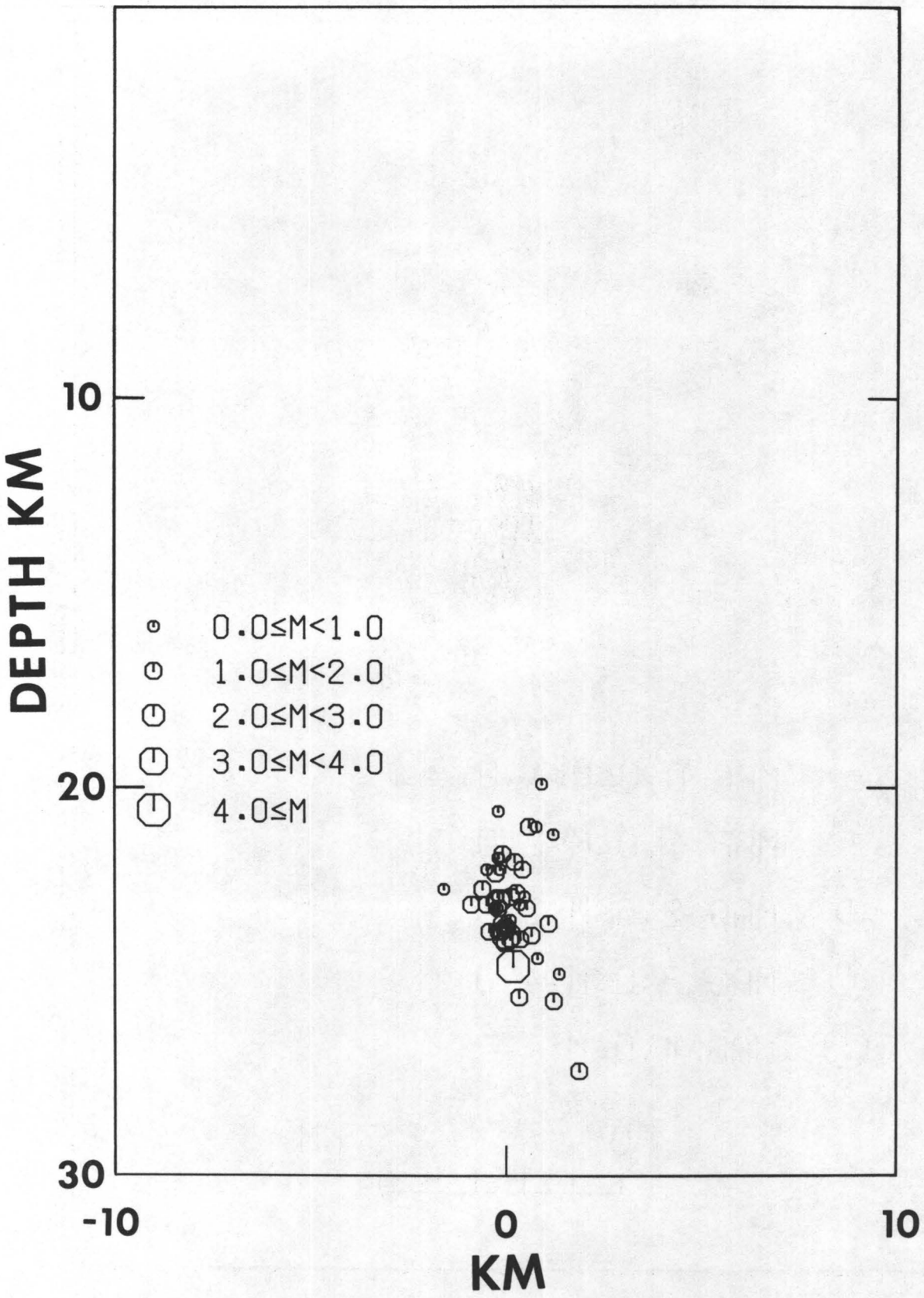
DEPTH KM
10
20
30
-10
0
10
KM
0.0≤M<1.0
1.0≤M<2.0
2.0≤M<3.0
3.0≤M<4.0
4.0≤M

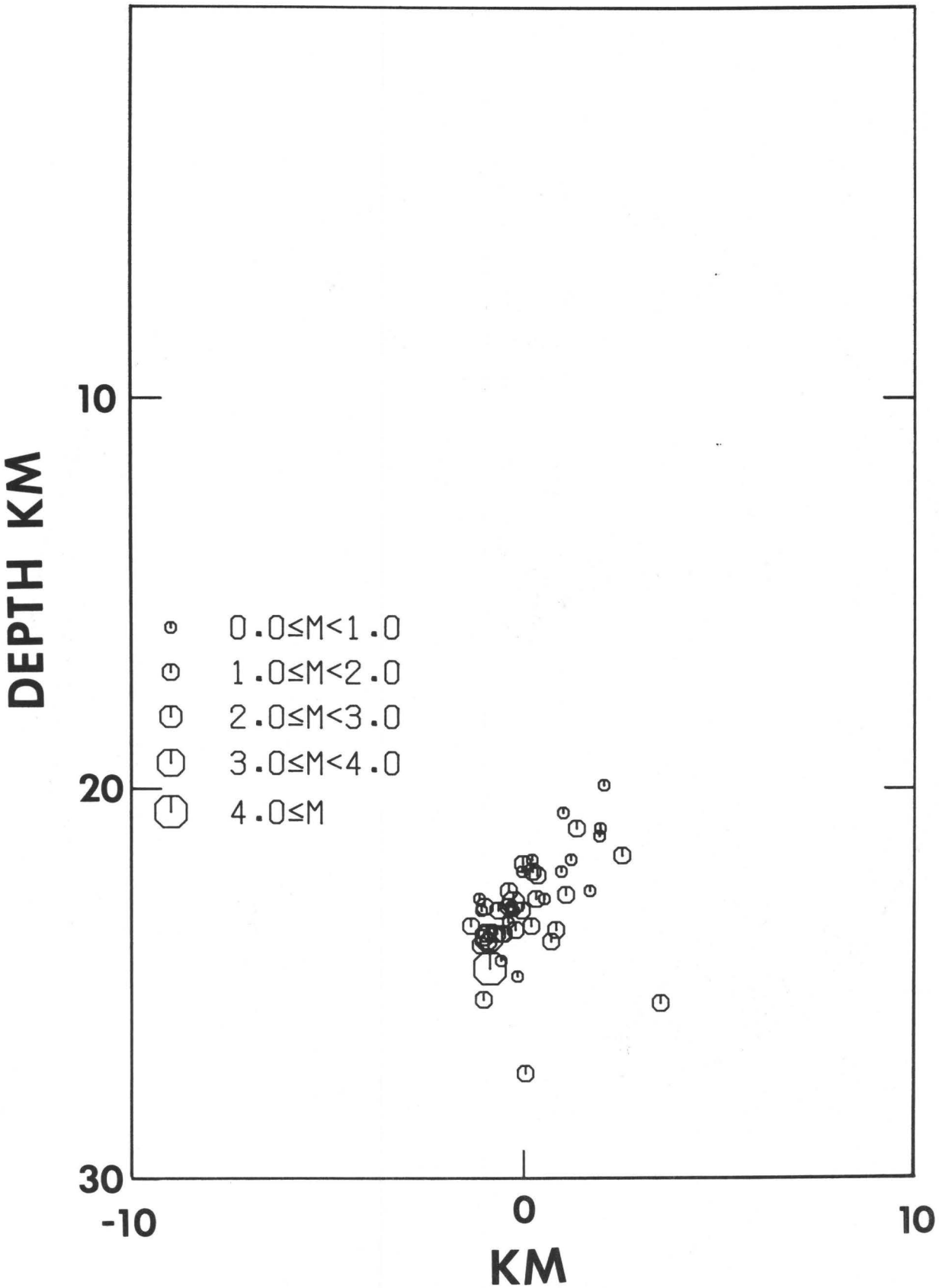
DEPTH KM
10
20
30
-10
0
10
KM
0.0≤M<1.0
1.0≤M<2.0
2.0≤M<3.0
3.0≤M<4.0
4.0≤M

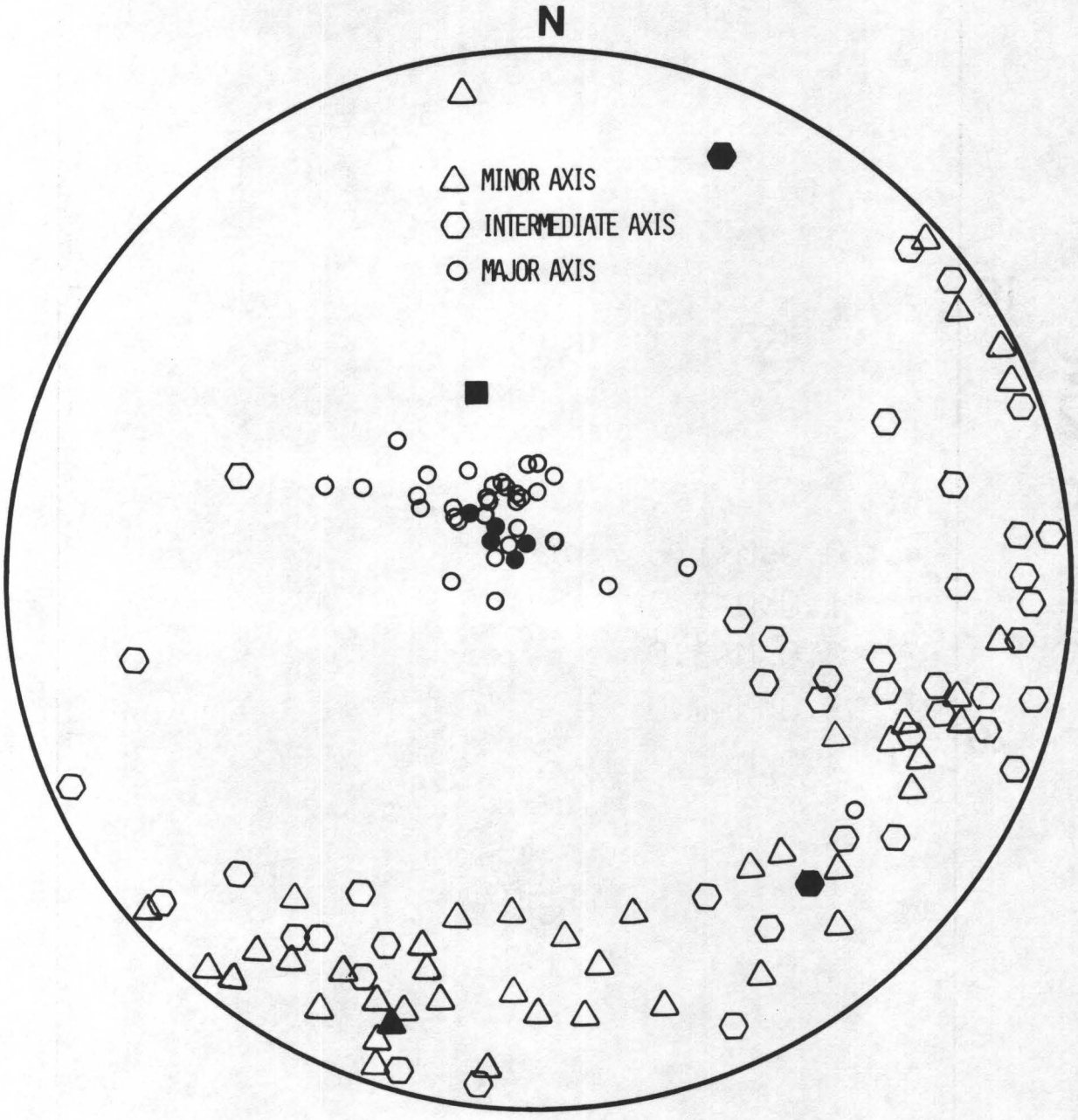
N
MINOR AXIS
INTERMEDIATE AXIS
MAJOR AXIS

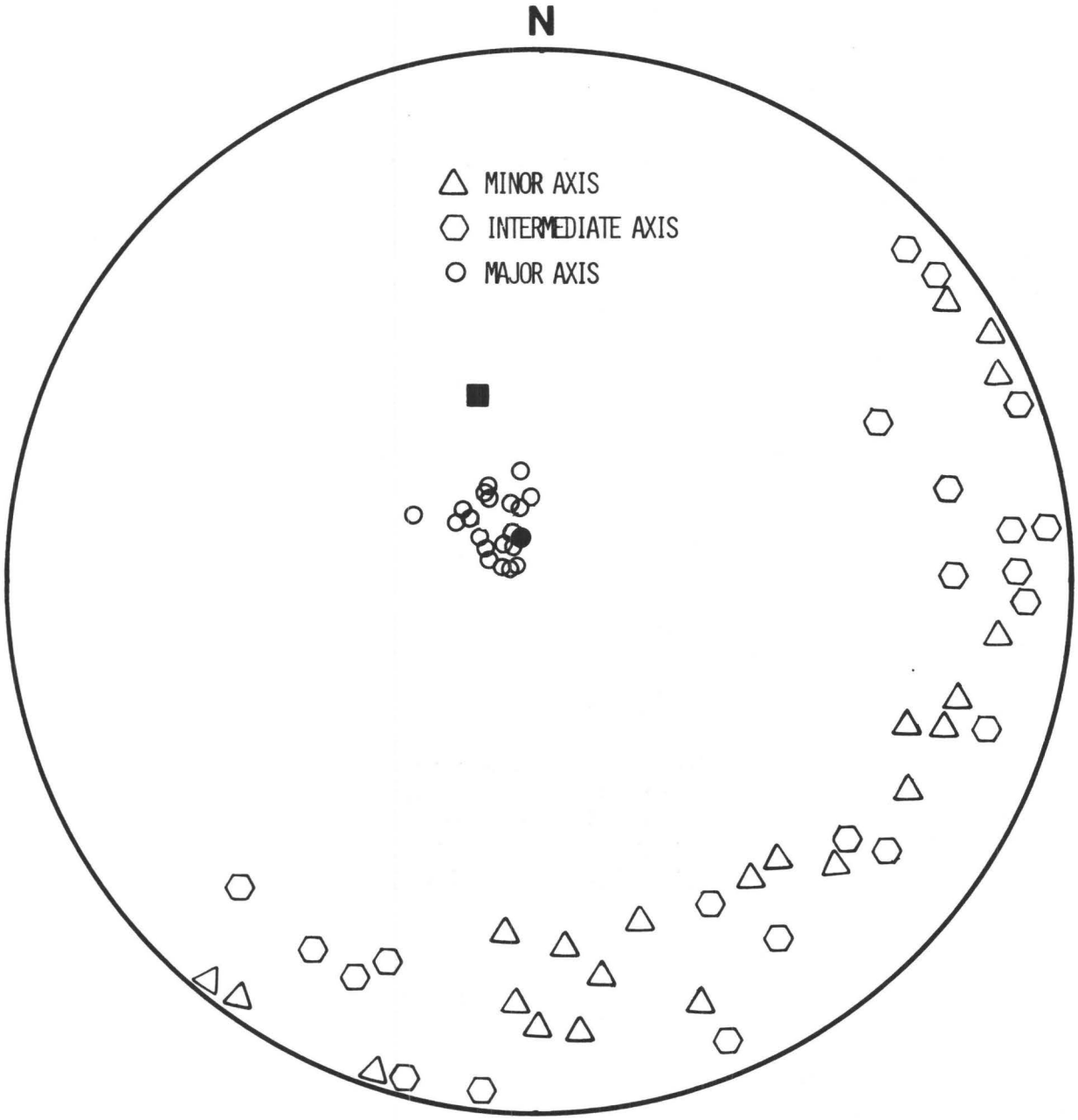
N
MINOR AXIS
INTERMEDIATE AXIS
MAJOR AXIS

# A Study of Puget Sound Strong Ground Motion

by

Charles A. Langston

Department of Geosciences
Geophysics Program
403 Deike Building
The Pennsylvania State University
University Park, Pennsylvania 16802

## Abstract

An attempt was made to model observed strong motion velocities and displacements from the April 29, 1965, magnitude 6.5 Puget Sound earthquake. Several different plane layered crustal models were assumed based on previous seismic refraction measurements. Source parameters for the 1965 event were taken from a previous study of teleseismic body waves. Teleseismic P waves recorded at Tumwater, Washington, near the Olympia strong motion site, were examined to place constraints on allowable interface contrasts and to determine whether lateral heterogeniety is a major factor affecting wave propagation. Because of the 60 km source depth and close epicentral distances for the strong motion sites, it proved adequate to approximate ground displacements and velocities by assuming an impinging P or S plane wave under the various crustal models and using a propagator matrix technique to compute the response. Amplitudes were scaled using the generalized ray theory result for direct P, SV, and SH waves from a point dislocation. Although strong motion models qualitatively showed many of the characteristics of near-vertical wave propagation in layered structures, the observed amplitude behavior of individual stations was quite complex. Data from Tacoma and Seattle sites, close to the epicenter, attained lower velocities and acceleration compared to Olympia which was three times as far. The amplitude behavior is consistent with higher attenuation under Tacoma and Seattle although this is not strictly required. The short-period P data recorded at Tumwater showed evidence of large

velocity contrast interfaces under the station, from large P to S conversions, consistent with those assumed in the crustal models. Comparison of both horizontal components for several teleseisms also indicated that dipping structure or other lateral heterogeniety is important for Olympia structure. Thus, it is likely that strong motion amplitudes and waveshapes are also controlled by scattering mechanisms to a large degree. Irrespective of these wave propagation problems, the largest single factor which has affected the level of strong ground motions in Puget Sound is the large source depth of past earthquakes. Using a simple geometrical spreading argument it is shown that if the 1965 event was only at 10 km distance from Olympia instead of 100 km, all other effects being equal, then greater than 1g accelerations would have been recorded. Thus, estimates of seismic hazard based on a direct interpretation of the strong motion data of the 1965 and 1949 events will be erroneously biased towards less hazard if there is potential for shallow faulting in the Puget Depression.

## Introduction

According to studies of historical seismicity (Algermissen, 1969; Milne, 1967; Howell, 1974), the Puget Sound area is one of high seismogenic potential and hazard, yet little is known of the geologic and geophysical factors which influence earthquake occurrence and resulting strong ground motions. The purpose of this paper is to investigate characteristics of strong ground motion recorded from the April 29, 1965, earthquake in an attempt to sort out factors important to wave propagation in the Puget depression. Recent work involving deterministic modeling of earthquake strong motions from shallow depth sourced has shown promise in estimating the effects of source when close to the source (e.g., Heaton and Helmberger, 1979) or in estimating structure effects on wave propagation when source parameters are known (Heaton and Helmberger, 1977; 1978). These studies have been most successful when modeling assumptions agree closely with the natural structure and when the long period band (e.g., displacements) is examined.

Because of limitations imposed by the relatively sparse strong motion data set and lack of geophysical control over small scale structures in Puget Sound, this study will necessarily be one of determining general characteristics of strong-motion wave propagation in southern Puget Sound within a deterministic framework. For example, a major purpose here is to determine whether plausible plane layered earth models can reproduce the duration and amplitude behavior of observed ground velocity from the 1965 event. Constraints on the source time function, orientation, and depth for the 1965 event are available from a study of teleseismic P and S

waves (Langston and Blum, 1977). Gross constraints on earth models are available from travel time and refraction studies (Crosson, 1976; Zuercher, 1975). Further, because of the fortuitous location of Tumwater station (TUM) near the Olympia strong motion site, assumptions regarding the homogeniety of earth structure can be tested directly by examining teleseismic P wave forms for off-azimuth arrivals and phase conversions (Langston, 1977). Once a set of earth and source models is produced for the 1965 event, they can then be evaluated for implications involving other assumed sources.

The 1949 magnitude 7.1 event and the 1965 magnitude 6.5 event were significant in size yet produced rather low accelerations and damage compared to like magnitude events in Southern California (Algermissen et al, 1965; Mullimeax et al, 1967). Their unusually large depths (70 and 60 km, respectively) will be shown to be the largest single factor in explaining these observations. Thus, it may be that the greatest problem in evaluating seismic risk in Puget Sound concerns not the effects of similar deep events but the effects of possible shallow, near surface, faulting.

Structural Setting

Algermissen et al (1965), Crosson (1972), and Langston and Blum (1977) give several general and topical descriptions of the geology and tectonics of the Puget Sound region. Of primary interest here are the characteristics of crustal structure in the Puget depression. The early pioneering refraction work of Tatel and Tuve (1955) indicated that the crust was rather thin in

Southern Puget Sound, having Moho depths of only about 20 km. Subsequent refraction work by Berg et al (1966) in the Oregon Coast Ranges and by Zuercher (1975) in Southern Puget Sound and the Olympic Peninsula confirm this shallow Moho depth. However, crustal structure studies in central Puget Sound based on earthquake travel time residuals (Crosson, 1976) and unreversed refraction (Zuercher, 1975) indicate that the Moho may be depressed by as much as 15 km obtaining 35 km depths. Indeed, Zuercher (1975) showed that crustal thicknesses and upper crustal velocities may vary considerably in Puget Sound. Implied dips from his structure interpretation may be as great as $45^{o}$.

Gravity and magnetic studies also indicate considerable variation in large scale crustal structures. Danes[v] et al (1965) proposed a northwest-southeast horst structure trending through the center of Puget Sound with flanking deep sedimentary basins. The unconsolidated sediment thickness map compiled by Hall and Othberg (1974) mimics Danes[v] structure and shows greater than 1 km sediment thicknesses under Seattle and Tacoma (see Figure 1 also). Gradients in the thickness are very steep in places, especially near Seattle.

An indication of the nature of short period (1 hz) wave propagation in Puget Sound was obtained in a study of teleseismic pP from the April 1965 event by Langston and Blum (1977). They noticed a dramatic amplitude reduction in short period pP, relative to direct P, even for stations where P was nodal and long period pP was several times larger than direct P. The absence of short period pP seemed to correlate with sediment thickness at its reflection point. An effective Q of 65 was inferred for the structure

between the hypocenter and surface although the amplitude depletion may have been due to scattering as well.

Thus, from all indications, the crustal structure of Puget Sound appears to be heterogeneous and profoundly affects short period wave propagation. The analysis of strong motion data and teleseismic body wave data will show that these heterogenities are probably significant in shaping wave forms and amplitudes although many of the general characteristics in the data can be explained by plausible crustal models.

Strong Motion Data from the 1965 Event

Three-component strong-motion acceleration data were recorded at three locations within Puget Sound from the 1965 earthquake (Figure 1). Additionally, the Tacoma and Seattle sites contained Carder displacement meter instrumentation which recorded horizontal motion. Table 1 lists the station locations, distances and azimuths from USCGS and ISC epicenters for the 1965 events. Table 2 displays instrumentation parameters. Corrected accelerogram data for the Olympia site was obtained in digital format from the Earthquake Engineering Research Laboratory of California Institute of Technology. Techniques and errors involved in processing these data are described by Trifunac et al (1973) and Trifunac and Lee (1974). Analogue copies of the acceleration and displacement meter recordings at Tacoma were obtained from the Solid Earth Data Center in Boulder, Colorado, since these were unavailable in digital form. Further, the Seattle data were unavailable from both sources and were obtained from high quality reproductions displayed in Algermissen et al (1965). The analogue data were

manually digitized at an uneven time increment and then interpolated to an equal time spacing of 0.01 seconds. The data were then corrected for instrument responses and band-passed filtered to remove baseline and digitizing noise. Amplitudes above 25 hz and below 0.05 hz were removed to be consistent with the Ormsby filtering operation described by Trifunac et al (1973). Acceleration and velocities were computed from the accelerogram data and velocity and displacement computed from the Carder displacement meter data. Figures 2, 3, and 4 display the processed accelerogram data for Olympia, Seattle, and Tacoma, respectively. Figures 5 and 6 display the processed Carder displacement meter data for Seattle and Tacoma, respectively.

Consistency between wave shapes for ground velocities derived from the acceleration and Carder data is generally good except for Tacoma NS components; the Tacoma NS Carder data was low amplitude and more difficult to digitize. Velocity amplitudes derived from the Carder data are also about 20% lower than those derived from the acceleration data. This is consistent with differences observed in comparisons of other similar data made by Trifunac and Lee (1974) and Heaton and Helmberger (1977) and is probably due to slight instrument miscalibration.

The acceleration data of Figures 2, 3, and 4 are very similar in form to local earthquake recordings. Indeed, there is no reason to treat them other than high-amplitude local earthquake seismograms. For example, in Figure 4 the vertical component appears to have an initial 'P' arrival and after about 5 seconds,a later 'S' arrival. This is more apparent in

the horizontal components where the S arrival at about 6 to 7 seconds into the record is several times larger than the first arrival. Tacoma is only about 20 km from the epicenter (Table 1) and the source is 60 km deep. This implies an S-P time of about 7 seconds which is consistent with the S- trigger time observed in Figure 4. Further, since the receiver is directly above the hypocenter, incident angles should be steep. P waves should be largest on the vertical component and S waves should predominate on the horizontal components Indeed, this is the case for all three recording sites.

The vertical and EW velocities for Tacoma are particularly simple consisting of a prominent double pulse (Figure 4). Displacements (Figure 6) show a show a prominent S wave pulse polarized entirely westward. Although velocities for Seattle (Figures 3 and 5) are somewhat more complicated than Tacoma, displacements (Figure 5) again show a relatively simple S pulse. Seattle is at approximately the same distance from the epicenter as Tacoma (Table 1), so it might be expected that the observations should be qualitatively similar.

Olympia accelerations show apparent anomalous amplitude behavior (Figure 2). Compared to Seattle, horizontal accelerations are approximately a factor of two larger at Olympia. The difference between Olympia and Tacoma is even more striking, being a factor of 3 to 4. The difference in velocity amplitudes is less striking. Figures 2, 3, and 4 also clearly show that Olympia horizontal accelerations are enriched in high frequencies compared to Tacoma and Seattle. Since Olympia is further from the source

(~70 km) these observations suggest that attenuation may play an important role in local wave propagation under the Tacoma and Seattle sites. This will be discussed in a later section.

Teleseismic Data Recorded at Tumwater, Washington

There are several particular structural properties which are of direct interest to the study of strong ground motions. First, we wish to know the nature of velocity and density contrasts under specific strong motion sites which affect wave propagation in the frequency band of about 1 to 10 hz. Observations concerning the extent and magnitude of lateral heterogeniety are also crucial since there must be a check on the validity of assumptions made in any wave calculations using simple plane-layer models. Through fortuitous circumstances, the University of Washington has been operating a three-component short-period seismic station at Tumwater, Washington (TUM). TUM is located only a few kilometers from the Olympia strong motion site (see Figure 1). Proper analysis of teleseismic body wave data recorded at TUM may therefore yield independent insight into structure appropriate for Olympia.

The basic approach in deducing structure under TUM is to compare the three components of ground motion for an incident teleseismic P wave. Because incident angles within the mantle for teleseismic rays are only $10^{o}$ to $20^{o}$, P to S conversions from boundaries under the station will be predominent on the horizontal components and can be seen directly through comparison with the vertical component (Burdick and Langston, 1977). The relative amplitudes of these conversions indicate velocity contrast and their timing, layer

thickness. Further, a comparison of both horizontal components can be used to determine whether the structure is laterally homogeneous or not (Langston, 1977). In a system of isotropic plane layers horizontal motion due to an incident P plane wave should be polarized in the radial direction only. In the presence of layer dip or other lateral heterogeniety, side refractions and S wave polarization angle changes at reflection and transmission will cause tangential ground motions as well. This will give rise to dissimilar waveshapes for observed horizontal components. A simple glance at the data can therefore reveal whether structure under the station is laterally heterogeneous.

With these techniques in mind, data from several teleseismic events recorded at TUM station were obtained from the University of Washington. Data for three events were chosen and digitized on the basis of high signal-to-noise ratio and simplicity of the P pulse on the vertical component. This last criterion is important since effective source function complexities may mask later arriving P-to-S conversions (Burdick and Langston, 1977). Table 3 lists the teleseismic events digitized in this study and instrument characteristics for the three components at TUM. Figure 7 displays the wave form data. Table 3 indicates that the horizontal instruments are nominally matched but are slightly longer period than the vertical. Also, the gains between vertical and horizontal instruments are radically different. Some compensation for the gains was obtained by dividing the data by the stated magnification. This correction is undoubtably in error, however, since the gains in Table 3 are only approximate (Norman Rasmussen, personal communication, 1979). The vertical-to-radial amplitude ratios displayed on

Figure 7 show unrealistic values indicating that there are problems with instrument calibration. Considering the ray azimuth of approach polarities of the initial P pulse are also inconsistent for the NS and EW components for the 12-27-67 and 7-25-68 events, respectively. Nevertheless, these amplitude problems do not mask the large differences in waveshape seen between horizontal and vertical components. The 12-27-67 event displays a very simple two-second duration pulse on the vertical component followed by virtually no other arrivals for the remainder of the recording (Figure 7). The horizontal components, however, show several major P to S conversions after the initial P wave arrival. Two of the clearer arrivals are indicated by arrows. Note also that the second marked arrival on the NS component is conspicuously absent from the EW component. This is a clear indication that lateral heterogeniety is a contributing factor in shaping short period wave forms. Data from the other two events also show high relative amplitude Ps arrivals on the horizontal components and gross differences in wave shapes between the horizontal components. Thus, we can conclude from this qualitative examination of the teleseismic data that there must be one or more high velocity contrast interfaces in the upper crust under TUM and that these structures are likely to be dipping or otherwise laterally heterogeneous.

Strong Ground Motion Modeling

Although there is direct evidence from the teleseismic data that lateral heterogeniety is significant for short period wave propagation in Puget Sound, we will approach the problem of computing strong ground motions by first assuming simple plane-layered models. Other than being more

computationally tractable and efficient, plane-layered models can yield important physical insights on the major effects of structure on wave propagation.

Figure 8 displays several earth models that were assumed for wave calculations. P wave velocities for models M1 and M2 were taken from Zuercher (1975) and S wave velocities were computed assuming a Poisson solid. Densities are also assumed but are based on empirical velocity-density relations. The variation in crustal thickness for Puget Sound was the basis for assuming thickness variation between models M1 and M2. Model M3 was constructed to introduce plausible velocity variations and more wave complications to compare with the simplier models M1 and M2. In the computations to be presented, two more earth models designated M1-A and M2-A, were used to evaluate the effect of the thick unconsolidated sedimentary section. These were constructed by adding a one kilometer thick layer of low velocity material ($V_p$=3.0 km/sec, $V_s$=1.5 km/sec, $\rho$=2.0 gm/cm$^3$) to the tops of model M1 and M2, respectively.

The relatively unusual circumstance of having all three strong motion sites within the distance of one source depth from the epicenter allows a significant simplification on how wave responses may be computed. Generally, for these types of studies involving shallow sources, the response due to a point source or collections of point sources is calculated using generalized ray theory, mode theory, or wave number integration techniques. Wave propagation from shallow sources to nearby receivers is often quite complicated involving diffracted waves and surface waves. Hence, a rather

robust method is needed for their computation. For Puget Sound strong motion calculations it proved adequate to simply assume a plane wave with the appropriate ray parameter impinging on the crustal model from below. Figure 9 demonstrates that there are minor differences between responses computed using generalized ray theory (Helmberger, 1974; Langston and Helmberger, 1975) and responses computed using the simple propagator matrix formulation of Haskell (1960, 1962). Model M1 was assumed for the calculations of Figure 9 for the Olympia strong motion site (Table 1). The generalized ray calculation involved summing 47 rays for the radial component and 18 for the tangential. A 60 km depth dislocation point source with the orientation derived by Langston and Blum (1977) was also assumed (Table 1). The Haskell response was computed assuming the ray parameter for the direct S wave. All impulse responses were convolved with the velocity time function, V(t), shown in Figure 10.

The major differences between the two kinds of calculations lie principally in geometric spreading changes for converted waves such as Sp. The difference in ray parameter between rays is of little importance because of the small incident angles involved. Besides being computationally inexpensive, the propagator matrix formulation also has the advantage of naturally including all rays within the structure, an important limitation of generalized ray theory in this study. The differences in responses become less as the epicentral distance decreases. Note that this approximation is only valid because source depth is large compared to epicentral distances and typical wave lengths.

For sake of clarity in understanding the theoretical effects of structure on wave propagation, a simple velocity time function was assumed based on the

far-field time function inferred by Langston and Blum (1977). Figure 10 displays a smoothed version of their far-field time function, S(t) and its derivative, V(t). Because of the 60 km source depth and the high frequencies considered, the seismic response is dominated by far-field terms so that displacements may be computed by

$$u_i(t) = S(t) * E_i(t) \tag{1}$$

where $u_i(t)$ is the ith displacement component and $E_i(t)$ is the structure impulse response for the ith component. Ground velocity $v_i(t)$ will therefore be

$$v_i(t) = V(t) * E_i(t) \tag{2}$$

This, of course, assumes a point dislocation source; directivity effects are ignored here.

Figure 11 displays theoretical velocity ground motions for the Olympia site assuming incident P and S waves under the different crustal models of Figure 8. All amplitudes have been normalized depending on incident wave type and displacement component. Radial velocity responses due to an incident P wave have been normalized to the P vertical component and vertical responses due to an incident SV wave have be normalized to the radial. All SH responses have been normalized. To obtain absolute velocity (or displacement) each component is scaled to the amplitude expected for the direct ray. For example, after Langston and Helmberger (1975), the high frequency radial response, q(t) for the direct SV wave is given by

$$q(t) = \frac{M_o}{4\pi\rho_o} \frac{\sqrt{p}}{\eta_\beta} \frac{R(p)\, R_{sr}}{(-2 \frac{d^2t}{dp^2})^{\frac{1}{2}}} \sum_{j=1}^{3} A_j(\theta,\delta,\lambda)\, SV_j \quad V(t) \qquad (3)$$

where,

$R(p)$ = product of generalized reflection and transmission coefficients

$R_{sr}$ = radial SV wave receiver function

$A_j(\theta,\delta,\lambda)$ = horizontal radiation pattern coefficients

$SV_j$ = SV wave vertical radiation pattern coefficient.

$p$ = ray parameter

$M_o$ = seismic moment.

Definitions of these and other parameters may be found in Helmberger (1974) and Langston and Helmberger (1975).

Vertical P waves and tangential SH waves are relatively unaffected by structure, having only minor reverberations occurring after the major direct arrival. Radial P shows many large P to S conversions and reverberations from the interfaces in the earth models. Radial SV shows a long coda of waves which are about 25% the amplitude of the large direct SV pulse. The vertical SV response rings a great deal but is only 20% to 30% the amplitude of the vertical. The extreme ringing in the vertical SV response is due to trapped S to P conversions within the crustal model. The ray parameter for incident S waves is greater than 1/8 sec/km so that converted S to P waves have greater than critical incident angles at the lowermost boundary in all models. Note that all models give similar results and that

effect of including low velocity sediments (models M1-A and M2-A) serves only to increase the coda in the radial P and vertical SV responses somewhat. Inclusion of more layer interfaces (model M3) also does little to increase complexity. Returning to the Olympia strong motion data, Figure 2, we see that these models are in qualitative agreement with the observations. The vertical component shows smaller S packet amplitudes (20% to 30%) relative to the horizontals, and is of longer duration with considerable ringing. The complexity of the observed horizontal components may be partially explained by appealing to a more complicated velocity function but this probably can't explain the relatively long codas of each.

Synthetics appropriate to the Tacoma and Seattle sites are shown in Figure 12. Wave effects are similar to those in Figure 11 except that incident angles are steeper for these close stations. There are also no critical angles for S to P conversions which dramatically reduces the ringing in both radial and vertical SV wave responses. This kind of behavior is qualitatively reflected in the Tacoma data of Figure 4. The S pulse seen in the EW component is relatively simple with little later reverberations. The S wave arrival on the vertical component is very small and comparable to the large radial/vertical SV wave amplitude ratio seen in Figure 12. The SN component, however, shows low amplitudes, which is probably an artifact of S polarization angle, but a long duration coda. This coda is undoubtably a result of scattering not unlike that seen in the teleseismic P wave data.

The velocities at Seattle (Figure 3) are much more complex than those at Tacoma and certainly more complex than those of the models in Figure 12.

Although some of this may be due to the seismic source function there is indirect evidence from displacement amplitudes, presented in a later section, that severe scattering may be occurring under the Seattle site.

Figure 13 presents a suite of synthetic seismograms for the teleseismic P data recorded at TUM. A two-second duration pulse similar to that of the 12-27-67 event (Figure 7) was convolved with earth responses calculated for each model. Although this calculation is only approximate, considering the evidence for lateral heterogeniety in the teleseismic data, it nevertheless should be adequate to determine whether the large velocity contrasts in the upper parts of the earth models are reasonable or not. Calculations of responses in moderately dipping structures indicate that tangential component waveshapes are most affected by the structure but that the radial usually only changes in detail (Langston, 1977). Since tangential motions are usually smaller than radial, horizontal motions composed of both should also be largely unaffected especially in the beginning portions of the records. Figure 13 shows that later arriving P to S conversions in the radial component do indeed attain amplitudes comparable to those seen in the data of Figure 7. In fact, model M2, which should be most appropriate for TUM, shows relative amplitude, waveshape, and timing behavior which is nearly identical to the first 15 records of the 12-27-67 data. This is a remarkable and heartening result since models M1 and M2 were constructed a priori from the refraction results of Zuercher (1975).

Strong motion velocity and displacement amplitudes were computed using the orientation and seismic moment determined by Langston and Blum (1977) (Table 1) and the time functions displayed in Figure 10. The maximum

amplitude of each velocity trace is compared to its expected value in Table 4. Amplitudes for displacements are taken from the height of the observed and calculated S wave pulse. Because the S wave responses in Figure 12 primarily show only the direct wave the displacements are nearly identical to the time function, S(t) (Figure 10). They are therefore not shown. The USCGS epicenter was assumed for the station-source geometry. Using the ISC epicenter changes these amplitudes by only 20%. Acceptable variations in the source mechanism can also affect individual amplitudes by as much as 50% but the vector sum of direct S amplitudes usually changes only $\pm$20%.

The expected large horizontal velocities at Tacoma and Seattle are most variant with the data. In the model, these are largely controlled by source orientation where the stations are near maxima in the SH wave radiation pattern. This is little affected by plausible and allowable variations in the dip of the auxilliary plane of the focal mechanism since each station is directly above the source and the inferred fault plane is nearly vertical. Although the velocity time function is oversimplified it is not likely that directivity effects could cause such a difference in amplitudes. The primary evidence for this comes from the previous study of teleseismic P waves (Langston and Blum, 1977). It was observed that although short-period pP was attenuated relative to direct P for some data, short-period pP and sP were readily apparent for stations further from the source. Body waves for these stations had near vertical incidence angles. Thus, the large changes in amplitude observed for pP could not be explained by directivity models since these changes were occurring over ray angle changes of only about $10^{o}$.

Other evidence for near receiver structure affecting these strong motion amplitudes comes from the comparison of displacements for Seattle

and Tacoma (part B, Table 4). Although Seattle model displacements are reasonable in terms of amplitude, the model fails to predict the polarity of the S58°W S pulse (see also Figure 5). This polarity is mainly a function of the large SH wave predicted by the radiation pattern and cannot be changed by any reasonable manipulation of the source mechanism. Instrument polarity is probably not to blame since velocities computed using the Carder and accelerometer data agree (Figures 3 and 5). Thus, this polarity reversal represents a major deficiency in the model and may be due to extreme lateral heterogeniety in the structure at Seattle. The predicted S wave at Tacoma is about three times larger than observed and its polarization angle allows too much displacement on the NS component. As in the case of predicted velocities and observed accelerations, Tacoma again exhibits lower than expected amplitudes.

Discussion

The preceding modeling experiments all point to the conclusion that several underlying assumptions on earth structure and, perhaps, source mechanism must be grossly inadequate. Taken individually, data at each station exhibit characteristics expected for near-vertical wave propagation in layered structures. However, the general observation that the closer stations have smaller amplitudes than the further station is contradictory to all intuition and modeling. If we take the factor of 5 discrepancy between observed and calculated velocities at Tacoma to be true and appeal to an attenuation mechanism to reduce the model velocities, a Q of about 28 is obtained for a one hertz S wave traveling along the entire path between

the hypocenter and station. This qualitatively agrees with the effective $Q_\alpha$ of 65 obtained from teleseismic pP attenuation for the Puget Sound event (Langston and Blum 1977). If the attenuation is confined within the upper layers of the crust and, in particular, the thick sediments under Tacoma or Seattle, then exceptionally low values are obtained (~1). These low Q values would not explain the same factor of 5 difference between 5 to 10 hertz accelerations at Olympia and Tacoma, however, unless Q was frequency dependent. In any case, since there is little to constrain the high frequency portion of the source spectrum, it can only be said that the amplitude discrepancies between stations and between models and data are consistent with higher attenuation under Seattle and Tacoma relative to Olympia.

In a recent comparative study of strong ground motion from the 1965 and 1949 Puget Sound events, Shakal and Toksoz (1980) suggest that attenuation is a major factor in wave propagation under the Seattle site compared to Olympia. They make this claim on the basis of low accelerations consistently observed at Seattle between both events. Although this type of model is supported here by the data and amplitude discrepancies between model and data, a further independent study is needed to definitively prove this. If there is an equal chance that the amplitude effect is due to source directivity or receiver structure attenuation, for each event, then there is a 1 in 4 chance that the observed effect is due to directivity rather than attenuation. A detailed study of teleseismic sources recorded at several broad-band stations in these areas of Puget Sound could answer this important question.

The results of this study fall considerably short of goals desired in most wave form studies. The anomalies observed between data and synthetics are partly due to the inadequacies of the source time history which was assumed. However, the large differences in amplitude and even polarity between observe and calculated displacements are particularly bothersome since they are caused by stable aspects of the model. Tacoma and Seattle are close to the source and amplitudes should be dominated by the maximum of the SH wave radiation pattern. On the basis of past seismic, gravity, and magnetic studies of crustal structure in Puget Sound and on the basis of the qualitative analysis of teleseismic P wave forms at TUM, it does seem clear that lateral heterogeniety is probably the major factor in these anomalies. Further work into wave propagation in Puget Sound should be performed to map out these heterogenieties in detail. One particularly simple method would be to use the P particle motion recorded from teleseismic sources on a dense broad-band three-component array. The analysis of off-azimuth arrivals could yield considerable information to the nature of velocity discontinuities , including layer dip and velocity contrasts, below the station. Thus type of information is indispensable to understanding ground motions from local earthquakes.

Irrespective of discrepant details, some order-of-magnitude estimates can be made concerning the gross characteristics of strong ground motion in Puget Sound. For example, even if the Olympia acceleration data are considered (Figure 2), it is evident that maximum accelerations were relatively low for a magnitude 6.5 earthquake. A maximum of only about 0.2g is observed compared to the greater than 1g accelerations observed at some stations for

the 1971 San Fernando earthquake or the 1979 Imperial Valley earthquake. The major difference between the 1965 event and these other events is depth. If it is reasonably assumed that the 1965 accelerations are dominated by body waves then they may be approximately corrected back to a point near the source using geometrical spreading. If the source was 10 km from Olympia rather than about 100 km, accelerations could have been as high as 2g using this simple technique. Figure 14 displays acceleration and velocities recorded at Olympia for the 1949 event. This event occurred at 70 km depth (Nuttli, 1952) and shows acceleration slightly larger than observed for the 1965 event. If the source was shallower at 10 km rather than 70 the geometric spreading correction again gives values greater than 2g. Although this is an approximate analysis, it does indicate that the level of strong ground motion in Puget Sound has, in the past, been controlled by large source depths rather than low intensity source radiation.

Second order wave propagation considerations, such as attenuation or lateral heterogeniety, may therefore be moot to the true seismic hazard of Puget Sound. The past strong ground motion record of Puget Sound is probably biased on the low side because of previous large source depths. Shallow earthquakes with possible surface or near-surface faulting may well overshadow the destructive effects of past historical events in the Puget Depression. Although the late Quaternary sedimentary cover in the area has hampered seismotectonic studies of near surface faulting, there is evidence that recent shallow faulting near the eastern Olypmic mountains has occurred (Wilson, et al 1979) and may well be currently active.

## Conclusions

The general behavior of observed strong motion velocities and displacements from the 1965 Puget Sound earthquake can be explained by near-vertical body wave propagation in plausible plane-layered crustal models. Some aspects of the data are poorly modeled, however. The lower velocity and displacement amplitudes observed at Tacoma and Seattle, relative to Olympia, are contrary to the synthetic calculations and physical intuition. The amplitude behavior is suggestive of high attenuation under Tacoma and Seattle.

Short-period teleseismic body wave data recorded nearby at Tumwater, Washington show large P to S conversions consistent with assumed crustal structures. They also show large off-azimuth P to S arrivals which indicate substantial deviation from plane-layered models. In conjunction with past geologic and geophysical studies, these data then suggest that scattering may play an important role in local wave propagation.

The largest single factor which has controlled past strong ground motion levels in Puget Sound is source depth. Large shallow earthquakes may be expected to be associated with significantly larger accelerations than previously experienced in Puget Sound in accordance with shallow events elsewhere.

Acknowledgments

I would like to thank Norman Rasmussen of the University of Washington for his kind assistance in procuring the data for Tumwater station and Walter Arnold for his help in processing the digital strong motion data. This research was supported by the U.S. Department of the Interior, Geologic Survey, under contract No. 14-08-0001-18235.

## REFERENCES


Algermissen, S. T. (1969). Seismic risk studies in the United States, Proc. 4th World Conf. Earthquake Eng., p. 1-20.

Algermissen, S. T., S. T. Harding, K. V. Steinbrugge, and W. K. Cloud (1965). The Puget Sound, Washington earthquake of April 29, 1965, U.S. Department of Commerce, Coast and Geodetic Survey, Rockville, Maryland.

Crosson, R. S. (1972). Small earthquakes, structure, and tectonics of the Puget Sound region, Bull. Seismol. Soc. Am. 62, 1133-1171.

Crosson, R. S. (1976). Crustal structure modeling of earthquake data 2. Velocity Structure of the Puget Sound region Washington, Jour. Geophys. Res., 81, 3047-3054.

Danes, Z. F., M. M. Bonno, E. Brau, W. D. Gilham, T. F. Hoffman, D. Johansen, M. H. Jones, B. Malfair, J. Masten, and G. O. Teague (1965). Geophysical investigation of the Southern Puget Sound area, Washington, Jour. Geophys. Res. 70, p. 5573-5580.

Hall, J. B. and K. L. Othberg (1974). Thickness of unconsolidated sediments, Puget lowland, Washington, Geologic Map GM-12, State of Washington Department of Natural Resources, Olympic, Wash.

Haskell, N. A. (1960). Crustal reflection of plane SH waves, Jour. Geophys. Res., 65, p. 4147-4150.

Heaton, T. H. and D. V. Helmberger (1977). A study of the strong ground motion of the Borrego Mountain, California, earthquake, Bull. Seismol. Soc. Am., 67, p. 315-330.

Heaton, T. H. and D. V. Helmberger (1978). Predictability of strong ground motion in the Imperial Valley: Modeling the M 4.9, November 4, 1976 Brawley earthquake, Bull. Seismol. Soc. Am., 68, p. 31-48.

Heaton, T. H. and D. V. Helmberger (1979). Generalized ray models of the san Fernando earthquake, Bull. Seismol. Soc. Am., 69, p. 1131-1341.

Helmberger, D. V. (1974). Generalized ray theory for shear dislocation, Bull. Seismol. Soc. Am., 64, p. 45-64.

Howell. B. F., Jr. (1974). Seismic regionalization in North America based on average regional seismic hazard indix, Bull. Seismol. Soc. Am., 64, p. 1509-1528.

Langston, C. A. (1977). The effect of planar dipping structure on source and receiver responses for constant ray parameter, Bull. Seismol. Soc. Am., 67, 1029-1050.

Langston, C. A. and D. E. Blum (1977). The April 29, 1965, Puget Sound earthquake and the crustal and upper mantle structure of Western Washington, Bull. Seismol. Soc. Am., 67, 693-711.

Langston, C. A. and D. V. Helmberger (1975). A procedure for modelling shallow dislocation sources, Geophys. J. R. astr. Soc., 42, p. 117-130.

Milne, W. G. (1967). Earthquake epicenters and strain release in Canada, Canadian Jour. Earth Sci., 4, p. 797-814.

Mullineaux, D. R., M. G. Bonilla, and J. Schlocker, (1967). Relation of building damage to geology in Seattle, Washington, during the April 1965 earthquake, U.S. Geol. Survey Prof. Paper 575-D, p. D183-D191.

Nuttli, O. W. (1952). The western Washington earthquake of April 13, 1949, Bull. Seismol. Soc. Am., 42, 21-28.

Shakal, A. F. and M. N. Toksoz (1980). Amplification and attenuation of site structure: Puget Sound strong motion, [abstract] Earthquake Notes, 50 p. 20.

Tatel, H. E. and M. A. Tuve (1955). Seismic exploration of a continental crust, Geol. Soc. Am. Spec. Paper 62, 35-50.

Trifunac, M. D., F. E. Udwadia, and A. G. Brady (1973). Analysis of errors in digitized strong-motion accelerograms. Bull. Seismol. Soc. Am., 63, 157-187.

Trifunac, M. D. and V. W. Lee (1974). A note on the accuracy of computed ground displacements from strong-motion accelerograms, Bull. Seismol. Soc. Am., 64, 1209-1219.

Wilson, J. R., M. J. Bartholomew, R. J. Carson (1979). Late Quaternary faults and their relationship to tectonism in the Olympic Peninsula, Washington, Geology, 7, p. 235-239.

Zuercher, H. (1975). A study of the crust in Puget Sound using a fixed seismic source, M.S. thesis, University of Washington, Seattle, Wash.

Table 1

Strong Motion Stations and Source Parameters

| Site | Location | Δ, km | | Azimuth, Degrees | | Back Azimuth, Degrees | |
|---|---|---|---|---|---|---|---|
| | | USCGS | ISC | USCGS | ISC | USCGS | ISC |
| Olympia Highway Test Lab | 47.03°, 122.90°W | 69 | 79 | 234 | 238 | 54 | 58 |
| Seattle Federal Office Building | 47.60°N, 122.33°W | 23 | 21 | 13 | 352 | 193 | 172 |
| Tacoma County-City Building | 47.25°N, 122.45°W | 18 | 25 | 198 | 225 | 18 | 45 |

April 29, 1965 epicenters

USCGS: 47.4°N 122.4°W

ISC: 47.41°N 122.29°W

Source Orientation : dip = 70°, rake = -75°, strike = 344°

Seismic Moment : $1.4 \times 10^{26}$ dyne-cm

Table 2

Strong Motion Instrumentation

| Site | Component | Instrument | Free Period (sec) | Damping Ratio | Static Magnification |
|---|---|---|---|---|---|
| Olympia Highway Test Lab | vertical | SMA | --- | --- | --- |
| | S 86°W | SMA | --- | --- | --- |
| | S 04°E | SMA | --- | --- | --- |
| Seattle Federal Office Building | vertical | SMA | 0.084 | 10 | 112 |
| | S 32°E | SMA | 0.083 | 10 | 119 |
| | S 58°W | SMA | 0.084 | 11 | 127 |
| | S 58°W | CDM | 2.45 | 10 | 0.8 |
| | N 32°W | CDM | 2.51 | 9 | 0.8 |
| Tacoma County-City Building | vertical | SMA | 0.078 | 10 | 114 |
| | E | SMA | 0.078 | 8 | 118 |
| | S | SMA | 0.076 | 10 | 120 |
| | E | CDM | 3.90 | 13 | 1.0 |
| | N | CDM | 4.01 | 10 | 1.0 |

SMA - Strong motion accelerometer

CDM - Carder displacement meter

Table 3

TUM station characteristics and teleseismic P data

location: 47.015N 122.9083W

instrumentation:

SPZ Wilson-Lamison Seismometer
$T_o$ = 1.0sec, $T_g$ = 0.95sec,
MAG = 50K at 1sec

SPNS EW Sprengnether, $T_o$ = 1.4sec,
$T_g$ = 1.4sec, MAG = 1800 at 1sec,

Teleseismic Event P Data:

| DATE | TIME | LAT (o) | LONG (o) | M | h | LOCATION |
|---|---|---|---|---|---|---|
| 12/27/67 | 9:17:50 | 21.29S | 68.20W | 6.3 | 91 | Chile |
| 7/25/68 | 7:23:02 | 30.97S | 178.13W | 6.5 | 17 | Kermadec |
| 10/15/67 | 8:00:53 | 11.92N | 85.98W | 6.2 | 181 | Nicaragua |

Table 4

Expected Strong Motion Amplitudes

A. Velocities

| | Component | Amplitude Observed (cm/sec) | Amplitude Calculated (cm/sec) |
|---|---|---|---|
| Olympia | Vertical | 3.0 | 5.3 |
| | S86° W | 12.7 | 16.8 |
| | S04° E | 8.0 | 0.2 |
| Tacoma | Vertical | 4.8 | 4.0 |
| | East | 9.8 | 50.4 |
| | South | 4.1 | 18.5 |
| Seattle | Vertical | 3.5 | 1.1 |
| | S32° E | 8.2 | 24.5 |
| | S58° W | 12.5 | 14.7 |

B. Displacements

| | Components | Amplitude Observed (cm) | Amplitude Calculated (cm) |
|---|---|---|---|
| Tacoma | East | -5.2 | -16.0 |
| | North | (~0.5) | -5.9 |
| Seattle | S58° W | -7.5 | 4.7 |
| | N32° W | +4.5 | 7.8 |

## Figure Captions

Figure 1: Index map of the Puget Sound Area showing the locations of three strong motion sites, Tumwater station (TUM), and epicenters for the 1965 and 1949 earthquakes. Contours show unconsolidated sediment thickness in feet (after Hall and Othberg, 1974).

Figure 2: Corrected acceleration and velocity recorded at the Olympia Highway Test Laboratory for the 1965 earthquake.

Figure 3: Corrected acceleration and velocity recorded at the Seattle Federal Office Building for the 1965 event.

Figure 4: Corrected acceleration and velocity recorded at the Tacoma County-City Building for the 1965 event.

Figure 5: Corrected velocity and displacement from the Carder displacement meter data at Seattle for the 1965 event.

Figure 6: Corrected velocity and displacement from the Carder displacement meter data at Tacoma for the 1965 event.

Figure 7: Teleseismic P waveforms from three earthquakes recorded at Tumwater station. 'BAZ' is the theoretical back azimuth of the ray approach to the station. The arrows indicate several major P to S converted phases.

Figure 8: Crustal models assumed in the wave calculation.

Figure 9: Comparison of responses calculated using generalized ray theory (Cagniard) and the propagator matrix approximation (Haskell) for a 70 km receiver distance and 60 km source depth in model M1.

Figure 10: Smoothed far-field source time function, S(t), obtained by Langston and Blum (1977) for the 1965 event. V(t) is its time derivative.

Figure 11: A suite of synthetic seismogram calculations appropriate for Olympia velocities assuming each crustal model. $P_V$ and $P_R$ are the vertical and radial responses, respectively, due to an incident P wave. $SV_V$ and $SV_R$ are the vertical and radial responses, respectively, due to an incident SV wave.

Figure 12: Synthetic velocities appropriate for Tacoma and Seattle. Same scheme as Figure 11.

Figure 13: Synthetic seismograms assuming several crustal models for Tumwater teleseismic data. A simple pulse-like wave form, similar to the vertical component of the 12/27/67 event of Figure 7 was convolved with each impulse response.

Figure 14: Corrected acceleration and velocity recorded at the Olympia site for the 1949 earthquake.

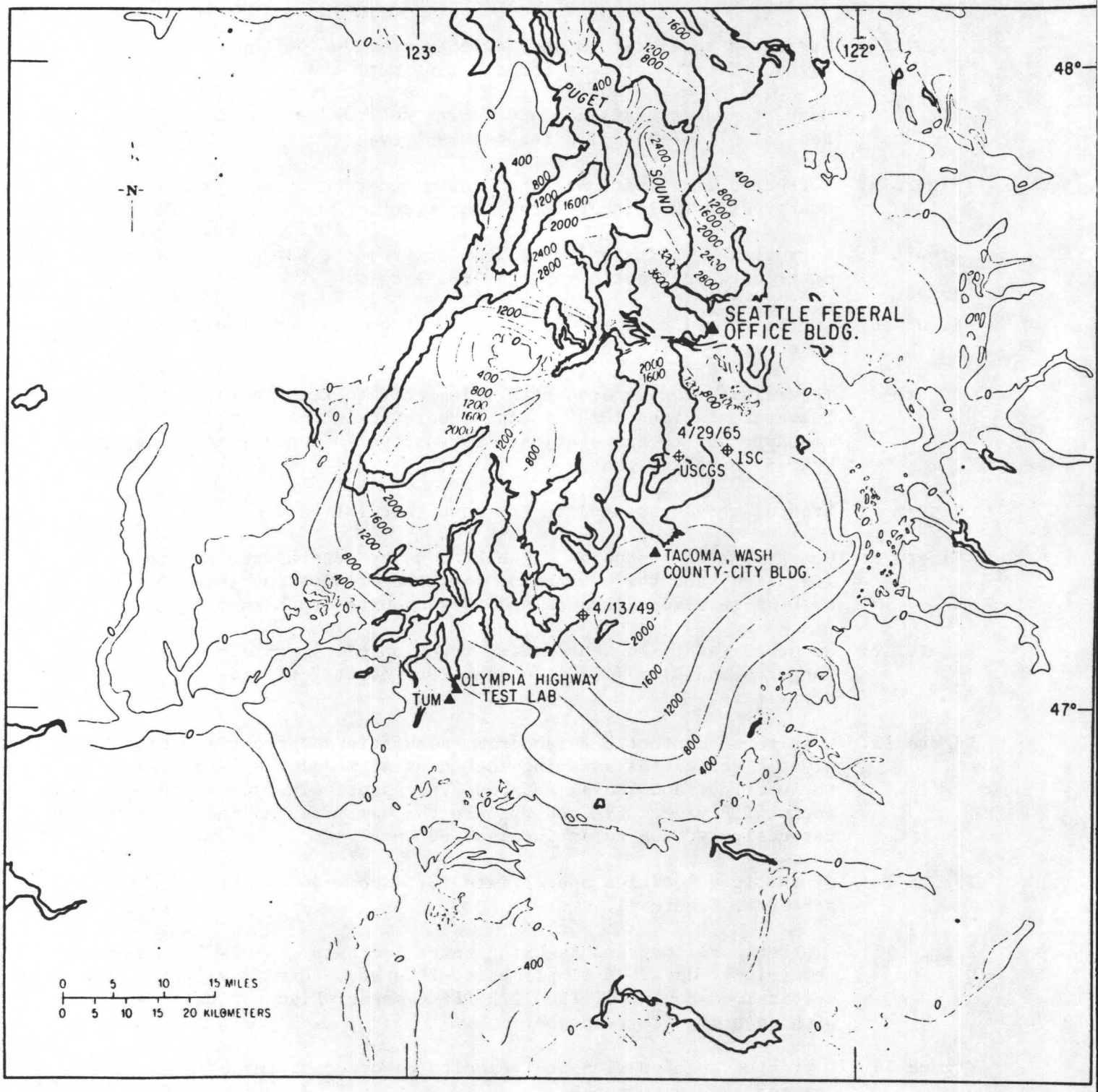
123°
122°
48°
47°
PUGET SOUND
N
SEATTLE FEDERAL OFFICE BLDG.
4/29/65
ISC
USCGS
TACOMA, WASH COUNTY-CITY BLDG.
4/13/49
OLYMPIA HIGHWAY TEST LAB
TUM
0 5 10 15 MILES
0 5 10 15 20 KILOMETERS

Fig. 1

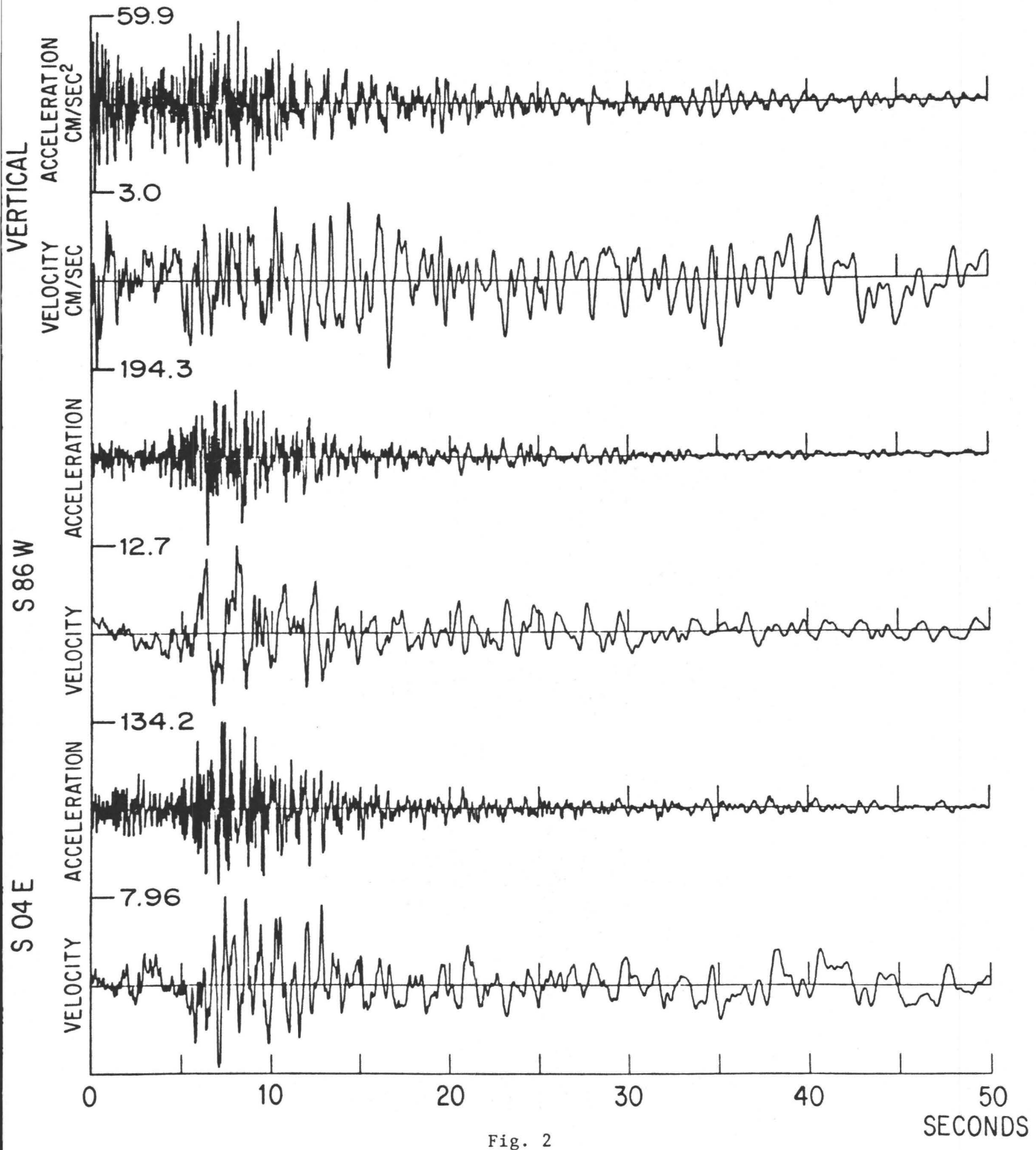
VERTICAL
59.9
ACCELERATION CM/SEC²
3.0
VELOCITY CM/SEC
194.3
S 86 W
ACCELERATION
12.7
VELOCITY
134.2
S 04 E
ACCELERATION
7.96
VELOCITY
0
10
20
30
40
50
SECONDS

Fig. 2

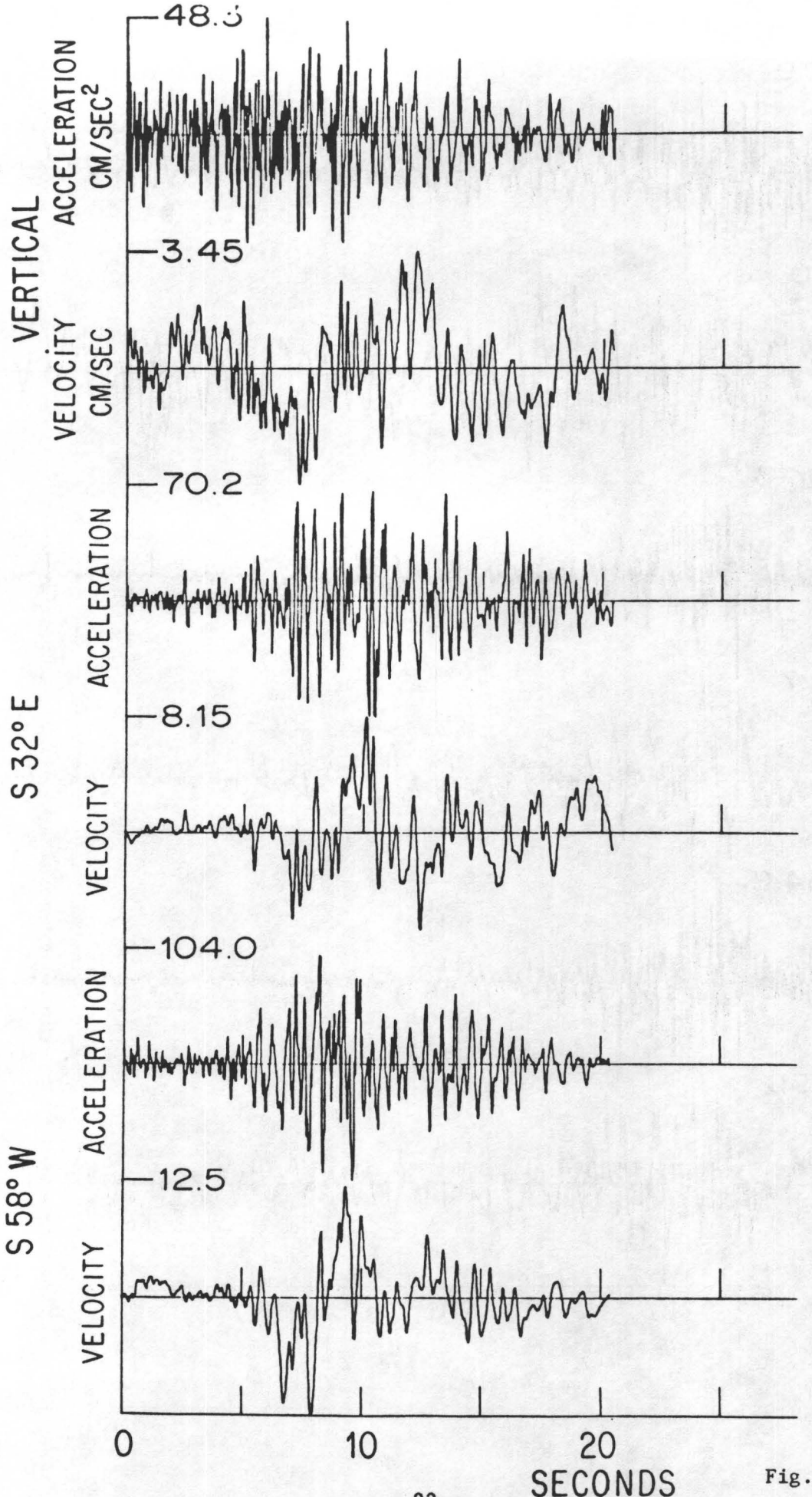
VERTICAL
ACCELERATION CM/SEC²
48.3
VELOCITY CM/SEC
3.45
S 32° E
ACCELERATION
70.2
VELOCITY
8.15
S 58° W
ACCELERATION
104.0
VELOCITY
12.5
0
10
20
SECONDS

Fig. 3

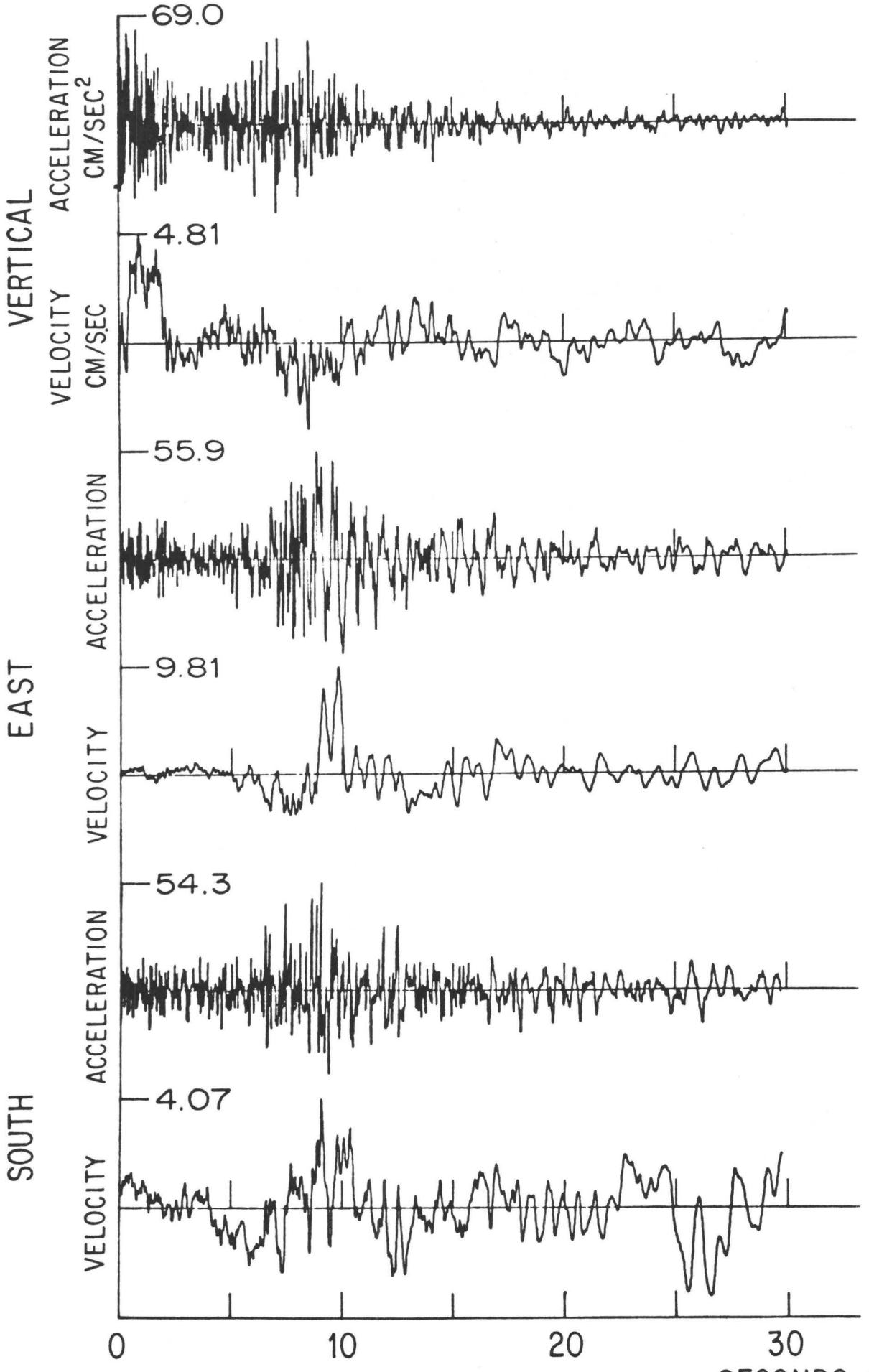
VERTICAL
ACCELERATION CM/SEC²
69.0
VELOCITY CM/SEC
4.81
EAST
ACCELERATION
55.9
VELOCITY
9.81
SOUTH
ACCELERATION
54.3
VELOCITY
4.07
0
10
20
30
SECONDS

Fig. 4

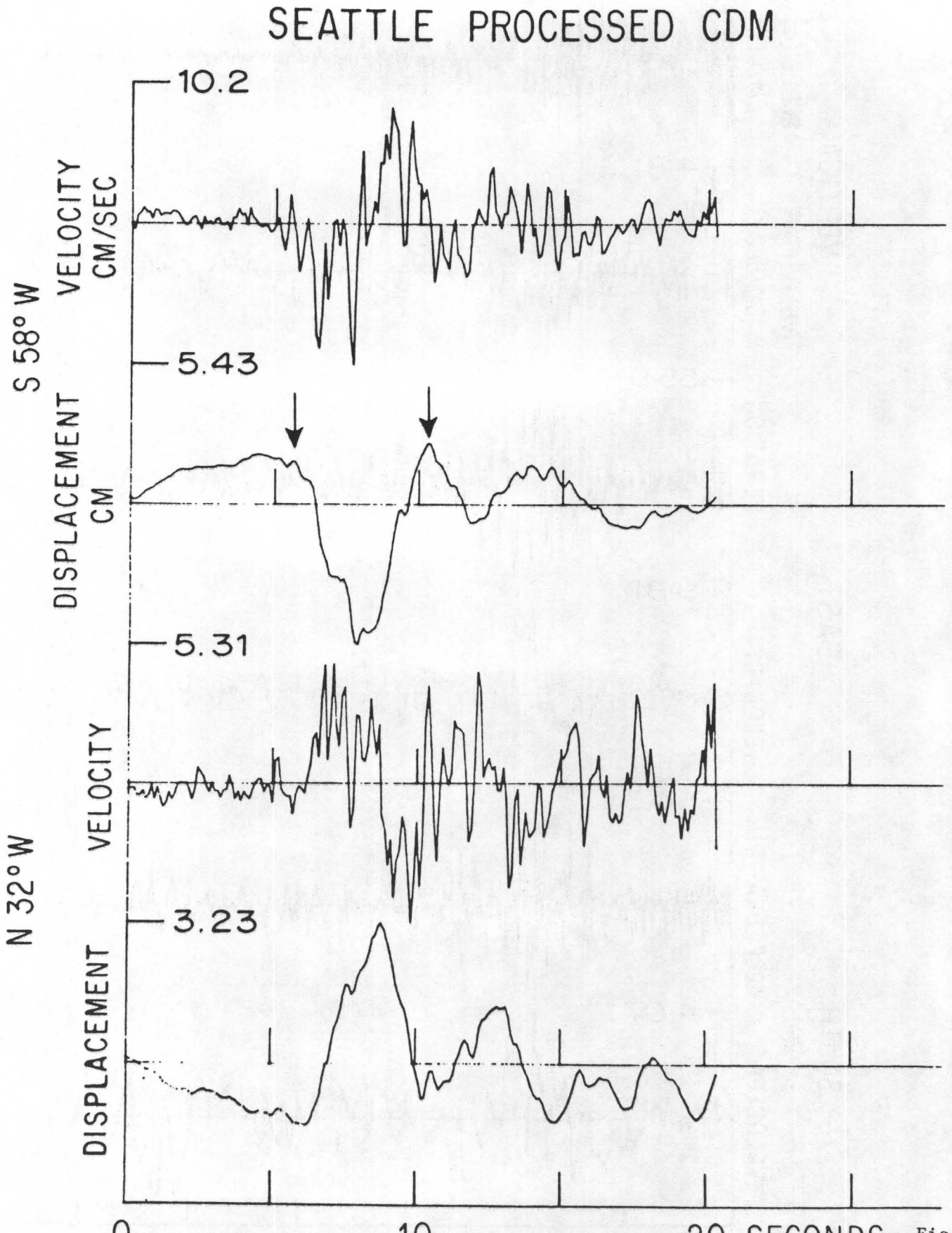
SEATTLE PROCESSED CDM
10.2
S 58° W
VELOCITY
CM/SEC
5.43
DISPLACEMENT
CM
5.31
N 32° W
VELOCITY
3.23
DISPLACEMENT
0
10
20 SECONDS

Fig. 5

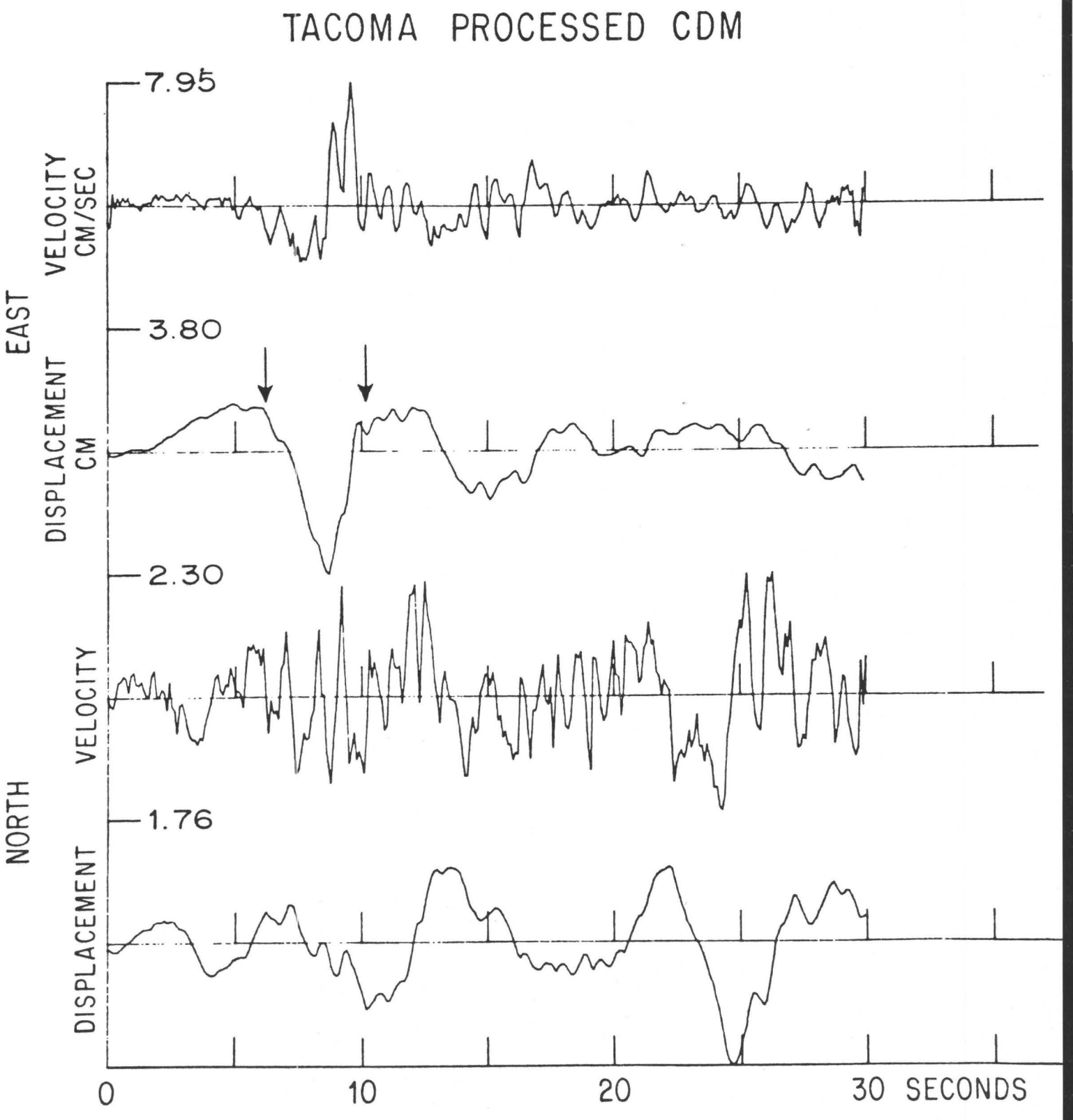
TACOMA PROCESSED CDM
7.95
VELOCITY CM/SEC
EAST
3.80
DISPLACEMENT CM
2.30
VELOCITY
NORTH
1.76
DISPLACEMENT
0
10
20
30 SECONDS

Fig. 6

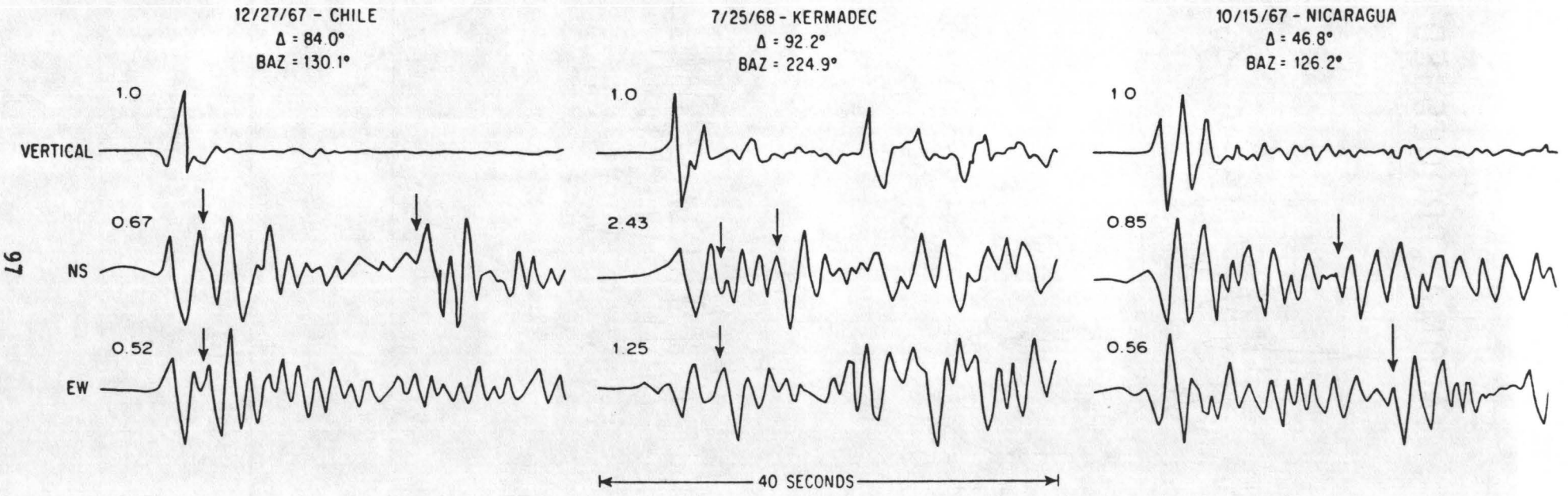
12/27/67 - CHILE
Δ = 84.0°
BAZ = 130.1°
7/25/68 - KERMADEC
Δ = 92.2°
BAZ = 224.9°
10/15/67 - NICARAGUA
Δ = 46.8°
BAZ = 126.2°
1.0
VERTICAL
0.67
NS
0.52
EW
1.0
2.43
1.25
1.0
0.85
0.56
40 SECONDS

Fig. 7

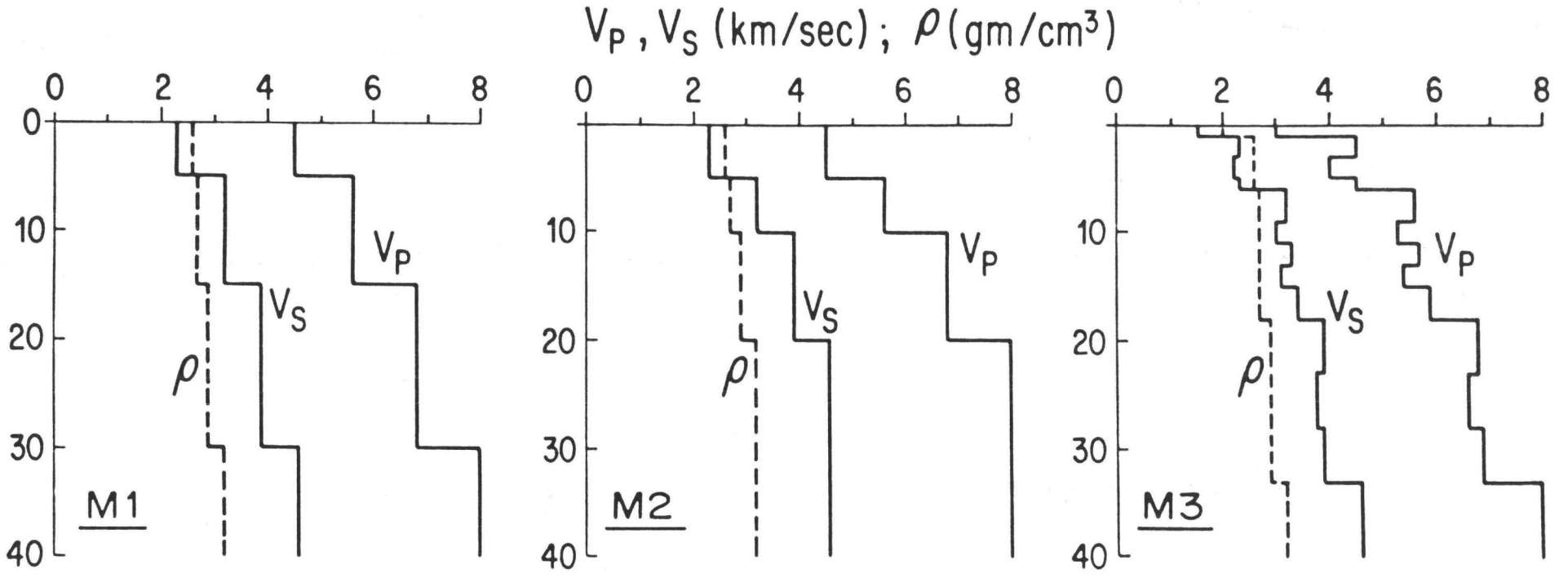


Fig. 8

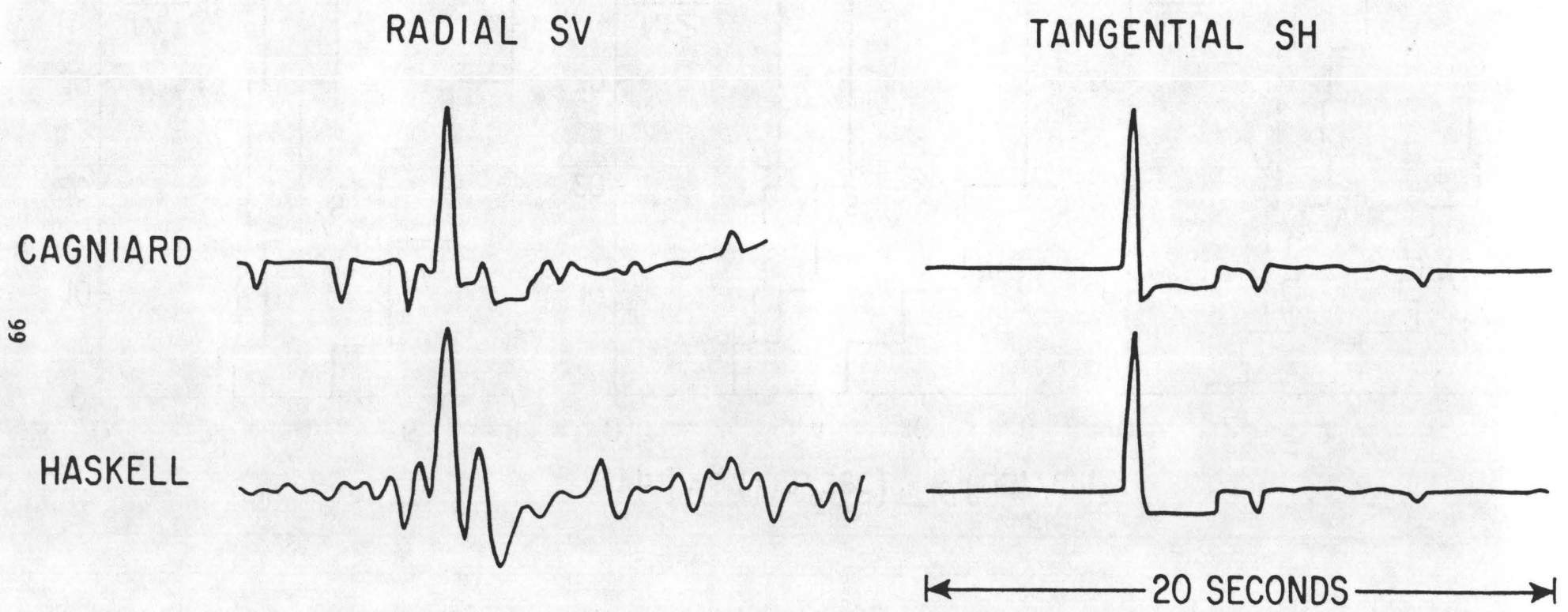




Fig. 9

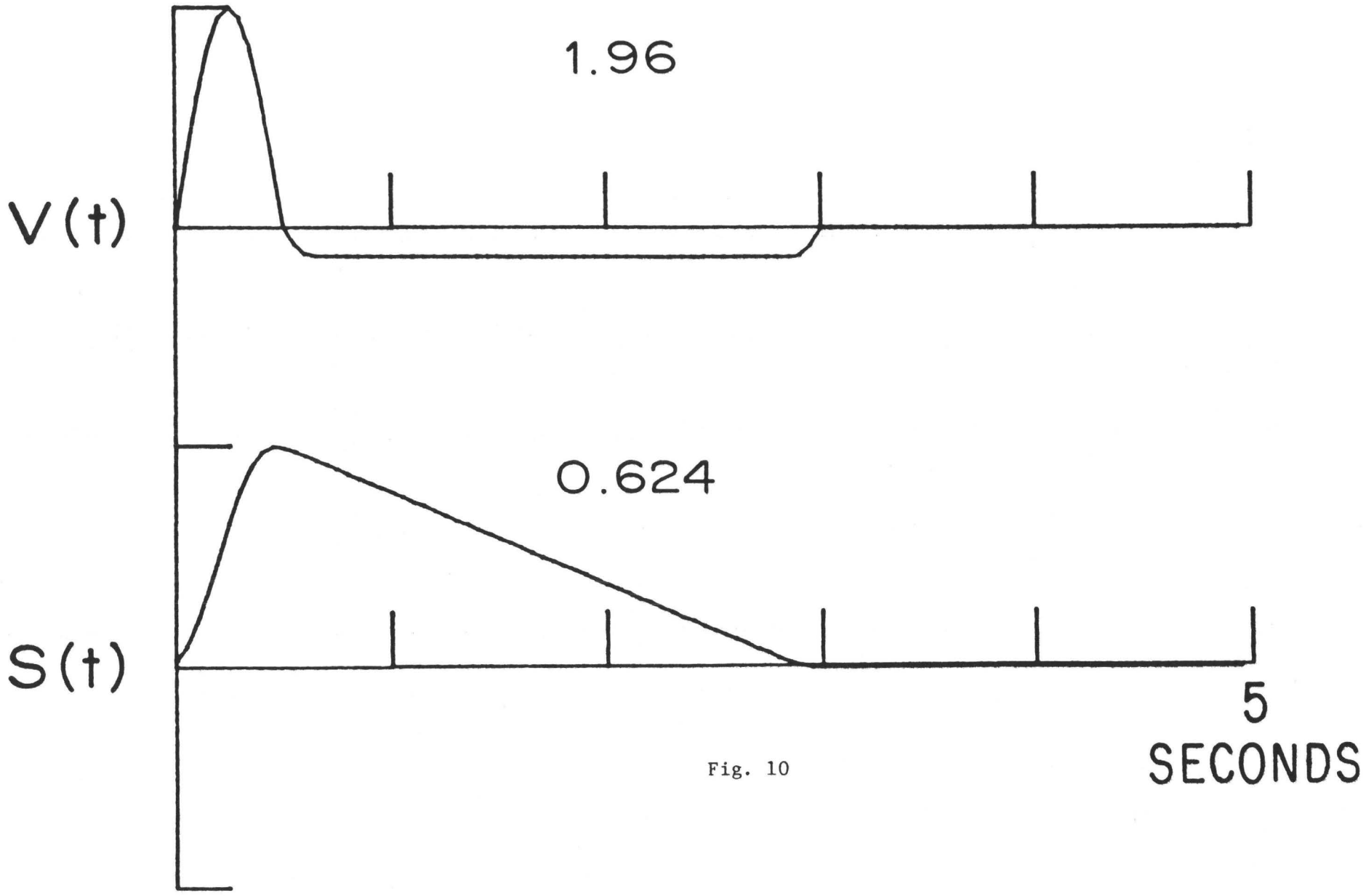


Fig. 10

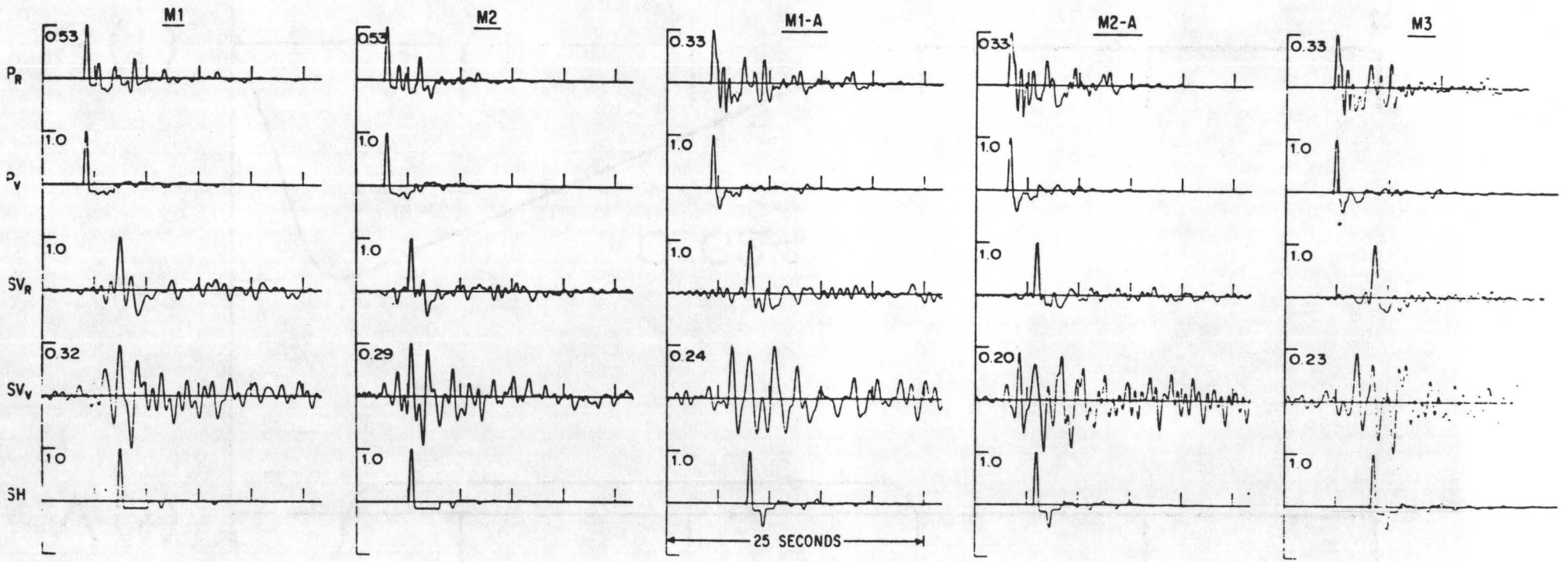
M1
M2
M1-A
M2-A
M3
P_R
P_V
SV_R
SV_V
SH
0.53
0.53
0.33
0.33
0.33
1.0
1.0
1.0
1.0
1.0
1.0
1.0
1.0
1.0
1.0
0.32
0.29
0.24
0.20
0.23
25 SECONDS

Fig. 11

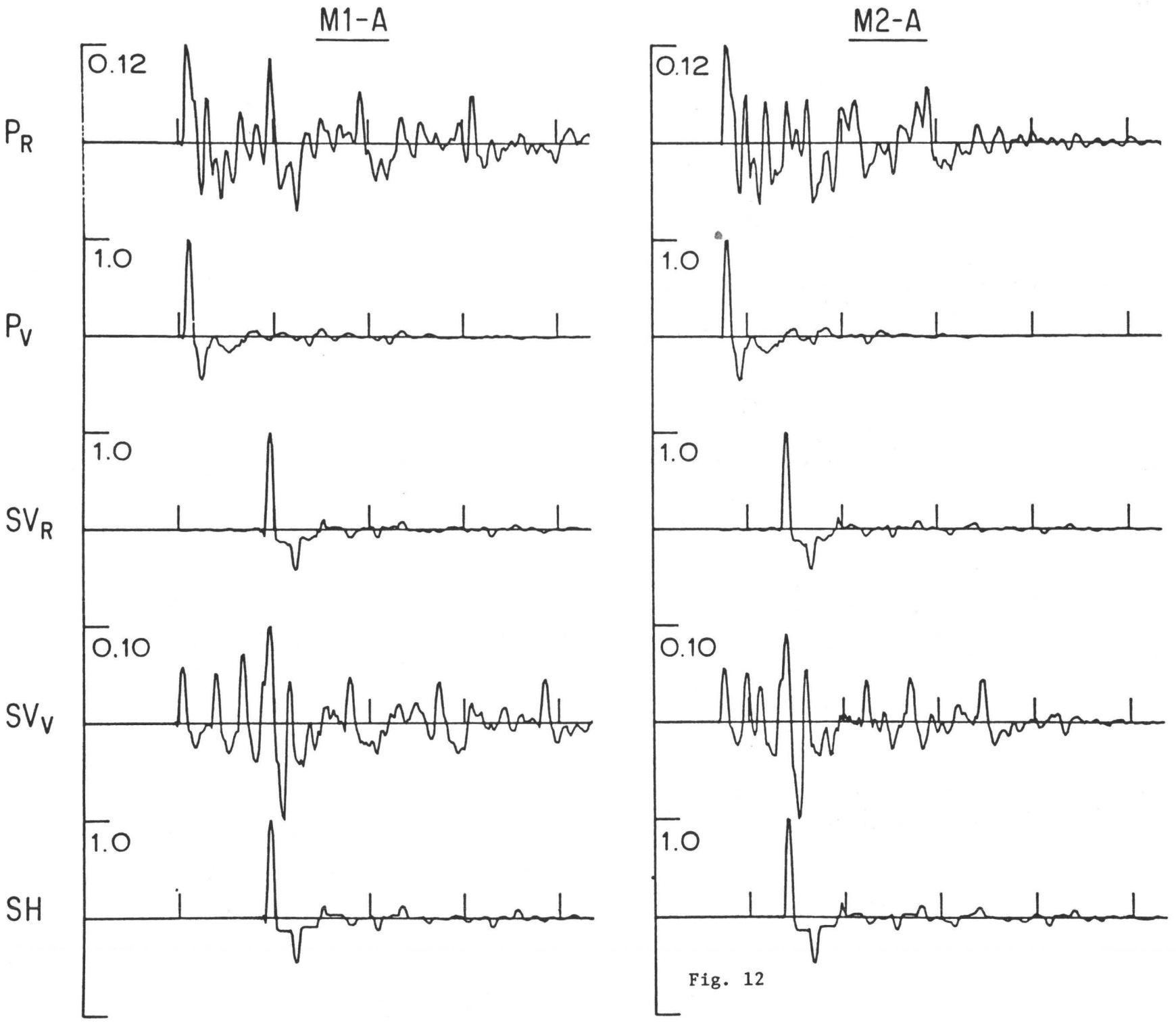


Fig. 12

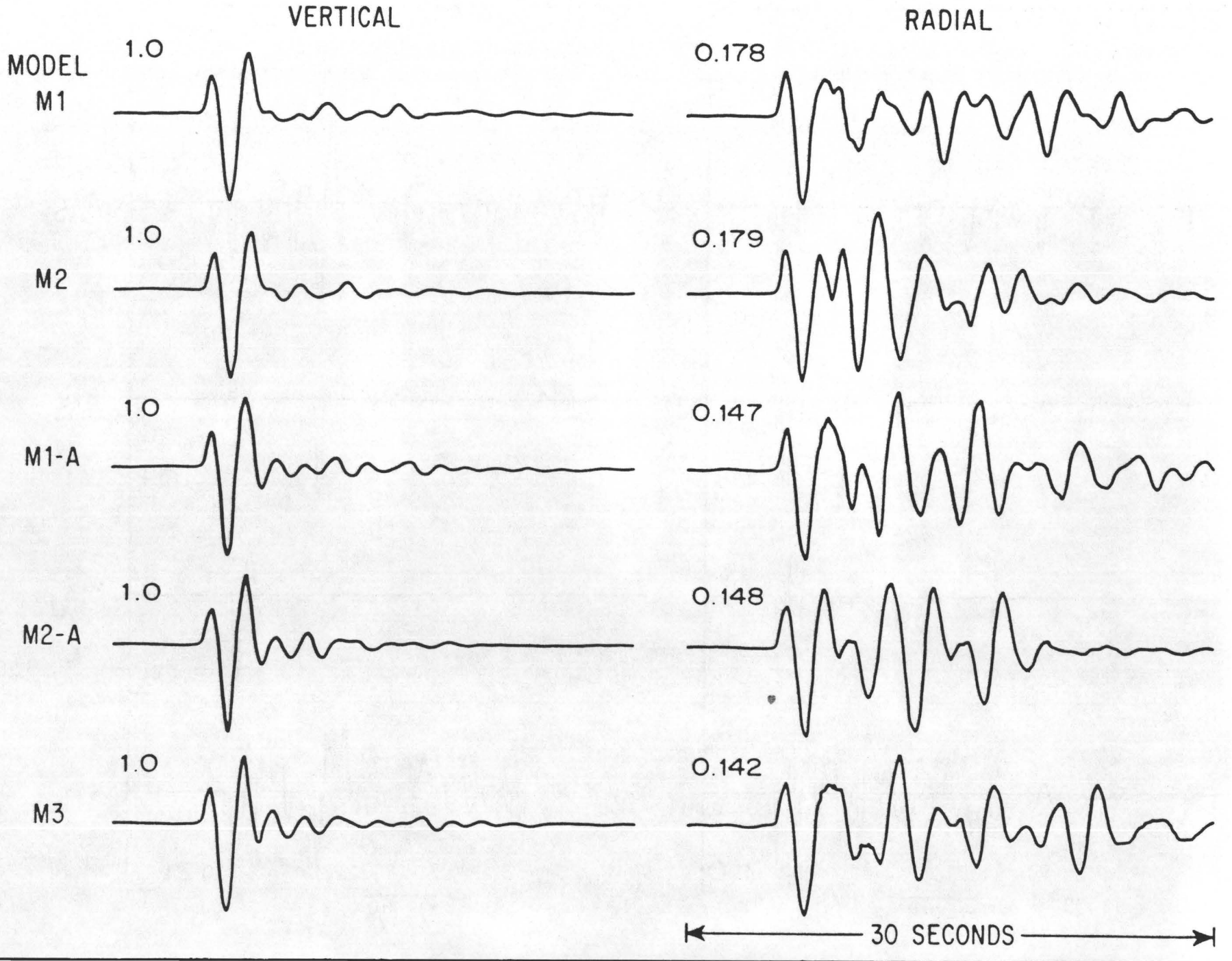
VERTICAL
RADIAL
MODEL
M1
1.0
0.178
M2
1.0
0.179
M1-A
1.0
0.147
M2-A
1.0
0.148
M3
1.0
0.142
30 SECONDS

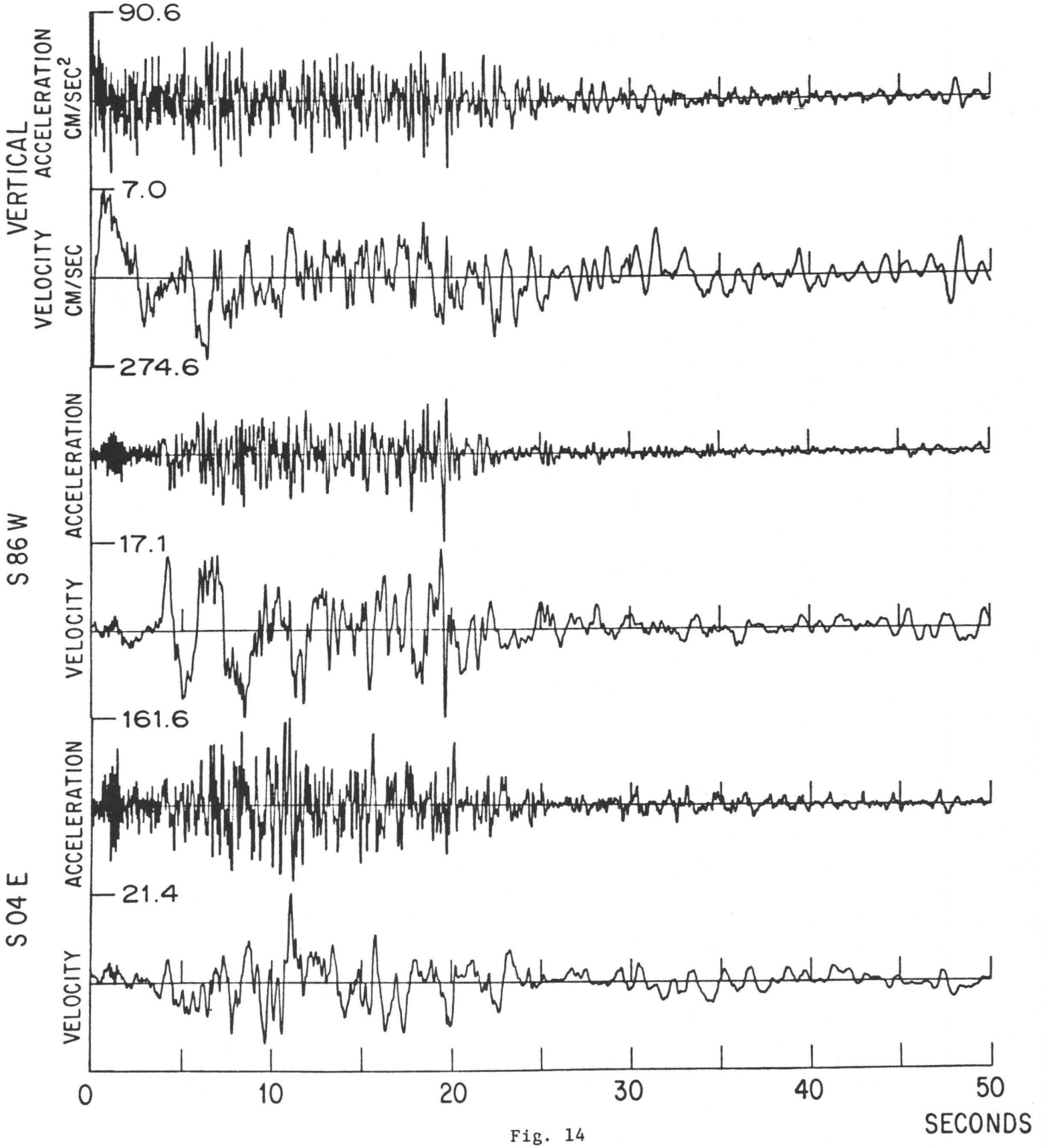
VERTICAL
ACCELERATION CM/SEC²
90.6
VELOCITY CM/SEC
7.0
274.6
S 86 W
ACCELERATION
17.1
VELOCITY
161.6
S 04 E
ACCELERATION
21.4
VELOCITY
0
10
20
30
40
50
SECONDS

Fig. 14

# A COMPARISON OF THE RATE OF SEISMIC ACTIVITY AND SEVERAL ESTIMATES OF DEFORMATION IN THE PUGET SOUND AREA

D.H. Weichert and R.D. Hyndman
Pacific Geoscience Centre
P.O. Box 6000
Sidney, B.C., Canada V8L 4B2

## Introduction

The Puget Sound - southern Georgia Strait area has the highest seismicity of the Oregon, Washington, southern British Columbia region. The continental margin in this area marks the zone of convergence between the Juan de Fuca and America plates and the seismicity has generally been associated with this convergence or subduction. In this article we compare the rate and pattern of seismic activity with several estimates of deformation associated with this interaction.

## Rates of Faulting from Seismicity

Brune (1968) has given an expression for the relation between the average fault slip during an earthquake and its seismic moment $M_o$. Subsequently, a number of authors have used this formulation to estimate the average slip rates on fault systems from the seismic record. For example, Davis and Brune (1968) in a global summary, and Reichle et al. (1976) for the Gulf of California, have summed the moments of all of the earthquakes that have been recorded on a fault zone for a particular time period. It turns out that the dominant contribution to the sum comes from the largest earthquakes which, because they are rare and occur at random time intervals, have a large statistical uncertainty of occurrence. For comparison with rates from longer term geological data or from plate tectonic models, the estimate of slip rate from a direct summation over individual events thus appears very uncertain.

It is tempting to seek a more stable estimate by introducing additional assumptions if these can be justified. For instance, the Richter $\log N = a - bM$ recurrence relation could be used to provide a more stable estimate of regional seismicity up to some maximum magnitude, $M_x$, and the total moment obtained by integration. This relation usually represents the observed data quite well and has been theoretically and experimentally justified. The now explicitly introduced uncertainty of $M_x$ was already implictly present in the discrete summation approach.

The integral approach to the total or time average seismic moment has been used by Smith (1976) to estimate the maximum magnitude of events that must be expected from geologically observed slip rates and from the recurrence relation derived from the observed seismicity. Molnar (1979) and Anderson (1979) start with slip rates from geological data or plate tectonic models and assumed or independently

estimated maximum magnitudes, and calculate recurrence intervals. In a recent paper (Weichert and Hyndman, 1980), we used the observed seismicity and estimated values of $M_x$ in the spreading ridge-transform fault system west of Vancouver Island and along the Queen Charlotte fault in order to obtain slip rates which could then be compared to plate tectonic model slip rates. Agreement was found to well within the uncertainties of the method which appear to be about a factor of two.

In this paper we attempt a comparison of the magnitude and direction of deformation in the Puget Sound - southern Georgia Strait area from the seismicity, from repeated geodetic surveys and from plate tectonic models for the Juan de Fuca - America convergence.

Earthquake Data

For comparison purposes we adopt the seismic zones, seismicity data and recurrence relations similar to those by Milne et al. (1978) and modified by Milne et al. (1981) for use in seismic risk evaluation. The recurrence relations have been computed using the method of Weichert (1980). Two seismic zones are considered, Puget Sound and Cascades (Fig. 1), with recurrence relations and maximum magnitudes $M_x$ given by:

Cascades

$$\log N = 2.74 - 0.75M;\ M_x = 7\text{-}1/4 \text{ (preferred)}$$

$$\text{or } \log N = 2.94 - 0.81M;\ M_x = 7\text{-}3/4$$

Puget Sound

$$\log N = 2.38 - 0.63M;\ M_x = 7\text{-}1/4 \text{ (preferred)}$$

$$\log N = 2.42 - 0.65M;\ M_x = 7\text{-}3/4$$

The areas are $2.84 \times 10^4$ km$^2$ and $13.9 \times 10^4$ km$^2$ and the lengths parallel to the margin are 200 and 400 km for the Puget Sound and Cascades zones respectively. The total seismicity in the two zones is similar but the maximum depth is less and the area normalized activity is considerably lower in the Cascade zone. Here we shall be mainly concerned with the Puget Sound seismicity.

Seismic Moment Rate

The integration per se over the recurrence relation up to the maximum magnitude is straight forward and Molnar (1979) and Anderson (1979) have given details. However, several points bear further attention. Firstly, different workers have integrated variously over moment, logarithmic moment or over magnitude. For unique deterministic relations between these quantities, there is no difference. However, the moment-magnitude relation is at best stochastic, and it is probably also regionally variable. While the scatter of data points for

any individual relation is only perhaps a factor of two or three, the difference among the relations given in the literature is more, perhaps as much as a factor of five. This is probably caused by true regional variability. With the usual choice of handling the upper limit of the integration as a simple truncation, different results are obtained by integrations over different variables. We take magnitude as the basic measured parameter and thus integrate over magnitude.

We have reviewed the available empirical moment-magnitude relations that have been given in the literature and find that the log-linear relation $\log M_o = c + dM$, with $c = 9.0$ and $d = 1.5$ in S.I. units is a good average. Most of the relations are from California data.

The second point concerns the asymmetry of the moment-magnitude relation. This tends to be overlooked because usually the log-moment is plotted and the log moment appears to scatter symmetrically about the best linear relation. But the average log-moment leads to an average moment, and hence to an average displacement, that is greater than just the anti-log, approximately by the factor $\exp(-s^2/2)$, where s is the variance of the distribution. This factor is exact if the log moment is normally distributed. For a rms of log 3 in the log moment-magnitude relation, the inclusion of the effect of stochasticity increases the calculated displacement by 80%. In seismic risk calculations a similar asymmetry exists and its effect is often included, as for instance in the program by McGuire (1976).

The last mathematical point concerns the difference between truncation at the maximum magnitude of either the cumulative event recurrence or the event density, or incremental recurrence curve. For instance, Molar (1979) truncates the cumulative, while Anderson (1979) truncates the density function. The first approach leads to a physically unacceptable density function with a delta function spike at the maximum magnitude, as shown in Fig. 2. We use the truncation of the density function but realize fully that even smoother cut-offs could be justified. If one integrates the two distributions shown in Fig. 2, and if we accept the average moment-magnitude relation as given above, we find that the moment contribution from the spike amounts to a factor of d/b. (see Fig. 3). For the values of $d = 1.5$ and $b = 0.75$ as in our area, the factor is about 2.

The uncertainty in the correct moment-magnitude relation for our region gives a moment uncertainty of about a factor of two. Admission of stochasticity would increase a simple total moment estimate by roughly a factor of two, finally use of incremental rather than cumulative truncation will decrease the estimate by a factor of two and vice versa.

Figures 4 and 5 show the cumulative recurrence distributions and resulting moment ratios for the Cascades and Puget Sound zones. These curves correspond to linear incremental or density relations with truncation at the maximum magnitude Mx. For the Puget Sound Mx values of 7-1/4 (moment rate per year $0.33 \times 10^{18}$ Nm) and of 7-3/4 ($0.80 \times 10^{18}$ Nm) are shown. We think that Mx lies between these limits, probably closer to 7-1/4 and take a moment rate of $0.5 \times 10^{18}$ Nm. For the Cascades zone an Mx of 7-1/4 gives a moment rate of $0.10 \times 10^{18}$ Nm and an Mx of 7-3/4 a moment rate of $0.35 \times 10^{18}$ Nm. We think that Mx is close to 7-1/4 and take a moment rate of $0.1 \times 10^{18}$ Nm. To obtain rates of motion we divide by the rigidity and, in the case of strike-slip boundaries, by the slip area. In a converging regime we need another factor of about 1/2, depending on the statistics of angle between convergence and fault plane directions. (cf. Molnar, 1979). The 1/2 is for an average 45° angle which is probably too large an angle but is an adequate approximation.

The length of the Cascade zone is about 400 km, that of the Puget Sound zone about 200 km; one could argue these lengths because the distribution of earthquakes is not constant along the lengths of the zones. We take a rigidity of $3.3 \times 10^{10}$ Pa appropriate for the crust. A higher value appropriate for the mantle would give lower rates of motion. The thickness of the seismogenic layer is a critical parameter, and one that is difficult to estimate. For the Cascades we take 30 km on the assumption that there is sufficient strength for deformation to occur through earthquakes from the surface to a depth of about 30 km. Below 30 km the temperature is high enough for deformation to occur plastically. Recent earthquake data support this depth range. In the Puget Sound zone the situation is more complex because of the presence of probable Benioff-Wadata type seismicity, in the underthrusting oceanic lithosphere, that extends to about 50 km depth. We have computed the seismic moment rate first assuming that the seismicity extends uniformly from the surface to 50 km and secondly assuming that most of the seismicity occurs over a 10 km depth range within the underthrusting oceanic lithosphere.

The computed convergence rates are

$$u_{CAS} = \frac{1}{2} \frac{0.1 \times 10^{18} \text{ Nm}}{3.3 \times 10^{10} \text{ Pa} \times 400 \text{ km} \times 30 \text{ km}} = 0.13 \text{ mm a}^{-1}$$

$$u_{PGT} = \frac{1}{2} \frac{0.5 \times 10^{18} \text{ Nm}}{3.3 \times 10^{10} \text{ Pa} \times 200 \text{ km} \times 50 \text{ km}} = 0.76 \text{ mm a}^{-1} \text{ (50 km thickness)}$$

$$\text{or} = 3.8 \text{ mm a}^{-1} \text{ (10 km thickness)}$$

These deformation rates could be increased by a factor of 2 or possibly at very most a factor of 4 through the inclusion of the effect of stochasticity and through the uncertainties in the various other parameters. However, we feel they cannot be increased to the rates from other deformation estimates as discussed below which are an order of magnitude higher.

Before discussing these deformation estimates and the reasons for the inconsistency, we want to show results of seismic moment-deformation rate calculations for two other areas along the west coast, that give rates close to those from plate tectonic models. For the Queen Charlotte fault zone we get a moment rate of $12.3 \times 10^{18}$ Nm (Fig. 6), which for an area of 360 km x 25 km give a slip rate of 42 mm $a^{-1}$. This is quite compatible with the plate tectonic model estimates of about 55 mm $a^{-1}$. Along the offshore northern Juan de Fuca ridge-fault system including the Wilson-Dellwood, Revere-Dellwood, Sovanco and Nootka fault zones, the moment rate is about $1.5 \times 10^{18}$ Nm (Fig. 7). For an area of 450 km x 4 km the slip rate estimate is about 25 mm $a^{-1}$. The average plate tectonic rate is about 45 mm $a^{-1}$. Inclusion on the effect of stochasticity could increase these moment estimates by up to a factor of 2, so the agreement between the seismic moment and plate tectonic slip rates is very good in both areas.

Earthquake Mechanisms and Direction of Deformation

Through earthquake mechanism solutions the earthquake data contain information on the orientation of faulting and by inference the stress orientation. Summaries of earthquake mechanism solutions have been given by Crosson (1972), Malone et al. (1975), Rogers (1979) and Crosson (1981, this volume). A common feature to most solutions is an inferred north-south compression in areas as distant as mid Vancouver Island, Puget Sound and the Columbia Plateau. Several of the deeper Puget Sound events have down dip tension inferred to be in the descending oceanic lithosphere. The clear thrust type events that one might expect in a simple convergent regime are missing.

Geodetic, Plate Tectonic and other Convergence Estimates

Savage et al. (1980) reported geodetic measurements of strain in the state of Washington for the interval 1972 to 1979. Across the southern Puget Sound near Seattle they find a N 71°E compression of $0.13 \pm 0.01$ microstrain per year. Their array extends about 100 km in the direction of compression so the total shortening rate is about 13 mm $a^{-1}$. In south central Washington over a 60 km distance they find compression at a rate of $0.04 \pm 0.01$ microstrain per year at N 54°E. If this rate is assumed to represent the rate for the some 300 km width of the Cascade zone, excluding Puget Sound, the shortening rate is very approximately 12 mm $a^{-1}$. Under this assumption the total compression is about 25 mm $a^{-1}$ in a roughly NE-SW direction across Washington.

The deformation of deep sea sediments along the continental margin is an additional measure of part of the convergence between the Pacific sea floor and North America. The estimates have a large uncertainty and range from 7 to 27 mm $a^{-1}$ (Silver; 1972; von Heune and Kulm, 1973; Barnard, 1978). These rates may refer to the rate of underthrusting along the margin, and hence should be added to the continental compresion discussed above to give the total plate convergence rate. Of course the different data are from very different time intervals.

Plate tectonic arguments give a convergence rate between the Juan de Fuca and North America plates of 35 to 46 mm $a^{-1}$ decreasing to the south from southernmost British Columbia to southern Washington. (see Riddihough, 1977; and references given there). Oblique convergence at N 50° E to N 62° E is predicted off Washington so the orthogonal component is somewhat less and there may be a component of N-S shear transmitted across the margin. In addition to the simple plate convergence, N-S compression may be generated in the underthrusting oceanic lithosphere because of the re-entrant corner in the continental margin (e.g. Keen and Hyndman, 1979). The plate descending into this corner must shorten, either by overlap, thickening or otherwise deforming, thus probably setting up a N-S compression at a rate of a few mm $a^{-1}$ (Fig. 8).

Discussion

We believe that the method of integrating the seismic moment contributions over magnitude using the recurrence relation is superior to summing the contributions of individual events. We have discussed a number of critical factors that require careful consideration for meaningful results to be obtained. Even so, uncertainties of a factor of two and bias factors of up to a factor of two are not difficult to explain. The credibility of the method is supported by the slip rates computed from the seismicity being in good agreement with plate tectonic estimates for two examples, the northern Juan de Fuca system ('Offshore') and the Queen Charlotte fault zone. This agreement forces us to take the results for the Puget Sound region as a serious constraint.

For convenience, we now list the constraints for any realistic model of deformation and earthquake generation in the Puget Sound region.

1. The Juan de Fuca - America convergence rate from plate tectonic models is 35 to 45 mm $a^{-1}$ at an azimuth of 50° to 62°. Roughly N-S compression of a few mm $a^{-1}$ in the underthrusting Juan de Fuca plate must result from the plate descending into the corner of the margin in this area. This compression may be transferred to the overlying continental plate, but we doubt that the coupling can be very efficient.

2. The strain rate from geodetic measurements in southern Puget Sound is about 13 mm $a^{-1}$ at an azimuth of 71° over a 100 km wide zone. A lower compressive strain rate may extend across much of Washington state.

3. The deformation of deep sea sediments along the edge of the shelf suggests underthrusting rates of 7 to 27 mm $a^{-1}$. The underthrusting plus the continental deformation should equal the plate model convergence rate if the process has been constant over the corresponding time intervals.

4. Earthquake mechanisms of shallow earthquakes have predominantly N-S dilational quadrants, and most are strike-slip thus implying N-S compression. Several deep normal mechanisms appear to reflect down-dip tension in the descending oceanic lithosphere. The N-S compression holds from Vancouver Island to the Columbia Plateau. This pattern appears to contradict the plate model and geodetically measured convergence directions which are roughly E-W, although it is consistent with N-S compression generated by the oceanic lithosphere descending into a corner in the margin.

5. The convergence rates computed from the seismicity are about a factor of 10 lower than the rates estimated from plate models, from sediment deformation along the shelf edge and from geodetic measurements. They are about the same as the rate of N-S compression generated by the oceanic lithosphere descending into a corner in the margin.

Our analysis provides quite clear evidence that the seismicity of Puget Sound does not reflect in a simple way the plate convergence between the Juan de Fuca and North America plates. The seismic moment rates are too low by about a factor of 10 and the stress from fault mechanism solutions is in the wrong direction compared to the other convergence estimates. We must ascribe the few mm of computed displacement to N-S compression. i.e. somewhere in the dilational quadrant of the earthquake mechanism solutions. The actual constraint on the direction of implied compression depends on the friction on pre-existing NW faults postulated in this area compared to the rock strength. Unfortunately we are unable to differentiate the moment rates in different directions. In any case, we are left with the apparent paradox that the small NS component of convergence is reflected in the seismicity while the larger EW component is not.

One obvious explanation for the low seismic moment rates is that convergence and subduction has very recently stopped. However, the compression indicated by the geodetic measurements does not readily allow this. Also the subsidence in Puget Sound and uplift along the coast determined by Ando and Balasy (1979) argue for continued convergence. Ando and Balasy's interpretation of the subsidence and uplift pattern is also not consistent with pre-seismic elastic strain build up.

The only reasonable hypothesis that we can suggest is that both underthrusting and continental compression are occurring largely through aseismic creep. This may be a consequence of the oceanic lithosphere being young, thin and hot as it descends beneath the continent. The seismicity that does occur and that appears to arise through N-S compression may be produced by N-S compression in the oceanic lithosphere as it descends into the corner of the margin in this region. This mechanism does not readily generate the inferred N-S compression in the overlying continental lithosphere, unless mechanical coupling is invoked between it and corrugations in the underthrusting oceanic lithosphere. Corrugations or breaks in the underthrusting plate generated by the corner in the margin (as in Figure 8) may be oblique to the direction of convergence, thus

generating the required tractions. The restriction of corrugations or breaks in the underlying plate to near the corner in the margin would explain why the seismicity is greater in the Puget Sound region compared to the regions to the north and south where the plate convergence rates are similar.

References


Anderson, J.G. 1979. Estimating the seismicity from geological structure for seismic risk studies. BSSA, 69, pp. 135-158.

Ando, M., and E.I. Balazs, 1979. Geodetic evidence for aseismic subduction of the San Juan de Fuca plate, J. Geophys. Res., 84, 3023-3028.

Barnard, W.D. 1978. The Washington continental slope: Quaternary tectonics and sedimentation. Marine Geology, 27, 79-114.

Brune, J.M. 1968. Seismic moment, seismicity and rate of slip along major fault zones. J. Geophys. Res., 73, 777-784.

Crosson, R.S., 1972. Small earthquakes, structure, and tectonics of the Puget Sound region. BSSA, 62, 1133-1172.

Davis, G.F. and J.N. Brune, 1971. Regional and global fault slip rates from seismicity. Nature, 229, 101-107.

Keen, C.E. and R.D. Hyndman, 1979. Geophysical review of the continental margins of eastern and western Canada. Can. J. Earth Sci., 16, 712-747.

Malone, S.D., G.H. Rothe and S.W. Smith, 1975. Details of micro-earthquake swarms in the Columbia Basin, Washington. BSSA, 65, 855-864.

McGuire, R.K., 1976. Fortran computer program for seismic risk analysis. U.S. Geological Survey Report 76-67.

Milne, W.G., G.C. Rogers, R.P. Riddihough, G.A. McMechan and R.D. Hyndman, 1978. Seismicity of Western Canada. Can. J. Earth Sci., 15, 1170-1193.

Milne, W.G., D.H. Weichert, P.W. Basham, M.J. Berry, and H.S. Hasegawa, 1981. Seismic zoning in Canada - some modifications, in press.

Molnar, P. 1979. Earthquake recurrence intervals and plate tectonics. BSSA, 69, 115-133.

Reichle, M.S., G.J. Sharman and J.N. Brune, 1976. Sonobuoy and teleseismic study of Gulf of California transform fault earthquake sequences. BSSA, 66, 1623-1641.

Riddihough, R.P., 1977. A model for recent plate interactions off Canada's west coast. Can. J. Earth Sci., 14, 384-396.

Rogers, G.C. 1979. Earthquake fault plane solutions near Vancouver Island. Can. J. Earth Sciences, 16, 523-531.

Savage, M., Lisowski, and W.H. Prescott, 1980. Geodetic strain measurements in Washington. J. Geophys. Res., in press.

Silver, E.A. 1972. Pleistocene tectonic accretion of the continental slope off Washington. Marine Geology, 13, 239-249.

Smith, S.U., 1976. Determination of maximum earthquake magnitude. Geoph. Res. Letters, 3, 351-353.

von Heune, R. and L.D. Kulm, 1973. Tectonic summary of DSDP leg 18. In Initial Reports of the Deep Sea Drilling Project V. 28, Washington, U.S. Government Printing Office, 961-976.

Weichert, D.H. and Hyndman, R.D. 1980. Seismicity and rates of motion along fault zones of western Canada. Pacific Northwest Am. Geophys. Union Meeting, Sept. 1980, Victoria, B.C.

Weichert, D.H. 1980. Estimation of the earthquake recurrence parameters for unequal observation periods for different magnitudes. Seism. Soc. Am. Bull., 70, 1337-1346.

Figures

Figure 1. Zones of seismicity of the Pacific Northwest as employed in the analyses.

2. The effect of different truncations of recurrence relation. Note the Delta function implied in the density recurrence if the cumulative recurrence is truncated.

3. Effect of different truncations on integrated moment. The d/b factor is required for cumulative truncation.

4. Recurrence data and curves for the Cascades. The integrated seismic moment per year is given for Mx = 7-1/4 and 7-3/4. Standard error estimates are given for the data points assuming a Poissonian distribution.

5. Recurrence data and curves for the Puget Sound. The integrated seismic moment per year is given for Ma = 7-1/4 and 7-3/4.

6. Recurrence data and curves for the Queen Charlotte fault. The integrated seismic moment per year is given for Mx = 8-1/4 and 8-3/4.

7. Recurrence data and curves for the Offshore zone. The integrated seismic moment per year is given for Mx = 6-3/4 and 7-1/4.

8. Model showing compression generated in a plate descending into a re-entrant corner of the continent. Folds or corrugations in the underlying lithosphere are an alternative to the break shown in this model.

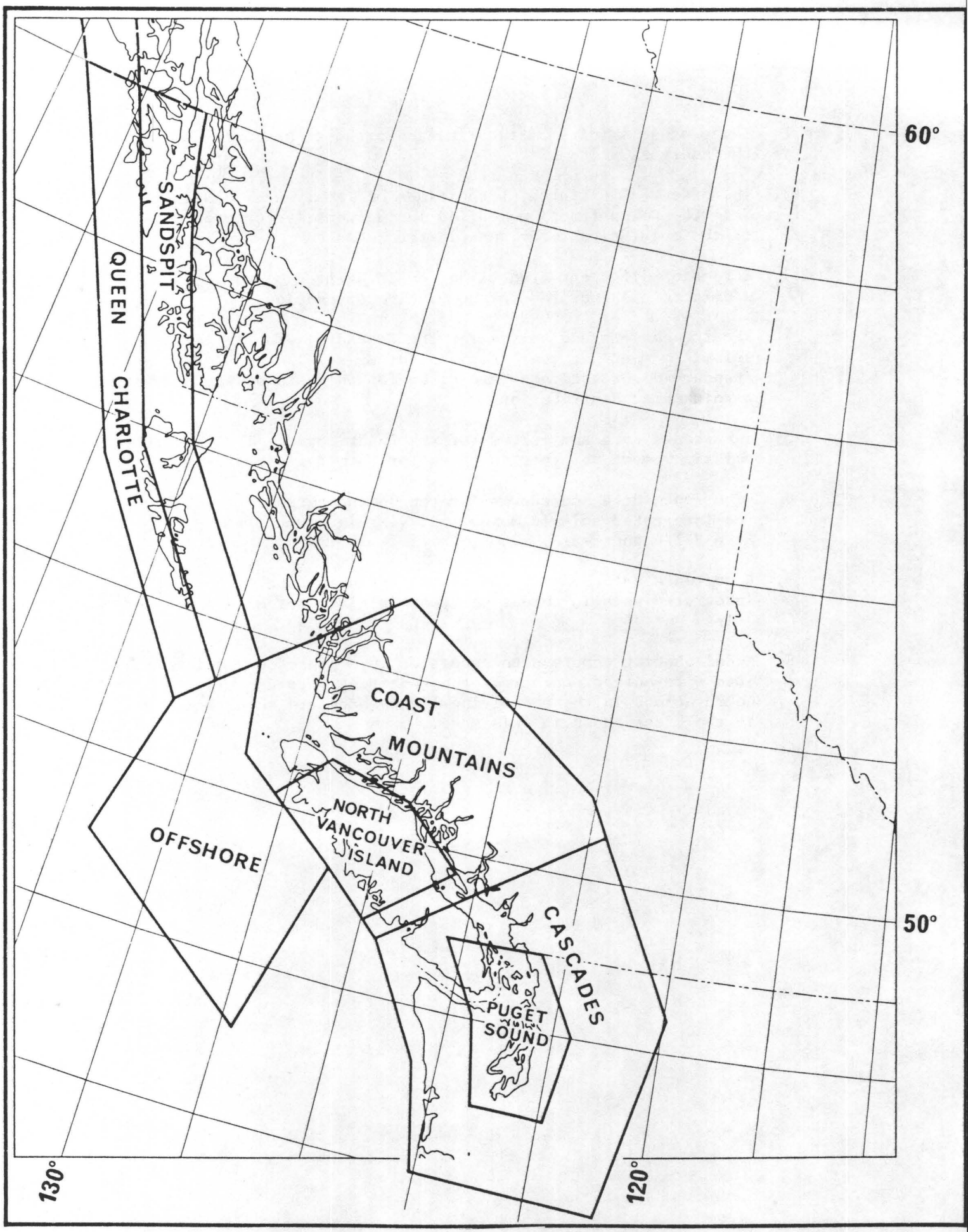
60°
50°
130°
120°
QUEEN CHARLOTTE
SANDSPIT
COAST MOUNTAINS
NORTH VANCOUVER ISLAND
OFFSHORE
CASCADES
PUGET SOUND

Fig. 1.

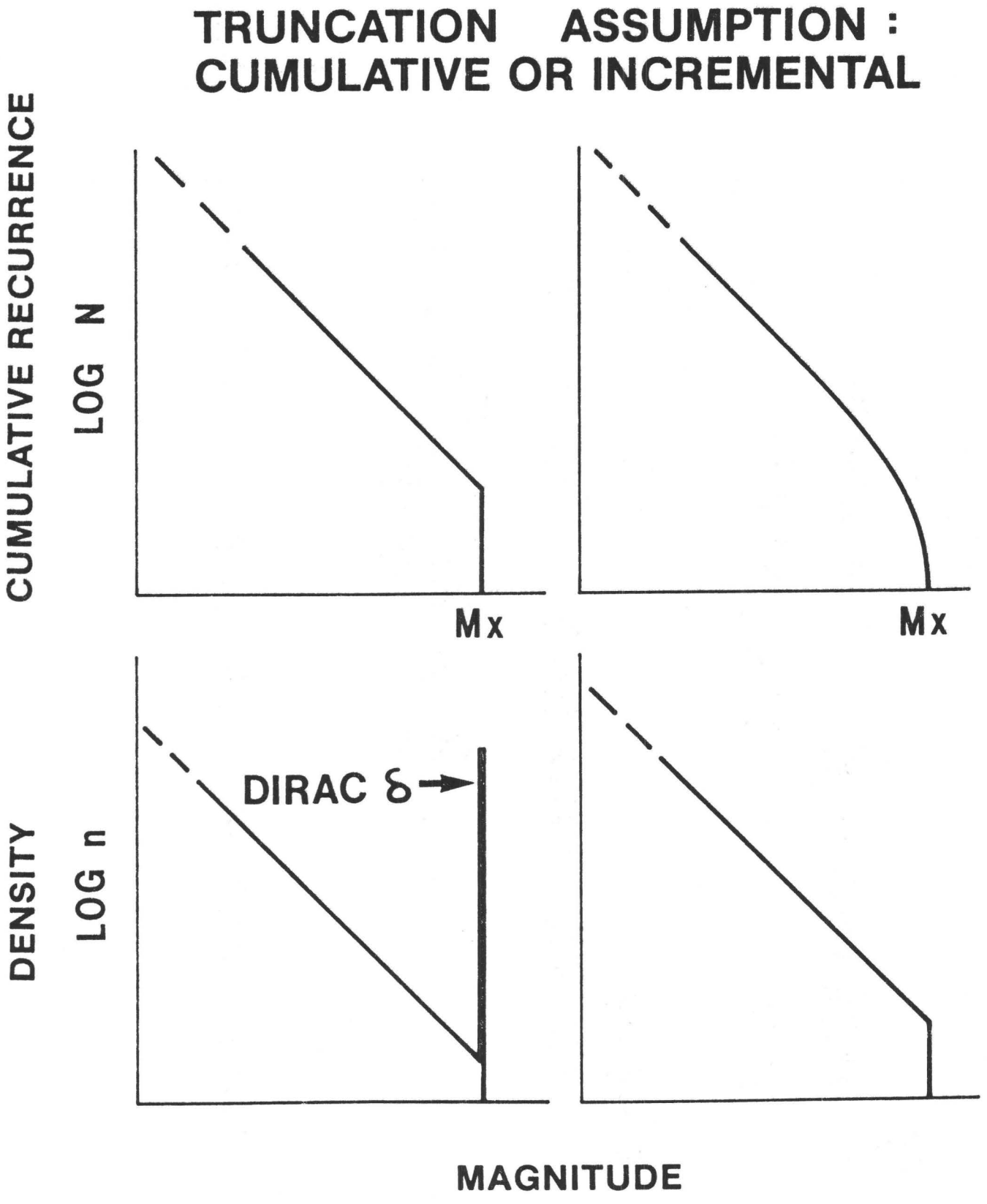
TRUNCATION ASSUMPTION :
CUMULATIVE OR INCREMENTAL
CUMULATIVE RECURRENCE
LOG N
Mx
Mx
DENSITY
LOG n
DIRAC δ
MAGNITUDE

Fig. 2.

**IF**

$$\text{MOMENT} = Y_0 e^{d' \times \text{Magnitude}}$$

$$\text{E.G.:} \quad = 10^9 \times 10^{3/2\,M}$$

**THEN**

TOTAL MOMENT, FOR $d > b$

$$= \frac{d}{b} \times \frac{e^{(d'-b')M_x}}{d'-b'} \times Y_0 n_0$$

*THIS FACTOR FOR CUMULATIVE TRUNCATION*



Fig 3

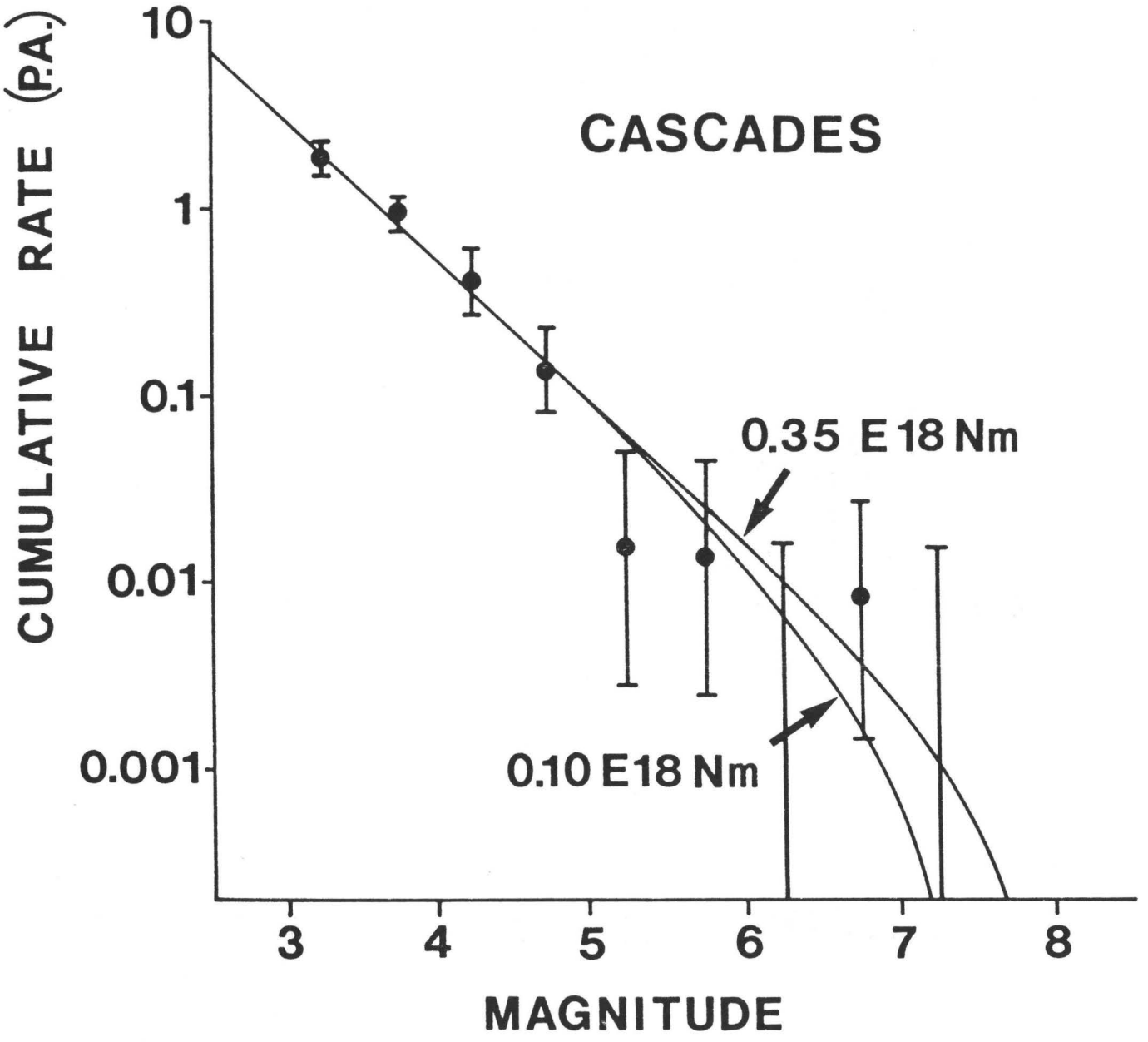
CASCADES
CUMULATIVE RATE (P.A.)
10
1
0.1
0.01
0.001
0.35 E 18 Nm
0.10 E18 Nm
3
4
5
6
7
8
MAGNITUDE

Fig. 4

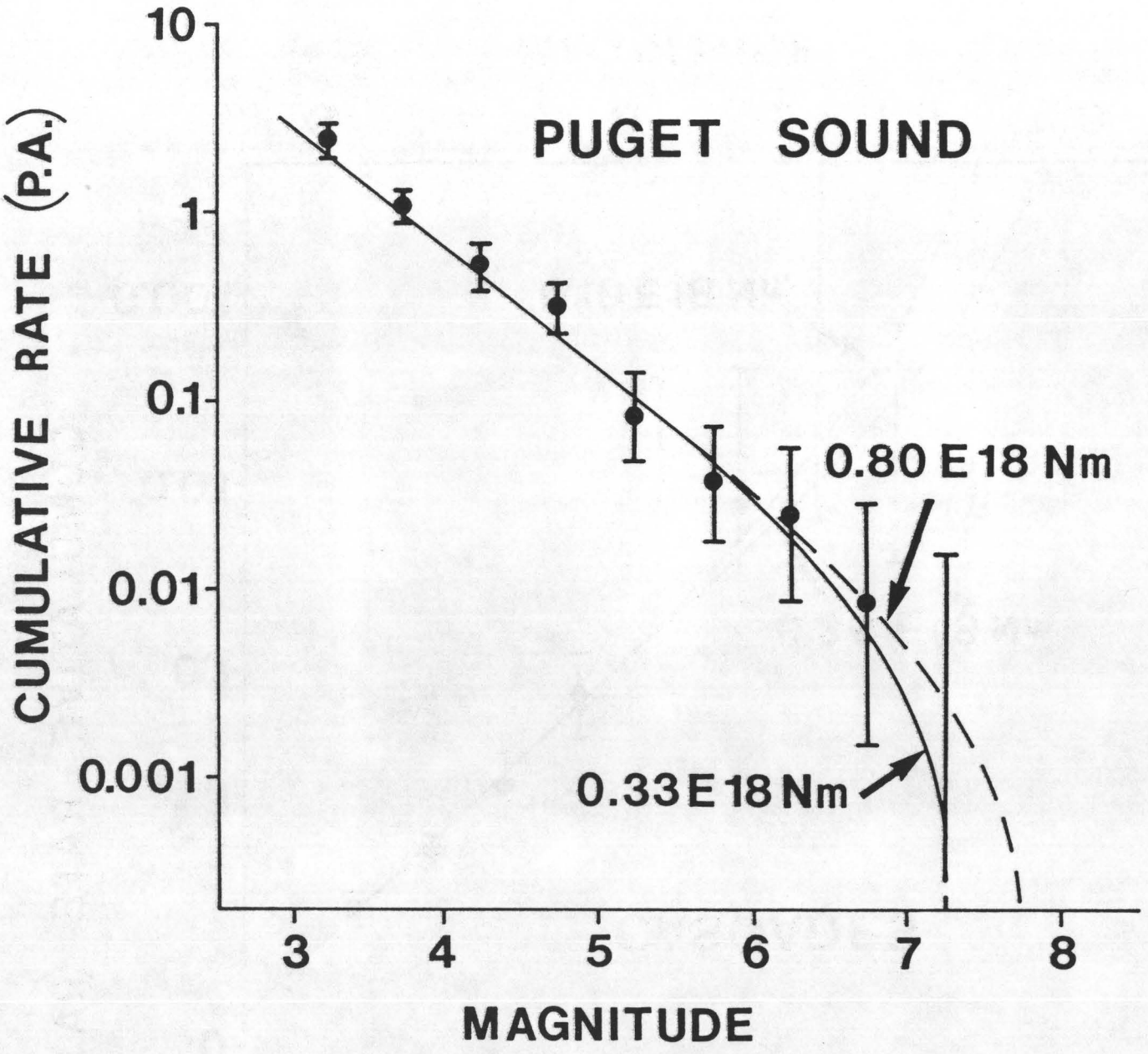
PUGET SOUND
CUMULATIVE RATE (P.A.)
10
1
0.1
0.01
0.001
0.80 E 18 Nm
0.33 E 18 Nm
3
4
5
6
7
8
MAGNITUDE

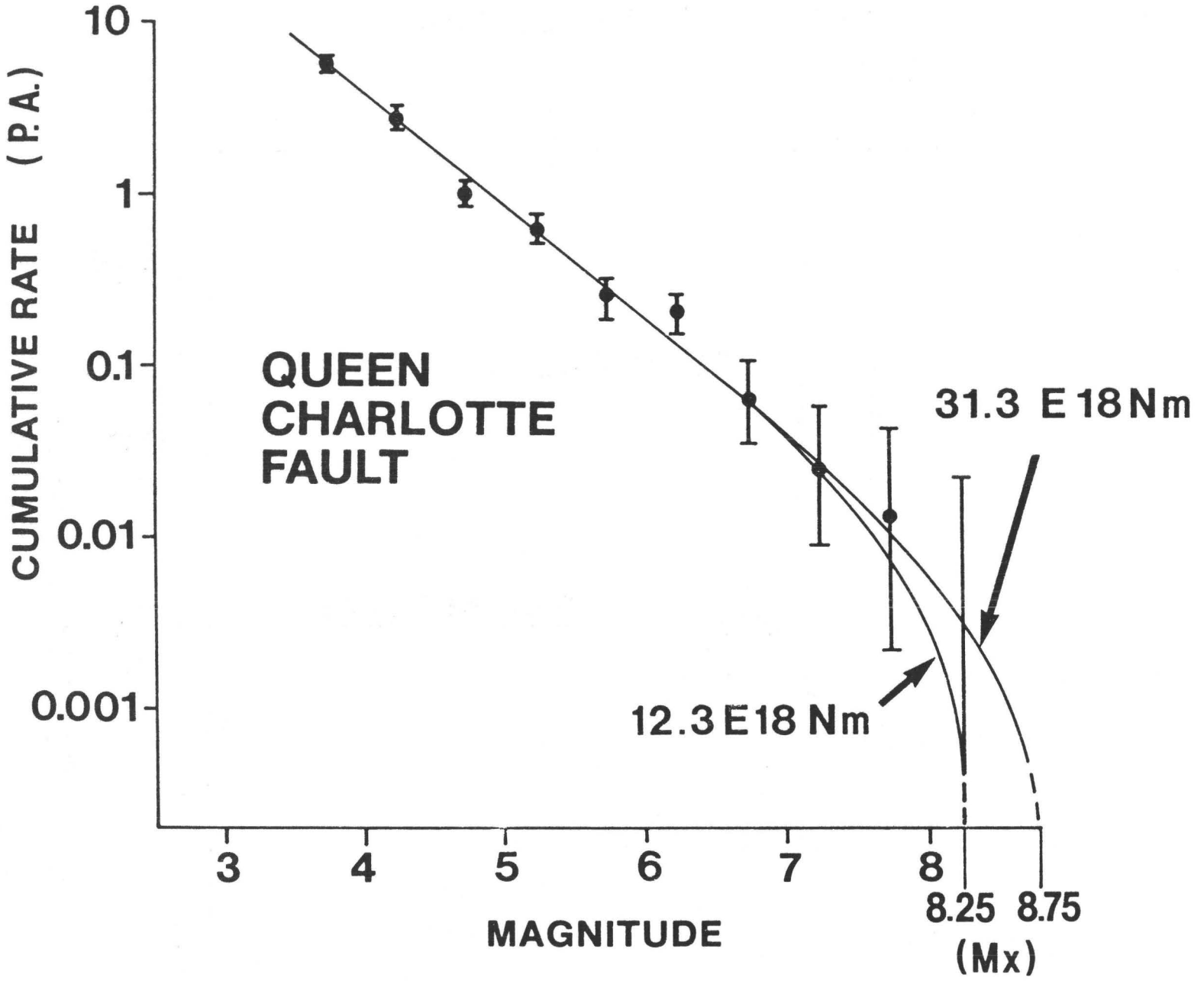
10
1
0.1
0.01
0.001
CUMULATIVE RATE (P.A.)
QUEEN
CHARLOTTE
FAULT
31.3 E 18 Nm
12.3 E18 Nm
3
4
5
6
7
8
8.25
8.75
(Mx)
MAGNITUDE

Fig. 6.

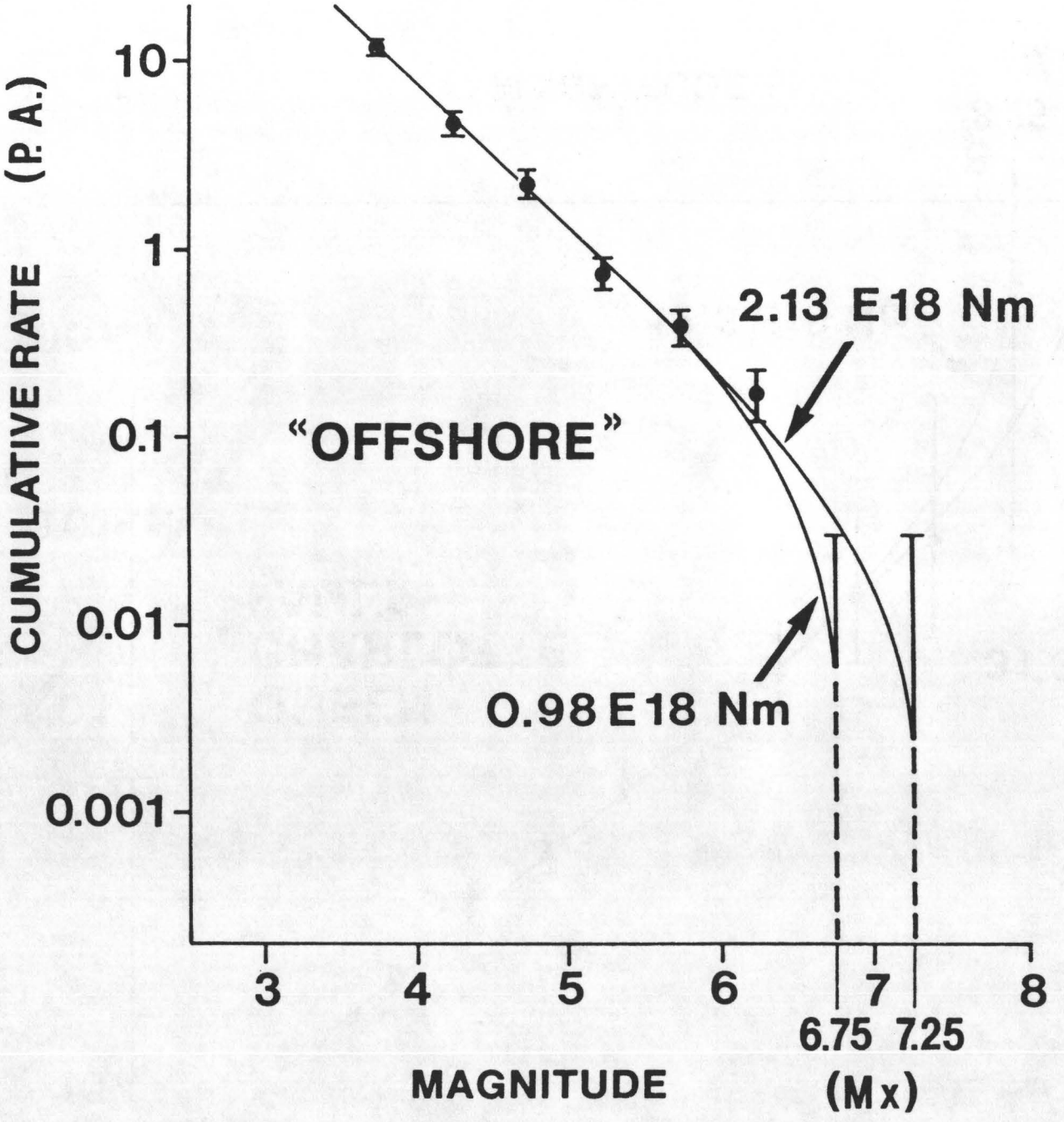
CUMULATIVE RATE (P. A.)
10
1
0.1
0.01
0.001
"OFFSHORE"
2.13 E18 Nm
0.98 E18 Nm
3
4
5
6
7
8
6.75
7.25
MAGNITUDE
(Mx)

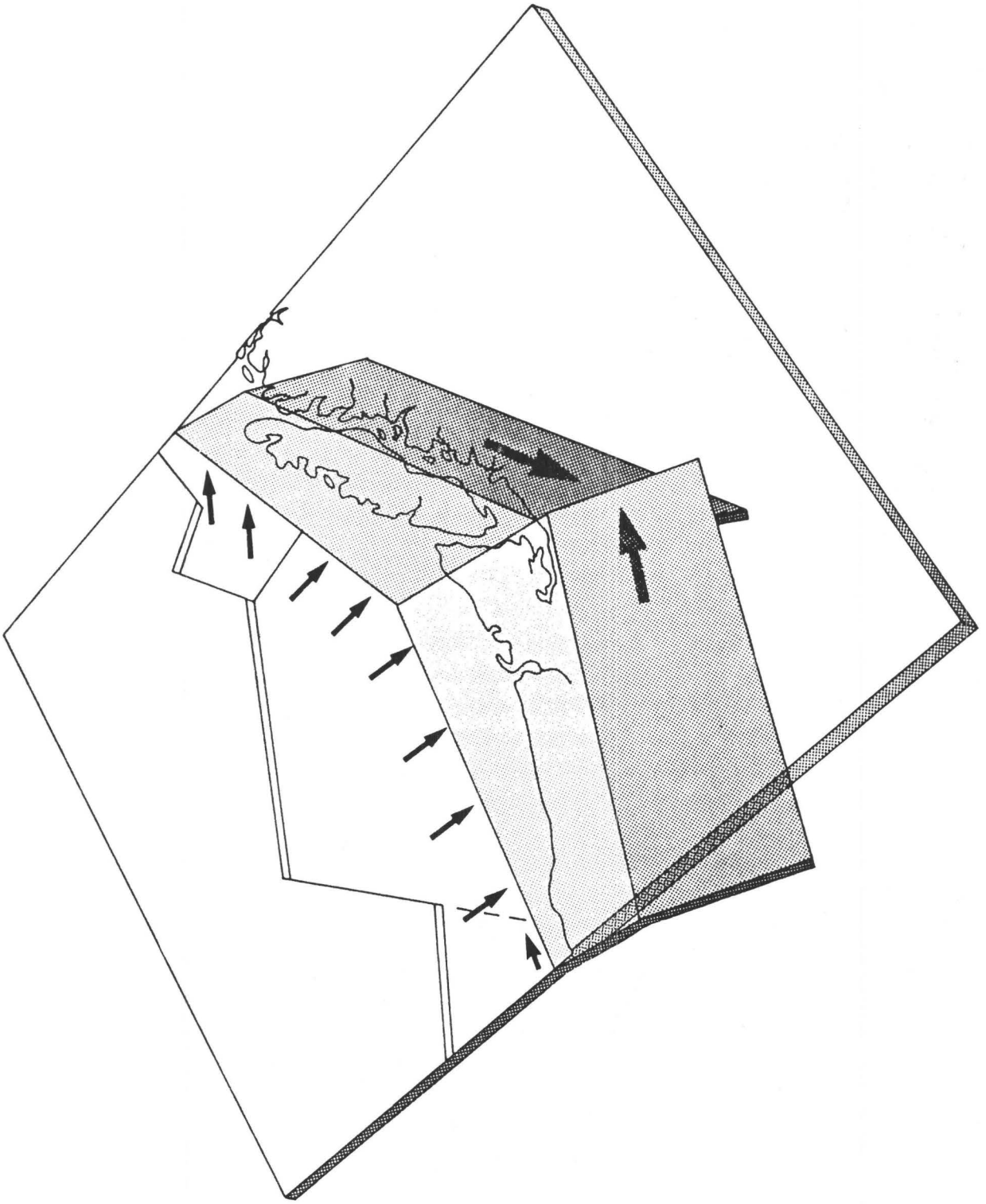

Fig. 8.

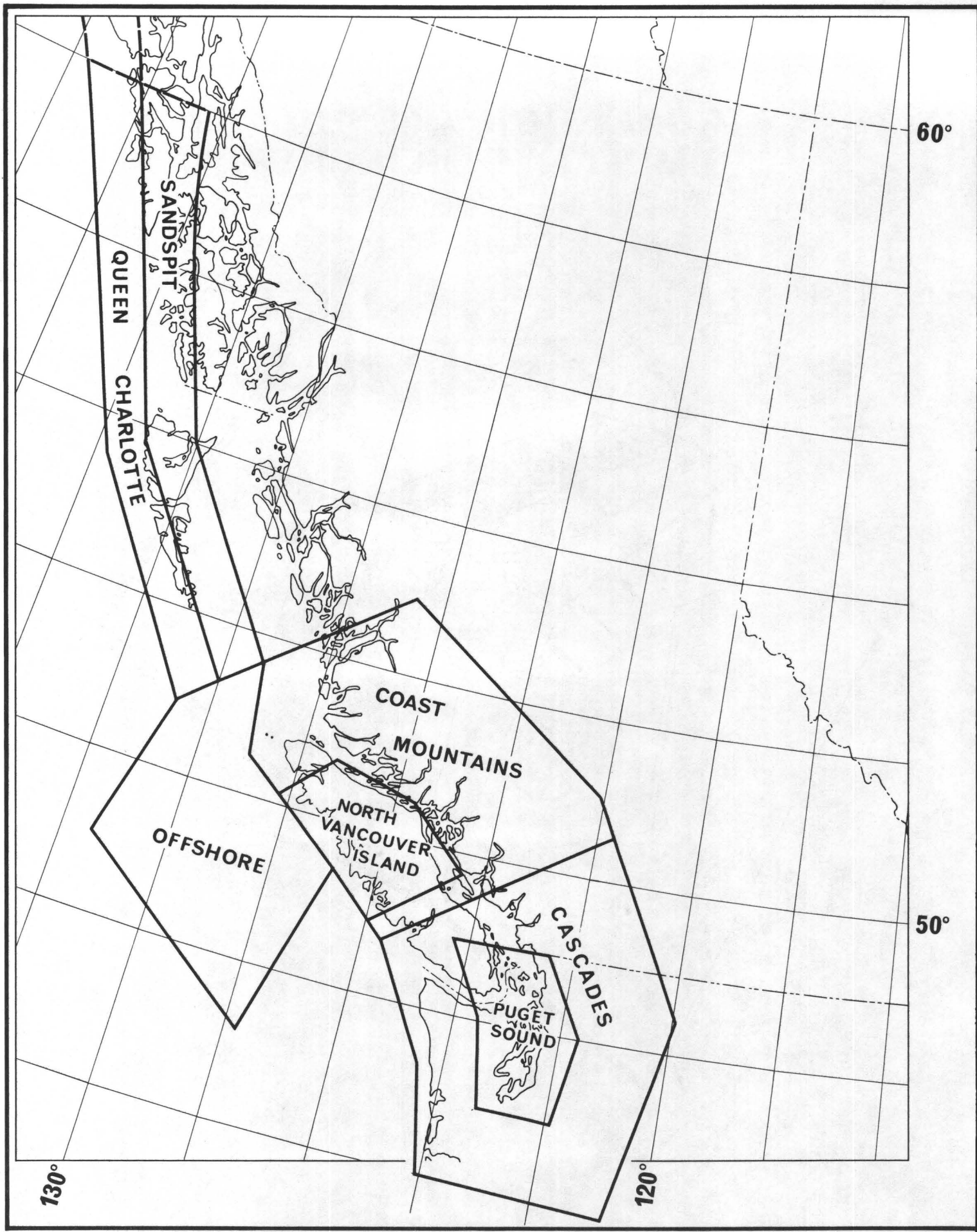
60°
50°
130°
120°
QUEEN CHARLOTTE
SANDSPIT
COAST MOUNTAINS
NORTH VANCOUVER ISLAND
OFFSHORE
CASCADES
PUGET SOUND

# TRUNCATION ASSUMPTION : CUMULATIVE OR INCREMENTAL

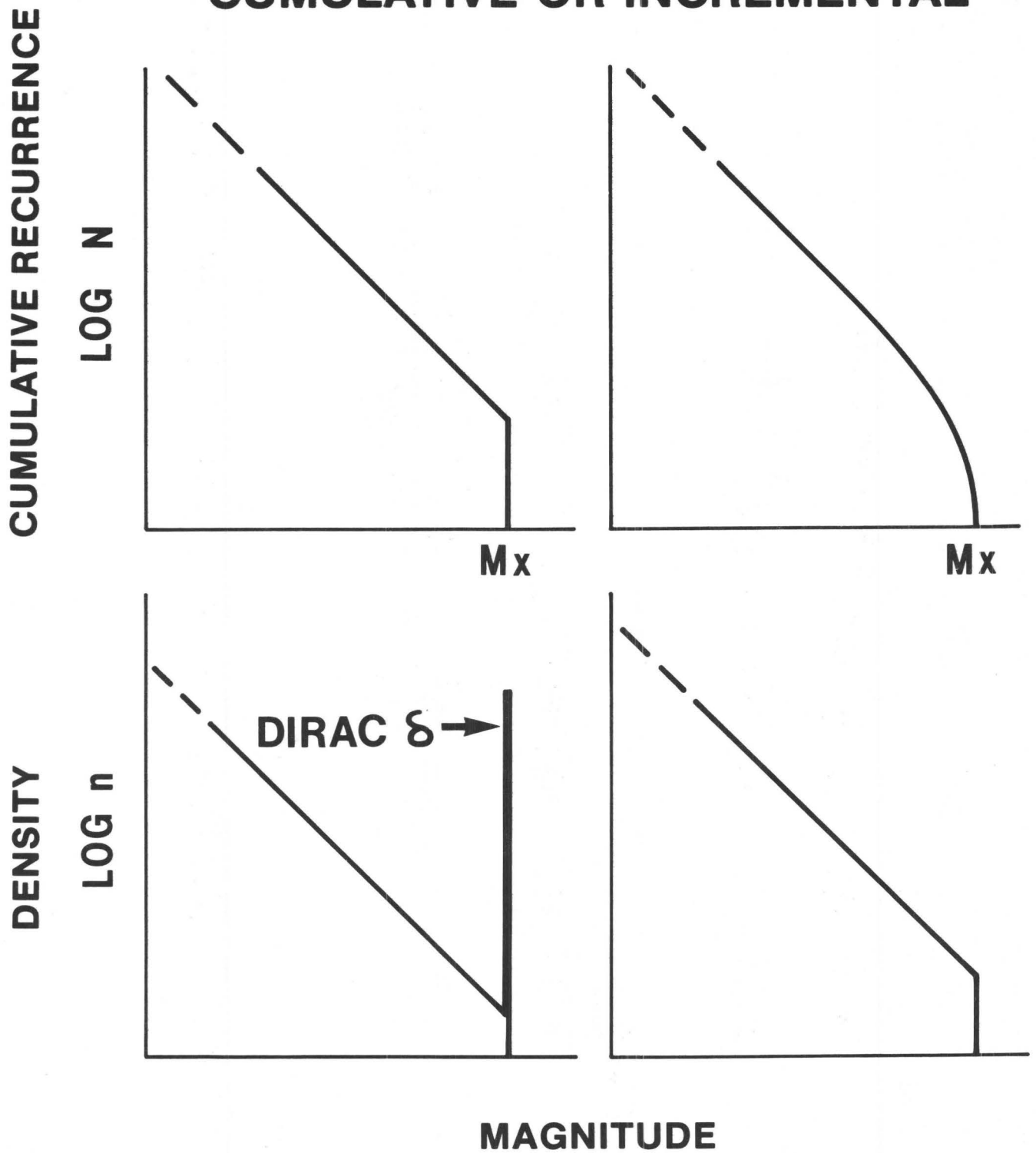

**IF**

$$\text{MOMENT} = Y_0 e^{d' \times \text{Magnitude}}$$

$$\text{E.G.:} \quad = 10^9 \times 10^{3/2\,M}$$

**THEN**

$$\text{TOTAL MOMENT, FOR } d > b$$

$$= \frac{d}{b} \times \frac{e^{(d'-b')M_x}}{d'-b'} \times Y_0 n_0$$

***THIS FACTOR FOR CUMULATIVE TRUNCATION***

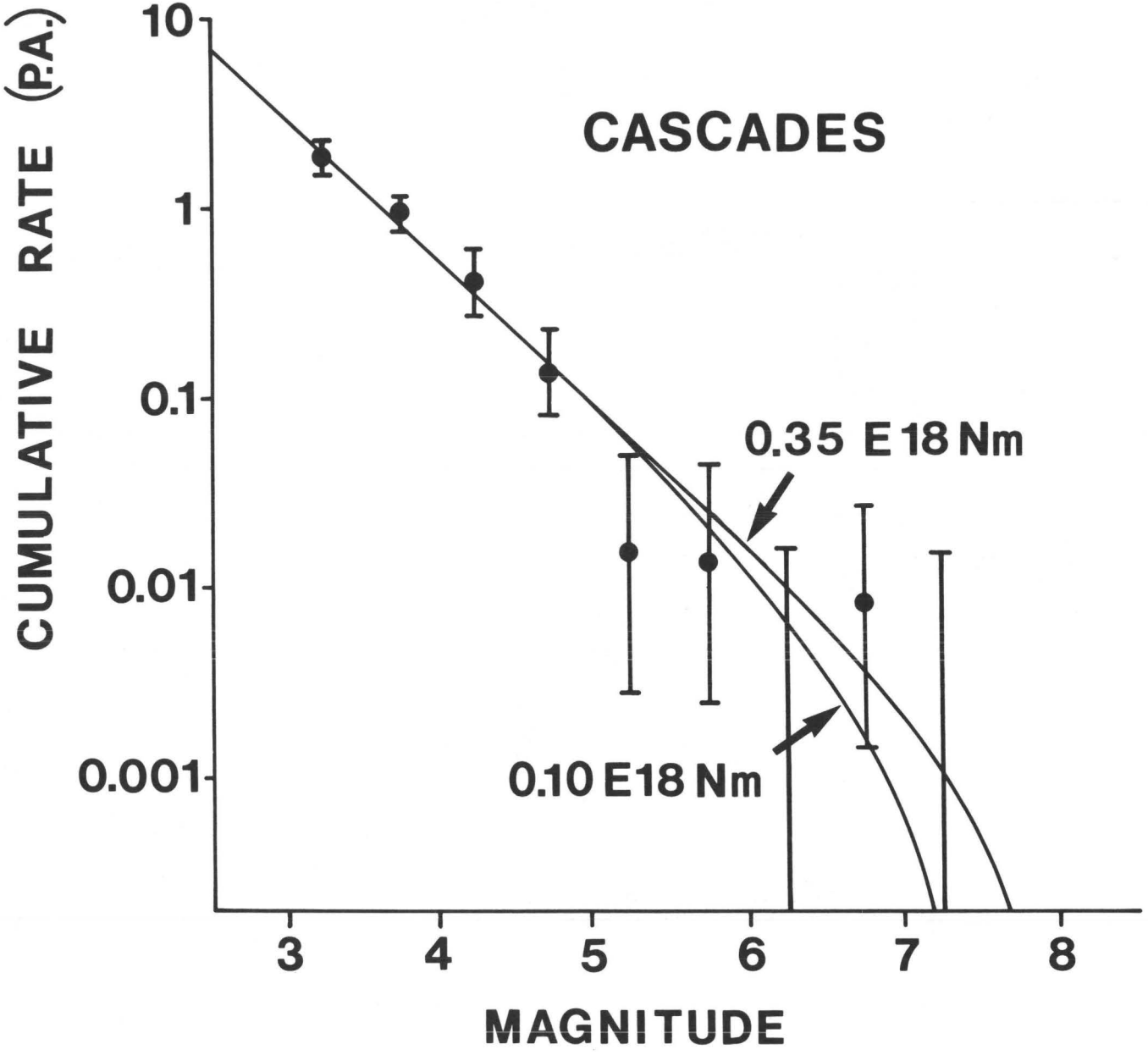
CASCADES
CUMULATIVE RATE (P.A.)
10
1
0.1
0.01
0.001
0.35 E18 Nm
0.10 E18 Nm
3
4
5
6
7
8
MAGNITUDE

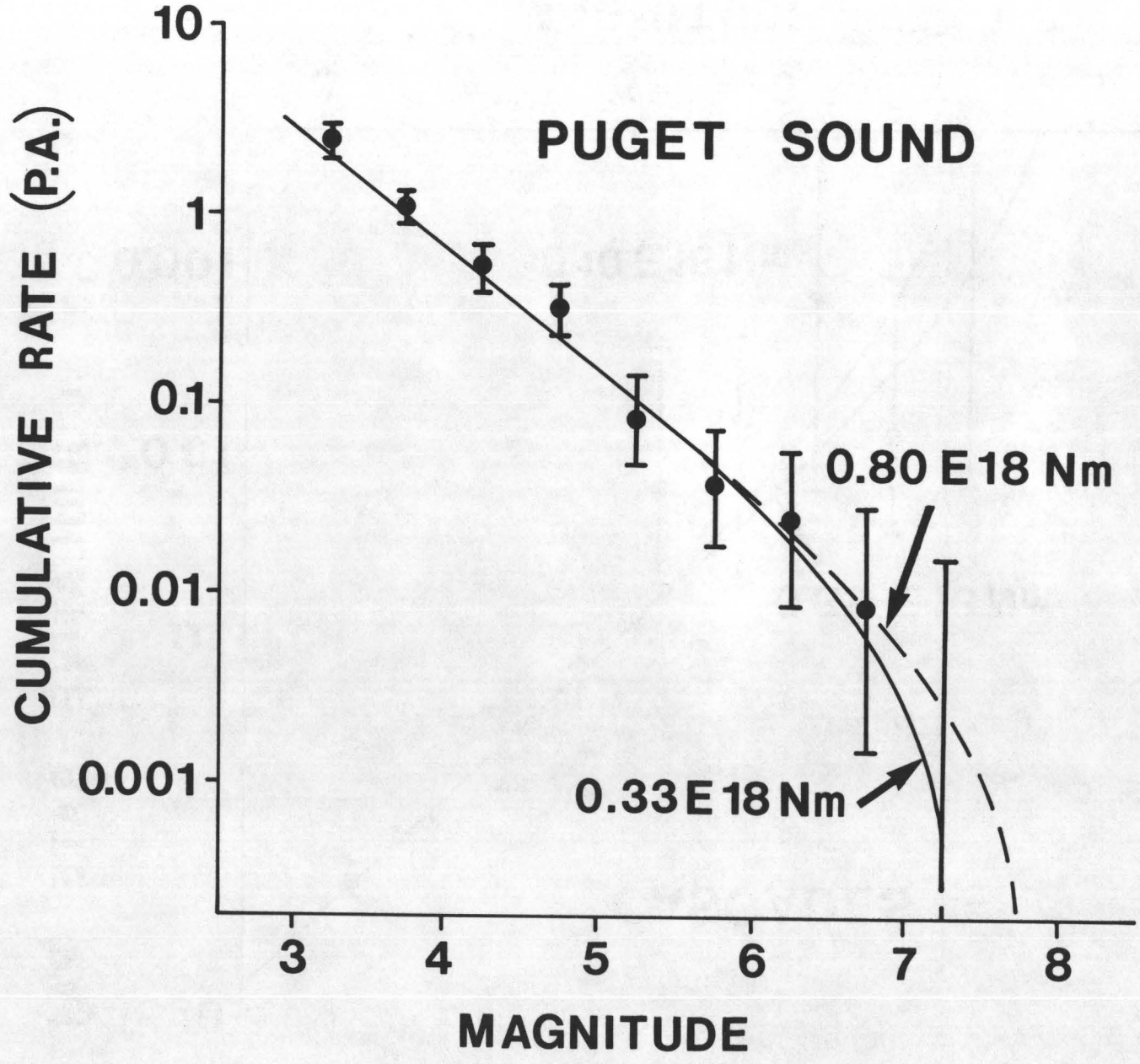
PUGET SOUND
CUMULATIVE RATE (P.A.)
10
1
0.1
0.01
0.001
0.80 E 18 Nm
0.33 E 18 Nm
3
4
5
6
7
8
MAGNITUDE

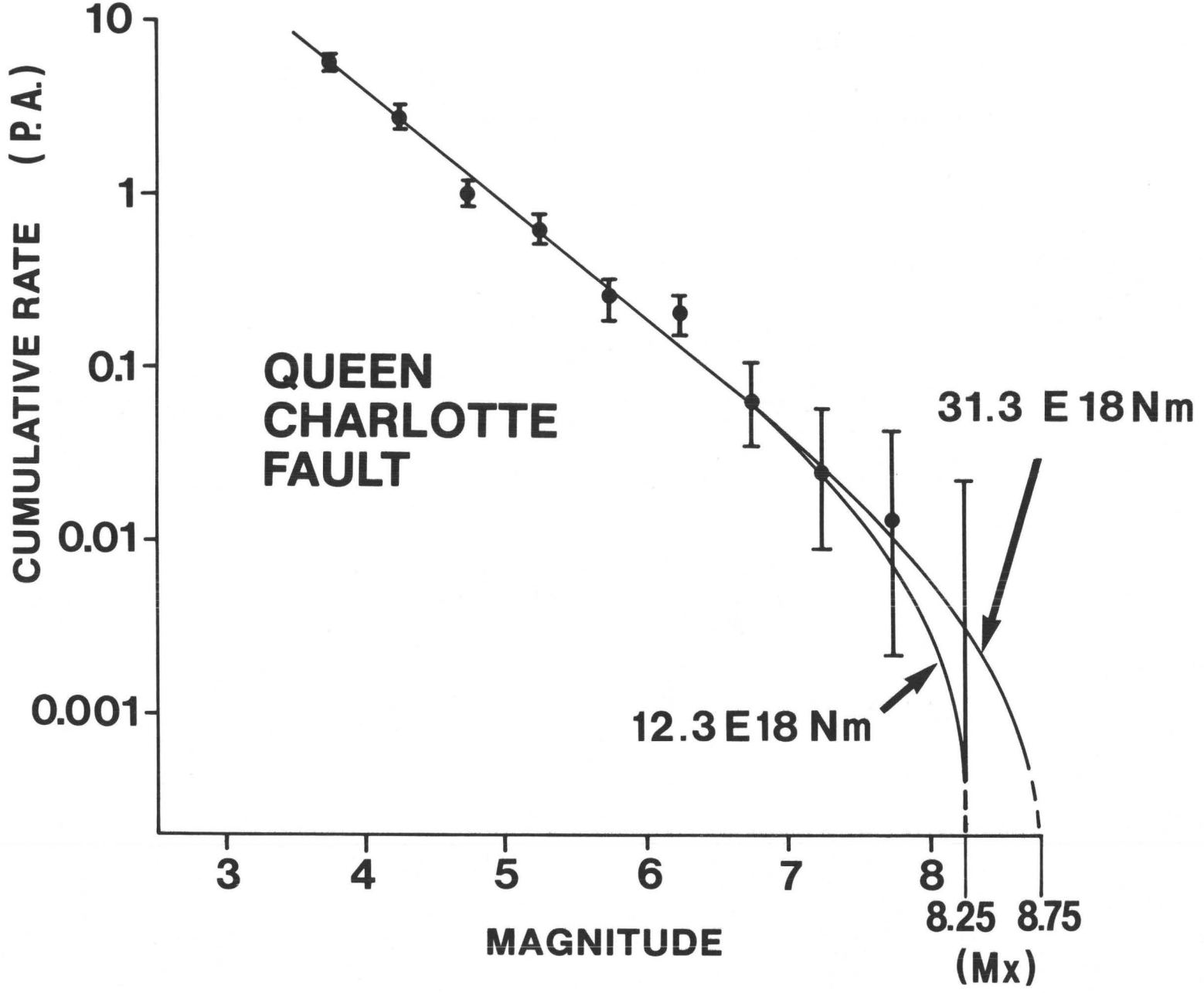
10
1
0.1
0.01
0.001
CUMULATIVE RATE (P.A.)
QUEEN
CHARLOTTE
FAULT
31.3 E 18 Nm
12.3 E 18 Nm
3
4
5
6
7
8
8.25
8.75
(Mx)
MAGNITUDE

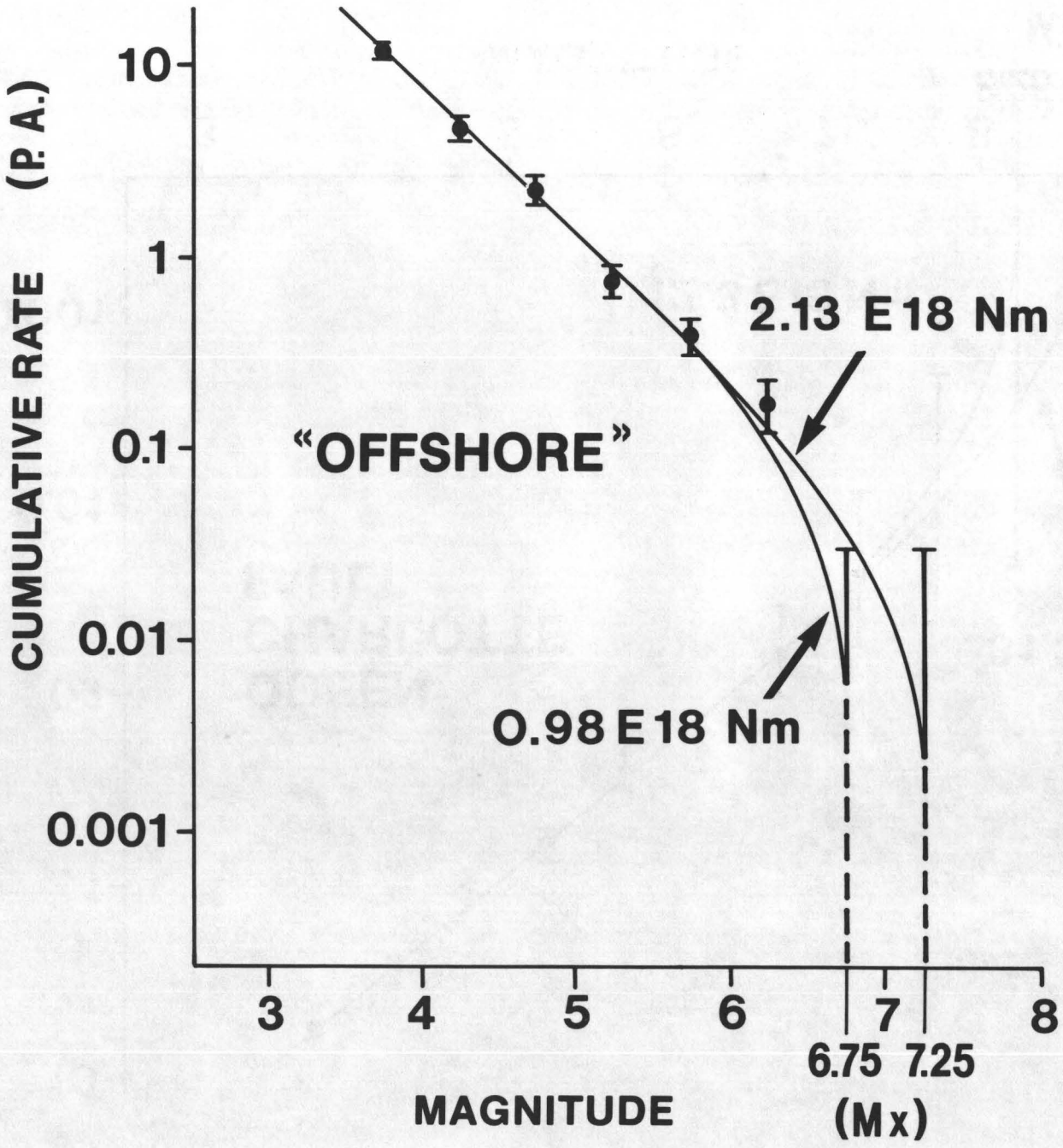
CUMULATIVE RATE (P. A.)
10
1
0.1
0.01
0.001
"OFFSHORE"
2.13 E 18 Nm
0.98 E 18 Nm
3
4
5
6
7
8
6.75
7.25
MAGNITUDE
(Mx)

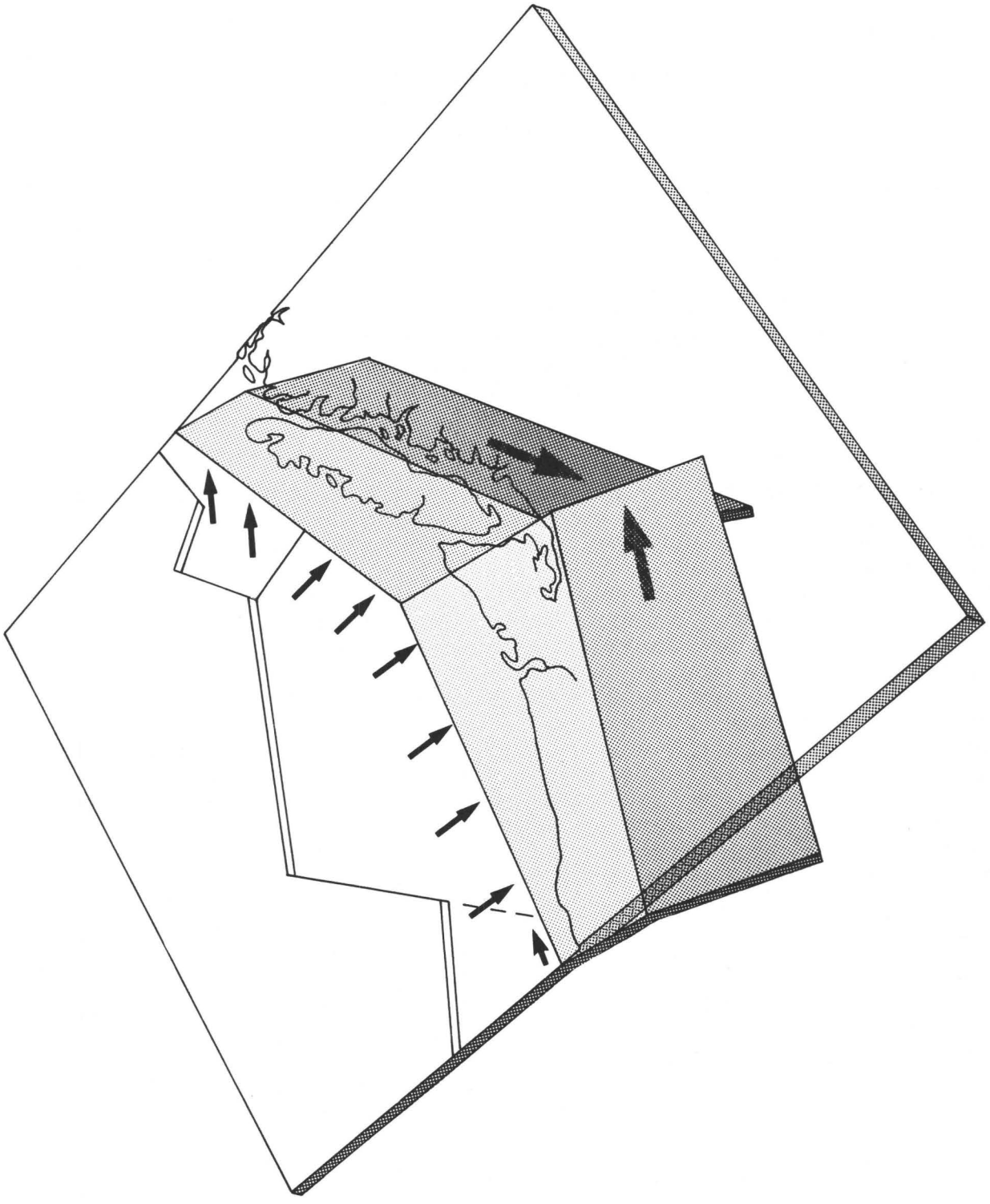

# ELEVATION CHANGES RELATED TO SEISMIC HAZARD EVALUATION WITH THE USE OF GRAVITY METERS

By

Norman H. Rasmussen
Seismologist, Geophysics Program
University of Washington
Seattle, Washington

## Abstract

Western Washington, in particular the Puget Sound area, is an active seismic region. Both geologic and seismic evidence point to the fact that vertical tectonic movement is likely to be significant in this region. Recognizing this, the Geophysics Program has been trying for several years to determine rates of tectonic movement from repeated precision gravity surveys. A network of permanent gravity reference monuments have been installed, and annual resurveys were completed in 1977 and 1978. Unfortunately, the equipment used was inadequate for the determination of relative vertical motion. A LaCoste & Romberg G meter designed primarily for exploration work was available and a LaCoste & Romberg D meter--more appropriate for geodetic work because of its greater reading accuracy--was borrowed from the U. S. Army Corps of Engineers. Data presented in a later section illustrates the drift problems that exist with this D meter. The measurement of vertical tectonic movement in this region has unusual significance for the basic understanding of tectonic processes here and for the investigation of earthquake related phenomena.

## Seismicity

The western portion of Washington State is seismically active, having experienced over 1,080 felt earthquakes in the past 135 years. In historic time there has been an intensity VIII (magnitude about 6.5) earthquake in 1877, near the Oregon-Washington border. There have been magnitude 6.3, 7.1, and 6.5 shocks in the central area of Puget Sound in 1946, 1949, and 1965, respectively. A map of these and other earthquakes of intensity VI or greater, or felt over 10,000 square miles, is shown in Figure 1.

The bedrock geology of the most seismically active area is not well know, due to Pleistocene glacial deposits resulting from the repeated episodes of continental and associated alpine glaciation. Evidence for surface faulting directly related to historic seismic activity is lacking in this area due to thick vegetation, relatively few populated areas over 100 years old, the thick unconsolidated and semiconsolidated glacial deposits, and the depth of the larger earthquakes. The depth of the 1877 shock is not known; however, the

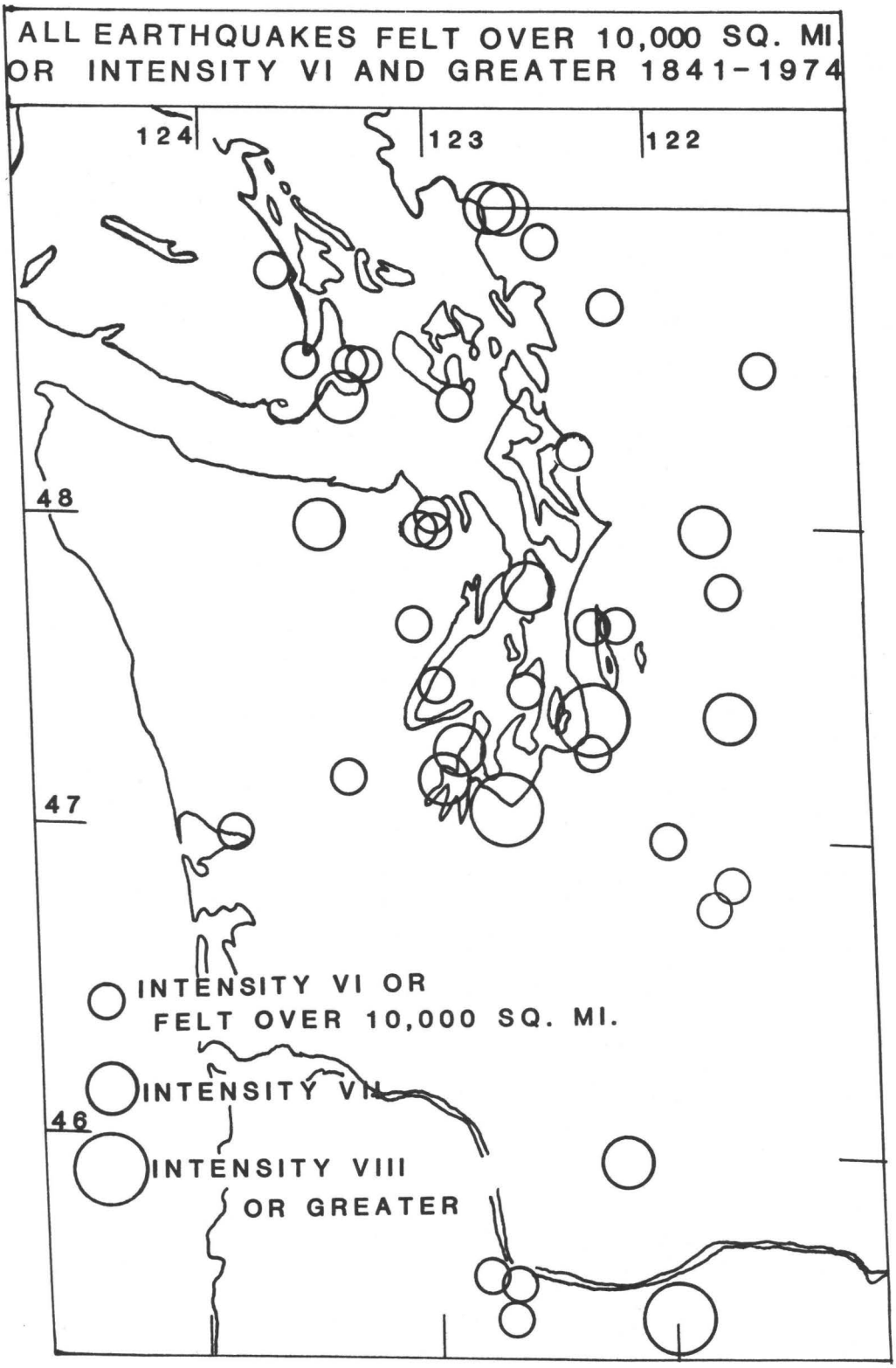
ALL EARTHQUAKES FELT OVER 10,000 SQ. MI.
OR INTENSITY VI AND GREATER 1841-1974
124
123
122
48
47
46
INTENSITY VI OR
FELT OVER 10,000 SQ. MI.
INTENSITY VII
INTENSITY VIII
OR GREATER

Figure 1

1946 and 1949 earthquakes were at least 40 kilometers deep and probably deeper. The 1965 earthquake had a 60 kilometer depth.

The regional tectonic stress is complex, but focal mechanisms have a common feature of north-south compression (Crosson, 1972). There are, however no linear seismic trends paralleling mapped surface faults reflected from past epicenter locations, nor do present foci line up along gravity or magnetic anomalies. Although there has been speculation by some investigators regarding correlation between steepening of gravity gradient and recent earthquakes, we fail to see any significant relationships.

A seismic network is now operating in western Washington, and earthquake locations and focal depth reliability is much improved since 1970. A number of programs, both geologic and seismologic, are currently underway to provide a better understanding of the tectonic picture in this area.

## Previous Studies

Extensive work has been done in compiling a complete listing of all earthquakes. These earthquakes date back to about 1840 and are fairly complete for the larger earthquakes of intensity VII or greater. Prior to 1900, intensity VI shocks and smaller are not complete, except in the populated areas. Since 1970, small earthquakes can be located from the seismic network established by Crosson (1972). From both the historic and recent network studies, earthquake listings of magnitude, or intensity, have been used to construct recurrence curves.

Seismic evaluation studies have been done by several researchers. The U. S. Geological Survey has studied earthquake risk in the large population centers of western Washington and related predicted ground motion to potential damage (USGS, 1975). The Geophysics Program has finished a study aimed at future planning and land use where potential earthquake damage is related to surface conditions, magnitude, and depth of the earthquake (Rasmussen et al, 1974). There has been a great deal of excellent gravity work done over the years in the area of interest (Stewart, 1961; Danes, 1968; Rogers, 1970). This has been brought together and published (Boninni, Hughes, and Danes, 1974). A compilation of data on depth to bedrock has been published by the Department of Natural Resources of Washington State using information from seismic reflection and refraction work and oil and water well data (Hall & Othberg, 1974).

Attempts have been made to subdivide the western Washington area into several tectonic provinces. These provinces are usually defined by topography, areal geology, or gravity. Different weight is given for each criterion depending on the investigator's background and intuition. Unfortunately, none of these divisions seem very closely related to seismicity (i.e., present-day tectonic activity). This is due to the limited amount of seismic data available and the short time interval for recording historic information on large earthquakes.

Several first- and second-order leveling surveys have been done by the U. S. Coast and Geodetic Survey in the past. These are shown in Figure 2. Couch (1965-66) showed some elevation changes from the 1947 and 1965 surveys between Chehalis and Bellingham, Washington. These may be related to the seismic activity of the 1949 and 1965 earthquakes.

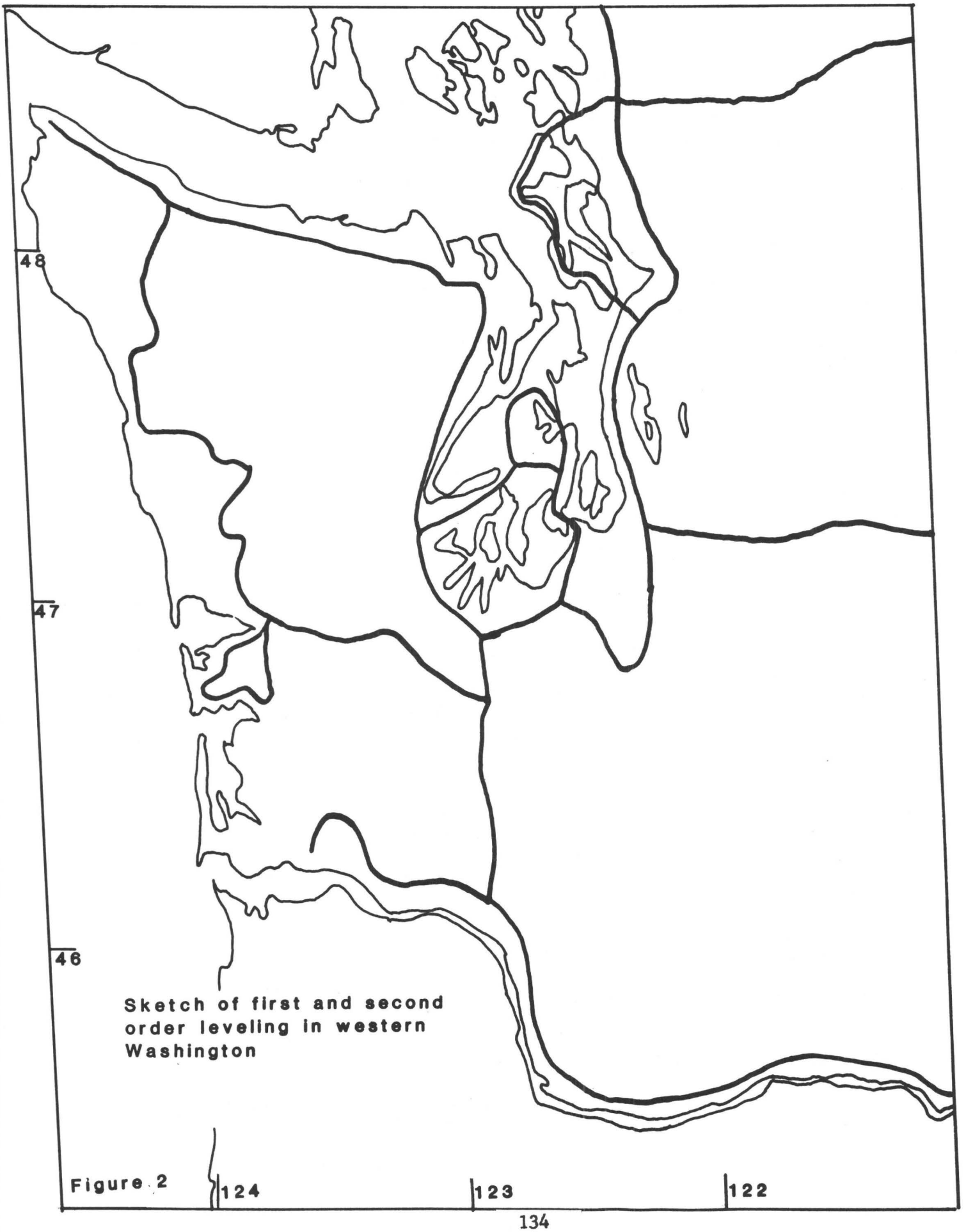


Sketch of first and second order leveling in western Washington

Figure 2

Any tilt in western Wasington should reflect tectonism and not isostatic rebound from past ice loading during the Pleistocene glaciation (Mathew, Fyles, and Nasmuth, 1970) since the rebound in the region was essentially complete some six to seven thousand years ago. Precision leveling is one means of outlining areas of relative present day tectonic activity. This approach is rather costly when first- and second-order leveling are the only tools. Alternatively, repeated measurement of a gravity network can give information on vertical crustal movement if a suitable gravity reference can be found (Whitcomb, 1976).

Study of the distribution in time and space of seismicity in Japan has led to the discovery that changes in the level of the land surface are associated with the occurrence of seismicity. For example, Hagiwara and Rikitake (1967, figure 2) suggest a precursive connection in time of changes in land level and the occurrence of a major seismic event at Niigata. As a result of such observations, the government of Japan intends to run 20,000 kilometers of first-order level surveys embracing all of Japan every five years.

## Present Study

The Geophysics Program at the University of Washington has installed approximately fifty gravity bench marks (Figure 3). They have all been installed on solid bedrock and are next to paved county, state, or federal highways for easy access and rapid reading.

With a LaCoste & Romberg D meter we have recorded over 30 days of continuous earth-tide data at four separate locations in western Washington and have compared this recorded data with a theoretical earth-tide program we have used for past gravity studies. The recorded earth-tide was filtered by a low pass filter having a cutoff of 0.001 Hz to eliminate high frequency noise. The comparison shows only a small phase shift most likely a result of ocean loading. The discrepancy is generally about five to ten microgals; however, at times when the tidal effect is large, the error can be as much as twenty to thirty microgals.

In our present study, we are investigating the phase change and are determining appropriate earth tidal corrections for the western Washington area. The objective of this is to provide an accurate gravity determination and thus improve the chance of observing relative vertical movement in the region.

With our own LaCoste & Romberg G-type and D-type meter borrowed from the U.S. Army Corps of Engineers, selected loops on the previously mentioned gravity bench marks have been run. The results of these readings show that the D meter we used was not stable; in spite of careful car transportation, we experienced short-term (i.e., less than one hour) drift almost twice that of our own G- type meter. Both meters are extremely stable when not being transported. During the four separate 30 or more days recordings of earth tides, there was no apparent drift like the type observed during the occupation of our own gravity stations. See Figure 4 for comparison drift during one day's readings.

After several years of attempting to carry out this project, we have

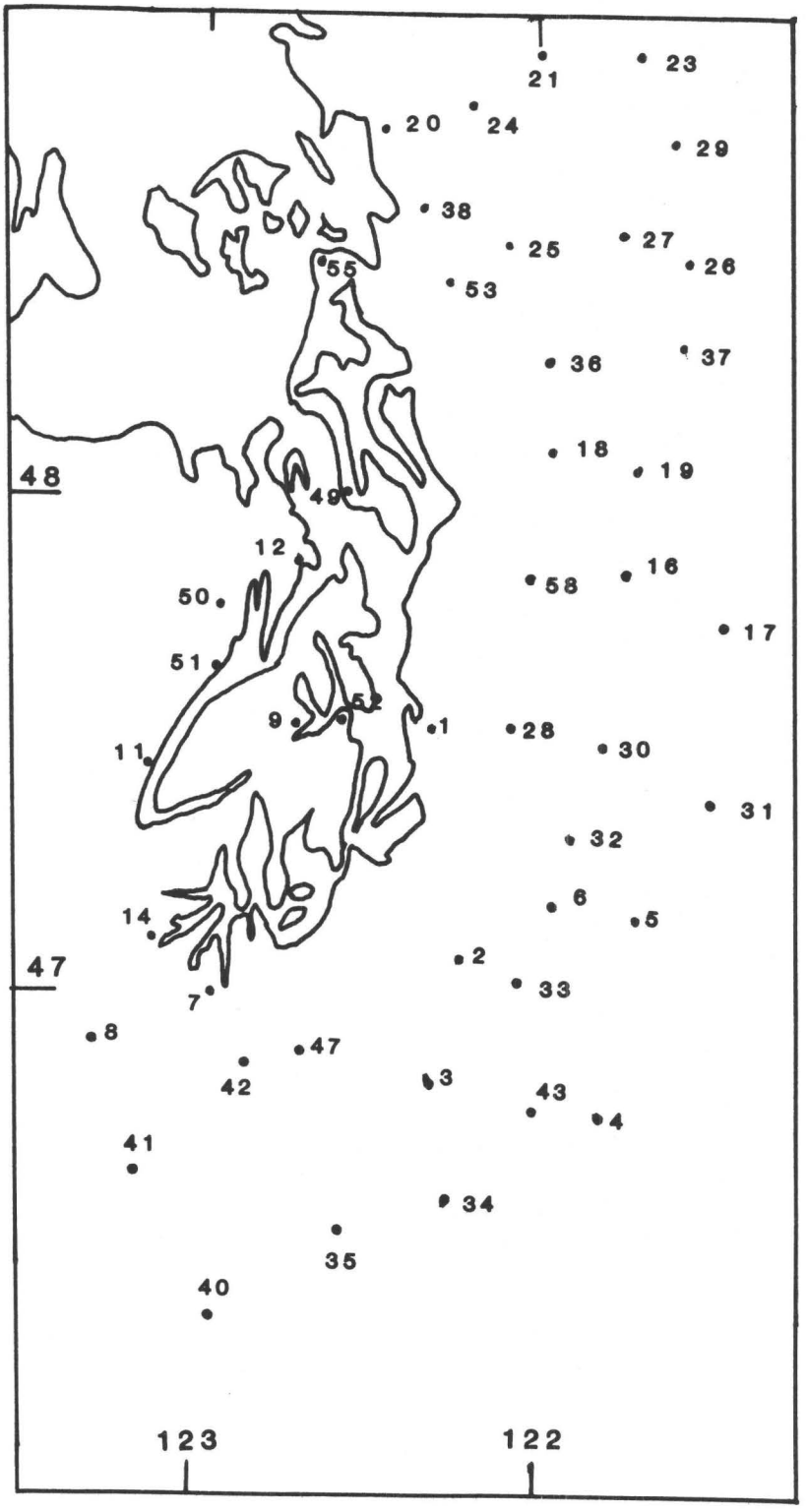


Figure 3

Location of gravity bench marks in western Washington

concluded that suitable data cannot be obtained with borrowed equipment. We have purchased our own D-type LaCoste & Romberg gravity meter so that stability can be assured through careful calibration and proper handling. With our own D-type meter the short-term drift due to transport can be reduced to about $\pm$ 0.010 milligals, we can theoretically see elevation changes at our gravity bench marks of $\pm$ 3 cm. We have decided on two possible methods of occupying our established gravity stations. The first is the much used method of looping (i.e., observe station 1, ahead to station 2, looping back to 1, then on again to 2, then on to 3, back to 2, ahead to 3, on ahead to 4, and etc.) This method was used during some test runs and was found to be relatively slow but acceptable. We found that we could complete four stations in a 12- to 15-hour day.

A second and much faster method is with an established base station. This method is to start at the base station and then proceed to observe station 1, back to the base station, then to station 2, back to base, on to 3, back to base, and etc. With this second method, six to seven stations can be included in one day, including the base station.

The second method would be accomplished using our G meter, our new D meter, and using the previously borrowed D meter as a continuous recording base station where it appears to be stable enough if not transported. We will install a recording gravity meter at the base station in order to continuously record the real earth-tide for that area in which we are working so as to include the effects of ocean loading which cannot be fully accounted for using theoretical earth-tide corrections.

In order to occupy the fifty stations using method one, it would take 30 days in the field. Each loop is tied to two adjacent loops. Using the second method it takes 17 days. The second method is superior for two reasons. First, meter transport time per day is actually reduced, and by being able to observe all the stations in 17 days, the entire net could be occupied in a shorter time and less miles driven. Secondly, the tide correction would be from the actual observed earth-tide recorded at the base station.

We are going to reoccupy these easily accessible bedrock bench marks each year for several years until we can determine if elevation changes are actually occurring. At a time when we may see elevation changes, we expect to redesign the network to focus on these specific regions. We have spent much time and effort installing gravity bench marks on solid bedrock and then trying different approaches to occupy and reduce the data received. This has been accomplished over the last three years. We now feel that we will be able to see elevation changes, if they are occuring by the methods outlined above.

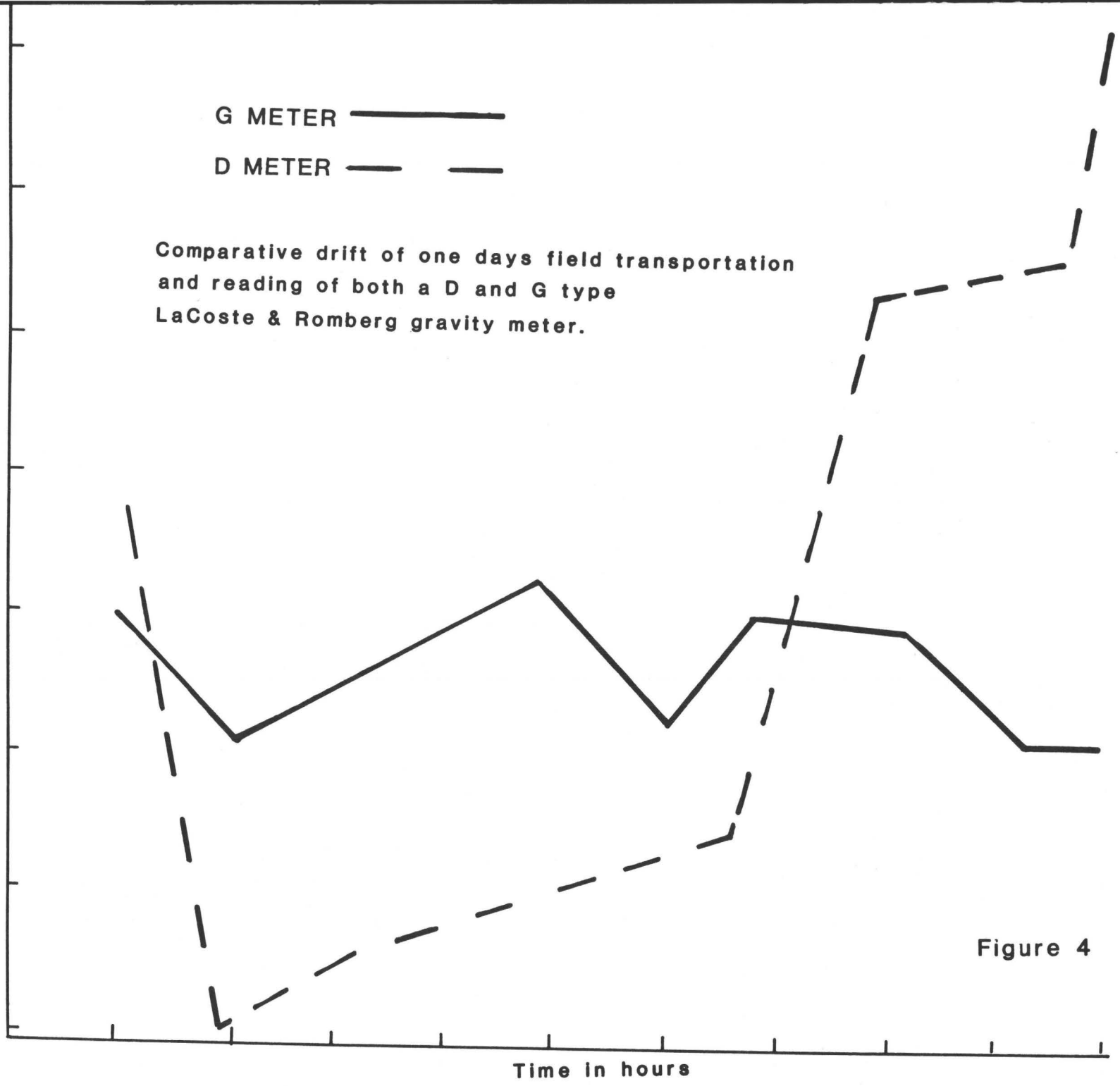
G METER
D METER
Comparative drift of one days field transportation
and reading of both a D and G type
LaCoste & Romberg gravity meter.
Drift in .025 milligal units
Time in hours

Figure 4

REFERENCES

Algermissen, S. T. and Harding, S. T., Preliminary seismological report,in Steinburgge, K. and Cloud, W., Preliminary engineering report: The Puget Sound, Washington earthquake of April 29, 1965: U. S. Dept. Commerce, U. S. Coast and Geodetic Survey, 1965.

Berg, J. W. and Baker, C. D., Oregon earthquakes, 1841 through 1958: Seis. Soc. Amer. Bull., v.53, no 1, p. 95-108, January, 1963.

Bonni, W. E., Hughes, D. W., and Danes, Z. F., Complete Bouguer gravity anomaly map of Washington: Washington Dept. Natural Resources, Olympia, Washington, 1974.

Bostrom, R. C., Couch, R. W., Rasmussesn, N. H., and Sherif, M. Level Changes and the incidence of seismicity in the Puget Sound area: Trend in Engineering, v. 20, p. 4-10, April, 1968.

Bowie, W., Isostatic investigations and data for gravity stations in the United States established since 1915: U. S. Coast and Geodetic Survey Spec. Pub. 99, 1924.

Campbell, C. D., Washington Geology and Resources Information Circular, No. 22R, Washington Dept. Conservation, 1962.

Castle, R. O., Alt, J. N., Savage, J. C., and Balazs, E. I., Elevation changes preceding the San Fernando earthquake of February 9, 1971: Geology, v. 2, p. 61-66, 1974.

Coombs, H. A., A summary of Washington earthquakes: Seis. Soc. Amer. Bull., v. 43, no. 1, p. 1-6, January 1953.

Couch, R., Preliminary observations of temporal gravity variations in the Puget Sound regions (abstract): Amer. Geophys. Union Trans., v. 47, no. 4, p. 629, 1967.

Crandell, D. R., The glacial history of western Washington and Oregon: Int. Assoc. Quaternary Res., Review Vol. for VIII Congress, Part I, 1965.

Crosson, R. S., Small earthquakes, structure, and tectonics of the Puget Sound Region: Seis. Soc. Amer. Bull., v. 62, no. 5, p. 1133-1172, October 1972.

Danes, Z. F., Bonno, M., Brau, E., Gilbram, W. D., Hoffman, T., Johansen, D., Malfait, M., Masten, J., and Teague, G., Geophysical investigations of the southern Puget Sound area, Washington: Jour. Geophys. Res., v. 7, 1965.

Danes, Z. F., Gravity surveys in western Washington: Amer. Geophys. Union Trans., v. 49, 1968.

Danes, Z. F., Gravity results in western Washington: Trans. Am. Geophys. Union, v. 50, no. 10, p. 548-550, 1969.

Dehlinger, P. E., Chiburis, E. F., and Collver, M. N., Local travel-time curves and their geologic implications for the Pacific Northwest states: Seis. Soc. Amer. Bull., v. 55, p. 587-607, 1965.

Easterbrook, D. J., Pleistocene chronology of the Puget lowland and San Juan Island, Washington: Geol. Soc. Amer. Bull., v. 80, 1969.

Hagiwara, T. and Rikitake, T., Japanese program on earthquake prediction: Science, v. 157, p. 761-768, 1967.

Hall, John B. and Othberg, Kurt L., Thickness of Unconsolidated Sediments, Puget Sound Lowland, Washington, Geologic Map GM-12, Dept. of Natural Resources, Olympia, WA, 1974.

Hudson, D. E., Local distribution of strong earthquake ground motions: Seis. Soc. Amer. Bull, v. 62, no. 6, p. 1765-1786, December, 1972.

Mathew, W. H. Fyles, J. G., and Nasmuth, N., Post glacial crustal movements in southwestern British Columbia and adjacent Washington State: Canad. Jour. Earth Sci., v. 7, no. 2, p. 690-702, 1970.

Neumann, F., Crustal structure in the Puget Sound area: Publications de

Bureau Central Seismologique International, Ser. A Tranaux Sci., Fasc. 20.

Oliver, H. W., Robbins S. L., Grannell, R. B., Alewine, R. W., and Biehler, Shawn, in press, Surface and subsurface movements determined by remeasuring gravity, Chap. 10 (p. 195-211 in Oakshott, G. G., (Ed.), San Fernando earthquake of Feb. 9, 1971): Calif. Div. Mines and Geology Bull. 196.

Rasmussen, N. H., Washington State earthquakes 1840 through 1965: Seis. Soc. Amer. Bull., v. 57, no. 3, p. 463-475, June, 1967.

Rasmussen, N. H., Millard, R., and Smith, S., Earthquake hazard evaluation of the Puget Sound region, Washington State: Univ. Washington Press, 1974.

Rogers, W. P., Geological and geophysical study of the central Puget Sound lowland: Univ. Washington Thesis, 1970.

Stewart, D. J., Gravity study of crustal structure in western Washington: U. S. Geol. Survey Prof Paper 424-C, p. C-273-276, 1961.

Tatel, H. E., and Tuve, M., Seismic exploration of a continual crust: Crust of the Earth: Geol. Soc. Amer. Spec. Paper 62, p. 35-50, 1955.

U. S. Air Force, Gravity select report no. 2101, D.O.D.: Gravity Series Branch, 1973.

U. S. Geological Survey, A Study of Earthquake Losses in Puget Sound, Washington, Area Open File Report 75-375, 1975.

Whitcomb, James H., New vertical geodesy, Jour. Geoph. Res., 4937-4944, September, 1976.

# HORIZONTAL TECTONIC STRESS DURING THE LATE CENOZOIC IN THE NORTHWESTERN UNITED STATES

Kenneth F. Fox, Jr.
U.S. Geological Survey, Menlo Park, CA 94025

and

David C. Engebretson
U.S. Geological Survey, Menlo Park, CA 94025
and
Dept. of Geophysics, Stanford University, Stanford, CA 94305

## ABSTRACT

The Miocene through Holocene tectonic stress pattern in northwestern United States, as deduced from the orientation of folds, basin-and-range structures, and from photoelastic modeling, is dominated by a set of principal compressive stress trajectories radiating horizontally outward to the north, east, and southeast from the contact of the North American plate with the Juan de Fuca plate. A second set, located farther to the east, sweeps out of the northeast and curves to a southward trend at the southern limit of the study area.

The fold and fault pattern indicates that an isotropic point was located in north-central Oregon during much of the late Cenozoic. The isotropic point probably shifted position as the direction of spreading of the Juan de Fuca plate with respect to the Pacific plate changed from eastward, parallel to the Mendocino fracture zone, to east-southeastward, parallel to the Blanco fracture zone. Sets of folds recording different stress trajectories in south-central Washington may result from superposition of the stress patterns developed during the periods of relative dynamic stability before and after this change in direction of sea-floor spreading.

Comparison with photoelastic modeling suggests that the observed stress pattern reflects a compressive force transmitted across the contact between the Juan de Fuca plate and the North American plate. Furthermore, this force must have been applied in a direction at least roughly comparable to the direction of relative motion between these two plates, rather than to that of the relative motion between the Pacific and North American plates.

The study area is classified into three structural domains, depending on the inferred magnitudes of the two horizontal principal tectonic stresses relative to each other and to the vertical tectonic stress. Tectonic stress is here defined as being roughly equivalent to the difference between actual stress and the stress in a conceptual standard state in which stress is due solely to the lithostatic load. In the Puget Sound area of northwestern Washington, both the maximum and minimum horizontal tectonic stresses exceeded the vertical tectonic stress during Holocene time. The area also seems to correspond to a zone of high shear stress which originates at the triple

junction near Vancouver Island and fades out along its southeast trend in northwestern Washington.

We speculate that future deformation of the Puget Sound area will form a conjugate set of diagonal-slip shear faults with a component of reverse slip, striking roughly 30° to either side of the maximum horizontal principal-stress trajectories. At the east and south boundaries of the Puget Sound area, there should be a transition to a tectonic style characterized by thrust or reverse faults striking orthogonal to the trajectories of the principal horizontal tectonic stress.

## INTRODUCTION

This study deduces the orientations of the principal horizontal components of tectonic stress in northwestern Washington, as they existed from Miocene through Holocene time, using the orientation of geologic structures of those ages as guides. Because the stress pattern in this area is probably sensitive to forces transmitted across the nearby boundary between the North American and Juan de Fuca plates, it seemed desirable to include within the area of interest the entire region immediately east of the Juan de Fuca plate. Hence, the study area was enlarged to include Washington, Oregon, and northern California (Fig. 1).

The data base becomes larger the farther back in time the analysis is extended, but so does the risk of superimposing deformational features produced in unlike tectonic settings and unlike stress fields. In choosing the beginning of the Miocene as the older limit, several large gaps appear where data are absent or scanty, most notably in northwestern California and northern Washington. Hence, photoelastic analogs of the Juan de Fuca-Pacific-North American plate junction were used to improve our estimate of the orientation of stress trajectories in these gaps, and also better to understand how the stress pattern relates to regional plate geometry.

## PREVIOUS WORK

Zoback and Zoback (1980) reviewed seismic, *in situ*-, and geologic evidence of stress orientation within the conterminous United States. The reader is referred to their study for an account of previous work within the region. Their compilation of Pliocene and younger stress indicators shows a west-southwest orientation of the least horizontal stress direction during this time in western Washington and northwestern California, and west-northwest in Nevada. The latter orientation is consistent with late Cenozoic extension in Nevada and adjacent parts of Utah, as documented by Stewart (1980). Zoback and Thompson (1978) report fairly convincing evidence that in central Nevada the least compressive stress rotated 45° or so from west-southwest to the present west-northwest direction between 15 and 6 m.y. B.P. In Arizona, the least compressive stress was oriented roughly east-northeast in late Cenozoic time (Rehrig and Heidrick, 1976, p. 210).

The orientation of the principal horizontal stresses in California was discussed by Stone (1970), who concluded that the direction of maximum compression shifted from east-northeast to the present northward direction during the Eocene. In Idaho, Furlong (1979) chose a direction of maximum compression of northeast on the basis of orientation of such late Tertiary

features as normal faults, and the nodal planes of earthquake fault-plane solutions. In southeastern Washington and northeastern Oregon, Taubeneck's (1970) analysis of trends of dikes indicates that the direction of maximum compression was northerly. In western Washington, Crosson (1972) concluded, on the basis of earthquake fault-plane solutions, that the present direction of maximum compression is northerly.

Analytical solutions for horizontal stresses in the entire lithosphere were reported by Solomon, Sleep, and Richardson (1975). Their study indicates that a northerly orientation of the principal horizontal stress in the part of the North American plate we identify with British Columbia and the northwestern United States is consistent with world-wide plate velocities and currently popular models of the driving forces.

The photoelastic method has previously been applied to studies of the San Andreas fault by Nikonov and others (1975), and to the region in the vicinity of the triple junction at Cape Mendocino by Fox (1979).

## CRUSTAL MODEL

We assume that the upper part of the lithosphere--perhaps the upper 10-30 kilometers--constitutes a relatively strong elastic shell within which most of the horizontal loads within the entire lithosphere are supported (Kusznir and Bott, 1977). Within this shell stresses are resolvable into principal stresses of varying magnitude. Below this shell, the lithosphere is probably ductile, deforming by flow on a geologically short time-scale (Kusznir and Bott, 1977).

## DEFINITION OF TECTONIC STRESS

In the following discussion, we borrow heavily from Anderson (1942), Hafner (1951), Couples (1977), and Greiner and Illies (1977). We assume that there is a standard state of stress within the elastic upper part of the lithosphere. In this standard state, the only force producing stress is the gravitational attraction of the Earth. Hence, one principal stress direction (z) is vertical, with magnitude at any depth of

$$S_z = p\underline{g}z$$

where $\underline{g}$ is the acceleration due to gravity and p is the average density of the lithosphere from the surface to a depth z. In other words, the vertical stress in this standard state is equivalent to that caused by the lithostatic load.

The other principal stress directions (x and y) at a given point are horizontal and of equal magnitude. We define the standard state to be that in which the strains in the x and y directions within this elastic body are zero. The lateral support necessary to so confine a segment of this lithosphere will be provided if the horizontal principal stresses

$$S_x = S_y = \frac{u}{1-u} \cdot S_z$$

where u is Poisson's ratio. If, for example, a value of 0.25 is assumed for u (Hafner, 1951; Couples, 1977), the horizontal stresses in this standard state would be 1/3 the vertical stresses. However, Anderson (1942) and Hafner (1951) take 0.5 to characterize their standard state, at which value the horizontal and vertical stresses are equal.

In the real world, we observe places where the lithosphere has thinned through extensional faulting, and other places where it has thickened through folding and thrust faulting. Hence we infer that in places the actual horizontal stresses must be less than--and in other places greater than--this hypothetical standard state. We suppose that this difference between the standard state and the actual stress is caused chiefly by application of what we loosely refer to as tectonic forces. If so, the actual stress at a given point in this elastic upper part of the lithosphere contains a component representing the standard state, plus increments representing tectonic stress and incidental stresses--the latter including residual stresses and stress resulting from minor density inhomogeneities, topographic irregularities, and so on.

The incidental stresses are those stresses which are both self-canceling within a given region and of too small a magnitude measurably to influence the development of geologic structures. We define tectonic stress to be

$$S_{Tect} = S_{Actual} - (S_{Standard\ state} + S_{Incidental})$$

As defined, the incidental stresses are small, and in many regions--specifically the region here considered--they can be ignored. Hence,

$$S_{Tect} \cong S_{Actual} - S_{Standard\ state}$$

To make a concise statement of general applicability about what tectonic stress is and how it originates is more difficult. Within the region of interest here, we identify the tectonic stress as being that part of the actual stress which originates as body forces within and outside the region and is transmitted by end loads and tractions from, to, and through the elastic part of the lithospheric plate within the region.

The actual stress at a given point will ordinarily be resolvable into the three principal components $S_{ax}$, $S_{ay}$, and $S_{az}$. Presuming that the tractions at the base of the elastic layer in the lithosphere are small relative to end loads, and that the thickness of this part of the crust is small relative to its lateral extent (for example, 20 km versus 500-2500 km or more), $S_{az}$ will be approximately vertical and $S_{ax}$ and $S_{ay}$ approximately horizontal. That being so,

$$S_{az} \cong S_z = \rho g z$$

and

$$S_{ztect} \cong S_{az} - S_z \cong 0$$

That is, the vertical component of tectonic stress will ordinarily be close to zero. On the other hand,

$$S_{xtect} \cong S_{ax} - \frac{u}{1-u} \cdot S_z$$

and $$S_{ytect} \tilde{=} S_{ay} - \frac{u}{1-u} \cdot S_z$$

That is, the horizontal components of tectonic stress are approximately equal to the difference between the actual horizontal stress and the part of the stress elastically contributed by the lithostatic load.

A hypothetical example may help illustrate what we have in mind. Suppose that at some point at a depth of 10 km in this elastic part of the lithospheric plate the actual principal stresses are:

$$S_{ax} = 900 \text{ bars}$$

$$S_{ay} = 800 \text{ bars}$$

$$S_{az} = 2650 \text{ bars}$$

Given that the density (p) equals 2.7 g/cm$^3$, and acceleration due to gravity ($\underline{g}$) equals 9.8 x 10$^2$ cm/sec$^2$, then

$$S_z = (2.7)\ (9.8 \times 10^2)\ (10^6) \text{ dynes/cm}^2 = 2646 \text{ bars}$$

Hence $S_{ztect} = 2650 - 2646 \cong 0$

Assuming further that Poisson's ratio (u) of this material is 0.25,

$$S_{xtect} \cong 900 - (1/3)\ (2646) \cong + 20 \text{ bars}$$

$$S_{ytect} \cong 800 - (1/3)\ (2646) \cong - 80 \text{ bars}$$

The principal horizontal tectonic stresses of 20 bars annd -80 bars in this example seem small, but are probably realistic if the stress drops measured in earthquakes--commonly on the order of 10 to 100 bars (Caputo and Console, 1980)--represents total or near total release of the tectonic stress (Raleigh and Evernden, 1980).

The horizontal components of tectonic stress may be positive, zero, or negative. Assuming that, in general, the horizontal components will be unequal, we identify the larger as $S_{hmax}$ and the smaller as $S_{hmin}$. Five cases appear to be particularly relevant, as follows:

Case 1; $S_{hmax} > S_{hmin} > 0$

Case 2; $S_{hmax} > S_{hmin} = 0$

Case 3; $S_{hmax} > 0 > S_{hmin}$

Case 4; $S_{hmax} = 0 > S_{hmin}$

Case 5; $0 > S_{hmax} > S_{hmin}$

The structural geometries we observe within the region and their inferred correlation with the five cases listed above are shown in Figure 2. The correlation is based on the assumption that the direction of maximum crustal extension (or thickening, in response to compressional stress) implied by

these structures will be the direction of minimum tectonic stress. In Case 1, contraction in both of the principal horizontal tectonic stress directions is compensated by vertical extension. In Case 2, contraction in the direction of maximum horizontal tectonic stress is compensated by crustal extension both vertically and in the direction of minimum horizontal tectonic stress. In Case 3, contraction in the direction of maximum horizontal tectonic stress--and, to a lesser extent, in the vertical direction--is compensated by crustal extension in the direction of minimum horizontal tectonic stress. In Case 4, contraction in the direction of maximum tectonic horizontal stress and also vertically is compensated by crustal extension in the direction of minimum horizontal tectonic stress. In Case 5, vertical contraction is compensated by crustal extension in the direction of minimum horizontal tectonic stress, and to a lesser extent, also in the direction of maximum horizontal tectonic stress.

The five cases outlined above are not all-inclusive. We do not treat, for example, the situation where forces at the boundary or at the base of a given region exert a net horizontal torque (possibly causing development of throughgoing wrench faults).

## TECTONIC SETTING

The evolution and stability of the stress pattern during the late Cenozoic in that part of the North American plate occupied by southernmost British Columbia, Washington, Oregon, and northern California are closely tied to the manner in which the plate configuration of this region evolved during this time. As is now well known, this region abuts and is being underthrust by the Juan de Fuca plate along an ill-defined subduction zone (Fig. 1)--a subduction zone terminating to the south at a triple junction at Cape Mendocino and to the north at a triple junction near Vancouver Island. South of the Mendocino triple junction and north of the Vancouver triple junction, the North American plate contacts the northwestward-moving Pacific plate along right-lateral faults, the San Andreas fault to the south, and the Queen Charlotte fault to the north. Because of the differing directions of movement of the three plates--North American, Juan de Fuca, and Pacific--stresses generated through tractions at their mutual contacts are expected to have radically different directions and magnitudes.

Stresses generated by tractions at the base of lithospheric plates are probably small relative to those transmitted across plate boundaries (Melosh, 1977). We therefore assume that the stress pattern in small plates and in small parts of larger plates is dominated by stresses originating outside the region. In particular, we assume that the stress pattern in the region under consideration is dominated by stresses transmitted through or into the region from across the plate boundaries on the west and from the greater expanse of the North American plate to the east.

For these reasons, the stress pattern within the region is probably quite sensitive to changes in relative movement and configuration of the Juan de Fuca plate, and particularly to the location of its bounding triple junctions. As explained by Atwater (1970), the Juan de Fuca plate formed through splitting of the Farallon plate after about 30 m.y. B.P. (by the time scale of LaBreque and others, 1977) when that part of the Pacific plate south

of the Mendocino fracture zone first contacted the North American plate. Subsequent steady (according to the constant-motion model of Atwater, 1970) or unsteady (Atwater and Molnar, 1973) northwestward movement of the Pacific plate relative to the North American plate brought the triple junction formed by this contact and marking the southern termination of the Juan de Fuca plate to its present position at Cape Mendocino.

The history of the northern triple junction is both more complex and more controversial. Part of the complexity results from the apparent growth at the northern tip of the Juan de Fuca plate of a small independent plate called the Explorer plate (Riddihough, 1977; Hyndman, Riddihough, and Herzer, 1979). Part of the controversy stems from contradictory views of whether the triple junction at the northern tip of the Juan de Fuca plate moved southeastward or northwestward during the Tertiary. Atwater's (1970) reconstruction, if taken literally in spite of her disclaimers, implies that this triple junction moved southeastward, traversing the entire western coast of British Columbia.

Had the triple junction moved southeast, however, a convergent tectonic regime with subduction zone and coeval volcanic arc should have prevailed in western British Columbia throughout much of the Tertiary time. The apparent absence of subduction-related volcanic rocks of Tertiary age within this area--except for extreme southwestern British Columbia--indicates that the boundary between this part of the North American plate and oceanic plates to the west was a strike-slip fault, not a subduction zone. Moreover, Riddihough's (1977) analysis of the spreading history of the Explorer plate indicates that the triple junction forming its northern tip--a ridge-transform fault-subduction zone triple junction--was nearly stationary about 10 m.y. ago, remained so for about 5 m.y., then began moving slowly northwestward, accelerating to 1.8 cm/year in the late Pliocene. A triple junction may remain stationary if spreading at the ridge adds sufficient new oceanic crust exactly to offset northwestward movement of the Pacific plate along the Queen Charlotte fault.

Fox (in press) has correlated the formation of the melanges of the Olympic Peninsula of early and middle Miocene age with transit of the triple junction formed through intersection of the Aja fracture zone (See Naugler and Wageman, 1973) and the Queen Charlotte fault between roughly 22 and 16 m.y. ago. This triple junction was by necessity a transform-transform-subduction zone triple junction and hence could not remain stationary; it must have moved northwestward with the Pacific plate, causing the subducted slab following the triple junction to plow up the adjacent part of the North American plate (Fox, 1976). Equating the Olympic melanges with the products of this process places the triple junction near its present position off the coast of northern Washington and southern British Columbia about 16 m.y. ago. Hence it seems likely that this triple junction has been near its present position since the middle Miocene, and that before that time a radically different tectonic situation prevailed.

Magnetic anomalies within the Juan de Fuca plate and adjacent parts of the Pacific plate reveal one and possibly more significant changes in spreading direction since the middle Miocene (see maps by Raff and Mason, 1961, and Atwater and Menard, 1970). The greatest change took place when the Juan de Fuca plate veered some 20° or so from an eastward course (relative to

the Pacific plate), parallel to the Mendocino fracture zone, to an east-southeastward course (Menard and Atwater, 1968).

Menard and Atwater (1968) correlate this change in direction of sea-floor spreading with the formation of anomaly 4, which occurred about 7 m.y. ago according to the time scale of LaBreque and others (1977). The Blanco fracture zone, however, which formed as a result of this change in spreading direction, seems to be traceable through anomaly 5, indicating that the spreading direction had begun to change by 10 m.y. ago.

## STRUCTURAL DOMAINS AND STRESS PATTERN

In Figure 1, we present a compilation of fold axes, axial trends of basin and range structures, and selected volcanic alinements within the study area. The structures shown involve Miocene or younger rocks. Thus, we include structures formed in rocks as old as about 22 m.y. We would have preferred to limit the compilation to structures developed in rocks not older than 16 m.y., to avoid including structures developed during the catastrophic formation of the melanges of the Olympic Peninsula in early Miocene. We partially correct for this problem by omitting entirely all structures within the Olympic Peninsula. The overall pattern is fairly coherent, though problem areas exist, of which the most notable are areas of interfering folds in south-central Washington and east-central Oregon.

Also outlined (Fig. 1) are structural domains I-III, corresponding to cases I-III outlined above. The analysis is in part based on structural details shown in the reports from which the data are taken, which could not be shown at the scale of Figure 1. Furthermore, the outline of these domains is partly based on our expectation that transition between domains should be gradual; domain I should not abut domain III.

South-central Washington and adjacent parts of Oregon appear to exemplify domain II. Here the Columbia River Basalt Group is folded into a series of well-defined anticlines and synclines with reverse faults striking parallel to the axial traces of the folds (Newcomb, 1970). Locally, strike-slip faults transect the folds at angles of $60^{\circ}$ to $80^{\circ}$ from the fold axes.

Southeastern Oregon probably exemplifies domain III. In this area, elongate basins are faulted down against the intervening ranges on conjugate northwest- and north-northeast trending fault sets (see Walker, 1977). The fault sets were contemporaneous and movement occurred concurrently along both sets (Donath, 1962; Lawrence, 1976). Though the latest movement was dip slip, Donath cites evidence of horizontal offsets of 500 to 1500 ft (1962, p. 5) and reasons that this offset occurred during an episode of strike-slip movement--in response to north-south compression--prior to the dip-slip movement. According to our model of stress domains, a component of strike-slip movement on some of the faults is required in order to produce north-south contraction of the crust concurrent with its east-west extension. Faults in a part of west-central Nevada that we equate with domain III form a conjugate set of diagonal slip faults having components of both strike slip and normal dip slip (Thompson and Burke, 1973), and so provide an analog to the situation in southeastern Oregon.

An example of domain V can be found in southeastern California, south of our study area (south of the map area shown in Fig. 1). In the part of California between the Garlock and San Andreas faults (see Jennings, 1977) the reticulate or grid pattern of basin-and-range structures indicates crustal extension in the direction of both of the principal horizontal tectonic stresses.

## PHOTOELASTIC EXPERIMENTS

In the experiments reported here, two-dimensional models of the mutually contiguous parts of the Pacific, Juan de Fuca, and North American plates were constructed using gelatin as the photoelastic medium. Gelatin can be used to analyze stress because it is optically isotropic where unstressed, but is anisotropic where stressed. Hence, when plane-polarized light is transmitted through the stressed gelatin and viewed through an analyzer, interference colors are produced whose order is proportional to the magnitude of the shear stress (Frocht, 1941).

The apparatus (Fig. 3) is simple but effective. An ordinary light table was used as a source of white light, with appropriate filters functioning as polarizer and analyzer. The model is contained within an aluminum enclosure with a glass window at the base. The parts of the three lithospheric plates of interest are represented by a layer of gelatin about 15 to 25 mm thick, cast within this enclosure and segmented so as to represent the surface geometry of the area of intersection of these three plates. To eliminate tractions at the base of the plates, the gelatin floats upon a thin layer (5-10 mm thick) of liquid composed of sodium disilicate (water glass) diluted with water. A rubber-band-powered piston drives the "Juan de Fuca" plate (JDF) in the desired direction (for example, S. 65° E., the orientation of the Blanco fracture zone), and a second piston embedded in the "North American" plate (NAP) drives this plate southward with respect to the "Pacific" plate (PP).

The contact between the "Pacific" plate and the "North American" plate represents the San Andreas fault (SAF) on the southeast and the Queen Charlotte fault (QCF) on the northwest. This contact is modeled as a straight, vertical plane to eliminate stress concentrations that might be produced solely by irregularities in the fault surfaces. Because boundary conditions on the east and south sides of the region are not specified, these boundaries in the model were established at considerable distance from the area of interest, and stresses on them were kept small.

Several gelatin formulations were used, including various proportions of water, gelatin, and ethylene glycol (antifreeze). All the mixtures were prepared by combining their respective constituents and heating until a clear liquid was obtained, which was then poured into an enclosure of appropriate shape. After cooling and gelling, the gelatin slabs were emplaced over the water glass, the pistons actuated, and the resulting stress pattern photographed at intervals through a 90° rotation of the stage.

Though the various gelatin mixtures differ significantly in modulus of elasticity and photoelastic sensitivity (see Farquharson and Hennes, 1940), the stress patterns obtained were similar. The 85 percent water-15 percent (by weight) gelatin mixture was considered the best because it is easy to

prepare, has high transparency, and is sufficiently strong to withstand the necessary handling. However, it is less than ideal, in that it does degrade where it contacts the waterglass, so once begun, the experiment must be conducted quickly.

## MODEL SIMILARITY

The model is scaled so that the distance between MTJ and VTJ represents the distance between the Mendocino triple junction and the Vancouver triple junction. Angular relations are the same as those in nature, except that the contact between PP and JDF is given either the azimuth of the Blanco fracture zone or that of the Mendocino fracture zone. In summary, the model is considered geometrically similar (as defined by Hubbert, 1937, p. 1466) to a much stylized version of the area of intersection of the Pacific, Juan de Fuca, and North American plates.

The applicability of the modeling experiments is limited by the degree to which the stress distribution in lithospheric plates can be approximated by a two-dimensional stress system. As noted previously, it is assumed that the lateral dimensions of lithospheric plates are large relative to their thickness and that the plates are elastic bodies floating on a viscous substratum. It is further assumed that basal tractions are small relative to end loads. If these assumptions are correct, then it is probable that the horizontal components of the regional tectonic stress distribution within the plates can be approximated by a two-dimensional stress system. However, this generalization does not hold in certain areas where the plate geometry clearly requires a three-dimensional representation. For example, the contact between JDF and NAP, modeled as a vertical plane, represents an inclined subduction zone in nature. Hence, the stress distribution in the immediate vicinity of this contact must be considerably more complex than is suggested by the model.

Frocht (1948, p. 174-201) has experimentally verified that "...in plane problems dealing with simply connected bodies subjected only to known boundary forces the stresses are independent of the physical constants of the material" (Frocht, 1948, p. 199). In the experiments reported here, however, the ability to achieve a given boundary condition does depend in part on the thickness and physical properties of the gelatin layer and also on the nature of the lubricating substance. The similarity of these materials to their natural counterparts is unknown. Furthermore, the magnitudes of neither the actual boundary forces nor the friction along the actual San Andreas and Queen Charlotte faults are known. For these reasons, no claim is made that the model is dynamically similar (as defined by Hubbert, 1937, p. 468). Finally, the model represents a static situation, so that time is not a factor in the model similarity.

## RESULTS

With JDF driven S. 65° E. and NAP driven southward against PP, shear stress concentrations form near VTJ and MTJ (Fig. 4). In the stress pattern depicted in Figure 4, the black band passing through I is an isoclinic, representing the loci of points at which the tangents to the principal stress trajectories are parallel to the optic directions of the analyzer and polarizer, here oriented north-south and east-west, respectively. As the model is rotated through 90° in the horizontal plane, the isoclinic sweeps

across the field and shows the orientation of the stress trajectories throughout the entire field. The isotropic point (I) remains dark during this rotation.

The map (Fig. 5) shows that the stress trajectories sweep around the isotropic point, and form a complex pattern of curved lines. At the isotropic point the stress is hydrostatic, that is, the shear stress is zero and the magnitude of the horizontal stress is the same in all directions. The position of this point can be varied by varying the forces applied by the pistons or by varying the direction of movement of JDF.

## INTERPRETATION

Figure 6 shows the trajectories of maximum horizontal tectonic stress existent during the formation of most of the late Cenozoic structures within the study area. In constructing this figure, we assumed that the maximum stress was (1) orthogonal to fold axes, (2) parallel to the long axis of the extensional valleys of the Basin and Range province, and (3) parallel to the alinement of recent volcanic vents and dikes. The presence of areas of interfering folds and discordant structures indicates that the stress pattern revealed by these trajectories is a composite of two or more distinct patterns.

The observed (Fig. 6) and experimental (Fig. 5) stress patterns are dominated by a group of principal compressive stress trajectories that radiate inland from the Juan de Fuca-North American plate boundary. Farther inland, a second group sweeps out of the north-northeast and, curving to a more north-south trend, extends through the southern margin of the region. The stress trajectories veer away from an isotropic point located east of JDF (the analogue of the Juan de Fuca plate) in the model studies and in north-central Oregon (Fig. 6) in the observed pattern.

The similarities between the modeled and observed stress patterns support the conclusion that the observed stress pattern reflects a compressive force transmitted across the contact between the Juan de Fuca plate and the North American plate. Furthermore, modeling and observed fold patterns suggest that this force must be applied in a direction at least roughly comparable to the direction of relative motion between these two plates, rather than to that of the relative motion between the Pacific and North American plates.

Many of the fold axes shown on Figure 1 are developed in strata of early and middle Miocene age. Hence, it is necessary to ask whether the conclusions of the preceding paragraph also apply to late Miocene and Pliocene time. The critical area is that offshore (west) of Oregon and California, because the east-west compression (revealed by the north-trending folds) of this area cannot be reconciled with the north-south compression indicated by the geologic structures of eastern Washington and eastern Oregon unless an isotropic point is present in between. If such a point exists, the stress pattern would resemble that revealed by the model studies.

Snavely and others (1977, p. 21) state that upper Miocene and Pliocene strata are broadly folded in many places on the Oregon and Washington outer continental shelf. On the outer part of the shelf, fold axes tend to parallel the base of the slope (Silver, 1972), and on the inner part, folds are more

closely parallel to those in older Tertiary rocks (Snavely and others, 1977, p. 21).

We conclude that the structural data do indicate continued impingement of the Juan de Fuca plate and transmission of a compressive stress to the North American plate through late Miocene and Pliocene. In the absence of evidence to the contrary, we expect that the Pleistocene and Holocene stress pattern(s) will prove to be similar to that of the Miocene and Pliocene.

This conclusion is critical to any understanding of present west coast tectonics and of course, there are contrary views. For example, the stress pattern shown here (Fig. 6) and the conclusions stated above differ from those of Zoback and Zoback (1980). They state (p. 366) that the north-south compression in the Pacific Northwest is not consistent with northeast-southwest convergence between the North American and Juan de Fuca plates.

As we noted above, the discordance in direction of certain folds and other structures suggests that the observed stress pattern is a composite reflecting more than one orientation of stress. This composite probably represents the dominant position of a pattern that shifted from place to place during the late Cenozoic. In this context, the location of the isotropic point is an important feature of the stress pattern, because, were we able to pinpoint it, we would be able to register the composite stress pattern to its actual position in the study area at any given time.

The isotropic point was probably located in north-central Oregon (Fig. 6) during much of the late Cenozoic. This position, though well defined by the pattern of folds in strata of this age, may not be a good candidate for the present position of the isotropic point because it is within a region of moderate seismic activity (Couch and Lowell, 1971; Smith, 1978). Because the horizontal shear stresses at the isotropic point are zero and in the region near it are low, the elastic upper part of the lithosphere at and near this point should be characterized by very low seismicity.

In the model studies, the position of the isotropic point is quite sensitive to changes in applied forces and to changes in the direction of movement of JDF. A shift in position of the isotropic point in nature should have occurred concurrently with the change in spreading direction of the Juan de Fuca plate and the formation of the Blanco fracture zone, a change which probably started about 10 m.y. ago. However, our data are not sufficiently refined to recognize this shift.

We do not have a good explanation for the discordancy in fold directions in southeastern Oregon. Many of these folds are developed in regionally extensive Pliocene ash-flow tuffs (Walker, 1977). The aberrant folds may signal a local departure from our initial assumption of negligible tractions at the base of the elastic part of the lithospheric plate. Very low seismic activity within region (Couch and Lowell, 1971; Smith, 1978), however, suggests that shear stresses are small. If the aberrant folds developed over some sort of mantle hot spot, plume, or zone of asthenospheric counterflow, then that feature is probably either no longer present or not currently active at this location.

To sum up, the pattern of folds and of basin-and-range structures as shown on Figure 1, even though restricted to Miocene and younger strata, reflects in its discordancies and interfering folds the superposition of two (or more) similar stress patterns, hypothetically corresponding to the two major plate-dynamic regimes that existed during this time span. Conceivably, each of the two stress patterns in turn represents the merging of many short-term fluctuations or perturbations into an average pattern. The two patterns probably have the same basic style; we expect that they differ only in their geographic position. Unfortunately, our data do not permit us to resolve the individual location of the multiple patterns--we see only a dominant or average pattern, with an isotropic point located in north-central Oregon.

In Figure 6, we equate the central part of the zone of high shear stress found in the model studies east of the triple junction near Vancouver Island with the zone of high seismicity of southwestern British Columbia and northwestern Washington (as depicted by Milne and others, 1978, Figs. 3 and 4). The zone of high shear stress develops where the northeast corner of the Juan de Fuca plate impinges on the North American plate, as noted by Crosson (1972).

Only a few recently active faults have been found in western Washington. Those investigated by Wilson and others (1979) in the west part of the Puget Sound area appear to be a conjugate set of reverse faults, which indicate crustal shortening in the direction of both of the principal horizontal tectonic stresses. Hence, at least this part of the Puget Sound area has been in structural domain I during the Holocene. We take the outer boundary of the zone of high seismicity to be the boundary between domains I and II; thus we include the entire Puget Sound area within domain I. This hypothesis is consistent with hypocentral solutions of small earthquakes located within the upper 30 to 40 km of the lithosphere in the Puget Sound area, which seem to show oblique slip with a marked component of reverse motion (Crosson, 1972). The 1949 and 1965 earthquakes, with magnitudes of 7.1 and 6.5, respectively (Hodgson and Storey, 1954; Algermissen and Harding, 1965), probably occurred within the subducted extension of the Juan de Fuca plate at depths of about 60 km (Bolt, 1979; McKenzie and Julian, 1971), below the stress regime we characterize in this paper.

In the following paragraphs we offer some predictions about the future style of faulting within the region, assuming that new or recurrent faulting will resemble the faults typifying the various structural domains during the late Cenozoic.

Assuming that the elastic upper part of the crust is characterized by an angle of internal friction of roughly $30^{\circ}$ we use the stress trajectories shown in Figure 6 to derive trajectories showing the expected orientation of conjugate shears (Fig. 7). In domain I, we expect faults developing parallel to these trajectories to be oblique slip-faults with a component of reverse slip. In domain II, faults with this orientation will be strike-slip, and in domain III, oblique-slip with a component of normal slip. In domains IV and V, the greater weakness of the crust in tension evidently causes normal faults to develop parallel to the maximum principal horizontal tectonic stress rather than to the shear-fault trajectories.

The boundary between these domains is a diffuse zone within which the difference between the magnitude of one of the horizontal tectonic stresses and the vertical tectonic stress becomes negligibly small. The directions of the maximum and minimum horizontal tectonic stresses need not change markedly at such a boundary.

In the Pacific Northwest, the seismogenic boundary between domains I and II probably marks an important change in structural style. At this boundary--which may lie within the area of high shear stress developed east of the northern corner of the Juan de Fuca plate--there will probably be a transition from numerous earthquakes occurring largely on oblique-slip reverse faults of the Puget Sound area, to fewer but possibly more energetic earthquakes occurring on thrust or reverse faults striking orthogonal to the trajectories of the maximum horizontal tectonic stress.

East-trending thrust or reverse faults younger than 3.7 m.y. in central Washington (recently described by Waitt, 1979) are properly oriented and situated to be part of this class of faults. We speculate that the 1872 earthquake of intensity VIII+ located near Lake Chelan (according to D. C. Dale, written communication cited by Bolt, 1979) may have occurred on a fault within and related to this transition zone.

The decrease in the level of horizontal shear stress to the east and south of the Puget Sound area implies a concomitant decrease in the maximum horizontal tectonic stress. Hence the probability of thrust or reverse faulting is greatest near the transition between domains I and II.

## REFERENCES CITED


Algermissen, S. T., and Harding, S. T., 1965, The Puget Sound, Washington earthquake of April 29, 1965: U.S. Coast and Geodetic Survey Preliminary Report, p. 1-26.

Anderson, E. M., 1942, The Dynamics of faulting: London, Oliver and Boyd, 183 p.

Atwater, Tanya, 1970, Implications of plate tectonics for the Cenozoic tectonic evolution of western North America: Geological Society of America Bulletin, v. 81, p. 3513-3536.

Atwater, Tanya, and Menard, H. W., 1970, Magnetic lineations in the northwest Pacific: Earth and Planetary Science Letters, v. 7, p. 445-450.

Atwater, Tanya, and Molnar, Peter, 1973, Relative motion of the Pacific and North American plates deduced from sea-floor spreading in the Atlantic, Indian, and South Pacific Oceans, in Kovach, R. L., and Nur, Amos, eds., Proceedings of the conference on tectonic problems of the San Andreas fault system: Stanford University Publications in Geological Sciences, v. 13, p. 136-148.

Bolt, B. A., 1979, Seismicity of the western United States: Geological Society of America, Reviews in Engineering Geology, v. 4, p., 95-107.

Caputo, Michele, and Console, Rodolfo, 1980, Statistical distribution of stress drops and faults of seismic regions: Tectonophysics, v. 67, p. T13-T20.

Couch, R. W., and Lowell, R. P., 1971, Earthquakes and seismic energy release in Oregon: Ore Bin, v. 33, p. 61-84.

Couples, Gary, 1977, Stress and shear fracture (fault) patterns resulting from a suite of complicated boundary conditions with application to the Wind River Mountains: Pure and Applied Geophysics (Pageoph), v. 115, p. 113-133.

Crosson, R. S., 1972, Small earthquakes, structure, and tectonics of the Puget Sound region: Seismological Society of America Bulletin, v. 62, p. 1133-1171.

Donath, F. A., 1962, Analysis of basin-range structure, south-central Oregon: Geological Society of America Bulletin, v. 73, p. 1-16.

Farquharson, F. B., and Hennes, R. G., 1940, Gelatin models for photoelastic analysis of stress in earth masses: Civil Engineering, v. 10, no. 4, p. 211-214.

Fox, K. F., Jr., 1976, Melanges in the Franciscan Complex, a product of triple junction tectonics: Geology, v. 4, p. 737-740.

-----, 1979, The experimental determination of stress patterns in the North American plate in the region near the triple junction at Cape Mendocino, using photoelastic models (abs.): Geological Society of America Abstracts with Programs, v. 11, no. 3, p. 78.

Fox, K. F., in press, Melanges and their bearing on late Mesozoic and Tertiary subduction and interplate translation at the western edge of the North American plate: U.S. Geological Survey Professional Paper 1198.

Frocht, M. M., 1941, Photoelasticity, Volume 1: New York, John Wiley and Sons, Inc., 411 p.

-----, 1948, Photoelasticity, Volume II: New York, John Wiley and Sons, Inc., 505 p.

Furlong, K. P., 1979, An analytic stress model applied to the Snake River Plain (northern Basin and Range province, U.S.A.): Tectonophysics, v. 58, p. T11-T15.

Greiner, Gerhard, and Illies, J. H., 1977, Central Europe: active or residual tectonic stresses: Pure and Applied Geophysics (Pageoph), v. 115, p. 11-26.

Hafner, W., 1951, Stress distributions and faulting: Geological Society of America Bulletin, v. 62, p. 373-398.

Hodgson, J. H., and Storey, R. S., 1954, Direction of faulting in some larger earthquakes of 1949: Seismological Society of America Bulletin, v. 44, p. 57-83.

Hubbert, M. K., 1937, Theory of scale models as applied to the study of geologic structures: Geological Society of America Bulletin, v. 48, p. 1459-1520.

Hyndman, R. D., Riddihough, R. P., and Herzer, R., 1979, The Nootka fault zone--a new plate boundary off western Canada: Geophysical Journal of the Royal Astronomical Society, v. 58, p. 667-683.

Jennings, C. W., 1977, Geologic map of California: California Division of Mines and Geology, scale 1:750,000.

Kusznir, N. J., and Bott, M. H. P., 1977, Stress concentration in the upper lithosphere caused by underlying viscoelastic creep: Tectonophysics, v. 43, p. 247-256.

LaBrecque, J. L., Kent, D. V., and Conde, S. C., 1977, Revised magnetic polarity time scale for Late Cretaceous and Cenozoic time: Geology, v. 5, p. 330-335.

Lawrence, R. D., 1976, Strike-slip faulting terminates the Basin and Range province in Oregon: Geological Society of America Bulletin, v. 87, p. 846-850.

McCulloch, D. S., Clarke, S. H., Jr., Field, M. E., Scott, E. W., and Utter, P. M., 1977, A summary report on the regional geology, petroleum potential, and environmental geology of the southern proposed lease sale 53, central and northern California outer continental shelf: U.S. Geological Survey Open-File Report 77-593, 57 p.

McKenzie, Dan, and Julian, Bruce, 1971, Puget Sound, Washington, earthquake and the mantle structure beneath the northwestern United States: Geological Society of America Bulletin, v. 82, p. 3519-3524.

Melosh, Jay, 1977, Shear stress on the base of a lithospheric plate: Pure and Applied Geophysics (Pageoph), v. 115, p. 429-439.

Menard, H. W., and Atwater, T., 1968, Changes in the direction of seafloor spreading: Nature, v. 219, p. 463-467.

Milne, W. G., Rogers, G. C., Riddihough, R. P., McMechan, G. A., and Hyndman, R. D., 1978, Seismicity of western Canada: Canadian Journal of Earth Sciences, v. 15, p. 1170-1193.

Minster, J. B., and Jordan, T.H., 1978, Present-day plate motions: Journal of Geophysical Research, v. 83, p. 5331-5354.

Naugler, F. P., and Wageman, J. M., 1973, Gulf of Alaska: magnetic anomalies, fracture zones, and plate interaction: Geological Society of America Bulletin, v. 84, p. 1575-1584.

Newcomb, R. C., 1970, Tectonic structure of the main part of the basalt of the Columbia River Group, Washington, Oregon, and Idaho: U.S. Geological Survey Miscellaneous Geological Investigations Map I-587, scale 1:500,000.

Nikonov, A. A., Osokina, D. N., and Tsvetkova, N.Yu., 1975, Recent movements and stress fields in the San Andreas fault system by the results of modelling: Tectonophysics, v. 29, p. 153-159.

Raff, A. D., and Mason, R. G., 1961, Magnetic survey off the west coast of North America, 40° N., latitude to 50° N. latitude: Geological Society of America Bulletin, v. 72, p. 1267-1270.

Raleigh, C. B., and Evernden, J., 1980, The case for low deviatoric stress in the lithosphere, in Magnitude of deviatoric stresses in the Earth's crust and upper mantle, Proceedings, Conference IX, July-August 1979: U.S. Geological Survey Open-File Report 80-625, p. 168-198b.

Rehrig, W. A., and Heidrick, T. L., 1976, Regional tectonic stress during the Laramide and Late Tertiary intrusive periods, Basin and Range province, Arizona: Arizona Geological Society Digest, v. 10, p. 205-228.

Riddihough, R. P., 1977, A model for recent plate interactions off Canada's west coast. Canadian Journal of Earth Sciences, v. 14, p. 384-396.

Silver, E. A., 1972, Pleistocene tectonic accretion of the continental slope off Washington: Marine Geology, v. 13, p. 239-249.

Smith, R. B., 1978, Seismicity, crustal structure, and intraplate tectonics of the interior of the western Cordillera, in Smith, R. B., and Eaton, G. P., eds., Cenozoic tectonics and regional geophysics of the Western United States: Geological Society of America Memoir 152, p. 111-144.

Snavely, P. D., Jr., Pearl, J. E., and Lander, D. L., 1977, Interim report on petroleum resources potential and geologic hazards in the outer continental shelf--Oregon and Washington Tertiary province, with a section on Resource appraisal estimate by E. W. Scott: U.S. Geological Survey Open-File Report 77-282, 68 p.

Solomon, S. C., Sleep, N. H., and Richardson, R. M., 1975, On the forces driving plate tectonics: inferences from absolute plate velocities and intraplate stress: Geophysical Journal of the Royal Astronomical Society, v. 42, p. 769-804.

Stewart, J. H., 1980, Regional tilt patterns of late Cenozoic basin-range fault blocks, western United States: Geological Society of America Bulletin, Part 1, v. 91, p. 460-464.

Stewart, J. H., and Carlson, J. E., 1978, Geologic map of Nevada: U.S. Geological Survey, scale 1:500,000.

Stone, D. S., 1970, Principal horizontal stress in the central Rocky Mountains versus California: Mountain Geologist, v. 7, no. 2, p. 69-87.

Taubeneck, W. H., 1970, Dikes of Columbia River Basalt in northeastern Oregon, western Idaho, and southeastern Washington, in Gilmour, E. H., and Stradling, Dale, eds., Proceedings of the second Columbia River Basalt symposium, Eastern Washington State College, Cheney, Washington, March 1969, p. 73-96.

Thompson, G. A., and Burke, Dennis, 1973, Rate and direction of spreading in Dixie Valley, Basin and Range province, Nevada: Geological Society of America Bulletin, v. 84, p. 627-632.

Waitt, R. B., Jr., 1979, Late Cenozoic deposits, landforms, stratigraphy, and tectonism in Kittitas Valley, Washington: U.S. Geological Survey Professional Paper 1127, 18 p.

Walker, G. W., 1977, Geologic map of Oregon east of the 121st meridian: U.S. Geological Survey Miscellaneous Geologic Investigations Map I-902, scale 1,500,000.

Wells, F. G., and Peck, D. L., 1961, Geologic map of Oregon west of the 121st meridian: U.S. Geological Survey Miscellaneous Geologic Investigations Map I-325, scale 1:500,000.

Wilson, J. R., Bartholomew, M. J., and Carson, R. J., 1979, Late Quaternary faults and their relationship to tectonism in the Olympic Peninsula, Washington: Geology, v. 7, p. 235-239.

Zoback, M. L., and Thompson, G. A., 1978, Basin and range rifting in northern Nevada: clues from a mid-Miocene rift and its subsequent offsets: Geology, v. 6, p. 111-116.

Zoback, M. L., and Zoback, Mark, 1980, Interpretative stress map of the coterminous United States, in Magnitude of deviatoric stresses in the Earth's crust and upper mantle, Proceedings, Conference IX, July-August 1979, U.S. Geological Survey Open-File Report 80-625, p. 353-433.

## Figure Captions

Figure 1. Fold axes, basin and range trends, and selected volcanic alinements of Miocene through Holocene age in the northwestern United States. Also shown are structural domains I, II, and III (see text). The map is based on data from the compilations of Jennings (1977), McCulloch and others (1977), Stewart and Carlson (1978), Walker (1977), Wells and Peck (1961), Snavely and others (1977), and Taubeneck (1970). In continental Washington, the map is based on data from numerous primary sources, to be listed in a forthcoming compilation by Fox (in prep.). Localities mentioned in text: a, area of late Quaternary faults (Wilson and others, 1979); b, area of post-4 m.y. B.P. faults in Kittitas Valley (Waitt, 1979); c, intensity VIII isoseismal of 1872 earthquake (D. C. Dale, written commun. cited by Bolt, 1979). Explorer plate configuration from Hyndman and others (1979). Oblique Mercator projection about lat. 48.77° N. and long. 73.91° W., the pole of rotation between the North American and Pacific plates (Minster and Jordan, 1978).

Figure 2. Diagrams showing structures typical of various stress regimes within the region.

Figure 3. Experimental set-up. Light table (concealed below stage) provides white light, and sheets of polarizing film serve as polarizer and analyzer. Model in circular enclosure with glass bottom is placed on rotating stage with camera above.

Figure 4. Model with gelatin in place and under compression by piston advancing S. $5^{\circ}$ W. and by JDF advancing S. $65^{\circ}$ E. JDF, Juan de Fuca plate; PP, Pacific plate; NAP, North American plate; MTJ, triple junction at Cape Mendocino; VTJ, triple junction near Vancouver Island; SAF, San Andreas fault; QCF, Queen Charlotte fault.

Figure 5. Sketch of stress pattern showing trajectories of maximum (compressive) principal stress as graphically determined (using rapid method described by Frocht, 1941, p. 198-199) from position of isoclinics (not shown) recorded at $10^{\circ}$ intervals. Symbols same as in Figure 4.

Figure 6. Dominant stress pattern in the northwestern United States during the late Cenozoic. Trajectories shown are those of maximum (compressive) horizontal tectonic stress.

Figure 7. Trajectories showing expected strike of conjugate fault sets of late Cenozoic age in the northwestern United States.

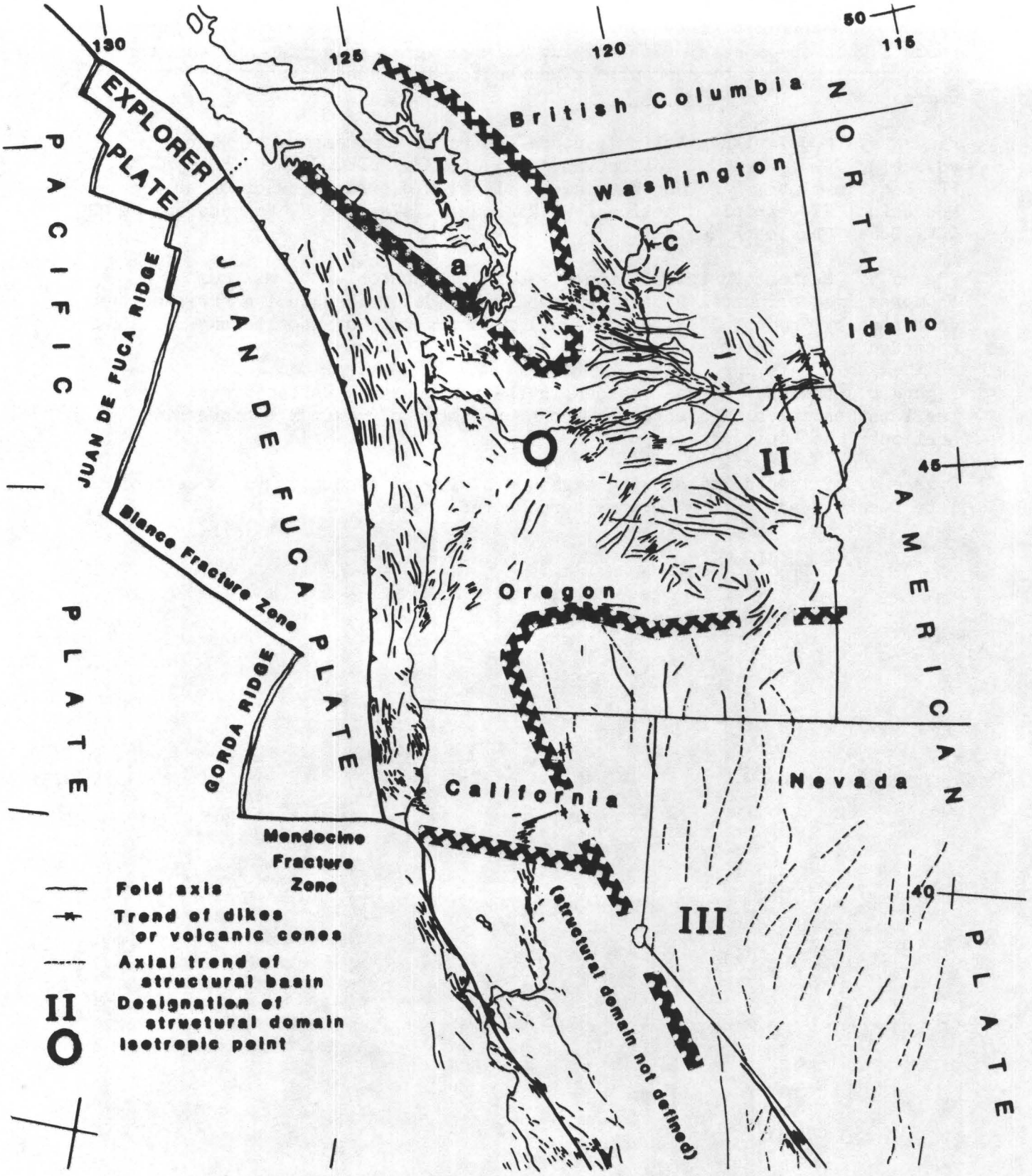
130
125
120
115
50
45
40
EXPLORER PLATE
JUAN DE FUCA RIDGE
JUAN DE FUCA PLATE
Blanco Fracture Zone
GORDA RIDGE
Mendocino Fracture Zone
PACIFIC PLATE
NORTH AMERICAN PLATE
British Columbia
Washington
Idaho
Oregon
California
Nevada
I
a
b
c
II
III
(structural domain not defined)
Fold axis
Trend of dikes or volcanic cones
Axial trend of structural basin
Designation of structural domain
Isotropic point

FIGURE 1.-

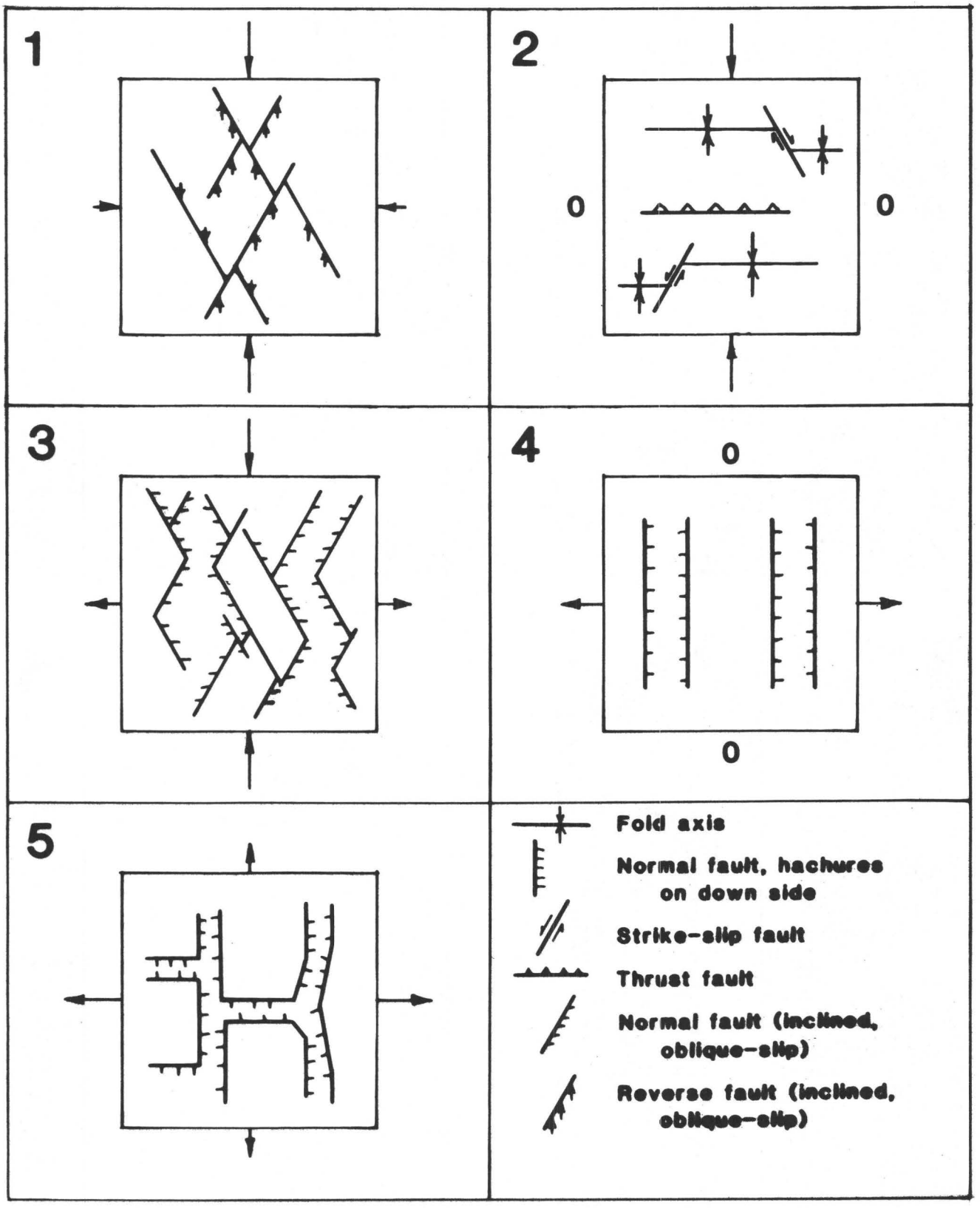
1
2
0
0
3
4
0
0
5
Fold axis
Normal fault, hachures on down side
Strike-slip fault
Thrust fault
Normal fault (inclined, oblique-slip)
Reverse fault (inclined, oblique-slip)

**FIGURE 2.-**

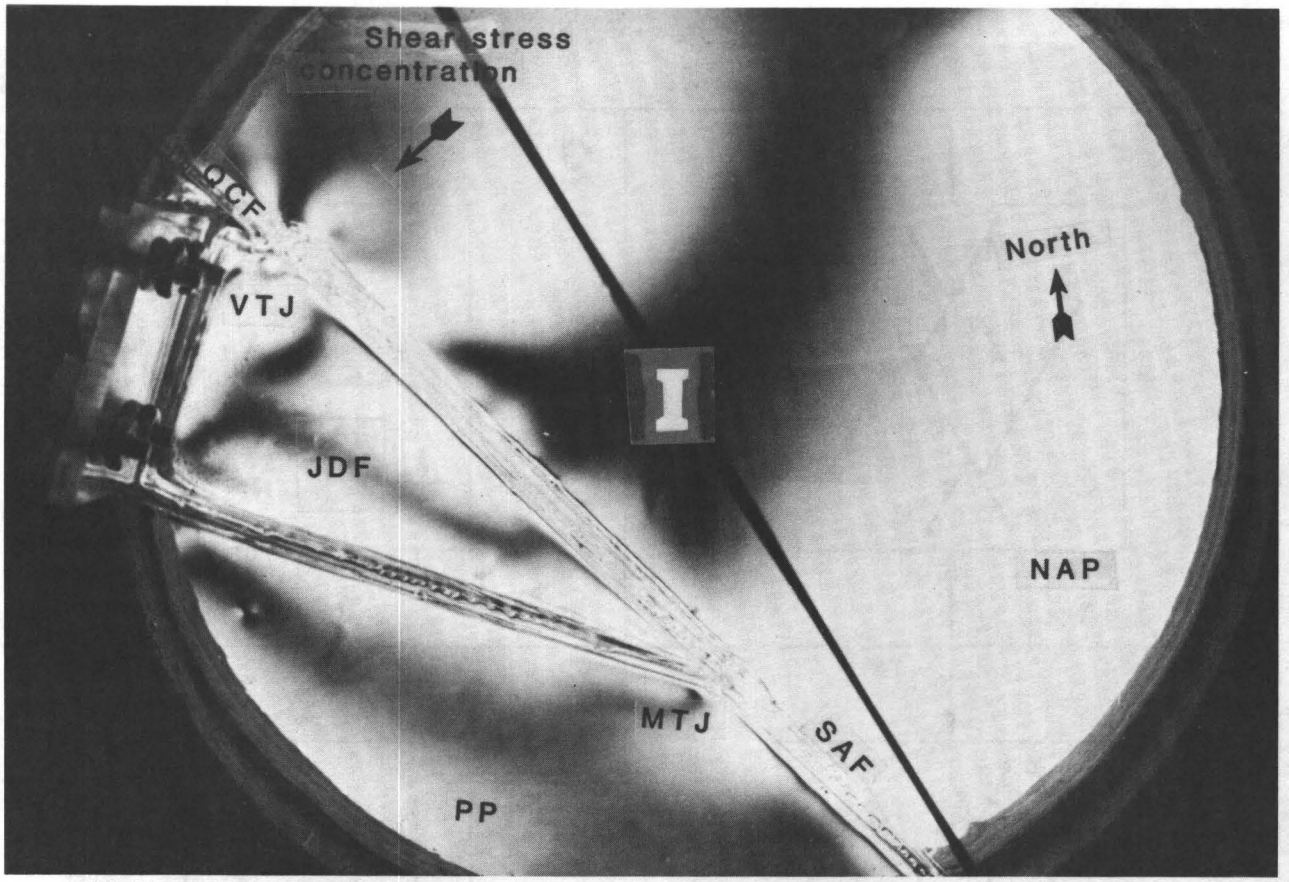


FIGURE 3.-

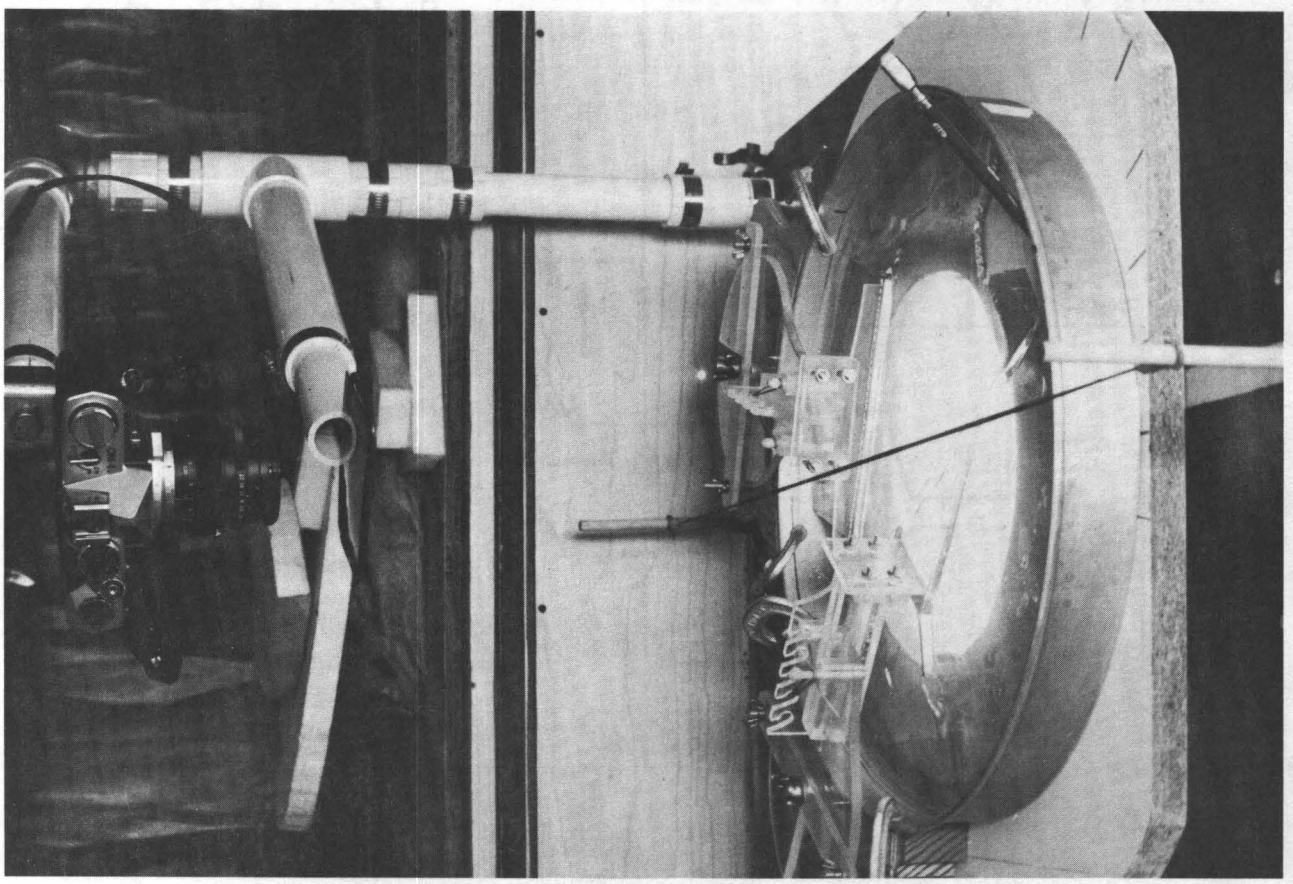

FIGURE 4.-

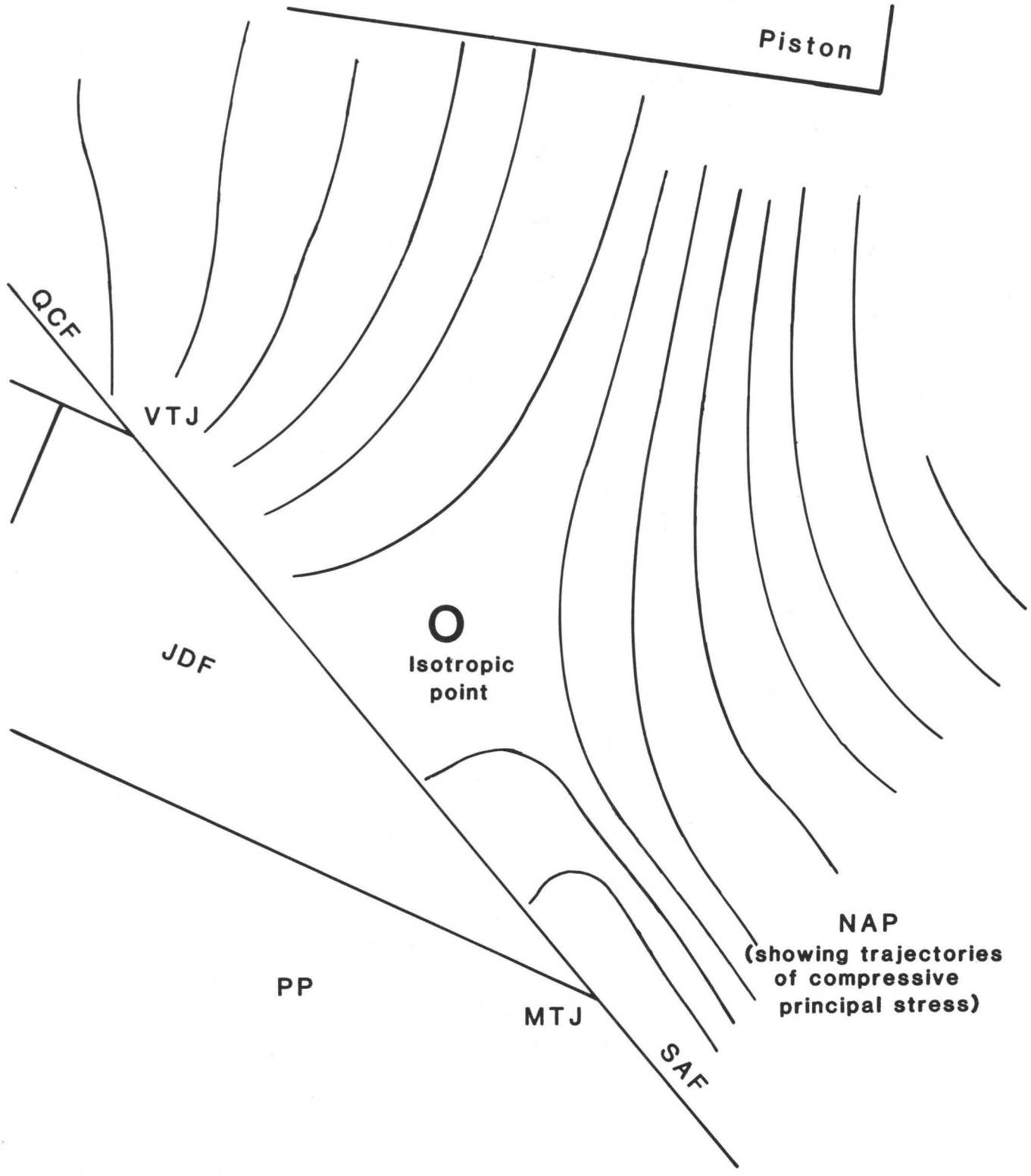
Piston
QCF
VTJ
JDF
O
Isotropic
point
NAP
(showing trajectories
of compressive
principal stress)
PP
MTJ
SAF

FIGURE 5.-

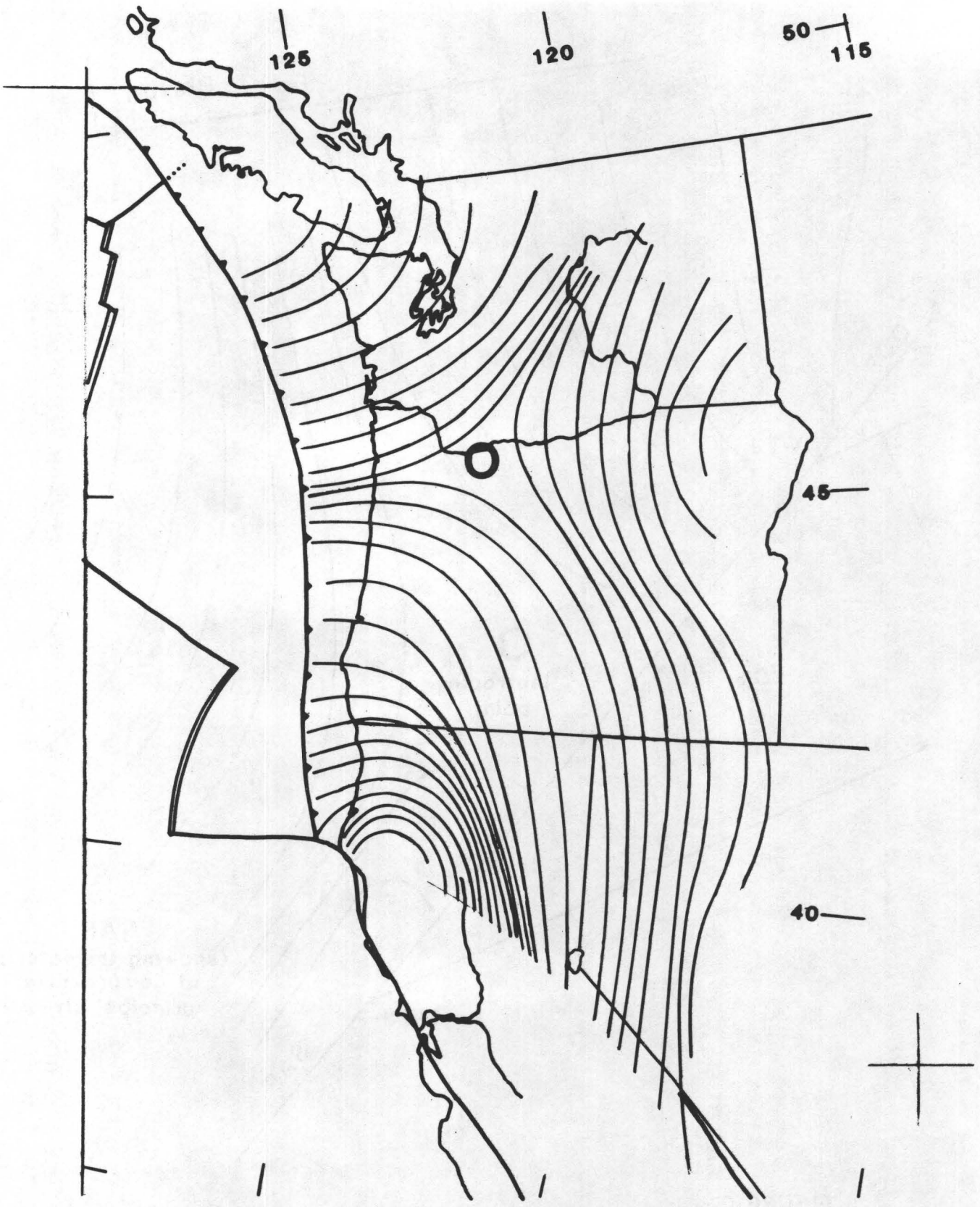


**FIGURE 6.-**

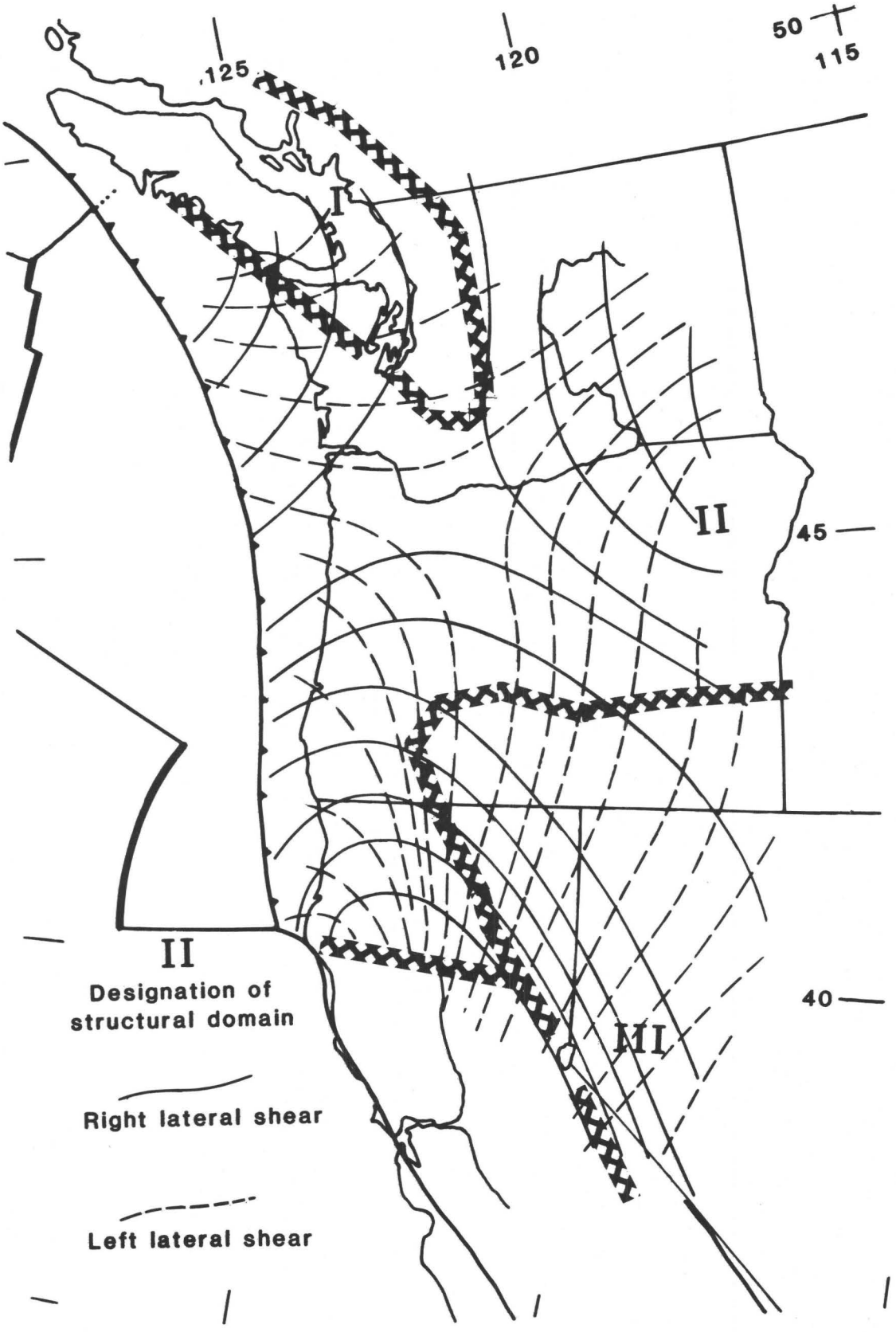
125
120
115
50
45
40
I
II
II
III
Designation of structural domain
Right lateral shear
Left lateral shear

FIGURE 7.-

# RELATIONSHIPS BETWEEN LATE QUATERNARY FAULTS AND EARTHQUAKES IN THE PUGET SOUND, WASHINGTON AREA

Joseph R. Wilson
Department of Geology
Washington State University
Pullman, Washington 99164

## ABSTRACT

Three definite faults and a fourth possible fault have been recognized in the southeastern Olympic Peninsula, Washington, between Lake Cushman and Hood Canal. The Saddle Mountain East fault is oriented N22°E,75°SE with 3.5 m of reverse offset. The Saddle Mountain West fault is oriented N19°E, 67°SE with 1.8 m of reverse offset. The Dow Mountain fault is oriented N58°W, 59°NE with 1.7 m of reverse offset. Offsets of pre-Fraser and Vashon tills show that movement along all of these faults is late Quaternary, and movement on the Saddle Mountain East fault may be as recent as 1240 yr ago. The Cushman Valley fault (?) is a N57°E-trending straight valley that may represent a strike-slip fault.

The Saddle Mountain faults occur along the trend of an older zone of fracturing and may have developed in this pre-existing structure.

The Dow Mountain and Cushman Valley (?) faults match focal mechanism solutions for modern earthquakes. Movement along all of the faults is compatible with north-south compression of the Puget Lowland. An attempt to use equations for fault length vs. earthquake magnitude on these faults shows the difficulties in using this method. However, these equations suggest that an earthquake associated with movement along the Saddle Mountain East fault may have had a maximum magnitude of about 6.5 to 7.0 but may have been much smaller.

## INTRODUCTION

Holocene faulting in the Puget Lowland region was first reported by Carson (1973). Since then, three definite faults and a fourth possible fault of late Quaternary age have been recognized in the same area (Wilson, 1975).

The area of faulting (Fig. 1) is located along the eastern edge of the Olympic Peninsula between Hood Canal and Lake Cushman in northern Mason County, Washington. Bedrock is the upper basalt unit of the Eocene Crescent Formation, primarily a pillow basalt in the study area. The unit dominantly strikes northeast and dips moderately to steeply southeast. The bedrock is mostly covered by Vashon drift (Vashon Stade, Fraser Glaciation) except on the unglaciated top of Dow Mountain. Vashon drift also overlies at least three older tills from both Fraser and pre-Fraser glaciations. The pre-Fraser tills are similar to the "Salmon Springs till" of Carson (1970) but no definite correlation has been made. Peat and lake deposits overlie Vashon drift at Price Lake and Lilliwaup Swamp.

## LATE QUATERNARY FAULTS

### Saddle Mountain East Fault

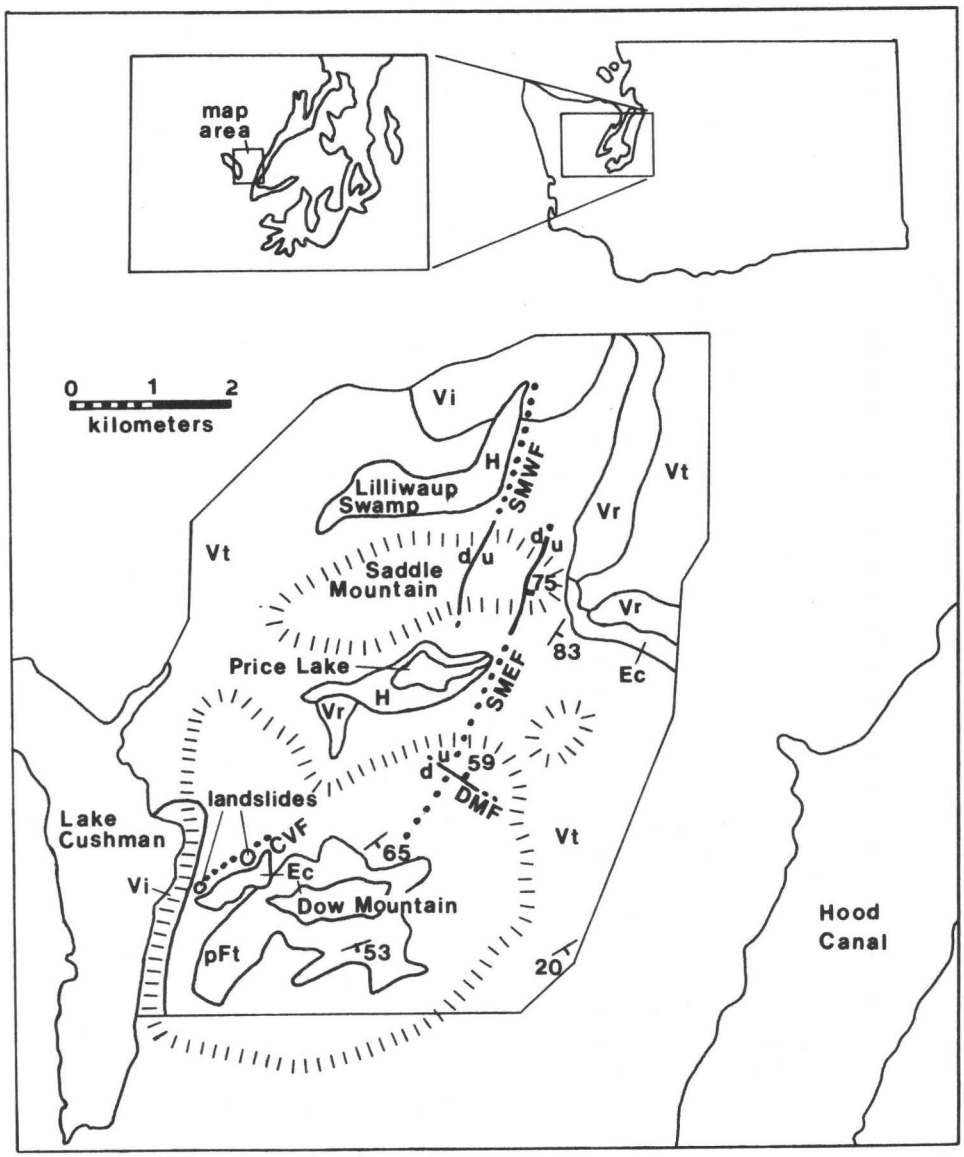


Figure 1. Geologic map of area of late Quaternary faulting. Symbols: H, Holocene lake deposits; Vr, Vashon recessional outwash; Vi, Vashon ice-contact stratified drift; Vt, Vashon till; pFt, pre-Fraser till; Ec, Eocene Crescent Formation; CVF, Cushman Valley fault (?); DMF, Dow Mountain fault; SMEF, Saddle Mountain East fault; SMWF, Saddle Mountain West fault.

The Saddle Mountain East fault is recognized by a N26°E-trending, 1.5 km-long, west-facing scarp across the east end of Saddle Mountain. The scarp is 1 to 3 m high near the flanks of the mountain and increases to 8 m on the crest of the ridge. In a trench excavated across the scarp on the south side of Saddle Mountain, the fault plane is part of a 1 m wide zone of fault gouge and brecciated basalt that is oriented N22°E, 75°SE and shows 3.5 m of apparent reverse offset of Vashon till. Faint striations on the fault plane have a pitch of 66°SW, suggesting a left-lateral component to the movement. Aerial photographs show a possible offset of the Dow Mountain fault scarp (not verified in the field) along with other faint lineaments on Dow Mountain along the trend of the Saddle Mountain East fault. These lineaments suggest a possible extended scarp length of 4.3 km.

Movement along the fault may have raised the level of Price Lake as well as forming small ponds along the scarp both north and south of Saddle Mountain. Radiocarbon ages of organic material taken from these ponds (Wilson and others, 1979) yield ages of 1315 ± 80, 1155 ± 85, and 5100 ± 500 yr B.P. Analytical problems with the last sample make its age questionable. A sample of charcoal from colluvium along the scarp was dated at 1600 ± 200 yr B.P. (J. D. Sims, personal communication). The first two ages suggest that movement along the Saddle Mountain East fault probably occurred at about 1240 to 1235 yr B.P., however several movements may have occurred beteen 1600 and 1155 yr B.P.

Saddle Mountain West Fault

The surface expression of the Saddle Mountain West fault is a 1.3 km-long, northeast-trending, west-facing scarp that crosses Saddle Mountain 0.7 km west of the Saddle Mountain East fault scarp. The scarp is 1 to 2 m high along the sides of the mountain and 3 to 4 m high as it crosses the mountain. A trench excavated across the scarp on the south side of Saddle Mountain exposed a 1.8 m-high, west-facing wall of basalt buried by colluvium that is interlayered with pre-Fraser till on the west side of the scarp. The height of this wall probably reflects offset along the fault. A three point geometric construction of the scarp gives a strike of N19°E and a dip of 67°SE for the fault plane. A northerly extension of the scarp corresponds to the eastern edge of Lilliaup Swamp and suggests that the swamp may have been formed or enlarged due to damming by the scarp. The possible length of this extended scarp is 4.0 km.

The interlayered pre-Fraser till and colluvium in the trench suggests that movement may have occurred during the pre-Fraser glaciation. Post-Vashon movement is suggested by the 8715 ± 185 yr B.P. radiocarbon age (Wilson and others, 1979) of organic material taken from Lilliwaup Swamp.

Dow Mountain Fault

The Dow Mountain fault is expressed as a 0.7 km-long, northwest-trending, southwest-facing scarp on a northeastern ridge of Dow Mountain. The scarp is 5 to 8 m high on the ridge and disappears on the flanks of the mountain. A trench excavated across the scarp exposed a narrow zone of fault gouge and brecciated basalt oriented N58°W, 59°NE. A gray

sandy-gravel layer within pre-Fraser till shows 1.7 m of relative reverse offset.

Offset of the pre-Fraser till and apparent obliteration of the scarp at lower elevations by the Vashon glacier bracketed the latest movement of the Dow Mountain fault between the pre-Fraser glaciation and the Vashon Stade of the Fraser Glaciation.

Cushman Valley Fault (?)

A possible fourth fault may be expressed as a 1.2 km-long, N57°E-trending, southwest draining valley on the northwest flank of Dow Mountain that is oblique to and cuts other geomorphic features in the area. The valley is straight but contains two 75 m high basalt hills that are probably slide blocks. Small intermittent ponds are present on the northeast sides of these hills. There is no glacial material on a series of truncated spurs that make up the southeast side of the valley or on the valley floor. Conversely, four different tills are exposed on the northwest side of the valley. The valley appears to truncate a network of north-flowing abandoned glacial meltwater channels. The valley ends abruptly into Vashon outwash to the northeast and a kame terrace to the southwest.

This anomalous valley is interpreted to be the surface expression of a fault with a strike of about N57°E. Although the dip of the fault is not known, a steep to nearly vertical dip is implied by the straight shape of the valley. The type of movement along the fault is also not known, but strike-slip movement is believed to be most likely because there is no scarp, as is the case with the reverse faults in the area, and its trend correlates with a strike- slip direction postulated from earthquake data to be discussed later.

The time of movement along the fault is uncertain. The abrupt termination of the valley into Vashon drift and the way it truncates meltwater channels suggests that the valley formed during the retreat of the Vashon glacier. However, the fault movement could have predated formation of the valley by a significant length of time.

RELATIONSHIPS BETWEEN THE FAULTS AND OLDER STRUCTURES

The Saddle Mountain faults approximately parallel the strike and dip of bedding in the area and may be developed along pre-existing weaknesses in this direction. However, these faults may also be related to other older structures in the area. A northerly projection of the Saddle Mountain faults corresponds to the zone of fractured basalt mapped by Glassley (1974). Cady (1975) believed fracturing to be the result of cooling in a transitional zone between the lower and upper basalt members of the Crescent Formation. However, comparison of the pattern of the contact (Tabor and Cady, 1978) and the zone of fractured basalt (Glassley, 1974) shows that the zone of fractured basalt appears nearly straight while the contact is folded and more sinuous (Fig. 2). Just north of Saddle Mountain this contact swings to the west-southwest and the zone of fracturing appears to continue straight and is developed only in the upper unit. The Saddle Mountain faults may be developed in a southern extension of the zone of fractured basalt.

All four of the faults are approximately parallel to numerous topographic lineaments in the Puget Lowland and Olympic Peninsula (Fig.

3). Some of these features, such as the Hood Canal, have been suggested in the past to be related to tectonic features, but no tectonic origin has ever been demonstrated. However, the abundance of these lineaments suggests that there may be a common origin between them and the late Quaternary faults.

## RELATIONSHIPS BETWEEN THE FAULTS AND EARTHQUAKE FOCAL MECHANISM SOLUTIONS

Although the Puget Sound region as a whole is a seismically active region, there appears to be little or no activity on the faults. Early records (Coombs, 1953; Rasmussen, 1967) show no recognized earthquakes with epicenters in the area. Records of more recent earthquakes (Crosson, 1974, 1975; Crosson and Millard, 1975; Crosson and Nelson, 1978a, 1978b, 1979) show a little activity nearby but no earthquakes within the study area. Although the faults are now seismically inactive, their young ages suggest that their past movements and modern earthquake activity are related.

Several focal mechanism solutions have been proposed (Table 1) to describe the stresses associated with Puget Sound earthquakes. These mechanisms and the late Quaternary faults are plotted for comparison on Figure 4 in the general area of their occurrence. Nuttli (1952) reported directions of faulting for the magnitude 7.1 earthquake of April 13, 1949 centered southwest of Tacoma. Hodgson and Storey (1954) included some additional data and recalculated the focal mechanisms for the earthquake. Algermissen and Harding (1965) calculated mechanisms for the deep-focus April 29, 1965, magnitude 6.5 earthquake centered south of Seattle. Isacks and Molnar (1971) recalculated focal mechanisms for this earthquake.

Crosson (1972) studied small earthquakes on the Puget Sound region in 1970 and 1971. Crosson used 55 events ranging in magnitude from 1 to 4 with an average depth of 20 km to define three focal mechanism solutions (Table 1). His group A consisted of 20 events northeast of Seattle, group B used 24 events west of Seattle, and group C used 11 events centered between Seattle and Tacoma.

Crosson (1972) and other workers (U. S. Geological Survey, 1975) concluded that the distribution of numerous minor earthquakes with few major events is a result of a broad deformation of a large amount of crust rather than movement along definite fault zones. Furthermore, they concluded that this deformation indicates major compressional stress of the Puget Lowland oriented north-south (Crosson, 1972, p. 1164) or N35°W (U. S. Geological Survey, 1975, p. 34). The faults in the study area are compatible with the focal mechanism solutions and regional stress system of the region.

The Dow Mountain fault (N58°W, 59°NE) approximates one nodal plane (N52°W, 58°NE) of Crosson's group B focal mechanism solution. Both exhibit dominantly high-angle reverse movement. This similarity of attitudes and movement suggests that the Dow Mountain fault and Crosson's group B earthquakes are expressions of similar regional stresses.

The Cushman Valley fault (?) (N57°E, inferred steep dip) matches one nodal plane (N57°E, 70°SE) of Crosson's group C focal mechanism solution. This mechanism exhibits left-lateral strike-slip movement. Movement along the Cushman Valley fault (?) is not known but is believed to be strike-slip. Thus, the Cushman Valley fault (?) appears to be an expression of the same stresses that caused the group C earthquakes. Both

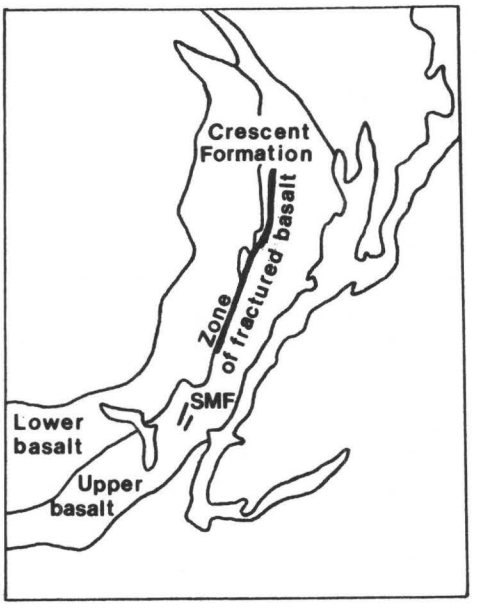


Figure 2. Map of selected structural features in the southeastern Olympic Peninsula. Geologic contacts after Tabor and Cady (1978); zone of fractured basalt after Glassley (1974); SMF, Saddle Mountain faults.

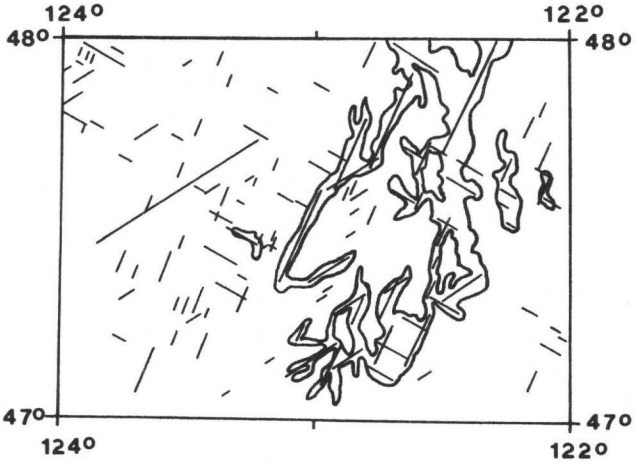


Figure 3. Map of Puget Lowland and eastern Olympic Peninsula showing possible lineaments that parallel late Quaternary faults.

the Cushman Valley fault (?) and the focal mechanism solution are similar to one nodal plane from each solution for the 1949 earthquake (N60°E, 78°NW (Nuttli, 1952); N49°E, 83°NW (Hodgson and Storey, 1954)) and all may be related to a similar stress orientation. All of the above correlations are by necessity only tentative because geographic distance, depth and age differences between the faults and earthquakes prevent any definite correlations.

The Saddle Mountain faults do not match any of the earthquake focal mechanism solutions in Table 1. However, the Saddle Mountain East fault plane (N22°E, 75°SE), with its dominant reverse with some left-lateral movement, and its orthogonal auxillary plane (N84°E, 29°NW) are consistent with the north to northwest regional compressive stress direction (Crosson, 1972; U. S. Geological Survey, 1975). Therefore, movement along all of the faults in the study area are probably the result of stresses similar to those now active in the Puget Sound region.

## POSSIBLE MAGNITUDE OF EARTHQUAKES ASSOCIATED WITH FAULTS

There have been several attempts in recent years to correlate the size of a fault with the maximum earthquake that could have been produced by movement along the fault. In one of the earlier analyses, Tocher (1958) plotted data from 10 California and Nevada earthquakes and performed a least squares fit of the data to obtain an equation correlating the log of fault length, L, to earthquake magnitude, M. Later workers have used this method on other data to derive different equations (Table 2) and evaluate possible errors in the data.

Wyss (1979) used the earthquake source area, A, rather than fault length to determine magnitude. He defined $A = W \cdot L$ where W is the width of the fault or the rupture distance in the dip direction. He used source area because the surface rupture length of a fault may not be the same as the source length and because faults with greater widths can create larger earthquakes even though their lengths may be the same or shorter than other faults. The use of source area is probably more accurate than using fault length if both W and L are known. However, without earthquake data this cannot be determined. Thus, approximating W adds an extra uncertainty to the problem.

A parameter that might be useful to incorporate into these equations is the amount of offset along the fault. It seems likely that faults having greater offsets, but similar lengths, than other faults would, like source width, cause larger earthquakes. This is a value that, unlike source width, can be determined for older faults. Tocher (1958) used fault offset in some of his equations of earthquake magnitude and energy. It is surprising that no one has continued using fault displacement.

Another problem that has received little consideration is the type of fault. Are the length and source area relative to magnitude the same for a strike-slip fault as for a normal or reverse fault? The data of Bonilla and Buchannan (1970) are based on strike-slip faulting, but other workers have not separated types of faults. Perhaps in the future there will be different sets of equations for each type of faulting.

Several problems are encountered in trying to evaluate the magnitude of earthquakes that occurred with movement of the faults in the study area: 1) The most obvious problem is determining the actual length of surface break along the faults. Time and erosion have surely reduced the length of the scarps, particularly on the Dow Mountain fault. Therefore,

Table 1. Earthquake focal mechanism solutions and orientations of late Quaternary faults.

| Earthquake | Reference | Solution |
|---|---|---|
| 1949 | Nuttli (1952) | N21°W, 52°NE<br>N60°E, 78°NW |
| 1949 | Hodgson and Storey (1954) | N76°W, 12°SW<br>N49°E, 83°NW |
| 1965 | Algermissen and Harding (1965) | N53°W, 35°SW<br>N18°W, 69°NE |
| 1965 | Isacks and Molnar (1971) | N15°W, 72°NE<br>N54°W, 23°SW |
| Group A | Crosson (1972) | N83°W, 70°SW<br>N12°E, 52°NW |
| Group B | Crosson (1972) | N52°W, 58°NE<br>N88°W, 38°SW |
| Group C | Crosson (1972) | N31°W, 85°SW<br>N57°E, 70°SE |
| Saddle Mountain East fault auxillary plane | | N22°E, 75°SE<br>N84°E, 29°NW |
| Saddle Mountain West fault | | N19°E, 67°SE |
| Dow Mountain Fault | | N58°W, 59°NE |
| Cushman Valley fault (?) | | N57°E, steep dip |

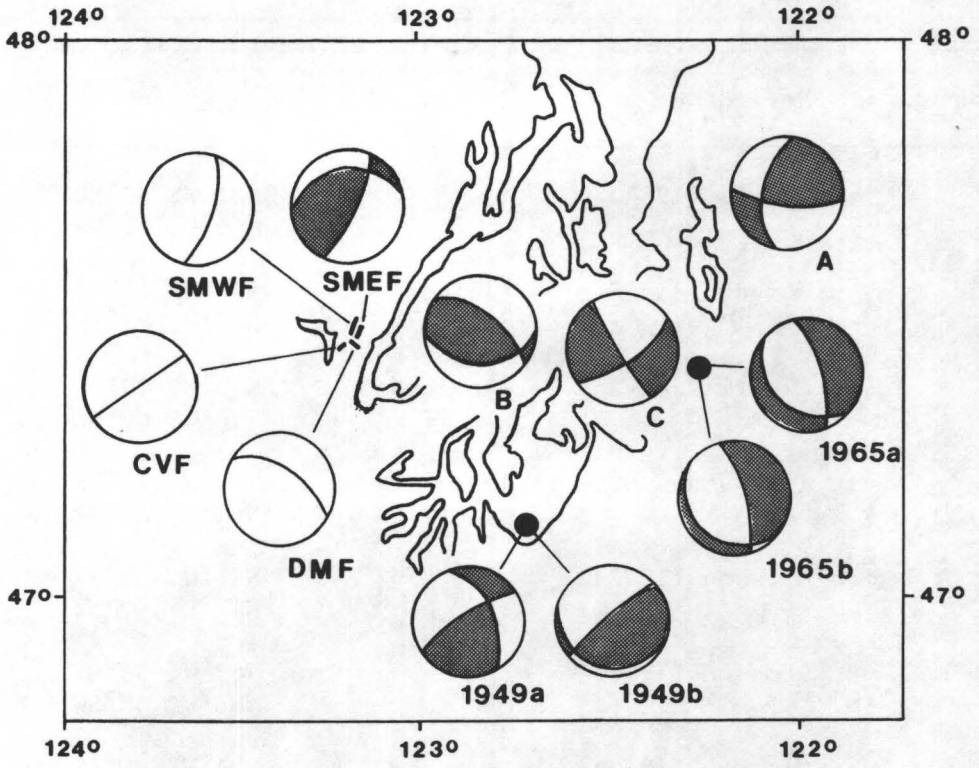


Figure 4. Map showing locations and orientations of earthquake focal mechanism solutions and late Quaternary faults in the Puget Lowland. Symbols: A, B, C, Crosson (1972); 1949a, Nuttli (1952); 1949b, Hodgson and Storey (1954); 1965a, Algermissen and Harding (1965); 1965b, Isacks and Molnar (1971); CVF, Cushman Valley fault (?); DMF, Dow Mountain fault; SMEF, Saddle Mountain East fault and its orthogonal auxillary plane; SMWF, Saddle Mountain West fault.

Table 2. Possible maximum magnitude of earthquake associated with Saddle Mountain East fault.

| Equation | Reference | Magnitudes L = 1.5 A = 2.25 | Magnitudes L = 4.3 A = 9.25 |
|---|---|---|---|
| $M = 5.65 + 0.98 \cdot \log L$ | Tocher (1958) eq. 1 | 5.8 | 6.3 |
| $M = 5.22 + 0.53 \cdot \log LD$ | Tocher (1958) eq. 5 | 6.7 | 6.9 |
| $\log L = 1.915 + .389 \cdot M$ | Bonilla and Buchana (1970) | 3.2 | 4.4 |
| $M = 1.235 + 1.243 \cdot \log L$ | Mark (1977) | 5.2 | 5.8 |
| $M = 6.03 + 0.76 \cdot \log L$ | Bolt (1978a) | 6.2 | 6.5 |
| $M = 3.415 + 0.825 \cdot \log L$ | Bolt (1978b) | 3.6 | 3.9 |
| $M = 4.38 + 0.93 \cdot \log A$ | Wyss (1979) | 4.7 | 5.3 |
| $M = 4.532 + 0.887 \cdot \log A$ | Singh and others (180) | 4.8 | 5.4 |

L is in km.
A is in sq. km.
Equations 3 and 4 require  in m.
D = 383 cm.

only the youngest and best exposed fault, the Saddle Mountain East fault, is used in Table 2. Even with this fault there are difficulties, thus both the visible scarp length (1.5 km) and the projected fault length (4.3 km) are used for comparison. 2) Determining the width of the fault is impossible. Geller (1976) plotted length versus width and decided that the best fit line was L = 2W, but there was considerable scatter from this line. However, since there is no other information on width of the Saddle Mountain East fault, Geller's relationship is used here. 3) The maximum amount of offset along the fault is uncertain. The scarp height is in places considerably higher than the recognized offset in the trench, but the height could be increased by erosion. The offset in the direction of the striations, 3.83 m, is therefore used in the calculations as the best approximation of maximum offset. 4) We do not know that all the offset along the fault occurred at the same time. If several movements occurred, the associated earthquakes could have been much smaller.

Table 2 shows the equations derived by several workers and magnitudes calculated for both possible lengths of the Saddle Mountain East fault. Due to the uncertainties of the models, these magnitudes show considerable variation and are open to interpretation.

The equations are generally designed to give the maximum magnitude earthquake that is likely to occur with a given fault. Yet, there are too many uncertainties to say that is the case with the Saddle Mountain East fault. If faulting occurred as several smaller movements, a possibility considering the radiocarbon dates for the fault, several smaller earthquakes could have occurred. If the present exposure is only a portion of the rupture length, the associated earthquake could have been larger. However, the magnitude differences between the two fault lengths for each equation are minor compared to the ranges between different equations.

It is difficult to distinguish which equation is best. Each is a best fit for the data it represents, but there is no indication as to how well the Saddle Mountain East fault fits with the data for the curves. There is a minimum magnitude for which each curve is accurate. Some of the smaller magnitudes in Table 2 are probably below their minimum. For example, Wyss (1979) suggested a minimum magnitude of 5.6 for his equation, well above the values calculated in Table 2. Thus, many of the magnitudes may be too small to be used with any certainty.

It is suggested that the values in Table 2 represent the range of possible earthquake magnitude that could have occurred with a single movement along the Saddle Mountain East fault. The maximum earthquake that could have occurred could thus have had a magnitude of about 6.5 to 7.0 but may have been much smaller.

## ACKNOWLEDGMENTS

Reviewed by John Watkinson. Robert J. Carson and Mervin J. Bartholomew provided invaluable assistance in the field and during the early writing of this report. Field work was funded by U. S. Geological Survey grant 14-08-0001-G-322 through the Washington Division of Geology and Earth Resources.

## REFERENCES CITED

Algermissen, S. T., and Harding, S. T., 1965, Preliminary seismological

report: in The Puget Sound, Washington earthquake of April 29, 1965: Washington, D.C., U. S. Government Printing Office.

Bolt, B. A., 1978a, Earthquakes: A primer: San Francisco, W. H. Freeman and Co., 241p.

_____, 1978b, Incomplete formulations of the regression of earthquake magnitude with surface fault rupture length: Geology, v. 6, p. 233-235.

Bonilla, M. G., and Buchanan, J. M., 1970, Interim report on world-wide historic surface faulting: U. S. Geological Survey Open-File Report, 32p.

Cady, W. M., 1975, Tectonic setting of the Tertiary volcanic rocks of the Olympic Peninsula, Washington: U. S. Geological Survey Journal of Research, v. 3, p. 573-582.

Carson, R. J., 1970, Quaternary geology of the south-central Olympic Peninsula, Washington (Ph.D. dissert.): Seattle, University of Washington, 67p.

_____, 1973, Holocene faulting, southeastern Olympic Peninsula, Washington: Geological Society of America Abstracts with Programs, v. 5, p. 568-569.

Coombs, H. A., 1953, A summary of Washington earthquakes: Seismological Society of America Bulletin, v. 43, p. 1-5.

Crosson, R. S., 1972, Small earthquakes, structure, and tectonics of the Puget Sound region: Seismological Society of America Bulletin, v. 62, p. 1133-1171.

_____, 1974, Compilation of earthquake hypocenters in western Washington: Washington Division of Geology and Earth Resources Information Circular 53, 25p.

_____, 1975, Compilation of earthquake hypocenters in western Washington - 1973: Washington Division of Geology and Earth Resources Information Circular 55, 14p.

Crosson, R. S., and Millard, R. C., 1975, Compilation of earthquake hypocenters in western Washington - 1974: Washington Division of Geology and Earth Resources Information Circular 56, 14p.

Crosson, R. S., and Nelson, L. J., 1978a, Compilation of earthquake hypocenters in western Washington - 1975: Washington Division of Geology and Earth Resources Information Circular 64, 12p.

_____, 1978b, Compilation of earthquake hypocenters in western Washington - 1976: Washington Division of Geology and Earth Resources Information Circular 65, 13p.

_____, 1979, Compilation of earthquake hypocenters in western Washington

- 1977: Washington Division of Geology and Earth Resources Information Circular 66, 12p.

Geller, R. J., 1976, Scaling relations for earthquake source parameters and magnitudes: Seismological Society of America Bulletin, v. 66, p. 1501-1523.

Glassley, W. E., 1974, Geochemistry and tectonics of the Crescent volcanic rocks, Olympic Peninsula, Washington: Geological Society of America Bulletin, v. 85, p. 785-794.

Hodgson, J. H., and Storey, R. S., 1954, Direction of faulting in some larger earthquakes of 1949: Seismological Society of America Bulletin, v. 44, p. 57-83.

Isacks, B., and Molnar, P., 1971, Distribution of stresses in the descending lithosphere from a global survey of focal-mechanism solutions of mantle earthquakes: Reviews of Geophysics and Space Physics, v. 9, p. 103-174.

Mark, R. K., 1977, Application of linear statistical models of earthquake magnitude versus fault length in estimating maximum expectable earthquakes: Geology, v. 5, p. 464-466.

Nuttli, O. W., 1952, The western Washington earthquake of April 13, 1949: Seismological Society of America Bulletin, v. 42, p. 21-28.

Rasmussen, N., 1967, Washington state earthquakes 1840 through 1965: Seismological Society of America Bulletin, v. 57, p. 463-476.

Singh, S. K., Bazan, E., and Esteva, L., 1980, Expected earthquake magnitude from a fault: Seismological Society of America Bulletin, v. 70, p. 903-914.

Tabor, R.W., and Cady, W. M., 1978, Geologic map of the Olympic Peninsula, Washington: U. S. Geological Survey Miscellaneous Investigations Map I-994.

Tocher, D., 1958, Earthquake energy and ground breakage: Seismological Society of America Bulletin, v. 48, p. 147-153.

U. S. Geological Survey, 1975, A study of earthquake losses in the Puget Sound, Washington, area: U. S. Geological Survey Open-File Report 75-375, 298p.

Wilson, J. R., 1975, Geology of the Price Lake area, Mason county, Washington (M.S. thesis): Raleigh, N. C. State University, 79p.

Wilson, J. R., Bartholomew, M. J., and Carson, R. J., 1979, Late Quaternary faulting and its relationship to tectonism in the Olympic Peninsula, Washington: Geology, v. 7, p. 235-239.

Wyss, M., 1979, Estimating maximum expectable magnitudes of earthquakes from fault dimensions: Geology, v. 7, p. 336-340.

# OFFSHORE QUATERNARY GEOLOGY OF THE NORTHERN PUGET SOUND - EASTERN STRAIT OF JUAN DE FUCA REGION WASHINGTON

by

H. C. Wagner and M. C. Wiley
Pacific-Arctic Branch of the Office of Marine Geology
U. S. Geological Survey-MS99
345 Middlefield Road
Menlo Park, California 94025

The interpretation of a series of major faults on marine gravity and magnetic maps in the northern Puget Sound-eastern Strait of Juan de Fuca region (Snavely and others, 1976b; MacLeod and others, 1977) led the office of Earthquake Studies of the U. S. Geological Survey to sponsor a study in 1978 of all available offshore seismic reflection profiles in the area. The study was aimed at delineating the major Quaternary offshore faults and relating them to earthquake activity since 1961 and to known faults onshore. Speculations concerning the geologic significance or evolution of the generally westward- or southwestward-tilted upper surfaces of bathymetric highs (Fig. 1) and their relationship to the series of major faults were also to be a part of the investigation. Bottom sediment data from National Ocean Survey charts provided information for lithologic and gross facies interpretation, as other bottom samples were not available.

## COLLECTION OF SEISMIC-REFLECTION PROFILE DATA

Most of the seismic reflection profiles upon which this study is based (Fig. 2) were obtained during a joint U. S. - Canadian geophysical cruise aboard the Canadian Survey Ship PARIZEAU in 1972 (Snavely and Tiffin, 1980). Additional data were obtained during a cruise of the U. S. Geological Survey Research Vessel DON J. MILLER in 1976 (Snavely and others, 1976a). Data concerning power systems, navigation, and filters used are given in Appendix I.

Twenty-three track lines with a total length of approximately 700 km were run in the area (Fig. 2) during the cruise of the CSS PARIZEAU. Three recorders operated simultaneously to record high-resolution (0.25 sec. sweep) and single-channel sparker (1-sec. and 2-sec. sweep) seismic-reflection profiles. About 80 km of high-resolution (0.25 sec. sweep) profile data were recorded by the R/V MILLER. Using sea-water velocity, vertical exaggerations on the records ranged from about 5:1 to 10:1, depending on sweep rate, on the PARIZEAU records and 10:1 on the MILLER records.

## INTERPRETATION OF INTERMEDIATE-PENETRATION SEISMIC-REFLECTION PROFILES

All CSS PARIZEAU and R/V MILLER seismic reflection profiles were reduced to fit on roll-vellum of 9-inch width. Geologically pertinent acoustic data were traced onto plastic overlays, and care was taken to eliminate multiple- and hyperbolic-derived reflections. Most of the stratigraphic and structural correlations were from CSS PARIZEAU single-channel data recorded at a 1-second sweep. The sparker system produced a very broad bubble pulse (Appendix II). The time interval between the initial bubble formation and final bubble collapse ("noise" or "ringing"), made the single-channel records particularly difficult to interpret (Figs. 3-4).

Line drawings showing similar structural features interpreted from the data were organized into 5 figures located in the northwestern, north-central and eastern, southwestern, south-central and southeastern parts of the study area (Figs. 5-9). These figures are outlined on Figure 10 by dotted lines. Brief descriptions of the structures and relationships in each of these areas follow.

Figure 5 shows line drawings from the northwestern part of the area, illustrating interpreted features that have sufficient similarity to be distinctive. These features define domains that are indicated by two separate stipple patterns on each line. The structure represented by the left-hand pattern is interpreted as a broad syncline that is faulted in part. South (left) of this structure is a sequence of faults and folds. North (right) of the syncline is a domain indicated by a darker pattern. It is interpreted as an anticlinal feature which clearly persists from line to line in Figure 5. The anticline is faulted locally along its northern and southern edges. These correlations and other structural features are plotted on Figure 10.

As shown in Figure 6, this entire structure can be correlated into the central and northeastern parts of the study area where it becomes somewhat more complex; but the same basic geologic features are present. The syncline has broadened and is cut locally by more faults. The anticline is still present and is faulted near its crest mainly along its southern flank. Other structural features also have become more obvious, such as the zone of small folds just south of the major syncline (Fig. 6, lines 37 and 38). Areas of complex faulting also carry from line to line as does a distinctive small feature that appears as a branching pair of reflectors (circled on lines 31, 33, 37, and 38 of Fig. 6). A very similar feature is recorded on several lines in the southern part of the area (Figs. 8 and 9) but as yet no clear evidence is present to indicate that they are correlative. In general, correlations are made and followed without great difficulty once the basic pattern has been recognized.

The structural and stratigraphic features of the acoustic reflection profiles in the southern part of the area (Figs. 7-9) are interpreted as a channel-fill feature (light stipple pattern) at the southern (left) ends of profiles 24-27 (Fig. 7). Lack of penetration and overriding multiple reflections of the seafloor masked the base of the channel-fill on lines 24 and 25. The presence of other geologic features associated with the channel,

though, allowed the position of the channel to be approximated (Figs. 7, 8). To the east, the northern part of this channel is no longer truncated by the fault (Fig. 9). The triangular, fault(?)-bounded feature toward the northern part of this segment can be delineated on several of the lines; the northern boundary appears to be vertical in Figure 8, while in Figure 9, lines 38 and 43, the boundary lies at a low angle. Other structural features, however, retain their relative positions and the correlations seem acceptable.

Figure 11 illustrates the correlations between the structurally similar domains depicted on Figure 10. Two contrasting regions of structural style are revealed. To the north, the units have been deformed, presumably by E-W compression, into broad folds whose axes trend roughly N-S; some axes are overturned toward the west (Fig. 10). South of these, the limbs of folds appear as discrete, isolated blocks and may represent two units now offset by multiple NW-trending faults (Fig. 10). As interpreted from the seismic-reflection profiles, these folded structures may affect strata at depths as much as 500 m beneath the seafloor; however, this "apparent" depth may also be attributed to multiples and may, in reality, be much less. If the deeper structures are real, the depth at which this deformation occurs suggests that these faults, anticlines, and synclines have been generated by two or more periods of tectonism affecting Pliocene(?) and Pleistocene sediments (Figs. 10, 11). The age of strata underlying the study area can be surmised only, but is based, in part, upon data from exploratory wells drilled on Dungeness Spit and Whidbey Island. In these wells, Miocene strata lie at depths greater than 650 m (2000 ft) below the sea floor and Pliocene strata may occur at shallower depths.

In addition to the tectonic origin, it is also possible that these large folded and faulted structural features are of glacial origin. They are similar to the straight or slightly arcuate ridges of ice-stagnation drift composed of kettled, hummocky gravel and boulder till reported upon by Thorson (1980) directly south of the study area in the Puget lowland. Ice-contact stratified drift, deposited during the recession of the Vashon ice lobes, formed deposits reaching 120 m in height. Ice-marginal channels parallel these ridges. The ridges may also be "glacio-tectonic" (Moran, 1971) in origin, such as glacial drift that has been contorted by ice push or bed shear into faults and folds with minor displacements. If this were the case, the direction of folding can be used as an indicator of direction of glacial flow. Kupsch (1962) documented ice-thrust ridges in Saskatchewan which have curved shapes similar to the trends shown in Figure 11 and with amplitudes of 20 to 40 km. The overturned limbs of the folded zone in the northern part of the study area could have formed during the maximum of the Vashon Stade of the Fraser Glaciation when the Cordilieran Ice Sheet sent lobes both southward beyond Olympia and westward through the Strait of Juan de Fuca to the Pacific Ocean (Heusser, 1973). The Juan de Fuca lobe, near its eastern end, is estimated to have extended to a height of more than 1000 m along the northern flanks of the Olympic Mountains (Brown and others, 1960) and to have been between 900 and 1200 meters thick near Victoria (Heusser, 1973, p. 288). Kupsch (1962, p. 591-592) estimated a maximum thickness of glacier ice where ice-thrust ridges were formed in the Dirt Hills area of Saskatchewan to have been between 137 and 275 meters. Kupsch believes that this thickness alone is insufficient to have formed the ice-thrust ridges unless they developed

parallel to the front of a relatively thin but actively-flowing glacier moving up-slope or pushing against valley walls, thus increasing the compressive-flow regime near the ice margins and terminus. The major structures in the northern Puget Sound-eastern Strait of Juan de Fuca area may, then, also be the result of deformation by ice-shove as the Juan de Fuca lobe advanced westward toward the constriction between Victoria, B. C. and Port Angeles, WA. exerting considerable lateral pressure against the sediments flanking the San Juan Islands. Thorson (1980) speculated on the origin of Dallas Bank and suggests that the Juan de Fuca ice lobe may have grounded itself on the bank during recession and that much of the ice-contact stratified drift may have been deposited in the Strait at this time of stabilization.

## INTERPRETATION OF SHALLOW-PENETRATION, HIGH-RESOLUTION SEISMIC-REFLECTION PROFILES

The 0.25-second sweep seismic-reflection profiles provided by the CSS PARIZEAU and R/V MILLER cruises reveal a wealth of information concerning Pleistocene glacial sedimentation, post-depositional folding and faulting, areas of slumps and landslides, and possible entrapment of methane(?) gas. The locations of selected parts of the high-resolution profiles used as illustrations are shown on Figure 12.

### Glacial sedimentary facies.

The depositional facies, processes and environments interpreted from the profiles will be discussed first because later figures will show them modified by folding, faulting, or other geologic phenomena. Figure 13 shows a series of near-horizontal reflectors (between 2218 and 2222) that are interpreted to represent interbedded glacio-marine or glacio-lacustrine sediments, possibly sands and silts. The sequence is about 2.5 m thick and is underlain by about 10 meters of irregular or lenticular reflectors that may represent intertonguing gravelly and silty sediments. The underlying, essentially non-bedded sequence is interpreted as till or morainal deposits. East (left) of 2214 is an 8-m thick sequence of reflectors that dip eastward to the edge of the record. The sequence is overlain by about 12 meters of unbedded material followed upward by 2 to 5 m of good reflectors that dip similarly eastward. An essentially unbedded sequence overlies these reflectors until the seafloor is reached. At a depth of roughly 20 meters beneath the 12-m thick material (at 2211) is a series of hyperbolic reflectors that trend upward toward 2215. This surface is interpreted as representing the irregular top of glacial moraine or a till sequence. A slight change in level of the seafloor at about 2214 is interpreted as a fault of Holocene age with the east (left) side down roughly 2 meters. The 12-m thick well-bedded unit appears to occur only on the east side of the fault. Small hyperbolic reflections, generated below the change in seafloor at the ends of the reflectors that make up the well-bedded unit, also suggest the presence of a fault at that position. Another fault is interpreted at approximately 2217.5. The location of Figure 13 is shown near the southeastern corner of Figure 12.

On Figure 14, between 0340.2 and the south (right) end of the figure, the rough surface of the seafloor is interpreted to reflect the presence of a

gravel-covered surface. A similar seafloor surface appears between the north (left) end of the figure and 0336.5 where the seafloor rises and becomes a smooth surface but has changes in level. The reflectors beneath the seafloor are continuous throughout the distance shown in the figure and the beds below the changes in level are not faulted. The reflectors suggest the presence of deltaic sediments (with foreset bedding) interbedded with glacio-marine beds.

Figure 15 shows somewhat irregular seafloor topography underlain by two or more thin sequences of bedded gravelly moraine deposits east (left) of 2025; the uppermost sequence dips eastward from 2020.2. Similarly, at least two upper Pleistocene bedded sequences underlie the seafloor between 2027.5 and 2030.1. These bedded sequences appear unconformably to overlie an older Pleistocene(?) unit in which folded beds (2025) are truncated by an irregular erosional surface.

Figure 16 shows at least four different facies, each indicative of different depositional processes and environments. The lowermost unit penetrated varies from a poorly bedded unit on the left (west) to an almost reflector-free unit on the right (east). The western unit probably consists of beds and lenses of pebbly mud and sand deposited by flowing water. The essentially unbedded eastern unit indicates homogeneous material such as mud or fine-grained till. Overlying these units (0.092-0.12 sec. depth) is a well-bedded unit that may reflect alternating layers of sand and mud, such as might develop in a ponded glacial lacustrine environment. Numerous small faults offset this unit and several extend into the underlying poorly bedded unit (till?). Minor faulting associated with glacial ice-contact (till) sediments is quite common and well documented (Thorson, 1980; McDonald and Shilts, 1973). Resting conformably upon this well-bedded sequence is another well-bedded unit that has been truncated by erosion at its west (left) edge (between 2200.5 and 2201.5 travel time). This unit was itself truncated at about 2201 and channeled at 2159.9. The uppermost (youngest) unit appears to be a prograding deposit with foreset beds and an irregular hummocky surface. The deposit probably consists of stratified sand and mud and may be a delta front.

Figure 17 is an example of fairly well-bedded glacial sediments (1417-1420) that have been dissected by tidal-current or glacial-scour erosion along the western slope of Eastern Bank. These sediments are overlain by a thin veneer of material of probable Holocene age (1418-1420). Although the quality of this record is poor, the discontinuous, parallel-reflection character in parts of the sequence are interpreted as being composed of randomly laminated mud to poorly stratified mud and sand reflecting glaciofluvial and glaciomarine sedimentation. Other examples of bedded glacial deposits whose slopes have been truncated by glacial erosion, glacial scour, or interglacial erosion are shown in figures 13, 36, 39, 45, 52, 60, and 80.

Along the northeastern upper part of Hein Bank, the lack of continuity or non-bedded reflection character in the lower part of Figure 18, which lies below 0.22 seconds depth in the northern part of the record (0735-0740) suggests that the unit may be a poorly sorted, massive pebbly mud or till. Farther south, a drumlinoid or mound-like feature, which extends above the seafloor at 0732-0733, contains discontinuous bedding in the uppermost part of

the unit indicating transition to a glacial-fluvial environment. The near-horizontal material that truncates the older bed at 0730 may consist of a latest Pleistocene and possibly Holocene packet of sediment. This packet laps onto the drumlinoid(?) feature from both the north (right) and the south. Near the center (0734 at 0.21 sec. depth) is a small channel partially filled with slump(?) debris and overlain by essentially horizontal sediments. A smaller drumlinoid(?) feature occurs at 0735. Similar constructional glacial features are shown in Figures 20, 25, 26, 33, 41, 50, 64, 65, 67, 74, and 80.

At least two glacial depositional sequences are interpreted on Figure 19. The lower sequence is internally chaotic, lacks bedding, and may be a bouldery ice-contact sediment. The overlying sequence shows faint bedding and may be a pebbly mud or till. The surface between the two sequences is fairly sharp and seems to be offset by vertical faults at several places (0542, 0549.7, 0550.3, 0550.7, and 0551.4). The faults at 0549.7, 0550.3, and 0550.7 appear to offset the seafloor. The irregular topography between the faults at 0550.7 and 0551.3 may be a slump block that is moving down-slope southeastward away from the line of the profile.

The large mound-like structure in Figure 20 is constructional and plots (Fig. 12) along an elongate bathymetric surface (Fig. 1) on the Canadian Hydrographic Service Natural Resources Map (1976). Based on its external geometry and the discontinuous, chaotic nature of the reflectors, the mound may be an ice-contact or ice-thrust deposit. Younger, poorly stratified sediments on the north (left) side (at 2315 and 0.12-0.14 sec. depth) dip inward. The dip decreases upward through the horizontal until they dip outward in an onlap or offlap position. These latter sediments may have been ponded along the flanks, onlapping against the structure. Sediments composed of sub-parallel lenses of sand and mud were presumably deposited around the mound as outwash during recession.

Figure 21 provides an example of two or more glacial sequences interpreted as episodes of glacial stagnation during recession or possibly as reflecting minor local advances and retreats of the ice. The irregular paleotopography shown by the irregular surfaces beneath the near-horizontal poorly bedded sediments may also represent channeling or scour by ice.

Internal features within the sediments in Figure 22 are interpreted as being a slump overlying a sequence of well-bedded and poorly bedded units. The basal (glide) plane of the slump lies along the upper surface of continuous-bedded reflectors that reach the seafloor at about 2119. The sequence below the base of the slump is interpreted to consist of alternating sand and mud grading upslope into more poorly sorted sediments. A similar interbedded unit that occurs in the basal part of the slump is overlain unconformably by relatively reflection-free sediments (till?) whose upper surface is hummocky. It is presumed that the entire slump sequence has moved downslope in a southerly direction. A good reflector occurs within the slump at about 0.14 sec. depth at 2125 and slopes gently southward; it apparently buckled somewhat (2122) by internal flowage before reaching the sea floor. A vertical fault, which is apparently confined to the slump brings a bedded sequence in contact with the till(?) and forms a south-facing escarpment. The preservation of this fault scarp suggests that it is relatively young and that

the slump has been active in Holocene time.

Figures 23 and 24 are interpreted to represent irregular sea floor topography that is attributed to either a recessional moraine composed of bouldery till or a slump. The hummocky topography in Figure 23 may favor a till origin although slump deposits could also produce such surface irregularities. Underlying these sediments are continuous subparallel reflectors suggesting deposition in a fluvial environment such as in glacial outwash as described by Mitchum and others (1977, p. 123). In Figure 24, a well-bedded feature, which appears to be truncated along both sides, is interpreted as an erosional remnant or pinnacle (0908-0909) surrounded by poorly bedded to homogeneous sediments, such as a slightly bedded to massive till. A nearly horizontal reflector at 0.048 time depth may be offset by a fault at 0906.2. This fault apparently also offsets the sea floor. Similar irregular seafloor topography is also present in Figure 37. Figures 24 and 37 show the tops of San Juan and Smith Banks, respectively.

Mounds of bouldery gravel or bouldery till and lacking internal structure are shown in Figures 25 and 26. A bedded sequence laps onto each mound, conformably draping their tops and then top-lapping them. Both mounds have characteristics of diapirs. The bedded sediments overlying the mounds have been gently warped, their upper surfaces have been onlapped and are conformably overlain by upper Pleistocene(?) to Holocene sediments. In Figure 25 the well-bedded sediments grade laterally northward into an unbedded homogeneous sequence, possibly gravels or gas-charged sediments. The lower part of the well-bedded sequence at the west (right) side of Figure 26 has been downdropped by faulting (1950.1) against a reflectionless unit. Similarly, at 1951, a fault has brought this reflectionless unit in contact with a somewhat bedded unit. The upper well-bedded sequence is underlain by a unit with discontinuous reflectors which, in turn, is underlain by fairly good reflectors which drape the mound. These reflectors dip westward and overlie an irregular topographic surface that may be till or ice-contact deposits. Another example of a well-bedded sequence indicative of a fluvial environment that grades laterally into poorly bedded to non-bedded sediments is shown in Figure 27 (1104.5). The well-bedded sequence is near a bathymetric low (Figs. 1, 12) whereas the homogeneous (gas-charged?) material is rising southward toward Dallas Bank. A fault which terminates the reflectors in the upper unit appears also to offset the sea floor in the same direction, down toward the north.

Figures 28 and 29 illustrate a slightly rough sea floor that is presumed to be covered with a boulder lag winnowed from till, or possibly sediment waves across the surface. In both profiles, this irregular surface is underlain by a sequence of good reflectors that are divergent, convergent and parallel. Two uplifted areas on Figure 28 (2254.5 and 2257), with onlapping sediments on their sides, appear to be underlain by heterogeneous non-bedded sedimentary materials. The sediments in the synclinal feature (2253) and adjacent anticlinal feature to its east (right) are thought to be gas-charged (acoustically turbid) as are those in the broad area between 2248 and 2252. The absence of reflections within, and the drawdown of well-bedded reflectors surrounding, this anomalous unit in Figure 28 suggests that the compressional velocities within the acoustically turbid (homogeneous) unit have been

considerably reduced in relation to those in the adjacent unit (Schubel, 1974, p. 292) due to the presence of interstitial gas bubbles. Peat and coal beds can have similar effects (Milton Dobrin, personal communication, 1979). The well-bedded unit in Figure 29 is interpreted as being underlain by a glacio-lacustrine or glacio-fluvial non-bedded sedimentary sequence, probably a massive till composed of structureless pebbly mudstone or poorly bedded outwash. Faults terminate and offset reflectors in the lower part of the well-bedded sequence.

An interesting buildup of glacial sediments is shown in Figure 30. The mound is formed of at least two depositional sequences distinguished by their angular discordance with one another. The lower contact of the uppermost reflectors is interpreted as sediments whose thin, gently dipping foreset beds terminate by downlap against a lower surface; the upper surface varies from onlap to topset bedding. The presence of this upper sedimentary (topset) segment implies low sediment supply accompanied by a rapid rise in sea level (or rapid basin subsidence) in order to preserve the topset unit (Mitchum and others, 1977). The external geometry of this structure and the internal configurations suggest that the buildup may have resulted from a series of migrating sediment waves creating a dune-like feature. A relatively low-energy sedimentary regime is indicated by the reflection configuration; such a regime would be favorable to the formation of large-scale ripples and dunes. If this is a dune, its approximate height would be 28 to 30 m. The structure may also be some sort of mounded onlap or prograded fill within the trough or channel. The sequence overlies a lower unit that may be cut off by faulting at its west (left) end in the topographic low. This constructional feature is part of a narrow, north-trending elongate high between Dungeness and Dallas Banks (Fig. 1).

Figure 31 displays a south-dipping well-bedded unit which is abruptly terminated (0640) by a near-vertical fault that brings a poorly bedded sequence on the south in contact with the bedded unit. A lower strong reflector 0.01 sec. above the multiple appears also to be offset by the fault (at 0.18 sec. depth) but the offset is small. This suggests that movement on the fault was principally strike slip bringing the well-bedded (fluvial or lacustrine) sediments into juxtaposition with the poorly bedded (ice-contact) sediments. The ice-contact sediment may be till with interbedded sand or silt giving the poorly bedded appearance. Hyperbolic reflections and offset of these beds, particularly in the upper part, suggest another fault (at 0643). This latter fault however, does not cut bedding near the seafloor and could be related to sedimentation and compaction of the till above buried ice.

The sediments in Figure 32 are interpreted as having been deposited by glacial-fluvial processes. The reflections are fairly strong, sub-parallel to parallel, but change rapidly laterally. The pattern suggests uniform rates of deposition and may represent a thick sequence of outwash sediments (sand, silt, and gravel). This sedimentary sequence in places shows a crenulated or crumpled character, as at 1453.2 at time depth 0.19 and at 1456 at time depth 0.215. Unconformably overlying this glacial-fluvial unit is a large landslide that trends into an east-west modern channel north of Dungeness Spit. Faults are interpreted at 1453 and 1457 on the basis of changes in reflection character and hyperbolics.

Figure 33 provides a good example of foreset bedding related to basinward deltaic sedimentation toward the Strait of Juan de Fuca (1728-1733). The location of this sequence is slightly northeast of Ediz Hook at Port Angeles and only a few km offshore. Two large creeks enter the Strait of Juan de Fuca near this profile and the foreset beds and scour channels (1729.7 and 1727.5) may be related to past and present stream-flow and longshore current activity. The two faults shown at about 1728 may have been active in developing a zone of weakness along which erosion could have been more effective and appear to have modified the continuity of the seafloor by dropping the shoreward portion downward (note dashed line). The two seafloor surfaces are parallel but the basinward (northern) portion is now roughly 8 meters higher than the landward portion. Another feature shown in Figure 33 is the depositional high in the northern part of the figure. This high may be a moraine composed of till upon which both upper and uppermost Pleistocene bedded gravel and sand deposits have accumulated. Some of the debris in these younger deposits was probably furnished by the high itself, which is now being truncated by erosional action at the seafloor.

The mound-like feature shown in Figure 34 is interpreted to be a cross-sectional view through a lobe of Pleistocene or Holocene glacial material. The configuration is mounded; reflectors drape and offlap an internal lens suggesting the mass is a small fan, till-lobe or slump. The hummocky bathymetric surface is in the Admiralty Inlet area and, as shown on detailed bathymetric maps (Canada Hydrographic Service, 1976; Chrzastowski, 1980) is an area in which the contours are suggestive of a recessional moraine. Underlying this deposit is an older sequence, possibly early late Pleistocene in age, that was folded and truncated by erosion prior to the deposition or slumping of these overlying sediments. Another set of foreset beds is shown along the southeast flank of Hein Bank in Figure 35. Their gently sloping, prograding reflection configuration is interpreted as resulting from deposition in a low-energy sedimentary regime, possibly during a rapid rise in sea level to allow deposition and preservation of the topset unit. They overlie a smooth surface cut on a till sheet in which poor bedding is apparent locally.

Other constructional glacial features are bank-edge deltaic deposits that consist largely of foreset beds. As shown in Figures 36, 38, 39, 40, 41, 42, and 43, the bottoms of these deposits commonly begin slightly back from the slope edge and build forward to the previous slope face. The slope face in places shows truncated, nearly horizontal older beds (Fig. 36). These truncated beds were possibly cut into and eroded by glacial scour during the last major westward advance of the Juan de Fuca lobe during the Vashon Stade of Fraser Glaciation. A feature common to some of these off-bank deposits is a low area at or near their bank-top edge (Figs. 36, 38, 41 42, 43). At both Eastern Bank and Center Bank (Figs. 37, 39), foreset beds are noted on both edges of the banks. The lateral extent of these deposits on Eastern Bank (Fig. 37) cannot be determined because only one seismic-reflection profile crosses it. Deltaic over-bank deposits seem to cover the uppermost slopes of much of Center Bank (Figs. 36, 38, 39). The very rough acoustic signals from the northern part of the top of Eastern Bank (Fig. 37), as well as from the southern part of San Juan Bank (Fig. 24) suggest a surface covered with very large boulders or sand waves. Offset of the reflector underlying this

irregular bottom topography on Eastern Bank (Fig. 37) suggests faulting some of which may be as young as latest Pleistocene or Holocene. Other bank tops, such as Smith Bank (Fig. 40) and Dallas Bank (Fig. 41), also have young sediments that have been offset by faulting. However, the overbank deltaic deposit on the northwest side of Dallas Bank (Fig. 41) is younger than a fault lower in the section which does not offset its base.

Figures 41, 42 and 43 show multiple depositional sequences. In these figures, fluvial overbank deposits have prograded out across an older ice-scoured surface. The underlying unit is poorly bedded to non-bedded and may be till. In these Figures, as in Figures 36, 38, and 39, there appear to be areas of sagging or depression near the upper bank edge part of the feature (1820 on Fig. 41; 1208 on Fig. 42; 1444 on Fig. 43).

Figure 44, although a deltaic deposit, occurs not on a bank top but on the seafloor slope between Port Angeles and Dungeness Spit. The prograding sediments may be relict and represent a shoreline or delta front at a lower stand of sea level prior to the sea level rise following the last major glaciation in the Strait of Juan de Fuca. They may also be interpreted as accumulations of detrital sediment that was moving downslope from the mouths of several rivers flowing northward from the Olympic Mountains as the alpine glaciers melted.

Erosional features.

The effects of large scale glacial scour can be observed in Figures 17, 36, 38, 39, and 88, where the truncated ends of near-horizontal reflectors surface along the slopes of Eastern Bank, Center Bank, and San Juan Bank. Glacial scour probably also accounts for the relatively steep slopes bounding other banks in which truncation of the underlying massive to poorly bedded till and associated faulted and folded ice-contact deposits is obscure.

Other erosional features, well displayed in the seismic-reflection profiles, are channels many of which were scoured by glacial ice or meltwater flowing beneath the ice sheet. Small channels and ponded sediments are preserved on bank tops (Figs. 45, 46, 48, 52), but most channel deposits lie within incised topographic lows at the bases of the banks (Figs. 47, 49, 50, 51). Where channels are noted on two or more crossing lines over a bank top or along a slope, trends can be established. Such channels cross Dungeness Bank (Figs. 45, 46) and Dallas Bank (Fig. 50). This apparent relationship of channels that lie on bank tops and not within present topographic lows may merely reflect the positions of older channels which formed across once-continuous outwash deposits that have since been uplifted and glacially scoured into separate banks.

Many bank-related channels contain well-bedded near-horizontal deposits (Figs. 46, 47, 51, 52); others contain unbedded deposits (Figs. 48, 49), and some contain a combination of bedded and unbedded deposits (Figs. 45, 50). Generally, the meltwater channels appear to have established themselves early during deglaciation so that their positions were maintained during recession (and even during submergence as sea level rose and inundated the region).

Folded glacial deposits.

Two different types of folding have been interpreted from the single-channel sparker and high-resolution seismic-reflection profiles. Both types may be related in part to ice movement. The folds and deeper structures interpreted from the sparker records reveal a style of deformation that is subject to more than one interpretation. First, the series of large amplitude folds north of the North Whidbey Island fault of Gower (1980) may have resulted from compression during tectonic activity in Pleistocene time. A second possibility is that the folds, which are roughly 10 km in width, represent large-scale ice-thrust ridges formed by ice-push during successive advances of the Cordilleran ice lobes. Folds of similar or greater dimensions and attributed to ice push have been recorded in the Puget Lowland by Thorson (1980) and in the Missouri Coteau region of Saskatchewan by Kupsch (1962).

On the high-resolution, shallow-penetration profiles, well-bedded sediments commonly are folded as illustrated in Figures 53 to 65. These folds are generally less than 0.2 km in width and of low amplitude. They are interpreted to represent folded, glacio-fluvial and glacio-lacustrine sediments and generally are associated with ice-contact materials against which they are juxtaposed by faulting or post-depositional collapse. Their uppermost beds are presumed to be of latest Pleistocene age and occur not only high on the flanks of islands and banks (Figs. 53, 57, 58, 59, 64, 65), but at intermediate locations (Figs. 55, 56, 61, 62, 63) and in the glacial troughs (Figs. 54, 60). The different amplitudes of fold-type deformation can be observed in Figures 53 and 55; those in Figure 55 are approximately twice the amplitude of those in Figure 53. Figure 58 shows a lesser amplitude than in Figure 53. Figure 60 is interpreted as an example of an earlier period of ice-push folding whose folds have been truncated during glacial advance and ice scour of a later lobe (or possibly by erosion from contact with a more inland portion of the same lobe). Ice-push folding seems in places to be followed by normal or strike-slip faulting (Figs. 60, 61, 62, 64). The faults in these profiles could be interpreted as resulting from adjustments within the sediment body as masses of associated ice melted. Examples of sediments faulted as a result of melting of large bodies of ice beneath them have been described by McDonald and Shilts (1973) and Rust and Romanelli (1975). In many places, during withdrawal of the last ice lobe, the uneven upper surfaces of folded sediments were truncated by erosion and filled by younger sediment (Figs. 53, 55, 56, 58, 59, 63, 64).

Faulted glacial deposits.

Faulted glacial deposits on the high-resolution seismic-reflection profiles have been interpreted on many of the previously described illustrations (Figs. 13, 16, 19, 22, 24, 26, 27, 29, 31, 33, 37, 40, 41, 47, 49, 50, 52, 60, 61, 62). Many of these faults (Figs.13, 19, 22, 24, 27, 33, 37, 40, 41, 49, 52,) and those on illustrations to follow (Figs. 65, 68, 85, 86) apparently offset the sea floor and could be classed as active. Other faults that reach the sea floor but show no apparent sea floor offset are classed as Holocene if they offset a thin layer of sediment above the uppermost folded sediments or reflective units that are interpreted as gravelly, bouldery, or till-like (Figs. 26, 31, 32, 38, 40, 41, 50, 52, 61,

62, 67, 69, 70). Many faults on the 0.25-second seismic-reflection profiles do not appear to reach or extend beyond the base of this upper layer of sediments and are not considered to be Holocene in age. Faults classed as Holocene are indicated by the symbol "H" on the map of late Pleistocene(?) and Holocene geologic features (Fig. 94).

Figure 64 shows several faults that appear to offset an older morainal surface and younger reflectors but do not offset the good reflector that lies 4 to 8 m below the sea floor and is interpreted to represent the base of Holocene sediments. A similar older moraine-like feature is offset on Figure 65. The fault that offsets it also appears to offset the sea floor. Figures 66 and 70 provide good illustrations of well-bedded sequences that are faulted against non-bedded sequences such as till sheets. On Figure 66 the base of an old channel (between 0957 and 1006) also appears to have been offset by faults (1000 and 1002). The topographic high at 1005 appears to be underlain by a young channel that is filled with glacial outwash(?). The reflectors in Figure 67 are interpreted as showing an early erosional surface that has been offset by faults (indicated by terminations of reflectors, offset of deeper surfaces, and hyperbolics). These faults appear to cut Holocene sediments. Figure 68 contains evidence of several faults (shown by hyperbolics) that offset the base of probable latest Pleistocene sediments that fill ice-scoured or other erosional features cut in older till or glacial outwash. Only one fault (2146) appears to reach the sea floor, but no offset has been preserved. Sea floor offset is apparent, however, in Figure 69 near the north (left) end of the figure. The sea floor is downdropped to the south on the two southern faults and to the north on the northern one. The total effect is a small horst-like feature. In figure 70, offset reflectors indicate faults that extend to the seafloor at positions where the slope of the seafloor changes.

Slump and landslide deposits.

Many irregularities on the sea floor may represent slump or landslide deposits; however, some of them could also be interpreted as till sheets or morainal ridges. Only by observing the basal and internal features can they be properly differentiated, and even then some interpretations are questionable. The small hummocky feature at about 1153 on Figure 67 is interpreted to be a small slump; the bedding of the sediments to the south (left) can be observed to extend beneath the slump area to the fault where they end in a series of hyperbolic reflections. Movement on the fault may have generated the slumping of sediments near or at the sea floor; the movement was probably at an angle to the line of profile since no breakaway face is apparent. An example of a breakaway face is shown in Figure 71. Presumably downfolding of the sediments occurred as their underlying support was removed. The beginning of the basal glide plane beneath the landslide is shown on Figure 71 and continues on Figure 72 where the listric surface at its termination is evident. Post-movement erosion has truncated and leveled the irregular upper surface of the feature at its time of origin. The toe of a modern slump moving downslope is shown in Figure 73 at 1802. The modern failure plane may overlie an older slump deposit between 1758 and 1808.

Disrupted reflectors below an irregular sea floor are interpreted as

slumping in Figure 74. The disrupted reflectors appear to grade laterally into a well-bedded sequence toward the south (left). On Figure 75 between 0313 and 0315 small seafloor disruptions occur above a zone of sediment flowage in the upper part of a landslide. The glide plane of the landslide can be followed northward in the profile to a subsurface buttress (0304.5) and beyond to where it reaches the present sea floor (0303). The landslide is buckled into anticlinal or domal features where the buttressing effect occurs and the sediments beneath the buried sea floor are folded to conform with the shape of the buttress. A somewhat similar set of topographic features (mounds?) are shown in Figure 76. The low-dipping planar reflector below the upper unit is interpreted as an older seafloor surface that forms the basal contact between the slump(?) and the underlying sedimentary unit. However, the mounds may be morainal deposits lying on an older seafloor.

Figures 77 through 83 illustrate other interesting slump and landslide features. In figure 77, the breakaway scarp and basal plane of a landslide can be readily distinguished, as can an arching in the landslide. Disruption of bedding in the landslide is not apparent, but the slip plane below the landslide is disrupted and the underlying sediments appear to consist primarily of till(?). The reflectors observed below the glide surface are essentially parallel to that surface suggesting that the bedding below was semi-consolidated and readily folded to conform to the glide plane. The lower sediments within the arched part of the landslide lack reflections and may be homogeneous mud or may be gas-charged sediments. Figure 78 shows another example of a landslide that is completely detached from the upper slope and has come to rest at the base of the slope. The glide-plane has become crenulated near the east (right) end of the figure (1251 at 0.17 sec. depth). A small slump lies within the upper part of the landslide (1244-1245). Figure 79 gives another example of a breakaway face and basal plane of a landslide or slump almost 30 m thick. Another small slump appears to have slid within the upper part and a young fault has offset the basal surface of the lower slump (1517). Figure 80 provides an unusual illustration of a slump or landslide in which the toe fills an older channel or has excavated a space for its lower part. Bedding near the toe area of the landslide is missing below the base of the slide. Within the toe of the landslide the bedding is partly disrupted but one plane appears to be continuous and planar. The toe has ridden slightly upward on the eastern slope. Two upper Pleistocene(?) mound-like features show clearly below the landslide. They were lapped onto and overtopped by sediment prior to the development of the landslide.

In Figure 81 an area of jumbled bedding (1557.4-1559.7) between two areas of good reflectors is interpreted to have been mobilized and slumped downslope. The well-bedded area to the south (left) of the slump is bounded by near-vertical faults at 1556.3 and 1557.4. The fault at 1557.4 appears to bound the southern edge of the slump. The northern boundary of the slump is more gentle and is marked by the termination of bedding at about 1559.5. A smaller slump is interpreted to overlie glacio-fluvial and ice-contact sediments between 1555 and 1558. It overlies both faults as well as the southern part of the larger slump and is the youngest feature noted in the Figure.

Figures 82 and 83 provide examples of slumps on slopes. The slump in Figure 82 is apparently composed of till or bouldery gravel (non-bedded, many

hyperbolic reflections), whereas that in Figure 83 is well-bedded but with a rough upper surface. Figure 84 illustrates a possible landslide that appears to have scooped out and filled a depression. The beds on the south (left) side of the main part of the slump and partly beneath it have been folded, presumably as a result of its impact.

Gas-charged sediments.

The presence of possible gas-charged sediments is detected in seismic-reflection profiles as acoustic anomalies. Gas may appear as plumes that stream vertically or at angles in the water column above their places of venting, or they may show as turbid areas in the sedimentary sequence and completely obliterate the bedded signal vertically and laterally without the introduction of the moderately sized hyperbolic reflections common in till and bouldery gravel. They may ascend upward along fault traces as interpreted in Figures 85 and 86 where the lines of faulting are not obvious because of the possibly abundant gas. The presence of faults is assumed because of changes in level of the sea floor. The gas is outlined by small hyperbolic reflections; hyperbolics are also recorded within the gaseous area.

Figure 87 shows a much larger gaseous(?) emanation, and it is difficult to provide an alternative geologic interpretation for this acoustic feature. Evidence for the position of the sea floor occurs at and to the southwest (left) of 2235, at 2239.5 and at 2243.5 at the northeast (right) edge of the figure. Similar irregular features have been noted in the water column in other areas and were interpreted as schools of fish and/or kelp, but in these records such a hypothesis seems unjustified because of their positions in relation to faults, their intimate relation to the sea floor, and their absence as discrete bodies in the water column.

Figure 88 is of interest because it shows a mound of sediments on the profile which correlates with a dome-shaped bathymetric feature (Canada Hydrographic Service, 1976). The well-bedded sequences on the flanks of this domal feature lose their continuity toward the center. The non-bedded, vertically bounded zone is interpreted to be gas charged. A fault may be present in possible upper Pleistocene glacial sediments near 0845 and disrupted sediments are discernible at 0851 at 0.20 sec. depth.

Figures 89 through 93 show clearly the loss of bedded-reflectors laterally into a reflection-free, non-bedded part of the profile. This may reflect a normal lateral gradation from one sedimentary facies to another, or the impenetrable sediments (turbid) may be an indicator of interstitial gas. On-site studies by Schubel (1974) and Kvenvolden and others (1980) have determined that the presence of gas makes the sediments considerably more turbid-appearing and compressible (Schubel, 1974, p. 275, 287). In Figure 89 the gas is interpreted to have risen only to a position about 20 m below the sea floor before it encountered impermeable beds and then moved laterally upward into more permeable beds between 1425 and 1430. Figures 90 and 91 show similar lateral movement in an upward direction. The vertical contact at 1524.5 in Figure 90 may be a fault along which the gas moved upward as the poor bedding preserved in the gaseous sediments appears to be offset or to be discontinuous across the contact. A similar nearly vertical contact is apparent in Figure 92 (near 0420) where presumed gas-charged sediments may

have effected a slight upward bulge in the sea floor. The gaseous area is at least 3 km in width and appears to terminate (vertically) near the north (right) end of the Figure. Some of the bedded units at the gaseous contact appear to turn downward, seen also in Figure 93, suggesting a change to higher velocity in the direction of the gas-charged sediments. An illustration in Schubel (1974, Fig. 1) shows a similar turn down. Other examples of possibly gas-charged sediments are shown in Figures 25, 26, and 28.

A map depicting the results of the study of these 0.25-second seismic profiles is reproduced in Figure 94. Correlations of small features, such as discrete anticlines and synclines, could not be made with any certainty. The continuity of faults that cut and offset the sea floor was also difficult to make except very locally. Correlation of small folds with small amplitudes were made in order to determine the directions of ice push and the relation of ice push to bathymetric obstructions. The positions of slump masses and of presumed gas-charged sediments also are informative in relation to offshore drilling and construction sites.

## GROUND TRUTH

### Roadcut, quarry, and seacliff examination.

Following the interpretation of most of the seismic-reflection profiles, a geological field trip was made into the northern Puget Sound-eastern Strait of Juan de Fuca area to study roadcut, quarry and seacliff exposures of Pleistocene and Holocene sediments. The field trip was necessary in order to observe in nature the features seen in the seismic reflection profiles. Fred Pessl, Jr., and Ralph F. Keuler of the U. S. Geological Survey's Seattle Office kindly took us to many well-exposed Pleistocene glacial features in the study area and provided explanations of their genesis. Cross-bedded glacial outwash gravels, shingle-pebble outwash gravels, glacial till (Fig. 95 A-D), slump features (Fig. 96 A) and pre-consolidation folding structures in glacial outwash (Fig. 96, B, C, D) all had similar counterparts in the seismic-reflection profiles although observable on a somewhat smaller scale at the outcrop.

Figure 97 illustrates several depositional, glacial features observed in sea cliff exposures. Part A shows gravelly outwash with locally interlaminated sand beds one of which has moved downslope about 10 m (a on Figure 97, part A). Part B shows a sequence of interbedded glacio-marine and glacial outwash deposits. The glacio-marine deposits are mainly in the upper part of the photograph. In seacliff exposures these marine deposits generally exhibit vertical jointing and contain mollusk and other types of marine shell fragments locally. The outwash deposits are well-bedded to poorly bedded gravelly sediments with clasts as much as one-fourth meter in long dimension. In the glacial till observed in part C of Figure 97, angular, pebble-size fragments are scattered throughout a clay matrix. At this outcrop, the till is broken by a set of near-vertical and near-horizontal shears. Part D provides an illustration of the type of bedding brought out by weathering of a bedded, gravelly outwash deposit. The uppermost part is dark-gray humus-filled material indicative of a weathered soil zone.

Faulting was clearly seen in seacliff exposures (Fig. 98, A, B) and in

several quarry sites. As in many of the seismic-reflection profiles, the offset of correlative beds on opposite sides of faults was small (1-5 m) and the amount of horizontal movement was difficult to assess. The vertical component of movement was obvious in some exposures (Fig. 98A) but associated slickensides and/or contemporaneous crenulated bedding did not provide sufficient data to resolve the question of the presence, absence, or amount of oblique movement, or whether apparent faults were tectonically related or were associated with collapse of ice-contact sediments.

Textural differences between glacial deposits at the outcrop was very apparent in some outcrops. These differences included the presence or absence of cross bedding and foreset beds of deltaic deposits, lack of bedding and presence of angular rocks of wide range in composition and rounding (till). Other outcrops showed rounded and flattened or ovoid-shaped pebbles and boulders (glacio-fluvial or glacial outwash deposits), vertical jointing in sediments containing shell debris in some outcrops (glacio-marine deposits), and horizontal variations of one or another of the above features with or without a sharp contact (Figs. 95-98). Many outcrops had a soil zone developed at the top of the seacliff, roadcut, or quarry, and some had internal features resembling soil zones. Glacial scour was observed in a few outcrops where lateral truncation of bedding was well displayed, and on one bedrock (Jurassic?) exposure on Whidbey Island glacial striations were observed. The striae trended a few degrees south of west and suggested that basal ice movement of the Juan de Fuca lobe had already diverged from the Puget lobe during that particular period of glaciation. No direct evidence of the time of development of these glacial striations was apparent but they may certainly have developed during the Vashon Stade. Features such as soil zones or striations would not show on seismic-reflection profiles. Distinctive color differences, also obvious at the outcrops, would not be recorded on the profiles either.

Large (2-5 m diam.) erratics were scattered along many outcrops and could account for the very irregular topography and the generation of hyperbolic crescents at the seafloor on many profiles. Similarly, the knob and kettle topography, observed a few miles north of Sequim, provides an onshore example of the seafloor irregularities shown by Chrzastowski (1980) in the Admiralty Inlet area and observed on the seismic records.

Bottom Sediment Data.

No bottom samples were taken during the PARIZEAU or MILLER cruises. The only immediate source of bottom sediment data was that obtained from charts of the National Ocean Survey of the National Oceanographic and Atmospheric Administration. The charts used were Chart No. 18465 of the Strait of Juan de Fuca, Eastern Part, published in August 1978 at a scale of 1:80,000; Chart No. 18441 of the Admiralty Inlet and Puget Sound to Seattle area, published in October 1978 at a scale of 1:80,000; Chart No. 18464 of the Port Townsend area, published in March 1979 at a scale of 1:20,000; and Chart No. 18467 of the Discovery Bay and Sequim Bay area, published in June of 1979 at a scale of 1:40,000.

The data given on these maps included, in places, a composite of bottom sediments, for example gravel, sand and mud. In such cases, the largest size

material (gravel) was used in our compilation in an effort to obtain the greatest amount of information on material most likely to be represented by an irregular seafloor on the seismic records. All single notations were plotted at their proper positions. Lines were then drawn that generalized the outlines of areas of rock, gravel, and mud (which included sand in places). Blank areas contained no data.

The majority of areas where rock predominated were on bank tops such as San Juan Bank, Smith Bank, Partridge Bank, Eastern Bank, the northern parts of Hein and Middle Banks, Dungeness Bank and Dallas Bank (compare Figs. 1 and 99). Other notable areas of rock concentration were off Partridge Point, north and east of Port Townsend and south of Lopez Island. The relations of areas of gravel concentration to topography are not as clear. Gravel appears to form a band around the southern part of Eastern Bank, to flank the northwestern part of Dallas Bank, and to form small deposits west and east of Dungeness Bank, Smith Bank and Partridge Bank. Two deposits east and north of Port Angeles seem not to be related to topographic highs.

A few areas of mud concentration are worthy of particular attention. The largest areas are east of Dungeness Bay and between Smith and Partridge Banks and Whidbey Island. Presumably these are areas protected from strong bottom-current action by islands and banks that more or less surround them. Anomalous areas of mud concentration are those that occur atop Hein Bank, Center Bank and north of Constance Bank.

## Earthquake Activity

About 70 earthquakes with magnitudes ranging from less than 2 to greater than 3 have been recorded in the northern Puget Sound-eastern Strait of Juan de Fuca area between 1961 and 1978. Locations of the hypocenters (Fig. 100) were plotted from computer printouts furnished by the National Geophysical and Solar-Terrestrial Data Center (1979) and reports by Crosson (1974, 1975), Crosson and Millard (1975), Crosson and Noson (1978a, 1978b, 1979) Horner and others (1976), Milne and Smith (1962, 1963, 1966), Noson and Crosson (1980), Stevens and others (1976) and Wetmiller (1976a, 1976b).

Since the accuracy of the hypocenter locations depends upon the crustal model used, on the recording-station distribution, and on the quality of the arrival-time data, the locations of earthquakes recorded prior to 1970 and a few since then, may be a kilometer or more in error. However, the map is useful if only as an indication of the abundance of shallow earthquake activity between 1961 and 1978 (17 years) in the area. When plotted, the hypocenters cluster about a trend beginning at Victoria and extending SE to the concentration around and north of Smith Island. This alignment is approximately parallel to the trace of the Northern Whidbey Island fault (Gower, 1980) and although no hypocenter falls directly on its projected offshore trace as shown on Figure 11, the fault appears to lie between an alignment of hypocenters. Similarly, hypocenter locations are very close to and parallel the offshore mapped positions of deeper structures C, D, E, and G (compare Figs. 11 and 100). In particular, the most abundant offshore cluster of hypocenters occurs within 3 kilometers of Point Partridge to its southwest. This cluster nearly corresponds with the junction of two branches of the Southern Whidbey Island fault (Gower, 1980) and an east-striking fault

zone that is north-dipping and cuts stratified glacial deposits onshore at Ebeys Landing (Gower, 1980, map and p. 6).

## SUMMARY AND CONCLUSIONS

Interpretation of intermediate and shallow penetration (mainly 1-second sweep) seismic-reflection profiles has revealed a series of nearly identical geologic features (anticlines, synclines, channel-fills, foreset bedding, faults, etc.) on many adjacent profiles. Correlation of these features from profile to profile has resulted in maps that shows structural trends and sedimentary features of presumed Pleistocene age (Figs. 11, 94). The deformation of these sediments may be due to tectonism presumed to have occurred during late Pliocene or early to middle Pleistocene time.

The correspondence between faults mapped on Figure 11 and the deeper discontinuities mapped by MacLeod and others (1977) on the basis of magnetic data strongly suggests that some of these faults may be related to old, deeper structures. Some of the folded and faulted structural features could, however, reflect a late phase of tectonic activity that occurred either during middle or near the end of Pleistocene time. Many folded and faulted structures are near the westward projection of the Devils Mountain fault (Gower 1978, fault A) and of the Northern Whidbey Island fault (Gower, 1980). The folded structures north of the Northern Whidbey Island fault could be as young as late Pleistocene (Vashon Stade) in age and be the result of ice shove at the time of the last glacial maximum of the Cordilleran Ice Sheet.

In general, The major Pleistocene structural features, appear to have little or no genetic relationship to the submarine topography; most faults cut obliquely across parts of banks; also, the faults do not trend along bathymetric low areas. The slopes of the upper surfaces of the bathymetric highs (banks) vary greatly in direction and seem possibly to reflect differences in movement of separate sub-lobes during recession of the Juan de Fuca and Puget lobes of the Cordilleran ice sheet. They could be the products of large subglacial streams moving in different directions but generally to the west and southwest. When the stream velocities were checked at the positions of contact with sea water, the surfaces of the fan-like gravel deposits that formed sloped in the general direction of transport of the gravels.

The many occurrences of hyperbolic-derived surfaces and of foreset beds at the upper edges of banks suggest that these deposits were formed during glacial recession while the Juan de Fuca lobe still filled the interbank depressions and continued to furnish large glacially derived rock fragments and boulders to the upper-bank environment. In other parts of the bank tops, it appears that subglacial streams carved deep channels into the upper bank surface and along the flanks of the banks. These channels were presumably filled with debris from the glacial lobe or from the action of the seawater as it progressed over the bank top and redistributed the finer materials.

The relationship of earthquake hypocenter locations (Fig. 100) and the faults mapped by correlation of structural and stratigraphic features (Fig. 11) seems to be more than coincidental. The Northern Whidbey Island and

Southern Whidbey Island faults in particular have several earthquakes along their trends. Other alignments are also notable and appear to indicate the possibility that adjustment along these lines of structural weakness is still occurring. The presence of areas of possible gas-charged sediments, of landslides and slumps, and of possible faults that reach or offset the seafloor in Holocene sediments warrants additional investigation in areas where construction of large man-made features are planned.

We conclude that good quality moderate-penetration seismic reflection profiles are difficult to obtain in this glaciated area and that those obtained are difficult to interpret. High-resolution seismic-reflection profiles provide excellent opportunities to study glacial features and aid in the identification of areas of possible offshore geologic hazards.

## ACKNOWLEDGMENTS

We wish to acknowledge the useful discussions with, and helpful comments by, colleagues during the preparation of this report. We particularly appreciate the thoughtul review of James C. Yount whose comments improved the report measurably. We, of course, take full responsibility for the correlations made and the conclusions drawn.

REFERENCES

Brown, R. D., Jr., Gower, H. D., and Snavely, P. D., Jr., 1960, Geology of the Port Angeles-Lake Crescent Area, Clallam County, Washington: U. S. Geological Survey Oil and Gas Investigations Map OM-203, 1:62,500.

Canada Hydrographic Service, 1976, Natural Resources Map (bathymetry): Canada Hydrographic Service Bathymetric Chart 15783-A, 1:250,000.

Chrzastowski, M. J., 1980, Submarine features and bottom configuration, Port Townsend quadrangle Puget Sound region, Washington: U. S. Geological Survey Water-Resources Investigations, Open-File Report 80-14, 1:100,000.

Crosson, R. S., 1974, Compilation of Earthquake Hypocenters in Western Washington: State of Washington Department of Natural Resources, Information Circular 53, 25 p.

_____, 1975, Compilation of Earthquake Hypocenters in Western Washington-1973: State of Washington Department of Natural Resources, Information Circular 55, 14 p.

Crosson, R. S. and Millard, R. C., 1975, Compilation of Earthquake Hypocenters in Western Washington-1974: State of Washington Department of Natural Resources, Information Circular 56, 14 p.

Crosson, R. S., and Noson, L. J., 1978a, Compilation of Earthquake Hypocenters in Western Washington-1975: State of Washington Department of Natural Resources, Information Circular 64, 12 p.

_____, 1978b, Compilation of Earthquake Hypocenters in Western Washington-1976: State of Washington Department of Natural Resources, Information Circular 65, 13 p.

_____, 1979, Compilation of Earthquake Hypocenters in Western Washington-1977: State of Washington Department of Natural Resources, Information Circular 66, 12 p.

Gower, H. D., 1978, Tectonic map of the Puget Sound region, Washington: U. S. Geological Survey Open-File Report 78-426, 1:250,000.

_____, 1980, Bedrock geologic and Quaternary tectonic map of the Port Townsend area, Washington: U. S. Geological Survey Open-File Report 80-1174, 1:100,000.

Heusser, C. J., 1973, Environmental sequence following the Fraser Advance of the Juan de Fuca lobe, Washington: Quaternary Research, Vol. 3, p. 284-306.

Horner, R. B., Milne, W. G., and McMechan, G. A., 1976, Canadian earthquakes-1971: Seismological Service of Canada, Seismological Series No. 74, Ottawa, Canada, 34 p.

Kupsch, W. O., 1962, Ice-thrust ridges in western Canada: Journal of Geology, Vol. 70, p. 582-594.

Kvenvolden, K. A., Redden, G. D., Thor, D. R., and Nelson, C. H., 1980, Hydrocarbon gases in near-surface sediment of northern Bering Sea (Norton Sound and Chirikov Basin), in Larsen, M. C., Nelson, C. H., and Thor, D. R., Geological, geochemical, and geotechnical observations on the Bering Shelf, Alaska: U. S. Geological Survey Open-File Report 80-979, 28 p.

MacLeod, N. S., Tiffin, D. L., Snavely, P. D., Jr., and Currie, R. G., 1977, Geologic interpretation of magnetic and gravity anomalies in the Strait of Juan de Fuca, U.S.-Canada: Canadian Journal of Earth Sciences, v. 14, no. 2, p. 223-238.

McDonald, B. C. and Shilts, W. W., 1975, Interpretation of faults in glaciofluvial sediments, in Jopling, A. V. and McDonald, B. C., eds., Glaciofluvial and Glaciolacustrine Sedimentation: Society of Economic Paleontologists and Mineralogists Special Publication No. 23, p. 123-131.

Milne, W. G. and Smith, W. E. T., 1962, Canadian earthquakes-1961: Seismological Series, Dominion Observatory, 1961-4, 24 p.

_____, 1963, Canadian earthquakes-1962: Seismological Series, Dominion Observatory, 1962-3, 22 p.

_____, 1966, Canadian earthquakes-1963: Seismological Series, Dominion Observatory, 1963-4, 30 p.

Mitchum, R. M., Jr., Vail, P. R., and Sangree, J. B., 1977, Seismic stratigraphy and global changes of sea level, part 6--Stratigraphic interpretation of seismic-reflection patterns in depositional sequences in Payton, C. E., ed., Seismic stratigraphy--applications to hydrocarbon exploration: American Association of Petroleum Geologists Memoir 26, p. 117-133.

Moran, S. R., 1971, Glaciotectonic structures in drift, in Goldthwait, R. P. , ed., Till - a Symposium: Ohio State Univ. Press, p. 127-148.

National Geophysical and Solar-Terrestrial Data Center, 1979, Computer listing from earthquake data file - Oregon-Washington area 42-49 N, 117-125 W: 5 p.

National Ocean Survey, 1978a, Chart No. 18465, Strait of Juan de Fuca, Eastern Part: National Oceanographic and Atmospheric Administration, 1 sheet, 1:80,000.

_____, 1978b, Chart No. 18441, Admiralty Inlet and Puget Sound to Seattle area: National Oceanographic and Atmospheric Administration, 1 sheet, 1:80,000.

_____, 1979a, Chart No. 18464, Port Townsend area: National Oceanographic and Atmospheric Administration, 1 sheet, 1:20,000.

_____, 1979b, Chart No. 18467, Discovery Bay and Sequim Bay area: National Oceanographic and Atmospheric Administration, 1 sheet, 1:40,000.

Noson, L. L. and Crosson, R. S., 1980, Compilation of earthquake hypocenters in Western Washington-1978: State of Washington Department of Natural Resources Information Circular 72, 18 p.

Rust, B. R. and Romanelli, R., 1975, Late Quaternary subaqueous outwash deposits near Ottawa, Canada in Jopling, A. V. and McDonald, B. C., eds., Glaciofluvial and Glaciolacustrine Sedimentation: Society of Economic Paleontologists and Mineralogists, Special Publication no. 23, p. 123-131.

Schubel, J. R., 1974, Gas bubbles and the acoustically impenetrable, or turbid, character of some estuarine sediments, in Kaplan, J. R., ed., Natural gases in moraine sediments: Plenum Press, New York, p. 275-298.

Snavely, P. D., Jr., Gower, H. D., Yount, J. C., Pearl, J. E., Tagg, A. R., and Lee, J. W., 1976a, High-resolution seismic profiles adjacent to Whidbey and Fidalgo Islands, Washington: U. S. Geological Survey Open-File Report 76-187, 1 p., microfilm.

Snavely, P. D., Jr., MacLeod, N. S., Tiffin, D. L., and Currie, R. G., 1976b, Bouguer gravity anomaly map 15783-D, Strait of Juan de Fuca; Natural Resource Series: Canadian Hydrographic Service, Ottawa, 1:250,000.

Snavely, P. D., Jr., and Tiffin, D. L., 1980, Seismic reflection profiles from cooperative investigations in the Strait of Juan de Fuca by the U. S. Geological Survey and Geological Survey of Canada aboard the Canadian Survey Ship PARIZEAU between May 15 and June 13, 1972, Part 1 (Easternmost Segment): U. S. Geological Survey Open-File Report 80-239, 3 p., 1 microfilm.

Stevens, A. E., Milne, W. G., Horner, R. B., Wetmiller, R. J., Leblanc, G., and McMechan, G. A., 1976, Canadian earthquakes-1968: Seismological Service of Canada, Seismological Series, no. 71, Ottawa, Canada, 30 p.

Thorson, R. M., 1980, Ice-sheet glaciation of the Puget Lowland, Washington, during the Vashon Stade (late Pleistocene): Quaternary Research, Vol. 13, p. 303-321.

Wetmiller, R. J., 1976a, Canadian earthquakes-1973: Seismological Service of Canada, Seismological Series, No. 72, Ottawa, Canada, 28 p.

_____, 1976b, Canadian earthquakes-1974: Seismological Service of Canada, Seismological Series, no. 73, Ottawa, Canada, 35 p.

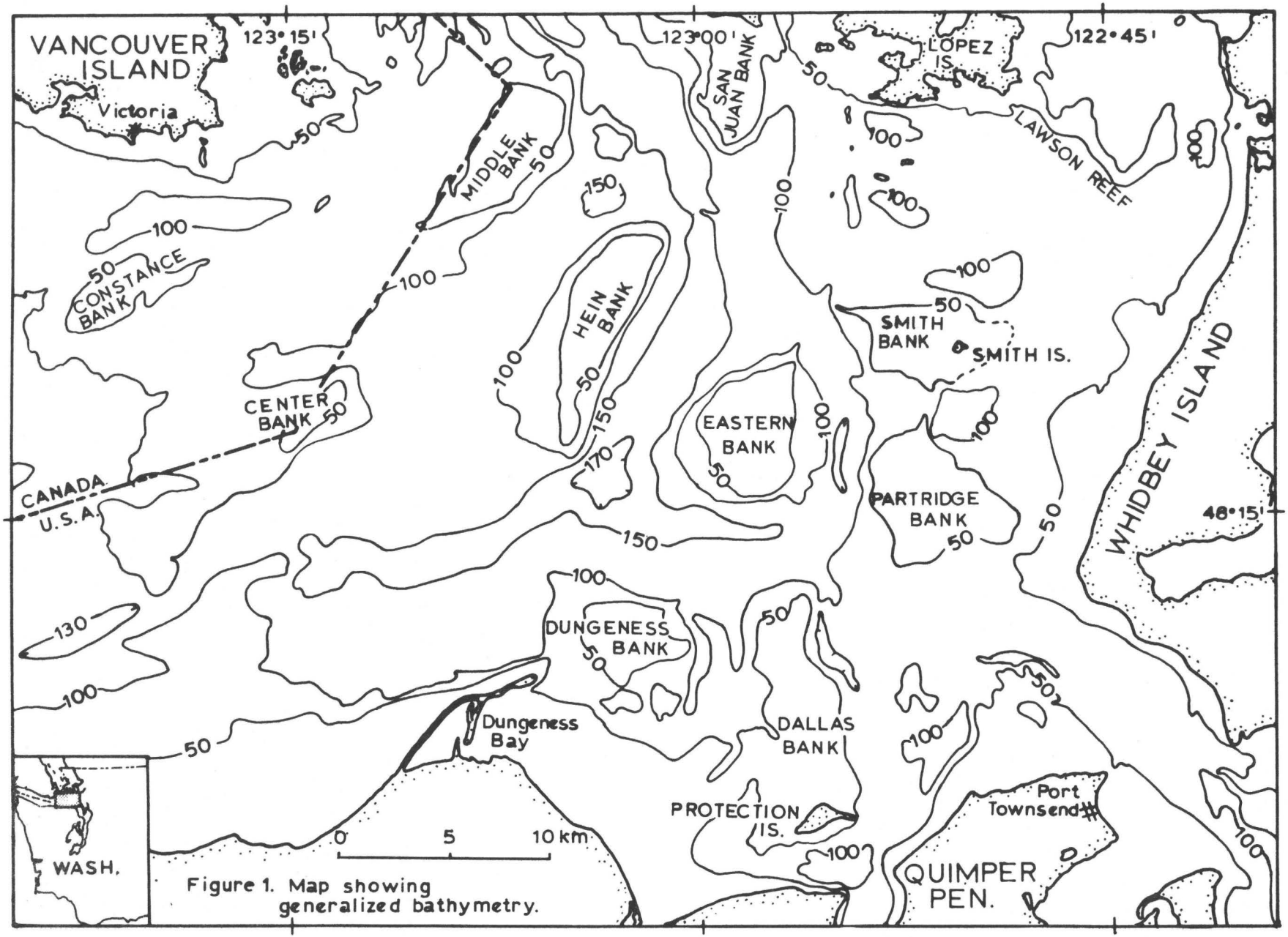


Figure 1. Map showing generalized bathymetry.

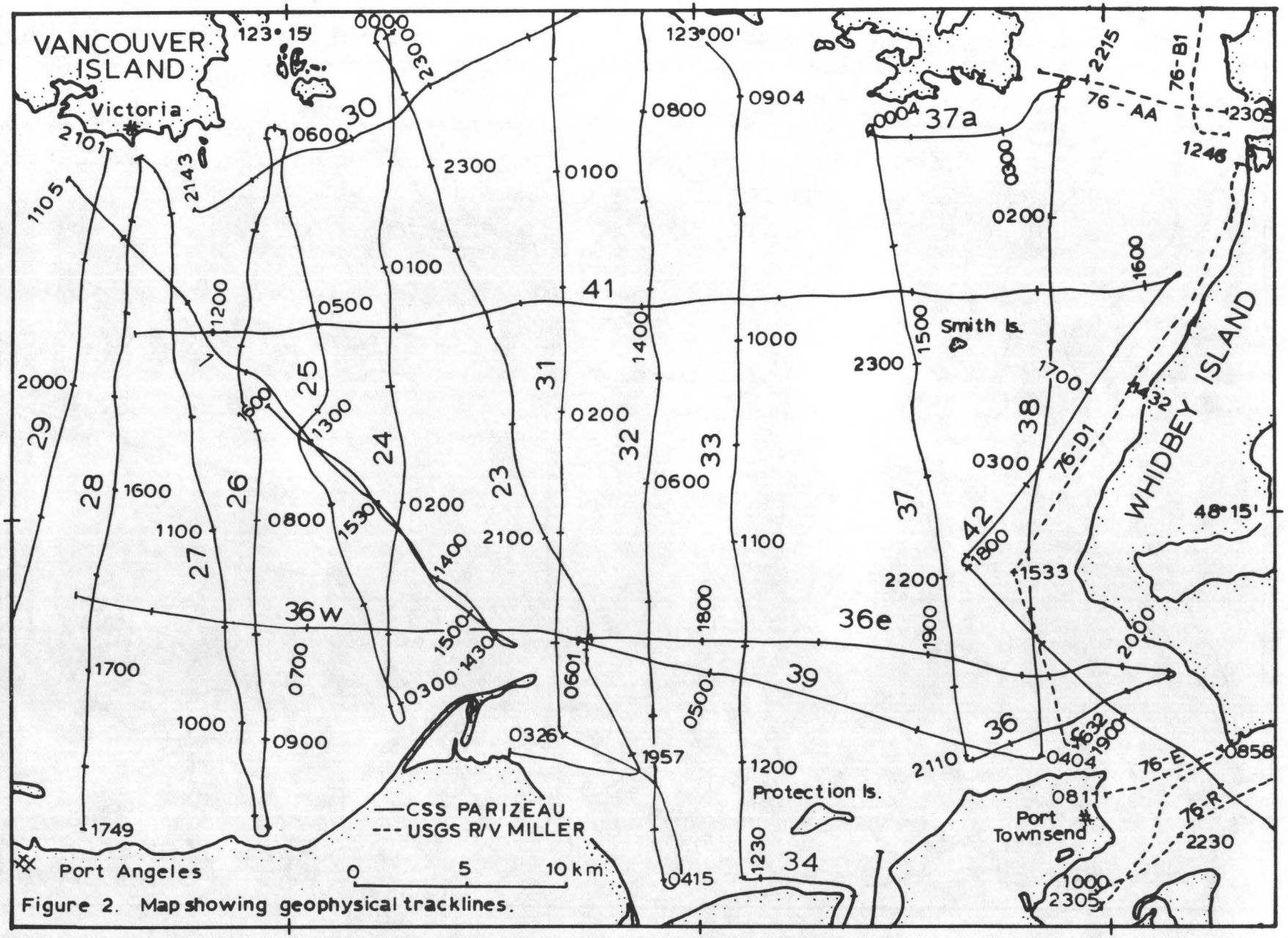


Figure 2. Map showing geophysical tracklines.

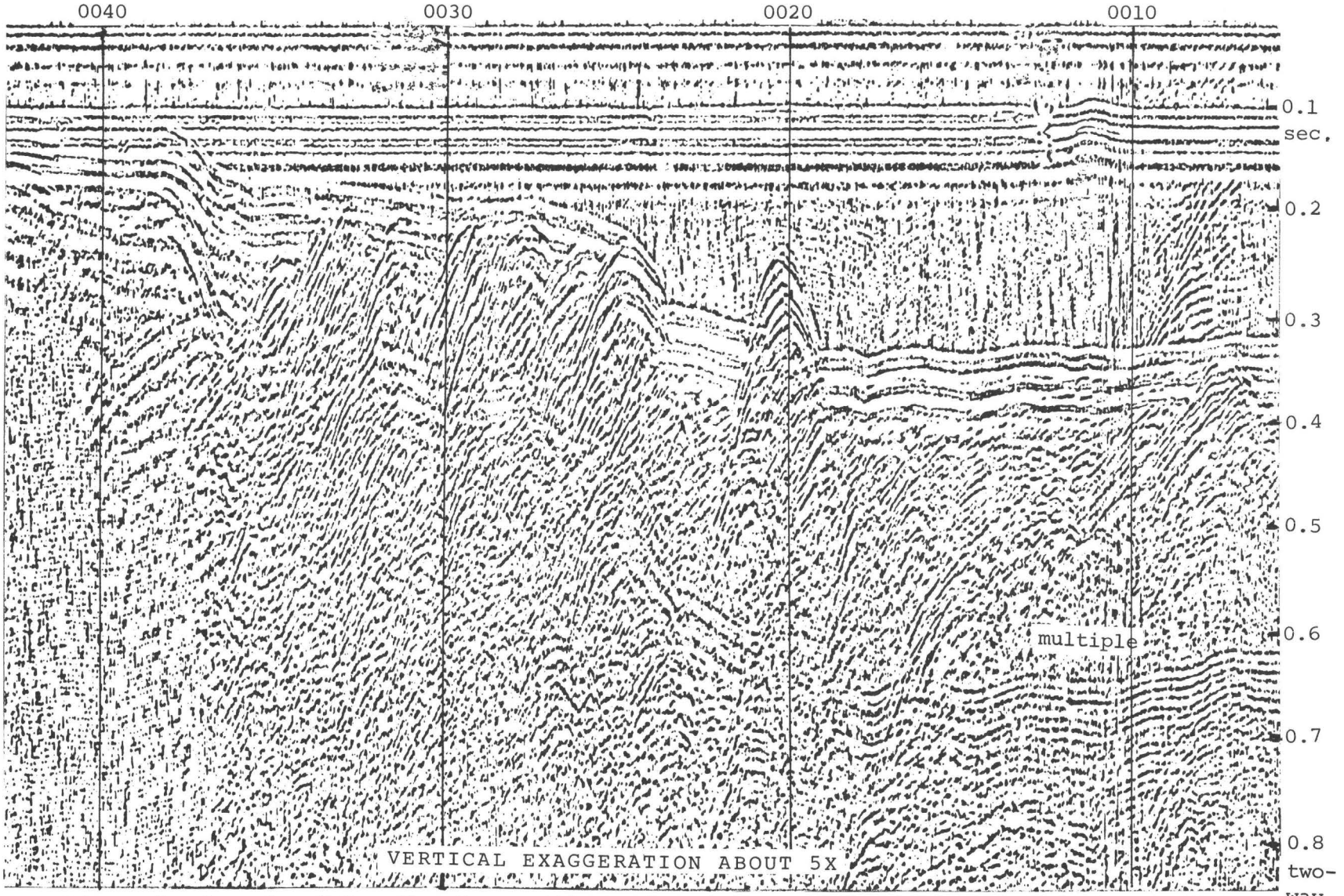


Figure 3. Example of Canadian Survey Ship Parizeau 1-second sweep seismic-reflection profile line 31.

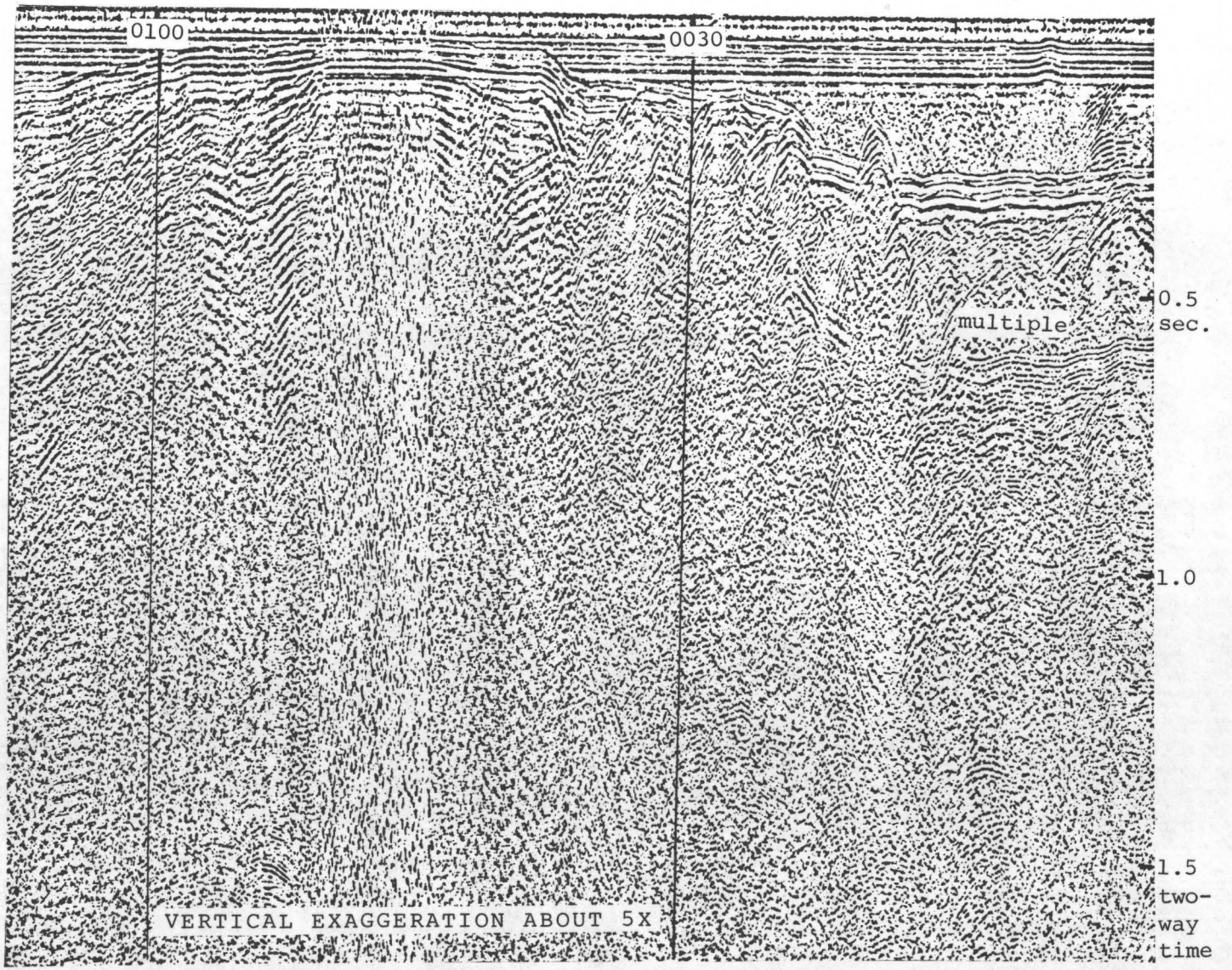


Figure 4. Example of Canadian Survey Ship Parizeau 2-second sweep seismic-reflection profile line 31.

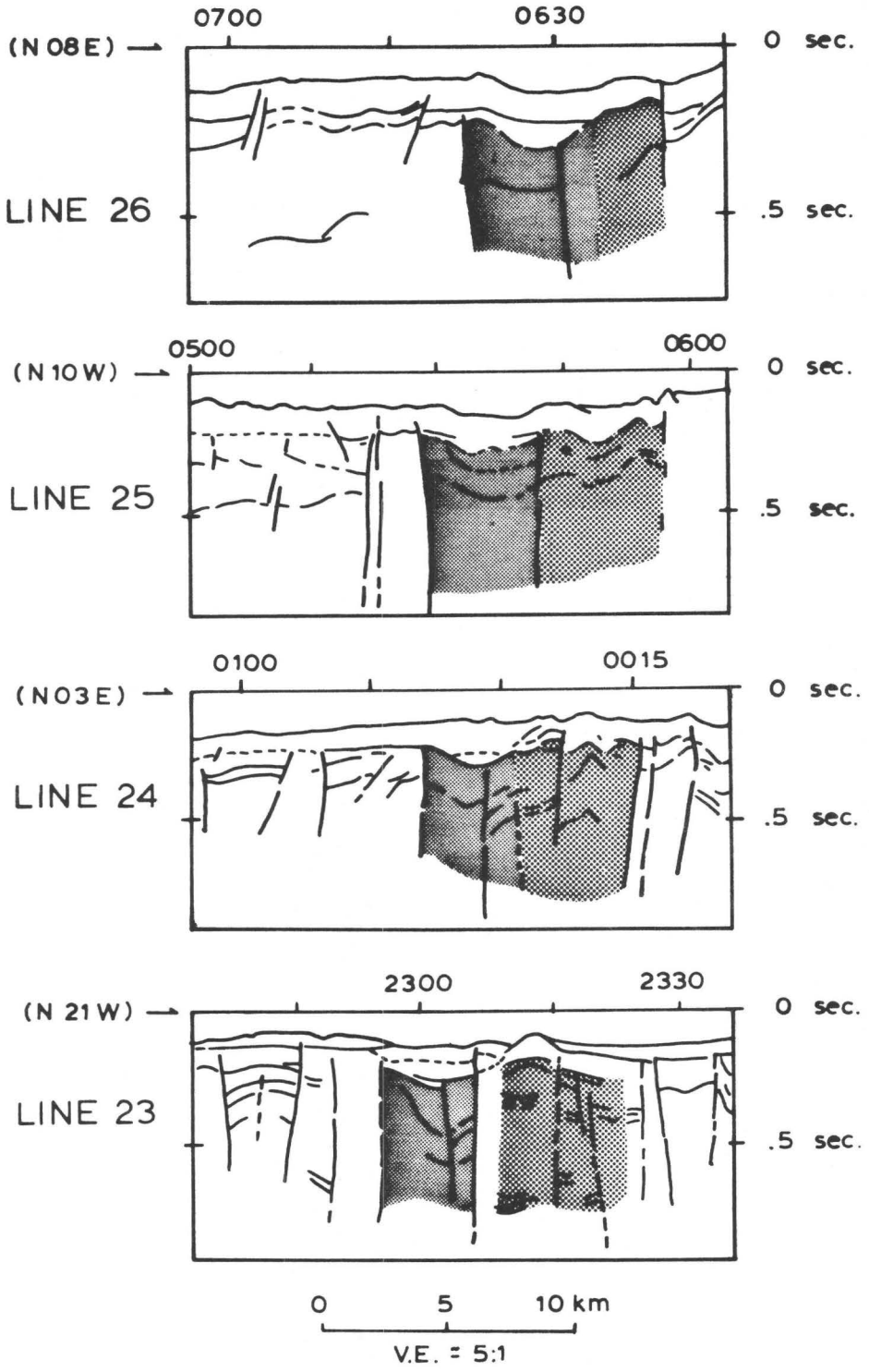


Figure 5. Line drawings of seismic-reflection profiles in the northwestern part of the area. Correlations in stipple pattern also indicated on Figure 11.

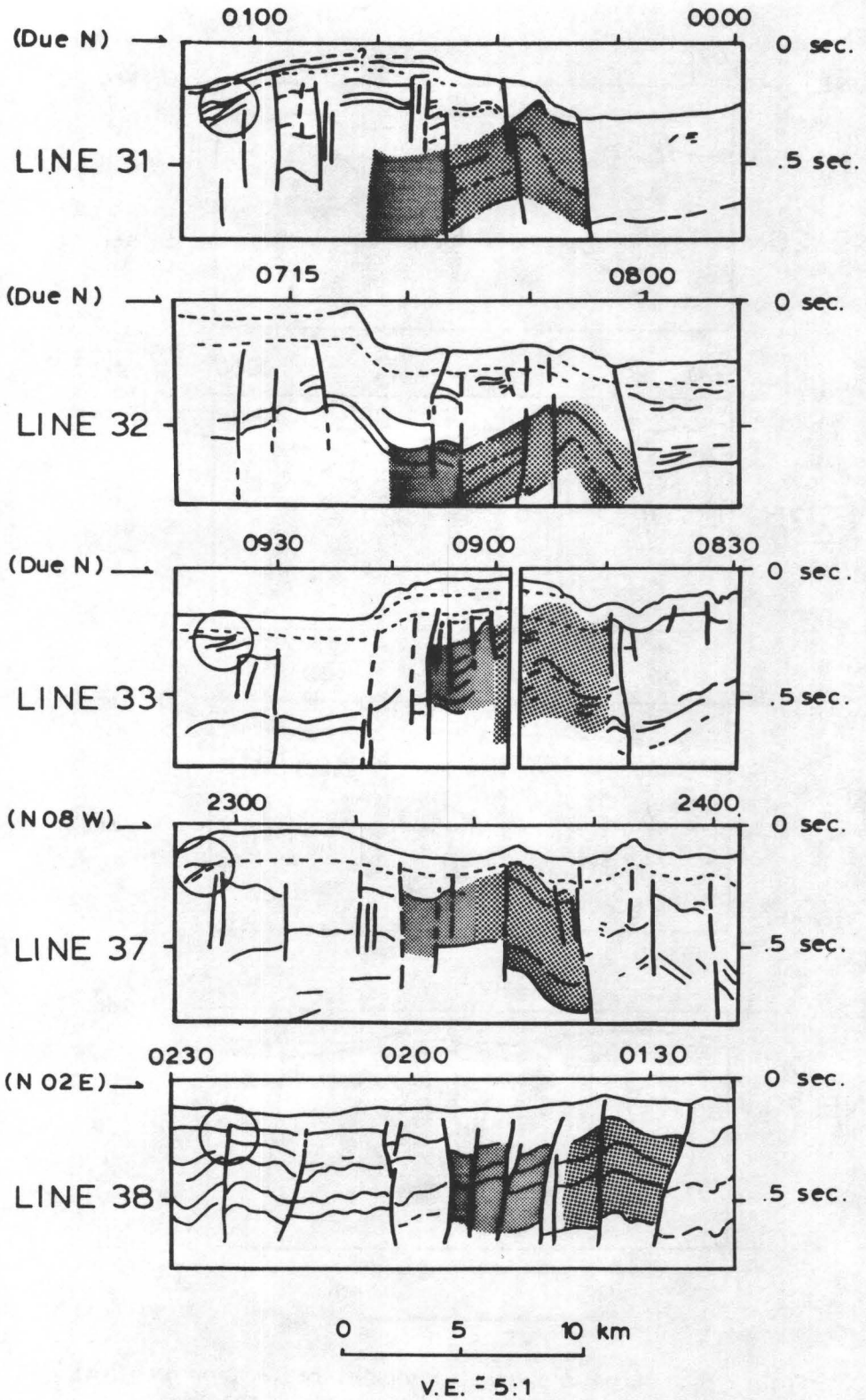


Figure 6. Line drawings of seismic-reflection profiles in the north-central part of the area.

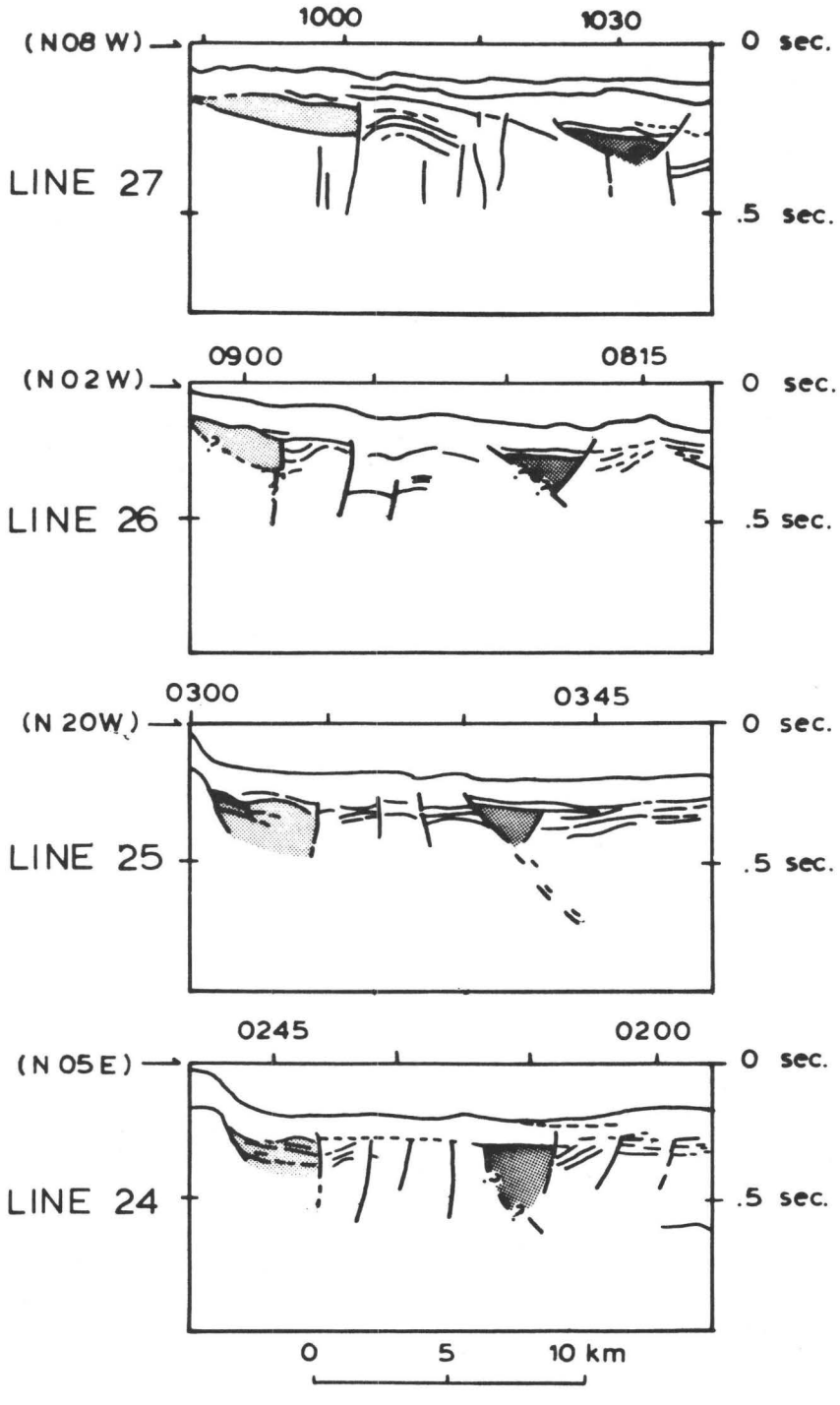


Figure 7. Line drawings of seismic-reflection profiles in the southwestern part of the area.

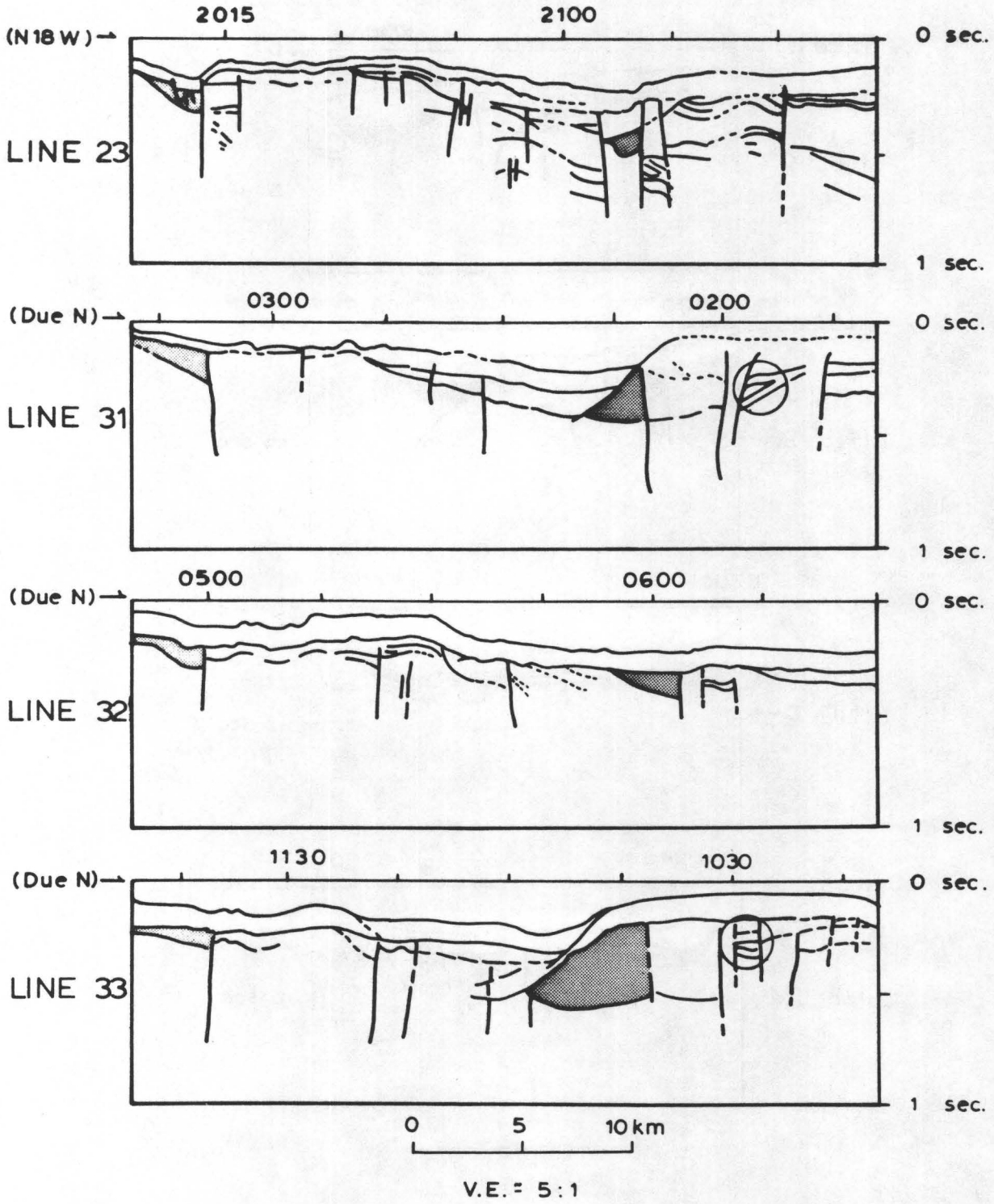


Figure 8. Line drawings seismic-reflection profiles in the south-central part of the area.

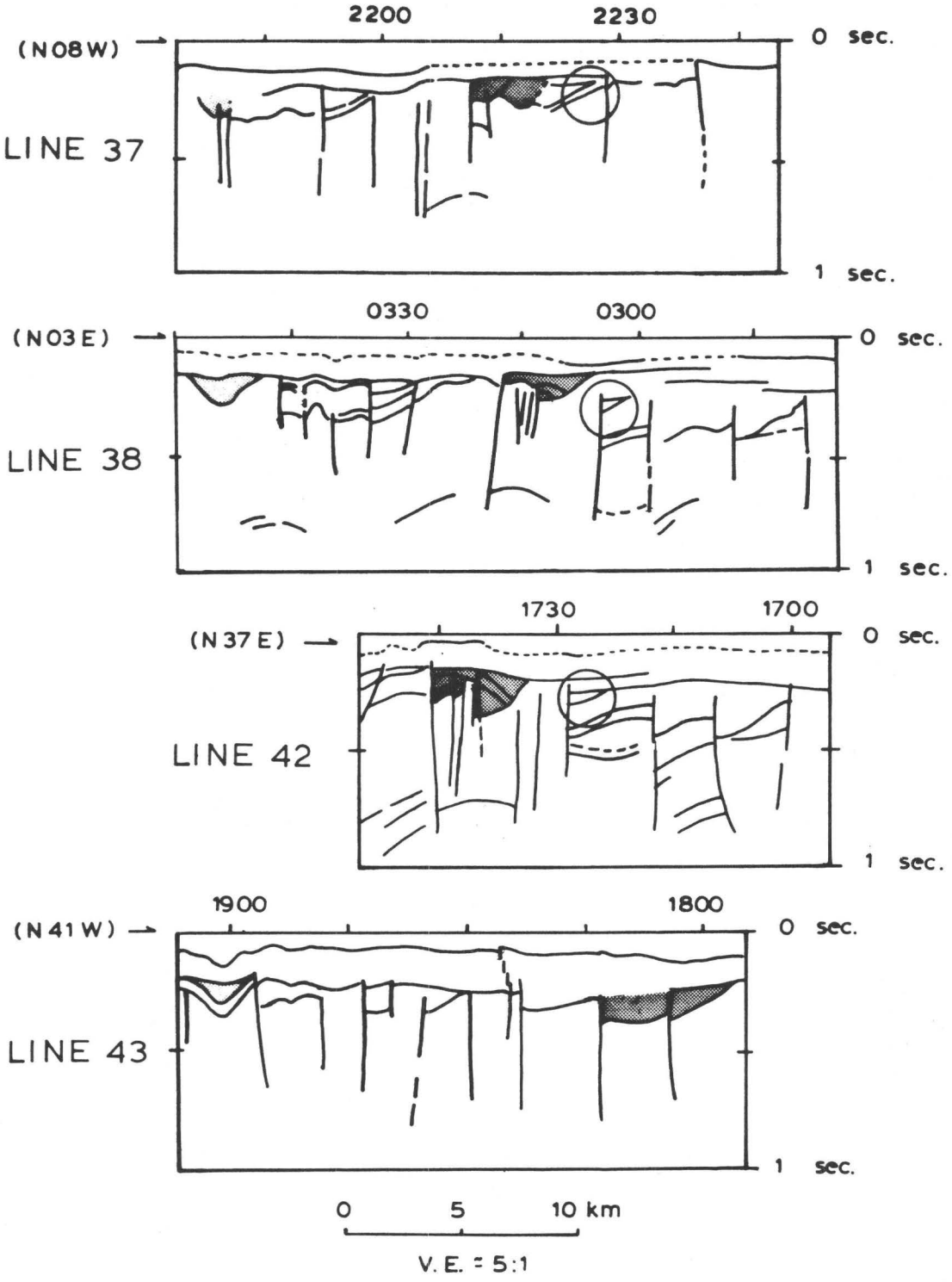


Figure 9. Line drawings of seismic-reflection profiles in the southeastern part of the area.

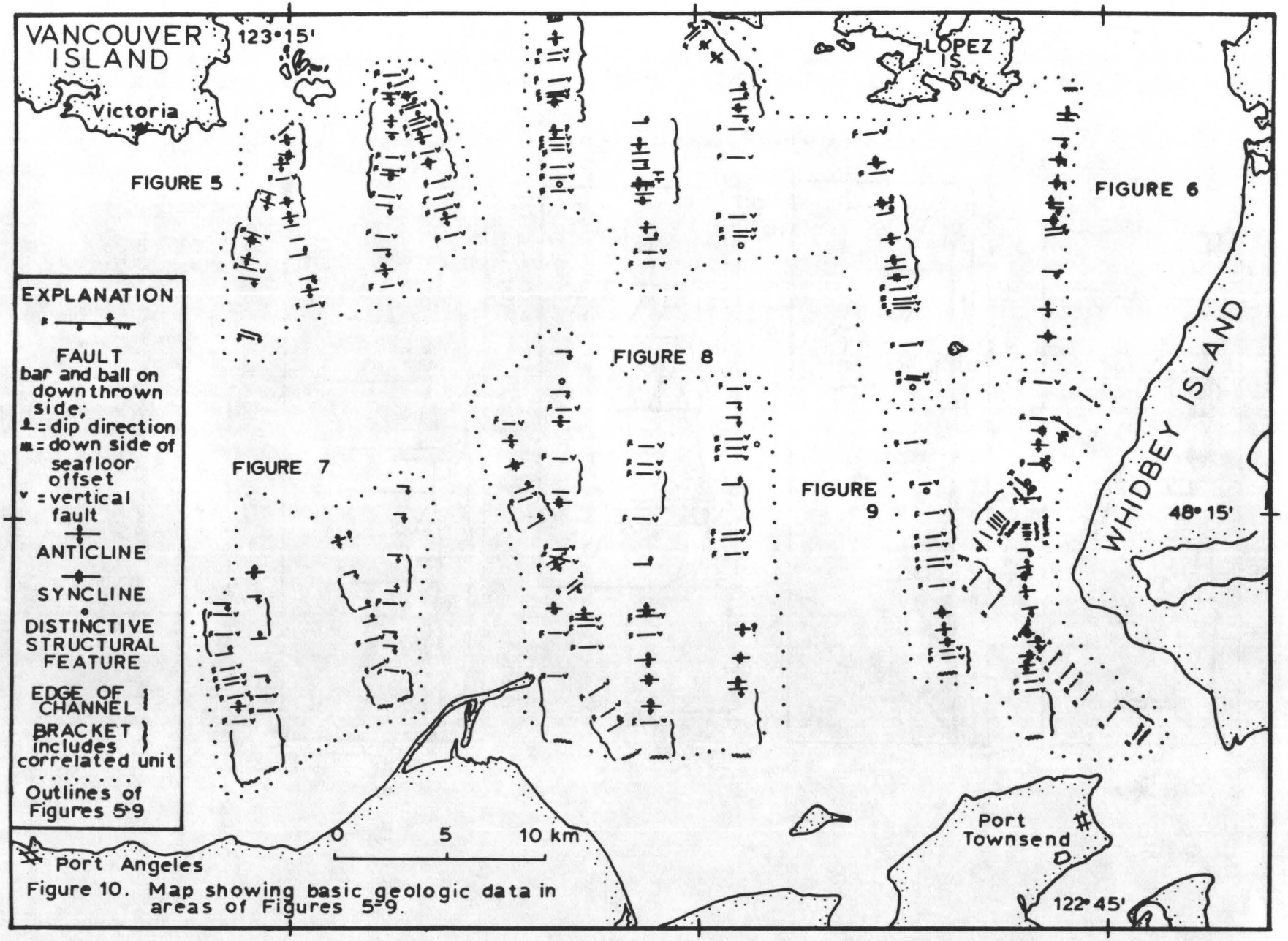


Figure 10. Map showing basic geologic data in areas of Figures 5-9.

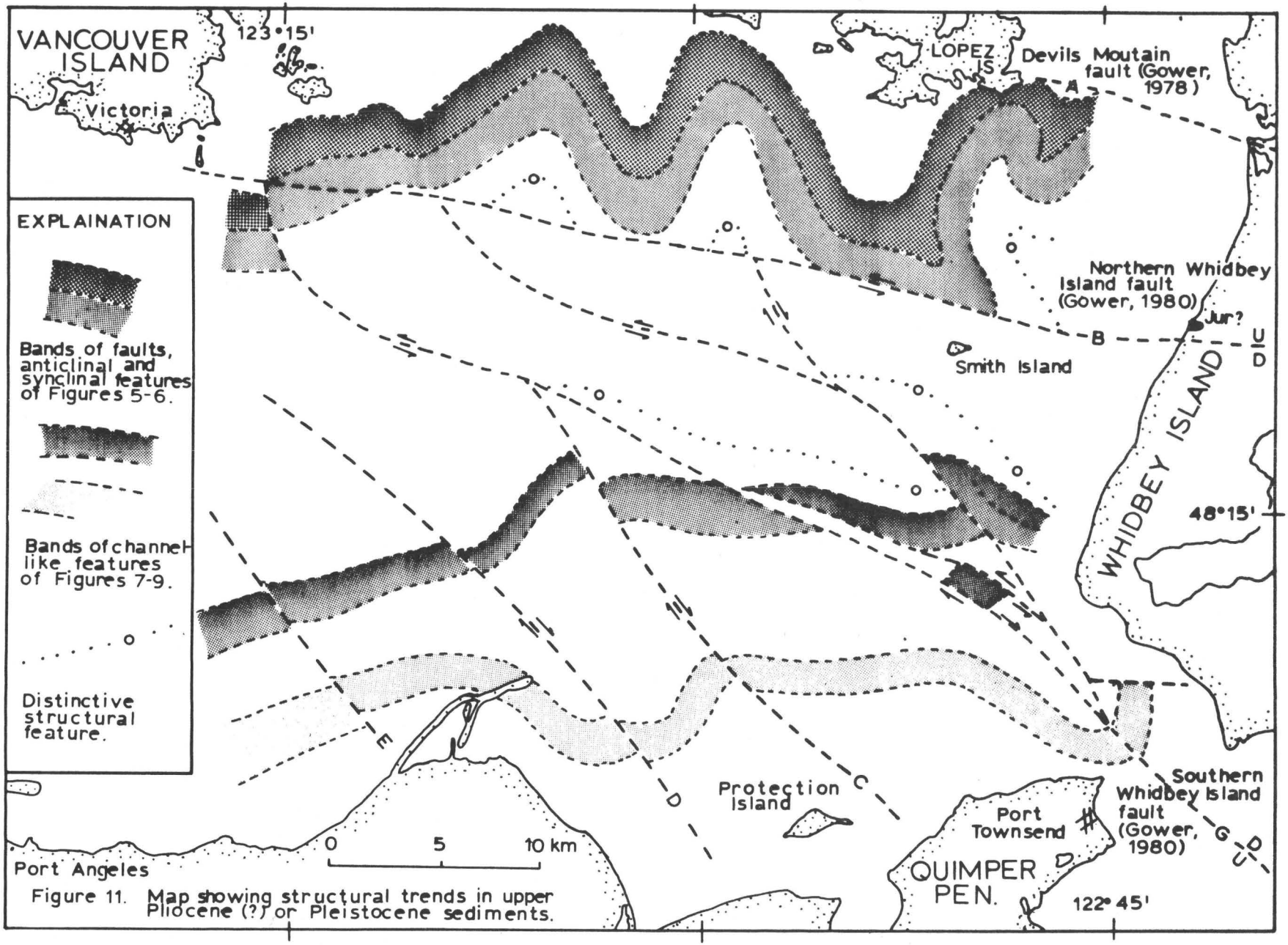


Figure 11. Map showing structural trends in upper Pliocene (?) or Pleistocene sediments.

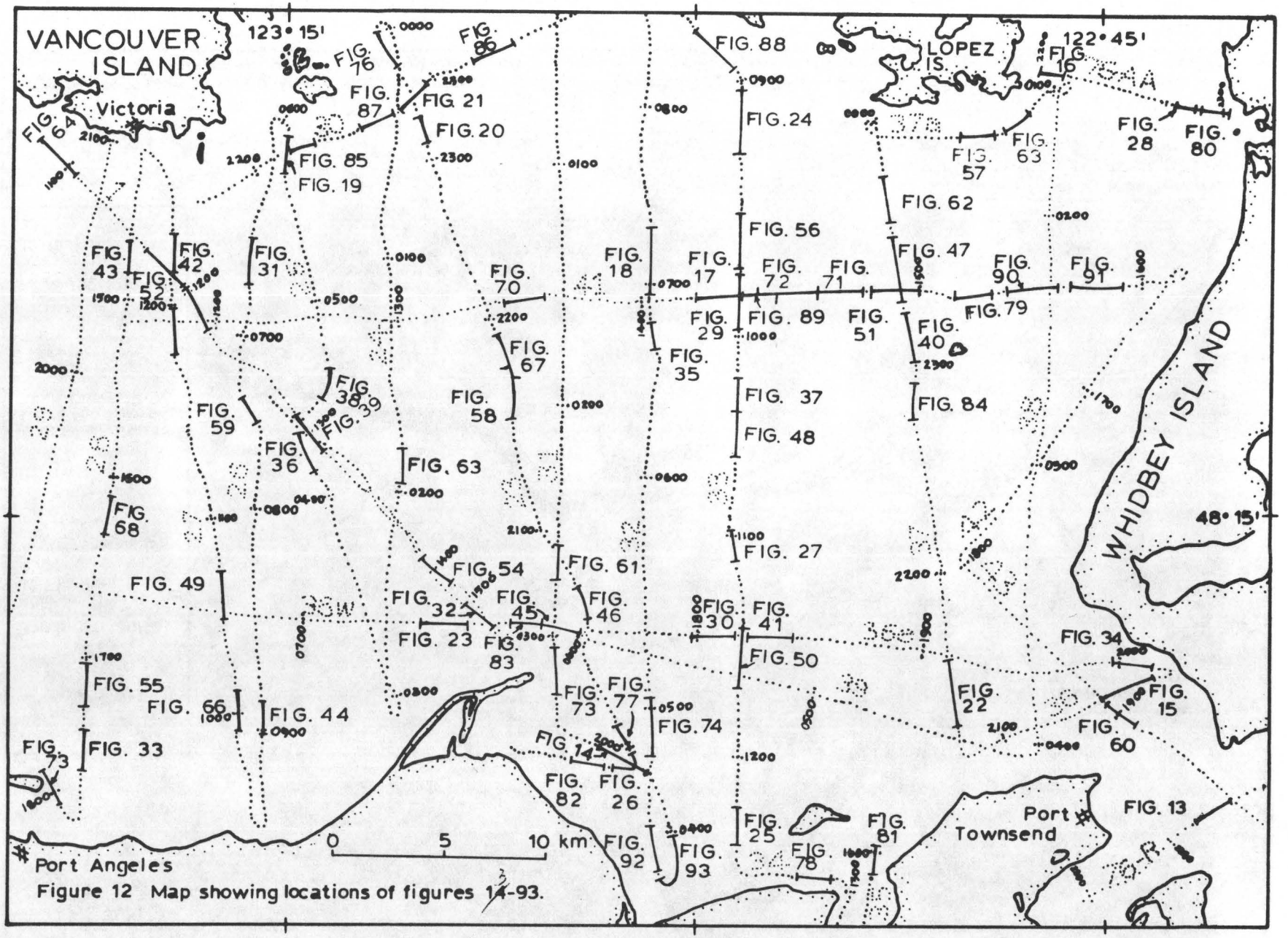


Figure 12 Map showing locations of figures 14-93.

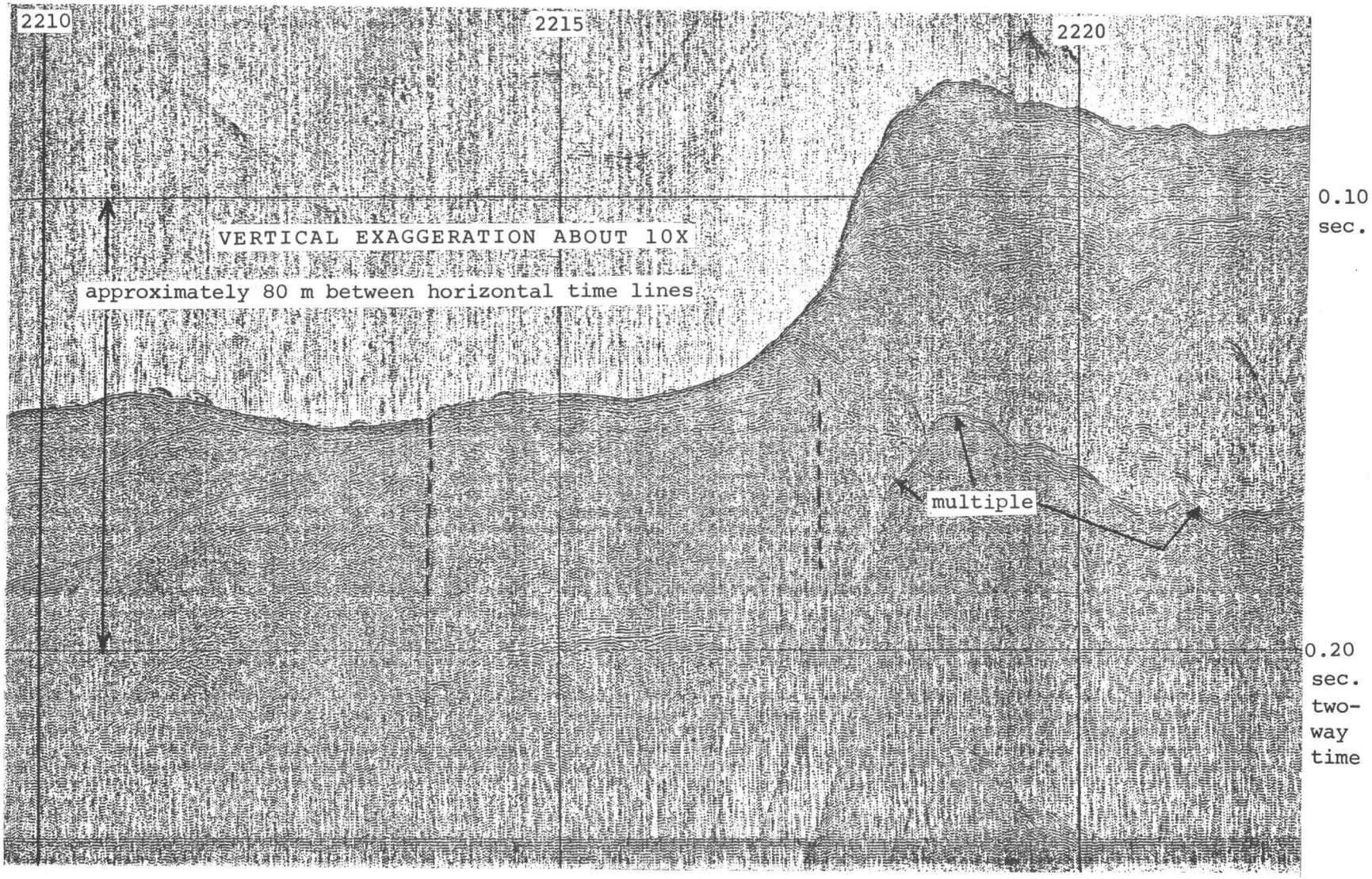


Figure 13. Seismic reflection profile of Miller line 76-R (0.25-sec. sweep) showing truncated upper Pleistocene sedimentary sequence with good reflectors in upper part (between 2218 and 2222) and eastwardly (left) dipping bedded sequence east of seafloor offset (fault) at 2214.

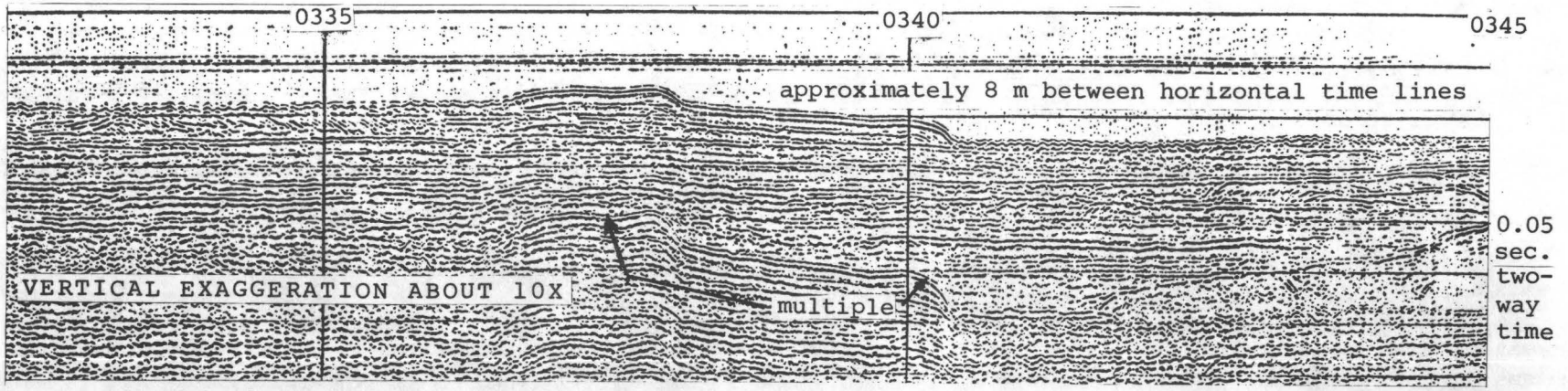


Figure 14. Seismic-reflection profile Parizeau line 31 (0.25-sec. sweep) showing possible upper Pleistocene gravel bed at sea floor (0340-0345) that overlies an erosional surface above a well-bedded to poorly bedded older Pleistocene sequence.

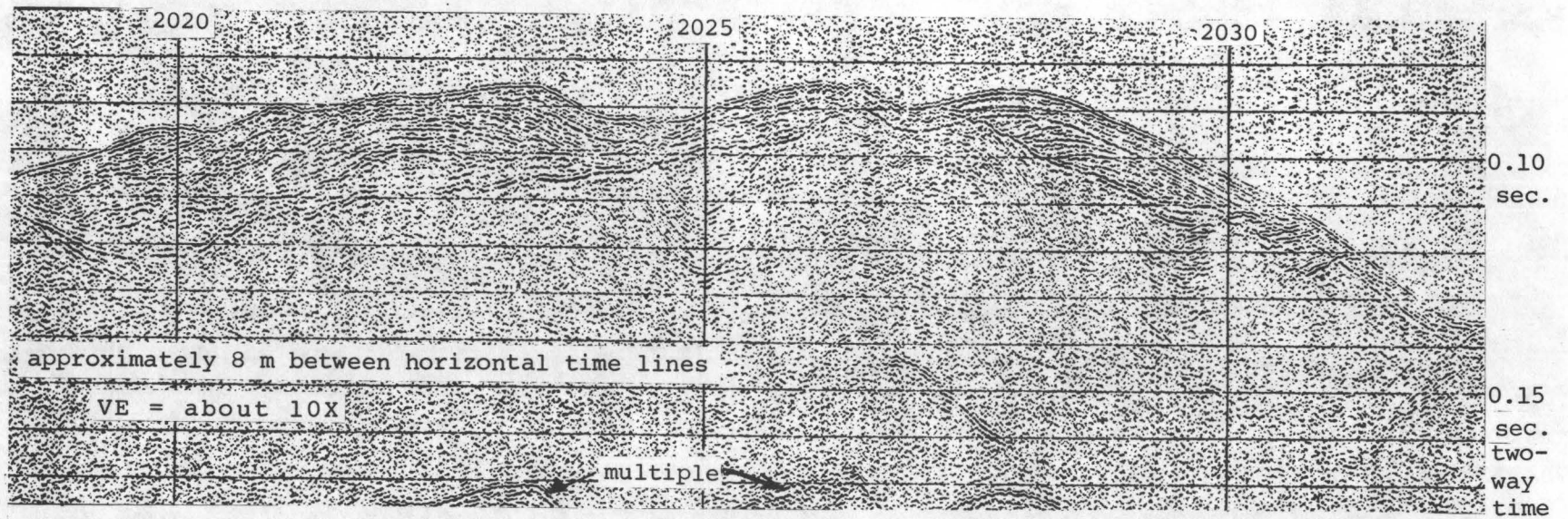


Figure 15. Seismic-reflection profile Parizeau line 36 (0.25-sec. sweep) showing upper Pleistocene glacial outwash and Holocene(?) sediments overlying folded older Pleistocene glacial sediments.

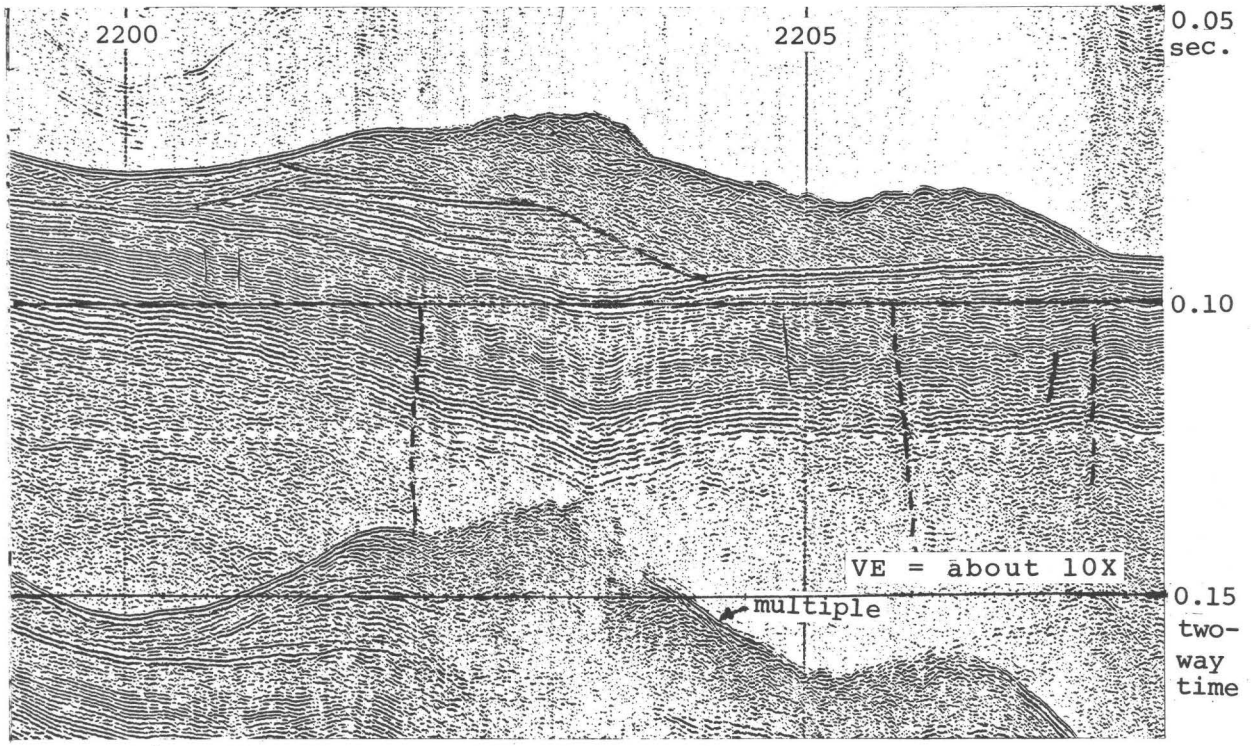


Figure 16. Seismic-reflection profile Miller line AA (0.25-sec. sweep) showing delta front that progrades out across an eroded and disrupted channel-fill sequence. Underlying bedded sequence is folded and fractured and underlain by thick poorly bedded till and gravel unit.

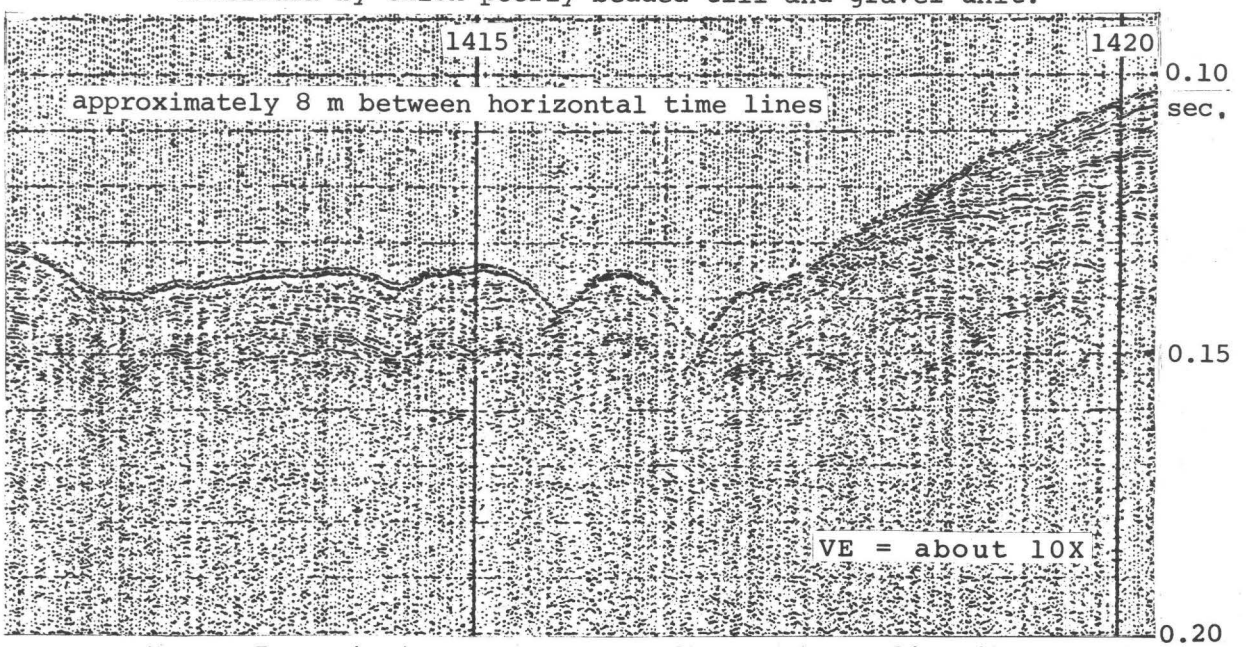


Figure 17. Seismic-reflection profile Parizeau line 41 (0.25 sec. sweep) showing erosional truncation (1419.20) of upper Pleistocene bedded sediments overlain by a veneer of Holocene sediments.

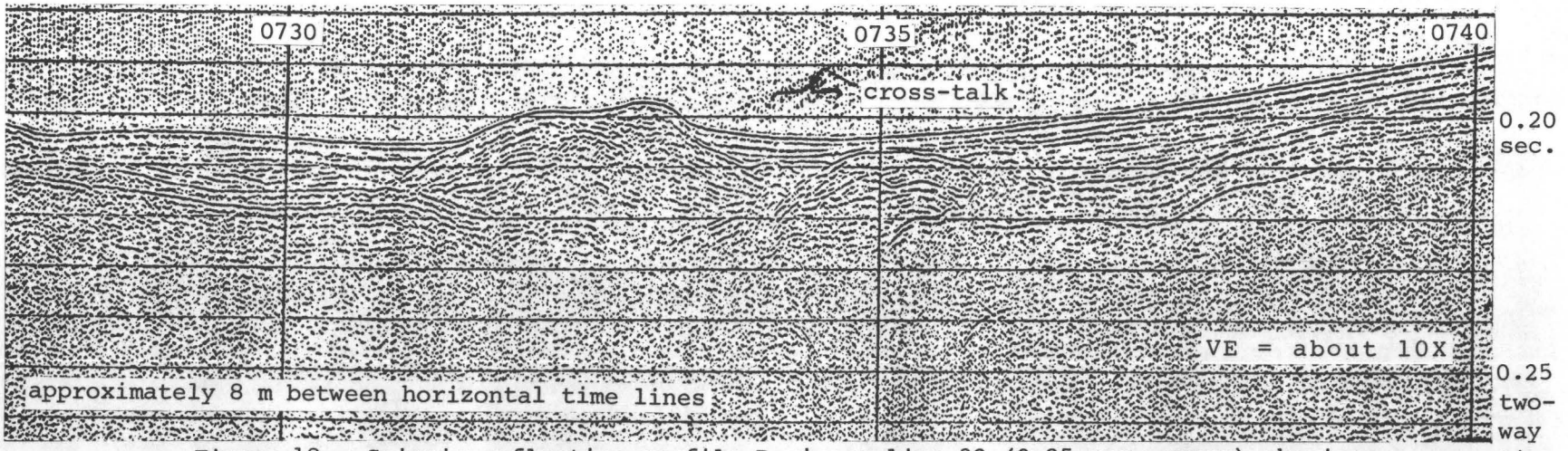


Figure 18. Seismic-reflection profile Parizeau line 32 (0.25-sec. sweep) showing drumlinoid (?) or recessional moraine feature in uppermost Pleistocene and Holocene (?) bedded sediments.

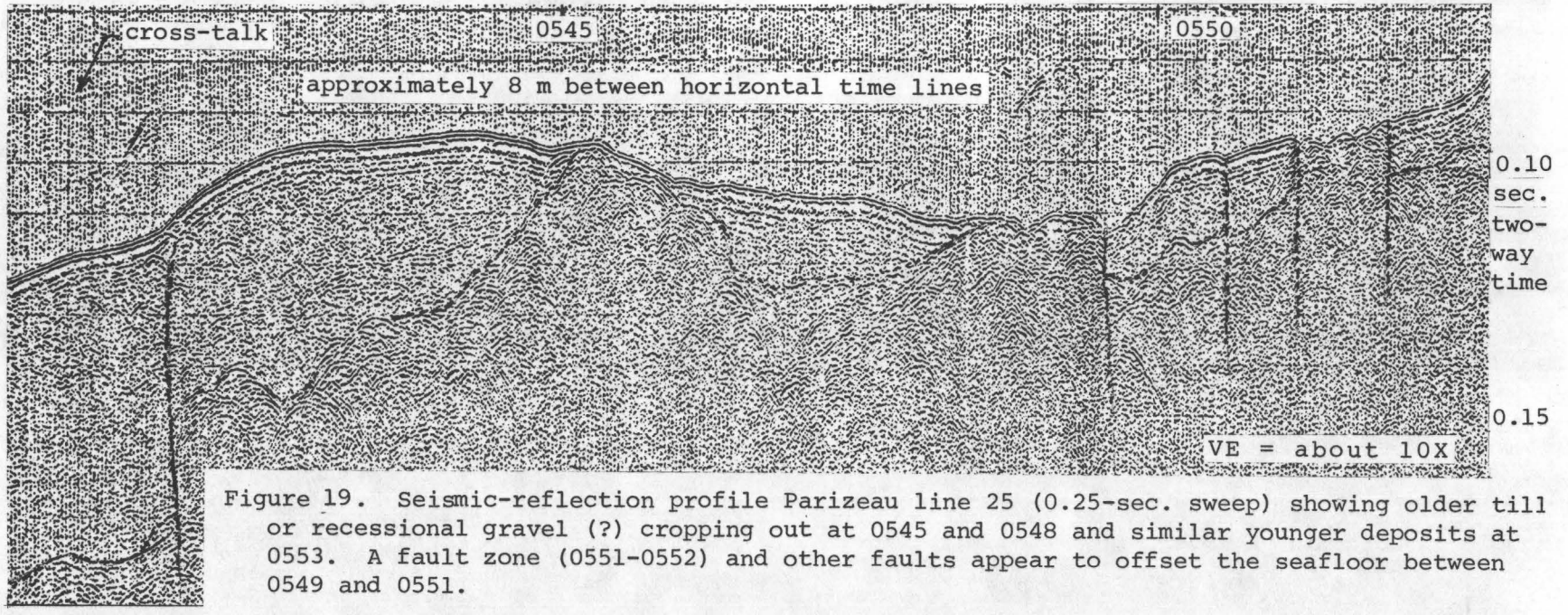


Figure 19. Seismic-reflection profile Parizeau line 25 (0.25-sec. sweep) showing older till or recessional gravel (?) cropping out at 0545 and 0548 and similar younger deposits at 0553. A fault zone (0551-0552) and other faults appear to offset the seafloor between 0549 and 0551.

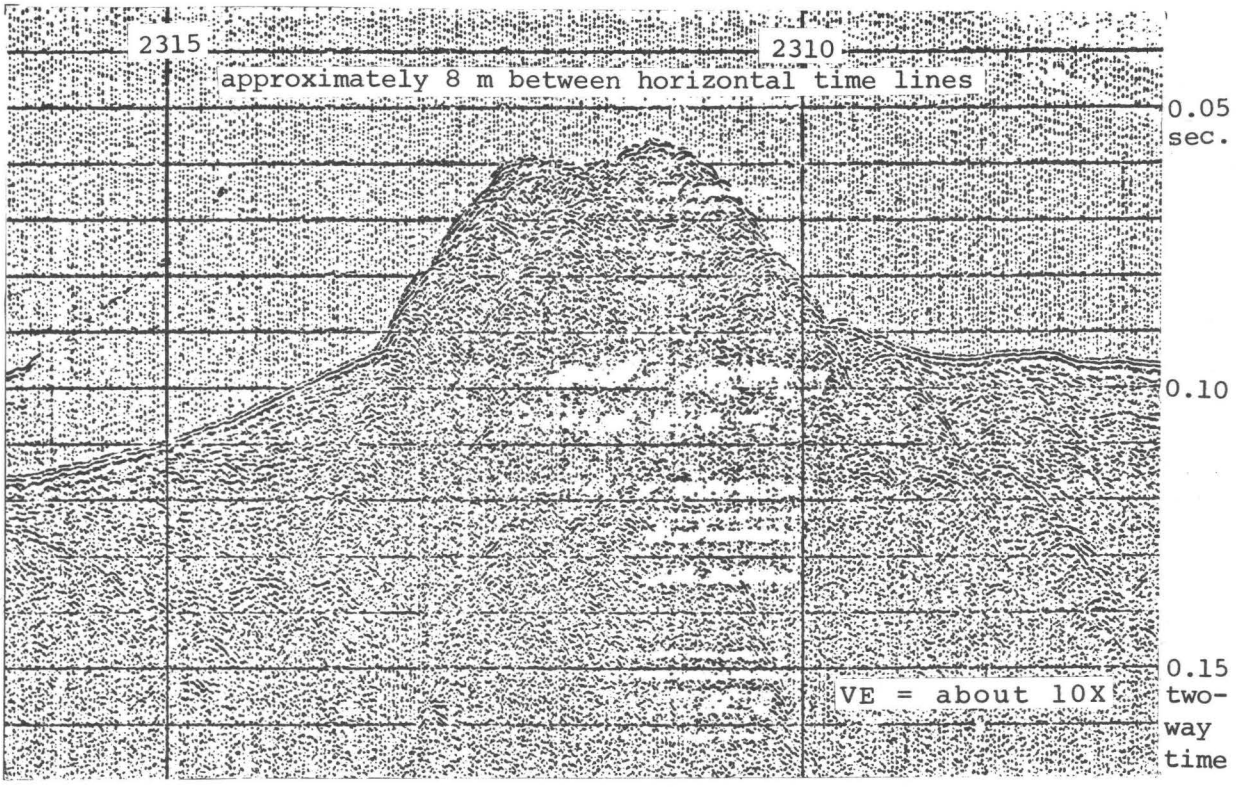


Figure 20. Seismic-reflection profile Parizeau line 23 (0.25-sec. sweep) showing mound-like feature that may represent a drumlin or moraine of latest Pleistocene age.

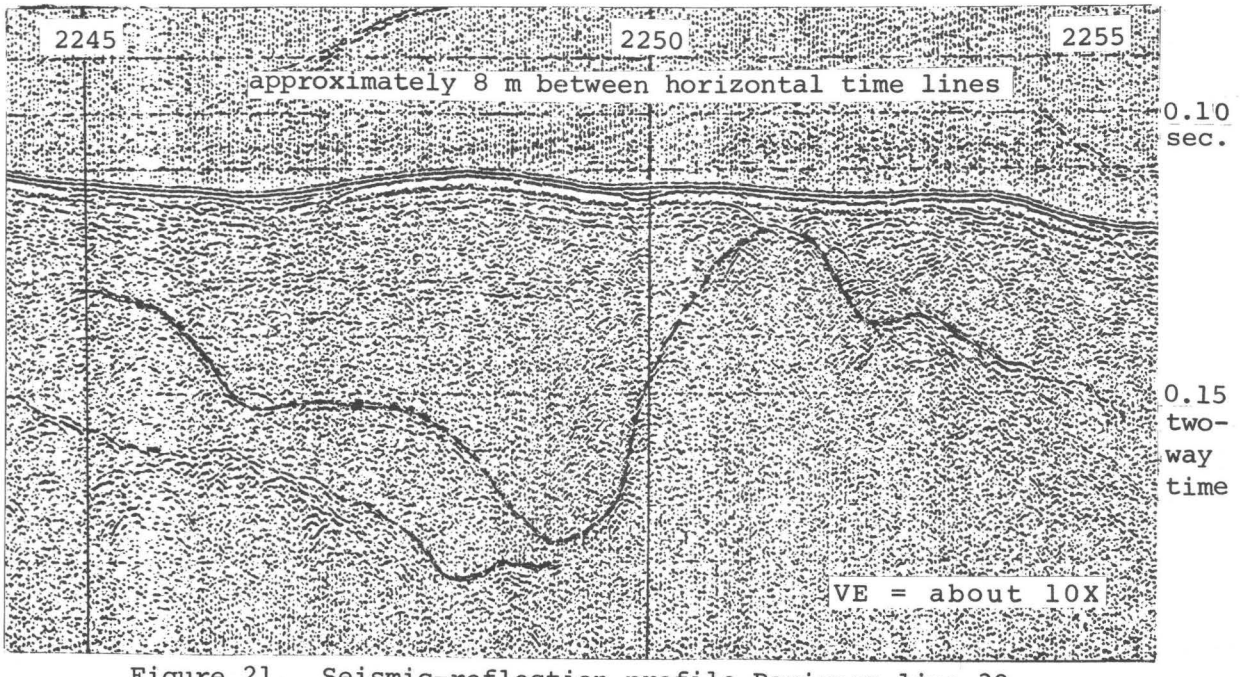


Figure 21. Seismic-reflection profile Parizeau line 30 (0.25-sec. sweep) showing relatively smooth seafloor. Irregular surfaces below seafloor represent older channels cut into till (?) deposits and filled by upper Pleistocene sediments.

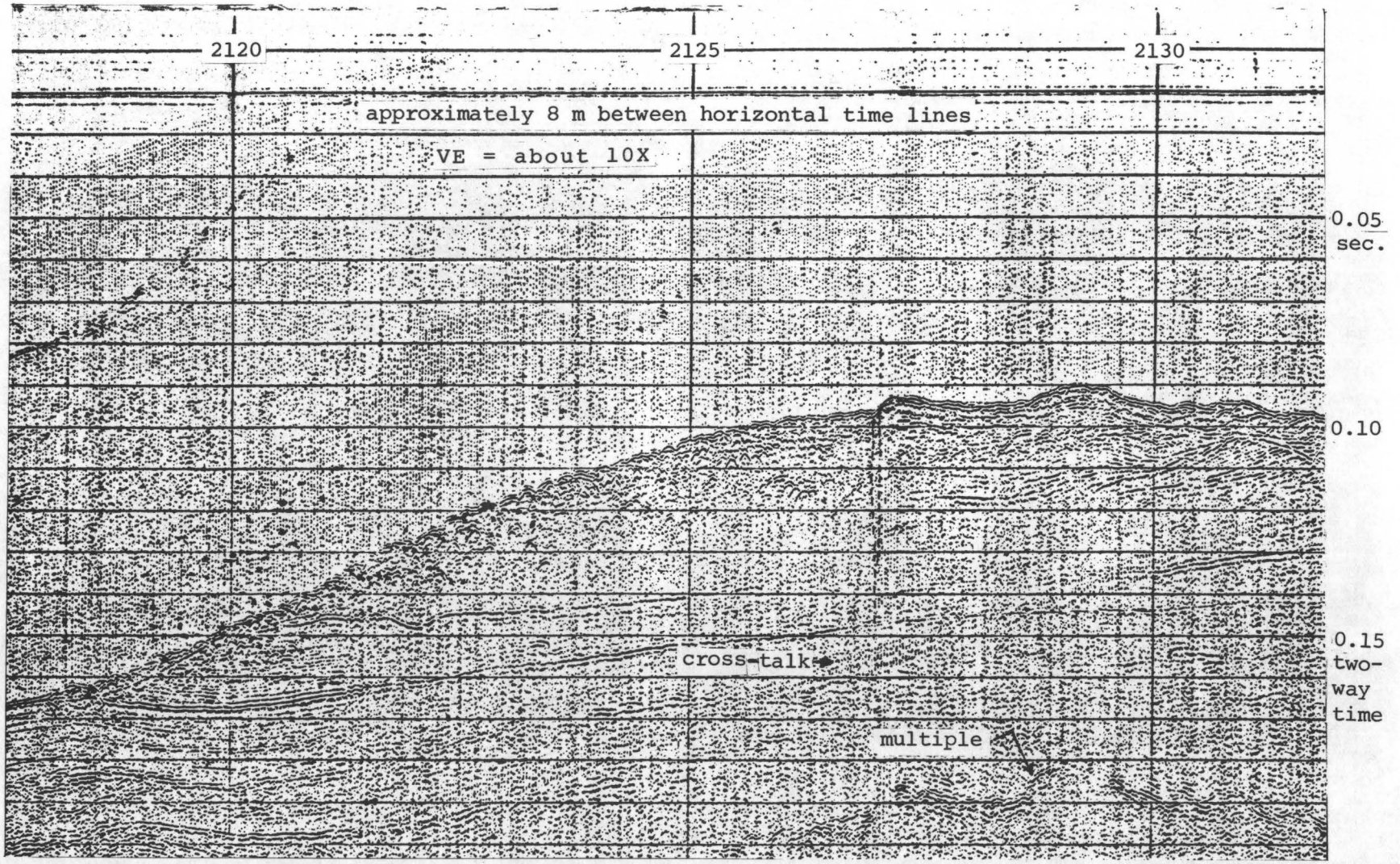


Figure 22. Seismic reflection profile Parizeau line 37 (0.25 sec. sweep) showing irregular glacial depositional surfaces. Bouldery till probably underlies the portion between 2118 and 2127; recessional outwash sediments underlie the portion between 2127 and 2133. Segment between 2118 and 2133 may be slump area with continuous reflector that surfaces at 2118 acting as glide plane.

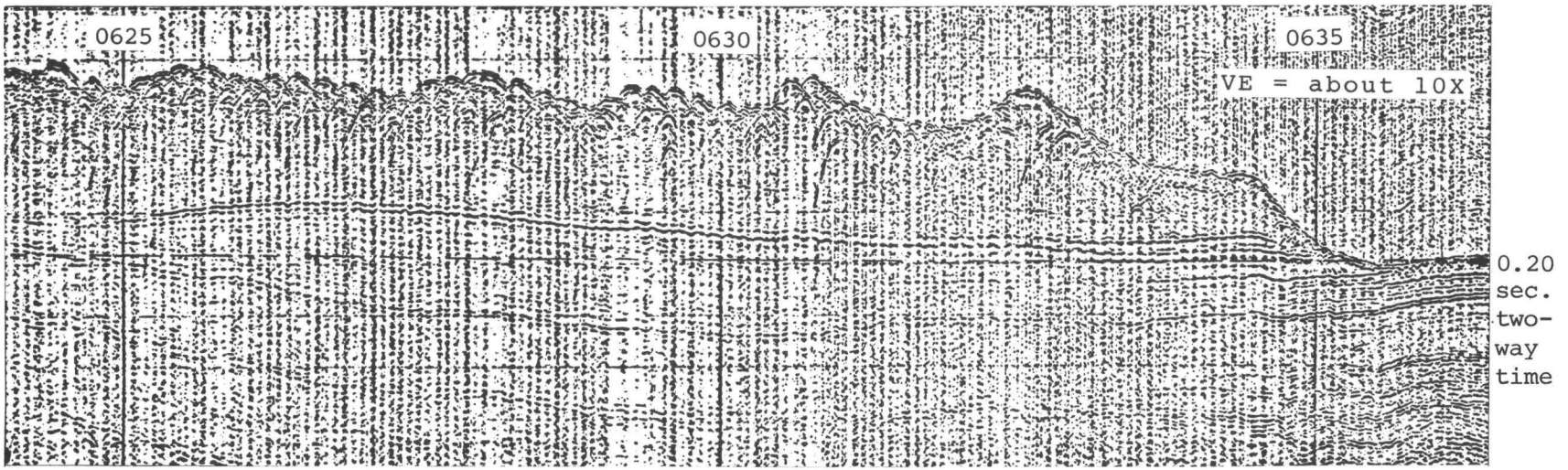


Figure 23. Seismic-reflection profile Parizeau line 36 w (0.25-sec. sweep) showing a possible bouldery till deposited upon lenticularly bedded glacial-deposits.

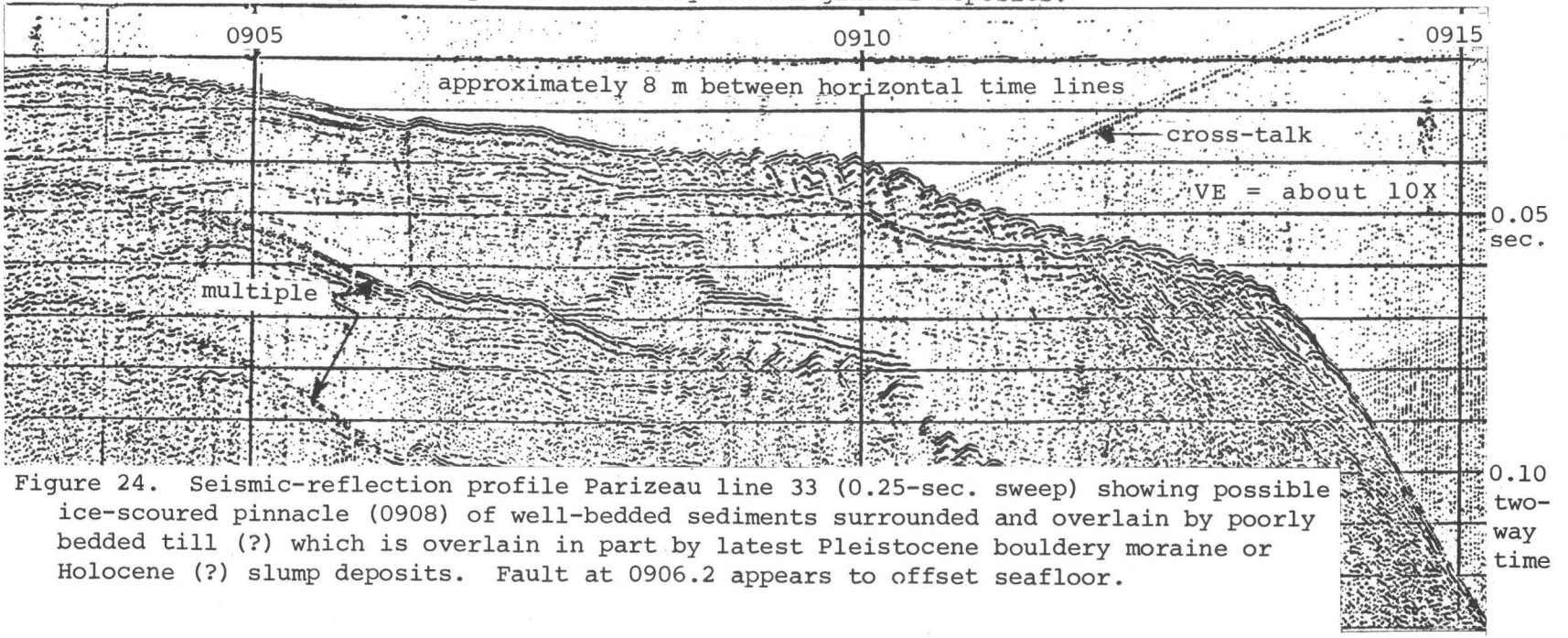


Figure 24. Seismic-reflection profile Parizeau line 33 (0.25-sec. sweep) showing possible ice-scoured pinnacle (0908) of well-bedded sediments surrounded and overlain by poorly bedded till (?) which is overlain in part by latest Pleistocene bouldery moraine or Holocene (?) slump deposits. Fault at 0906.2 appears to offset seafloor.

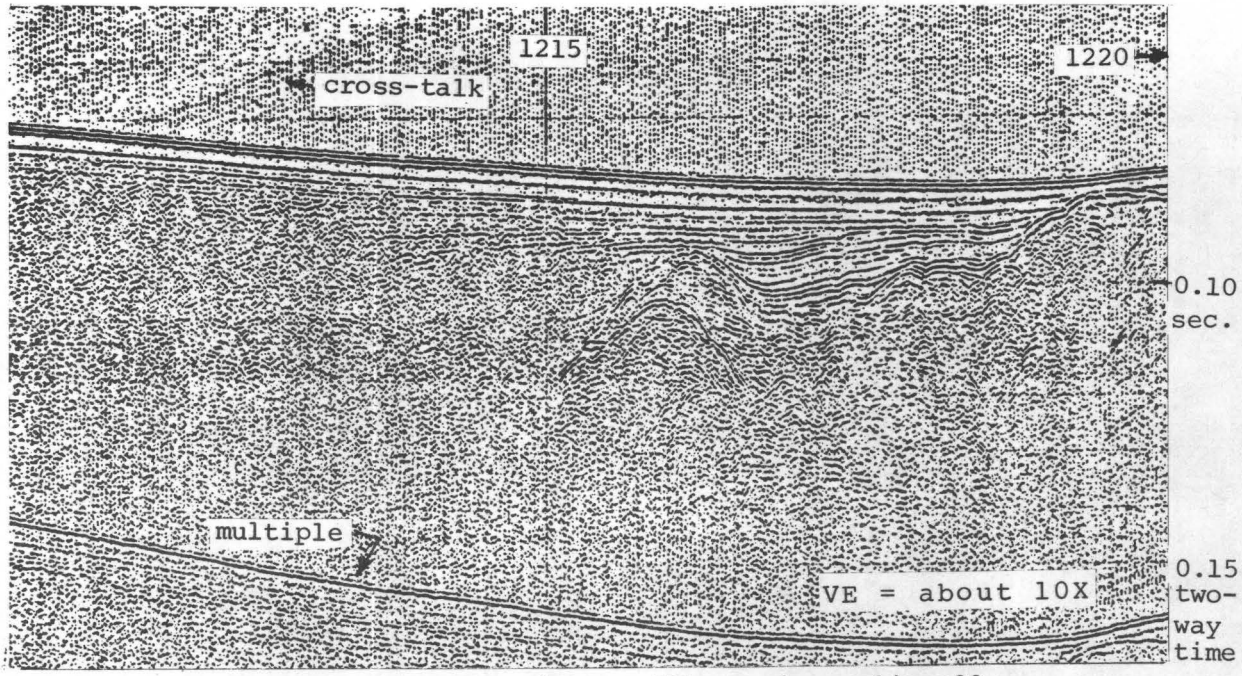


Figure 25. Seismic reflection profile Parizeau line 33 (0.25-sec. sweep) showing possible diapiric high (1216) with onlapping Pleistocene glacial sediments which become homogeneous or gas filled to south (left). Younger sediments overtop the high and lap out under Holocene(?) sediments.

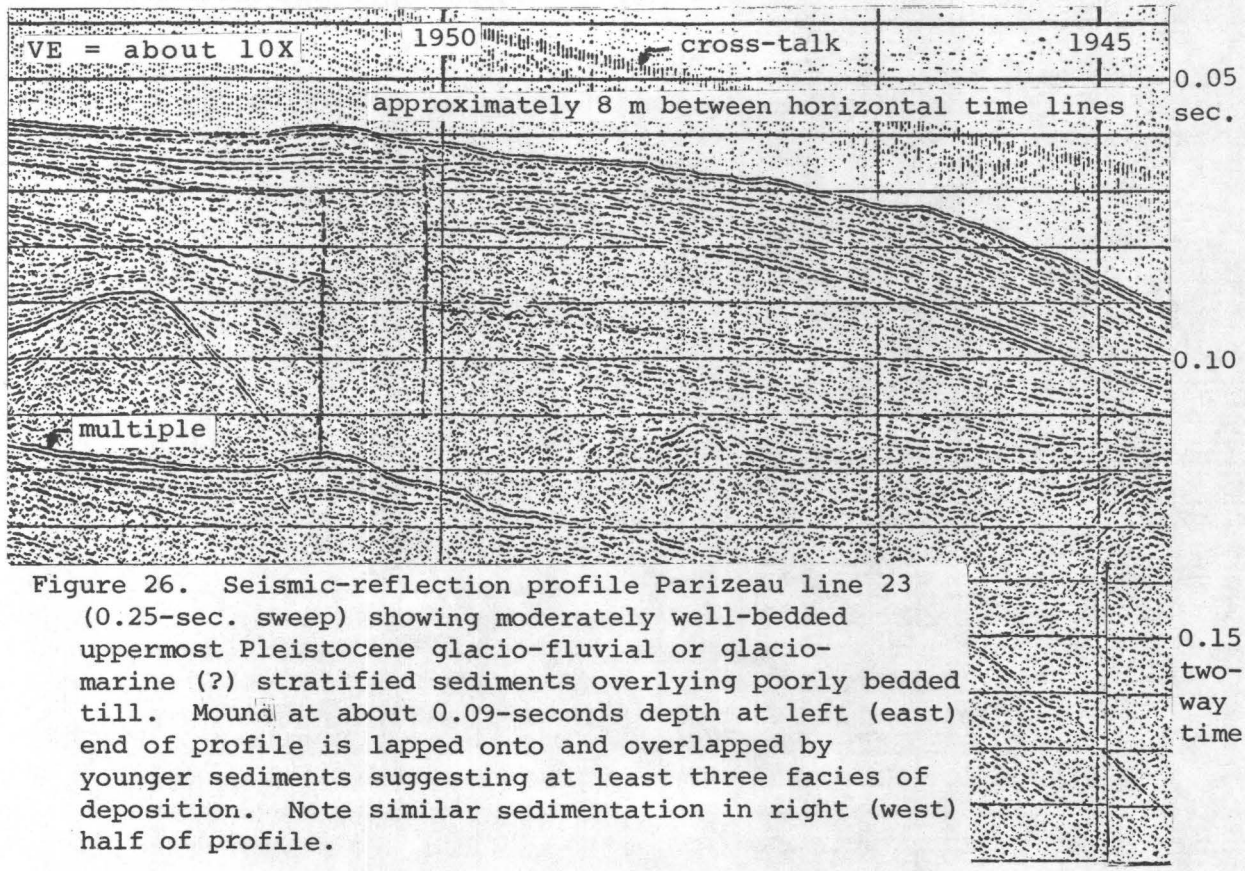


Figure 26. Seismic-reflection profile Parizeau line 23 (0.25-sec. sweep) showing moderately well-bedded uppermost Pleistocene glacio-fluvial or glacio-marine (?) stratified sediments overlying poorly bedded till. Mound at about 0.09-seconds depth at left (east) end of profile is lapped onto and overlapped by younger sediments suggesting at least three facies of deposition. Note similar sedimentation in right (west) half of profile.

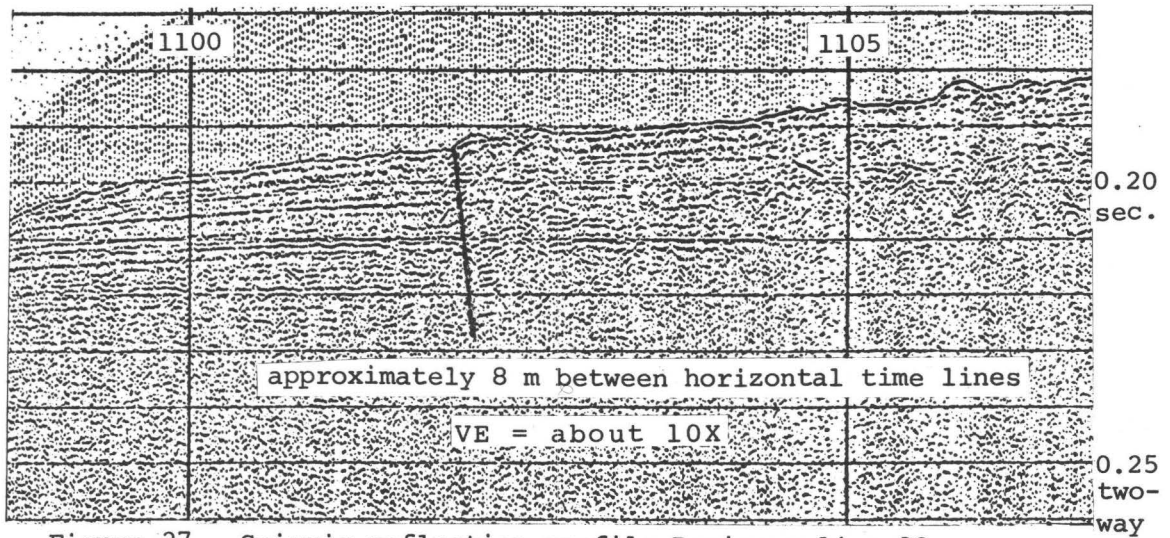


Figure 27. Seismic-reflection profile Parizeau line 33 (0.25 sec. sweep) showing well-bedded sequence that goes laterally into unbedded gravels (?) near north (right) edge of profile and gas (?)-filled sediments at depth between 1057 and 1105. Rough seafloor at right of profile suggests piles of bouldery sediments.

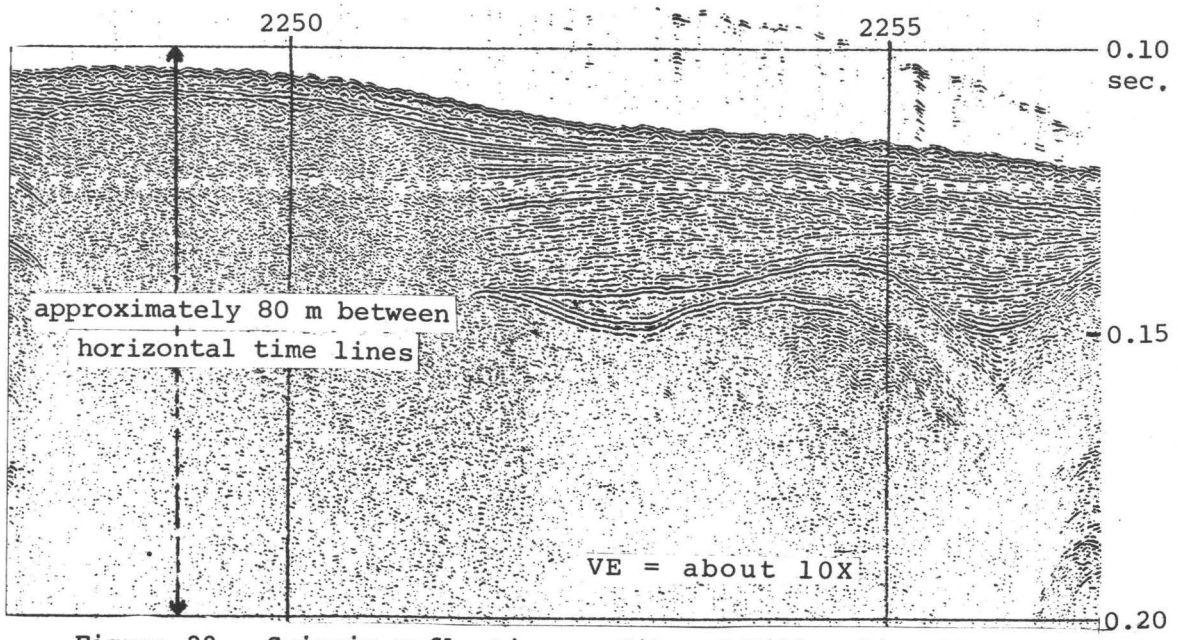


Figure 28. Seismic-reflection profile of Miller line AA (0.25-sec. sweep) showing irregular seafloor with gravelly or bouldery surface. Deeper reflectors abruptly terminate against a reflection-free area which is possibly charged with gas or is overlain by a layer of peat. Also shows erosional truncation or lenticular nature of older unit (2252).

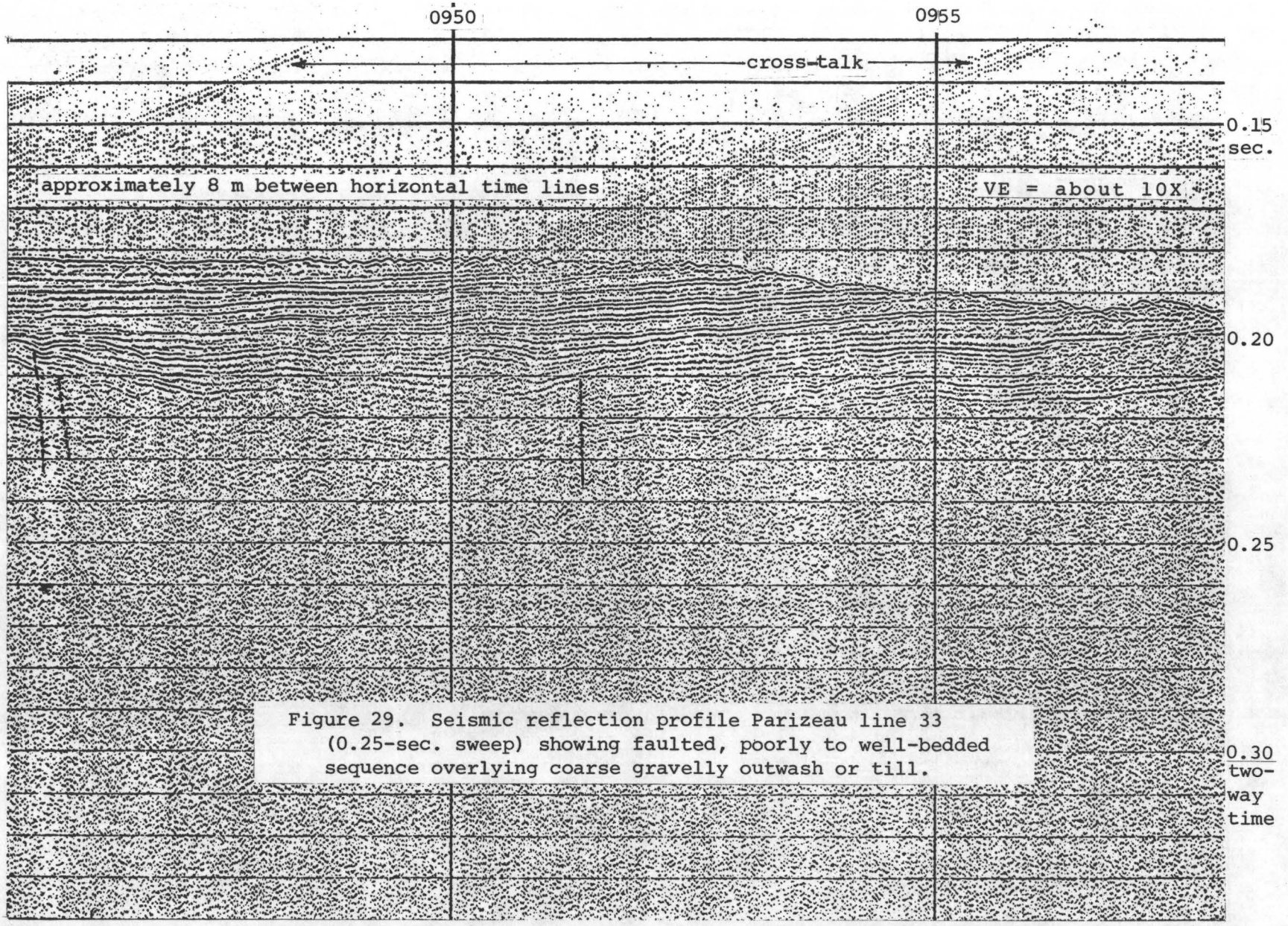


Figure 29. Seismic reflection profile Parizeau line 33 (0.25-sec. sweep) showing faulted, poorly to well-bedded sequence overlying coarse gravelly outwash or till.

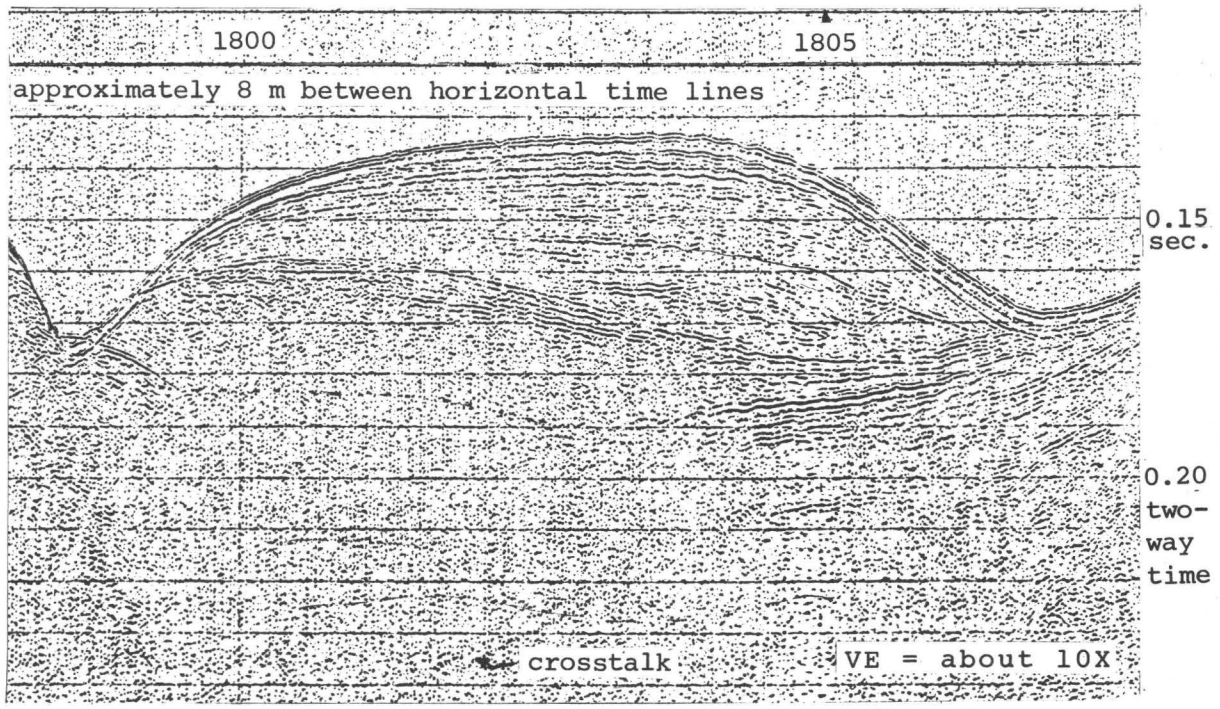


Figure 30. Seismic-reflection profile Parizeau line 36e (0.25-sec. sweep) showing separate depositional sequences bounded by unconformities and erosional channels (?).

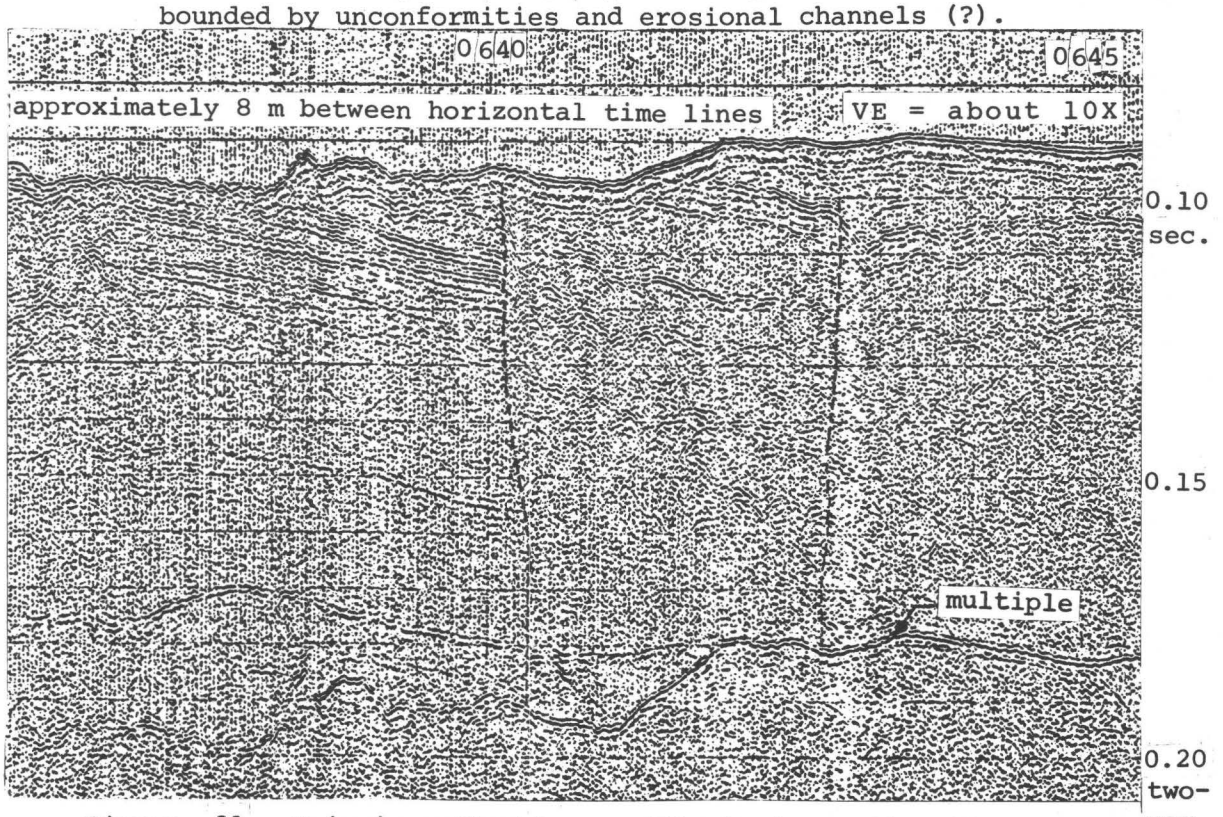


Figure 31. Seismic-reflection profile Parizeau line 26 (0.25-sec. sweep) showing bedded section offset by a fault (indicated by hyperbolics and terminations of reflectors).

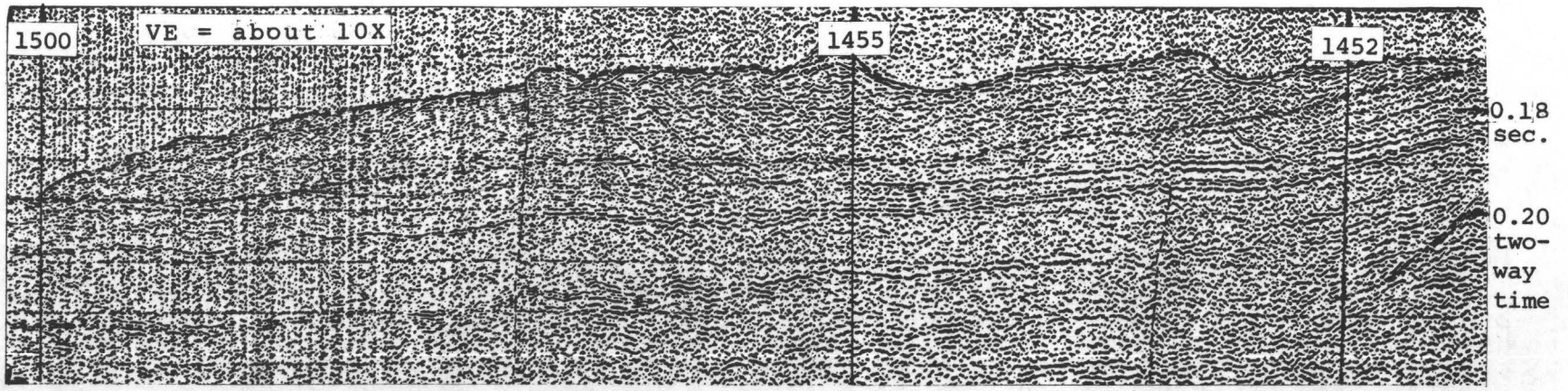


Figure 32. Seismic reflection profile Parizeau line 1A (0.25-sec. sweep) showing Holocene (?) landslide deposit resting upon slightly folded and locally truncated uppermost (?) Pleistocene sediments.

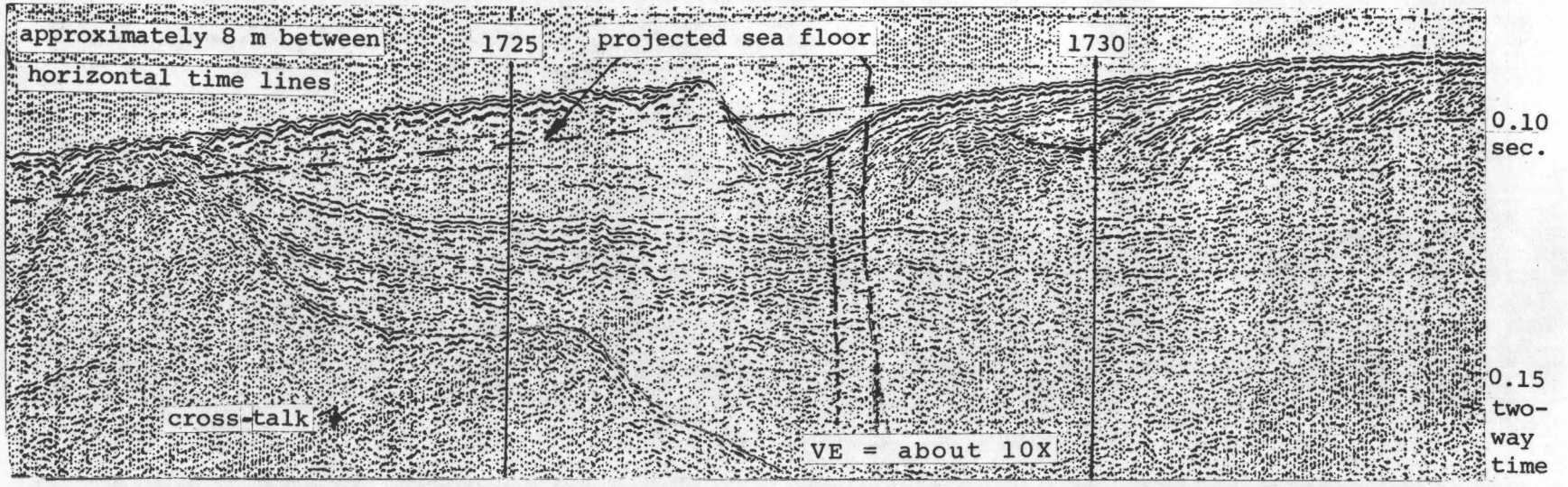


Figure 33. Seismic-reflection profile Parizeau line 28 (0.25-sweep) showing upper Pleistocene glacial outwash(?) overlain by prograding uppermost Pleistocene delta deposits (1730-1733). Holocene(?) channel (partly filled by rubble) occurs at apparent offset of seafloor where one young fault reaches the seafloor (1728). Other fault reaches base of rubble. Older constructional(?) glacial deposits reach the seafloor at 1722.

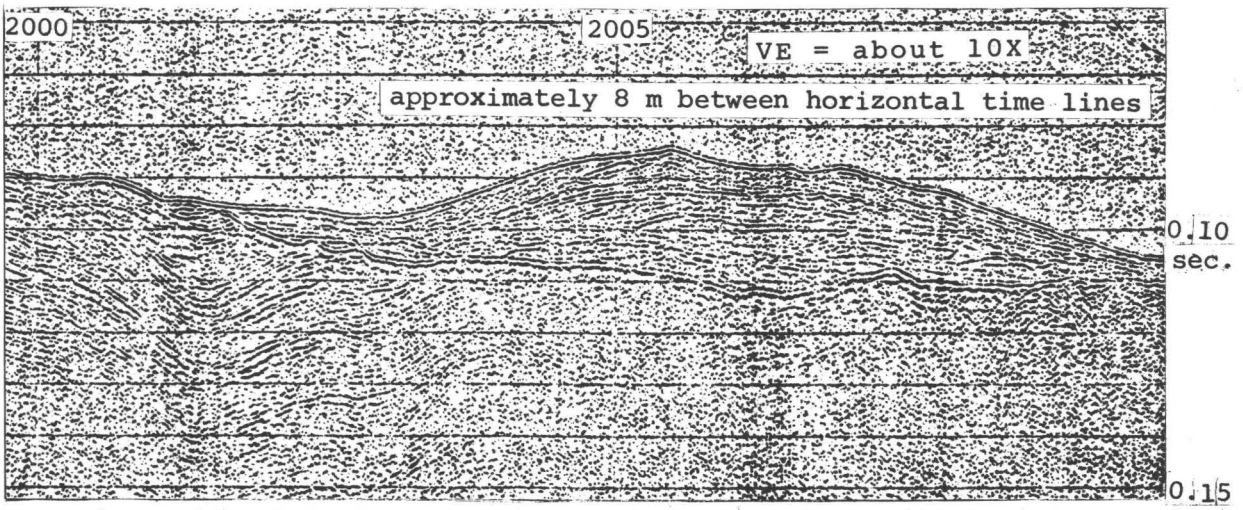


Figure 34. Seismic-reflection profile Parizeau line 36e (0.25-sec. sweep) showing upper Pleistocene glacial drift unconformably overlying older folded and truncated Pleistocene (?) sediments.

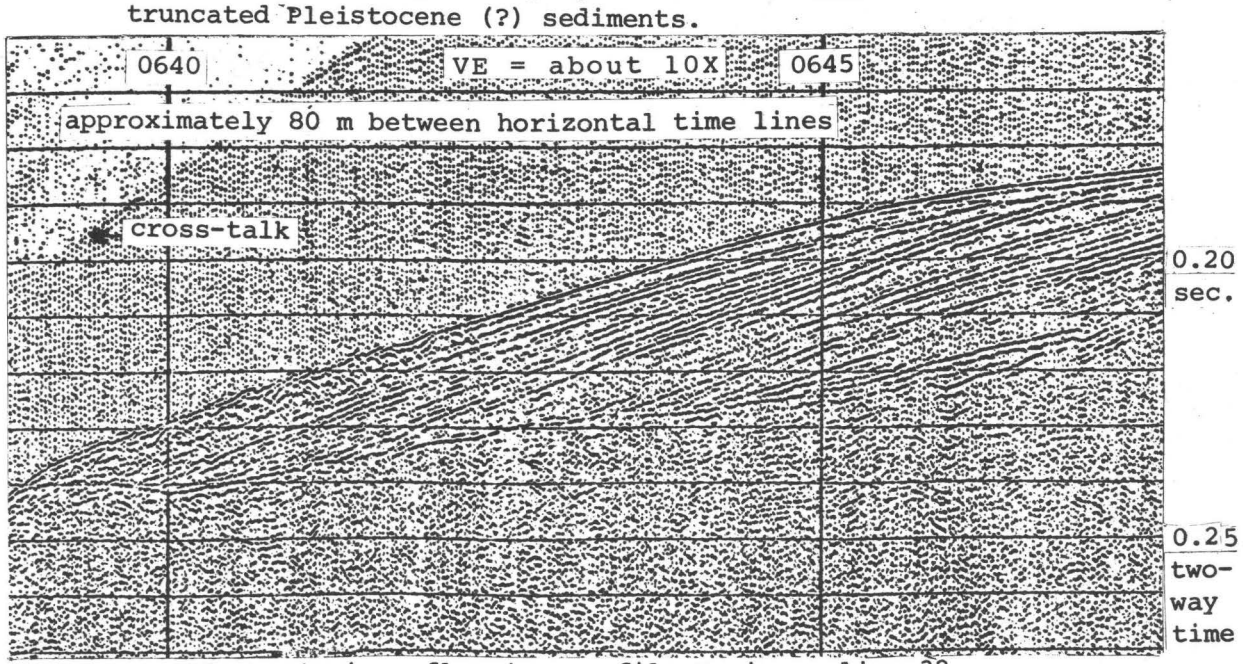


Figure 35. Seismic-reflection profile Parizeau line 32 (0.25-sec. sweep) showing gently sloping prograding reflection being deposited in a low-energy sedimentary regime possibly during a rapid rise in sea level to allow deposition and preservation of the top set unit.

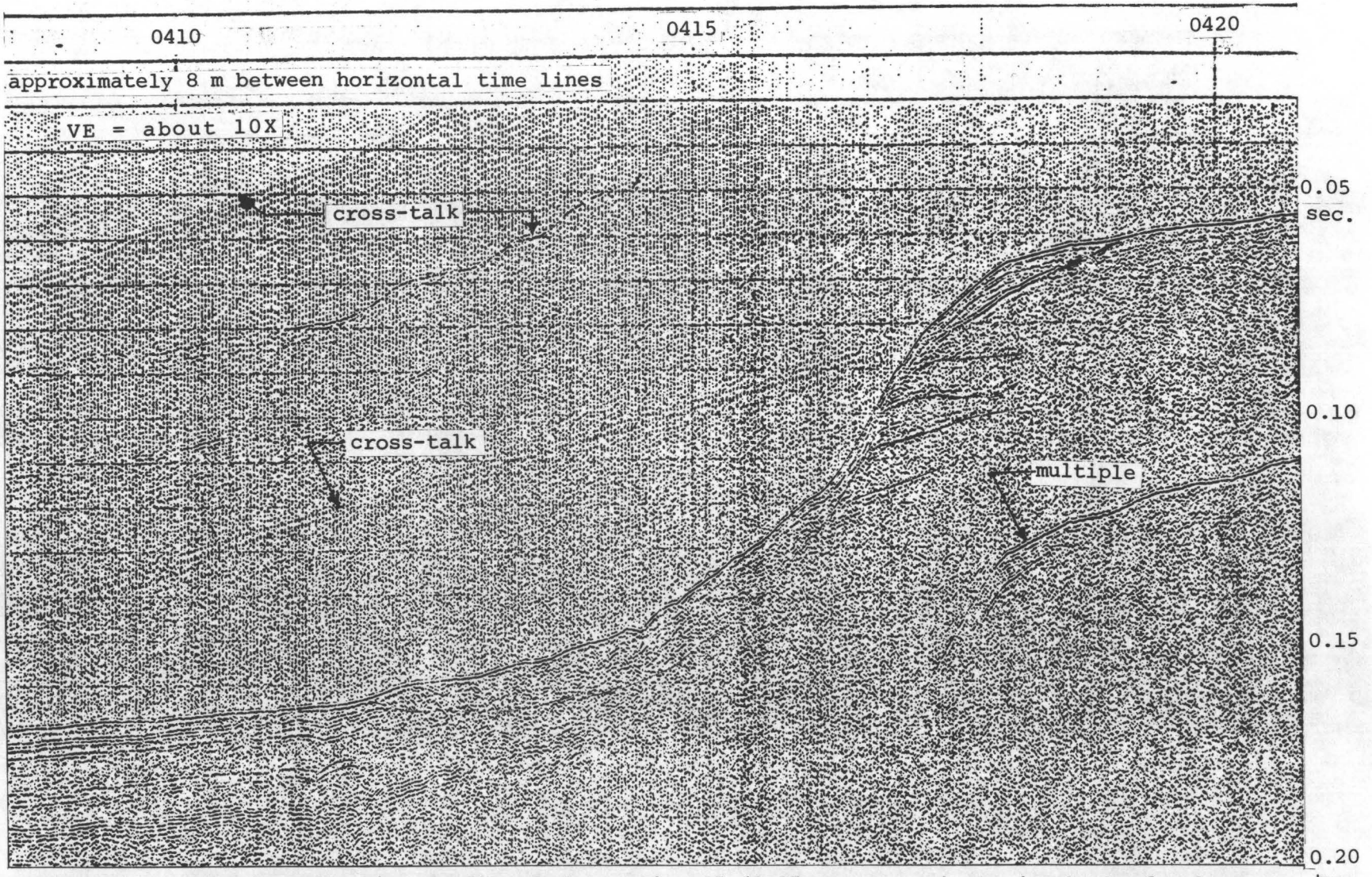


Figure 36. Seismic-reflection profile Parizeau line 25 (0.25-sec. sweep) showing bank edge lense of uppermost Pleistocene and Holocene (?) sediments (0418), truncated bank-slope deposits (0417), slump deposits (0412-0416) and related pressure fold (0411.5).

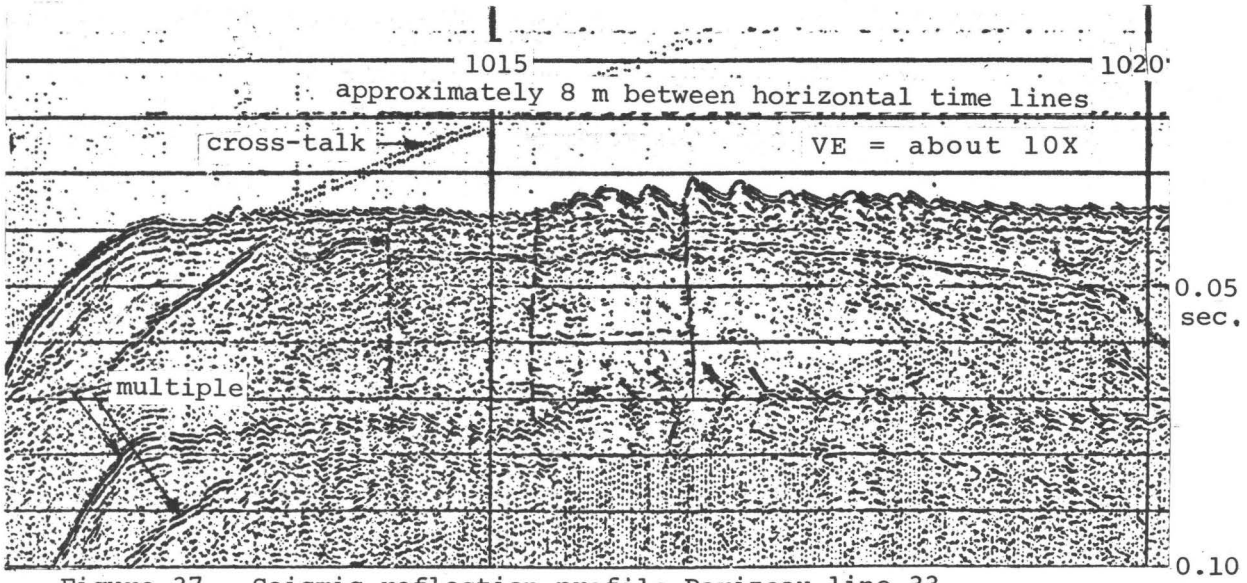


Figure 37. Seismic reflection profile Parizeau line 33 (0.25-sec. sweep) showing recessional-moraine (?) deposits on Eastern Bank on top of older ice-contact bank deposits with foreset deltaic beds (0.05-0.08 sec. depth) at south (right) end. Uppermost Pleistocene or Holocene (?) deltaic overbank deposits occur at north (left) end of bank. Faulting may offset older ridge top and possibly present ridge top as indicated.

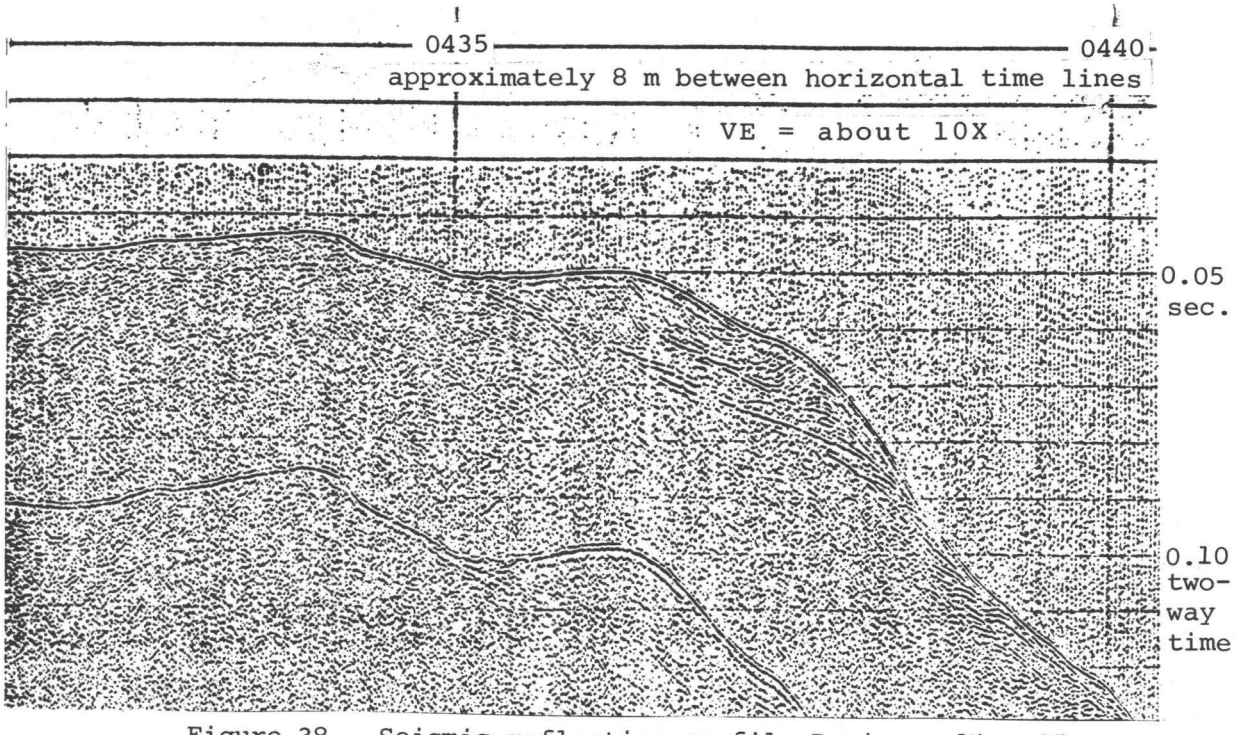


Figure 38. Seismic-reflection profile Parizeau line 25 (0.25 sec. sweep) showing the northern edge of Center Bank with an off bank top uppermost Pleistocene or Holocene (?) deposit.

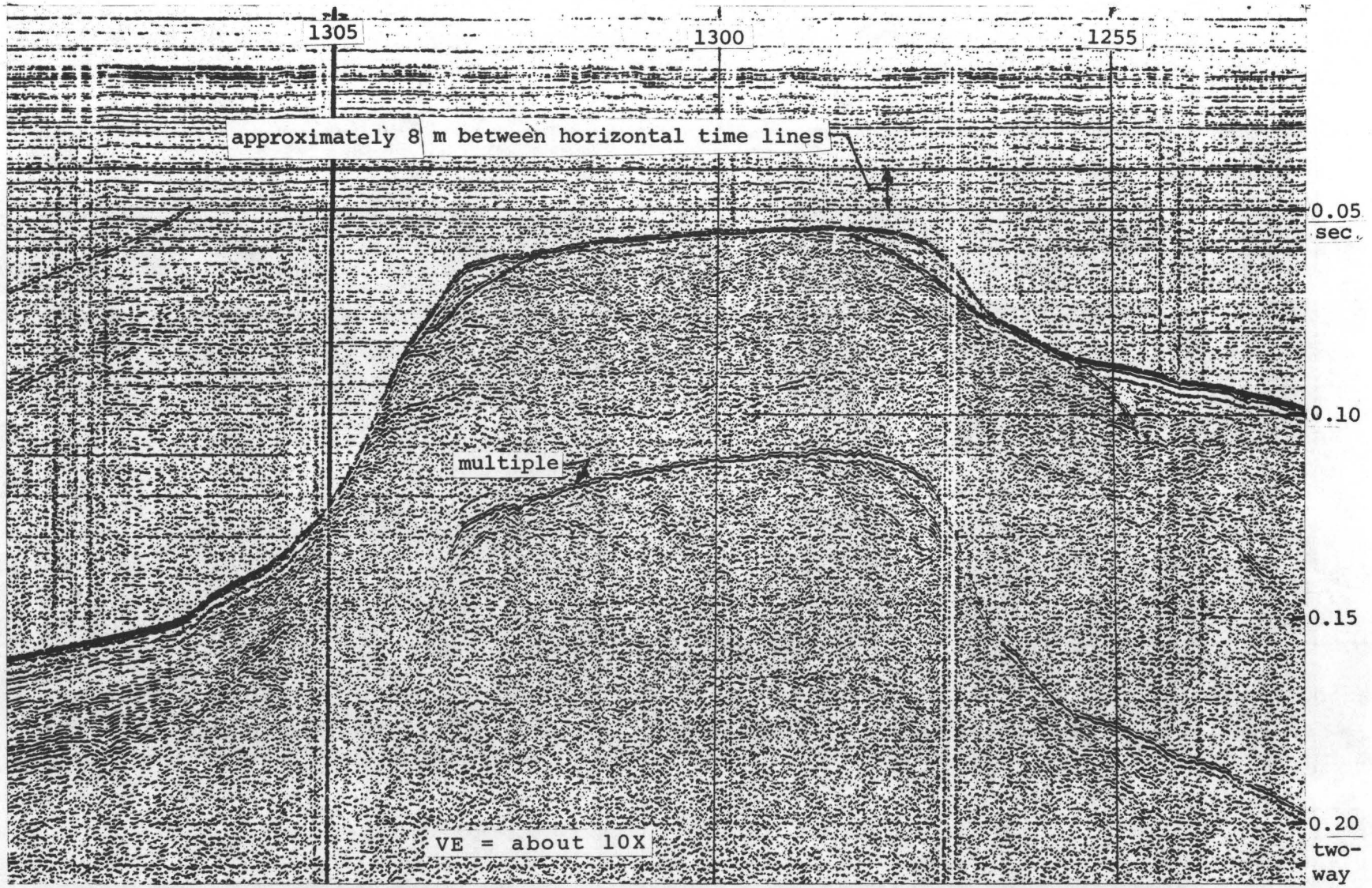


Figure 39. Seismic-reflection profile Parizeau line 1 (0.25-sec. sweep) showing part of Center Bank with uppermost Pleistocene and Holocene deltaic, bank-edge sediments on each side. Upper Pleistocene sediments on southeast (left) side were presumably truncated by ice-scour process during movement of the Juan de Fuca lobe.

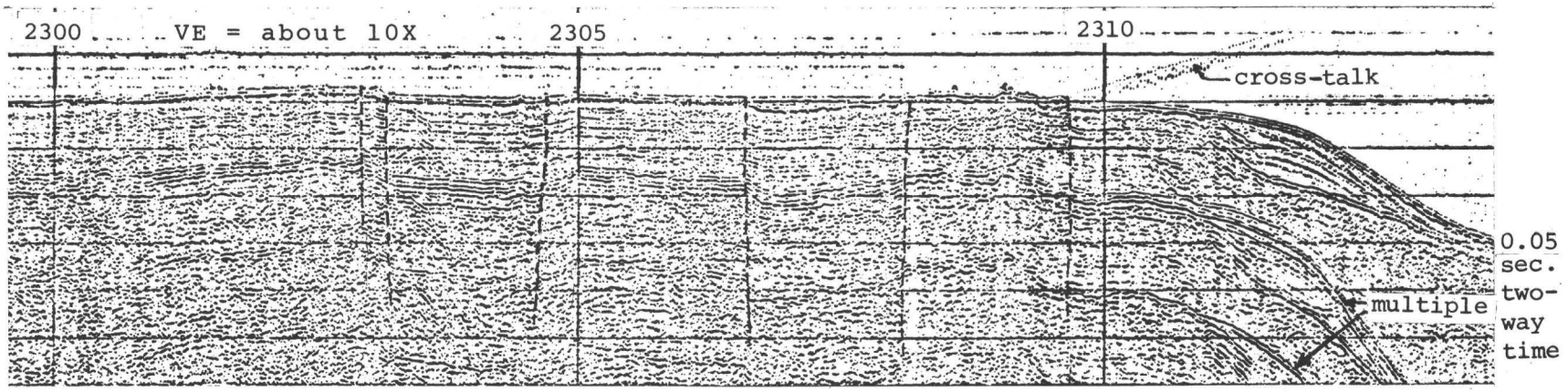


Figure 40. Seismic reflection profile Parizeau line 37 (0.25-See sweep) showing faulted and folded uppermost Pleistocene or Holocene sediments. Faults at 2303 and 2309.5 appear to offset seafloor (down to right). Lense of deltaic sediment occurs at break in slope.

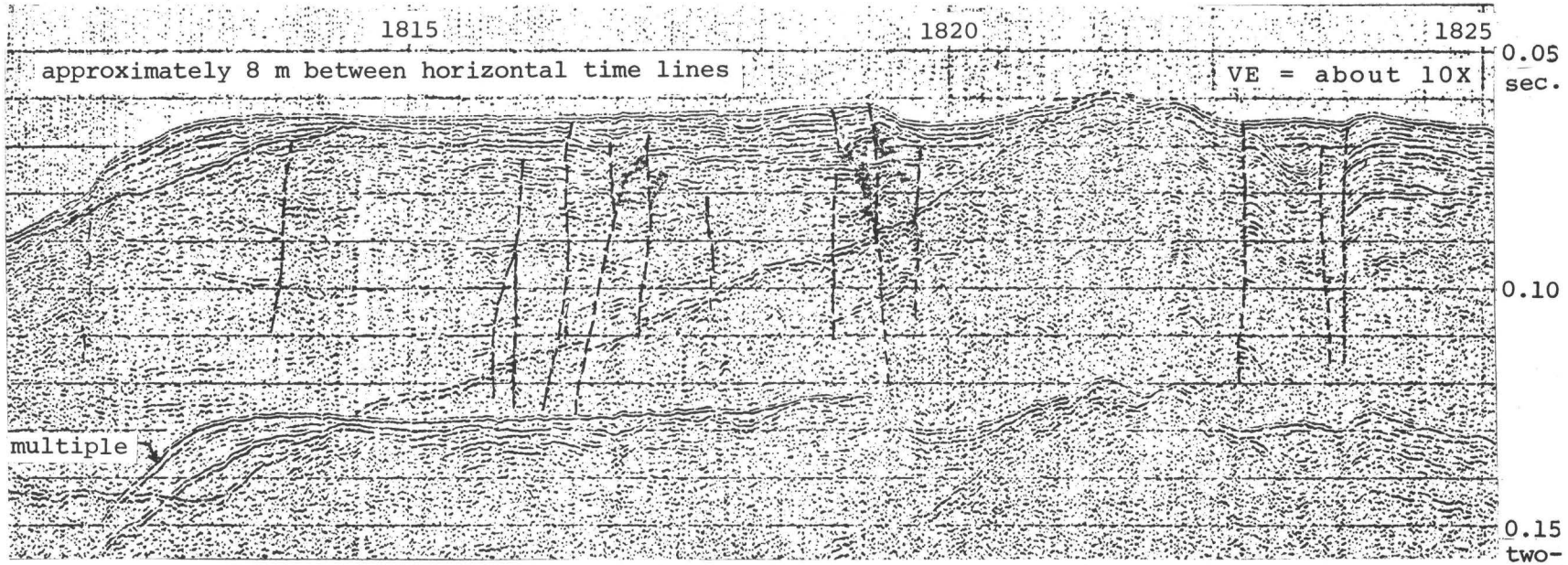


Figure 41. Seismic-reflection profile Parizeau line 36e (0.25-sec. sweep) illustrating multiple depositional sequences that are separated by unconformities. Post-depositional deformation from subsidence or faulting has occurred locally.

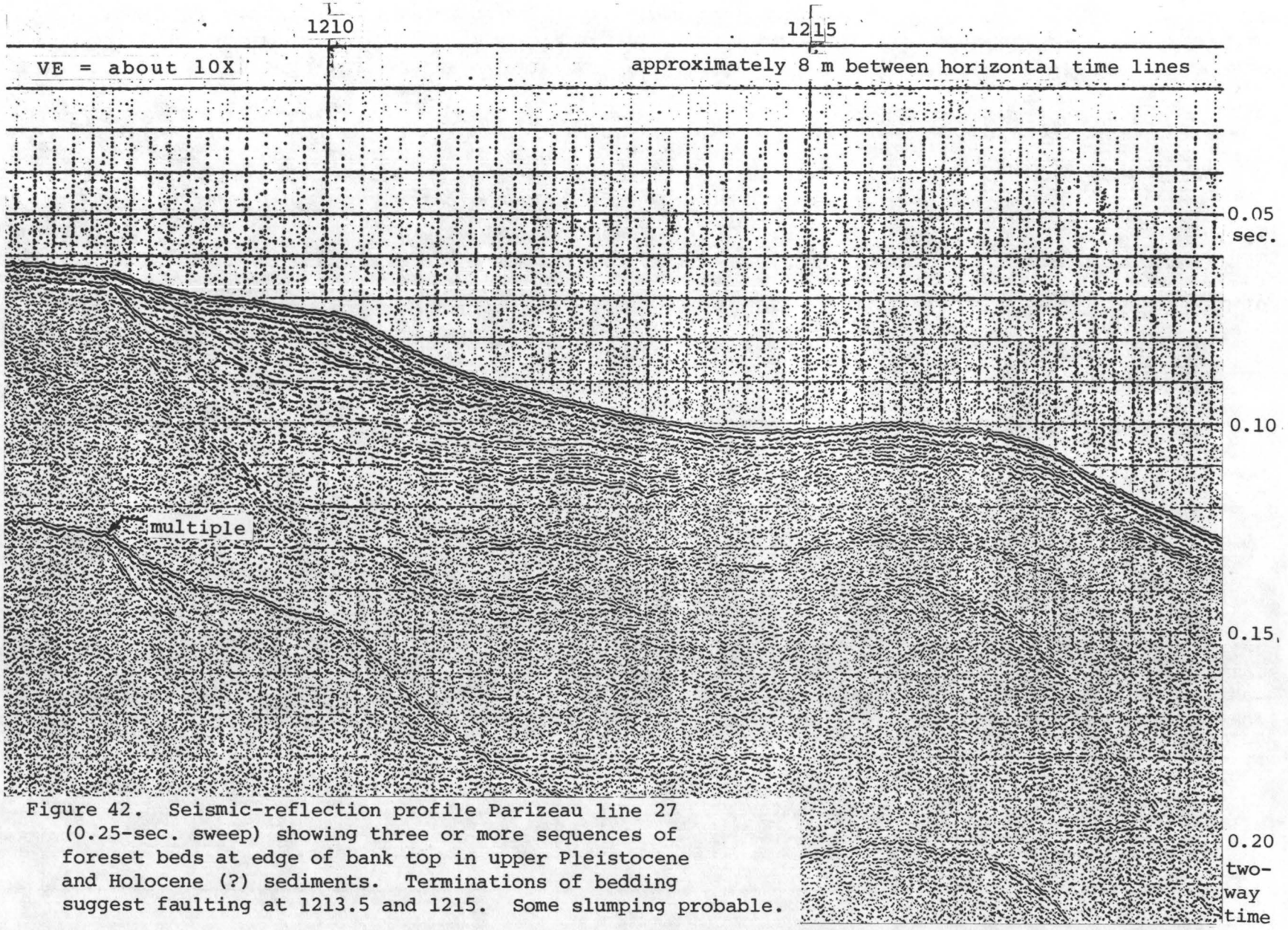


Figure 42. Seismic-reflection profile Parizeau line 27 (0.25-sec. sweep) showing three or more sequences of foreset beds at edge of bank top in upper Pleistocene and Holocene (?) sediments. Terminations of bedding suggest faulting at 1213.5 and 1215. Some slumping probable.

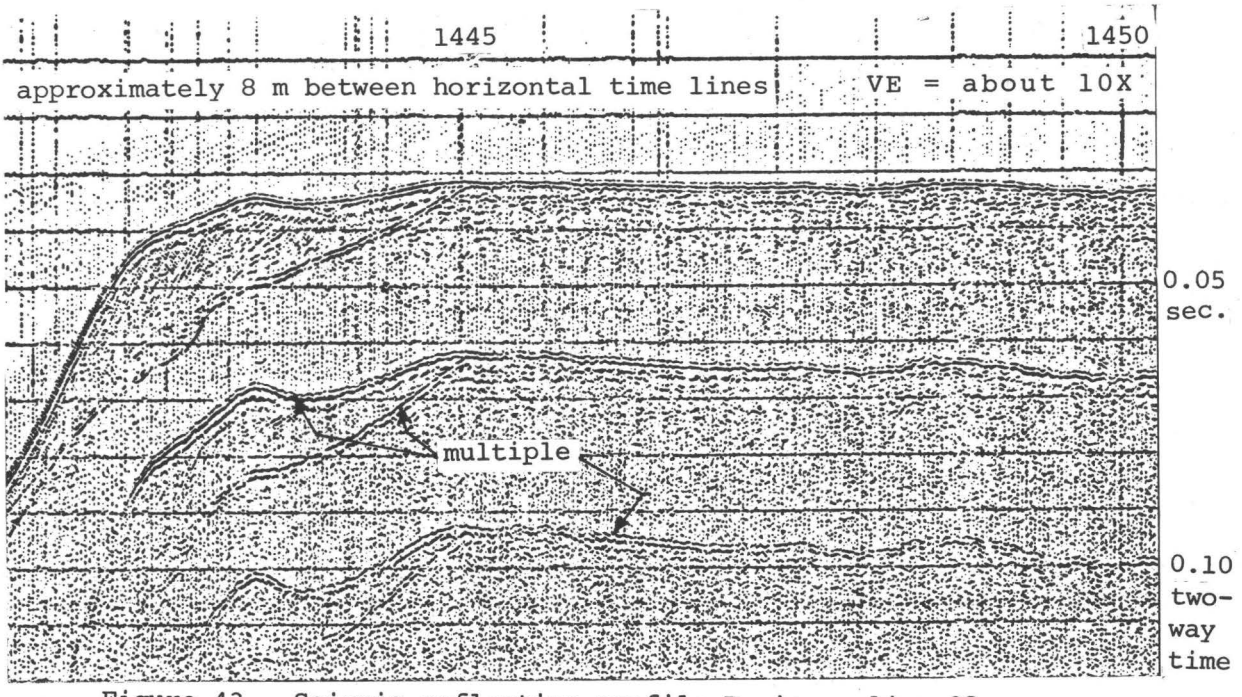


Figure 43. Seismic-reflection profile Parizeau line 28 (0.25-sec. sweep) showing deltaic bank-edge foreset beds of latest Pleistocene or Holocene (?) age overlying non-bedded till (?) on north side of Constance Bank.

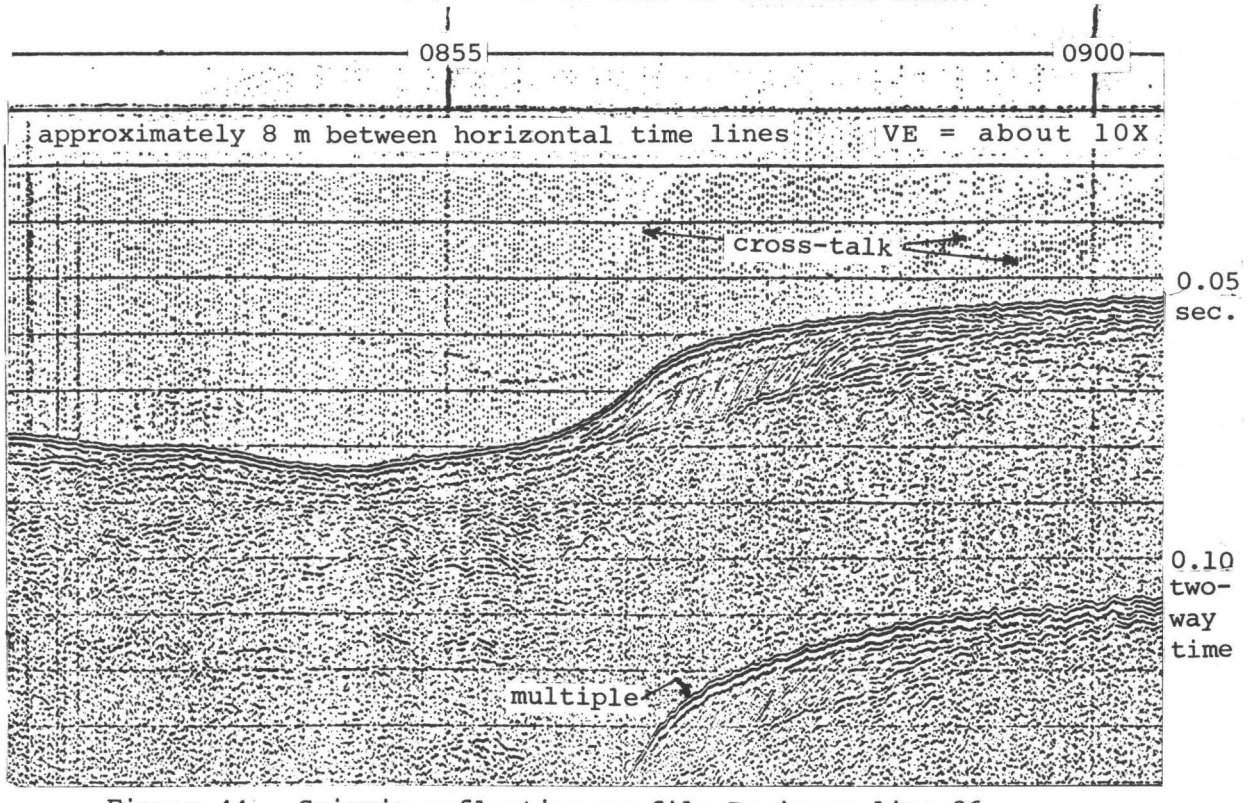


Figure 44. Seismic reflection profile Parizeau line 26 (0.25 sec. sweep) showing foreset beds in slope-edge deposit of latest Pleistocene age overlying sediments of unbedded till-like character.

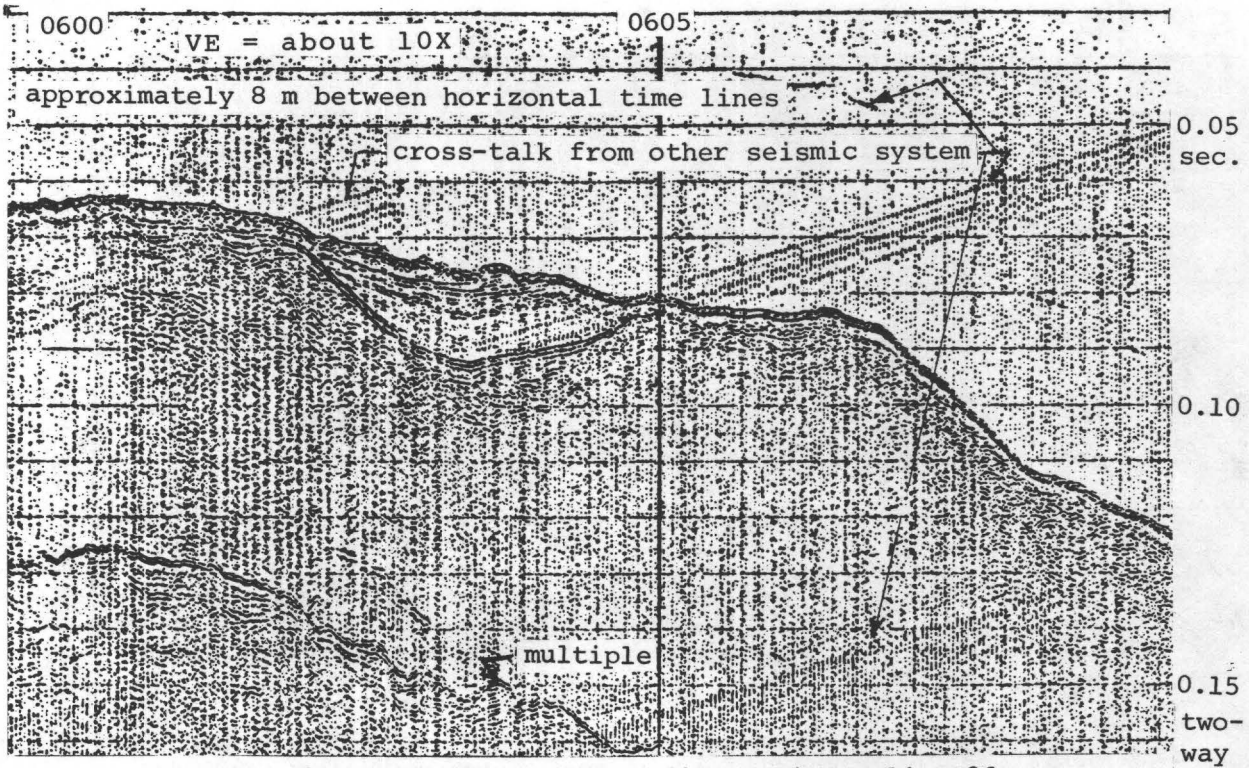


Figure 45. Seismic-reflection profile Parizeau line 36 w (0.25-sec. sweep) showing a channel-fill deposit near the top of a submarine topographic high (Dungeness Bank).

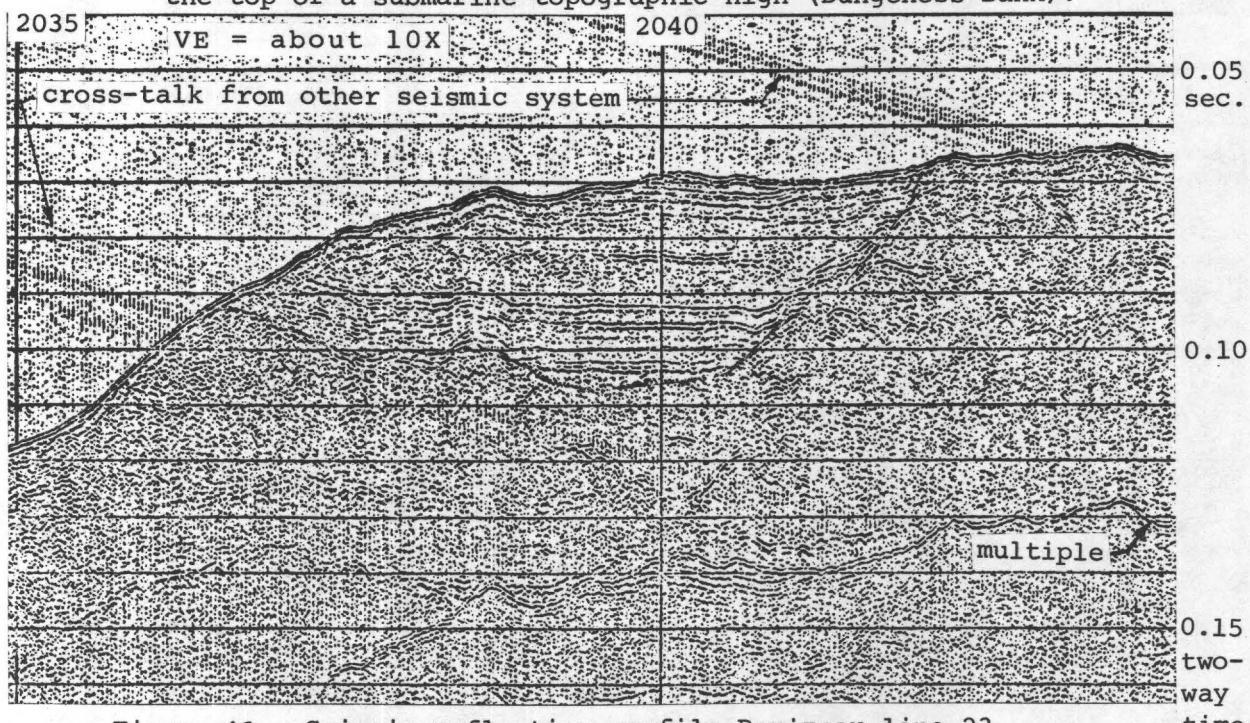


Figure 46. Seismic-reflection profile Parizeau line 23 (0.25-sec. sweep) showing uppermost Pleistocene sediments possibly ponded in erosional feature cut in older Pleistocene till-like sediments. Ponded (?) sediments have been truncated by Holocene (?) erosion at 2032.

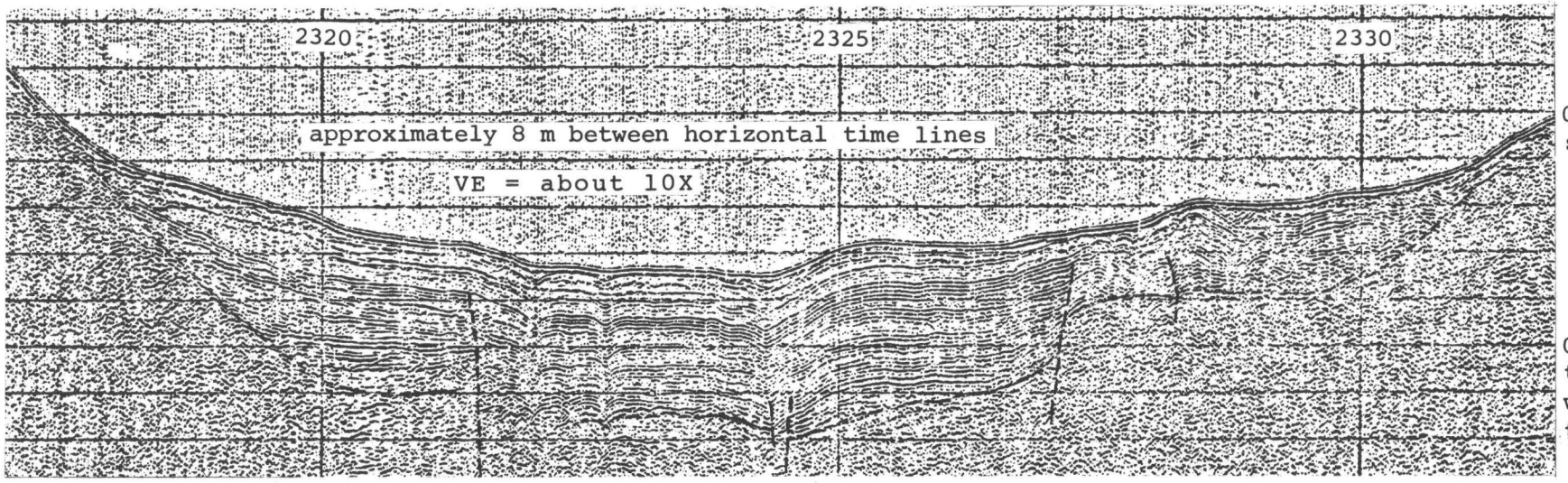


Figure 47. Seismic-reflection profile Parizeau line 37 (0.25-sec. sweep) showing a channel in which onlap filling and post-depositional latest Pleistocene settling and faulting of unconsolidated to semi-consolidated channel fill has occurred.

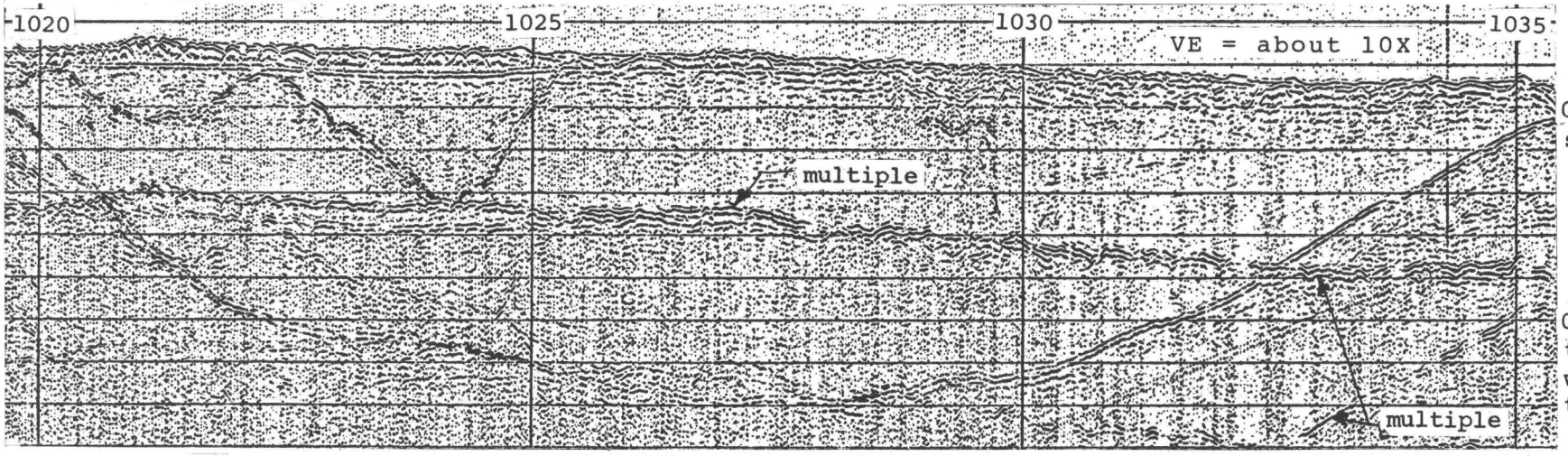


Figure 48. Seismic reflection profile Parizeau line 33 (0.25-sec. sweep) showing old channel surface filled with poorly sorted, non-bedded morainal (?) deposits from two periods of late Pleistocene (?) glaciation.

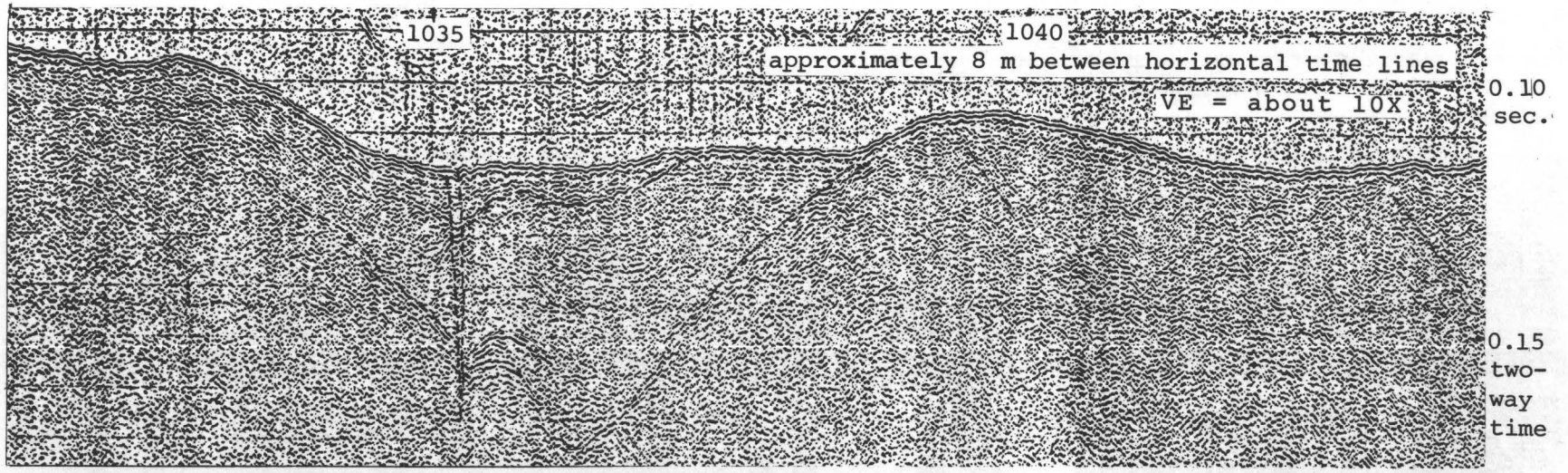


Figure 49. Seismic-reflection profile Parizeau line 27 (0.25-sec. sweep) showing channel-fill sediments folded and terminated by faulting at their south (left) side (1035). Seafloor appears to be downdropped slightly on left side at fault.

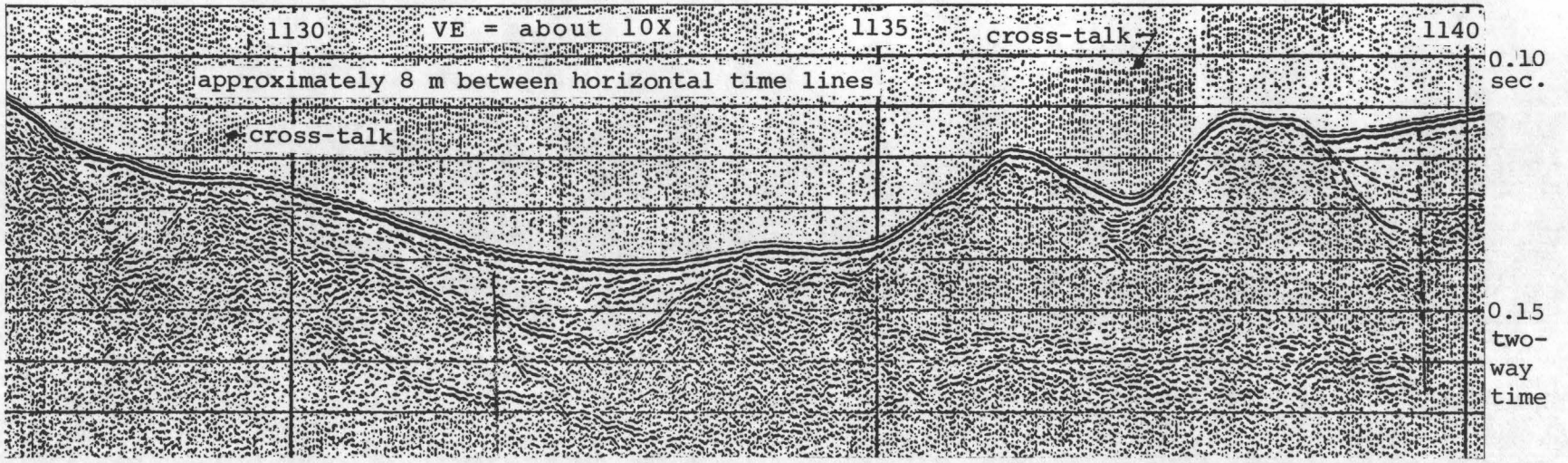


Figure 50. Seismic-reflection profile Parizeau line 33 (0.25-sec. sweep) showing channels of different depths filled with uppermost Pleistocene and Holocene (?) sediment. Overlies glacial gravels or tills of late Pleistocene age. Fault appears to terminate sediments at 1139.5 and offset correlative reflectors at 1132.

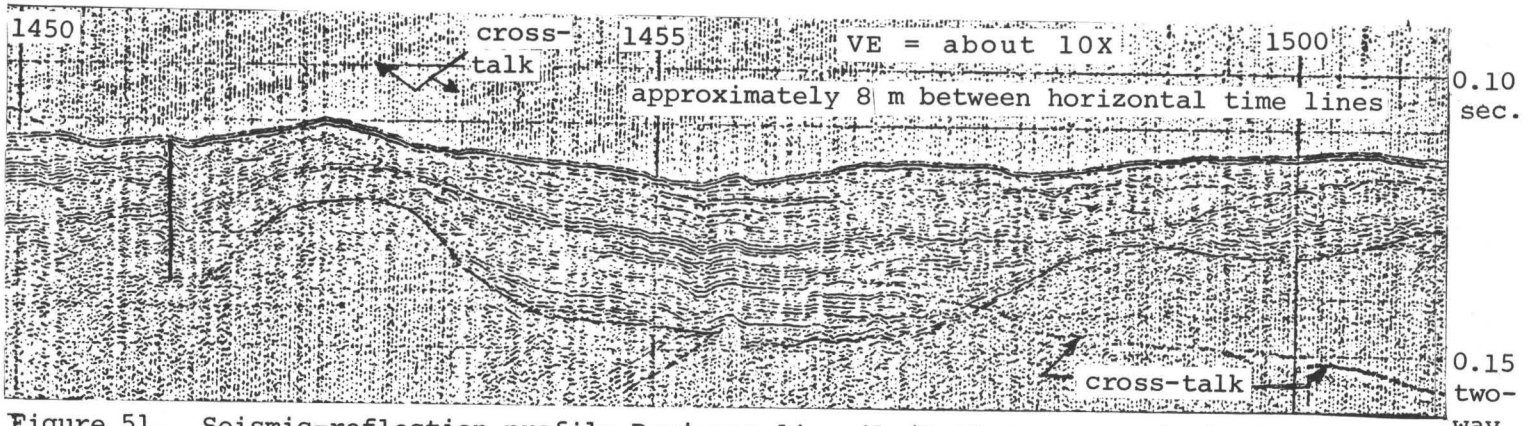


Figure 51. Seismic-reflection profile Parizeau line 41 (0.25-sec. sweep) showing channel-cut and -fill in upper Pleistocene glacial sediments. Uppermost sediments are probably Holocene in age.

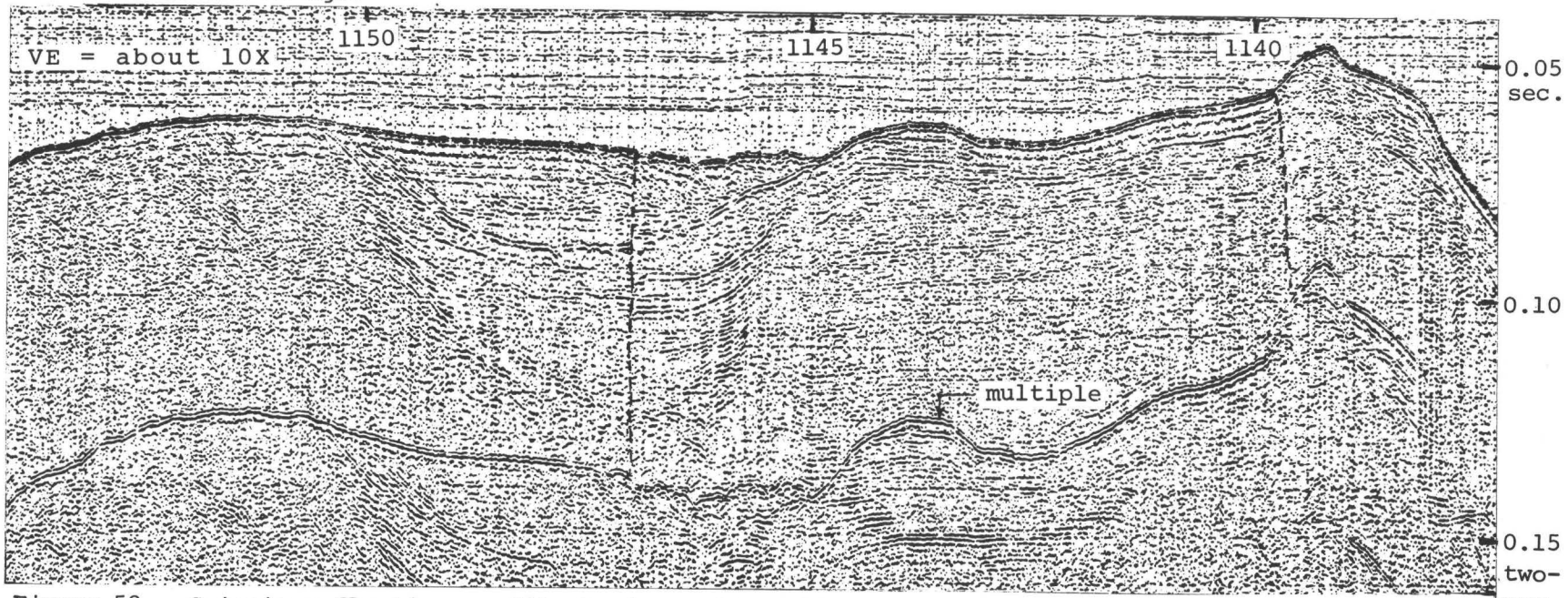


Figure 52. Seismic-reflection profile Parizeau line 1 (0.25-sec. sweep) showing ice-scour (?) erosional channel on top of Constance Bank. Channel filled with horizontally bedded sediments that are slumping downslope (northeastward) away from line of profile.

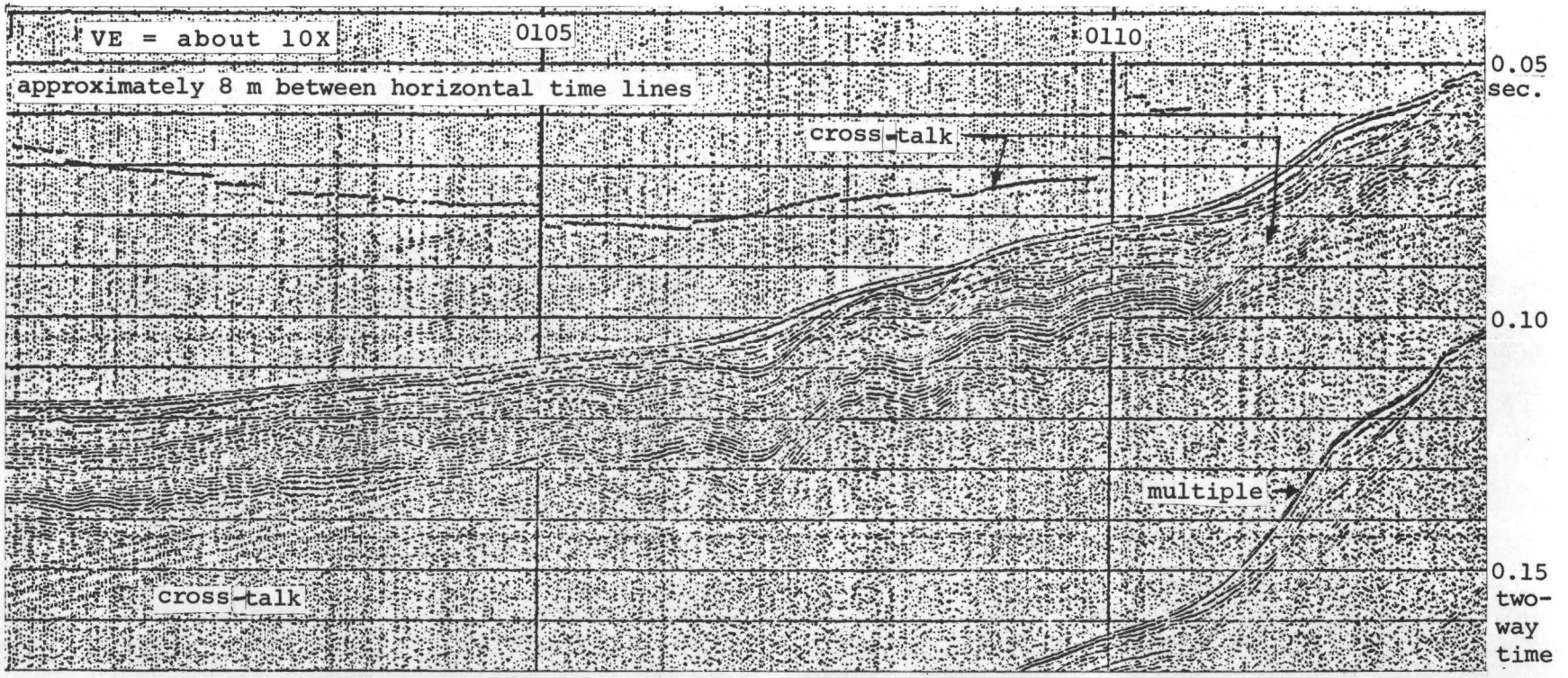


Figure 53. Seismic-reflection profile Parizeau line 37a (0.25 sec. sweep) showing folded uppermost Pleistocene (?) sediments in which the upper surfaces of the synclinal folds have been filled with presumed Holocene sediments.

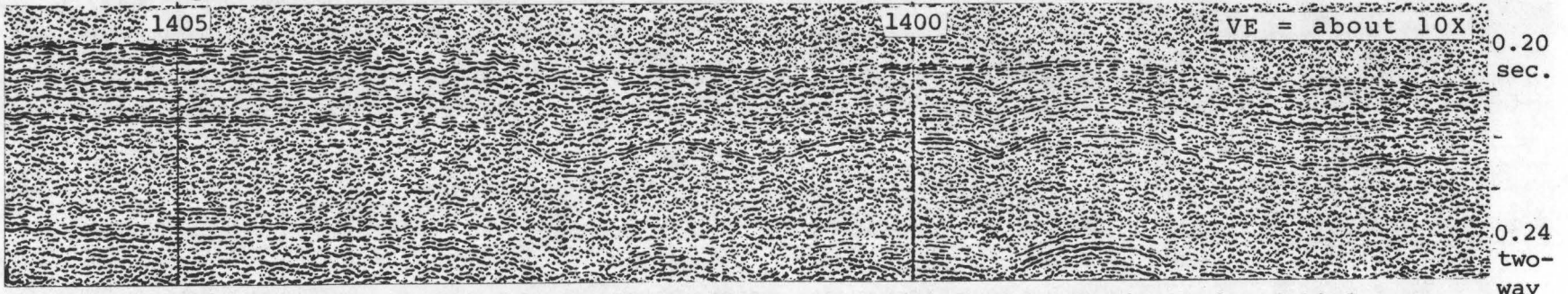


Figure 54. Seismic reflection profile Parizeau line 1 (0.25 sec. sweep) showing folded upper Pleistocene glacial sediments.

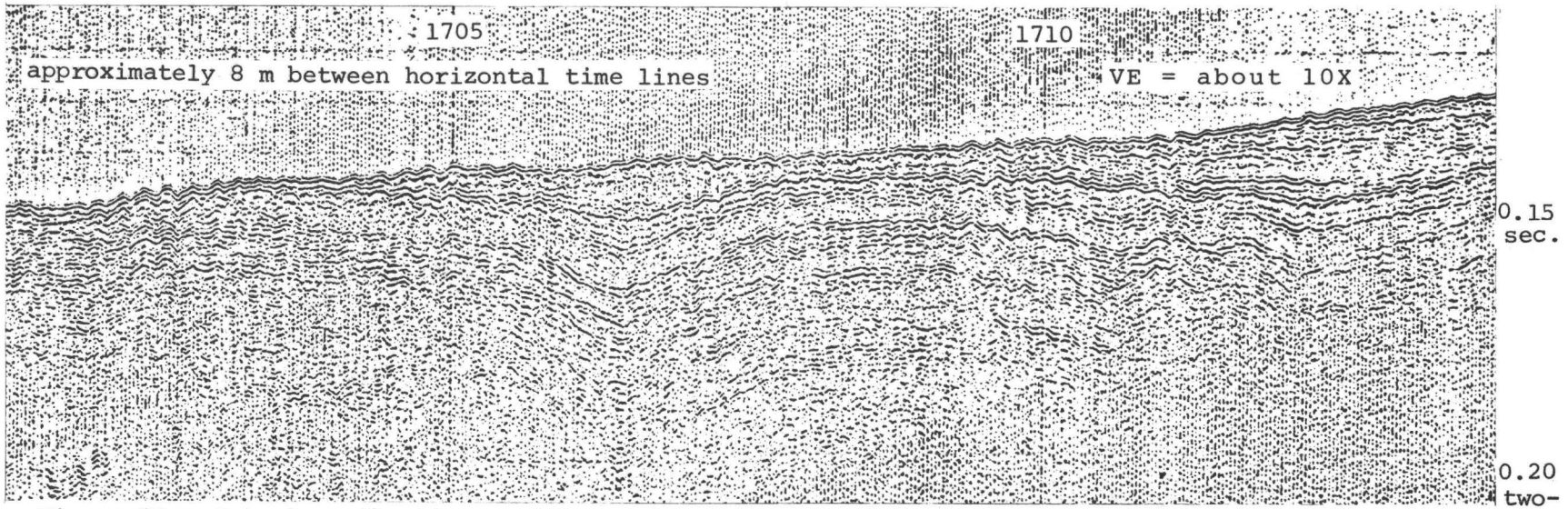


Figure 55. Seismic-reflection profile Parizeau line 28 (0.25-sec. sweep) showing folded uppermost Pleistocene sediments overlain by horizontal Holocene (?) beds in synclinal lows.

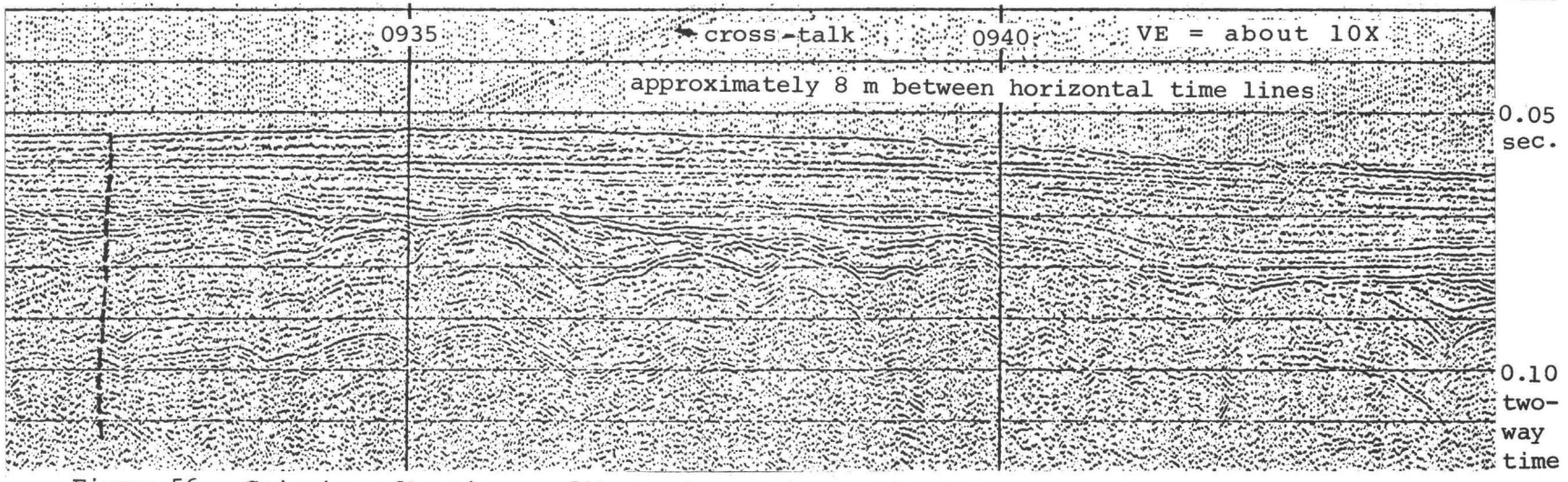


Figure 56. Seismic-reflection profile Parizeau line 33 (0.25-sec. sweep) showing folded Pleistocene semi-consolidated glacial sediments truncated and overlain by latest Pleistocene and Holocene sediments.

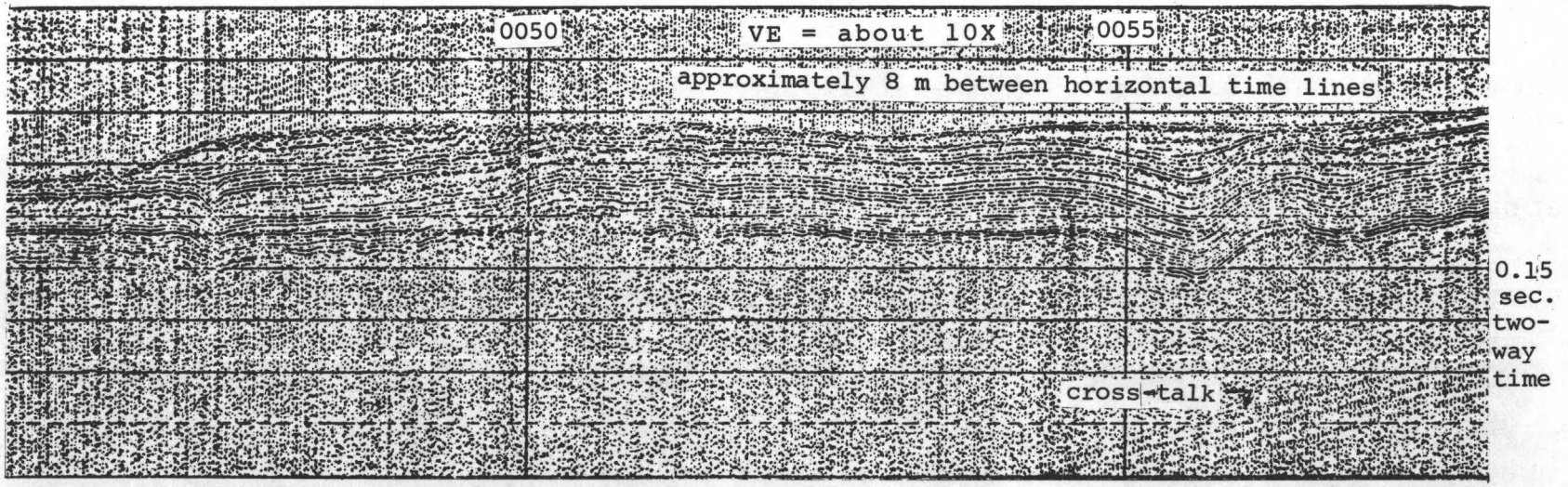


Figure 57. Seismic-reflection profile Parizeau line 37a (0.25 sec. sweep) showing folded uppermost Pleistocene (?) sediments overlain by gravelly or bouldery glacial deposits (or possibly landslide).

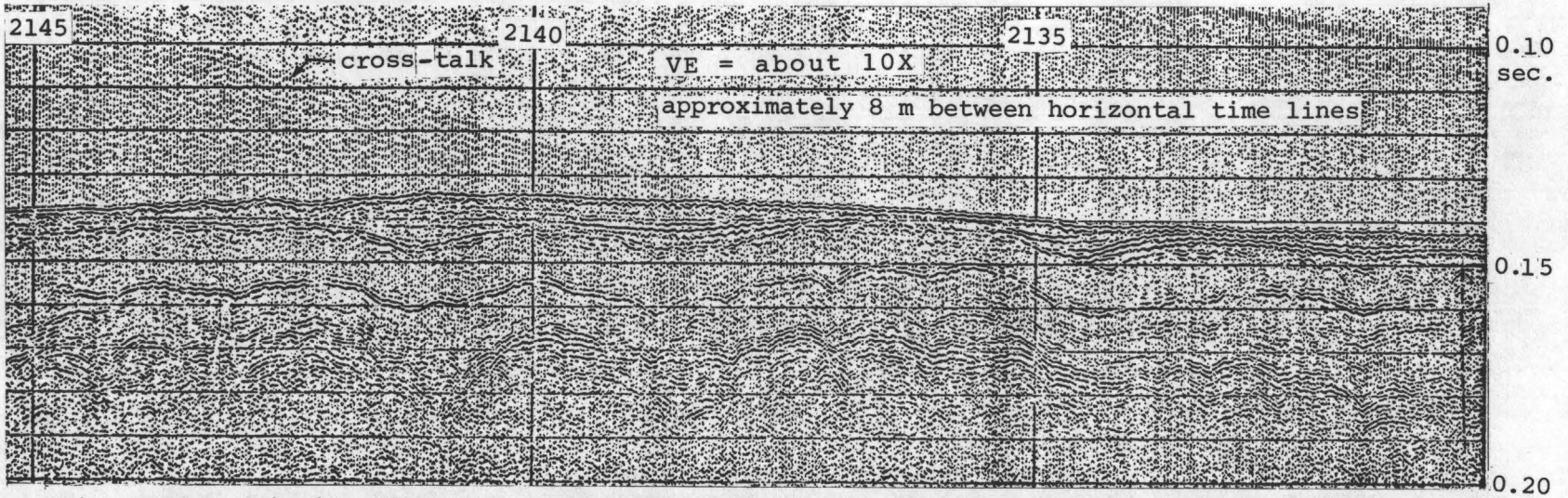


Figure 58. Seismic-reflection profile Parizeau line 23 (0.25-sec. sweep) showing folded and channeled upper Pleistocene stratified sediments overlain by uppermost Pleistocene and Holocene(?) channel-fill sediments.

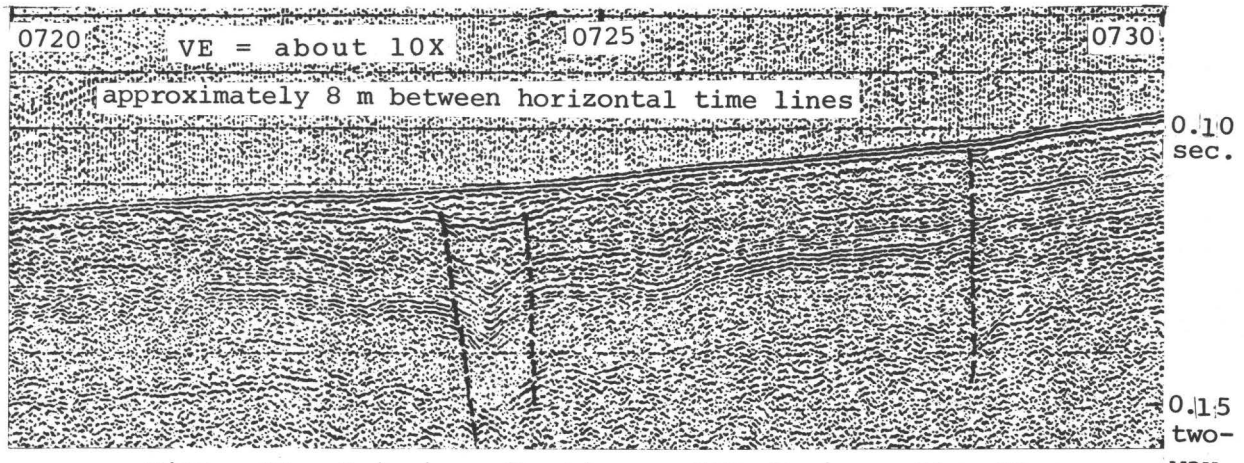


Figure 59. Seismic-reflection profile Parizeau line 26 (0.25 sec. sweep) showing folded uppermost Pleistocene gravelly and bedded sediments.

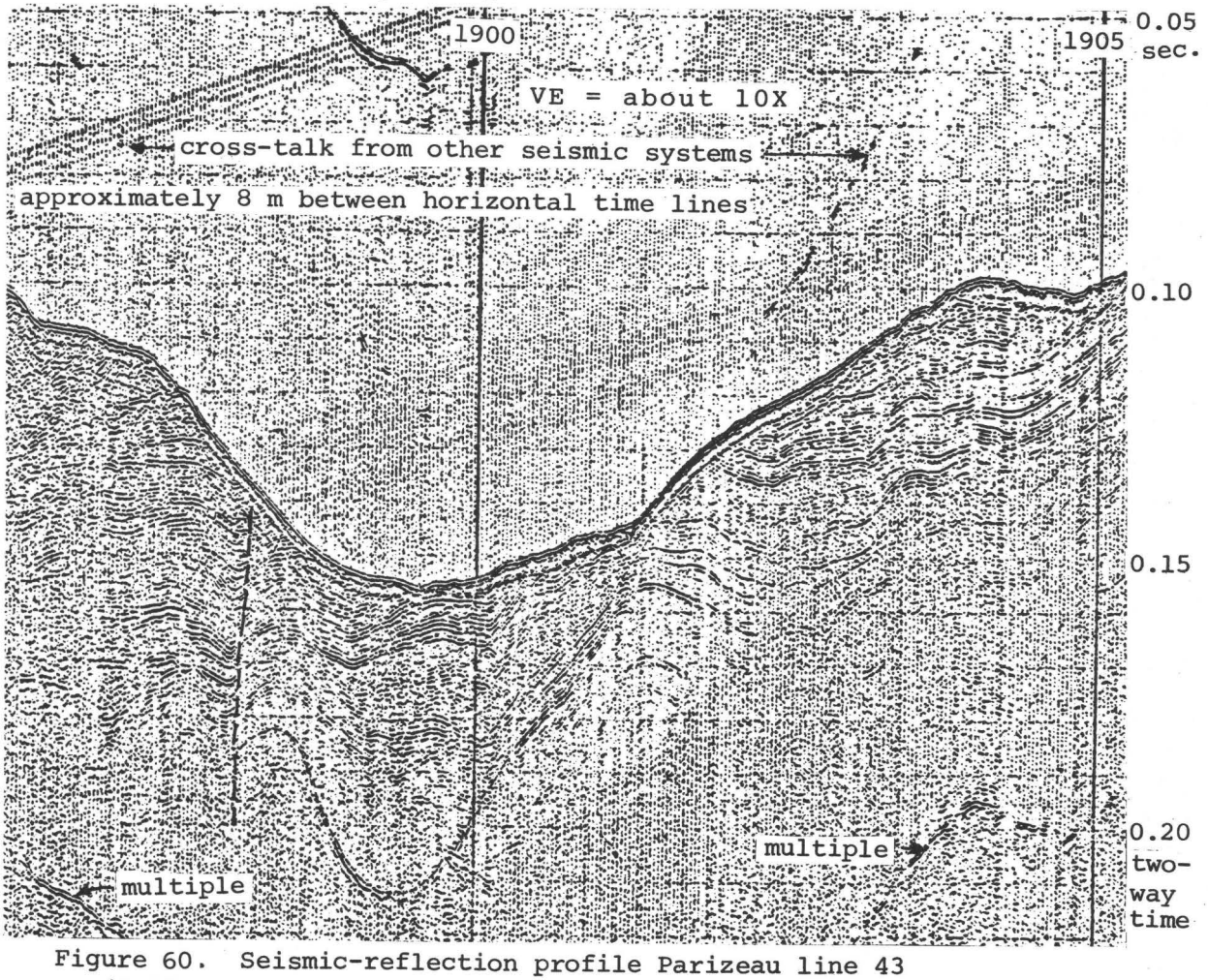


Figure 60. Seismic-reflection profile Parizeau line 43 (0.25-sec. sweep) showing erosion and channeling that has truncated folded glacial deposits. A small slump deposit is located on the southeast (right) side of the channel floor (1859-1902). Ice push may be responsible for some folding; faulting, as at 1858, may have contributed.

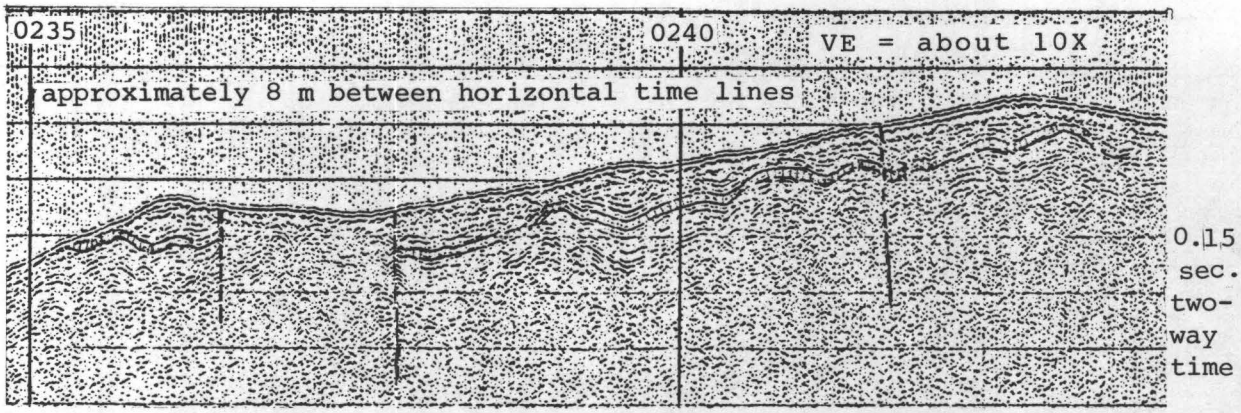


Figure 61. Seismic-reflection profile Parizeau line 31 (0.25-sec. sweep) showing uppermost Pleistocene (?) folded and faulted semi-consolidated sediments; faults offset and terminate key bed.

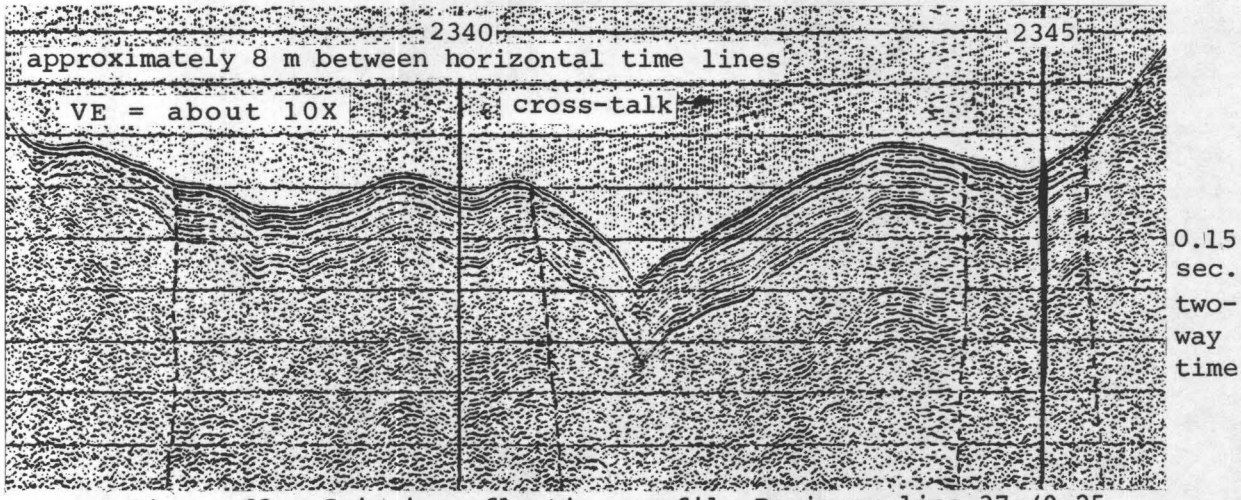


Figure 62. Seismic-reflection profile Parizeau line 37 (0.25-sec. sweep) showing well-bedded folded uppermost Pleistocene or Holocene sediments faulted against an unbedded sequence near left-side (2338) and right side (2345.5).

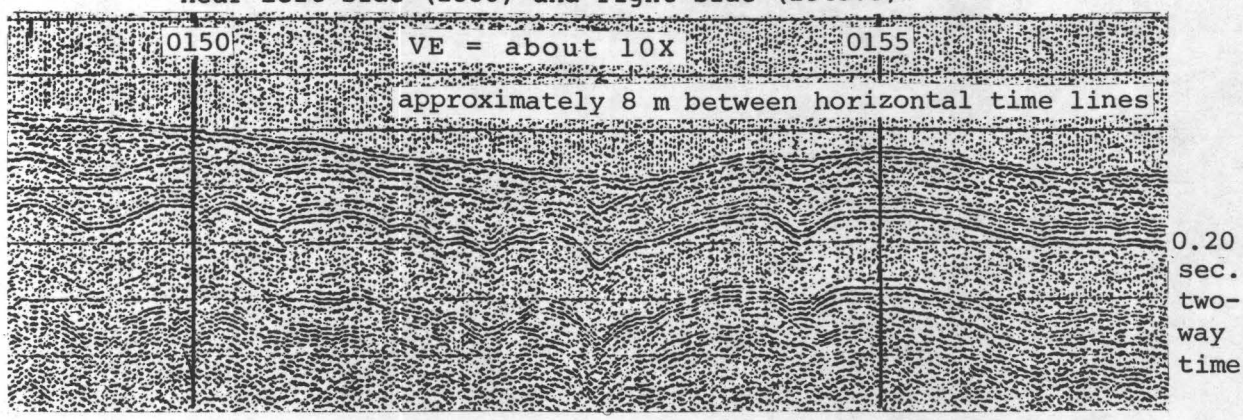


Figure 63. Seismic-reflection profile Parizeau line 24 (0.25-sec. sweep) showing irregular, continuous reflectors within upper Pleistocene glacial deposits; interpreted as post-depositional deformation of unconsolidated or semi-consolidated sediment.

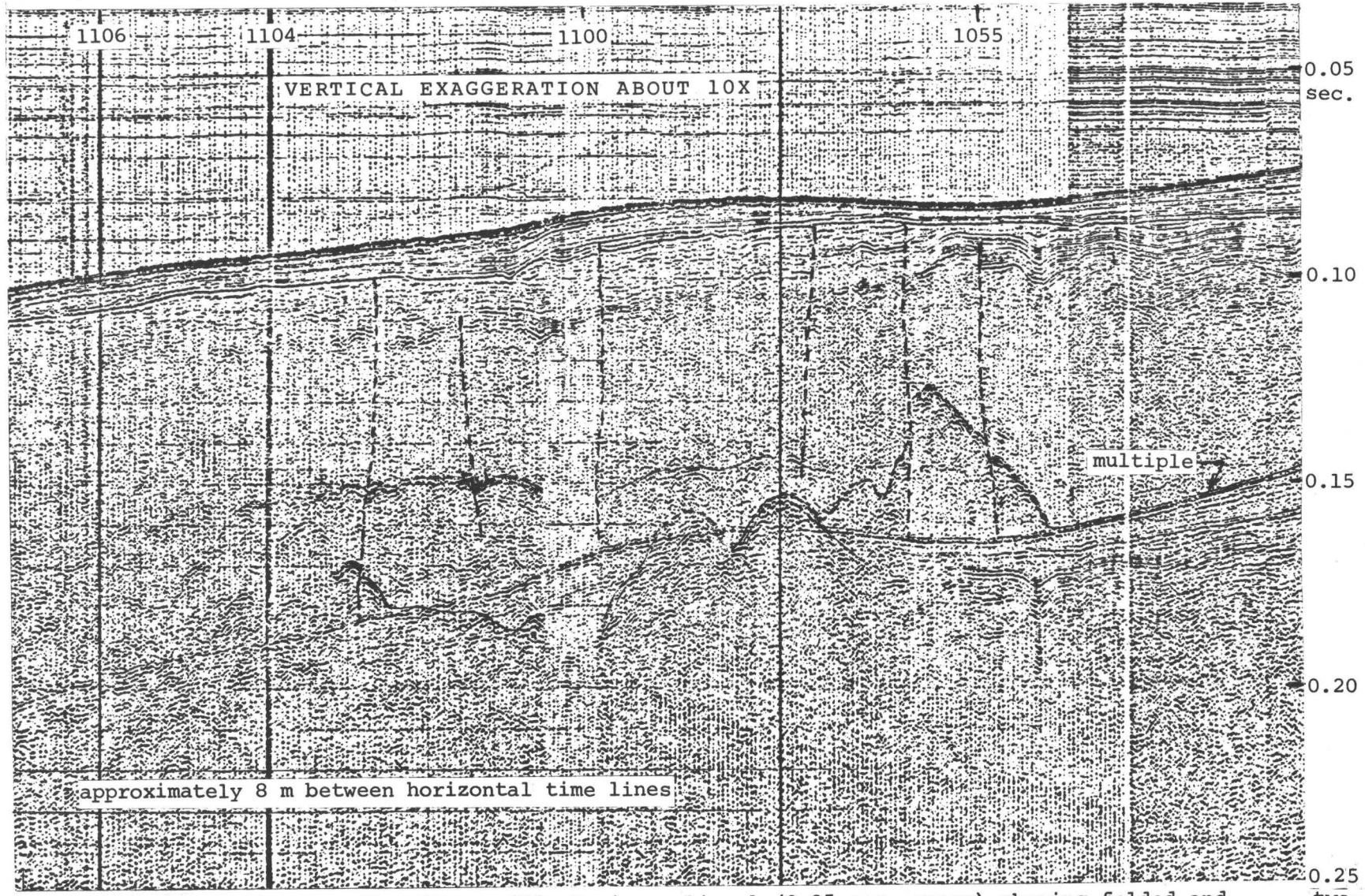


Figure 64. Seismic-reflection profile Parizeau line 1 (0.25-sec. sweep) showing folded and faulted glacial sediments of pre-latest Pleistocene age. Overlying sediments are probably of latest Pleistocene and Holocene age. An irregular surface of older glacial (?) deposits occurs deeper beneath the seafloor.

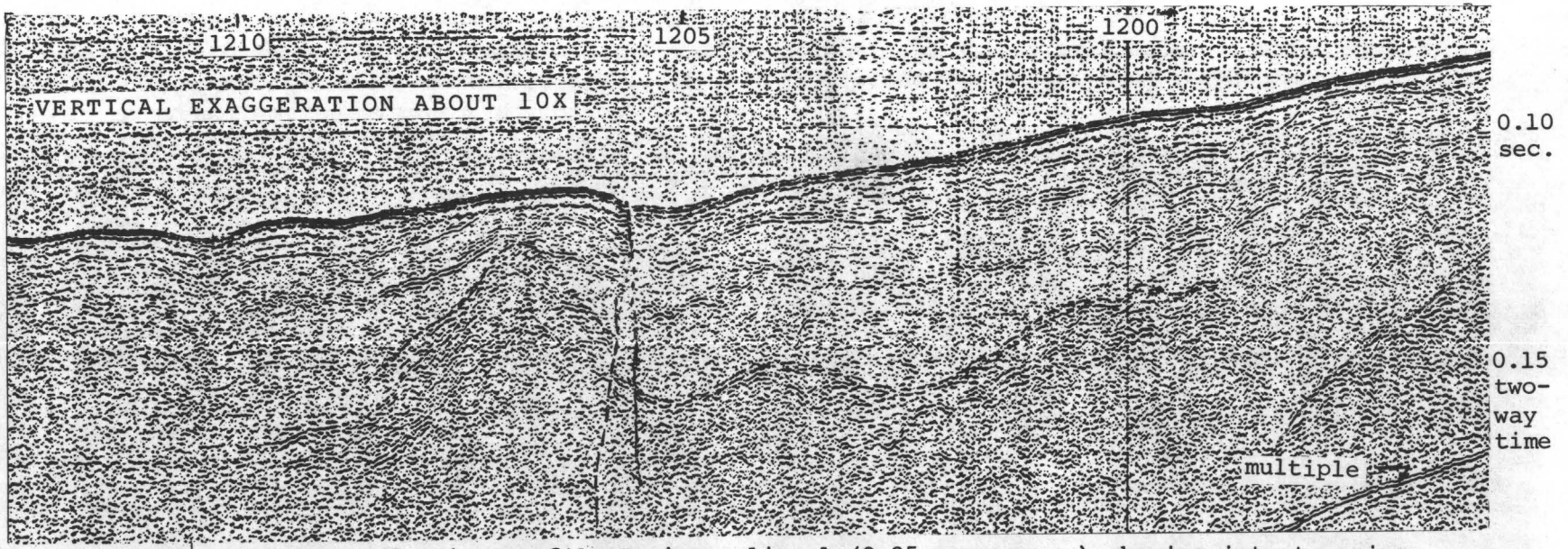


Figure 65. Seismic-reflection profile Parizeau line 1 (0.25-sec. sweep) showing intertonguing contact between bouldery gravelly sediments (1152-1155) and folded, bedded glaciomarine (?) sediments to southeast (left). Fault (1205.5) apparently offsets sedimentary beds and seafloor.

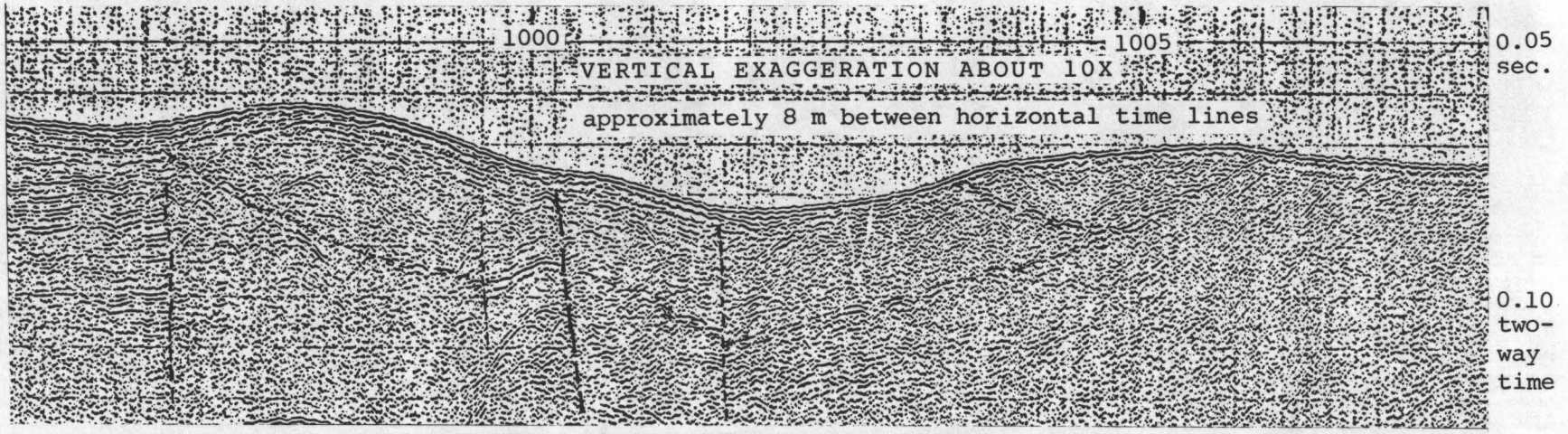


Figure 66. Seismic-reflection profile Parizeau line 27 (0.25-sec. sweep) showing termination of bedded sequence at 0957 and of till-like sequence at 1002.

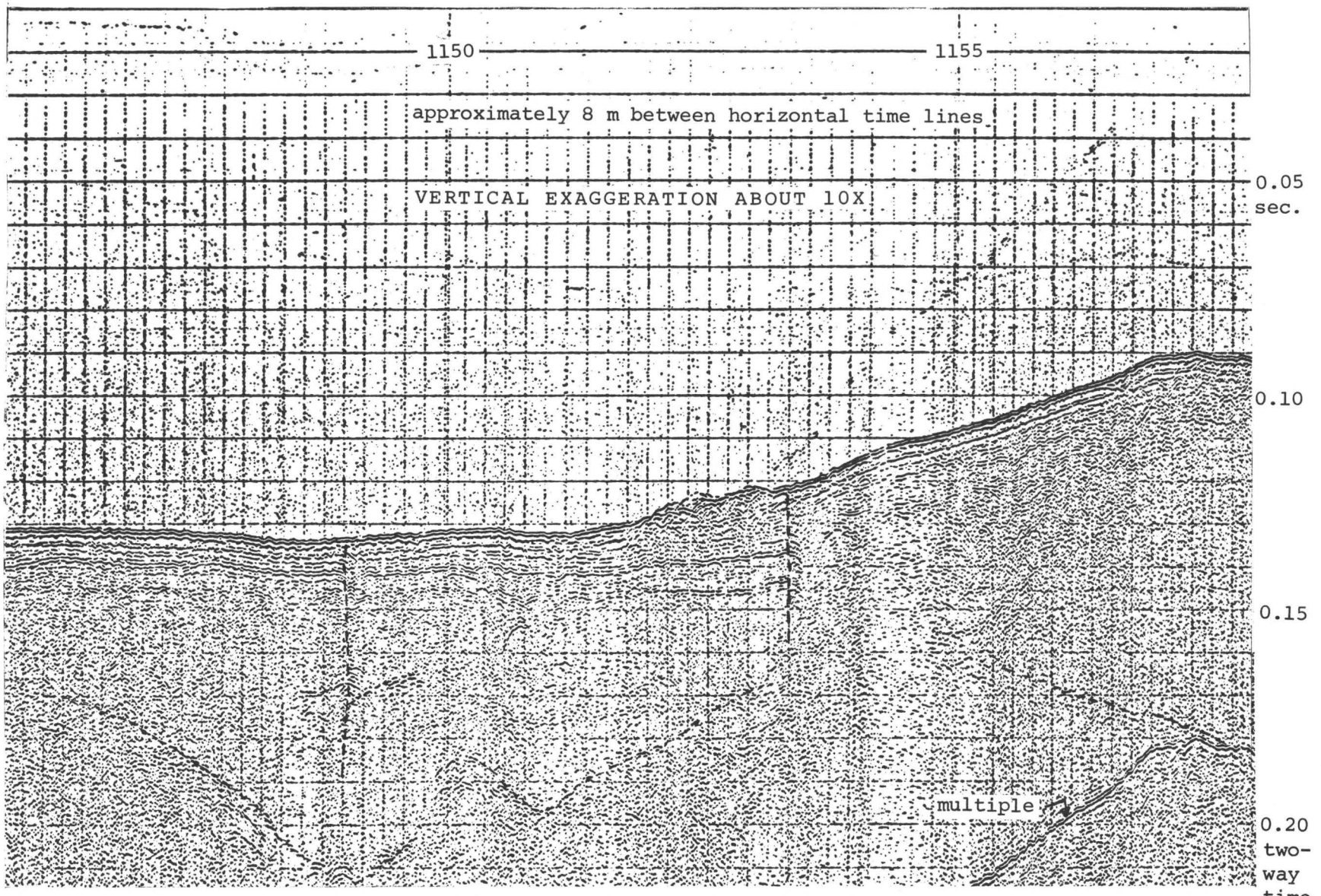


Figure 67. Seismic-reflection profile Parizeau line 27 (0.25 sec. sweep) showing Holocene slump deposit at 1152-1153 that may have been generated by movement of fault on north (right) side.

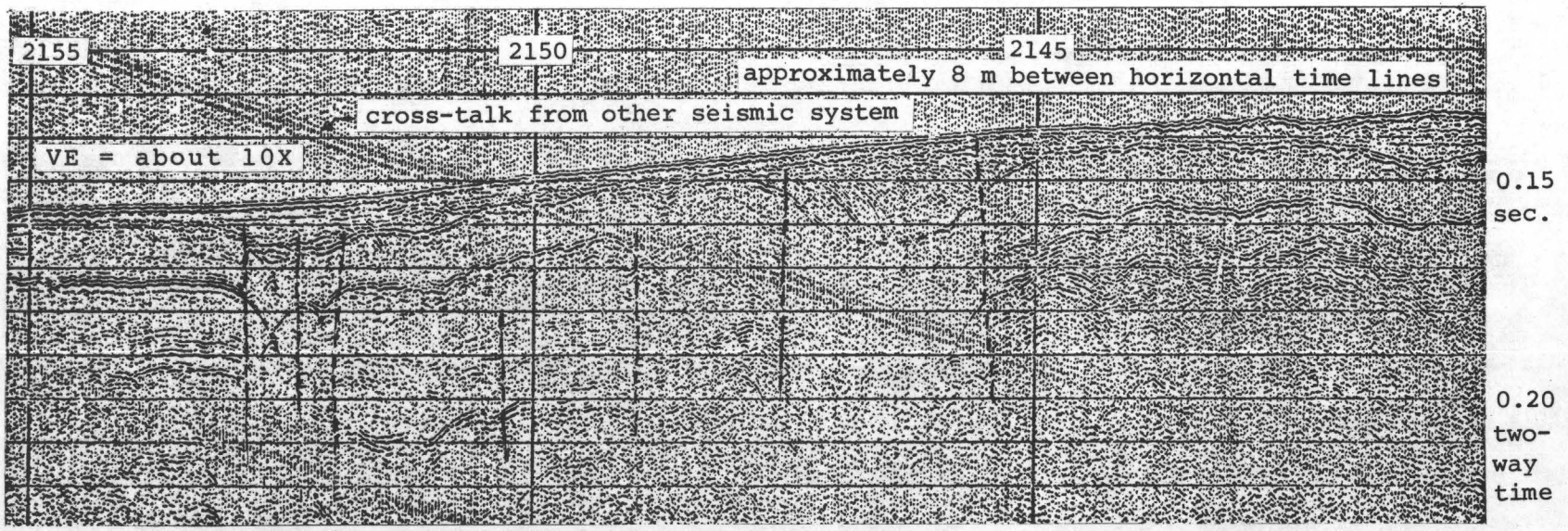


Figure 68. Seismic-reflection profile Parizeau line 23 (0.25-sec. sweep) showing folded and faulted upper Pleistocene sediments that are overlain by channels filled by uppermost Pleistocene and Holocene (?) sediments. Faults are indicated by hyperbolic signatures and terminations or offsets of beds.

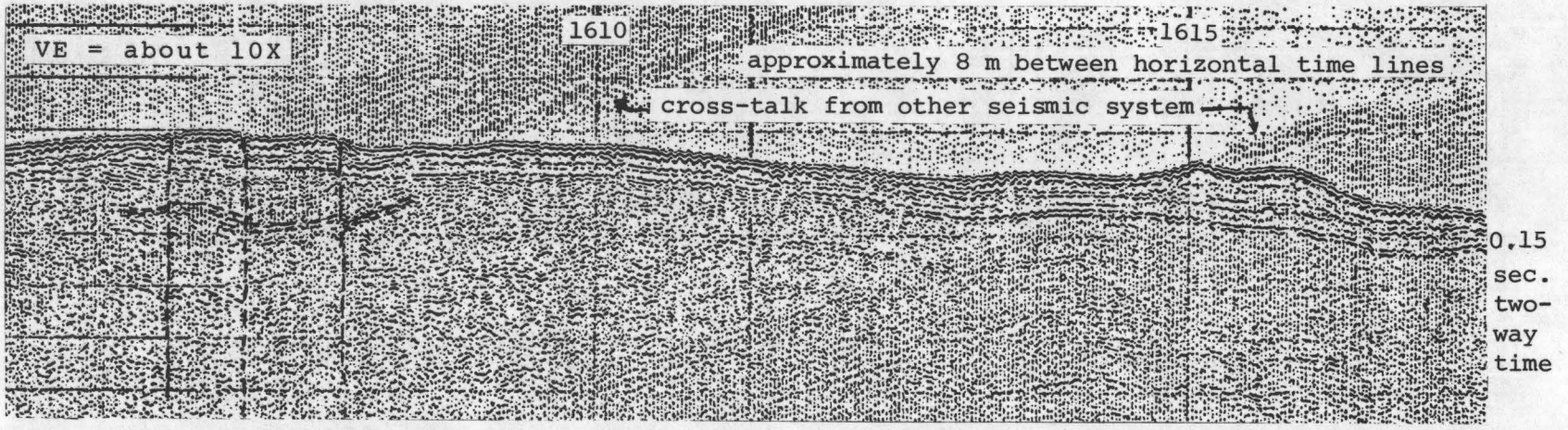


Figure 69. Seismic-reflection profile Parizeau line 28 (0.25-sec. sweep) showing three faults that apparently offset the seafloor (1606-1607) and a moraine-like deposit (1615-1616).

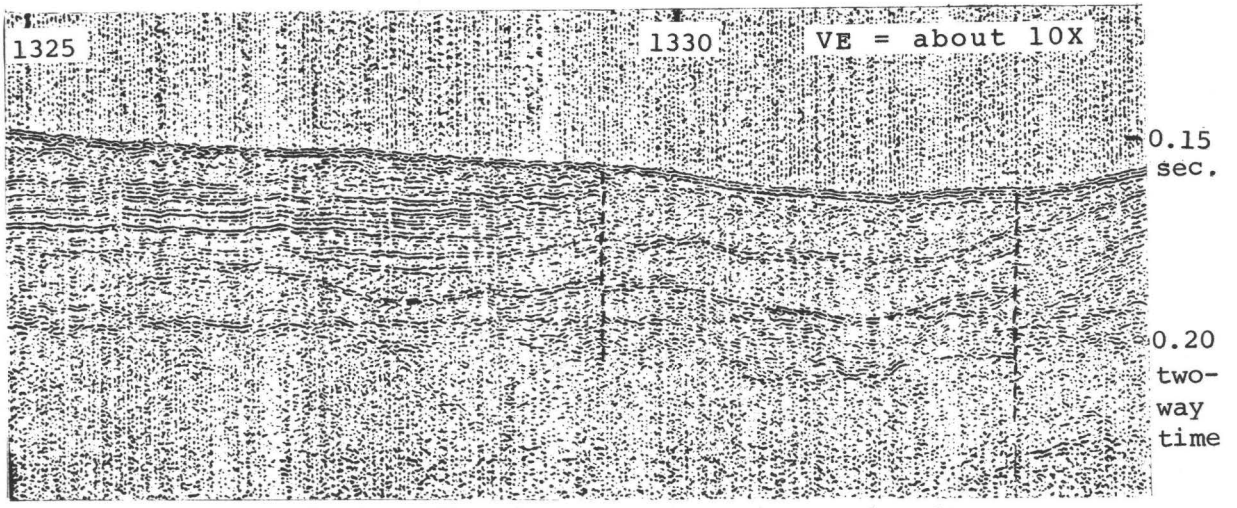


Figure 70. Seismic-reflection profile Parizeau line 41 (0.25-sec. sweep) showing faults (1329.5 and 1332.8) and folds in sediments of late Pleistocene and possible Holocene age. Lack of similarity of bedding across faults suggests lateral offset.

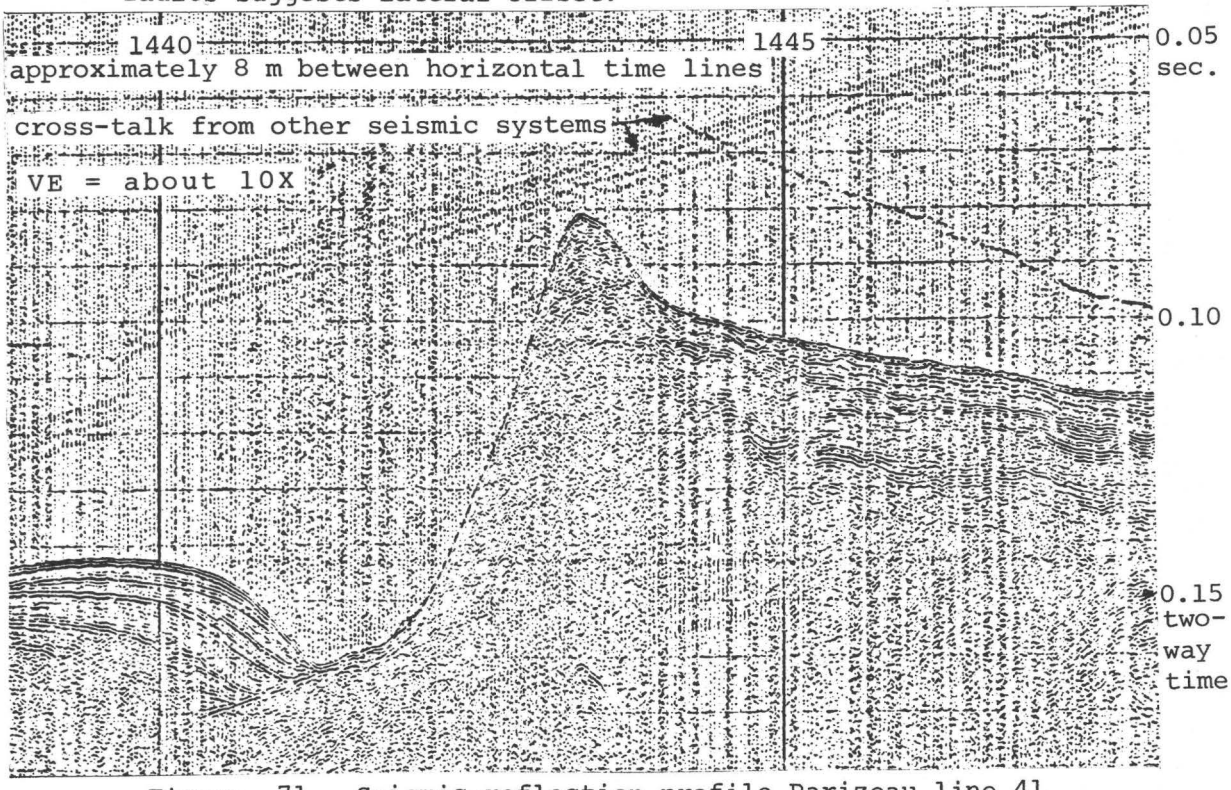


Figure 71. Seismic-reflection profile Parizeau line 41 (0.25-sec. sweep) showing break-away face of slump block shown in Figure 72.

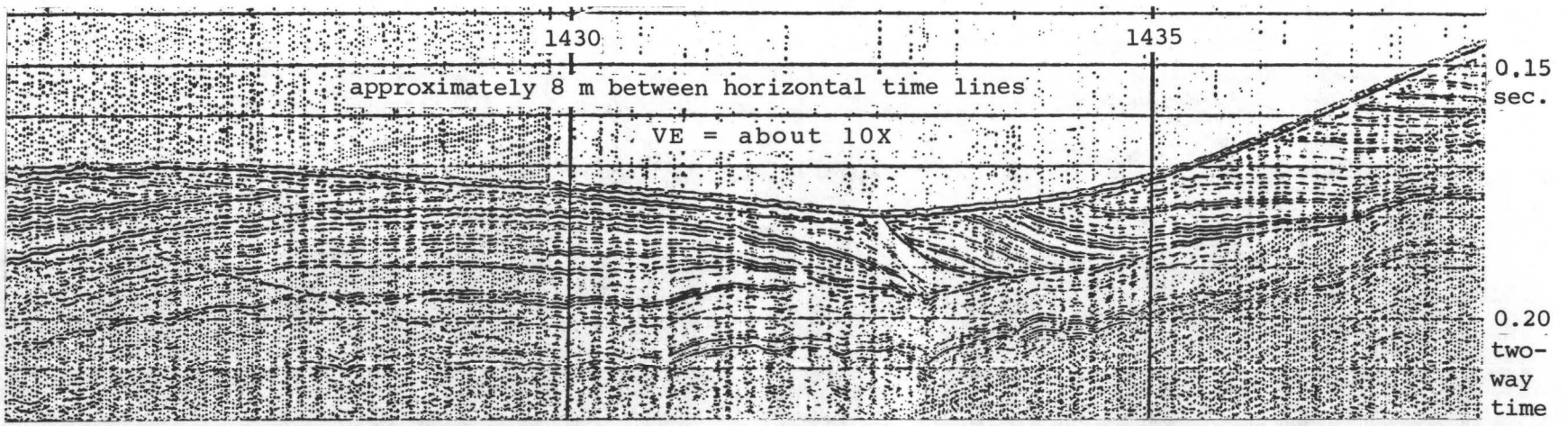


Figure 72. Seismic-reflection profile Parizeau line 41 (0.25-sec. sweep) showing truncated and folded slump deposits overlying a disrupted older surface.

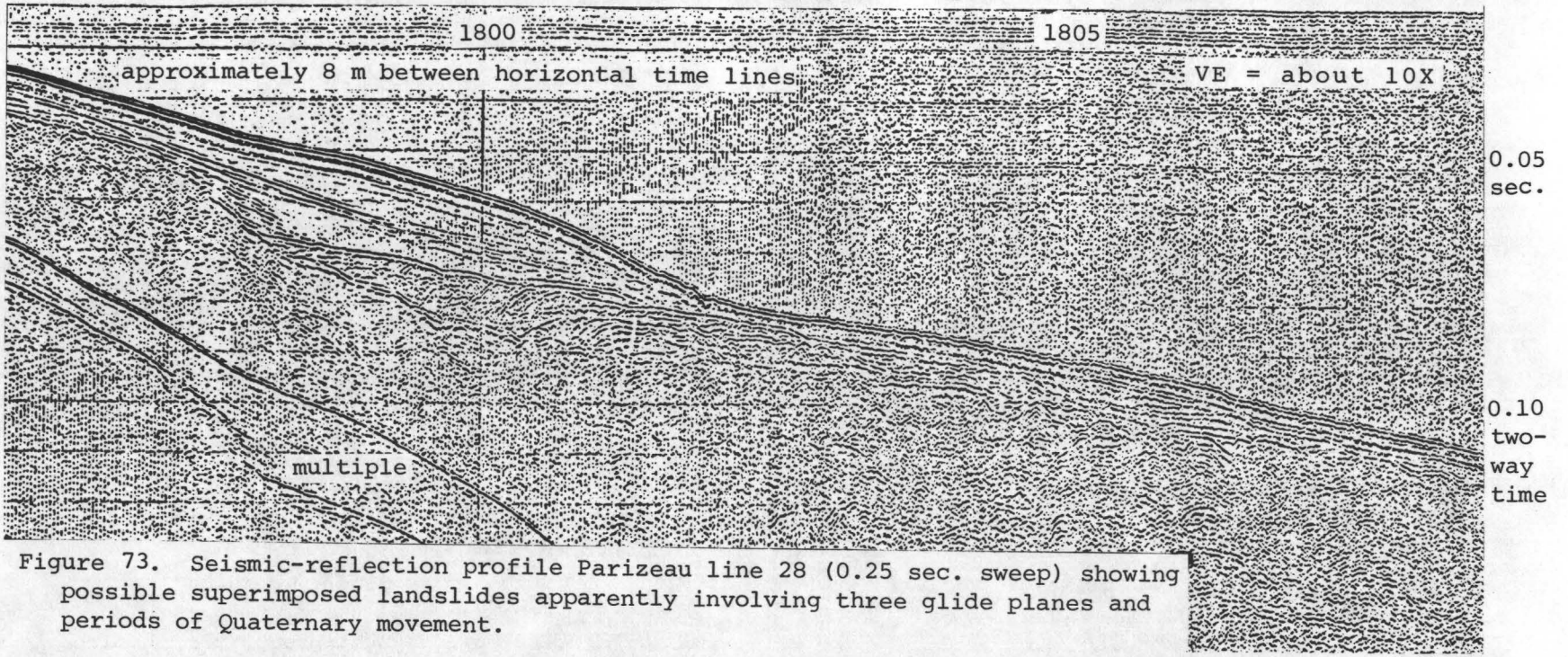


Figure 73. Seismic-reflection profile Parizeau line 28 (0.25 sec. sweep) showing possible superimposed landslides apparently involving three glide planes and periods of Quaternary movement.

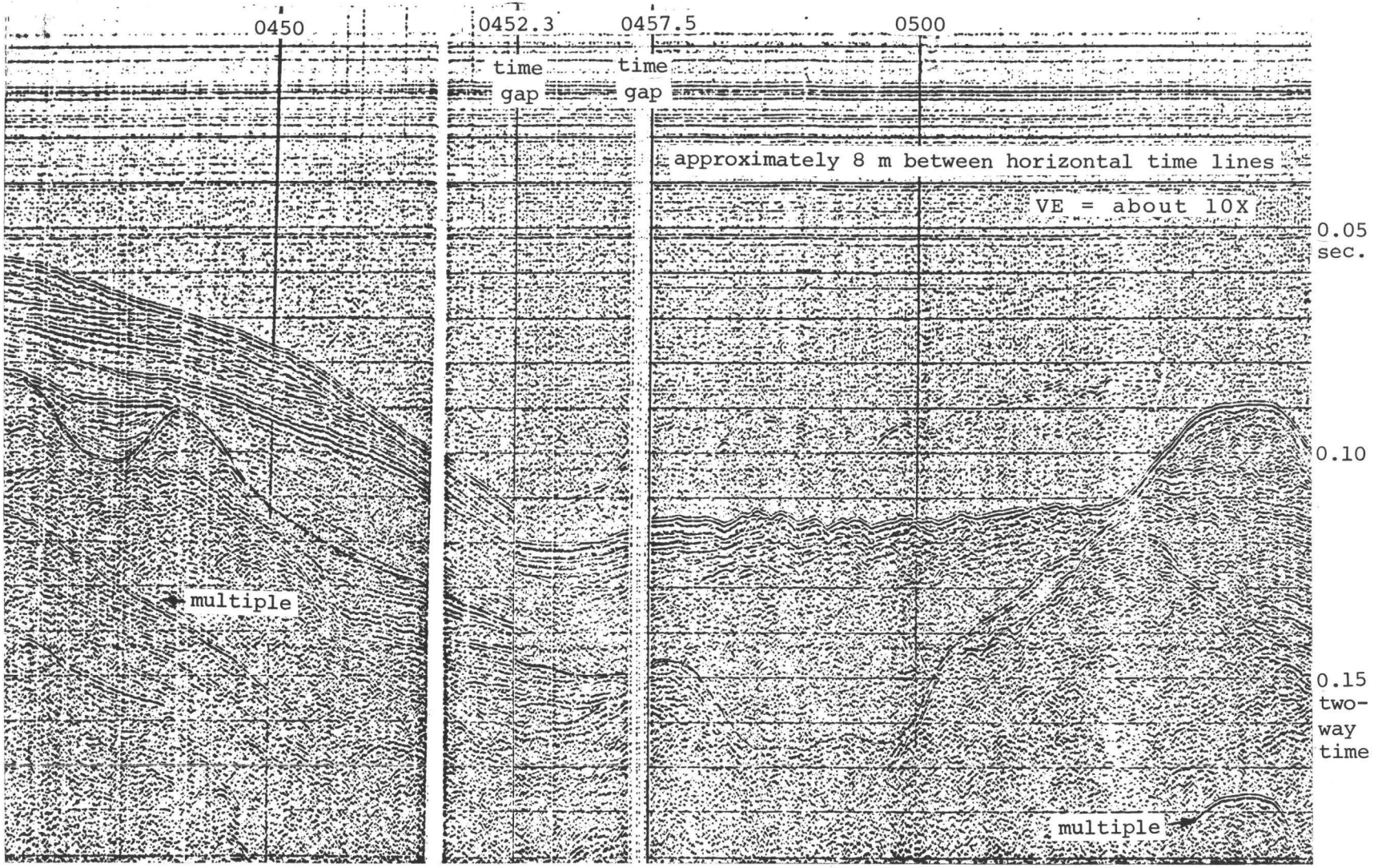


Figure 74. Seismic-reflection profile Parizeau line 32 (0.25-sec. sweep) showing an irregular older till surface that has been channeled, filled and overtopped by later glacial sediments which, in turn, have been truncated (0448-0451) and have partially slumped into an adjacent low-lying area (0458-0502).

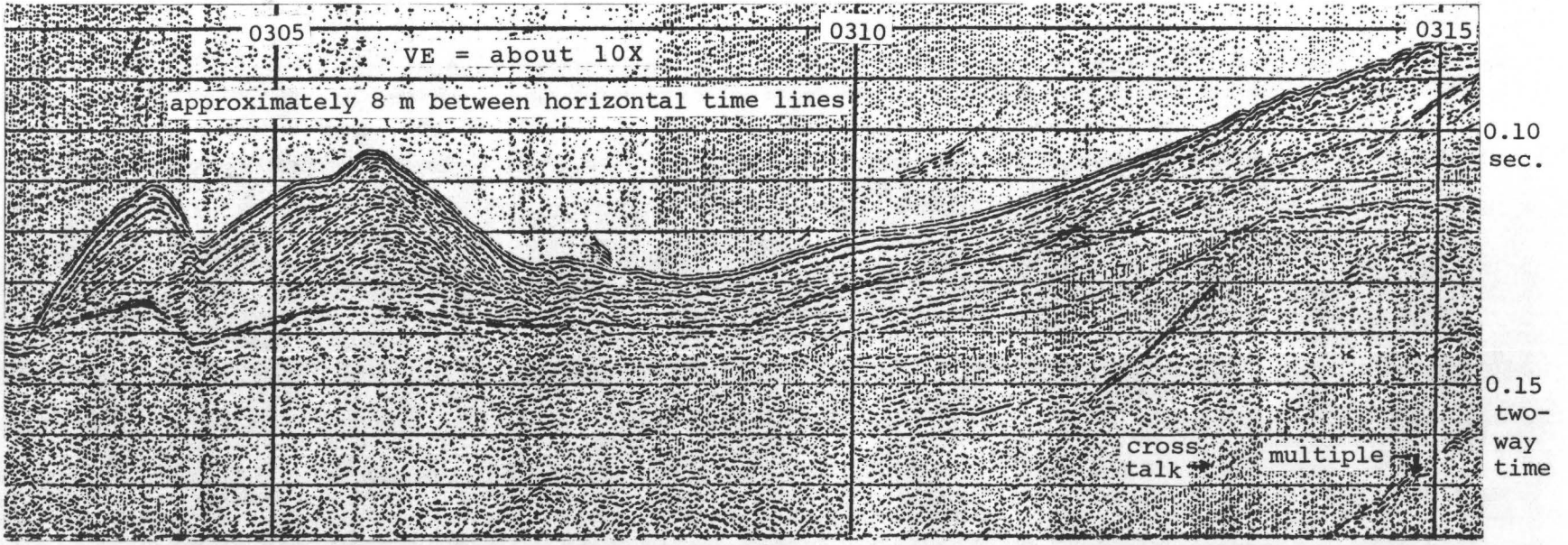


Figure 75. Seismic-reflection profile Parizeau line 31 (0.25 sec. sweep) showing toe and buckled portion of slumped uppermost Pleistocene and Holocene sediments (0303-0307) and break-up of bedding at pull-away segment high on the slope (0313-0316).



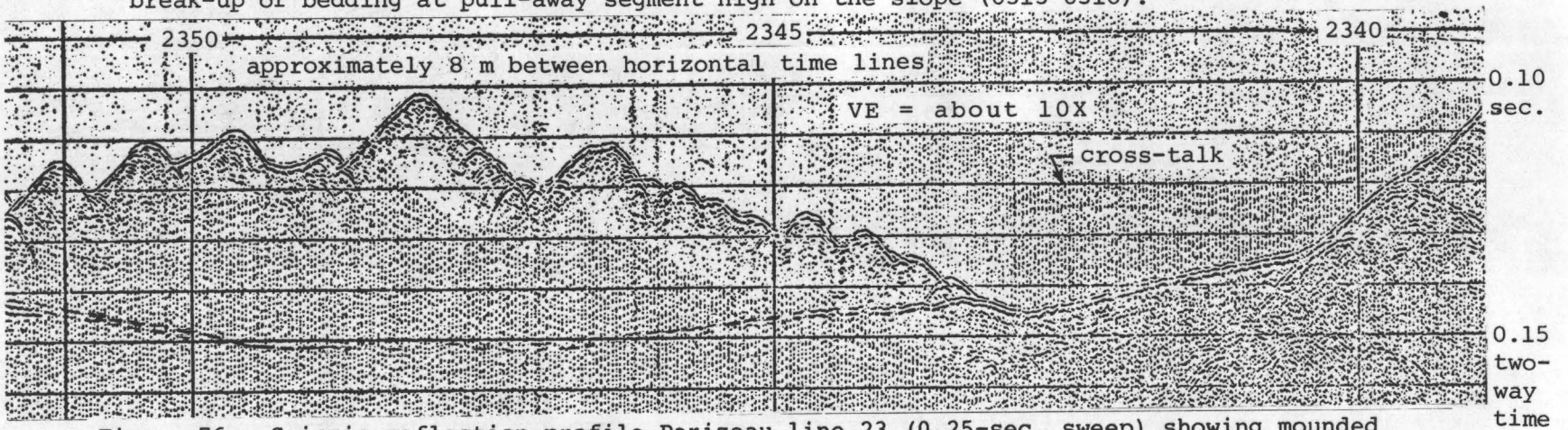


Figure 76. Seismic reflection profile Parizeau line 23 (0.25-sec. sweep) showing mounded irregular surface of probable slump and near-horizontal slip surface between 0.14 and 0.15 seconds depth. Alternatively, could be morainal mounds left during recession of Juan de Fuca lobe.

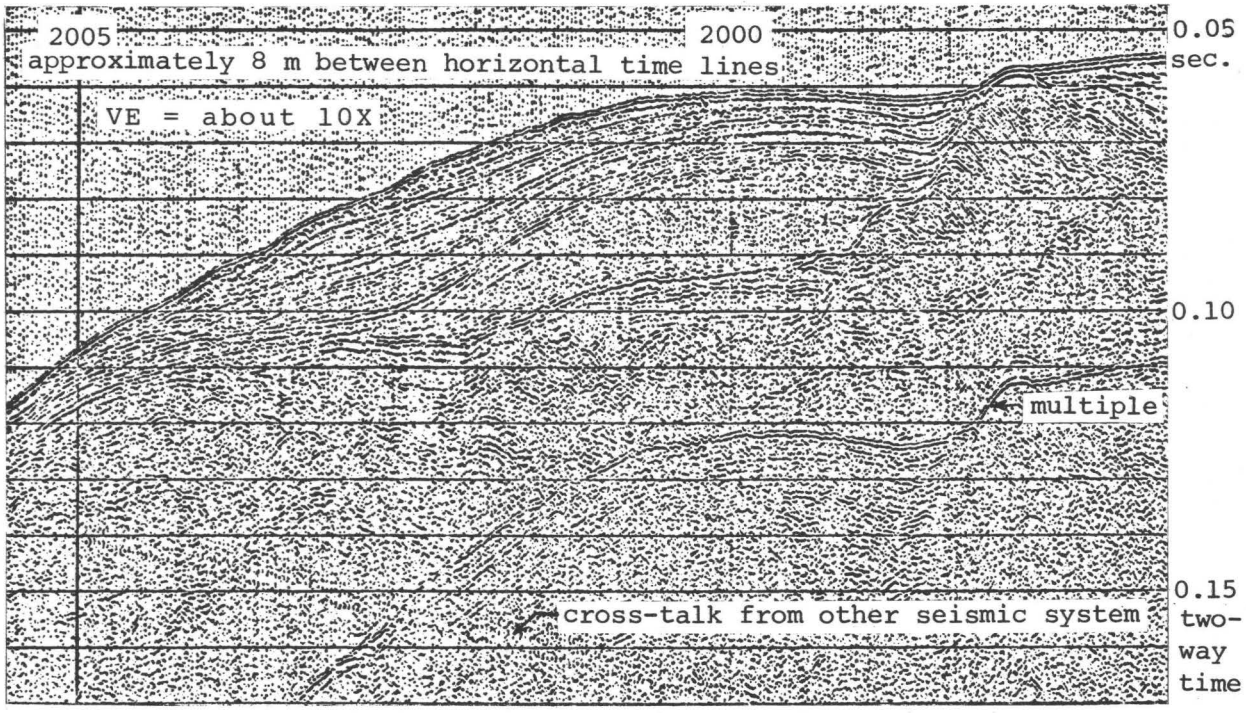


Figure 77. Seismic-reflection profile Parizeau line 23 (0.25-sec. sweep) showing slumped uppermost Pleistocene and Holocene (?) sediments that have been bowed slightly upward during downslope transport. Breakaway scarp is at 1958.

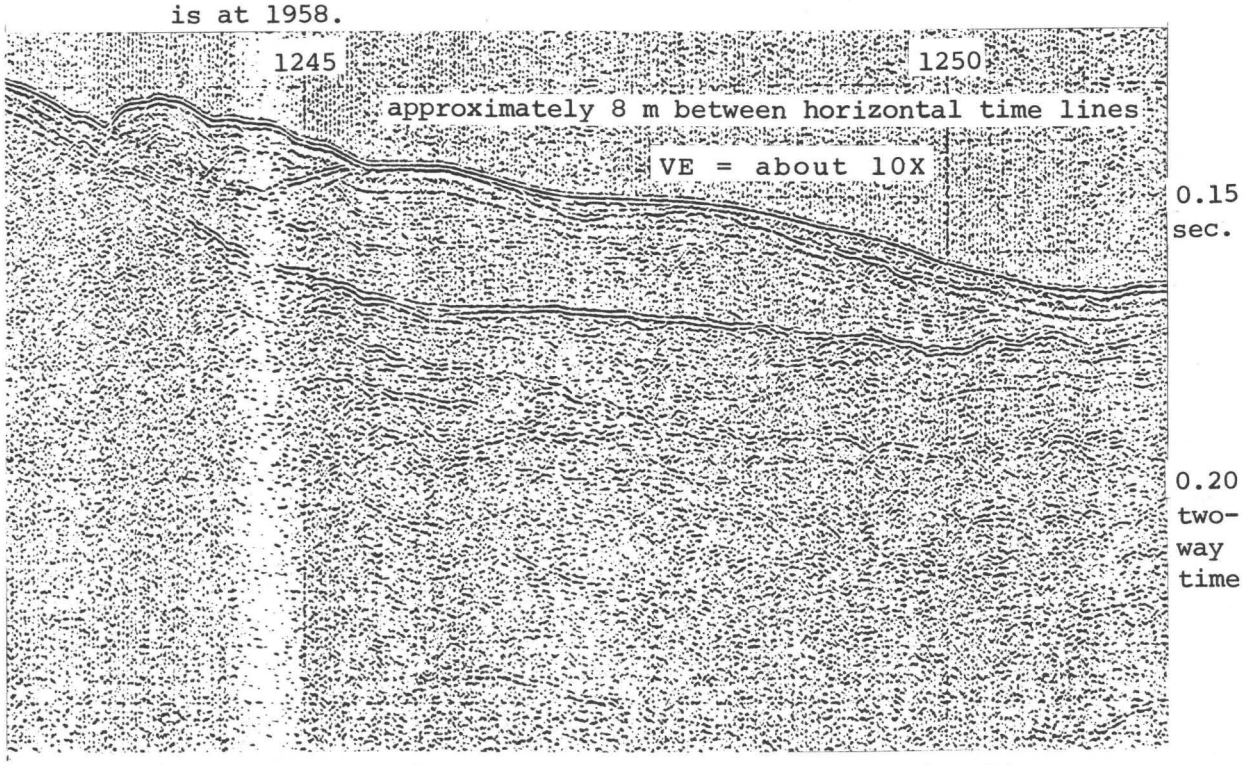


Figure 78. Seismic-reflection profile Parizeau line 34 (0.25 sec. sweep) showing Holocene slump (at left) and possible associated deformation of older sediments (at right).

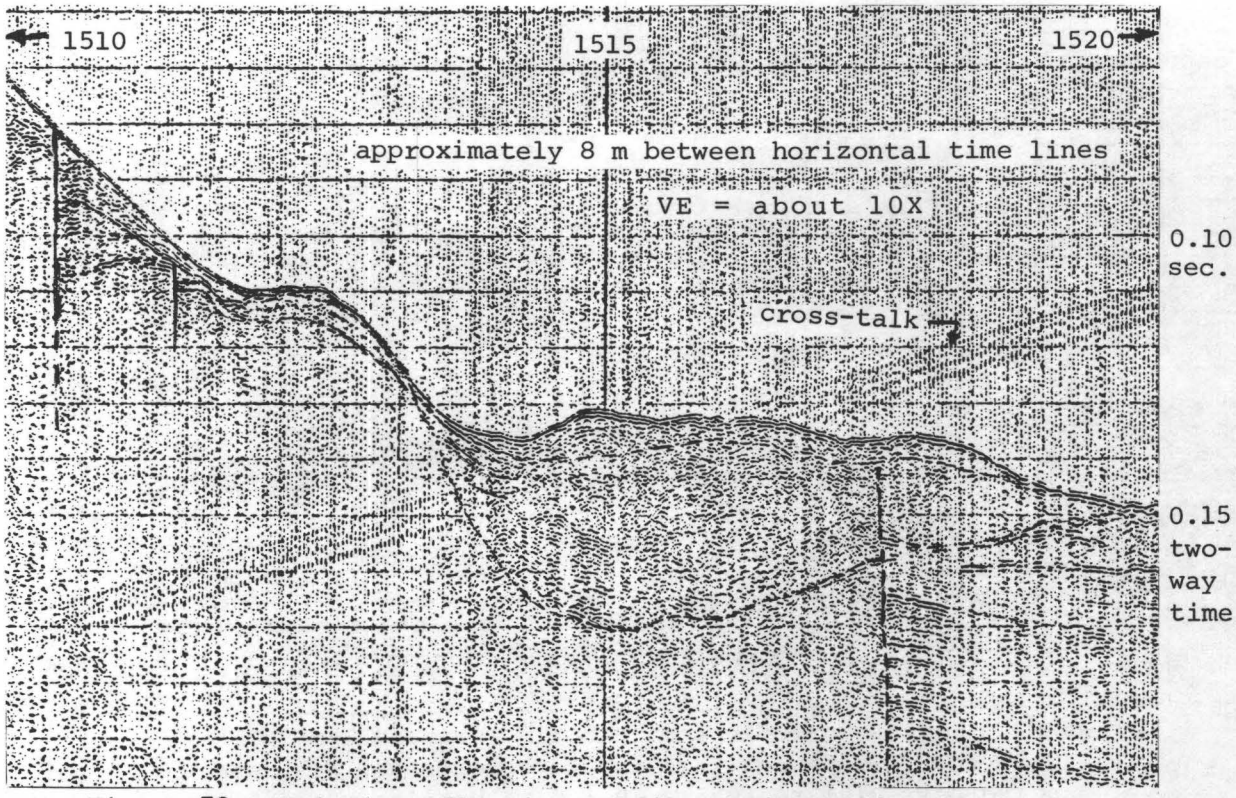


Figure 79. Seismic-reflection profile Parizeau line 41 (0.25-sec. sweep) showing probable upper Pleistocene channel-fill sediments that probably slumped in Holocene time. Faulted sediments (1517.1) are probably late Pleistocene in age. Fault at 1510.8 may reach seafloor and offset Holocene sediments.

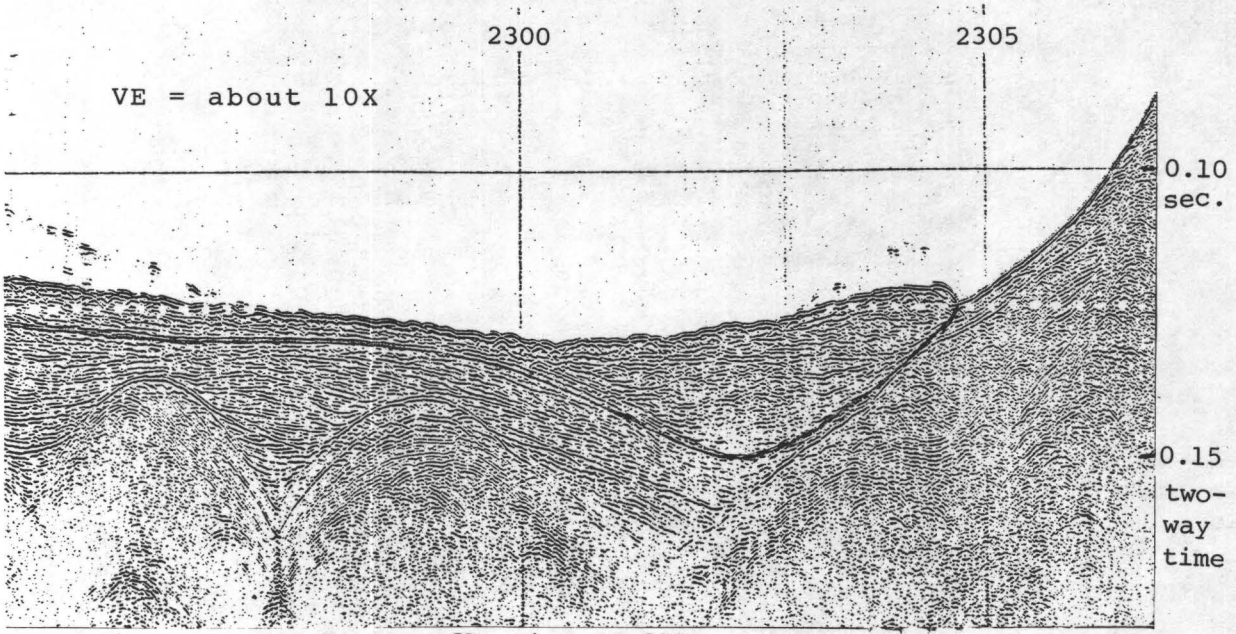


Figure 80. Seismic-reflection profile of Miller Line AA (0.25-sec. sweep) showing Holocene slump that overlies folded and disrupted upper Pleistocene sediments.

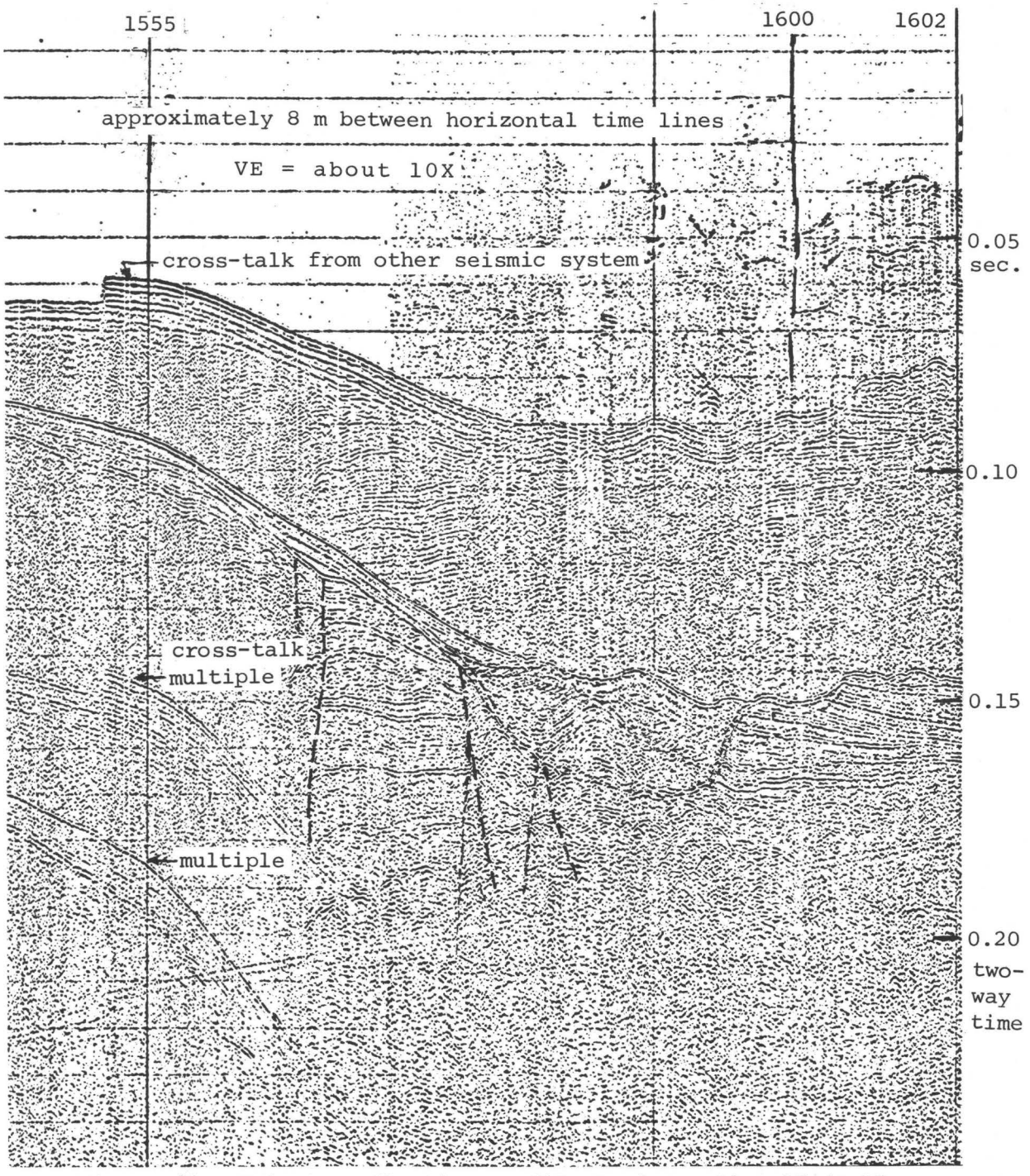


Figure 81. Seismic-reflection profile Parizeau line 35 (0.25-sec. sweep) showing slump or landslide (1600-1602) and fault (?) shown by terminations of bedding (1557).

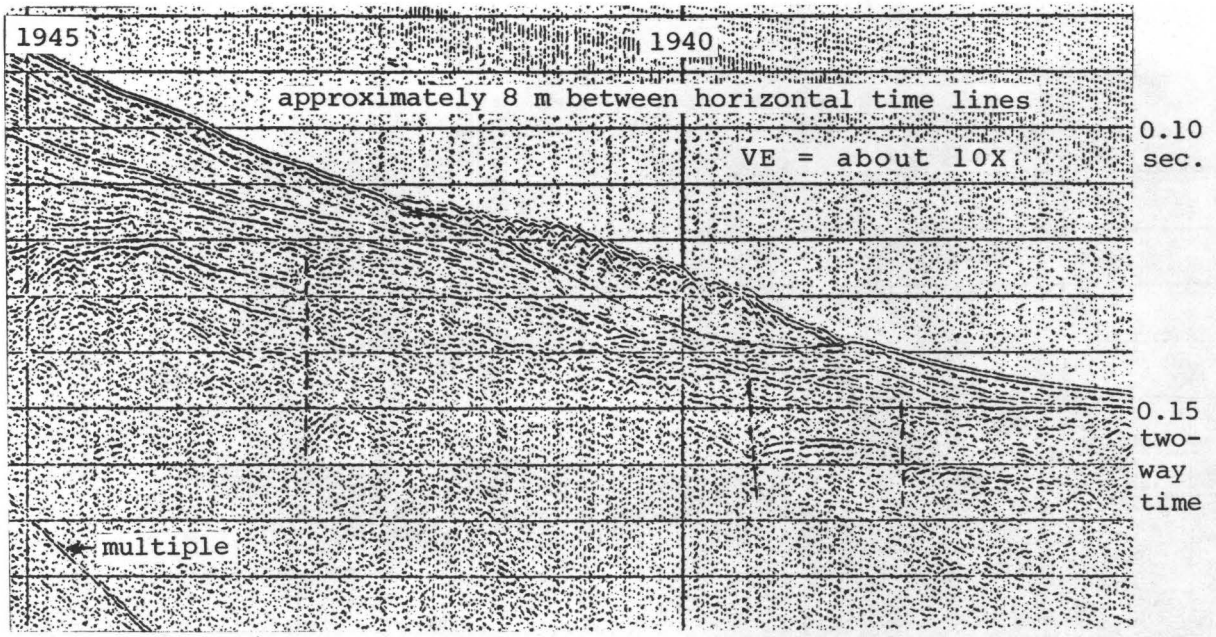


Figure 82. Seismic-reflection profile Parizeau line 23 (0.25-sec. sweep) showing Holocene (?) slump material with irregular upper surface overlying bedded uppermost Pleistocene glacial sediments which overlie generally unbedded older Pleistocene faulted sediments.

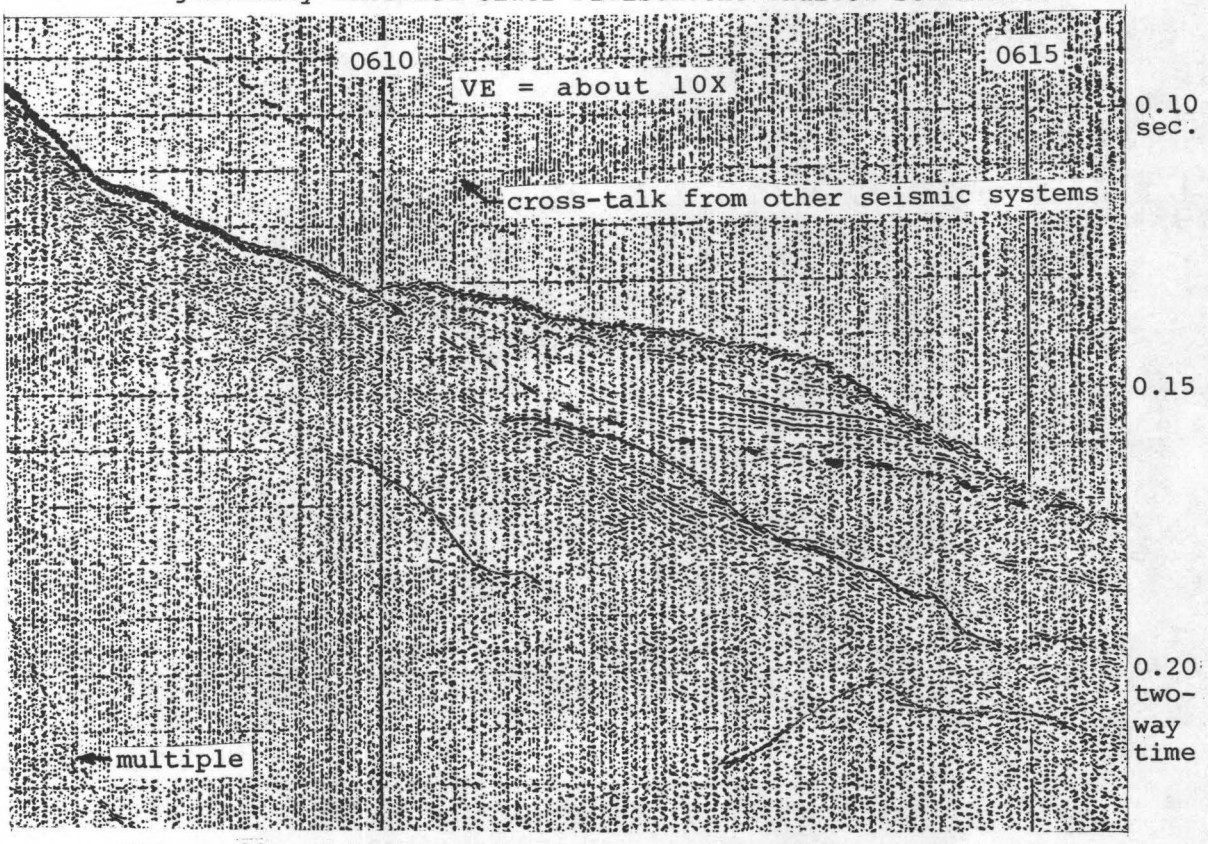


Figure 83. Seismic-reflection profile Parizeau line 36 w (0.25-sec. sweep) showing a landslide deposit of probable Holocene age.

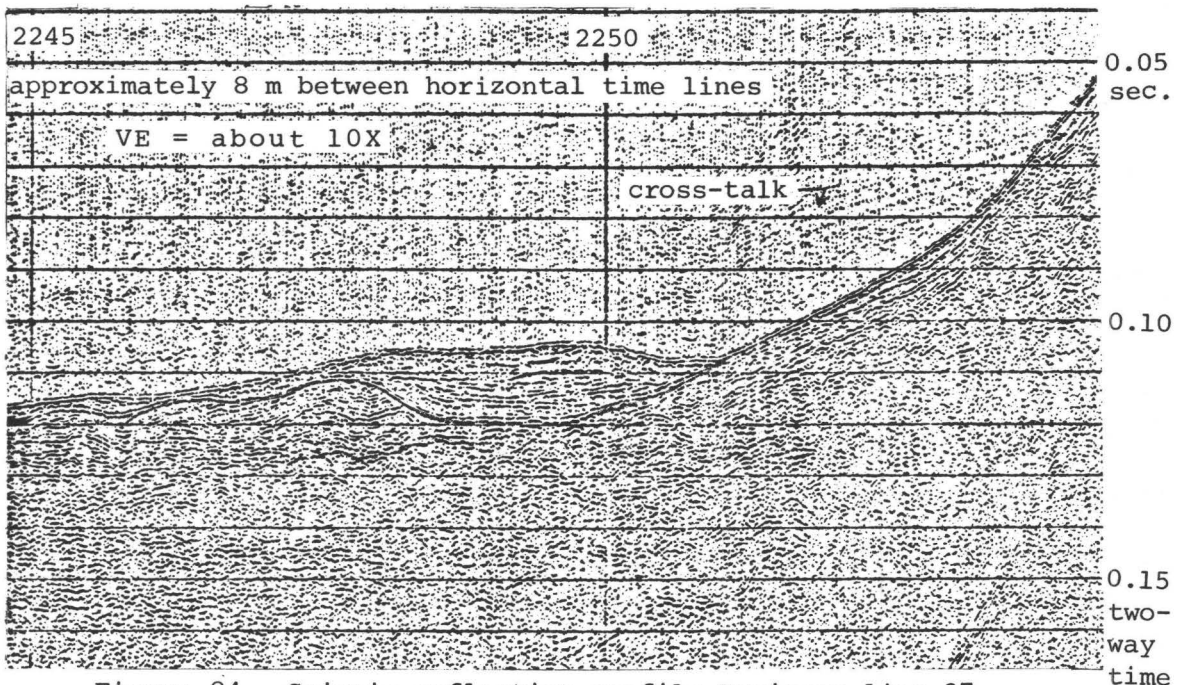


Figure 84. Seismic-reflection profile Parizeau line 37 (0.25-sec. sweep) showing possible Holocene landslide that scooped out and filled a depression cut into folded latest Pleistocene(?) unconsolidated sediments. Force of landslide may have been agent that folded the unconsolidated sediments.

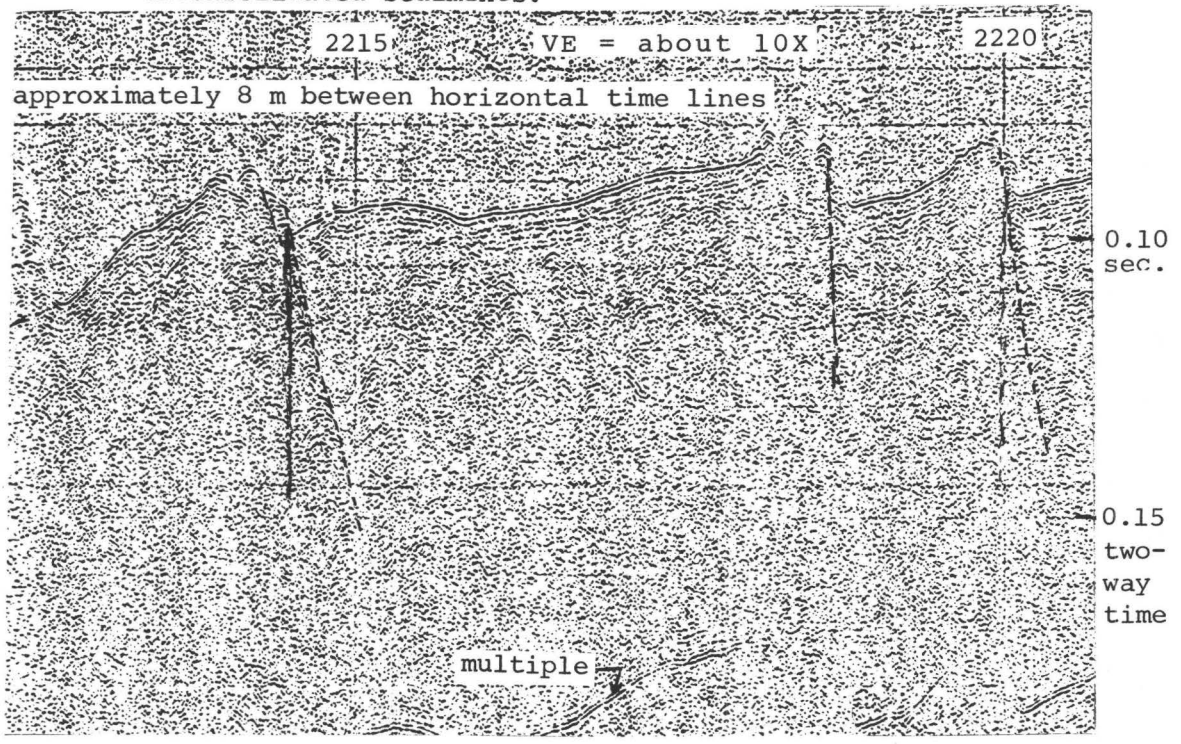


Figure 85. Seismic-reflection profile Parizeau line 30 (0.25-sec. sweep) showing apparent offsets of sea floor and possible gas seeps along faults (?).

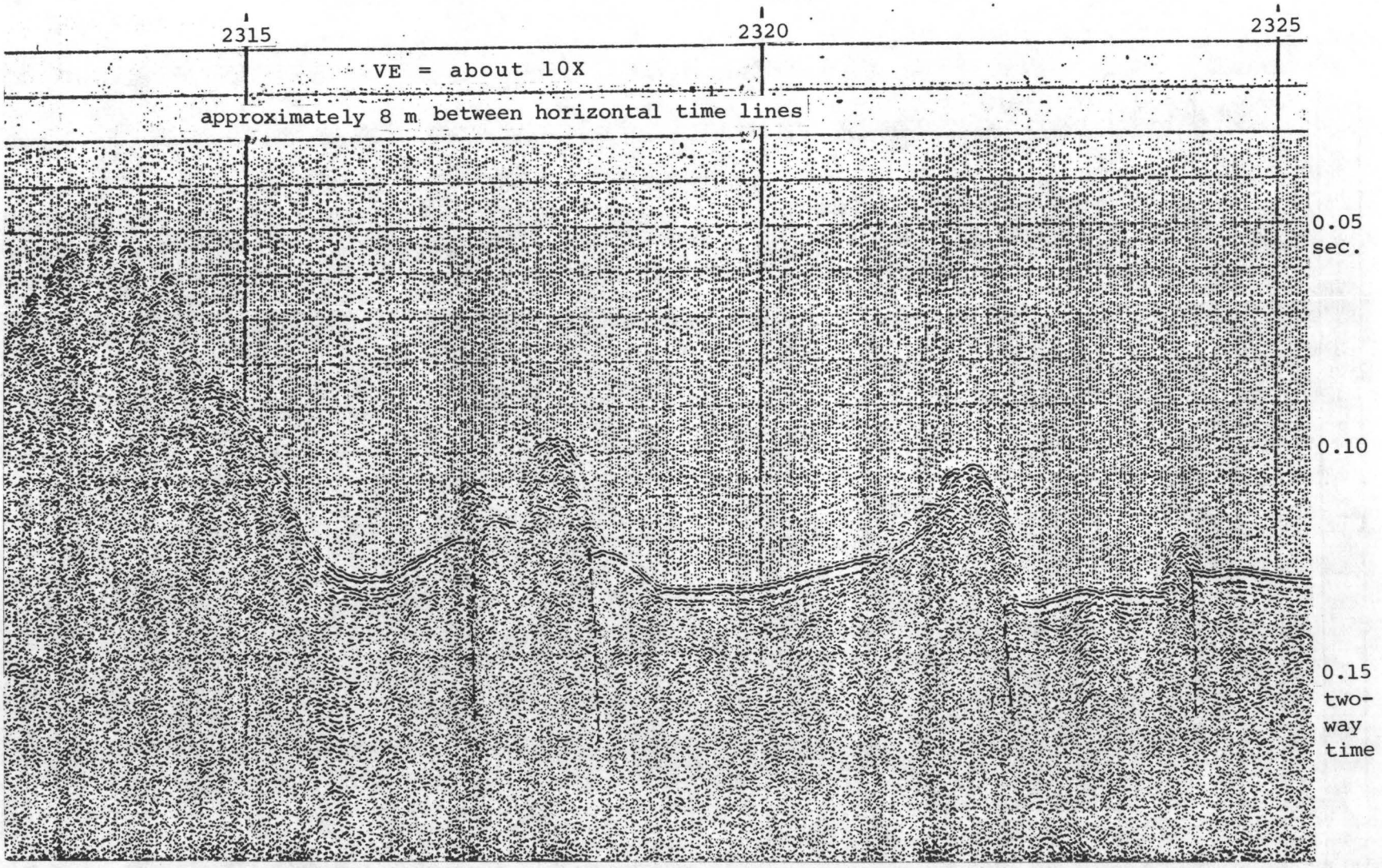


Figure 86. Seismic-reflection profile Parizeau line 30 (0.25-sec. sweep) showing apparent offsets of seafloor (assumed to be due to faulting) accompanied by possible gas seeps along faults (?). Hyperbolics and changes in dip at 2313 and 2317 on 1-second sweep records suggest faults at west edges of these gas (?) emanations also.

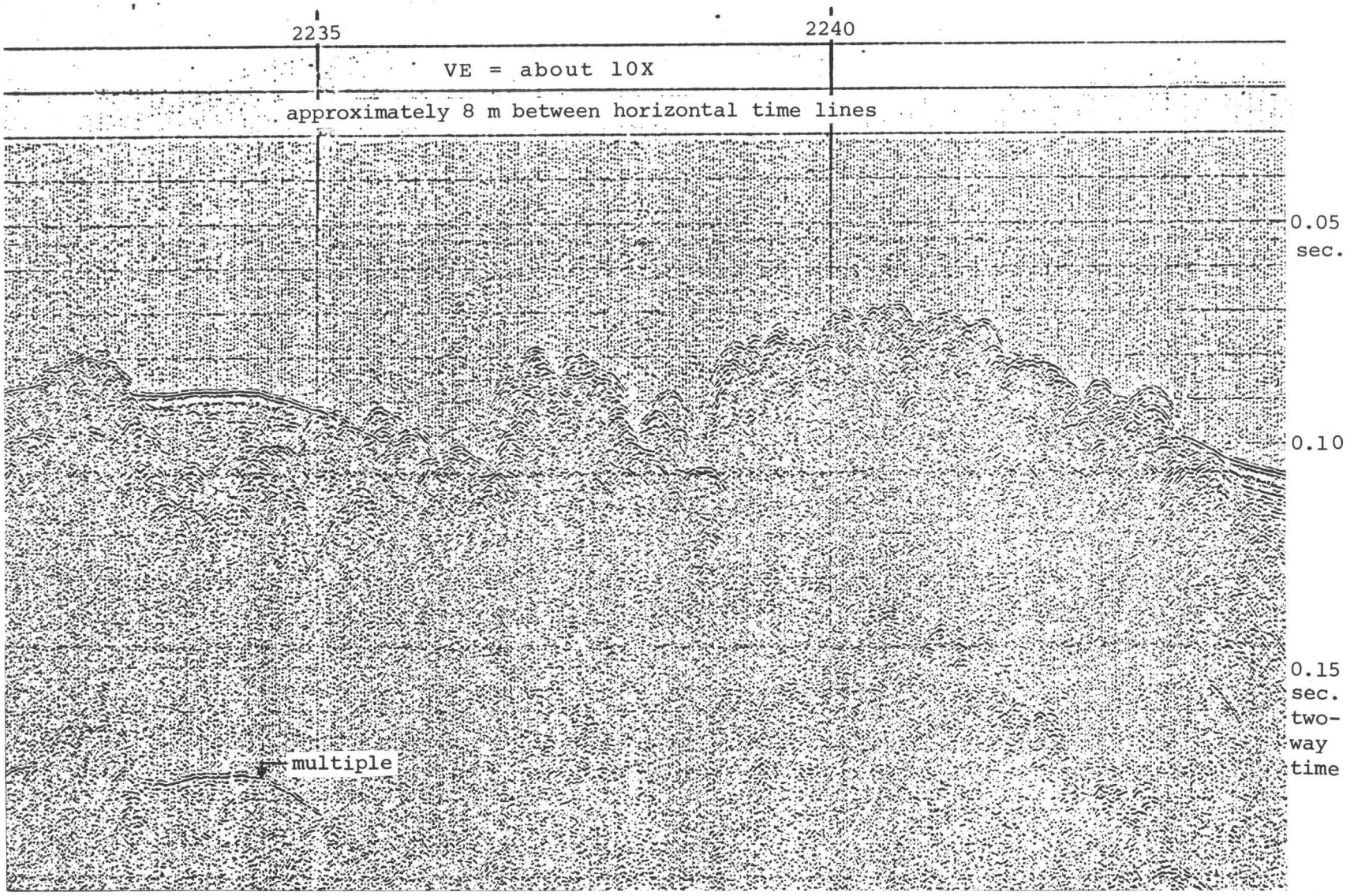


Figure 87. Seismic-reflection profile Parizeau line 30 (0.25-sec. sweep) showing possible large gaseous emanations at seafloor (or rough morainal topography). Adjacent area (2244-2246) is underlain by bedded sediments below seafloor.

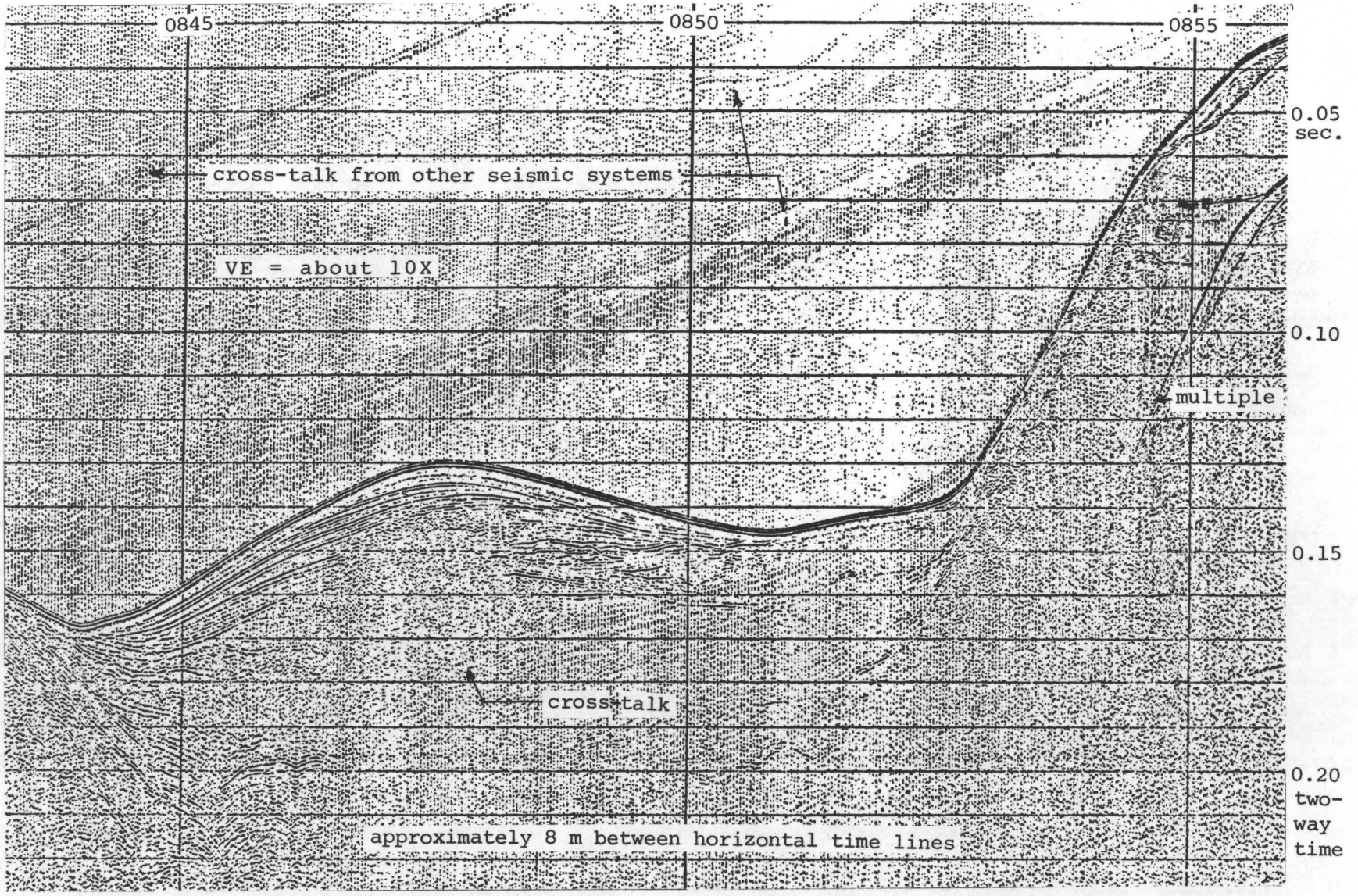


Figure 88. Seismic-reflection profile Parizeau line 32 (0.25-sec. sweep) showing partially gas-filled sediments in domed Holocene (?) landslide. Underlying late Pleistocene glacial sediments have been folded and disrupted.

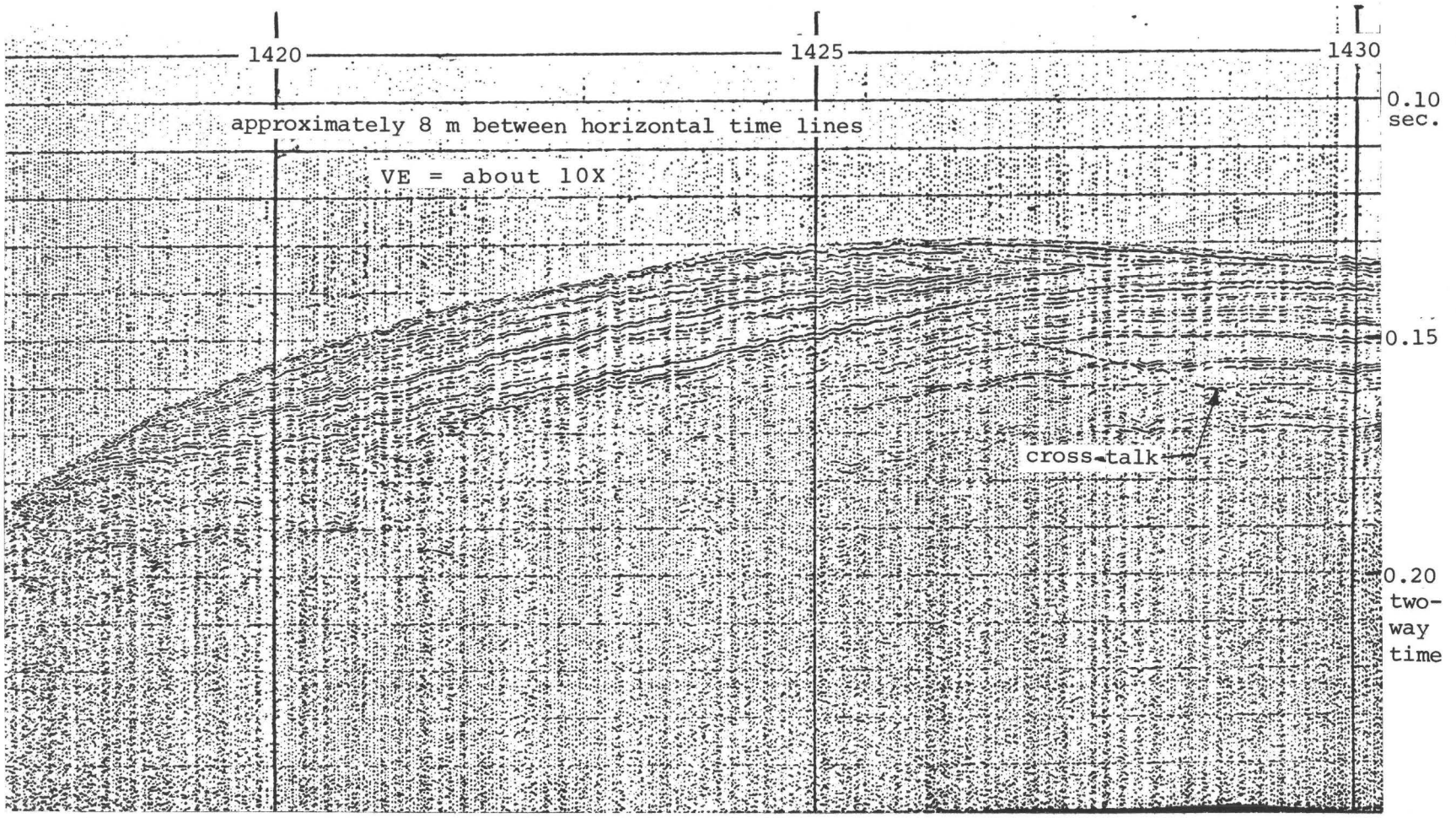


Figure 89. Seismic-reflection profile Parizeau line 41 (0.25-sec. sweep) showing well-bedded upper Pleistocene off-bank sediments. Change in lithology or presence of gas or peaty beds in sequence to left of 1425 deteriorates signal about one inch below sea floor.

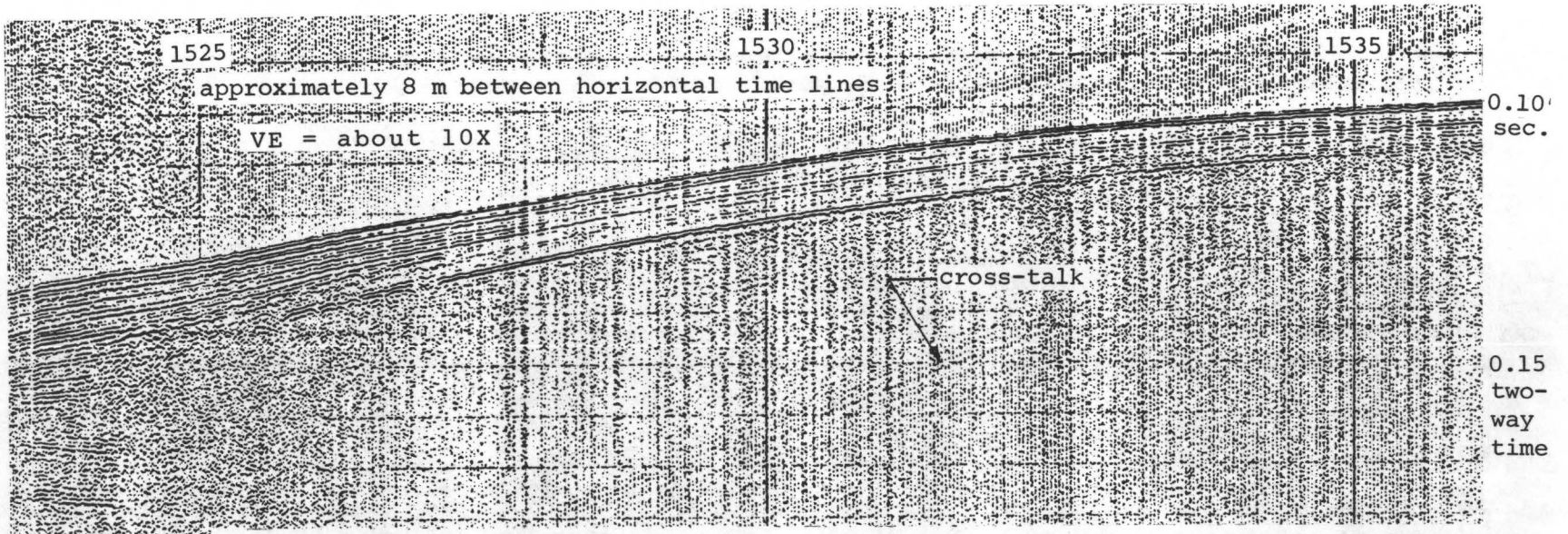


Figure 90. Seismic-reflection profile Parizeau line 41 (0.25-sec. sweep) showing abrupt change from well-bedded sequence to gas (?)-filled sediments to east (right) of 1524. Gas (?) probably infiltrates into lower part of upper sequence (Holocene?) between 1524 and 1528.

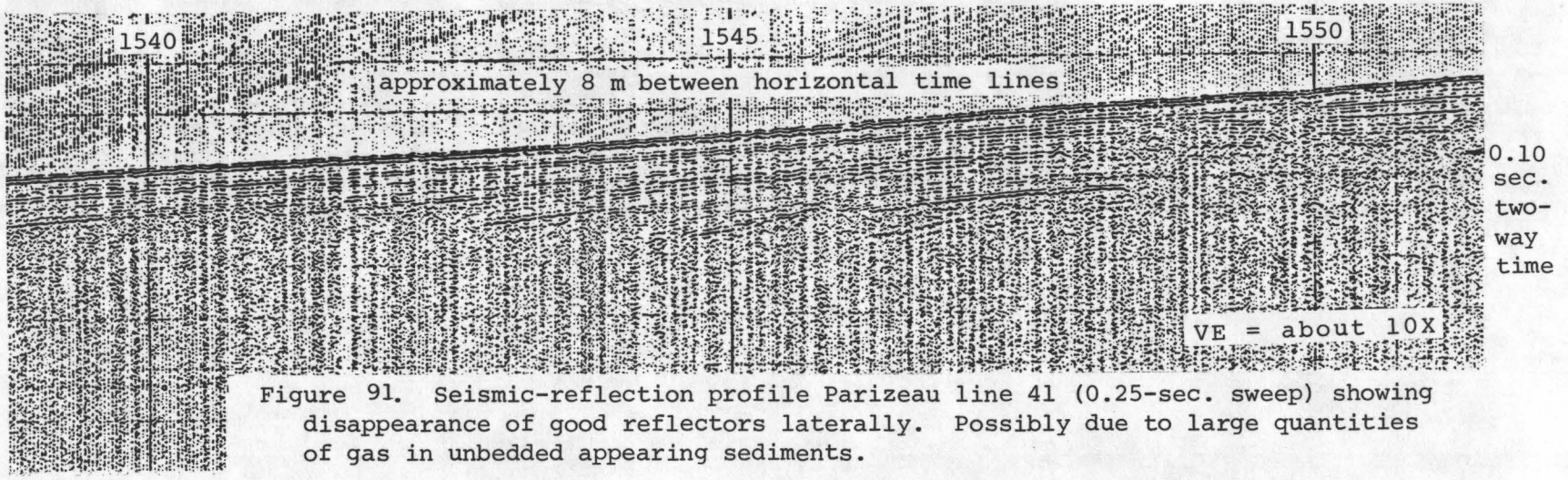


Figure 91. Seismic-reflection profile Parizeau line 41 (0.25-sec. sweep) showing disappearance of good reflectors laterally. Possibly due to large quantities of gas in unbedded appearing sediments.

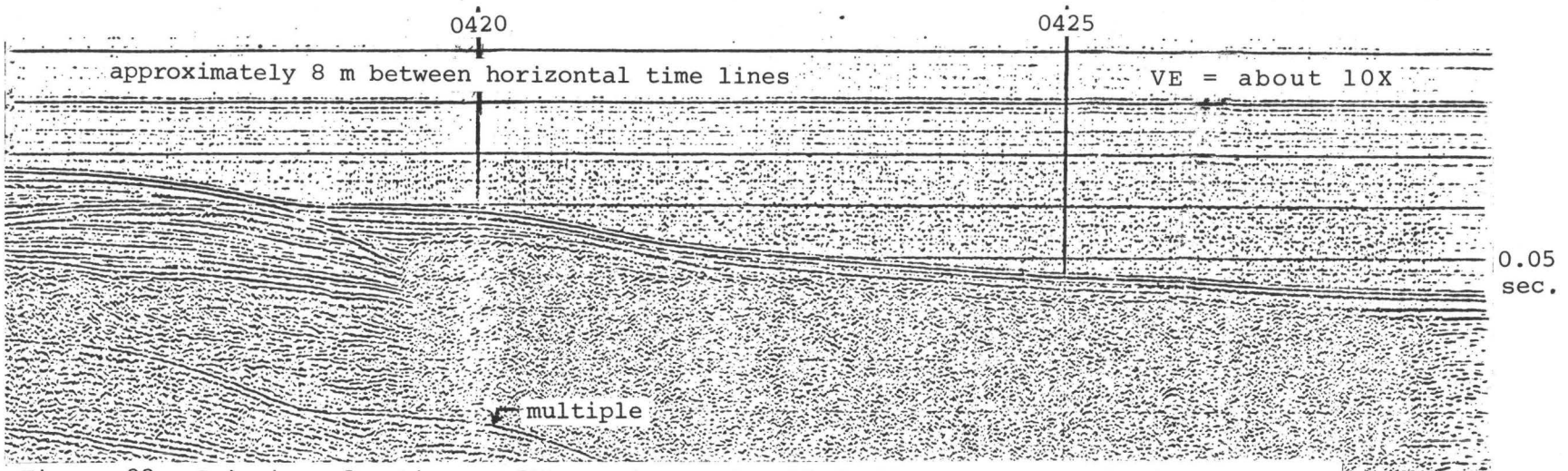


Figure 92. Seismic-reflection profile Parizeau line 32 (o.25-sec. sweep) showing a bedded sequence at north (right) end of profile. Bedded sequence changes fairly abruptly into non-bedded (gas-charged?) area to left.

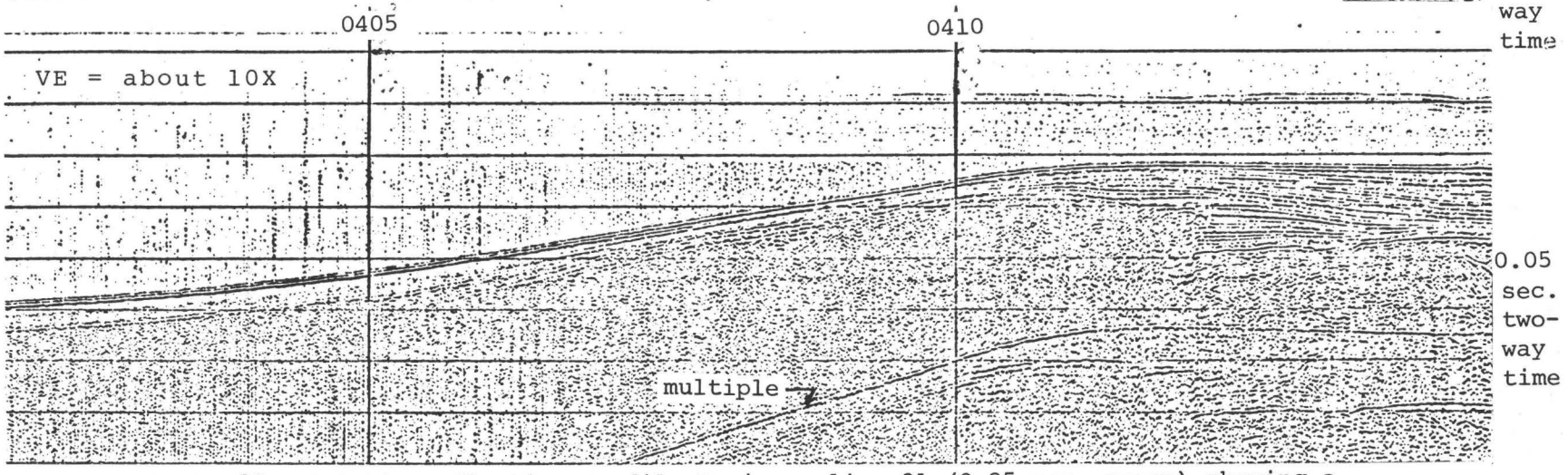


Figure 93. Seismic-reflection profile Parizeau line 31 (0.25-sec. sweep) showing a well-bedded sequence that abruptly becomes non-bedded. Non-bedded area is presumed to be gas-charged. Bedding reappears at north (right) end of profile.

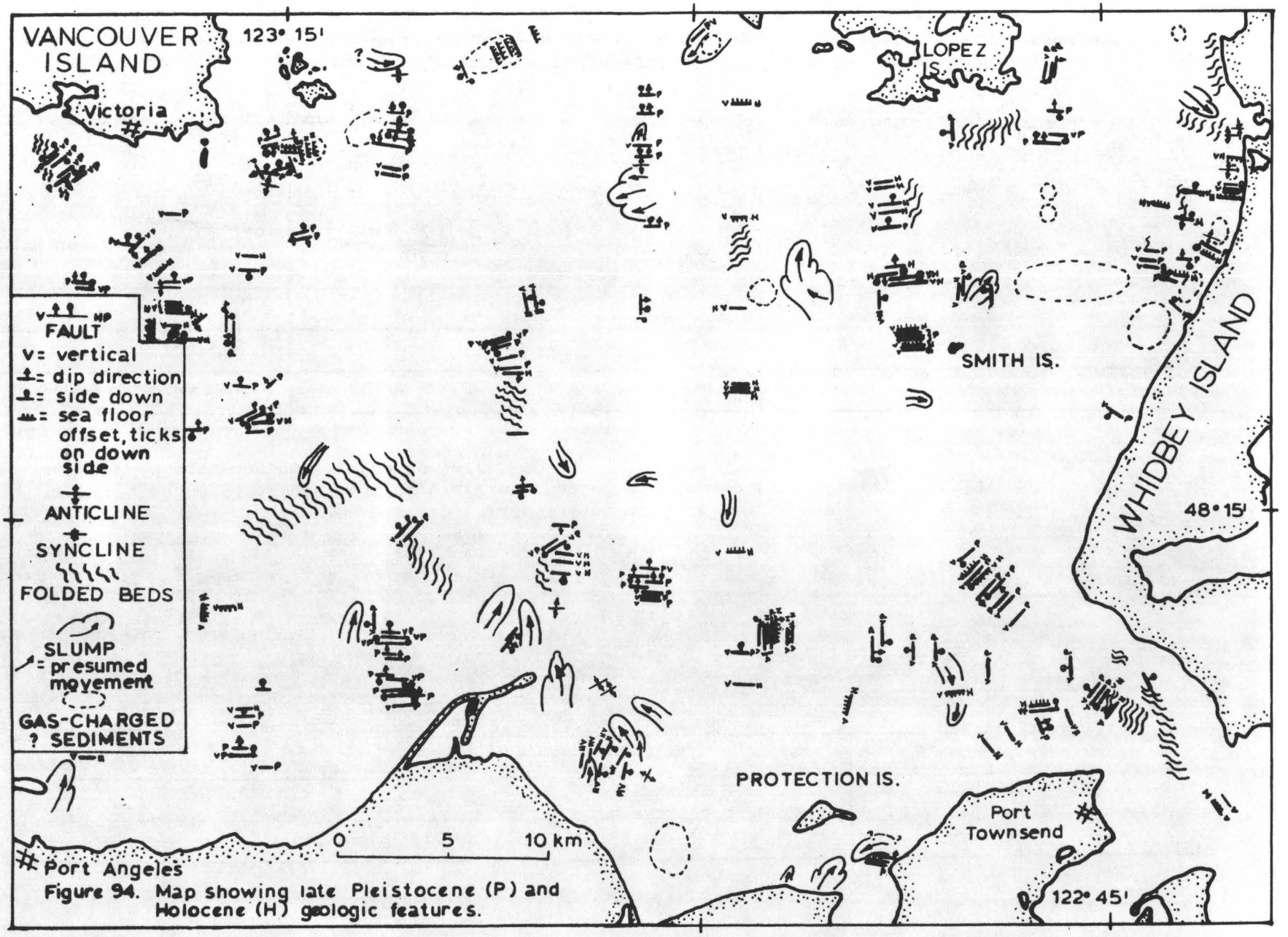


Figure 94. Map showing late Pleistocene (P) and Holocene (H) geologic features.

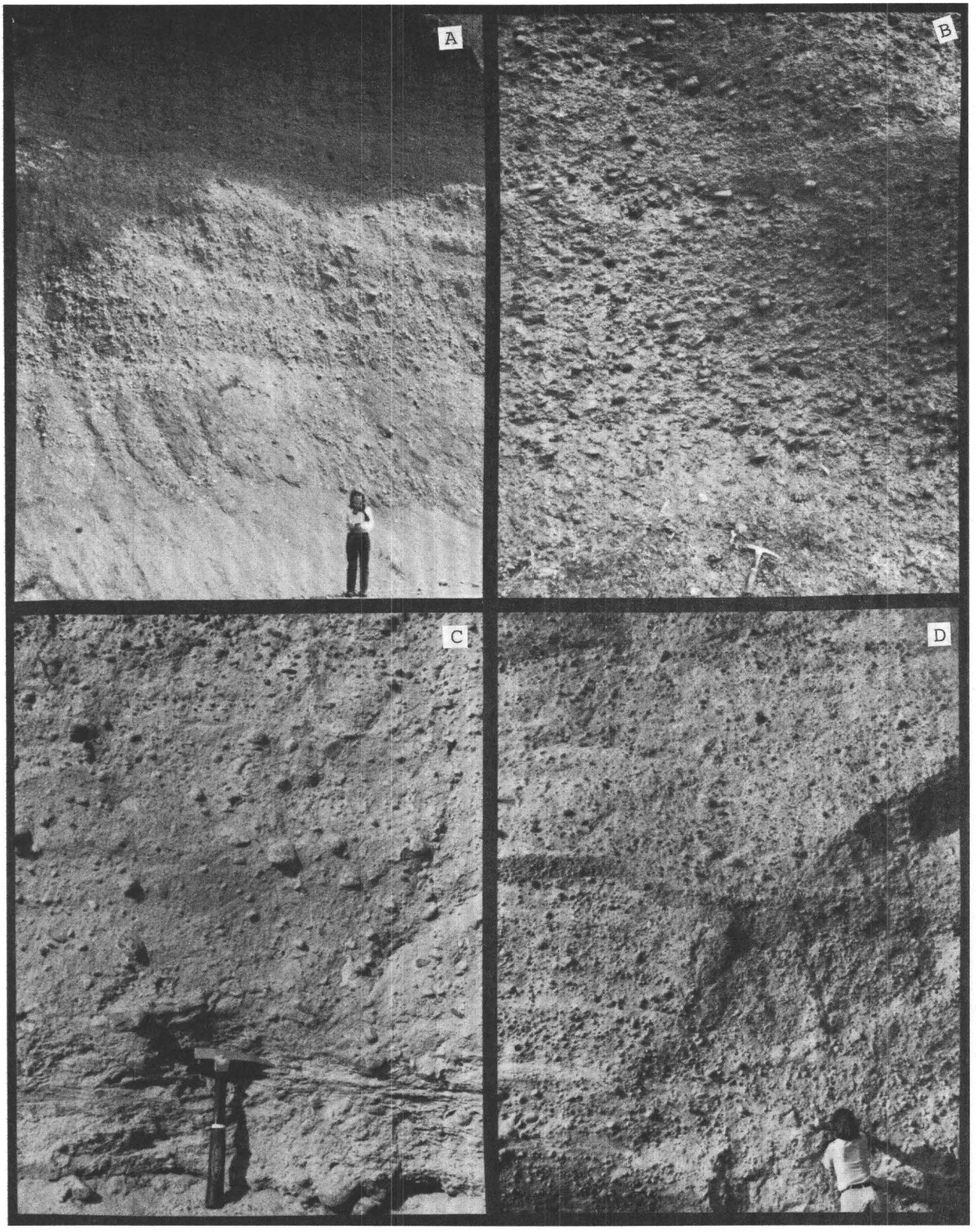


Figure 95. Road and seacliff exposures showing cross-bedded (at top) and even-bedded glacial outwash gravel (A), shingle-pebble outwash gravel (B), and glacial till (C, D).

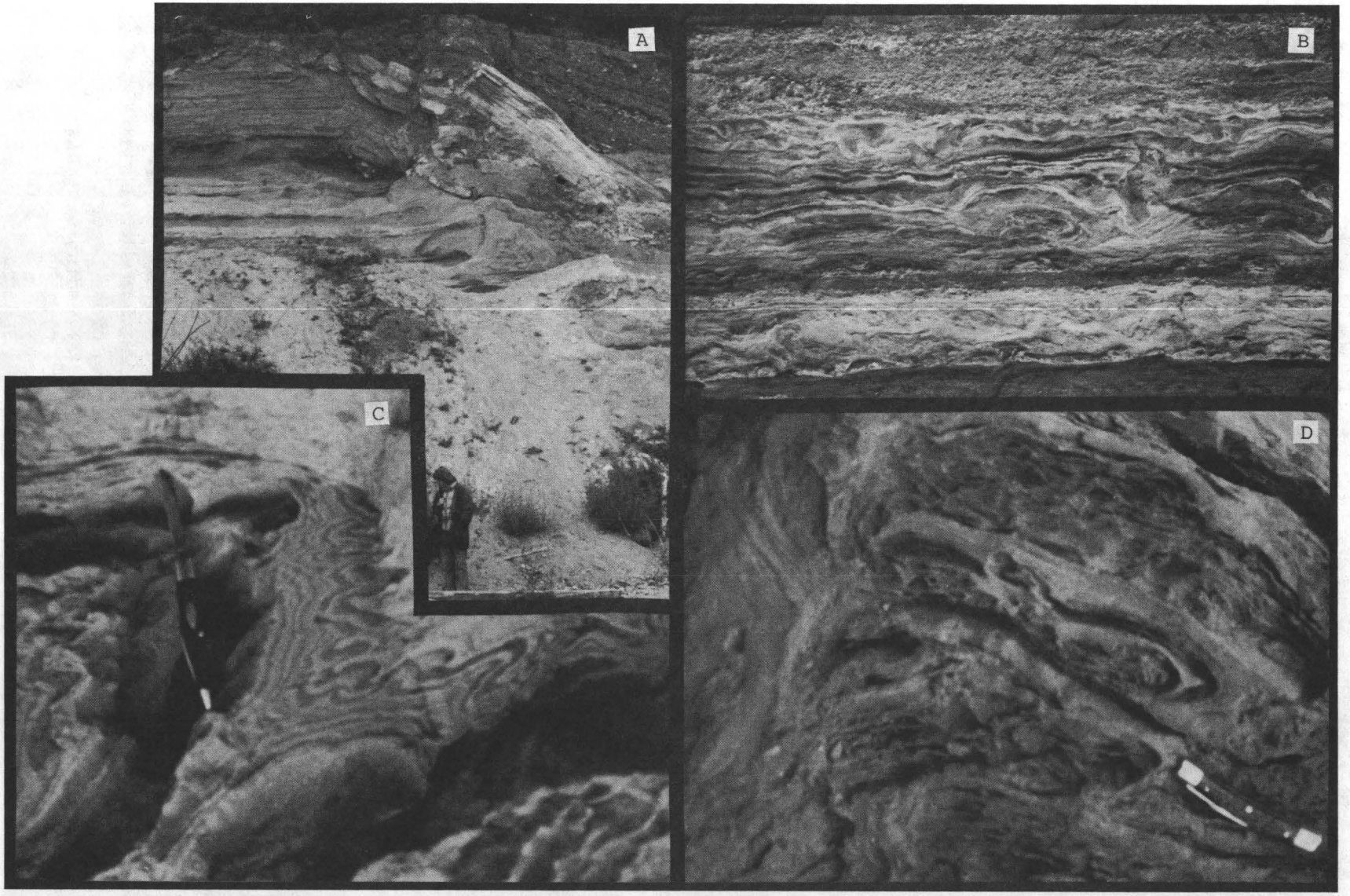


Figure 96. Seacliff exposures showing fault and slump features (A), and crenulated pre-consolidation fold and roll-up structures in glacial outwash (B, C, D).

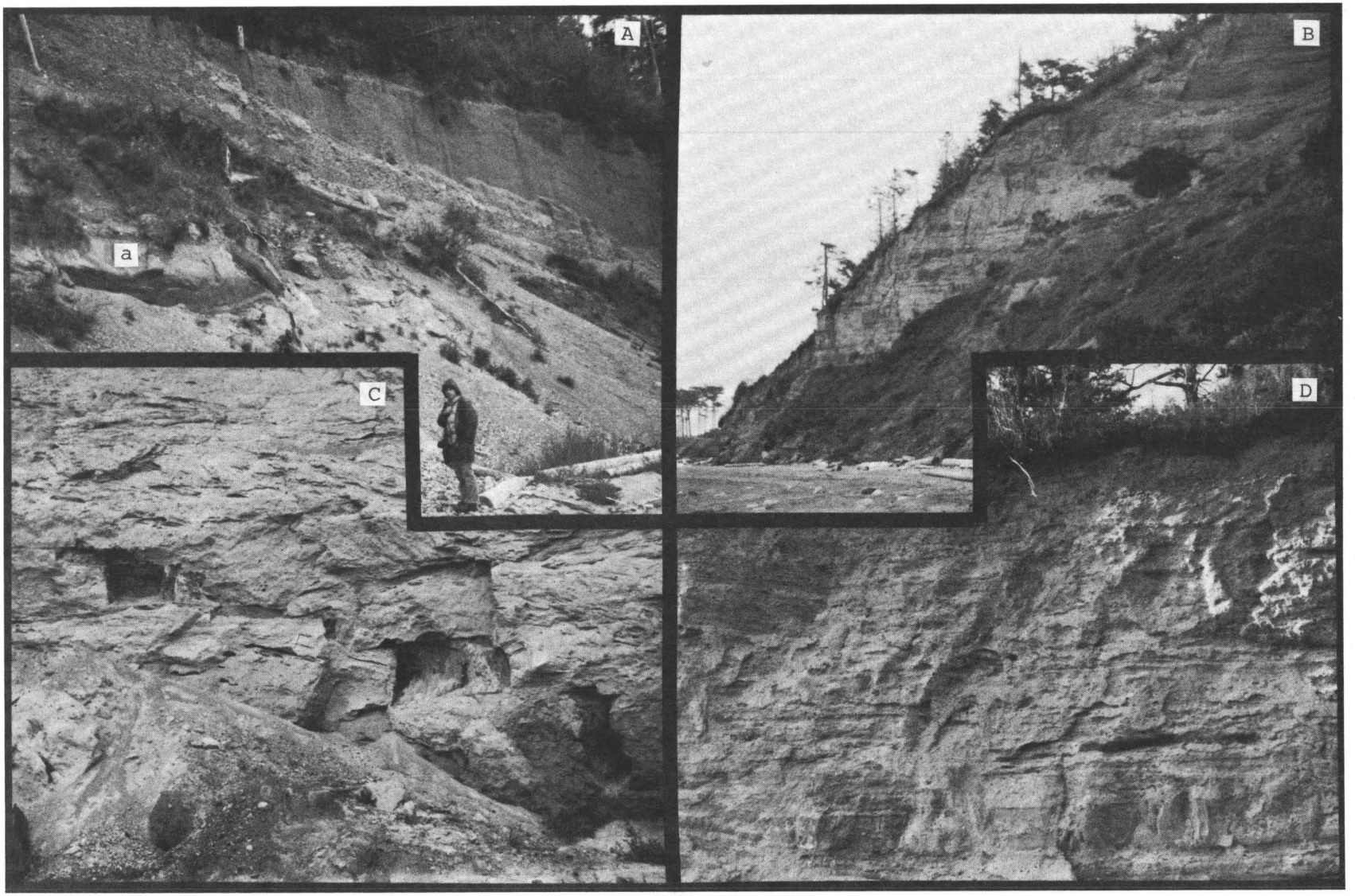


Figure 97. Seacliff exposures showing a slump block (a) and glacial gravel and weathering profile (A), interbedded glacio-marine and glacial outwash deposits (B), sheared and faulted glacial till (C), and bedded gravelly outwash with weathering profile (D).

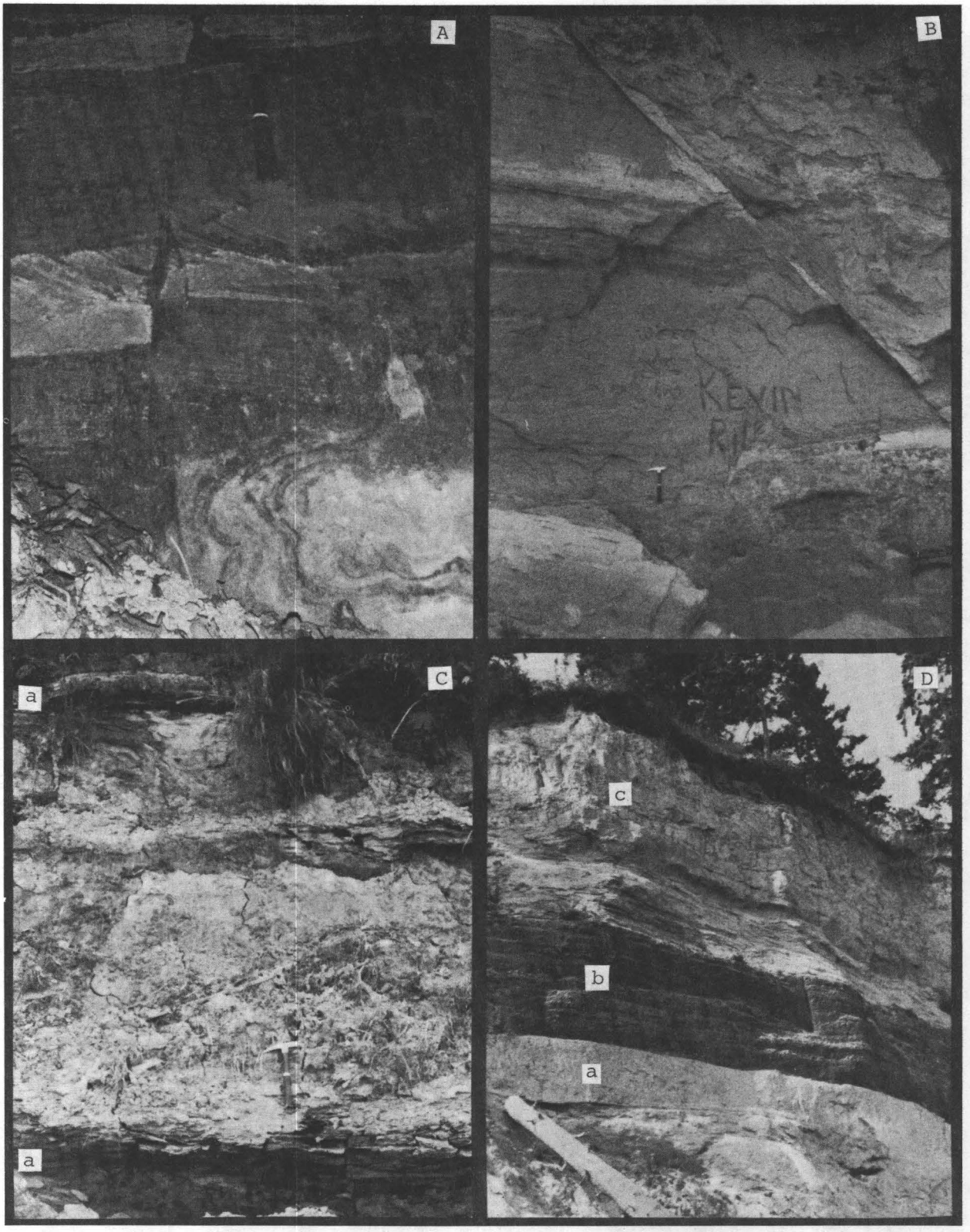


Figure 98. Seacliff exposures showing faulting (A, B), peat beds (a) in glacio-fluvial deposits (C), and glacial till (a) overlain by glacio-fluvial gravel (b) and glacio-marine sediments (c) and weathering profile (D).

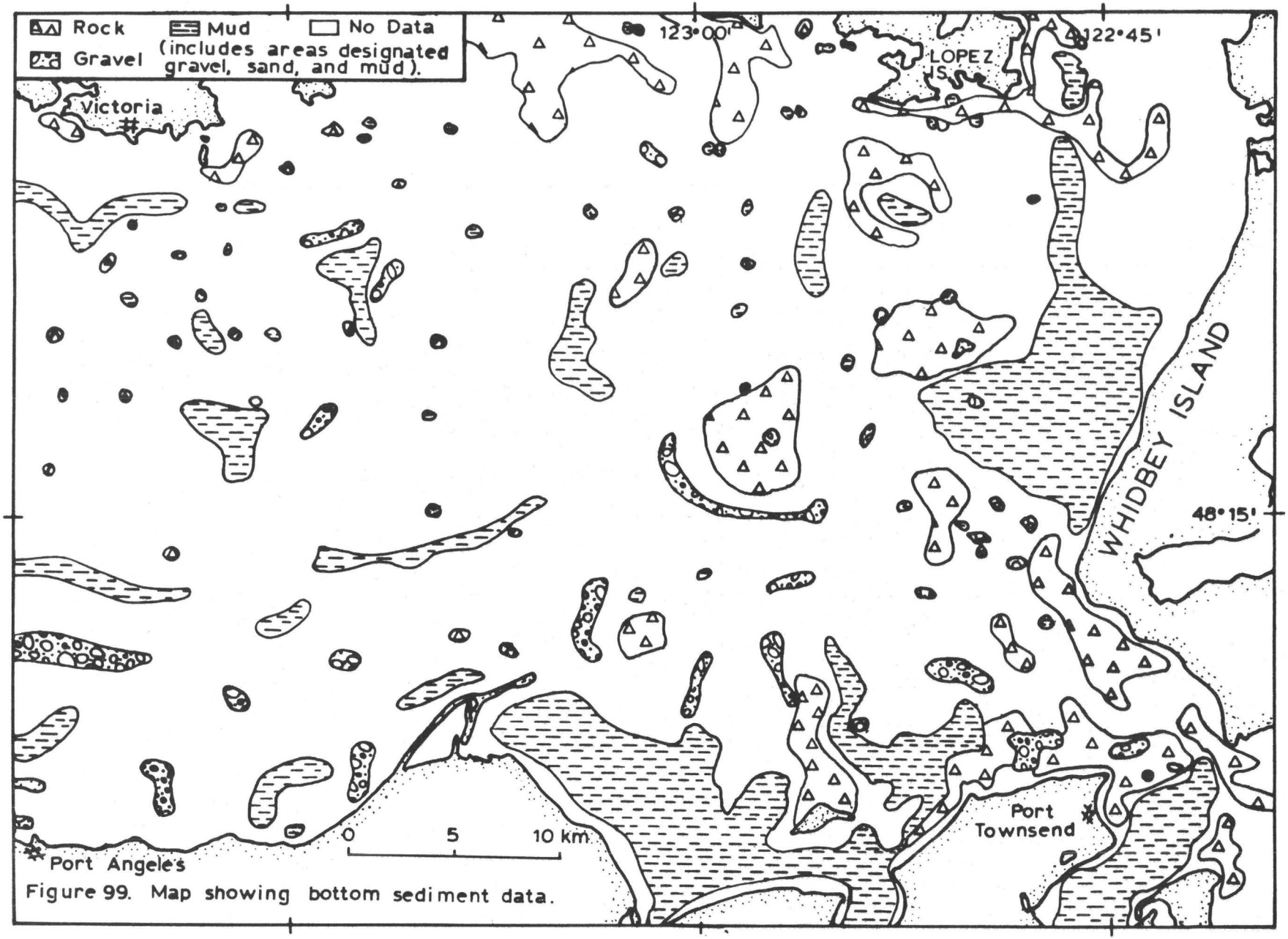


Figure 99. Map showing bottom sediment data.

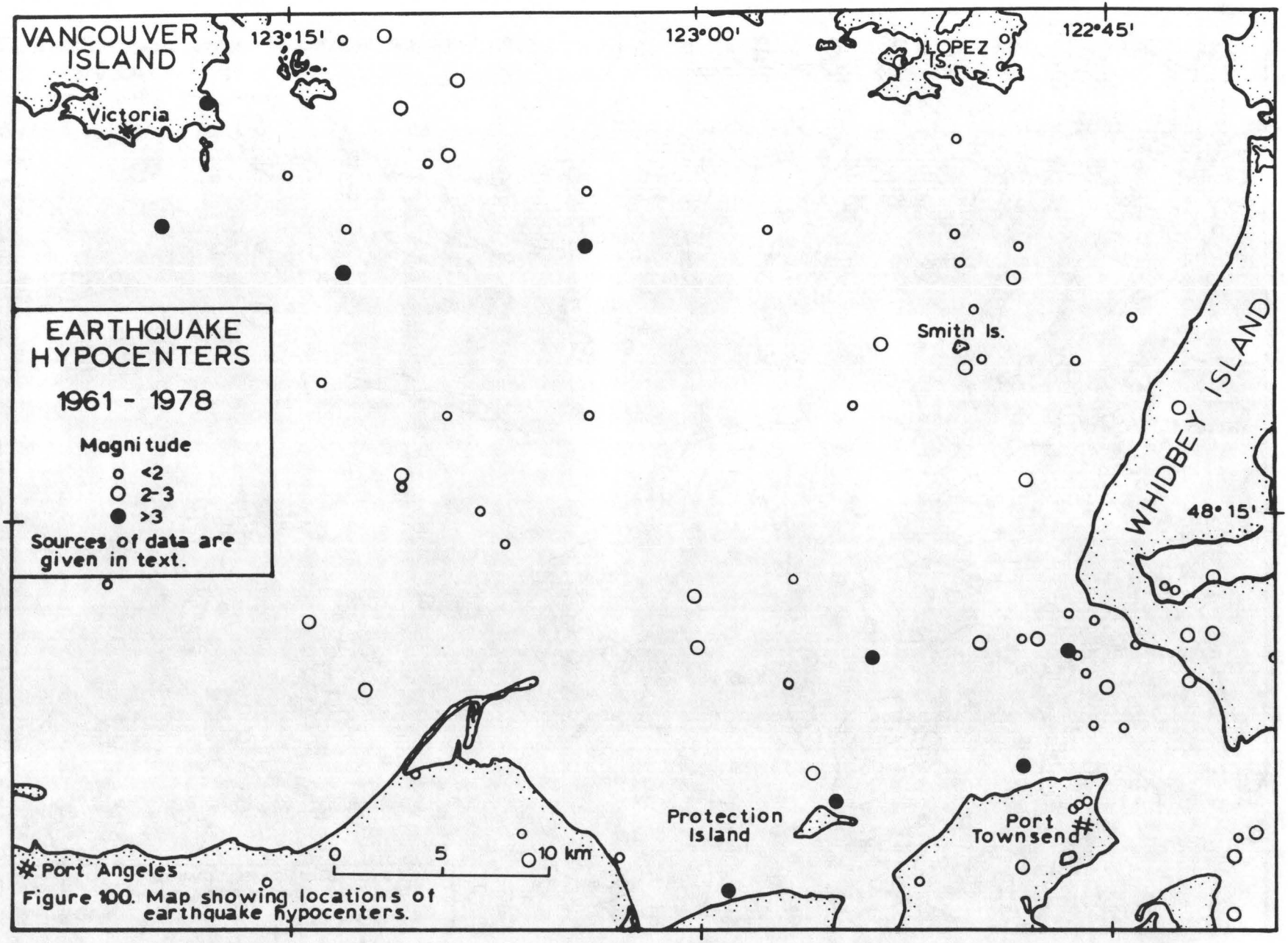


Figure 100. Map showing locations of earthquake hypocenters.

APPENDIX I
Operational Data

Canadian Survey Ship PARIZEAU.

The subbottom acoustic reflection data were obtained using three separate seismic systems; a moderately deep penetrating sparker system, a high resolution electromechanical device, and an echo-sounding device. The moderately deep penetrating sparker consisted of a van-mounted four-bank 40 to 160 kilojoule unit triggered from a single source. The triggered discharge of large capacitors traveled through six twin-electrode "ladders" trailed behind the ship. At their terminations in the sea water, these "ladders" created a spark that produced the high-intensity, low-frequency acoustic pulse. These pulses were reflected from the sea bottom and from subbottom surfaces and were received and preamplified by a 100-hydrophone streamer. They were then selectively filtered (average 160/31 Hz) and recorded graphically on two Raytheon recorders at one- and two-second sweeps.

The power source of the high-resolution system (Uniboom) consisted of an electrical discharge (capicitor bank) into a flat wound coil. The coil generated an eddy current with the same polarity as the encompassing aluminum disc. These similarly polarized electrical fields expelled the aluminum disc from the coil face thus delivering a mechanical pulse to the water. A rubber sheet immediately pulled the aluminum disc back to the coil face and the equipment was ready for the next electrical discharge. The returning signal was detected with a hydrophone and transferred to a Raytheon recorder. The dominant frequency was about 2500 hertz (range 700-14,000 Hz) and power demand was about 400 joules. The pulses ere selectively filtered at high settings of 1000 to 200 Hz (average 1500) and low of 400 Hz. A 3.5 kilocycle transducer system was used to obtain precision depth control.

Navigation for most of the track lines utilized a Decca Minifix system with an accuracy of 100 m or better.

U.S. Geological Survey Research Vessel DON J. MILLER

The source of seismic energy used was a 400 Joule double-back high-resolution (Uniboom) system with recorder sweep rate of 1/4-second and a 1/4-second firing rate. Filter settings for lines B and B-1 were 3000-6000 Hz (high) and 200-300 Hz (low). Ship's speed averaged about 5 knots.

Tracklines were located by a combination of precision transponder navigation system and ship's radar with variable range marker.

## APPENDIX II
## Interpretation Problems

Bubble Pulse. The sparker system produced a very broad bubble pulse, which results from the time interval between the initial bubble formation and the final bubble collapse. A noise or "ringing" effect is also made in single-channel records by reverberation between surfaces of different velocities such as air-water, water-seafloor, clay-sand, sand-gravel, etc. interfaces.

Multiples. In Figure 22 the lowermost surface (0.19 sec) shown by dark reflectors represents the first multiple. This multiple is recorded as a group of reflectors that bounced back a second time at twice the depth from sea level to the seafloor, thus taking twice the time to reach the position at which they are recorded. Multiples are also reproduced by strong subbottom reflectors where large sound velocity contrasts exist.

Cross-talk. A trio of straight, slanted group of dots that trend slightly upward across the records represent a sea-level signal from another seismic-reflection profile system that was in operation on the ship at the same time. Cross talk can also take the form of the water-seafloor and subbottom contacts.

Figure 81 shows another type of cross talk. The upper part of the subbottom profile is not the true record but is cross-talk from a larger profiling system in operation at the same time. The signal at the water-seafloor interface has five lines to it, rather than the two lines of the profile of the 0.25-second system which is observed at a time depth of about 0.95 sec. depth at the south (left) side of the figure. Each system has produced its multiple, and there is cross-talk from yet another system in the lower part of the record (diagonally down from 0.18 sec. at the north (right) side of the figure).

Time Gaps. Time gaps in profiles are periods when the ship was moving but the recorder had stopped; offsets of the sea floor or reflectors at such time gaps are meaningless geologically except tht they indicte a loss of data.

# GEOLOGIC UNITS THAT LIKELY CONTROL SEISMIC GROUND SHAKING IN THE GREATER SEATTLE AREA

James C. Yount
U. S. Geological Survey
345 Middlefield Road
Menlo Park, California 94025

## Introduction

Two moderately large earthquakes have occurred in Puget Sound in the past two decades (fig. 1), the 1949 Olympia earthquake (M=7.1, Nuttli, 1952) and the 1965 Seattle earthquake (M=6.5, Algermissen and others, 1965). These earthquakes highlighted the complicated role that both crustal and near surface geology play on resultant ground shaking in the Puget Sound region. Both earthquakes had relatively deep foci of 70 and 60 kilometers respectively (Nuttli, 1952; Algermissen and others, 1965) and produced ground shaking effects that were small for their respective magnitudes (Algermissen and others, 1965; Mullineaux and others, 1967; Langston, 1981). Large source depth (Langston, 1981) and thick unconsolidated sedimentary sections (Shakal and Toksoz, 1980) are thought to be most responsible for this generally diminished ground response.

In addition, specific consequences of ground shaking, such as building damage, appear to be highly variable over short distances and on lithologically similar geologic units, particularly in the 1965 event (Mullineaux and others, 1967). Building damage in 1965 was relatively heavy in the lower Duwamish River area and southern downtown region of Seattle where unconsolidated Holocene alluvium and artifical fill make up most of the substrate; but damage was relatively light in the upper Duwamish River valley just a few kilometers to the south, where similar geologic materials make up the substrate (fig. 1). Similarly, the most severe residential building damage, mostly to brickwork and chimneys, appeared to be concentrated in West Seattle, an area underlain by compact Pleistocene sands and silts; in contrast, only light damage was reported for nearby regions of Seattle such as Beacon Hill and Magnolia (fig. 1) underlain by similar compact Pleistocene sediments.

All of these observations suggest that subsurface geologic conditions play important roles in determining the ground response characteristics of sites in Puget Sound. The purpose of this report is to provide a basic description of the subsurface geology of the Seattle area with emphasis on: a) the configuration and depth of the Tertiary bedrock surface underlying the region, b) the depth to poorly consolidated, water-saturated sand units in the otherwise compact parts of the Pleistocene section that underlies much of Seattle, and c) the thickness of unconsolidated Holocene alluvium and man-made fill in the area. This information can serve as a guide for tentative explanations of observed ground response effects and can also be utilized for

locating instrumentation to better measure and understand the strong ground motion resulting from future earthquakes in Puget Sound.

## Geologic Setting of the Greater Seattle Area

The greater Seattle area is underlain by a complex configuration of steeply dipping Teriary sedimentary and volcanic rocks, and flat lying Quaternary glacial and non-glacial deposits of highly variable thickness. Sandstone, conglomerate, and volcanic breccia make up the Tukwila Formation (Mullineaux, 1970), a unit that crops out southeast of Seattle in the vicinity of Renton (fig. 1). The Tukwila Formation is overlain conformably by arkosic sandstone, shale, and coal of the Renton Formation (Mullineaux, 1970). These two formations, together forming the middle to upper Eocene Puget Group, dip gently south in a section that is at least 1500 meters thick just northeast of Renton (Mullineaux, 1965). Small bodies of porphyritic andesite intrude the Tukwila Formation northeast of Renton; small outcrops of similar andesite are found in the Duwamish River valley west of Allentown, but no intrusive relationship with Puget Group or younger rocks can be demonstrated there.

Marine and nonmarine volcanic sandstone, siltstone, and claystone of late Eocene and Oligocene age crop out along the east side of the Duwamish River valley and in the Rainier Valley and Seward Park regions south and east of Seattle (Waldron and others, 1962; Gower and Yount, in preparation). These rocks are at least 750 meters thick and, in general, dip steeply north and east, with dips becoming progressively steeper to the north (Gower and Yount, in preparation).

The bulk of the geologic section underlying Seattle consists of Quaternary glacial and nonglacial sediments that unconformably overlie the Tertiary rocks. At least two glacial drifts, predating deposits of the Fraser Glaciation (12,000 to 18,000 years b.p) are exposed in the Seattle area (fig. 2). Poor exposures of the oldest drift, including the Beacon Till of Stark and Mullineaux (1950), can be found near the base of the east wall of the Duwamish River valley just southeast of the Interstate 5-Spokane Street interchange. The drift is composed mainly of compact clayey till containing well-rounded pebble and cobble clasts (Stark and Mullineaux, 1950; Wegner, 1968). At least 25 meters of till was exposed in the abandoned Seattle Brick Company pit, but recent freeway construction and fill work have destroyed most of the exposure of this unit. A more widespread drift unit, including the Klinker Till of Stark and Mullineaux (1950), and associated glaciolacustrine silt and glaciofluvial sand and gravel crops out along the west wall of the Duwamish River valley and in the slopes and seacliffs surrounding Fauntleroy Cove. Much of West Seattle is presumably underlain by this drift unit. The till is very clay-rich, compact, and contains rounded pebbles and cobbles (Stark and Mullineaux, 1950). Associated glaciolacustrine sediments are composed mainly of cohesive, well-laminated silt and clay. Very compact, iron-stained medium to coarse-grained sand and sandy gravel have been found in the Lincoln Park- Fauntleroy Ferry Terminal area (Waldron, 1967), and are thought to represent a glaciofluvial facies within this drift unit. As much as 25 meters of till is exposed in the west wall of the Duwamish River valley near the north side of South Seattle Community College.

Interposed between drifts is a fine-grained section typically composed of compact varved to massive proglacial lacustrine silts and clays in the lower part, grading upward into lacustrine and fluvial medium to fine-grained sand

and peaty silt and clay (fig. 2). This unit, the Duwamish Formation of Stark and Mullineaux (1950), underlies most of the greater Seattle area, and is especially prominent in the bluffs surrounding West Seattle and in the slopes on the north end of Beacon Hill. Geotechnical investigations for high-rise buildings indicate that much of downtown Seattle is underlain by these fine-grained sediments. The thickness of the unit is variable owing to differential erosion by subsequent glaciations, but as much as 70 meters of Duwamish Formation is exposed in the west wall of the Duwamish River valley. One radiocarbon date (W-1979) from a cedar branch interbedded in Duwamish Formation alluvium from a downtown building excavation indicates that these sediments are greater than 42,000 years old (Marsters and others, 1969).

This section of glacial and nonglacial sediment is overlain, in most Seattle locales, by widespread fine and coarse-grained deposits of the Fraser Glaciation, the last major invasion of Cordilleran ice into the Puget Lowland. The resultant sediments, termed Vashon Drift (fig. 2) have been subdivided into two members, the Lawton Clay Member, and the overlying Esperance Sand Member (Mullineaux and others, 1965), both of which are well represented in the Seattle region. The Lawton Clay Member is often underlain by as much as 30 meters of interbedded silty clay, clayey silt, and crossbedded sand with abundant organic debris throughout the section (fig. 2). Radiocarbon dates of 18,100 ±700 (W-1186)to 22,400 ±800 years B.P. (W-1181) from organic debris in sediments beneath the Lawton Clay Member at its type section in the bluffs south of Fort Lawton, indicate that these sediments were deposited late in the period of interglaciation that preceeded the advance of Vashon ice into the Puget Lowland (Mullineaux and others, 1965). It is difficult, particularly utilizing subsurface data, to distinguish these interglacial sediments from the lithologically similar sediments of the underlying Duwamish Formation without recognition of an intervening drift unit, or radiocarbon ages from associated organic material.

The Lawton Clay Member is almost entirely composed of thinly laminated clay and silt, sometimes resembling varves. The organic content of the sediment is low and the unit is stiff and generally impermeable. Approximately 25 meters of Lawton Clay is exposed at its type section (Mullineaux and others, 1965), but as much as 45 meters of Lawton Clay underlies portions of West Seattle (Waldron, 1967). The contact between the Lawton Clay and the overlying Esperance Sand is gradational to distinct, with the transition to well-sorted, cross-bedded, fine- to medium grained sand usually taking place over an interval of less than 2 meters. The impermeable nature of the Lawton Clay and the well-sorted sandy character of the overlying Esperance Sand create water-saturated conditions along the Lawton-Esperance contact that are a major cause of spring-sapping and landsliding in the greater Seattle area (Tubbs, 1974). This water-saturated condition also exists in much of the subsurface underlying Seattle (fig. 3) and may be a contributing factor to intensified seismic ground shaking, particularly where Tertiary bedrock lies close to such sensitive sediments. the Esperance Sand ranges from 10 to 100 meters thick, with some 25 meters of horizontal and cross-bedded medium grained sand exposed at its type locality at Fort Lawton (Mullineaux and others 1965). The sand is loose, friable, and contains occasional lenses of pebble gravel. In the southwestern part of Seattle, the Esperance Sand grades upward into loose, well-bedded pebble and cobble gravel.

Glacial lodgement till caps these glaciofluvial and glaciolacustrine

sands and gravels. The till, formally named Vashon Till, consists of a very compact mixture of sandy clay and silt in the matrix, supporting numerous pebble to boulder-sized clasts of diverse lithology. The till can be as much as 10 meters thick, but is typically 2 to 3 meters thick. Minor amounts of loose, poorly sorted sandy pebble to cobble gravel, comprising ablation till and recessional outwash, overlie the lodgement till in a few places in the Seattle area, most notably near Fauntleroy, White Center, and east of Allentown.

The youngest geologic units of significance are the post-glacial alluvial and estuarine sediments that underlie the Duwamish River valley, and the extensive areas of man-made fill that form the substrate beneath much of the land area surrounding Elliot Bay, and the lower Duwamish River waterway. The Duwamish River alluvium is chiefly moderately sorted medium to fine sand and silt, with minor interbedded clay and peat. Shell-bearing estuarine sediments, of similar lithology underlie and interfinger with the alluvium up the Duwamish valley as far south as the Seattle City Limit near Boeing Field. The alluvial and estuarine sediments are loose, soft and generally water saturated. Duwamish River alluvium reaches thicknesses in excess of 50 meters in the southern part of Seattle, and fill and alluvium near the mouth of the Duwamish exceed 75 meters (fig. 4).

Extensive portions of downtown Seattle and Denny Hill were hydraulically removed near the turn of the century, mainly to lower street grades and enhance development. Much of the spoil was utilized as fill in the tidal regions of the Duwamish River estuary and along the water front surrounding Elliot Bay. Fill continued until approximately 20 years ago, resulting in large tracts of land, such as Harbor Island being reclaimed. Distinguishing hydraulic fill from natural alluvium in geotechnical borings can be difficult unless foreign material is encountered. Older fill tends to vary considerably in properties, depending on the variety of materials used. In general though, fill is soft, water-saturated, poorly to moderately sorted, muddy fine to medium sand with varying proportions of admixed and interbedded foreign matter (logs, woody debris, concrete, sawdust). More recent fill is of better quality, generally being medium to coarse sand which is better compacted than the older fill. Fill is typically 3 to 5 meters thick, but can attain thicknesses of as much as 10 meters.

## Depth Distribution of Important Geologic Units

Tertiary Bedrock: Water well and geotechnical drilling information gives an indication of the irregular nature of the bedrock surface lying beneath Seattle (fig. 5). The top of the Tertiary section is more than 1000 meters beneath sea level in the northern portion of the city but rises rapidly to the south beneath West Seattle and South Seattle. This configuration results from uplift on the south side of a major east-west trending gravity and aeromagnetic gradient which has been interpreted as a fault (Gower and Yount, in press). The effects of incision of the Duwamish River into this uplifted block are manifested by the NNW trending trough running beneath Boeing Field.
Lawton - Esperance Contact: The contact between Lawton Clay and Esperance Sand can be recognized in many geotechnical wells in the Seattle area. These units underlie most of West Seattle, Capitol Hill, Beacon Hill and portions of Rainier Beach. The contact is remarkably flat, generally lying between 40 and

80 meters above sea level (fig. 3). The gentle dips of the contact indicate that very little topography existed on the lake floor onto which the Esperance Sand was deposited.

In most wells that penetrate the Esperance Sand, the zone a few meters above the Lawton Clay is water-saturated, very soft, and shows very low penetration resistance (standard penetration usually less than 5 blows per foot).

## Correlation between ground shaking and distribution of subsurface lithologic units

As noted previously, the relation between ground shaking during the 1965 Seattle earthquake and the geologic unit immediately underlying the site, is not straight forward. The complicated problem of amplification effects for sites underlain by unconsolidated deposits over bedrock is beyond the scope of this geologic description (see Idriss and Seed, 1968; Borcherdt and others, 1975; Hays, 1980). One observation, however, may be important. Comparison of figures 3, 4, and 5 suggest that subsurface factors may play a part in controlling the observed ground shaking. Areas underlain by units with low impedence such as alluvium, fill, and water saturated Esperance Sand showed the strongest shaking effects where bedrock was near the sensitive unit. If a thick (greater than 100 meters) sequence of semi-consolidated Quaternary sediment was between the low impedence units and bedrock, ground shaking was attenuated (such as in the Magnolia area and Capitol Hill).

## References


Algermissen S. T. and Harding, S. T., 1965, The Puget Sound, Washington Earthquake of April 29, 1965: U.S. Coast and Geodetic Survey Preliminary Seismic Report, 26 p.

Borcherdt R. D., Joyner W. B., Warrick R. E., and Gibbs, J. F., 1975, Response of local geologic units to ground shaking: in U.S. Geological Survey Professional Paper 941-A, p. A52-A67.

Gower H. D. and Yount J. C., in preparation, Bedrock geology of the Seattle 1:100,000 map sheet, U.S. Geological Survey Miscellaneous Investigation Map.

Gower H. D. and Yount J. C., in press, Seismotectonic map of the Puget Sound region, Washington: U. S. Geological Survey Miscellaneous Geologic Investigations Map, scale 1:250,000.

Hays W. W., 1980, Procedures for estimating earthquake ground motions: U.S. Geological Survey, Professional Paper 1114, 77 p.

Idriss I. M. and Seed H. B., 1968, An analysis of ground motions during the 1957 San Francisco earthquake: Bulletin of the Seismological Society of America, v. 58, no. 6, p. 2013-2032.

Langston C. A., 1981, A study of Puget Sound Strong Ground Motion: Bulletin Seismolgical Society of America, v. 71, no. 3, p. 883-904.

Marsters, B., Spiker, E., and Rubin, M., 1969 U.S. Geological Survey Radiocarbon Dates X: Radiocarbon v. 11, no. 1, p. 210-227.

Mullineaux, D. R., 1965, Geologic map of the Renton Quadrangle, King County, Washington: U.S. Geological Survey, Geologic Quadrangle Map. GQ-405, scale 1:24,000.

Mullineaux D. R., 1970, Geology of the Renton, Auburn, and Black Diamond Quadrangles, King County, Washington: U.S. Geological Survey Professional Paper 672, 92 p.

Mullineaux D. R., Bonilla M. G., and Schlocker J.,1967, Relation of building damage to geology in Seattle, Washington during the April, 1965 Earthquake. U. S. Geological Survey Professional Paper 575-D, p. 183-191.

Mullineaux D. R., Waldron H. H., and Rubin M., 1965, Stratigraphy and chronology of late interglacial and early Vashon glacial time in the Seattle area, Washington: U.S. Geolgical Survey, Bull. 1194-O, 10 p.

Nuttli O. W., 1952, The western Washington earthquake of April 13, 1949; Seismological Society of America Bulletin, v. 42, p. 21-28.

Shakal, A. F., and Toksoz, M. N., 1980, Amplification and attenuation of site structure: (abstract), Earthquake Notes, v. 50, p. 20.

Stark W. J. and Mullineaux D. R., 1950, The glacial geology of the city of Seattle: M. S. thesis, University of Washington, Seattle, 88 p.

Tubbs, D.W., 1974, Landslides in Seattle: Washington Division of Geology and Earth Resources, Information Circular No. 52, 15p.

Waldron, H. H., 1967, Geologic map of the Duwamish Head Quadrangle, King and Kitsap Counties, Washington: U.S. Geological Survey Geological Quadrangle map GQ-706, scale 1:24,000.

Waldron, H. H., Liesch, B. A., Mullineaux, D. R., and Crandell, D. R., 1962, Preliminary geologic map of Seattle and vicinity, Washington: U.S. Geological Survey Miscellaneous Geologic Investigation Map. I-354, scale 1:31,680.

Wegner D. E., 1968, Glacial geology of Seattle Freeway: Washington State Highway Commission Department of Highways, unpublished report, 31 p.

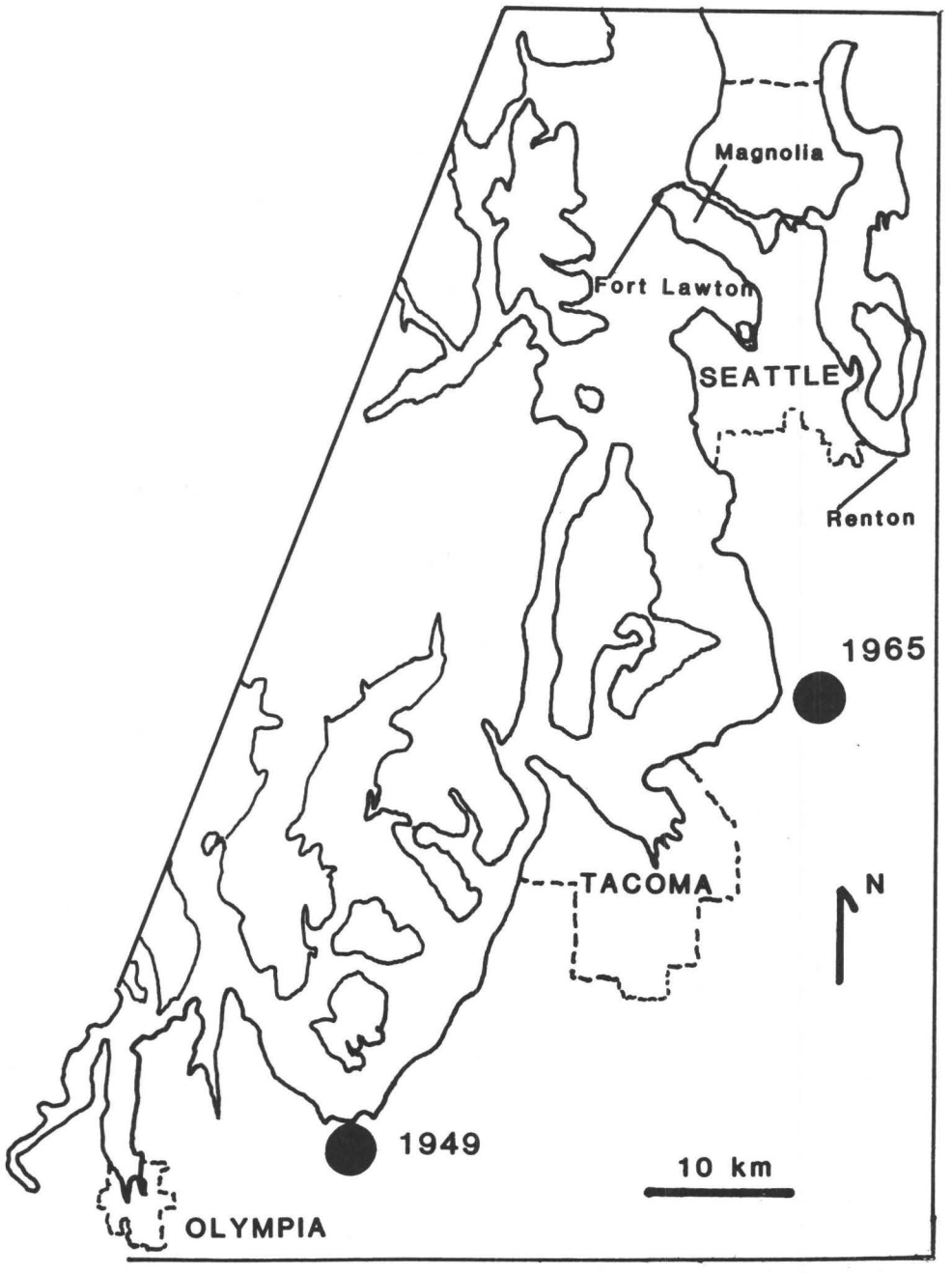


Figure 1A: Location map of Puget Sound. Epicenters for 1949 and 1965 earthquakes shown as filled circles.


Figure 1B: Principal geographic features of the greater Seattle area.

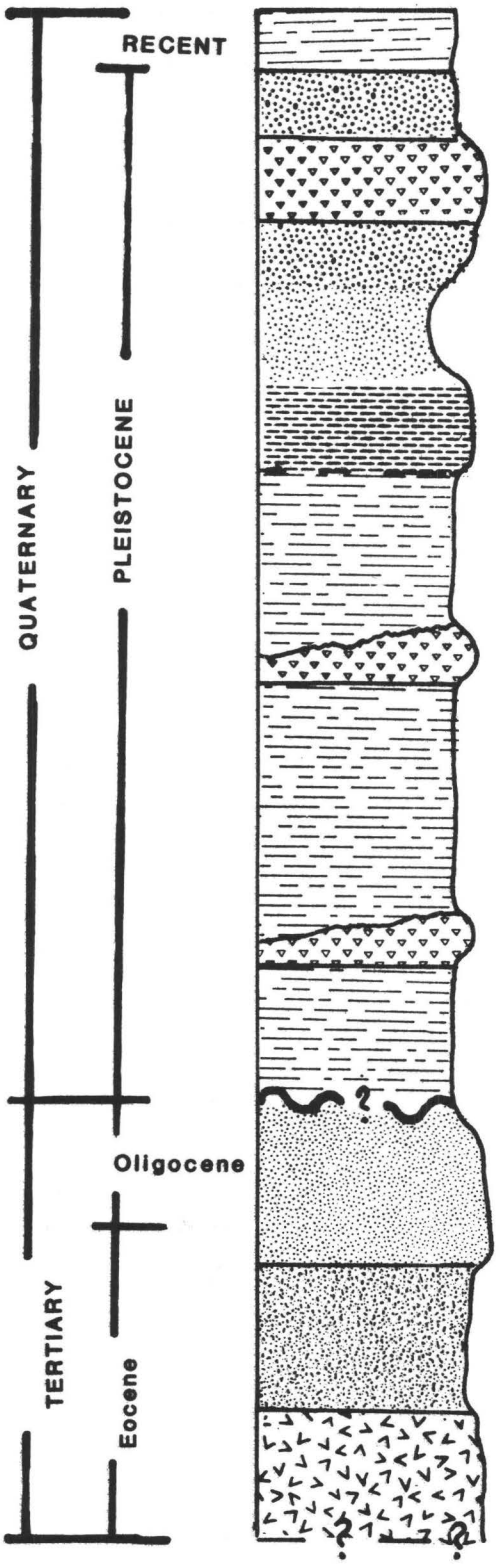


Alluvium

Vashon Recessional Outwash

Vashon Till

Vashon Advance Outwash

Esperance Sand Member

Lawton Clay Member

VASHON DRIFT

Olympia Nonglacial Sediments

Klinker Till

Duwamish Formation

Beacon Hill Till

unnamed sandstone and siltstone

Renton Formation

Tukwila Formation

Puget Group

no vertical scale

**Figure 2:**

**Composite Stratigraphic Column**
**Central Puget Sound**


Figure 3. Elevation above sea level of contact between Lawton Clay and Esperance Sand (in meters).

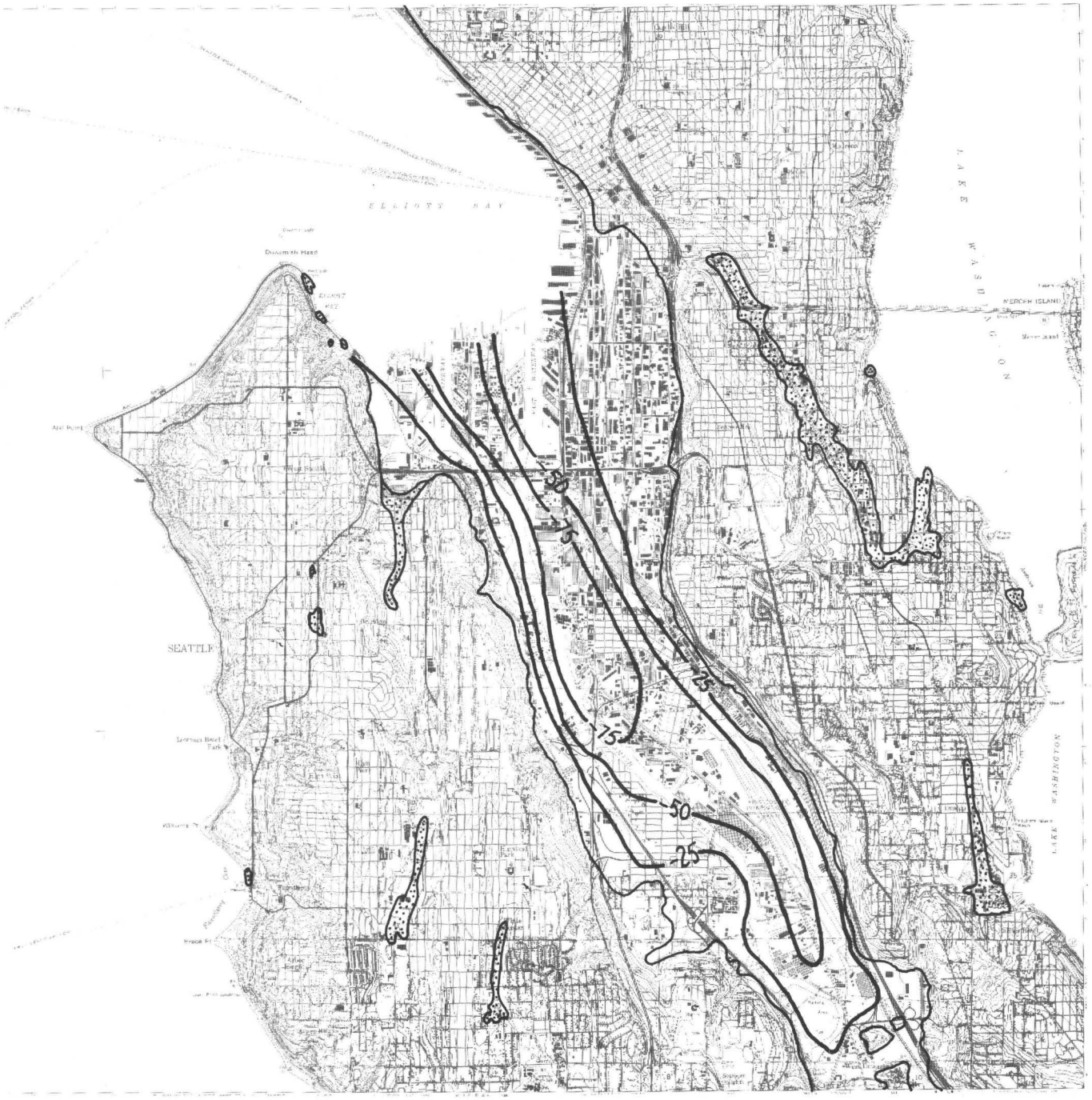


Figure 4: Elevation below sea level of base of Duwamish River alluvium and artifical fill (in meters). Areas underlain by thin alluvium (less than 10 meters) shown in stippled pattern.


Figure 5: Elevation relative to sea level of the top of Tertiary bedrock (in meters).

# LANDSLIDES, SOIL LIQUEFACTION, AND RELATED GROUND FAILURES IN PUGET SOUND EARTHQUAKES

David K. Keefer
U.S. Geological Survey
345 Middlefield Road
Menlo Park, California 94025

## ABSTRACT

This paper defines the common types and environments of earthquake-induced ground failures, discusses the occurrence of ground failures in the 13 April 1949 and 29 April 1965 Puget Sound earthquakes, and presents an evaluation of ground-failure susceptibilities of geologic environments in the Puget Sound region. Types and environments of ground failure were determined from a compilation of data on ground failures in 40 recent earthquakes including the 1949 and 1965 Puget Sound earthquakes. Data from the two Puget Sound earthquakes indicate that ground failures can occur throughout large areas in moderate or large earthquakes in this region. Geologic environments in the Puget Sound region with high susceptibilities to ground failure are areas of poorly compacted artificial fill; areas of Holocene alluvium, lacustrine sediments, or beach sediments; deltas of rivers emptying into Puget Sound; and rock or soil slopes steeper than 35° in the Puget Sound lowland or adjacent mountains.

## INTRODUCTION

Landslides, soil liquefaction, and related ground failures such as ground settlement and surface cracking are a major cause of property damage and loss of life in earthquakes. For example, a single landslide triggered by the 31 May 1970 Peruvian earthquake killed more than 18,000 people (Plafker and others, 1971), and several tens of thousands of people were killed by landslides in the 16 December 1920 earthquake in Kansu Province, China (Close and McCormick, 1922). Ground-failure damage exceeded $200 million in the 28 March 1964 Alaskan earthquake (Wallace Hansen, oral comm.) and $800 million in the 16 June 1964 Niigata, Japan earthquake (Lee and others, 1977).

Though historic earthquakes in the Puget Sound region have not produced ground-failure damage of this magnitude, ground failures in both the 13 April 1949 and the 29 April 1965 earthquakes did cause damage to buildings, highways, bridges, and other engineering structures. Similar earthquakes in the future can be expected to cause comparable damage; even greater ground-failure damage could occur in larger or shallower-focus

earthquakes or in earthquakes that occur in different parts of the Puget Sound region. This paper will first define the most common types and environments of earthquake-induced ground failures, then examine ground-failure occurrence in the 1949 and 1965 Puget Sound earthquakes, and finally define geologic environments in the Puget Sound region that have high susceptibilities to ground failure.

## GROUND-FAILURE DISTRIBUTION, TYPES, AND ENVIRONMENTS

Types and geologic environments of earthquake-induced ground failures are currently being determined from a global study of historic earthquakes (Keefer and others, 1978; Keefer, 1979); data from 40 earthquakes with magnitudes greater than 5 have been compiled from published and unpublished reports and from field investigations (Table 1). These earthquakes represent a sample drawn from most seismically active regions of the world and include several from the western United States. Data on numerous smaller earthquakes have been compiled from intensity reports on earthquakes in the United States during the 20-year period from 1958 through 1977[1].

### Distribution and Abundance

The number of ground failures and the size of the region affected by them in an earthquake depend on several factors including geologic conditions in the epicentral region, the size and focal depth of the earthquake, and characteristics of the ground shaking. Significant numbers of landslides and instances of ground settlement and surficial cracking occur in areas where shaking intensities are as low as MMI VI, and small numbers of such failures have been reported in areas where shaking intensities are as low as MMI V. We have not made similar correlations for soil liquefaction, but Kuribayashi and Tatsuoka (1977) found that soil liquefaction occurred at a minimum intensity of 5 on the JMA scale, which is equivalent to MMI VII to IX (Medvedev, 1962). Few ground failures are caused by earthquakes with magnitudes less than 5.0 whereas many earthquakes with magnitudes greater than 7.5 have caused tens of thousands of ground failures. Shallow-focus earthquakes generally cause more ground failures than deep-focus earthquakes of equal magnitude.

[1]The intensity reports are published annually under the title United States earthquakes. Prior to 1971, these were published by the U.S. Department of Commerce Coast and Geodetic Survey; between 1971 and 1974, they were published by the U.S. Department of Commerce National Oceanic and Atmospheric Administration (NOAA); and beginning in 1975, they have been published jointly by NOAA and the U.S. Geological Survey.

TABLE 1: HISTORIC EARTHQUAKES USED IN COMPILING GROUND FAILURE DATA

| Earthquake | Date | Magnitude[1] | Source of Data; Remarks |
|---|---|---|---|
| Assam, India | 15 Aug. 1950 | 8.6 | Published reports |
| Kansu, China | 16 Dec. 1920 | 8.5 | Published reports |
| Alaska | 27 Mar. 1964 | 8.4 | Published reports |
| Bihar-Nepal | 15 Jan. 1934 | 8.3 | Published reports |
| Chile | 22 May 1960 | 8.3 | Published reports |
| San Francisco, California | 18 Apr. 1906 | 8.25 | Published reports |
| Alaska | 10 July 1958 | 7.9 | Published reports |
| Hawke's Bay, New Zealand | 3 Feb. 1931 | 7.9[2] | Published reports |
| Tangshan, China | 27 July 1976 | 7.8 | Published reports |
| Peru | 31 May 1970 | 7.8 | Published reports |
| New Madrid, Missouri | 1811-1812 | | Published reports; Max. intensity = MMI XII |
| Khait, U.S.S.R. | 10 July 1949 | 7.6[2] | Published reports |
| Guatemala | 4 Feb. 1976 | 7.5 | Published reports |
| Niigata, Japan | 16 June 1964 | 7.5[3] | Published reports |
| Miyagi-ken-oki, Japan | 12 June 1978 | 7.4 | Field investigation |
| San Juan Province, Argentina | 23 Nov. 1977 | 7.4 | Field investigation |
| Kilauea, Hawaii | 29 Nov. 1975 | 7.1 | Published reports |
| Hebgen Lake, Montana | 17 Aug. 1959 | 7.1 | Published reports |
| Puget Sound, Washington | 13 April 1949 | 7.1[4] | Published and unpublished reports |
| Inangahua, New Zealand | 24 May 1968 | 7.1 | Published reports |

TABLE 1: HISTORIC EARTHQUAKES USED IN COMPILING GROUND FAILURE DATA (CONTINUED)

| Earthquake | Date | Magnitude[1] | Source of Data; Remarks |
|---|---|---|---|
| Imperial Valley, California | 19 May 1940 | 7.1 | Published and unpublished reports |
| Panama | 11 July 1976 | 7.0 | Published and unpublished reports |
| Madang, Papua New Guinea | 31 Oct. 1970 | 7.0 | Published reports |
| Khurgu, Iran | 21 Mar. 1977 | 6.9 | Published reports |
| Puget Sound, Washington | 29 Apr. 1965 | 6.5 | Published and unpublished reports |
| San Fernando, California | 9 Feb. 1971 | 6.5 | Published reports |
| Friuli, Italy | 6 May 1976 | 6.5 | Published reports |
| Borrego Mountain, California | 9 Apr. 1968 | 6.4[5] | Published reports |
| Santa Barbara, California | 29 June 1925 | 6.25[2] | Published reports |
| Honomu, Hawaii | 26 Apr. 1973 | 6.1 | Published reports |
| Indus-Kohistan, Pakistan | 28 Dec. 1974 | 6.2 | Published reports |
| Parkfield-Cholame, California | 27 June 1966 | 6.2 | Published reports |
| Mammoth Lakes, California | 25, 27 ~~June~~ May 1980 | 6.1, 6.2, 6.2 | Field investigation; Earthquake swarm |
| Fortuna-Rio Dell, California | 7 June 1975 | 5.7 | Field investigation |
| Santa Barbara, California | 13 Aug. 1978 | 5.6 | Field investigation |
| Mount Diablo, California | 24, 26 Jan. 1980 | 5.6, 5.4[5] | Field investigation; Earthquake swarm |
| Khulm, Afghanistan | 19 Mar. 1976 | 5.5 | Published reports |

TABLE 1: HISTORIC EARTHQUAKES USED IN COMPILING GROUND FAILURE DATA (CONTINUED)

| Earthquake | Date | Magnitude[1] | Source of Data; Remarks |
|---|---|---|---|
| Coyote Lake, California | 6 Aug. 1979 | 5.4 | Field investigation |
| Daly City, California | 22 Mar. 1957 | 5.3[5] | Published reports |
| Homestead Valley, California | 15 Mar. 1979 | 5.2[5] | Published reports |

[1]Surface wave magnitude ($M_s$) unless otherwise noted
[2]Magnitude determined by California Institute of Technology, Pasadena
[3]Magnitude determined by Japan Meterological Agency
[4]Body wave magnitude
[5]Local magnitude

## Landslides

The following types of earthquake-induced landslides are discussed in approximate order of decreasing total abundance in the earthquakes studied. Landslide names conform to those of Varnes (1978). The term rock as used in this report refers to firm bedrock that was intact and in place prior to failure. The term soil refers to any uncemented or poorly cemented aggregate of mineral grains, whether or not it contains any organic constituents.

Shallow slides and falls on steep slopes: The most common types of earthquake-induced landslides occur where individual boulders, blocks of soil, or masses of material up to a few meters thick are shaken loose from steep slopes and slide, roll, or move by free fall down the slopes. Rock falls and slides occur on slopes steeper than $35^{\circ}$ in almost every type of rock. These failures are most common where rocks are weathered, poorly cemented, or broken by joints or other discontinuities spaced less than one meter apart. Soil falls and slides occur on steep slopes such as streambanks or bluffs; they are most common in cohesionless or weakly-cemented granular soils. Rock and soil failures of these types frequently occur on artificially cut slopes, blocking roads and railroads and hindering relief efforts in the hours or days after an earthquake.

Slumps and block slides: Slumps and block slides, which involve the movement of relatively coherent blocks of soil or rock on discrete shear surfaces, are generally deeper seated than the shallow falls and slides discussed above. Block slides move in a translational manner; slumps move with a significant component of backward rotation. Slumps and block slides commonly occur on slopes steeper than $10^{\circ}$ in weathered, sheared, or weakly-cemented rocks, in fine-grained soils, and in poorly compacted or poorly drained artificial fills. Though many earthquake-induced slumps and block slides occur in areas with abundant preexisting slump and block slide deposits, few of the older deposits themselves are re-activated during earthquakes.

Lateral Spreads: In lateral spreads, blocks of soil move on layers of liquefied sand or silt or, in a few cases, on layers of weakened, sensitive clay. The blocks commonly break up as they move, and the subsidiary blocks may rotate, subside, or become partially liquefied. Many lateral spreads occur in areas where the overall surface slope is less than $2^{\circ}$; indeed at least one such failure moved a few centimeters up a slope of a fraction of a degree (Youd and Keefer, 1978). Most lateral spreads, however, are associated with locally steep free faces such as streambanks or bluffs.

Soil flows: Soil flows are fluid mixtures of water and soil that flow rapidly down slopes as gentle as a few degrees.

Materials with high susceptibilities to failures of this type are loose sands or silts, loess, volcanic ash, old landslide deposits, and uncompacted artificial fills. Soil flows commonly occur when seismic events coincide with periods of high rainfall; flows also occur on hillsides where soils are saturated or under artesian pore-water pressure at the time of an earthquake.

Rock and soil avalanches: Where ground shaking causes large masses of rock or soil to disintegrate, large rock or soil avalanches are formed. These avalanches, which generally have volumes of more than a million cubic meters, are capable of moving distances of several kilometers on slopes of a few degrees at velocities of several kilometers per minute. Thus, they are particularly hazardous to life and property. The landslide that killed 18,000 people in the 1970 Peruvian earthquake was a rock avalanche; the deaths in the 1920 Kansu Province earthquake were caused by soil avalanches. Rock avalanches occur on slopes several hundreds of meters high that are oversteepened by glacial, fluvial, or coastal erosion. Soil avalanches occur on steep slopes in weakly-cemented sands, loess, and volcanic pumice. Many soil avalanches have occurred in materials that form stable, near-vertical slopes under non-seismic conditions.

Subaqueous landslides: Subaqueous landslides are complex failures, involving components of slumping, lateral spreading and flow. They commonly occur in deltaic sediments, particularly where layers of liquefiable sand or silt are present. They are hazards to port and harbor facilities. For example, in the 1964 Alaska earthquake, subaqueous landslides caused significant damage to the ports of Valdez, Whittier, Seward, and Homer.

## Soil Liquefaction

Soil liquefaction is a primary or contributing cause in most lateral spreads, soil flows, and subaqueous landslides. Soil liquefaction also causes numerous other ground failure effects. These include ground settlement, settlement and tilting of engineering structures, flotation of buried structures such as pile foundations and tanks, surficial cracking, and erosion of cavities by fountains of soil and water under high pressure.

Soil liquefaction occurs in saturated sands and silts. Techniques for assessing liquefaction susceptibility on a regional basis developed by Youd and Perkins (1978) indicate that the liquefaction susceptibility of a sand or silt deposit is related to its age and depositional environment. According to Youd and Perkins (1978), river channel deposits, deltaic deposits, and uncompacted artificial fills less than 500 years old have "very high" liquefaction susceptibilities. Other materials less than 500 years old with "high" susceptibilities are flood plain, lacustrine, colluvial, dune, loess, tephra, sebka, estuarine, low-energy beach, lagoonal, and foreshore

sediments. Older sediments with "high" susceptibilities are Holocene river channel, tephra, and deltaic deposits; and Holocene and Pleistocene loess.

## Other Ground Failures

Ground settlements and surficial cracking also commonly occur during earthquakes in areas where soil liquefaction does not take place. The settlements are caused by vibrational compaction of loose soft soils and fills; much of the cracking is a manifestation of incipient landsliding. Earthquakes also trigger snow avalanches, generally in the same areas where snow avalanches occur under non-seismic conditions.

# GROUND FAILURES IN THE 1949 AND 1965 PUGET SOUND EARTHQUAKES

The two largest recent earthquakes in the Puget Sound regions were those of 13 April 1949 ($m_b$ = 7.1[1]) and 29 April 1965 ($m_b$ = 6.5; $M_s$ = 6.5[2]). Both earthquakes caused ground failures throughout large areas. Ground failures have also occurred in the earthquakes of 14-16 December 1872 (M. Hopper, oral comm., 1977), 13 November 1939 (Coombs and Barksdale, 1942), and 14 February 1946 (Barksdale and Coombs, 1946), but documentation of ground failures in these earthquakes is fragmentary. Hence, discussion of the historic record will concentrate on the 1949 and 1965 earthquakes. Ground failures in the 1949 earthquake were documented by engineering and intensity studies (Murphy and Ulrich, 1951; Hopper, unpub. data). Ground failures in the 1965 earthquake were documented by engineering and intensity studies (Steinbrugge and Cloud, 1965; von Hake and Cloud, 1967; Hopper, unpub. data) and, in Seattle, by geologic investigations (Mullineaux and others, 1967).

## Ground failures in the 13 April 1949 earthquake

The 13 April 1949 earthquake, which had an epicenter near Tacoma and a focal depth of 70 km (Nuttli, 1952), caused ground failures at sites scattered throughout an area of 30,000 $km^2$ (fig. 1). Soil liquefaction occurred up to 120 km from the epicenter, landslides occurred up to 180 km from the epicenter, and surficial cracking occurred up to 230 km from the epicenter. Most soil liquefaction occurred in areas with shaking intensities of MMI VIII; a few instances occurred in areas of MMI VII (Hopper, unpubl. data). Landslides, ground settlements, and surficial cracking occurred in areas with shaking intensities as low as MMI V. Ground failures damaged buildings, bridges, highways, railroads, and underground pipes; however, no quantitative estimate was made of the contribution of ground

[1]Body wave magnitude
[2]Surface wave magnitude

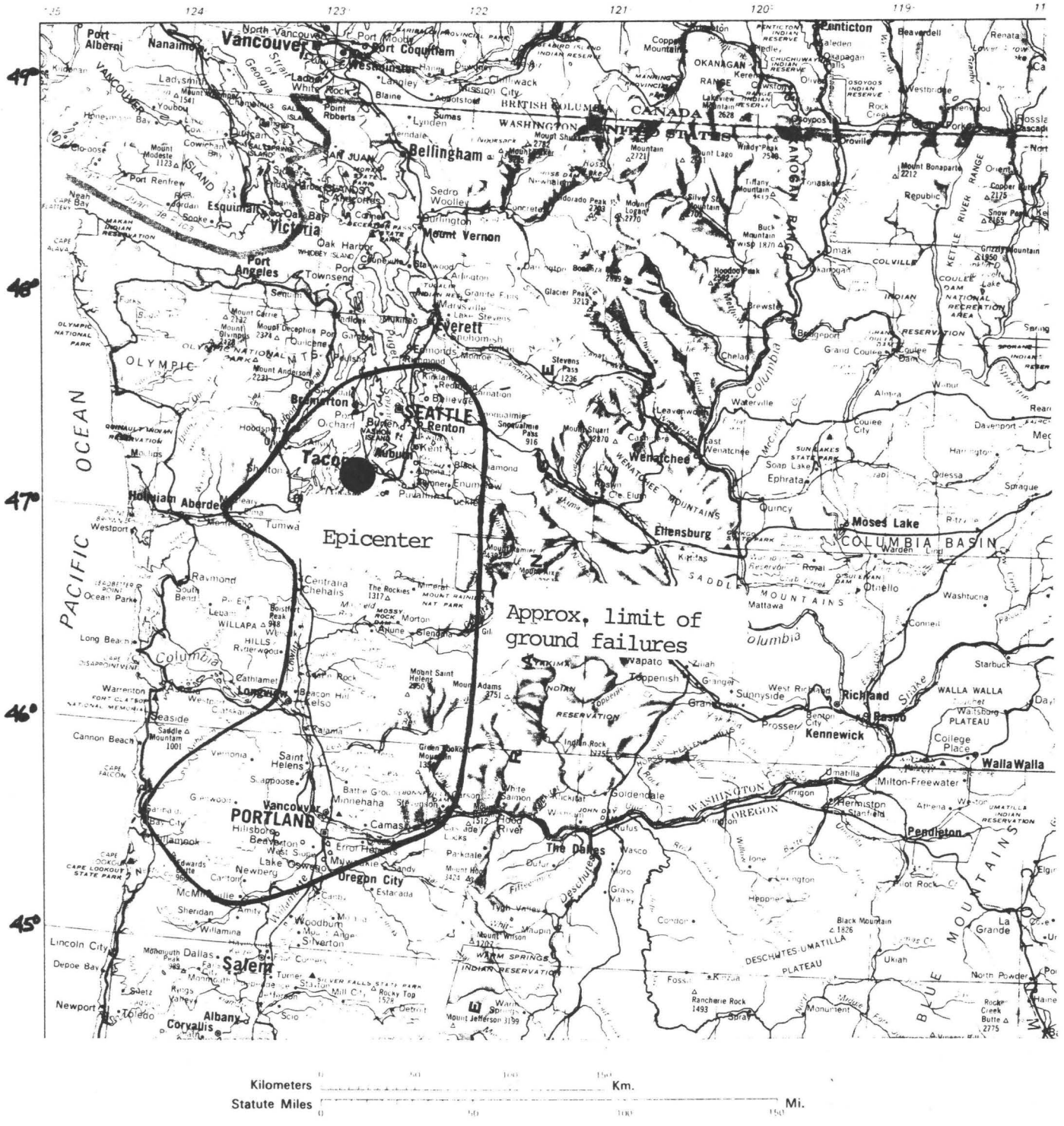


Figure 1: Area within which ground failures occurred in the 13 April 1949 Puget Sound earthquake

failures to the total earthquake damage of $25 million.

Data on the types, numbers, and geologic environments of ground failures in the 1949 earthquake are shown in Table 2. The most numerous ground failures were settlements and surficial cracking, some of which were caused by soil liquefaction. Most of the cracking occurred in artificial fill or Holocene alluvium consisting of soft sand, silt and clay; some cracking occurred in glacial till and outwash. Settlements occurred in artificial fill and in Holocene alluvium, deltaic, and beach deposits. Areas with high concentrations of damage due to cracking and settlement were the port area of Olympia, south Seattle, and the Duwamish Valley in Seattle.

Three days after the earthquake, a landslide with a volume of more than a million cubic yards (765,000 $m^3$), occurred on a bluff overlooking the Tacoma Narrows. The bluff was composed of glacial sand and gravel resting on a base of clay. This failure was probably a delayed response to weakening of the bluff by earthquake shaking. Other landslides triggered by the earthquake included four slumps and/or lateral spreads in artificial fill, Holocene alluvium, and peat; one subaqueous landslide in glacial drift and beach sand, and a dozen landslides of unknown type in artificial fill, Holocene alluvium and landslide deposits, and glacial till and outwash. A few landslides were reported in rock. Where slopes were described, the descriptions indicate that the landslides occurred on steep slopes. The earthquake also triggered snow avalanches on Mt. Rainier.

## Ground failures in the 29 April 1965 earthquake

The 29 April 1965 earthquake, which had an epicenter between Seattle and Tacoma and a focal depth of 59 km (Algermissen and Harding, 1965), caused ground failures at sites scattered throughout an area of 20,000 $km^2$ (fig. 2). Maximum distances from the epicenter to sites of ground failure were 36 km for soil liquefaction, 100 km for landslides, and 130 km for cracking of surficial materials. Soil liquefaction occurred in areas where the shaking intensity was MMI VII. Landslides, ground settlements, and surficial cracking occurred in areas with shaking intensities as low as MMI V (Hopper, unpubl. data). Approximately half of the reported ground failures were in Seattle. As in the 1949 earthquake, ground failures damaged buildings and other engineering structures, but the total damage due to ground failures was not determined. Total estimated damage from the 1965 earthquake was $12.5 million (Steinbrugge and Cloud, 1965).

As in the 1949 earthquake, the most numerous ground failures were settlements and surficial cracking (Table 3). In Seattle, these failures occurred in artificial fill, Holocene alluvium and landslide deposits, and glacial till and outwash. Damage due to

TABLE 2: GROUND FAILURES IN THE 13 APRIL 1949 PUGET SOUND EARTHQUAKE

LANDSLIDES

| Type | Number of Sites[1] | Geologic Materials and Environments[2] | Remarks |
|---|---|---|---|
| Rock falls | 2 | Steep slopes in Oligocene-Miocene andesite, basalt, and volcanic breccia | Several rock falls at each site |
| Landslides in rock; specific type not determined | 5 | Eocene- Miocene andesite, basalt, and volcanic breccia; Oligocene non-marine andesite conglomerate, tuff, and mudflow material; Jurassic-Cretaceous graywacke, argillite, siltstone, slate, volcanic rocks; rocks; Pre-Upper Jurassic greenschist metamorphic rocks, limestone, metaconglomerate, breccia, basic igneous rocks | Several landslides of two of the sites; one site on steep slopes, slopes at other sites undetermined |
| Soil slumps and/or lateral spreads[3] | 4 | Artificial fill, Holocene alluvium consisting of channel sand, flood plain silt and swamp deposits of silt, clay, and peat | |
| Subaqueous landslide | 1 | Sand spit and glacial drift | |
| Landslides in soil; specific type not determined | 12 | One large landslide (volume = 1 to 11 x $10^6$ yds $^3$) on bluff composed of glacial sand and gravel resting on base of clay. Other slides in Holocene alluvium composed of gravel, sand, silt, and clay; glacial till and outwash; Holocene landslide deposits; and artificial fill. | Multiple landslides at 6 sites; one or two sites on cut slopes; large landslide occurred 3 days after earthquake |

TABLE 2: GROUND FAILURES IN THE 13 APRIL 1949 PUGET SOUND EARTHQUAKE (CONTINUED)

SOIL LIQUEFACTION EFFECTS OTHER THAN LANDSLIDES

| Type | Number of Sites[1] | Geologic Materials and Environments[2] | Remarks |
|---|---|---|---|
| Settlements | 5 | Holocene alluvium; artificial fill; Holocene beach and deltaic deposits | |
| Surficial cracking | Several tens | Most in artificial fill; a few in Holocene alluvium; 2 to 4 sites possibly in glacial drift | |

OTHER GROUND FAILURES

| Type | Number of Sites[1] | Geologic Materials and Environments[2] | Remarks |
|---|---|---|---|
| Surficial cracking (soil and artificial fill) | Several tens | Most in artificial fill or Holocene alluvium; a few in glacial drift; a few in glacial outwash | |
| Settlements | 11 | Holocene alluvium; glacial drift; artificial fill | |
| Snow avalanches | Several | Steep slopes on Mt. Rainer | |
| Surficial cracking (rock) | 1 | Steep slope in Eocene andesite, basalt, or volcanic breccia | |

[1]Data from Murphy and Ulrich, 1951; Hopper, unpublished data

[2]Data from Washington Div. Mines and Geology, 1961

[3]Lateral spreads are caused by soil liquefaction

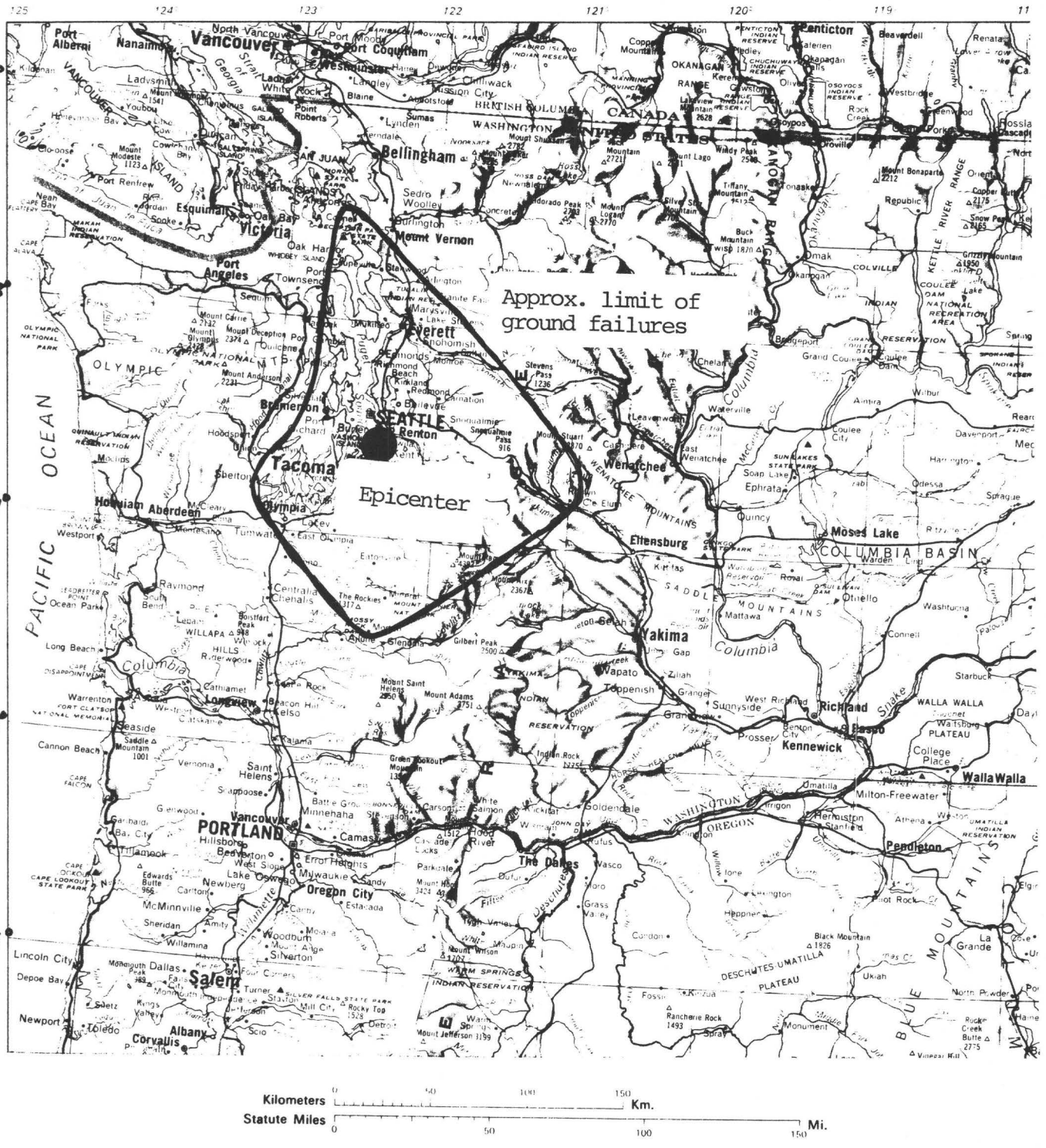


Figure 2: Area within which ground failures occurred in the 29 April 1965 Puget Sound earthquake

TABLE 3: GROUND FAILURES IN THE 29 APRIL 1965 PUGET SOUND EARTHQUAKE

LANDSLIDES

| Type | Number of Sites[1] | Geologic Materials and Environments[2] | Remarks |
|---|---|---|---|
| Landslides in rock; specific type not determined | 4 | Eocene sandstone, siltstone, shale, pyroclastic deposits, flow breccia, and volcaniclastic rocks; Jurassic-Cretacaeous graywacke, argillite, siltstone, slate, phyllite with local limestone and chert | 2 sites on steep slopes, slopes, slopes at other sites unknown |
| Soil slumps | 4 | Artificial fill; bluff composed of hard glacial till; steep slope composed of uncemented, loose, medium-grained Pleistocene sand ("Older Sand"); Holocene beach sand | |
| Landslides in soil, specific type not determined | 13 | Artificial fill; Holocene alluvium consisting of gravel, sand, silt with some peat and clay; glacial till and outwash; uncemented, loose, medium-grained Pleistocene sand ("Older Sand"); Holocene beach sand | One of fill failures was in rock fill |
| Lateral spreads[3] | 2 | Thin artificial fill overlying Holocene lacustrine sediments on lakeshore; fill of Harbor Island at mouth of Duwamish River | |

TABLE 3: GROUND FAILURES IN THE 1965 PUGET SOUND EARTHQUAKE (CONTINUED)

SOIL LIQUEFACTION EFFECTS OTHER THAN LANDSLIDES

| | | |
|---|---|---|
| Settlements | 2 | Artificial fill overlying Holocene alluvium; Holocene lacustrine sediments consisting of clay, silt, and fine sand |
| Surficial cracking | 4 | Artificial fill; Holocene lacustrine sediments consisting of clay, silt, and fine sand; Holocene alluvium |

OTHER GROUND FAILURES

| Type | Number of Sites[1] | Geologic Materials and Environments[2] | Remarks |
|---|---|---|---|
| Settlements and Surficial cracking (soil and artificial fill) | Several tens | Numerous failures in lower Duwamish Valley north of Spokane Street in artificial fill and Holocene alluvium consisting mostly of soft, saturated flood plain silt with some channel sand and swamp deposits of clay and peat. Numerous failures in West Seattle in uncemented, loose, Pleistocene medium sand ("Older Sand"); Holocene landslide deposits; hard glacial till and Pleistocene clay and gravel ("Vashon Till" and "Older Clay, Till, and Gravel"); and Pleistocene gravel ("Younger Gravel"). Some failures outside Seattle in glacial till and outwash; Holocene alluvium; and artificial fill | |

[1]Data from Steinbrugge and Cloud, 1965; von Hake and Cloud, 1967; Mullineaux and others, 1967; Hopper, unpublished data

[2]Data from Waldron and others, 1961; Washington Div. Mines and Geology, 1961; Steinbrugge and Cloud, 1965; Mullineaux and others, 1967

[3]Caused by soil liquefaction

ground failures was generally greatest at sites where soft, poorly compacted artificial fill overlay relatively soft Holocene alluvium. Damage was greatest in west Seattle and in the Duwamish Valley north of Spokane Street and the adjacent waterfront area. The Duwamish Valley area was also the location of concentrated damage in the 1949 earthquake as well as in the 14 February 1946 earthquake ($m_b$ = 5.8) (Barksdale and Coombs, 1946); this repetition of damage indicates that materials in these areas are particularly susceptible to ground failure. Outside Seattle, most sites of settlement and cracking were in glacial till and outwash; a few were in Holocene alluvium.

The earthquake also triggered landslides and soil liquefaction effects at several sites (Table 3). Slumps occurred in artificial fill and on steep slopes in glacial till and sand. Other landslides occurred in artificial fill, Holocene alluvium and beach deposits, and glacial till and outwash. Lateral spreads and liquefaction-induced ground settlements and surficial cracking occurred in artificial fill and in Holocene alluvium and lacustrine sediments. A few landslides were also reported in rock.

## DISCUSSION OF GROUND-FAILURE SUSCEPTIBILITIES OF GEOLOGIC ENVIRONMENTS IN THE PUGET SOUND REGION

The 1949 and 1965 earthquakes caused numerous reported incidents of settlement and surficial cracking but only small numbers of reported landslides. The sparsity of reported landslides is probably due, in part, to the properties of the materials in the epicentral region, in part to incomplete reporting, and in part to the deep foci of the earthquakes.

Data on ground failures in the two earthquakes are derived primarily from engineering and intensity surveys rather than from geologic field investigations. Thus, documentation of ground failures was not of uniform quality throughout the effected areas. Reporting appears relatively complete in populated areas but less complete in sparsely inhabited areas. Incomplete reporting probably explains the small numbers of landslides reported from steep rock slopes in the mountains bordering the Puget Sound lowland and from steep bluffs bordering Puget Sound itself. Studies of other historic earthquakes indicate that both of these environments have high susceptibilities to earthquake-induced landslides. Incomplete reporting may also explain why only one subaqueous landslide in Puget Sound was recorded in the two earthquakes; studies of other earthquakes indicate that delta fronts such as those bordering portions of Puget Sound also have high susceptibilities to landsliding.

Because both the 1949 and 1965 earthquakes were deep-focus events, significant attenuation of seismic energy probably took

place between the source and the ground surface. Thus, the earthquakes caused fewer landslides than would be caused by shallow-focus earthquakes of comparable magnitude. Many of the incidents of surficial cracking, however, were probably manifestations of incipient landsliding. If the ground shaking had been stronger or of longer duration, many more landslides would probably have occurred.

In populated areas of the Puget Sound lowland, Holocene alluvium and artificial fill demonstrated the highest susceptibilities to settlement, cracking, and landsliding in the 1949 and 1965 earthquakes. Because of the large proportion of failures in artificial fill, the most effective means of minimizing ground failures in future earthquakes are proper engineering control and compaction of fill and, where possible, avoidance of placing fill over soft alluvium.

Other materials for which smaller numbers of such ground failures indicate lower susceptibilities are Holocene beach and landslide deposits and glacial till and outwash deposits. Even allowing for possible incomplete reporting and the deep-foci of the earthquakes, the small numbers of landslides and incipient landslides that occurred in these materials indicate that, except on unusually steep slopes, they are only moderately susceptible to earthquake-induced landslides. Few descriptions in the intensity reports of the Puget Sound earthquakes are adequate for determining landslide types or slope inclinations. However, studies of other earthquakes in similar environments indicate that many of the landslides in soil and artificial fill were probably slumps that occurred on moderate to steep slopes.

Artificial fill and Holocene alluvium demonstrated the highest susceptibilities to soil liquefaction in the 1949 and 1965 earthquakes. Materials in the Puget Sound lowland that demonstrated somewhat lower, but still significant, susceptibilities were Holocene lacustrine, deltaic, and beach deposits. These results are consistent with findings in other earthquakes and with the criteria of Youd and Perkins (1978).

Areas with high concentrations of ground-failure damage in one or both earthquakes were the lower Duwamish Valley and the adjacent waterfront area, west Seattle, south Seattle, and the port area of Olympia. These areas are likely to sustain similar damage in future, moderate or large earthquakes.

## CONCLUSION

The historic record shows that landslides, soil liquefaction, settlements, and surficial cracking can occur throughout large areas in earthquakes in the Puget Sound region. The 13 April 1949 earthquake, the largest instrumentally recorded earthquake in the Puget Sound region, caused ground

failures of these types throughout an area of 30,000 $km^2$. Soil liquefaction occurred at sites within a radius of 120 km from the epicenter. Corresponding radii were 180 km for landslides and 230 km for surficial cracking.

Soil liquefaction effects in Puget Sound earthquakes have occurred in areas experiencing intensities as low as MMI VII. Landslides, ground settlements, and surficial cracking have occurred in areas with shaking intensities as low as MMI V. These correlations are consistent with results from historic earthquakes in other regions and provide an approximate means for estimating minimum levels of shaking intensity at which ground failures will occur in future earthquakes in the Puget Sound region.

The 1949 and 1965 earthquakes provide data on ground failures in the Puget Sound region under two particular sets of ground shaking conditions; studies of ground failures in other historic earthquakes provide additional information on ground failures in similar geologic environments under a wide variety of other ground shaking conditions.

Based on these two types of studies, it is concluded that the following geologic environments in the Puget Sound region are susceptible to earthquake-induced ground failure: (1) Holocene alluvium and artificial fill, especially poorly compacted fill, have high susceptibilities to landslides, cracking, settlement, and soil liquefaction. Types of landslides likely to occur on moderate to steep slopes in these materials are slumps, block slides, lateral spreads, and, to a lesser extent, shallow falls and slides. (2) Deltas bordering portions of Puget Sound have high susceptibilities to subaqueous landsliding and other soil liquefaction effects. (3) The steep bluffs bordering portions of Puget Sound have high susceptibilities to slumps, block slides, and shallow falls and slides. (4) Rock slopes steeper than $35^0$ in the Puget Sound lowland and adjacent mountains have high susceptibilities to rock falls and shallow rock slides, snow avalanches, and, to a lesser extent, to slumps and block slides. Very steep, high slopes in the mountains are susceptible to rock avalanches. (5) Holocene beach and landslide deposits and glacial till and outwash have moderate susceptibilities to landslides, settlement, and cracking except on steep bluffs or other slopes steeper than $35^0$ where susceptibilities are high. (6) In addition to artificial fill, and Holocene deltaic sediments and alluvium, Holocene beach and lacustrine sediments have high susceptibilities to soil liquefaction.

ACKNOWLEDGEMENT

The assistance of Nancy E. Tannaci in compiling data on the Puget Sound earthquakes is gratefully acknowledged.

## REFERENCES CITED


Algermissen, S. T., and Harding, S. T., 1965, Preliminary seismological report, in the Puget Sound, Washington earthquake of April 29, 1965: U.S. Dept. of Commerce Coast and Geodetic Survey, pp. 1-26.

Barksdake, J. D., and Coombs, H. A., 1946, The Puget Sound earthquake of February 14, 1946: Seismological Society of America Bulletin, v. 36, no. 4, p. 349-354.

Close, U. and McCormick, E., 1922, Where the mountains walked: National Geographic, v. 41, no. 5, p. 445-472.

Coombs, H. A., and Barksdale, J. D., 1942, The Olympic earthquake of November 13, 1939: Seismological Society of America Bulletin, v. 32, no. 1, p. 1-6.

Hopper, M., unpublished data.

Keefer, D. K., 1979, Landslides in historic earthquakes: Geological Society of America Abstracts with Programs, v. 11, no. 7, p. 454-455.

Keefer, D. K., Wieczorek, G. F., Harp, E., L., and Tuel D. H., 1978, Preliminary assessment of seismically induced landslide susceptibility: International Conference on Microzonation, 2d San Francisco, Proc., v. 1, p. 279-290. Reprinted in Brabb, E. E., (ed.), 1979, Progress on seismic zonation in the San Francisco Bay region: U.S. Geological Survey Circular 807, p. 49-60.

Kuribayashi, E., and Tatsuoka, F., 1977, History of Earthquake-induced soil liquefaction in Japan: Public Works Research Institute Bulletin, v. 31, 26 p.

Lee, K. L., Marcuson, W. F., III, Stokoe, K. H., II, Yokel. F. Y., (eds.), 1977, Research needs and priorities for geotechnical earthquake engineering applications: Report of workshop at Univ. of Texas, Austin, NSF Grant No. AEN77-09861, 134 p.

Medvedev, S. V., 1962, Engineering seismology: Trans., 1965, Israel Program for Scientific Translations, Jerusalem, U.S. Department of Commerce, Clearinghouse for Federal Scientific and Technical Information, TT 65-50011, 260 p.

Mullineaux, D. R., Bonilla, M. G., and Schlocker, J., 1967, Relation of building damage to geology in Seattle, Washington, during the April 1965 earthquake, in Geological Survey Research 1967: U.S. Geological Survey Professional Paper 575-D, pp. 183-191.

Murphy, L. M., and Ulrich, F. P., 1951, United States earthquakes 1949: U.S. Department of Commerce, Coast and Geodetic Survey, Serial 748, 64 p.

Nuttli, O. W., 1952, The western Washington earthquake of April 13, 1949: Seismological Society of America Bulletin, v. 42, no. 1, p. 21-28.

Plafker, G., Ericksen, G. E., and Concha, J. F., 1971, Geological aspects of the May 31, 1970, Peru earthquake: Seismological Society of America Bulletin, v. 61, no. 3, p. 543-578.

Steinbrugge, K. V. and Cloud, W. K., 1965, Preliminary engineering report, in the Puget Sound, Washington earthquake of April 29, 1965: U.S. Dept. of Commerce Coast and Geodetic Survey, pp. 27-51.

Varnes, D. J., 1978, Slope movement types and processes: in Schuster, R. L., and Krizek, R. J., (eds.), Landslides--analysis and control: Transportation Research Board Special Report 176, National Academy of Sciences, p.12-33.

von Hake, C. A., and Cloud, W. K., 1967, United States earthquakes, 1965: U.S. Dept. of Commerce Coast and Geodetic Survey, 91 p.

Waldron, H. H., Leisch, B. A., Mullineaux, D. R., and Crandell, D. R., 1961, Preliminary geologic map of Seattle and vicinity, Washington: U.S. Geological Survey, 3 sheets, scale 1:24,000.

Washington Division of Mines and Geology, 1961, Geologic map of Washington: 1 sheet, scale 1:500,000.

Youd, T. L., and Keefer, D. K., 1978, Liquefaction and landslides in the November 23, 1977, earthquake in San Juan, Argentina: Geol. Soc. America Abs. with Programs, Ann. Mtg., Toronto, Canada, v. 10, no. 3, p. 521.

Youd, T. L., and Perkins, D. M., 1978, Mapping liquefaction-induced ground failure potential: Journal of the Geotechnical Engineering Div., American Society of Civil Engineers, v. 104, no. GT4, p. 433-446.

# ISOSTATIC EFFECTS OF THE LAST GLACIATION IN THE PUGET LOWLAND, WASHINGTON

Robert M. Thorson
Puget Sound Earth Science Applications Project
U.S. Geological Survey
Seattle, Washington

present address:

University of Alaska Museum
Fairbanks, Alaska 99701

## ABSTRACT

During the Vashon Stade of the late Pleistocene Fraser Glaciation, the Puget lobe of the Cordilleran Ice Sheet advanced into western Washington, innundating the Puget lowland between the Cascade Range and Olympic Mountains. During systematic recession of the Puget lobe between about 14,000 and 13,000 years B. P., a complex system of proglacial lakes formed in the troughs of the Puget Sound region. Initially the lakes drained south via the Chehalis River to the Pacific Ocean, but lake drainage was later directed northward to the Strait of Juan de Fuca. Following deglaciation of the lowland about 13,000 years ago, marine waters invaded the areas formerly occupied by proglacial lakes.

The surfaces of the proglacial lakes (water planes) that formerly occupied the Puget lowland can be reconstructed from lake spillways that controlled the height of the lakes, and from outwash deltas built at the lake surfaces. The marine limit in the northern Puget lowland is also a nearly isochronous water plane, and can be reconstructed from the distribution of raised marine deltas, glacial-marine drift, and meltwater channels. The ancient marine and lacustrine water planes were determined independently, yet both indicate a regional gradual northward increase in the amount of postglacial deformation, reaching a maximum of about 140 meters in the northern Puget lowland. The major cause of postglacial deformation in the Puget lowland was a return to isostatic equilibrium following deglaciation. At least one, and possibly three, significant departures from the regional pattern of uplift near Seattle were probably caused by Holocene tectonic warping and (or) possibly by variations in the rate of glacier retreat.

Comparison of the predicted and observed isostatic responses indicates that the substratum below the Puget lowland responded rapidly to the mass imbalance caused by ice-sheet glaciation. As

much as 35 to 70 % of isostatic equilibrium apparently was attained at the glacial maximum, which occurred less than several thousand years after glaciers invaded the Puget lowland. This inferred rapid response is supported by relatively low estimates for the effective viscosity of the substratum obtained from minimum uplift rates following deglaciation (3 cm/yr). The large amount and rapid rate of isostatic rebound in the Puget lowland within the last 13,000 years may relate to regional crustal structure, Quaternary faulting, and recent seismicity.

# GEOLOGIC CONSTRAINTS ON THE MOVEMENT HISTORY OF THE STRAIGHT CREEK FAULT

Joseph A. Vance
Department of Geological Sciences
University of Washington
Seattle, Washington 98195

and

Robert B. Miller
Department of Geology
University of Kansas
Lawrence, Kansas 66045

## ABSTRACT

The Straight Creek fault is a major tectonic feature of the northwest Cordilleran region. This linear N-S trending, high-angle structure is approximately 200 km long in the northern Washington Cascades (Vance, 1957 and 1977; Misch, 1966 and 1977) and continues north a further 210 km into southern British Columbia as the Hope and Fraser River fault systems (Read, 1960; McTaggart and Thompson, 1967). In recent years the fault has become the object of much speculation with regard to the Cenozoic tectonics of the Pacific Northwest. Major strike-slip movement has been postulated on the fault (Misch, 1977). By some workers it has been considered a candidate structure for large prehistoric or potential earthquakes and one federal agency has declared it to be probably active (J. T. Whetten, press interview, 1978).

The Straight Creek fault system in Washington State is here treated as three large segments separated by Tertiary plutons. The northern segment lies between the Chilliwack batholith which straddles the International Border and the Monte Cristo pluton; the central segment lies between the Monte Cristo and the Snoqualmie batholith; and the southern segment extends from the Snoqualmie batholith to the central Washington Cascades about 15 km south of the Yakima River. On the northern segment the fault juxtaposes schists, migmatites, gneissess and plutonic rocks of the Skagit terrane east of the fault with a western assemblage including Jura-Cretaceous blueschists, greenschists, and phyllites (Easton Fm.), Paleozoic sedimentary and volcanic rocks (Chilliwack Fm.) and Jurassic ophiolitic rocks and their sedimentary cover. Deformed Eocene continental sediments (Chuckanut Fm.) are trapped in a discontinuous belt along the west side of the Straight Creek fault from the Suiattle River

north into British Columbia.

In the central segment the Straight Creek fault appears to have been largely obliterated by a N-S zone of Tertiary plutonic and volcanic rocks emplaced along the fault. We interpret the Evergreen Fault (Yeats, 1958 and 1977) which lies about 5 km east of the projection of Straight Creek as a major Straight Creek fault splay. The low contrast in metamorphic grade across the fault and the presence of 90 m.y. plutonic rocks of the Mt. Stuart batholith on both sides of the Evergreen fault preclude major strike-slip displacement on that structure. We interpret the Easton Schist as lying east of the Straight Creek fault in this segment.

In the southern segment the Straight Creek fault is represented by the Kachess fault north of the Yakima River and the Goat Peak fault to the south. Pre-Cenozoic units, including the Easton Schist and quartz dioritic gneisses, are restricted to the east side of the faults. Both faults cut Eocene units which are strongly deformed and overturned adjacent to the faults. The Goat Peak fault turns southeast into the Taneum Lake fault about 15 km south of the Yakima River. The fault has no expression in the middle Eocene Naches Formation and younger units along its projected southern continuation.

The length and remarkable linearity of the Straight Creek fault are consistent with major transcurrent movement. Moreover, the juxtaposition across the fault of terranes with markedly dissimilar histories, such as the high P/T Easton Schist and the amphibolite facies rocks of the Skagit Suite, is difficult to explain solely by dip-slip displacement. Misch (1966 and 1977) proposed approximately 200 km of right-slip movement based on apparent dextral drag patterns in the northern segment and metamorphic terranes offset between the Mt. Stuart area of the central Washington Cascades and the Harrison Lake area of southern British Columbia. Comparable dextral displacement is required if the north-directed fault systems of the San Juan Islands and Ingalls areas are correlative (Vance and others, 1980). Finally, at least 100 km of right-slip offset is implied by the displacement required to restore the Easton Schist east of the Straight Creek fault in the central and southern segments to a position adjacent to the Easton Schist of the northern segment.

Major transcurrent movement on the Straight Creek system post-dates 90 m.y. plutons which are offset by the fault. Most of this movement probably occurred in latest Cretaceous and Paleocene time during a magmatic hiatus in which the region west of the fault was coupled to a north-moving oceanic plate in a configuration analogous to the present day San Andreas system (Vance, 1977). Renewal of plate convergence and the transition to compressive tectonics was signaled by the onset of Eocene magmatic activity in the northwest at about 53 m.y. If strike-slip movement on the scale proposed is correct, the fault must continue south under the cover of middle Eocene and younger

beds. The 40 degree bend of the Goat Peak fault into the Taneum Lake structure is too sharp to accomodate large transcurrent movement. Thus, major strike-slip movement on the system must have ended by the middle Eocene. This conclusion is supported by the dominantly compressional nature of the deformation of the Naches Formation adjacent to the fault in the southern segment. This deformation is marked by tight overturned folds and high-angle east-dipping reverse faults.

Frizzell (1979) has suggested that Eocene continental sedimentary units in the east central Washington Cascades have been offset from correlative units in the northwest Cascades by major strike-slip on the Straight Creek fault. Too little is known, however, about the initial distribution and exact ages of these units to test this speculation. Mapping by Ashelman (1979) in the Kachess Lake area shows that fold axes in the early Eocene Swauk Formation swing from a northwest to a more northerly trend as they approach the Kachess fault, thus implying right-lateral movement. This drag effect, however, is not seen in the axes of folded middle Eocene Naches Formation adjacent to the fault. We believe that large strike-slip displacement on the Straight Creek system ended prior to middle Eocene time when it was supplanted by compressional tectonics and dip-slip movement on the fault. Similarly, Eocene Chuckanut conglomerates adjacent to the Straight Creek fault just north of Marblemount contain cobbles of meta-quartz diorite derived from a local source immediately east of the fault. Clearly no significant transcurrent movement has occurred here since the deposition of the conglomerates.

The Straight Creek fault system in the Washington Cascades is roughly coincident with a zone of shallow Oligocene and Miocene granitic plutons. Emplacement of many of these intrusions has been controlled by the fault. Field work demonstrates that several of these intrusions seal the fault and have not been broken by subsequent movement on the fault. There is no expression of the Straight Creek fault in rocks dated at about 33 m.y. (Misch, 1979) in the southern Chilliwack batholith. Similarly a 35 m.y. pluton has intruded the fault in southern British Columbia, but shows no offset on the projection of the fault (Richards and McTaggart, 1976). The Monte Cristo and Grotto plutons dated at about 25 m.y. (Yeats and Engels, 1971) have been emplaced along the fault but show no evidence of offset. The eastern Snoqualmie batholith similarly truncates the fault, but shows no internal expression of that structure (Ellis, 1959) and the Three Queens stock dated at 30 m.y. (R. W. Tabor, pers. comm.) was emplaced along the fault, but is not cut by it. We conclude that activity on the Straight Creek fault had ended on those segments intruded by the plutons by early Oligocene time and probably had ended on the entire system. It might be argued that the intervening segments remained active. In the absence of a through-going Straight Creek structure, however, any such activity could not have involved a significant strike-slip component, and even dip-slip displacement would be limited especially in proximity to the blocking plutons.

The absence of any expression of the Straight Creek fault in these Oligocene and Miocene plutons refutes tectonic models requiring young transcurrent movement on the Straight Creek system (e.g., Laubscher, unpublished report to WPPSS). Similarly it supports the gravitational, non-tectonic origin proposed for linear scarps described along the Straight Creek fault near Marblemount (Woodward-Clyde Consultants, 1978) and Kachess Lake (Ashelman, 1979).

## REFERENCES


Ashelman, J.C., 1979, The geology of the western part of the Kachess Lake Quadrangle, Washington: M.S. thesis, University of Washington, Seattle, Washington, 88p.

Ellis, R.C., 1959, The geology of the Dutch Miller Gap area, Washington: Ph. D. thesis, University of Washington, Seattle, Washington, 113p.

Frizzell, V.A., 1979, Petrology and stratigraphy of Paleocene nonmarine sandstones, central Cascades, Washington: Ph. D. thesis, Stanford University, Stanford, California, 151p.

McTaggart, K.C. and Thompson, R.M., 1967, Geology of part of the Northern Cascades in southern British Columbia: Canadian Journal of Earth Science, v. 4, p. 1199-1228.

Misch, Peter, 1966, Tectonic evolution of the North Cascades of Washington State-- A west Cordilleran case history: in A symposium on tectonic history and mineral deposits of the Western Cordillera in British Columbia and neighboring parts of the United States, H.C. Gunning, ed., Canadian Institute of Mining and Metallurgy, Special Paper No. 8, p. 101-148.

_____, 1977, Dextral displacements at some major strike faults in the Northern Cascades (abstract): Geological Association of Canada, Program with Abstracts, v. 2, p. 37.

_____, 1979, Geologic map of the Marblemount Quadrangle, Washington: State of Washington, Division of Geology and Earth Resources Geologic Map GM-23, scale 1:48,000.

Read, P.B., 1960, Geology of the Fraser River valley between Hope and Emory Creek, British Columbia: M.A.Sc. thesis, University of British Columbia, Vancouver, Canada, 145p.

Richards, T.A. and McTaggart, K.C., 1976, Granitic rocks of the southern coast plutonic complex and Northern Cascades of British Columbia: Geological Society of America Bulletin, v. 87, p.935-953.

Vance, J.A., 1957, The geology of the Swauk River area in the northern Cascades of Washington: Ph. D. thesis, University

of Washington, Seattle, Washington, 312p.

_____, 1977, Fault studies in the north Cascades: in Washington Public Power Supply System, Preliminary Safety Analysis Report-- WPPSS Nuclear Project No. 1, Amendment 23, Subappendix 2R D, Chapter 5.0, p. 2R D.5-1 to 2R D.5-32.

Vance, J.A., Dungan, M.A., Blanchard, D.P. and Rhodes, J.M., 1980, Tectonic setting and trace element geochemistry of Mesozoic ophiolitic rocks in western Washington: American Journal of Science, v. 280-A, Part 1, p. 359-388.

Woodward-Clyde Consultants, 1978, Straight Creek Fault Zone Study: 1872 Earthquake Studies for Washington Public Power Supply System, Nuclear Project Nos. 1 and 4, 75p.

Yeats, R.S., 1958, Geology of the Skykomish area in the Cascade Mountains of Washington: Ph. D. thesis, University of Washington, Seattle, Washington, 249p.

_____, 1977, Structure, plutonism, and volcanism of the central Cascades, Washington, Part I. General geologic setting of the Skykomish Valley: in Geologic Excursions in the Pacific Northwest, E.H. Brown and R.C. Ellis, eds., Geological Society of America Annual Meeting, 1977, Seattle, Washington, p. 265-275.

Yeats, R.S., and Engels, J.C., 1971, Potassium-argon ages of plutons in the Skykomish-Stillaguamish areas, north Cascades, Washington: U.S. Geological Survey Professional Paper 750-D, p. D34-D38.

GPO 687-040/14

## CONFERENCES TO DATE

| | |
|---|---|
| Workshop XV | A Workshop on "Preparing for and Responding to a Damaging Earthquake in the Eastern United States" Open-File No. 82-220 |
| Workshop XVI | The Dynamic Characteristics of Faulting Inferred from Recordings of Strong Ground Motion Open-File No. 82-591 |
| Workshop XVII | Workshop on Hydraulic Fracturing Stress Measurements Open-File No. 82-1075 |